SANDIA REPORT

SAND92–0700/4 • UC–721
Unlimited Release
Printed August 1993

Preliminary Performance Assessment for the Waste Isolation Pilot Plant, December 1992

Volume 4: Uncertainty and Sensitivity Analyses for 40 CFR 191, Subpart B

WIPP Performance Assessment Department

Prepared by
Sandia National Laboratories
Albuquerque, New Mexico 87185 and Livermore, California 94550
for the United States Department of Energy
under Contract DE-AC04-76DP00789

Issued by Sandia National Laboratories, operated for the United States Department of Energy by Sandia Corporation.

Available to DOE and DOE contractors from
Office of Scientific and Technical Information
PO Box 62
Oak Ridge, TN 37831

Prices available from (615) 576-8401, FTS 626-8401

Available to the public from
National Technical Information Service
US Department of Commerce
5285 Port Royal Rd
Springfield, VA 22161

NTIS price codes
Printed copy: A18
Microfiche copy: A01

SAND92-0700/4
Unlimited Release
Printed August 1993

Distribution
Category UC-721

Preliminary Performance Assessment for the Waste Isolation Pilot Plant, December 1992

Volume 4: Uncertainty and Sensitivity Analyses for 40 CFR 191, Subpart B

WIPP Performance Assessment Department
Sandia National Laboratories
Albuquerque, New Mexico 87185

ABSTRACT

Before disposing of transuranic radioactive waste in the Waste Isolation Pilot Plant (WIPP), the United States Department of Energy (DOE) must evaluate compliance with applicable long-term regulations of the United States Environmental Protection Agency (EPA). Sandia National Laboratories is conducting iterative performance assessments (PAs) of the WIPP for the DOE to provide interim guidance while preparing for a final compliance evaluation. This volume of the 1992 PA contains results of uncertainty and sensitivity analyses with respect to the EPA's *Environmental Protection Standards for Management and Disposal of Spent Nuclear Fuel, High-Level and Transuranic Radioactive Wastes* (40 CFR 191, Subpart B). Additional information about the 1992 PA is provided in other volumes. Volume 1 contains an overview of WIPP PA and results of a preliminary comparison with 40 CFR 191, Subpart B. Volume 2 describes the technical basis for the PA, including descriptions of the linked computational models used in the Monte Carlo analyses. Volume 3 contains values for input parameters used in consequence and probability modeling. Volume 5 contains uncertainty and sensitivity analyses of gas and brine migration for undisturbed performance. Finally, guidance derived from the entire 1992 PA is presented in Volume 6.

Results of the 1992 uncertainty and sensitivity analyses indicate that, conditional on the modeling assumptions, the choice of parameters selected for sampling, and the assigned parameter-value distributions, the most important parameters for which uncertainty has the potential to affect compliance with 40 CFR 191B are: drilling intensity, intrusion borehole permeability, halite and anhydrite permeabilities, radionuclide solubilities and distribution coefficients, fracture spacing in the Culebra Dolomite Member of the Rustler Formation, porosity of the Culebra, and spatial variability of Culebra transmissivity. Performance with respect to 40 CFR 191B is insensitive to uncertainty in other parameters; however, additional data are needed to confirm that reality lies within the assigned distributions.

ACKNOWLEDGMENTS

The Waste Isolation Pilot Plant (WIPP) Performance Assessment (PA) Department is comprised of both Sandia National Laboratories (SNL) and contractor employees working as a team to produce preliminary comparisons with Environmental Protection Agency (EPA) regulations, assessments of overall long-term safety of the repository, and interim technical guidance to the program. The on-site team, affiliations, and contributions to the 1992 performance assessment are listed in alphabetical order:

Performance Assessment Department

Name	Affil.*	Primary Author of Major Code	Area of Responsibility
R. Anderson	SNL		Department Manager
B. Baker	TEC		SECO2D, Hydrology, Office Manager
J. Bean	UNM		BRAGFLO, 2-Phase Flow
J. Berglund	UNM	CUTTINGS	Task Ldr., Cuttings/Cavings/ Spallings, Engr. Mech.
S. Bertram-Howery	SNL		PA Liaison with DOE, Criteria Document, Test Phase Plan
W. Beyeler	SAI	PANEL, GARFIELD	Geostatistics, Analytical Models, CAMCON Systems Codes
K. Brinster	SAI		Geohydrology, Conceptual Models
R. Blaine	ECO		SECO2D, SECOTP, & CAMCON Systems Codes
T. Blaine	GC		Drilling Technology, Exposure Pathways Data
K. Byle	UNM		Software and Analysis QA
J. Chapman	TRI		Documentation V.3
D. Duncan	MAC		Data QA
K. Economy	ECO		SECO2D, SECOTP, Hydrology &
D. Gallegos	SNL		Transport Task Ldr., Hydrology, Geostatistics, NEA, PSAG
D. Galson	GS		NEA Working Groups, PSAG, PAAG, Human Intrusion
J. Garner	API	PANEL	Source Term, Sens. Anal.
A. Gilkey	UNM		CAMCON Systems Codes
L. Gomez	SNL		Task Ldr., Safety Assessments
M. Gruebel	TRI		EPA Regulations, Documentation V.1, Editor V.1
R. Guzowski	SAI		Geology, Scenario Construction
J. Helton	ASU	CCDFPERM	Task Ldr., Uncert./Sens. Anal., Probability Models, Editor V.4
S. Hora	UHH		Expert Elicitation, Probability Models
H. Iuzzolino	GC	CCDFCALC CCDFPERM	LHS, CAMCON System Codes, Probability Models
R. Klett	SNL		EPA Regulations
P. Knupp	ECO	SECOTP	Comp. Fluid Dyn.
M. LaVenue	INT	GRASP-INV	Hydrology/Geostatistics
C. Leigh	SNL	GENII-S	Exposure Pathways

M. Marietta	SNL		Dep. Dept. Manager, Tech. Coord.
G. de Marsily	UP		Geostatistics Expert Group Chair
R. McCurley	UNM		CAMCON System Codes
B. Napier	PNL	GENII	Safety Assessments
A. Peterson	SNL		Task Ldr., Inventory
B. RamaRao	INT	GRASP-INV	Geostatistics
J. Rath	UNM		CAMCON System Codes
R. Rechard	SNL		Task Ldr., CAMCON, QA
P. Roache	ECO	SECO	Task Ldr., Comp. Fluid Dyn.
D. Rudeen	UNM		STAFF2D, SECOTP, Transport
J. Ruge	ECO		Multigrid Methods/BRAGFLO
T. Russell	ECO		Upscaling
K. Salari	ECO	SECOTP	Transport, Computational Fluid Dynamics
J. Sandha	SAI		INGRES, PA Data Base
J. Schreiber	SAI		BRAGFLO, 2-Phase Flow
D. Scott	TRI		Documentation V.2
P. Swift	TRI		Task Ldr., Geology, Climate Var., Editor V.1, 2, 4, & 5
M. Tierney	SNL		Task Ldr., CDF Constr., Probability Models, Ref. Data, Editor V.2 & 3
K. Trauth	SNL		Task Ldr., Expert Panels
P. Vaughn	API	BRAGFLO	Task Ldr., 2-Phase Flow & Waste Panel Chemistry, Editor V. 4 & 5
T. Zimmerman	GRA		Geostatistics Test Problem

The foundation of the annual WIPP performance assessment is the underlying data set and understanding of the important processes in the engineered and natural barrier systems. Other SNL Departments are the primary source of these data and understanding. Assistance with the waste inventory comes from Westinghouse Electric Corporation and its contractors. We gratefully acknowledge the support of our departmental and project colleagues. Some individuals have worked closely with the performance assessment team, and we wish to acknowledge their contributions individually:

H. Batchelder	WEC	CH & RH Inventories
R. Beauheim	SNL	Natural Barrier System, Hydrologic Parameters
D. Borns	SNL	Geology, Geophysics
B. Butcher	SNL	Engineered Barrier System, Unmodified Waste-Form Parameters, Disposal Room Systems Parameters
L. Brush	SNL	Engineered Barrier System, Source Term (Solubility) and Gas Generation Parameters
L. Clements	ReS	Computer System Support
T. Corbet	SNL	Natural Barrier System, Geologic & Hydrologic Parameters, Conceptual Models
P. Davies	SNL	Natural Barrier System, Hydrologic & Transport Parameters, & 2-Phase Flow Mechanistic Modeling
P. Drez	DEA	CH & RH Inventories
R. Finley	SNL	Repository Isolation Systems Parameters
F. Gelbard	SNL	Natural Barrier System, Retardation

E. Gorham	SNL	Natural Barrier System, Fluid Flow & Transport Parameters
R. Holt	CON	Geology
S. Howarth	SNL	Natural Barrier System, Hydrologic Parameters
R. Kehrman	WEC	CH & RH Waste Characterization
K. Lickliter	BEC	EPA Regulations
R. Lincoln	SNL	Room Modeling
F. Mendenhall	SNL	Engineered Barrier System, Unmodified Waste Form Parameters, Waste Panel Closure (Expansion)
D. Munson	SNL	Reference Stratigraphy, Constitutive Models, Physical & Mechanical Parameters
C. Novak	SNL	Natural Barrier Systems, Chemistry
E. Nowak	SNL	Room Modeling, Source Term
J. Orona	ReS	Computer System Support
A. Stevens	SNL	DOE Liaison
J. Tillerson	SNL	Repository Isolation Systems Parameters
W. Wawersik	SNL	Fracturing
S. Webb	SNL	2-Phase Flow Sensitivity Analysis & Benchmarking

* Affiliation

API = Applied Physics Incorporated
ASU = Arizona State University
BEC = Benchmark Environmental Corp.
CON = Consultant
DEA = Drez Environmental Associates
ECO = Ecodynamics Research Associates
GC = Geo-Centers Incorporated
GRA = GRAM, Inc.
GS = Galson Sciences
INT = Intera
MAC = MACTEC
PNL = Pacific Northwest Laboratory
ReS = ReSpec
SAI = Scientific Applications International Corporation
SNL = Sandia National Laboratories
TEC = Technadyne Engineering Consultants
TRI = Tech Reps, Inc.
UHH = University of Hawaii at Hilo
UNM = Univ. of New Mexico/New Mexico Engineering Research Institute
UP = University of Paris
WEC = Westinghouse Electric Corporation

Expert Panels

Futures

M. Baram	Boston University
W. Bell	Yale University
G. Benford	University of California, Irvine
D. Chapman	The World Bank, Cornell University
B. Cohen	University of Pittsburgh
V. Ferkiss	Georgetown University
T. Glickman	Resources for the Future
T. Gordon	Futures Group
C. Kirkwood	Arizona State University
H. Otway	Joint Research Center (Ispra), Los Alamos National Laboratory
M. Pasqualetti	Arizona State University
D. Reicher	Natural Resources Defense Council
N. Rosenberg	Resources for the Future
M. Singer	The Potomac Organization

Volume 3: J. Chapman (text); D. Pulliam (illustrations)
Volume 4: V. Gilliland, M. Minahan (text); S. Laundre-Woerner, A. Montano (illustrations)

D. Rivard and the Word Processing Department
R. Rohac, R. Andree, and the Illustration and Computer Graphics Departments
S. Tullar and the Production Department

Peer Review

Internal/Sandia
F. Mendenhall
L. Gomez

Management/Sandia
W. Weart

PA Peer Review Panel

R. Heath, Chair	University of Washington
R. Budnitz	Future Resources Associates, Inc.
T. Cotton	JK Research Associates, Inc.
J. Mann	University of Illinois
T. Pigford	University of California, Berkeley
F. Schwartz	Ohio State University

Department of Energy
J. Coffey

PREFACE

The *Preliminary Performance Assessment for the Waste Isolation Pilot Plant, December 1992* is currently planned to consist of six volumes. The titles of the volumes are listed below. All analyses reported in the 1992 Preliminary Performance Assessment, including those described in this volume, are based on computer modeling of disposal-system performance that was completed in November 1992.

This report is the fourth in a series of annual reports that document ongoing assessments of the predicted long-term performance of the Waste Isolation Pilot Plant (WIPP); this documentation will continue during the WIPP Test Phase. However, the Test Phase schedule and projected budget may change; if so, the content of the *1992 Preliminary Performance Assessment* report and its production schedule may also change.

Volume 1: Third Comparison with 40 CFR 191, Subpart B

Volume 2: Technical Basis

Volume 3: Model Parameters

Volume 4: Uncertainty and Sensitivity Analyses for 40 CFR 191, Subpart B

Volume 5: Uncertainty and Sensitivity Analyses of Gas and Brine Migration for Undisturbed Performance

Volume 6: Guidance to the WIPP Project from the December 1992 Performance Assessment

CONTENTS

FIGURES

Figure Page

Figure Page

Figure Page

TABLES

1. INTRODUCTION

The Waste Isolation Pilot Plant (WIPP) is planned as a research and development facility to demonstrate the safe disposal of transuranic (TRU) wastes generated by defense programs of the United States Department of Energy (DOE). Before disposing of waste in the WIPP, the DOE must evaluate compliance with applicable long-term regulations of the United States Environmental Protection Agency (EPA), including 40 CFR 191, Subpart B *(Environmental Radiation Protection Standards for the Management and Disposal of Spent Nuclear Fuel, High-Level and Transuranic Radioactive Wastes)* (EPA, 1985) and *40 CFR 268.6 (Petitions to Allow Land Disposal of a Waste Prohibited Under Subpart C of Part 268)* (EPA, 1986), which is the regulation implementing the *Resource Conservation and Recovery Act (RCRA)* that states the conditions for disposal of specified hazardous wastes. Performance assessment (PA) will form the basis for evaluations of compliance with these regulations.

The WIPP Performance Assessment Department of Sandia National Laboratories (SNL) is performing iterative preliminary PAs to provide guidance to the WIPP Project while preparing for final compliance evaluation. This volume is part of a multi-volume report documenting the third preliminary performance assessment for the WIPP, completed in December 1992. Preparation for preliminary performance assessments began with the December 1989 *Draft Forecast of the Final Report for the Comparison to 40 CFR Part 191, Subpart B for the Waste Isolation Pilot Plant* (Bertram-Howery et al., 1989) and *Performance Assessment Methodology Demonstration: Methodology Development for Evaluating Compliance with EPA 40 CFR 191, Subpart B, for the Waste Isolation Pilot Plant* (Marietta et al., 1989). The 1990 report (Bertram-Howery et al., 1990) and two supporting volumes (Rechard et al., 1990; Helton et al., 1991) presented preliminary results of evaluations that addressed only the long-term performance criteria for disposal specified in the radioactive-waste disposal standards (*40 CFR 191, Subpart B*, EPA, 1985). The 1991 version of the report (WIPP PA Division, 1991a, 1991b, 1991c; Helton et al., 1992) presented preliminary evaluations for comparison with the regulatory requirements of *40 CFR 191, Subpart B*. Results of the 1992 performance assessment are not suitable for final compliance evaluations because portions of the modeling system and data base are incomplete, and the level of confidence in the defensibility of the performance estimates has not been established. Results are, however, suitable for providing interim guidance to the WIPP Project as it moves toward final compliance evaluations.

Previous volumes of the December 1992 *Preliminary Performance Assessment* have provided an overview of the performance assessment and results of a preliminary comparison with Subpart B of *40 CFR 191* (Volume 1), a description of the technical basis for probability and consequence modeling (Volume 2), and the data base of parameter values used in modeling (Volume 3). This volume contains the results of uncertainty and sensitivity analyses performed with respect to *40 CFR 191B*. These analyses provide quantitative and qualitative insights on the relationships between uncertainty in the models and data used in the performance assessment and the resultant uncertainty in the results of the performance assessment. Additional uncertainty and sensitivity analyses of gas and brine migration for undisturbed conditions relevant to compliance evaluations for *40 CFR 268.6* are contained in Volume 5. Finally, Volume 6 contains guidance to the WIPP Project based on the 1992 performance assessment.

Uncertainty and sensitivity analysis is an important part of the WIPP PA and contributes to the overall analysis in the following areas: (1) assessment of the uncertainty in performance assessment results that must be used in regulatory compliance evaluations, (2) identification of modeling areas where reductions in uncertainty can increase confidence in performance assessment results, and (3) partial verification that the computational models used in the performance assessment system are operating properly. Because uncertainty and sensitivity analyses are inherently conditional on the models, data distributions, and techniques used to generate them, they cannot provide insight about parameters not sampled, conceptual and computational models not used in the analysis in question, or processes that have been oversimplified in the analysis. As discussed further in Volume 6, qualitative judgment about the modeling system must be used in combination with the results of analyses presented in this volume to set priorities for additional data acquisition and model development.

Organization of this volume is as follows:

- Chapter 2 provides an overview of the structure of the WIPP PA, including an introduction to the Kaplan and Garrick (1981) ordered-triple representation for risk. The definition of scenarios, the determination of scenario probabilities, and the calculation of scenario consequences are described in the context of the ordered-triple representation for risk. Additional information about the PA methodology is provided in Chapters 3 and 4 in Volume 2 of this report.

- Chapter 3 provides information about the imprecisely known variables selected for sampling in the 1992 PA. Detailed information about parameter values is provided in Volume 3 of this report.

- Chapter 4 contains a discussion of the modeling of undisturbed performance using a rectangular cross-section representation of the entire repository. Results are presented in terms of cumulative gas and brine migration and other two-phase flow performance measures. Radionuclide transport is not modeled because no brine that has been in contact with waste reaches the accessible environment during 10,000 yr of undisturbed performance. Discussions of two-phase flow and creep closure and detailed information about the BRAGFLO and SANCHO codes used in the modeling are provided in Chapter 7 and Appendices A and B in Volume 2 of this report.

- Chapter 5 contains a discussion of the modeling of disturbed performance (i.e., scenarios in which the waste-disposal region is intruded by an exploratory borehole) using a cylindrical representation of a single panel. Results in this chapter are presented in terms of cumulative gas and brine migration and other two-phase flow performance measures. Uncertainty and sensitivity analyses using radionuclide releases as the primary performance measure are discussed in Chapter 8. Modeling for disturbed performance uses the BRAGFLO and SANCHO codes, and also uses the PANEL code to model radionuclide mobilization in the waste-emplacement panel. PANEL is described in Chapter 7 and Appendix A in Volume 2 of this report.

- Chapter 6 contains a discussion of the modeling of groundwater flow and radionuclide transport in the Culebra Dolomite Member of the Rustler Formation above the repository. Radionuclide transport in the Culebra occurs only in human intrusion scenarios. Modeling is done using the SECO flow and transport codes, as described in Chapter 7 and Appendix C in Volume 2 of this report.

- Chapter 7 contains a discussion of the modeling of the release of radionuclides directly at the ground surface during the drilling of an exploratory borehole that intrudes into the waste-disposal region. As modeled, particulate waste is brought to the surface in the drilling fluid both as cuttings (material intersected by the drill bit) and cavings (material eroded from the borehole wall by the circulating drilling fluid). Cuttings and cavings are collectively referred to as cuttings in this report. Modeling is done using the CUTTINGS code, as described by Berglund (1992) and Chapter 7 in Volume 2 of this report.

- Chapter 8 contains uncertainty and sensitivity analysis results for radionuclide releases both from cuttings and groundwater transport. Alternative conceptual models are examined for transport in the Culebra, including transport in a single-porosity, fracture-only medium and transport in a dual-porosity, fracture plus porous-matrix system. For dual-porosity transport, releases are examined with and without the physical effect of clay linings in fractures and with and without chemical retardation by sorption. Cases considered here are a more complete set of those for which results were presented in Chapter 5 of Volume 1 of this report for preliminary comparison with the Containment Requirements of *40 CFR 191B*. Dual-porosity transport with both chemical and physical retardation in matrix and clay linings is the conceptual model believed by the WIPP PA Department to provide the most realistic representation for transport in the Culebra. Experimental and field data are not sufficient at this time to eliminate alternative conceptual models, and other cases are therefore analyzed here for comparison.

- Chapter 9 summarizes the results of the 1992 uncertainty and sensitivity analyses for *40 CFR 191B*, and identifies overall importance of individual parameters.

2. STRUCTURE OF WIPP PERFORMANCE ASSESSMENT

2.1 Conceptual Model

As proposed by Kaplan and Garrick (1981), the outcome of a performance assessment can be represented by a set R of ordered triples of the form

$$R = \{(S_i, pS_i, \mathbf{cS}_i), i=1, \ldots, nS\}, \qquad (2.1\text{-}1)$$

where

S_i = a set of similar occurrences,

pS_i = probability that an occurrence in the set S_i will take place,

$\mathbf{cS}_i$ = a vector of consequences associated with S_i,

nS = number of sets selected for consideration,

and the sets S_i have no occurrences in common (i.e., the S_i are disjoint sets). This representation formally decomposes the outcome of a performance assessment into what can happen (the S_i), how likely things are to happen (the pS_i), and the consequences of what can happen (the $\mathbf{cS}_i$). The S_i are typically referred to as "scenarios" in radioactive waste disposal. Similarly, the pS_i are scenario probabilities, and the vector $\mathbf{cS}_i$ contains environmental releases for individual isotopes, the normalized EPA release for all isotopes, and possibly other information associated with scenario S_i. The set R in Eq. 2.1-1 is used as the conceptual model for the WIPP performance assessment.

Although the expression in Eq. 2.1-1 provides a logical conceptual representation for risk, the set R by itself can be difficult to examine. For this reason, the risk results in R are often summarized with complementary cumulative distribution functions (CCDFs). These functions provide a display of the information contained in the probabilities pS_i and the consequences $\mathbf{cS}_i$. With the assumption that a particular consequence result cS in the vector $\mathbf{cS}$ has been ordered so that $cS_i \leq cS_{i+1}$ for i=1, ..., nS-1, the associated CCDF is shown in Figure 2.1-1. A consequence result of particular interest in performance assessments for radioactive waste disposal is the EPA normalized release to the accessible environment (EPA, 1985). As indicated in Figure 2.1-1, the EPA places a bound on the CCDF for normalized release to the accessible environment.

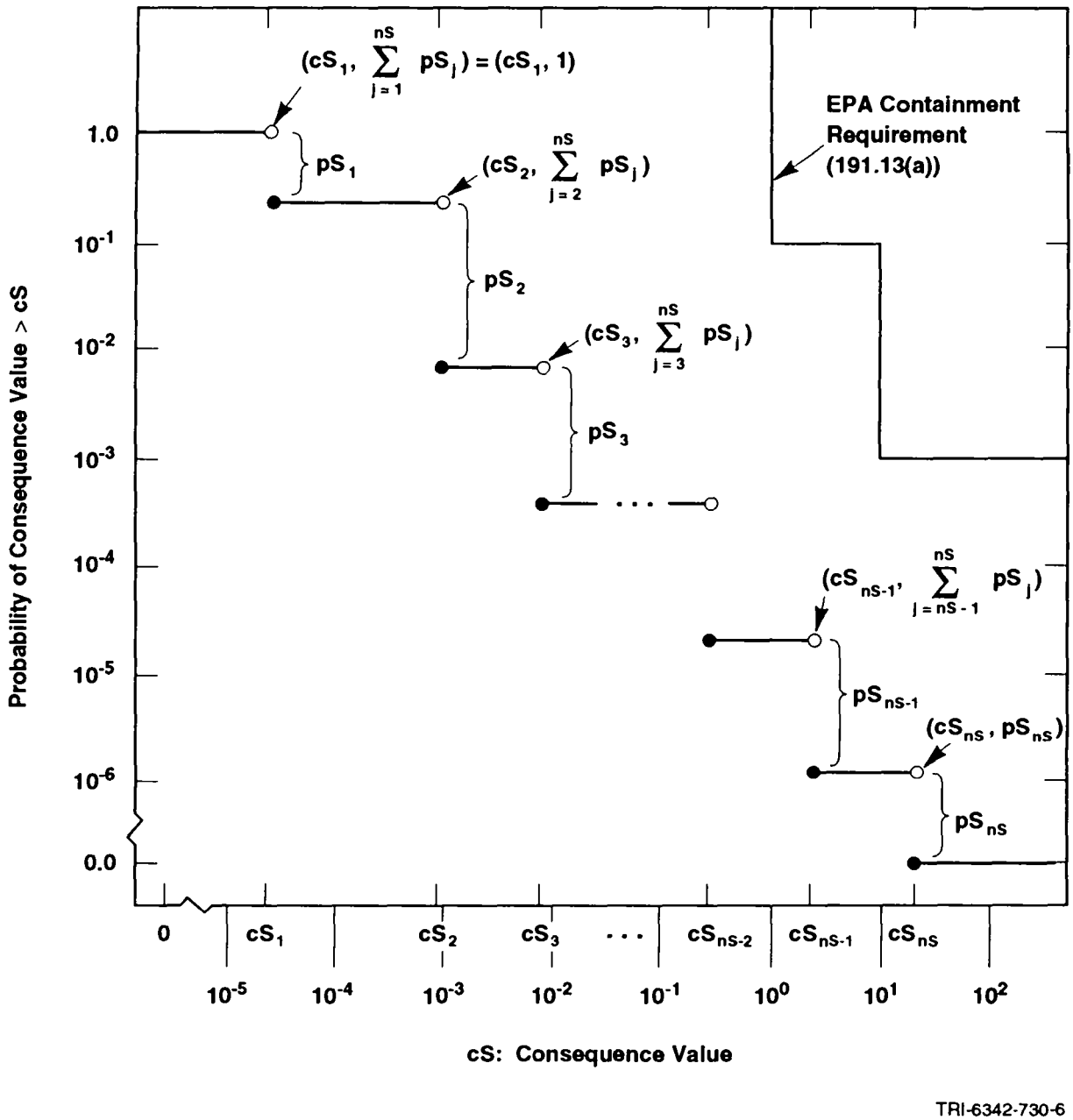

Figure 2.1-1. Estimated complementary cumulative distribution function (CCDF) for consequence result cS (Helton et al., 1991). The open and solid circles at the discontinuities indicate the points included on (solid circles) and excluded from (open circles) the CCDF.

In practice, the outcome of a performance assessment depends on many imprecisely known variables. These imprecisely known variables can be represented by a vector

$$\mathbf{x} = [x_1, x_2, \ldots, x_{nV}], \tag{2.1-2}$$

where each x_j is an imprecisely known input required in the performance assessment and nV is the total number of such inputs. As a result, the set R is actually a function of $\mathbf{x}$:

$$R(\mathbf{x}) = \{[S_i(\mathbf{x}), pS_i(\mathbf{x}), \mathbf{cS}_i(\mathbf{x})], i=1, \ldots, nS(\mathbf{x})\}. \tag{2.1-3}$$

As $\mathbf{x}$ changes, so will $R(\mathbf{x})$ and all summary measures that can be derived from $R(\mathbf{x})$. Thus, rather than a single CCDF for each consequence value contained in $\mathbf{cS}$, there will be a distribution of CCDFs that results from the possible values that $\mathbf{x}$ can take on.

The uncertainty in $\mathbf{x}$ can be characterized by a sequence of probability distributions

$$D_1, D_2, \ldots, D_{nV}, \tag{2.1-4}$$

where D_j is the distribution for the variable x_j contained in $\mathbf{x}$. The definition of these distributions may also be accompanied by the specification of correlations and various restrictions that further define the relations between the x_j. These distributions and other restrictions probabilistically characterize where the appropriate input to use in a performance assessment might fall given that the analysis has been structured so that only one value can be used for each variable.

Once the distributions in Eq. 2.1-4 have been developed, Monte Carlo techniques can be used to determine the uncertainty in $R(\mathbf{x})$ that results from the uncertainty in $\mathbf{x}$. First, a sample

$$\mathbf{x}_k = [x_{k1}, x_{k2}, \ldots, x_{k,nV}], k=1, \ldots, nK, \tag{2.1-5}$$

is generated according to the specified distributions and restrictions, where nK is the size of the sample. A performance assessment is then conducted for each sample element $\mathbf{x}_k$, which yields a sequence of risk results of the form

$$R(\mathbf{x}_k) = \{[S_i(\mathbf{x}_k), pS_i(\mathbf{x}_k), \mathbf{cS}_i(\mathbf{x}_k)], i=1, \ldots, nS(\mathbf{x}_k)\} \tag{2.1-6}$$

for k=1, ..., nK. Each set $R(\mathbf{x}_k)$ is the result of one complete performance assessment conducted with a set of inputs (i.e., $\mathbf{x}_k$) that the review process producing the distributions in Eq. 2.1-4 concluded was possible. Further, associated with each risk result $R(\mathbf{x}_k)$ in Eq. 2.1-6 is a probability or weight that can be used in making probabilistic statements about the distribution of $R(\mathbf{x})$. When random or Latin hypercube sampling is used, this weight is the reciprocal of the sample size (i.e., 1/nK).

In most performance assessments, CCDFs are the results of greatest interest. For a particular consequence result, a CCDF will be produced for each set $R(\mathbf{x}_k)$ shown in Eq. 2.1-6. This yields a distribution of CCDFs of the form shown in Figure 2.1-2.

An important distinction exists between the uncertainty that gives rise to a single CCDF in Figure 2.1-2 and the uncertainty that gives rise to the distribution of CCDFs in this figure. A single CCDF arises from the fact that a number of different occurrences (e.g., borehole intrusions) have a real possibility of taking place. This type of uncertainty is referred to as stochastic variation or uncertainty in this report. A distribution of CCDFs arises from the fact that fixed, but unknown, quantities (e.g., hydrologic properties) are needed in the estimation of a CCDF. The development of distributions that characterize what the values for these fixed quantities might be leads to a distribution of CCDFs. In essence, a performance assessment can be viewed as a very complex function that estimates a CCDF. As there is uncertainty in the values of some of the variables operated on by this function, there will also be uncertainty in the dependent variable produced by this function, where this dependent variable is a CCDF.

Both Kaplan and Garrick (1981) and a recent report by the International Atomic Energy Agency (IAEA, 1989) distinguish between these two types of uncertainty. Specifically, Kaplan and Garrick distinguish between probabilities derived from frequencies and probabilities that characterize degrees of belief. Probabilities derived from frequencies correspond to the probabilities pS_i in Eq. 2.1-1, while probabilities that characterize degrees of belief (i.e., subjective probabilities) correspond to the distributions indicated in Eq. 2.1-4. The IAEA report distinguishes between what it calls Type A uncertainty and Type B uncertainty. The IAEA report defines Type A uncertainty to be stochastic variation; as such, this uncertainty corresponds to the frequency-based probability of Kaplan and Garrick and the pS_i of Eq. 2.1-1. Type B uncertainty is defined to be uncertainty that is due to lack of knowledge about fixed quantities; thus, this uncertainty corresponds to the subjective probability of Kaplan and Garrick and the distributions indicated in Equation 2.1-4. Expressed another way, Type A uncertainty

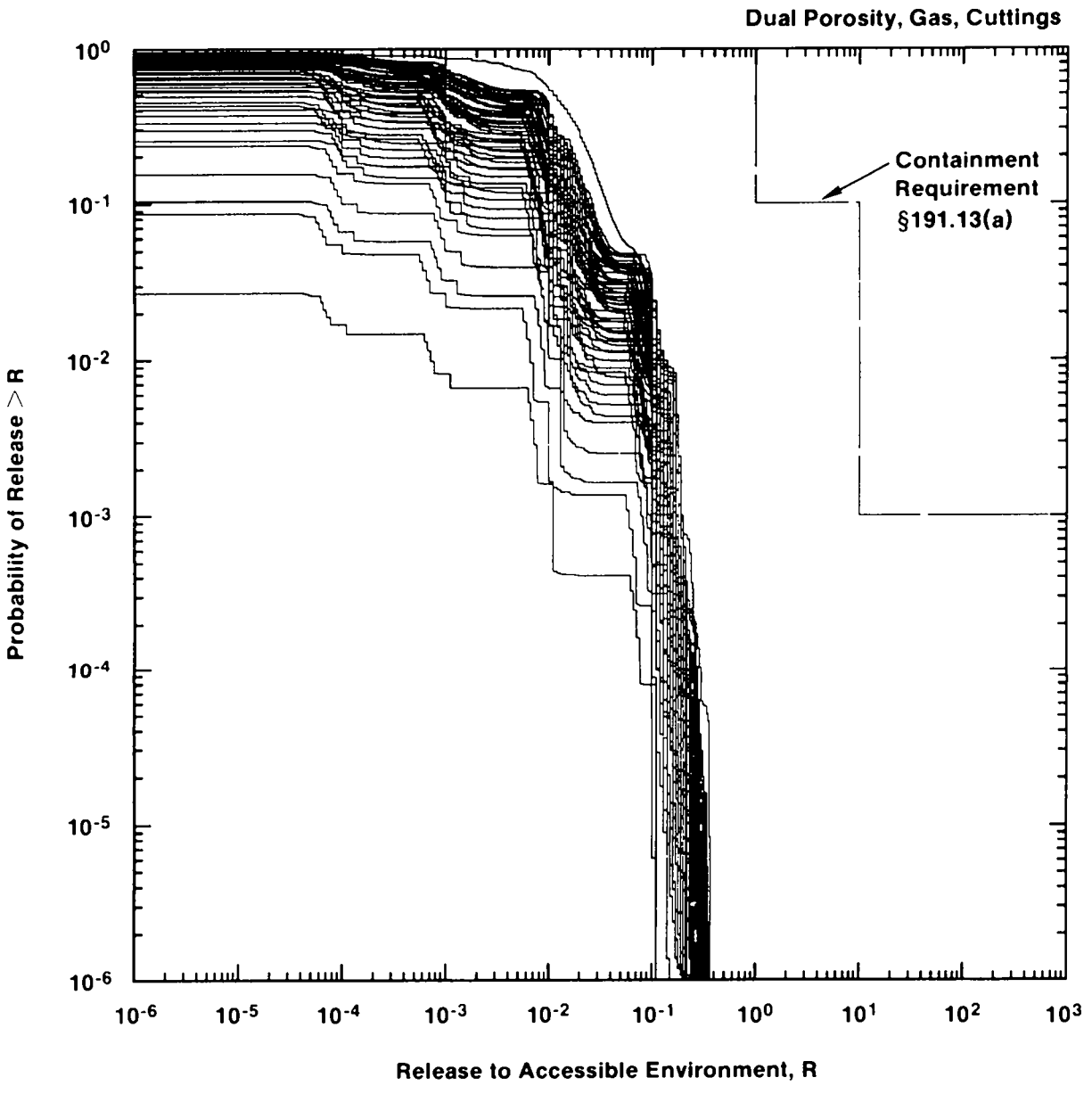

TRI-6342-1293-1

Figure 2.1-2. Distribution of complementary cumulative distribution functions (CCDFs) for normalized release to the accessible environment obtained in the 1991 WIPP performance assessment including both cuttings removal and groundwater transport with gas generation in the repository and a dual-porosity transport model in the Culebra Dolomite (Helton et al., 1992, Figure 2.1-2).

designates variability in a population; Type B uncertainty designates a lack of knowledge about this population and how to appropriately calculate associated results of interest. For the WIPP performance assessment, Type A uncertainty refers to all possible patterns of disruption that could occur over a 10,000 yr period, and Type B uncertainty refers to our lack of knowledge on how to characterize these patterns and calculate their consequences. This distinction has also been made by other authors, including Vesely and Rasmuson (1984), Paté-Cornell (1986), Parry (1988), Helton (1993b), and Helton and Breeding (1993).

As already indicated, the ordered-triple representation shown in Eq. 2.1-1 is used as the conceptual model for the WIPP performance assessment. In consistency with this representation, the scenarios S_i, scenario probabilities pS_i and scenario consequences $\mathbf{cS}_i$ used in the 1991 preliminary WIPP performance assessment are discussed in Sections 2.2, 2.3 and 2.4, respectively. Several specific definitions used for R in the 1992 WIPP performance assessment are then presented in Section 2.5.

The WIPP performance assessment endeavors to maintain a distinction between stochastic (i.e., Type A) uncertainty and subjective (i.e., Type B) uncertainty. The effect of stochastic uncertainty is represented by the probabilities pS_i discussed in Section 2.3. The characterization of the subjective uncertainty in the inputs to the 1992 WIPP performance assessment is discussed in Chapter 3. The primary focus of this report is the impact of subjective uncertainties on the outcomes of the 1992 WIPP performance assessment. These impacts will be investigated in Chapters 4 through 8. A concluding discussion is given in Chapter 9.

2.2 Definition of Scenarios

Scenarios constitute the first element S_i of the ordered triples contained in the set R shown in Eq. 2.1-1 and are obtained by subdividing the set

$$S = \{x\text{: } x \text{ a single 10,000-yr history beginning at decommissioning of the WIPP}\}. \qquad (2.2\text{-}1)$$

Each 10,000-yr history is complete in the sense that it includes a full specification, including time of occurrence, for everything of importance to performance assessment that happens in this time period. In the terminology of Cranwell et al. (1990), each history would contain a characterization for a specific sequence of "naturally occurring and/or human-induced conditions

that represent realistic future states of the repository, geologic systems, and ground-water flow systems that could affect the release and transport of radionuclides from the repository to humans." In the terminology of probability theory, the set S is called the sample space, the members of S are called elementary events, and the individual scenarios S_i are called events.

The WIPP performance assessment uses a two-stage procedure for scenario development (Chapter 4 of Volume 2). The purpose of the first stage is to develop a comprehensive set of scenarios that includes all occurrences that might reasonably take place at the WIPP. The result of this stage is a set of scenarios, called summary scenarios, that summarize what might happen at the WIPP. These summary scenarios provide a basis for discussing the future behavior of the WIPP and a starting point for the second stage of the procedure, which is the definition of scenarios at a level of detail that is appropriate for use with the computational models employed in the WIPP performance assessment. The scenarios obtained in this second stage of scenario development are referred to as computational scenarios. The development of summary scenarios is directed at understanding what might happen at the WIPP and answering completeness questions. The development of computational scenarios is directed at organizing the actual calculations that must be performed to obtain the consequences $\mathbf{cS}_i$ appearing in Eq. 2.1-1, and as a result, must provide a structure that both permits the $\mathbf{cS}_i$ to be calculated at a reasonable cost and holds the amount of aggregation error that enters the analysis to a reasonable level. Here, aggregation error refers to the inevitable loss of resolution that occurs when an infinite number of occurrences (i.e., the elements of S) must be divided into a finite number of sets for analysis (i.e., the subsets S_i of S). The following discussion describes the computational scenarios used in the 1992 WIPP performance assessment.

The development of summary scenarios for the 1992 WIPP performance assessment led to a set S of the form shown in Eq. 2.2-1 in which all disruptions were due to drilling intrusions (Chapter 4 of Volume 2). As a result, computational scenarios were defined to provide a systematic coverage of drilling intrusions. Specifically, computational scenarios were defined on the basis of (1) number of drilling intrusions, (2) time of the drilling intrusions, (3) whether or not a single waste panel is penetrated by two or more boreholes, of which at least one penetrates a pressurized brine pocket and at least one does not, and (4) activity level of the waste penetrated by the boreholes.

The construction of computational scenarios started with the division of the 10,000-yr time period appearing in the EPA regulations into a sequence

$[t_{i-1}, t_i]$, i = 1, 2, ..., nT, (2.2-2)

of disjoint time intervals. When the activity levels of the waste are not considered, these time intervals lead to computational scenarios of the form

$$S(\mathbf{n}) = \{x: x \text{ an element of } S \text{ for which exactly n(i) intrusions occur in time interval } [t_{i-1}, t_i] \text{ for i=1, 2, ..., nT (i.e., an E1 or E2-type scenario as described in Section 4.2.3.2 of Volume 2.)}\} \quad (2.2\text{-}3)$$

and

$$S^{+-}(t_{i-1},t_i) = \{x: x \text{ an element of } S \text{ for which two or more boreholes penetrate the same waste panel during the time interval } [t_{i-1}, t_i], \text{ with at least one of these boreholes penetrating a pressurized brine pocket and at least one not penetrating a pressurized brine pocket (i.e., an E1E2-type scenario as described in Section 4.2.3.2 of Volume 2)}\}, \quad (2.2\text{-}4)$$

where

$$\mathbf{n} = [n(1), n(2), \ldots, n(nT)]. \quad (2.2\text{-}5)$$

As discussed in Section 2.5, the 1992 WIPP performance assessment uses two different subdivisions of the 10,000-yr time period in the EPA regulations. In turn, these different subdivisions lead to different definitions for the set R in Eq. 2.1-1.

When the activity levels of the waste are considered, the preceding time intervals lead to computational scenarios of the form

$$S(\mathbf{l},\mathbf{n}) = \{x: x \text{ an element of } S(\mathbf{n}) \text{ for which the } j^{th} \text{ borehole encounters waste of activity level } \ell(j) \text{ for j=1, 2, ..., nBH, where nBH is the total number of boreholes associated with a time history in } S(\mathbf{n})\} \quad (2.2\text{-}6)$$

and

$$S^{+-}(\mathbf{l};t_{i-1},t_i) = \{x: x \text{ an element of } S^{+-}(t_{i-1},t_i) \text{ for which the } j^{th} \text{ borehole encounters waste of activity level } \ell(j) \text{ for j=1, 2, ..., nBH, where nBH is the total number of boreholes associated with a time history in } S^{+-}(t_{i-1},t_i)\}, \quad (2.2\text{-}7)$$

where

$$\mathbf{l} = [\ell(1), \ell(2), \ldots, \ell(nBH)] \text{ and } nBH = \sum_{i=1}^{nT} n(i). \qquad (2.2\text{-}8)$$

The computational scenarios $S(\mathbf{l},\mathbf{n})$ and $S^{+-}(\mathbf{l};t_{i-1},t_i)$ are used as the basis for the CCDFs for normalized release to the accessible environment presented in the 1992 WIPP performance assessment.

The definitions of $S^{+-}(t_{i-1},t_i)$ and $S^{+-}(\mathbf{l};t_{i-1},t_i)$ appearing in Eqs. 2.2-4 and 2.2-7 do not use the vector $\mathbf{n}$ designating the time intervals in which drilling intrusions occur that appears in the definitions of $S(\mathbf{n})$ and $S(\mathbf{l},\mathbf{n})$. However, vectors of this form can be incorporated into the definitions of $S^{+-}(t_{i-1},t_i)$ and $S^{+-}(\mathbf{l};t_{i-1},t_i)$. Specifically, let

$$S_i^{+-}(\mathbf{n}) = \{x: \text{ x an element of } S(\mathbf{n}) \text{ for which 2 or more boreholes penetrate the same waste panel during the time interval } [t_{i-1},t_i] \text{ (i.e., } n(i)\geq 2\text{), with at least one of these boreholes penetrating a pressurized brine pocket and at least one not penetrating a pressurized brine pocket}\}. \qquad (2.2\text{-}9)$$

Then,

$$S^{+-}(t_{i-1},t_i) = \bigcup_{\mathbf{n}\in A(i)} S_i^{+-}(\mathbf{n}), \qquad (2.2\text{-}10)$$

where $\mathbf{n}\in A(i)$ only if $\mathbf{n}$ is a vector of the form defined in Eq. 2.2-5 with $n(i)\geq 2$. The computational scenarios $S_i^{+-}(\mathbf{l},\mathbf{n})$ and $S^{+-}(\mathbf{l};t_{i-1},t_i)$ can be defined analogously for the vector $\mathbf{l}$ indicated in Eq. 2.2-8. In Section 2.3, conservative relations are presented (i.e., Eqs. 2.3-3 and 2.3-4) that bound the probabilities for $S^{+-}(t_{i-1},t_i)$ and $S^{+-}(\mathbf{l};t_{i-1},t_i)$ and are used in the construction of CCDFs of the form appearing in Figure 2.1-2. In Section 2.4, $S^{+-}(t_{i-1},t_i)$ and $S^{+-}(\mathbf{l};t_{i-1},t_i)$, $i = 1, \ldots, nT$, are assigned the groundwater releases (i.e., Eqs. 2.4-13 and 2.4-14) associated with

$$S_1^{+-}(2,0,\ldots,0),\ S_2^{+-}(0,2,\ldots,0),\ \ldots,\ S_{nT}^{+-}(0,0,\ldots,2), \qquad (2.2\text{-}11)$$

respectively; these releases are used in the construction of CCDFs of the form appearing in Figure 2.1-2. The subscripts in the preceding notation for $S_1^{+-}(2,0,\ldots,0)$ through $S_{nT}^{+-}(0,0,\ldots,2)$ are redundant and will be omitted in the remainder of this report.

Additional information on the construction of computational scenarios for the 1992 WIPP performance assessment is available elsewhere (Chapter 5 of Volume 2).

2.3 Determination of Scenario Probabilities

As discussed in Chapter 5 of Volume 2 and Helton (1993a), probabilities for computational scenarios were determined under the assumption that the occurrence of boreholes through the repository follows a Poisson process with a rate term λ. The probabilities $pS(\mathbf{n})$ and $pS(\mathbf{I},\mathbf{n})$ for the computational scenarios $S(\mathbf{n})$ and $S(\mathbf{I},\mathbf{n})$ are given by

$$pS(\mathbf{n}) = \left\{ \prod_{i=1}^{nT} \left[\int_{t_{i-1}}^{t_i} \lambda(t)dt \right]^{n(i)} / n(i)! \right\} \exp\left[-\int_{t_0}^{t_{nT}} \lambda(t)dt \right] \tag{2.3-1}$$

and

$$pS(\mathbf{I},\mathbf{n}) = \left[\prod_{j=1}^{nBH} pL_{\ell(j)} \right] pS(\mathbf{n}), \tag{2.3-2}$$

where $\mathbf{n}$ and $\mathbf{I}$ are defined in Eqs. 2.2-5 and 2.2-8, respectively, and pL_ℓ is the probability that a randomly placed borehole through a waste panel will encounter waste of activity level ℓ. Examples of probabilities $pS(\mathbf{n})$ calculated as shown in Eq. 2.3-1 are given in Section 2.5.

The probabilities $pS^{+-}(t_{i-1},t_i)$ and $pS^{+-}(\mathbf{I};t_{i-1},t_i)$ for the computational scenarios $S^{+-}(t_{i-1},t_i)$ and $S^{+-}(\mathbf{I};t_{i-1},t_i)$ are given by

$$pS^{+-}(t_{i-1},t_i) \triangleq \sum_{\ell=1}^{nP} \left\{ 1 - \exp\left[-\int_{t_{i-1}}^{t_i} \alpha_\ell(t)dt \right] \right\} \left\{ 1 - \exp\left[-\int_{t_{i-1}}^{t_i} \beta_\ell(t)dt \right] \right\} \tag{2.3-3}$$

and

$$pS^{+-}(\mathbf{I};t_{i-1},t_i) \triangleq \left[\prod_{j=1}^{nBH} pL_{\ell(j)} \right] pS^{+-}(t_{i-1},t_i), \tag{2.3-4}$$

where

$$\alpha_\ell(t) = [aBP_\ell]\lambda(t)/aTOT,$$

$$\beta_\ell(t) = [aTOT_\ell - aBP_\ell]\lambda(t)/aTOT,$$

aBP_ℓ = area (m^2) of pressurized brine pocket under waste panel ℓ,

$aTOT_\ell$ = total area (m^2) of waste panel ℓ,

aTOT = total area (m^2) of waste panels,

and

nP = number of waste panels.

For the 1992 WIPP performance assessment, each of the areas $aTOT_\ell$ and aBP_ℓ is assumed to be the same for all waste panels. This assumption is conservative in the sense that it increases the probability of E1E2-type scenarios as defined in Eq. 2.2-4 as the probability of the necessary pattern of drilling intrusions is zero for a waste panel that is underlain by no pressurized brine pocket or entirely underlain by a pressurized brine pocket.

The relations appearing in Eqs. 2.3-1 through 2.3-4 are derived in Chapter 5 of Volume 2 of this report and also in Helton (1993a) under the assumption that drilling intrusions follow a Poisson process (i.e., are random in time and space).

2.4 Calculation of Scenario Consequences

As indicated in Figure 2.4-1, the following nine computer models were used to estimate scenario consequences in the 1992 WIPP performance assessment: CUTTINGS, BRAGFLO, PANEL, SECO2D, SECOTP, GRASP-INV, CCDFPERM, GENII-S and SANCHO. Brief descriptions of these models are given in Table 2.4-1. More detailed descriptions of some of these models and their use in the 1992 WIPP performance assessment are provided in Chapters 4 through 7 and in additional references indicated in Table 2.4-1.

There are too many computational scenarios (e.g., $S(\mathbf{n})$ and $S(\mathbf{l},\mathbf{n})$) to perform a detailed calculation for each scenario with the models summarized in Table 2.4-1. For example, 3003 scenarios of the form $S(\mathbf{n})$ are required to reach a cumulative probability of 0.9994 when $\lambda = 3.28 \times 10^{-4}$ yr^{-1} and five time intervals of length 2000 yr are used (Helton et al., 1992, Table 2.3-1).

Construction of a CCDF for comparison against the EPA release limits requires the estimation of cumulative probability through at least the 0.999 level. Thus, depending on the value for the rate λ in the Poisson model for drilling intrusions, this may require the inclusion of computational scenarios involving as many as 10 to 12 drilling intrusions, which results in a total of several thousand computational scenarios. Further, this number does not include the effects of different activity levels in the waste. To obtain results for such a large number of computational scenarios, it is necessary to plan and implement the overall calculations very carefully. The following describes the approach used in the 1992 WIPP performance assessment (Helton and Iuzzolino, 1993).

As indicated in Eq. 2.2-2, the 10,000-yr time interval that must be considered in the construction of CCDFs for comparison with the EPA release limits is divided into disjoint subintervals $[t_{i-1}, t_i]$, $i = 1, 2, \ldots, nT$, in the definition of computational scenarios. The following results can be calculated for each time interval:

rC_i = EPA normalized release to the surface environment for cuttings removal due to a single borehole in time interval i with the assumption that the waste is homogeneous (i.e., waste of different activity levels is not present), (2.4-1)

rC_{ij} = EPA normalized release to the surface environment for cuttings removal due to a single borehole in time interval i that penetrates waste of activity level j, (2.4-2)

$rGW1_i$ = EPA normalized release to the accessible environment due to groundwater transport initiated by a single borehole in time interval i (i.e., an E2-type scenario), (2.4-3)

$rGW2_i$ = EPA normalized release to the accessible environment due to groundwater transport initiated by two boreholes in the same waste panel in time interval i, of which one penetrates a pressurized brine pocket and one does not (i.e., an E1E2-type scenario), (2.4-4)

with the assumption that the intrusions occur at the midpoints of the time intervals (e.g., at 1000 yr for the time interval [0, 2000 yr]). For the calculation of $rGW1_i$ and $rGW2_i$ in the 1992 WIPP performance assessment, the accessible environment is assumed to begin 2.65 km from the center of the waste panels (i.e., at the land-withdrawal boundary as shown in Figure 1-2 of Volume 1 of this report).

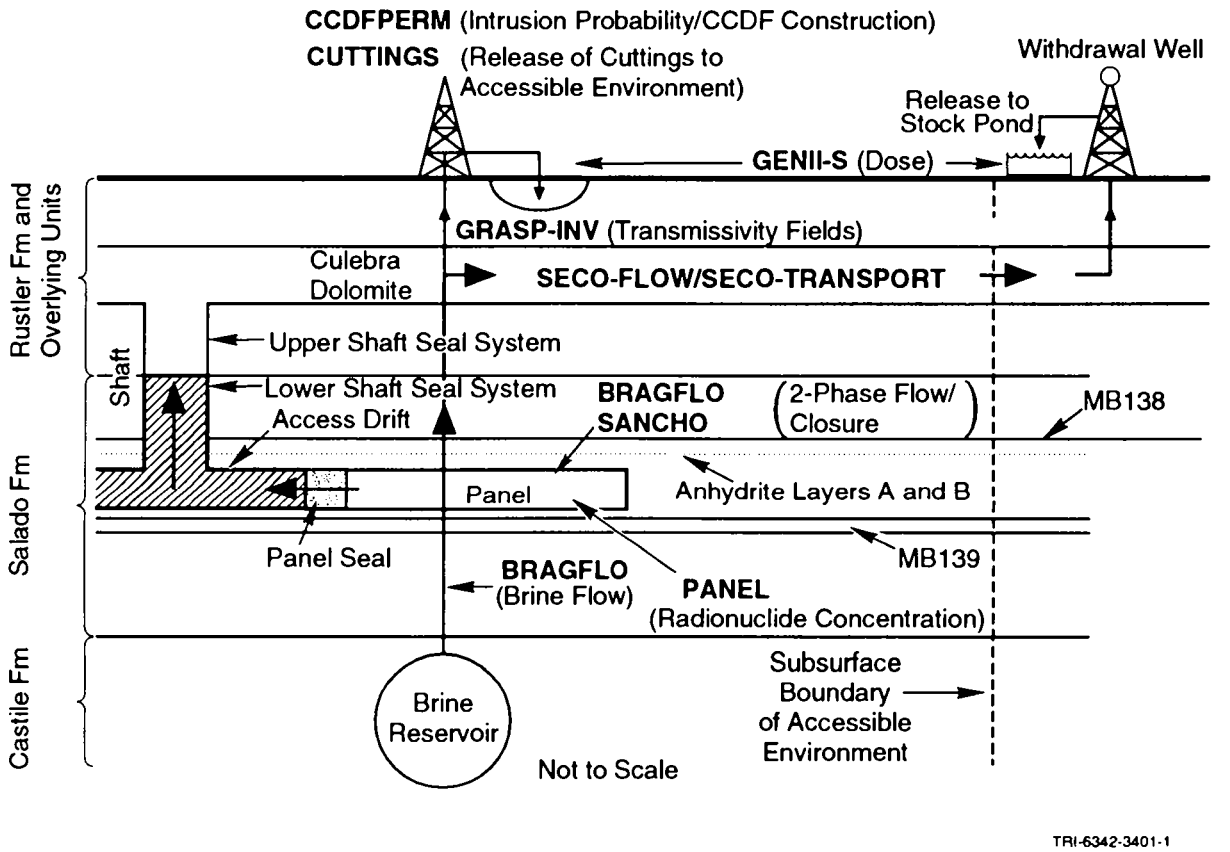

Figure 2.4-1. Models used in 1992 WIPP performance assessment to calculate scenario consequences. The names for computer models (i.e., computer codes) are shown in capital letters.

Table 2.4-1. Summary of Computer Models Used in the 1992 WIPP Performance Assessment to Calculate Scenario Consequences

Model	Description
BRAGFLO	Describes the multiphase flow of gas and brine through a porous, heterogenous reservoir. BRAGFLO solves simultaneously the coupled partial differential equations that describe the mass conservation of gas and brine along with appropriate constraint equations, initial conditions, and boundary conditions. Additional information: Chapters 4 and 5.
CCDFPERM	Constructs probabilities and consequences for various computational scenarios associated with human intrusion by exploratory drilling. Also constructs CCDFS. Additional information: Section 1.4.2 of Volume 3 and Helton and Iuzzolino, 1993.
CUTTINGS	Calculates the quantity of radioactive material brought to the surface in cuttings and cavings generated by an exploratory borehole that penetrates a waste panel. Additional information: Chapter 7.
GENII-S	Estimates potential radiation doses to humans from radionuclides in the environment. Additional information: Leigh et al., 1993.
GRASP-INV	Generates transmissivity fields (estimates of transmissivity values) conditioned on measured transmissivity values and calibrated to steady-state and transient pressure data at well locations using an adjoint sensitivity and pilot-point technique. Additional information: LaVenue and RamaRao, 1992.
PANEL	Calculates rate of discharge and cumulative discharge of radionuclides from a repository panel through an intrusion borehole. Discharge is a function of fluid flow rate, elemental solubility, and radionuclide inventory. Additional information: WIPP PA Division 1991b, Section 5.3.
SECO-FLOW	Calculates single-phase Darcy flow for groundwater-flow problems in two dimensions. The formulation is based on a single partial differential equation for hydraulic head using fully implicit time differencing. Additional information: Chapter 6.
SECO-TRANSPORT	Simulates fluid flow and transport of radionuclides in fractured porous media. Additional information: Chapter 6.
SANCHO	Solves quasistatic, large deformation, inelastic response of two-dimensional solids with finite element techniques. Used in the 1992 performance assessment to determine porosity of the waste as a function of time and cumulative gas generation. Additional information: Section 1.4.7 of Volume 3, Stone et al., 1985.

In general, rC_i, rC_{ij}, $rGW1_i$ and $rGW2_i$ will be vectors containing a large variety of information; however, for notational simplicity, a vector representation will not be used. For the 1992 WIPP performance assessment, the cuttings release to the accessible environment (i.e., rC_i and rC_{ij}) is determined by the CUTTINGS program, and the groundwater release to the accessible environment (i.e., $rGW1_i$ and $rGW2_i$) is determined through a sequence of linked calculations involving the BRAGFLO, PANEL, SECO-FLOW and SECO-TRANSPORT programs.

The cuttings releases

$$rC_1, rC_2, \ldots, rC_{nT} \tag{2.4-5}$$

correspond to the cuttings releases associated with the computational scenarios

$$S(1,0,\ldots,0), S(0,1,\ldots,0), \ldots, S(0,0,\ldots,1) \tag{2.4-6}$$

under the assumption that all waste is of the same average activity level. Similarly, the groundwater releases

$$rGW1_1, rGW1_2, \ldots, rGW1_{nT} \tag{2.4-7}$$

correspond to the groundwater releases associated with the preceding five scenarios, while

$$rGW2_1, rGW2_2, \ldots, rGW2_{nT} \tag{2.4-8}$$

correspond to the groundwater releases associated with the computational scenarios

$$S^{+-}(2,0,\ldots,0),\ S^{+-}(0,2,\ldots,0),\ \ldots,\ S^{+-}(0,0,\ldots,2). \tag{2.4-9}$$

In like manner, rC_{1j} corresponds to the cuttings release associated with the computational scenario $S(j;\ 1,0,\ldots,0)$; rC_{2j} corresponds to the cuttings release associated with $S(j;\ 0,1,\ldots,0)$, and so on.

The releases rC_i, rC_{ij}, $rGW1_i$ and $rGW2_i$ are used to construct the releases associated with the many individual computational scenarios that are used in the construction of a CCDF for comparison with the EPA release limits. The following assumptions are made:

(1) With the exception of E1E2-type scenarios, no synergistic effects result from multiple boreholes, and thus, the total release for a scenario involving multiple intrusions can be obtained by adding the releases associated with the individual intrusions.

(2) An E1E2-type scenario can take place only when the necessary boreholes occur within the same time interval $[t_{i-1}, t_i]$.

(3) An E1E2-type scenario involving more than two boreholes will have the same subsurface release as an E1E2-type scenario involving exactly two boreholes.

The preceding assumptions are used to construct the releases for individual computational scenarios.

For cuttings removal, Assumption (1) is the only pertinent assumption. As the only release associated with cuttings removal is the direct removal of cuttings and spallings to the surface, this assumption seems reasonable; the relatively small cross-sectional area intersected by a drilling intrusion makes the interaction of two or more drilling intrusions very unlikely. Further, should such an intersection occur, the assumption is conservative in the sense that it would tend to overestimate the total size of the release. For E2-type scenarios, Assumption (1) is again the only pertinent assumption. When one, and only one intrusion occurs into each of several waste panels, this assumption seems to be appropriate as there is little reason to believe that the release taking place from one waste panel would affect the release taking place from another waste panel. If anything, the assumption in this case would be conservative due to the limited amount of brine in the region surrounding the waste panels that is available for the potential transport of radionuclides up an intruding borehole; specifically, a single borehole may experience more brine flow than each of several boreholes. For several drilling intrusions into the same waste panel, Assumption (1) is probably conservative due to the limited amount of brine available for radionuclide transport and the possible inventory limits on the releases of some radionuclides. Assumptions (2) and (3) relate to E1E2-type scenarios. Assumption (2) places a limit on how far apart in time two drilling intrusions can occur and still give rise to an E1E2-type scenario. Such a limitation seems reasonable due to both the plugging of boreholes by natural processes and the depletion of the brine in a pressurized brine pocket. If anything, the relatively long time intervals (e.g., 2000 yrs) used in the WIPP performance assessment in conjunction with this assumption lead to overestimates of the probability of E1E2-type scenarios. Further, given this assumption, the relationships used in the WIPP performance assessment tend to overestimate the probability of an E1E2-type scenario. Assumption (3) should have a neutral effect on the analysis as multiple drilling intrusions do not

affect the amount of brine available for radionuclide transport up the intruding boreholes and the effect of the increased borehole cross-sectional area is small compared to the uncertainties that result from borehole permeability and elemental solubilities.

The normalized releases rC_i, rC_{ij} and $rGWl_i$ can be used to construct the EPA normalized releases for the scenarios $S(\mathbf{n})$ and $S(\mathbf{l},\mathbf{n})$. For $S(\mathbf{n})$, the normalized release to the accessible environment, $cS(\mathbf{n})$, can be approximated by

$$cS(\mathbf{n}) = \sum_{j=1}^{nBH} (rC_{m(j)} + rGWl_{m(j)}), \tag{2.4-10}$$

where m(j) designates the time interval in which the j^{th} borehole occurs. The vector

$$\mathbf{m} = [m(1), m(2), \ldots, m(nBH)] \tag{2.4-11}$$

is uniquely determined once the vector $\mathbf{n}$ appearing in the definition of $S(\mathbf{n})$ is specified. The definition of $S(\mathbf{n})$ in Eq. 2.2-3 contains no information on the activity levels encountered by the individual boreholes, and so $cS(\mathbf{n})$ was constructed with the assumption that all waste is of the same average activity. However, the definition of $S(\mathbf{l},\mathbf{n})$ in Eq. 2.2-6 does contain information on activity levels, and the associated normalized release to the accessible environment, $cS(\mathbf{l},\mathbf{n})$, can be approximated by

$$cS(\mathbf{l},\mathbf{n}) = \sum_{j=1}^{nBH} \left[rC_{m(j),\ell(j)} + rGWl_{m(j)} \right], \tag{2.4-12}$$

which does incorporate the activity levels encountered by the individual boreholes.

For $S^{+-}(t_{i-1},t_i)$, the normalized release to the accessible environment, $cS^{+-}(t_{i-1},t_i)$, can be approximated by

$$cS^{+-}(t_{i-1},t_i) = 2\, rC_i + rGW2_i, \tag{2.4-13}$$

where it is assumed that all waste is of the same average activity for cuttings removal. Similarly, the normalized release $cS^{+-}(\mathbf{I};t_{i-1},t_i)$ for $S^{+-}(\mathbf{I};t_{i-1},t_i)$ can be approximated by

$$cS^{+-}(\mathbf{I};t_{i-1},t_i) = \sum_{j=1}^{2} rC_{i,\ell(j)} + rGW2_i, \qquad (2.4\text{-}14)$$

which incorporates the activity level of the waste. The approximations for $cS^{+-}(t_{i-1},t_i)$ and $cS^{+-}(\mathbf{I};t_{i-1},t_i)$ in Eqs. 2.4-13 and 2.4-14 are based on exactly two intrusions in the time interval $[t_{i-1},t_i]$. More complicated expressions could be developed to define releases for multiple E1E2-type intrusions. However, due to the low probability of such patterns of intrusion (e.g., the probabilities for 2 and ≥2 boreholes in Table 2-6 of WIPP PA Division (1991b) for the time interval [0,2000 yr] with 100 yr of administrative control are 0.009022 and 0.009315, respectively), the use of such expressions would have little impact on the CCDFs used for comparison with the EPA release limits.

The construction process shown in Eqs. 2.4-10 and 2.4-13 to obtain the normalized releases $cS(\mathbf{n})$and $cS^{+-}(t_{i-1},t_i)$ for scenarios $S(\mathbf{n})$ and $S^{+-}(t_{i-1},t_i)$ is illustrated in Table 3-4 of Volume 3. Further, the construction process shown in Eqs. 2.4-12 and 2.4-14 to obtain normalized releases $cS(\mathbf{I},\mathbf{n})$ and $cS^{+-}(\mathbf{I};t_{i-1},t_i)$ for scenarios $S(\mathbf{I},\mathbf{n})$ and $S^{+-}(\mathbf{I};t_{i-1},t_i)$ is illustrated in Table 3-5 of Volume 3.

2.5 Performance Assessment Representations Used in 1992

As discussed in conjunction with Eq. 2.1-1, the outcome of a performance assessment can be represented by a set R of ordered triples. Sections 2.2, 2.3 and 2.4 provide general descriptions of the manner in which the individual elements of these triples are defined in the 1992 WIPP performance assessment. Due to computational constraints and the desire to present results obtained with different modeling assumptions, the set R is actually defined in two different ways in the 1992 WIPP performance assessment.

The computational cost of performing groundwater transport calculations precluded the consideration of a large number of intrusion times in the 1992 WIPP performance assessment. Specifically, the decision was made to consider intrusions at only a single time (i.e., 1000 yr) for the initiation of groundwater transport. A relatively early intrusion time was selected because of the reduced releases that occur for later intrusion times due to both increased radioactive decay and reduced time for groundwater transport

to the accessible environment. This decision led to scenarios defined on the basis of the time intervals [0, 2000 yr] and [2000, 10,000 yr], with the rate term (i.e., $\lambda(t)$) in the Poisson model for drilling intrusions assumed to be zero after 2000 yr. This definition produced a set R_1 defined by

$$R_1 = \{(S_i, pS_i, \mathbf{cS}_i), i=1,\ldots, nS\}, \tag{2.5-1}$$

where the intervals indicated in Eq. 2.2-2 are

$$[0, 2000 \text{ yr}], [2000, 10{,}000 \text{ yr}] \tag{2.5-2}$$

and the vector $\mathbf{n}$ appearing in Eq. 2.2-5 is of the form

$$\mathbf{n} = [n(1), n(2)]. \tag{2.5-3}$$

The scenarios $S(\mathbf{n})$, $S^{+-}(t_{i-1}, t_i)$, $S(\mathbf{l},\mathbf{n})$ and $S^{+-}(\mathbf{l}; t_{i-1}, t_i)$ in Eqs. 2.2-3, 2.2-4, 2.2-6 and 2.2-7 are then defined accordingly.

As already indicated, the rate term $\lambda(t)$ in the Poisson model for drilling intrusions is assumed to be zero for $t > 2000$ yr. With this assumption, the expressions in Eqs. 2.3-1 and 2.3-3 for scenario probability become

$$pS(n(1),n(2)) = \begin{cases} \{[\int_0^{2000} \lambda(t)dt]^{n(1)}/n(1)!\}\exp[-\int_0^{2000} \lambda(t)dt] & \text{if } n(2) = 0 \\ 0 & \text{if } n(2) \neq 0 \end{cases} \tag{2.5-4}$$

and

$$pS^{+-}(t_{i-1},t_i) \doteq \begin{cases} \sum_{\ell=1}^{nP} \{1-\exp[-\int_0^{2000} \alpha_\ell(t)dt]\}\{1-\exp[-\int_0^{2000} \beta_\ell(t)dt]\} & \text{if } i = 1 \\ 0 & \text{if } i = 2 \end{cases}, \tag{2.5-5}$$

respectively. As a reminder, the assumption of 100 yr of administrative control in which no drilling intrusions can occur is equivalent to assuming that $\lambda(t) = 0$ for $0 \leq t \leq 100$ yr. Thus, the assumptions of 100 yr of administrative control and a constant value λ for $\lambda(t)$ in the time interval [100, 2000 yr] leads to the scenario probabilities

$$pS(n(1),n(2)) = \begin{cases} [(1900\ \lambda)^{n(1)}/n(1)!]\exp[-1900\lambda] & \text{if } n(2) = 0 \\ 0 & \text{if } n(2) \neq 0 \end{cases} \quad (2.5\text{-}6)$$

and

$$pS^{+-}(t_{i-1},t_i) \doteq \begin{cases} \sum_{\ell=1}^{nP} (1-\exp[-1900\ \alpha_\ell])(1-\exp[-1900\ \beta_\ell]) & \text{if } i = 1 \\ 0 & \text{if } i = 2 \end{cases}, \quad (2.5\text{-}7)$$

where α_ℓ and β_ℓ are defined in conjunction with Eq. 2.3-3 with $\lambda(t) = \lambda$. Examples of the scenario probabilities pS(n(1),n(2)) defined in Eqs. 2.5-4 and 2.5-6 are given in Tables 2.5-1 and 2.5-2, respectively. Further, the time-dependent λ used in the determination of the probabilities in Table 2.5-1 is based on the time-dependent drilling rate shown in Figure 2.5-1. In particular, the drilling rate in Figure 2.5-1 is expressed in units of drilling intrusions per square kilometer per 10,000 yr (i.e., $1/(km^2 \times 10^4$ yr) or $(km^2 \times 10^4\ yr)^{-1}$). As used in this report, λ has units of drilling intrusions per year (i.e., 1/yr or yr^{-1}) and is obtained by multiplying the drilling rate in Figure 2.5-1 by 0.126 km^2 and performing the indicated division by 10^4 where 0.126 km^2 is the area of emplaced waste used in the 1992 WIPP performance assessment.

The scenario consequences $\mathbf{cS}_i$ for R_1 appearing in Eq. 2.5-1 are constructed as shown in Eqs. 2.4-10 through 2.4-14 for the scenarios S_i that have nonzero probabilities.

Once R_1 is determined, the information contained in the probabilities pS_i and consequences $\mathbf{cS}_i$ can be summarized in CCDFs as shown in Figure 2.1-1. The set R_1 and its associated CCDFs are determined with the assumption that $\lambda(t)=0$ for $t > 2{,}000$ yr. Except for small effects due to the approximations used for the probabilities of the scenarios $S^{+-}(0, 2000)$ and $S^{+-}(2000, 10{,}000)$, the same CCDFs result when $\lambda(t)$ is unchanged (i.e., $\lambda(t)$ is not set to 0 for $t > 2000$ yr) but the environmental releases rC_2, rC_{2j}, rGW_2 and $rGW2_2$ for intrusions in the time interval [2000, 10,000 yr] are set to 0.

The calculation of releases to the accessible environment due to cuttings removal was significantly less computationally demanding than the calculation of releases due to groundwater transport. As a result, the decision was made to consider the effects of cuttings removal at a sequence of intrusion times rather than only at the single intrusion time considered

Table 2.5-1. Probabilities for Scenarios Involving Multiple Intrusions over 10,000 yr for the Time-Dependent λ Shown in Figure 2.5-1, 100 yr Administrative Control, and the Time Intervals [0, 2000 yr], [2000, 10,000 yr]. The scenarios shown in this table are contained in the set R_1 defined in Eq. 2.5-1.

Scenario[a]	Prob with $\lambda \neq 0$[b]	Prob with $\lambda \to 0$[c]
	0 intrusions	
	(# Scenarios = 1)	
$S(0,0)$	8.703E-01	9.863E-01
Prob 0 intr[d]	8.703E-01	9.863E-01
Cum Prob[e]	8.703E-01	9.863E-01
	1 intrusions	
	(# Scenarios = 2)	
$S(1,0)$	1.199E-02	1.358E-02
$S(0,1)$	1.090E-01	0.000E+00
Prob 1 intr	1.209E-01	1.358E-02
Cum Prob	9.912E-01	9.999E-01
	2 intrusions	
	(# Scenarios = 3)	
$S(2,0)$	8.253E-05	9.353E-05
$S(1,1)$	1.500E-03	0.000E+00
$S(0,2)$	6.820E-03	0.000E+00
Prob 2 intr	8.403E-03	9.353E-05
Cum Prob	9.996E-01	1.000E+00
	3 intrusions	
	(# Scenarios = 4)	
$S(3,0)$	3.789E-07	4.294E-07
$S(2,1)$	1.033E-05	0.000E+00
$S(1,2)$	9.392E-05	0.000E+00
$S(0,3)$	2.846E-04	0.000E+00
Prob 3 intr	3.892E-04	4.294E-07
Cum Prob	1.000E+00	1.000E+00
	4 intrusions	
	(# Scenarios = 5)	
$S(4,0)$	1.304E-09	1.478E-09
$S(3,1)$	4.743E-08	0.000E+00
$S(2,2)$	6.467E-07	0.000E+00
$S(1,3)$	3.919E-06	0.000E+00
$S(0,4)$	8.907E-06	0.000E+00
Prob 4 intr	1.352E-05	1.478E-09
Cum Prob	1.000E+00	1.000E+00
	5 intrusions	
	(# Scenarios = 6)	
$S(5,0)$	3.593E-12	4.072E-12
$S(4,1)$	1.633E-10	0.000E+00
$S(3,2)$	2.969E-09	0.000E+00
$S(2,3)$	2.699E-08	0.000E+00
$S(1,4)$	1.227E-07	0.000E+00
$S(0,5)$	2.230E-07	0.000E+00
Prob 5 intr	3.758E-07	4.072E-12
Cum Prob	1.000E+00	1.000E+00
	6 intrusions	
	(# Scenarios = 7)	
$S(6,0)$	8.246E-15	9.346E-15
$S(5,1)$	4.498E-13	0.000E+00
$S(4,2)$	1.022E-11	0.000E+00
$S(3,3)$	1.239E-10	0.000E+00
$S(2,4)$	8.447E-10	0.000E+00
$S(1,5)$	3.072E-09	0.000E+00
$S(0,6)$	4.654E-09	0.000E+00
Prob 6 intr	8.704E-09	9.346E-15
Cum Prob	1.000E+00	1.000E+00

[a] $S(i,j)$ represents the scenario in which i and j drilling intrusions occur in the time intervals [0, 2000 yr], and [2000, 10,000 yr], respectively.
[b] Scenario probability calculated with $\lambda \neq 0$ over the time interval [100, 10,000 yr].
[c] Scenario probability calculated with $\lambda \neq 0$ over the time interval [100, 2000 yr] and $\lambda = 0$ over the time interval [2000, 10,000 yr].
[d] Probability of indicated number of intrusions.
[e] Cumulative probability for all scenarios.

Table 2.5-1. Probabilities for Scenarios Involving Multiple Intrusions over 10,000 yr for the Time-Dependent λ Shown in Figure 2.5-1, 100 yr Administrative Control, and the Time Intervals [0, 2000 yr], [2000, 10,000 yr]. The scenarios shown in this table are contained in the set R_1 defined in Eq. 2.5-1. (concluded)

Scenario[a]	Prob with $\lambda \neq 0$[b]	Prob with $\lambda \rightarrow 0$[c]
	7 intrusions (# Scenarios = 8)	
S(7,0)	1.622E-17	1.839E-17
S(6,1)	1.032E-15	0.000E+00
S(5,2)	2.815E-14	0.000E+00
S(4,3)	4.266E-13	0.000E+00
S(3,4)	3.878E-12	0.000E+00
S(2,5)	2.115E-11	0.000E+00
S(1,6)	6.409E-11	0.000E+00
S(0,7)	8.323E-11	0.000E+00
Prob 7 intr	1.728E-10	1.839E-17
Cum Prob	1.000E+00	1.000E+00
	8 intrusions (# Scenarios = 9)	
S(8,0)	2.793E-20	3.165E-20
S(7,1)	2.031E-18	0.000E+00
S(6,2)	6.462E-17	0.000E+00
S(5,3)	1.175E-15	0.000E+00
S(4,4)	1.335E-14	0.000E+00
S(3,5)	9.709E-14	0.000E+00
S(2,6)	4.413E-13	0.000E+00
S(1,7)	1.146E-12	0.000E+00
S(0,8)	1.302E-12	0.000E+00
Prob 8 intr[d]	3.002E-12	3.165E-20
Cum Prob[e]	1.000E+00	1.000E+00
	9 intrusions (# Scenarios = 10)	
S(9,0)	4.274E-23	4.844E-23
S(8,1)	3.497E-21	0.000E+00
S(7,2)	1.271E-19	0.000E+00
S(6,3)	2.697E-18	0.000E+00
S(5,4)	3.677E-17	0.000E+00
S(4,5)	3.343E-16	0.000E+00
S(3,6)	2.026E-15	0.000E+00
S(2,7)	7.893E-15	0.000E+00
S(1,8)	1.794E-14	0.000E+00
S(0,9)	1.812E-14	0.000E+00
Prob 9 intr	4.635E-14	4.844E-23
Cum Prob	1.000E+00	1.000E+00
	10 intrusions (# Scenarios = 11)	
S(10,0)	5.886E-26	6.671E-26
S(9,1)	5.350E-24	0.000E+00
S(8,2)	2.189E-22	0.000E+00
S(7,3)	5.306E-21	0.000E+00
S(6,4)	8.440E-20	0.000E+00
S(5,5)	9.207E-19	0.000E+00
S(4,6)	6.975E-18	0.000E+00
S(3,7)	3.623E-17	0.000E+00
S(2,8)	1.235E-16	0.000E+00
S(1,9)	2.495E-16	0.000E+00
S(0,10)	2.268E-16	0.000E+00
Prob 10 intr	6.441E-16	6.671E-26
Cum Prob	1.000E+00	1.000E+00

[a] S(i,j) represents the scenario in which i and j drilling intrusions occur in the time intervals [0, 2000 yr], and [2000, 10,000 yr], respectively.
[b] Scenario probability calculated with $\lambda \neq 0$ over the time interval [100, 10,000 yr].
[c] Scenario probability calculated with $\lambda \neq 0$ over the time interval [100, 2000 yr] and $\lambda = 0$ over the time interval [2000, 10,000 yr].
[d] Probability of indicated number of intrusions.
[e] Cumulative probability for all scenarios.

Table 2.5-2. Probabilities for Scenarios Involving Multiple Intrusions over 10,000 yr for $\lambda = 3.78 \times 10^{-4}$ yr^{-1}, 100 yr Administrative Control, and the Time Intervals [0, 2000 yr], [2000, 10,000 yr]. The scenarios shown in this table are contained in the set R_1 defined in Eq. 2.5-1, and $\lambda = 3.78 \times 10^{-4}$ yr^{-1} is the largest drilling rate considered in the 1992 WIPP PA.

Scenario[a]	Prob with $\lambda \neq 0$[b]	Prob with $\lambda \rightarrow 0$[c]
	0 intrusions	
	(# Scenarios = 1)	
$S(0,0)$	2.378E-02	4.879E-01
Prob 0 intr[d]	2.378E-02	4.879E-01
Cum Prob[e]	2.378E-02	4.879E-01
	1 intrusions	
	(# Scenarios = 2)	
$S(1,0)$	1.707E-02	3.501E-01
$S(0,1)$	7.185E-02	0.000E+00
Prob 1 intr	8.892E-02	3.501E-01
Cum Prob	1.127E-01	8.381E-01
	2 intrusions	
	(# Scenarios = 3)	
$S(2,0)$	6.123E-03	1.256E-01
$S(1,1)$	5.156E-02	0.000E+00
$S(0,2)$	1.085E-01	0.000E+00
Prob 2 intr	1.662E-01	1.256E-01
Cum Prob	2.789E-01	9.637E-01
	3 intrusions	
	(# Scenarios = 4)	
$S(3,0)$	1.464E-03	3.004E-02
$S(2,1)$	1.850E-02	0.000E+00
$S(1,2)$	7.789E-02	0.000E+00
$S(0,3)$	1.093E-01	0.000E+00
Prob 3 intr	2.072E-01	3.004E-02
Cum Prob	4.861E-01	9.937E-01
	4 intrusions	
	(# Scenarios = 5)	
$S(4,0)$	2.627E-04	5.390E-03
$S(3,1)$	4.424E-03	0.000E+00
$S(2,2)$	2.794E-02	0.000E+00
$S(1,3)$	7.844E-02	0.000E+00
$S(0,4)$	8.257E-02	0.000E+00
Prob 4 intr	1.936E-01	5.390E-03
Cum Prob	6.797E-01	9.991E-01
	5 intrusions	
	(# Scenarios = 6)	
$S(5,0)$	3.770E-05	7.735E-04
$S(4,1)$	7.937E-04	0.000E+00
$S(3,2)$	6.683E-03	0.000E+00
$S(2,3)$	2.814E-02	0.000E+00
$S(1,4)$	5.924E-02	0.000E+00
$S(0,5)$	4.989E-02	0.000E+00
Prob 5 intr	1.448E-01	7.735E-04
Cum Prob	8.245E-01	9.999E-01
	6 intrusions	
	(# Scenarios = 7)	
$S(6,0)$	4.508E-06	9.250E-05
$S(5,1)$	1.139E-04	0.000E+00
$S(4,2)$	1.199E-03	0.000E+00
$S(3,3)$	6.731E-03	0.000E+00
$S(2,4)$	2.126E-02	0.000E+00
$S(1,5)$	3.580E-02	0.000E+00
$S(0,6)$	2.512E-02	0.000E+00
Prob 6 intr	9.022E-02	9.250E-05
Cum Prob	9.147E-01	1.000E+00

[a] $S(i,j)$ represents the scenario in which i and j drilling intrusions occur in the time intervals [0, 2000 yr] and [2000, 10,000 yr], respectively.
[b] Scenario probability calculated with $\lambda = 3.78 \times 10^{-4}$ yr^{-1} over the time interval [100, 10,000 yr].
[c] Scenario probability calculated with $\lambda = 3.78 \times 10^{-4}$ yr^{-1} over the time interval [100, 2000 yr] and $\lambda = 0$ over the time interval [2000, 10,000 yr].
[d] Probability of indicated number of intrusions.
[e] Cumulative probability for all scenarios.

Table 2.5-2. Probabilities for Scenarios Involving Multiple Intrusions over 10,000 yr for $\lambda = 3.78 \times 10^{-4}$ yr^{-1}, 100 yr Administrative Control, and the Time Intervals [0, 2000 yr], [2000, 10,000 yr]. The scenarios shown in this table are contained in the set R_1 defined in Eq. 2.5-1, and $\lambda = 3.78 \times 10^{-4}$ yr^{-1} is the largest drilling rate considered in the 1992 WIPP PA. (concluded)

Scenario[a]	Prob with $\lambda \neq 0$[b]	Prob with $\lambda \to 0$[c]
	7 intrusions	
	(# Scenarios = 8)	
S(7,0)	4.621E-07	9.482E-06
S(6,1)	1.362E-05	0.000E+00
S(5,2)	1.721E-04	0.000E+00
S(4,3)	1.207E-03	0.000E+00
S(3,4)	5.084E-03	0.000E+00
S(2,5)	1.284E-02	0.000E+00
S(1,6)	1.803E-02	0.000E+00
S(0,7)	1.084E-02	0.000E+00
Prob 7 intr	4.819E-02	9.482E-06
Cum Prob	9.629E-01	1.000E+00
	8 intrusions	
	(# Scenarios = 9)	
S(8,0)	4.145E-08	8.504E-07
S(7,1)	1.396E-06	0.000E+00
S(6,2)	2.058E-05	0.000E+00
S(5,3)	1.733E-04	0.000E+00
S(4,4)	9.120E-04	0.000E+00
S(3,5)	3.072E-03	0.000E+00
S(2,6)	6.467E-03	0.000E+00
S(1,7)	7.780E-03	0.000E+00
S(0,8)	4.095E-03	0.000E+00
Prob 8 intr[d]	2.252E-02	8.504E-07
Cum Prob[e]	9.854E-01	1.000E+00
	9 intrusions	
	(# Scenarios = 10)	
S(9,0)	3.305E-09	6.780E-08
S(8,1)	1.252E-07	0.000E+00
S(7,2)	2.109E-06	0.000E+00
S(6,3)	2.072E-05	0.000E+00
S(5,4)	1.309E-04	0.000E+00
S(4,5)	5.511E-04	0.000E+00
S(3,6)	1.547E-03	0.000E+00
S(2,7)	2.791E-03	0.000E+00
S(1,8)	2.938E-03	0.000E+00
S(0,9)	1.375E-03	0.000E+00
Prob 9 intr	9.356E-03	6.780E-08
Cum Prob	9.948E-01	1.000E+00
	10 intrusions	
	(# Scenarios = 11)	
S(10,0)	2.371E-10	4.865E-09
S(9,1)	9.985E-09	0.000E+00
S(8,2)	1.892E-07	0.000E+00
S(7,3)	2.124E-06	0.000E+00
S(6,4)	1.565E-05	0.000E+00
S(5,5)	7.908E-05	0.000E+00
S(4,6)	2.775E-04	0.000E+00
S(3,7)	6.676E-04	0.000E+00
S(2,8)	1.054E-03	0.000E+00
S(1,9)	9.863E-04	0.000E+00
S(0,10)	4.153E-04	0.000E+00
Prob 10 intr	3.498E-03	4.865E-09
Cum Prob	9.983E-01	1.000E+00

[a] S(i,j) represents the scenario in which i and j drilling intrusions occur in the time intervals [0, 2000 yr] and [2000, 10,000 yr], respectively.
[b] Scenario probability calculated with $\lambda = 3.78 \times 10^{-4}$ yr^{-1} over the time interval [100, 10,000 yr].
[c] Scenario probability calculated with $\lambda = 3.78 \times 10^{-4}$ yr^{-1} over the time interval [100, 2000 yr] and $\lambda = 0$ over the time interval [2000, 10,000 yr].
[d] Probability of indicated number of intrusions.
[e] Cumulative probability for all scenarios.

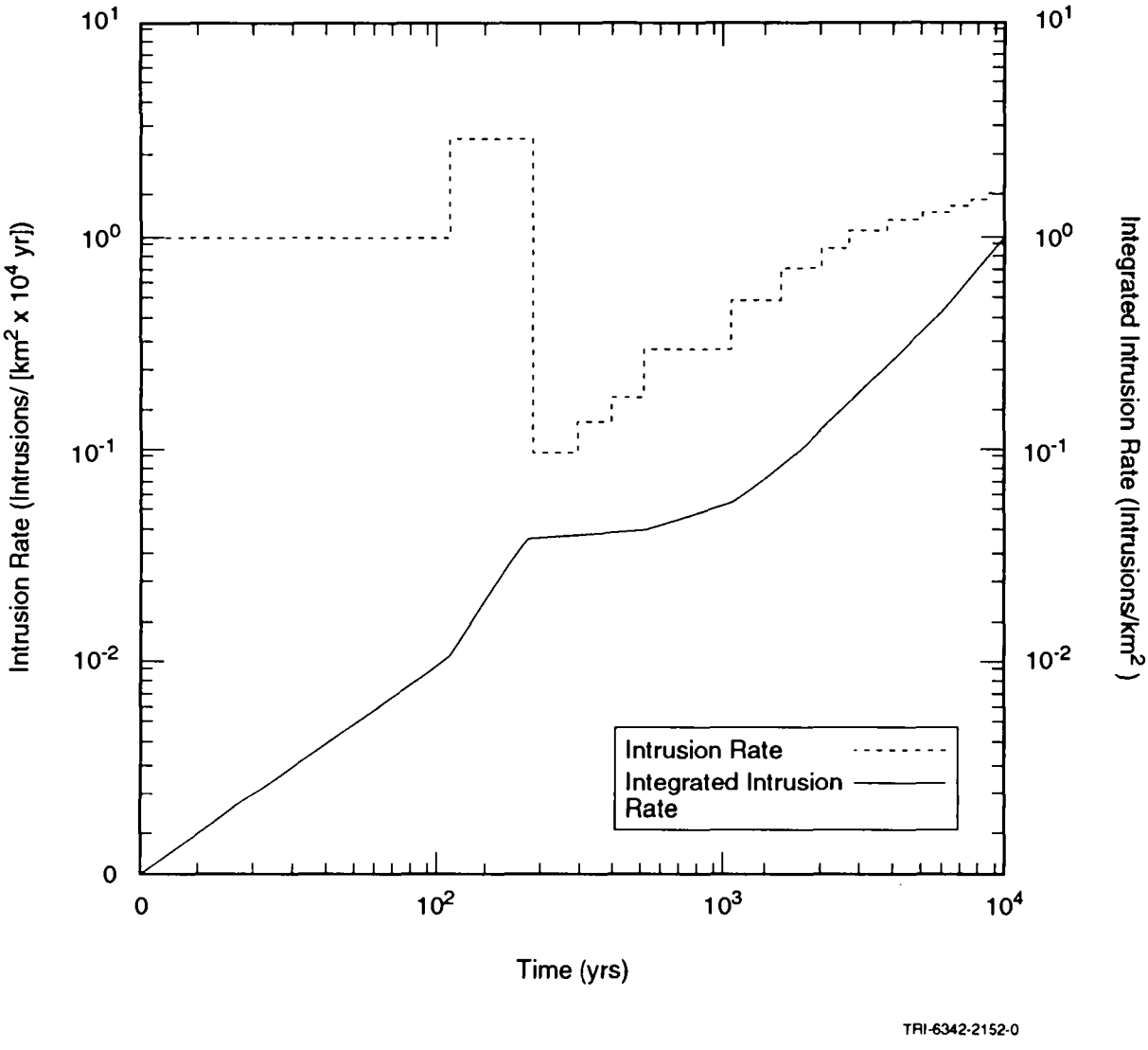

Figure 2.5-1. Example time-dependent rate term used in Poisson model for drilling intrusions in the 1992 WIPP performance assessment (Volume 3, Appendix D, Figure D-45). The rate $\lambda(t)$ as used in this chapter has units of yr^{-1} and is obtained by multiplying the rate indicated in this figure by 0.126 km^2 (i.e., the area of emplaced waste) and performing the indicated division by 10^4; further, $\lambda(t)$ is set to zero for the first 100 yrs when 100 yrs of administrative control is assumed. The rate $\lambda(t)$ was a sampled variable in the 1992 WIPP performance assessment; this figure shows the drilling rate with the largest integrated value (i.e., expected number of drilling intrusions) over 10,000 yr. In this and other similar figures, a hyperbolic sine transformation is used to generate the scales on the abscissa and ordinate; this transformation allows the plotting of zero, which is not possible when a logarithmic transformation is used.

for the initiation of groundwater transport. In particular, a set R_2 defined by

$$R_2 = \{(S_i, pS_i, \mathbf{cS}_i), i=1, \ldots, nS\} \tag{2.5-8}$$

was used in the 1992 WIPP performance assessment to investigate the effects of cuttings removal, where the time intervals indicated in Eq. 2.2-2 are

$$[0, 150 \text{ yr}], [150, 200 \text{ yr}], [200, 500 \text{ yr}], [500, 1500 \text{ yr}], [1500, 4500 \text{ yr}], [4500, 10{,}000 \text{ yr}] \tag{2.5-9}$$

and the vector $\mathbf{n}$ appearing in Eq. 2.2-5 is of the form

$$\mathbf{n} = [n(1), n(2), n(3), n(4), n(5), n(6)] \; . \tag{2.5-10}$$

The time intervals in Eq. 2.5-9 were selected to provide increased resolution at early times when the inventory of radionuclides with relatively short half lives (e.g., Pu-238 and Am-241) is changing rapidly. With the assumption of 100 yr of administrative control, the first time interval in Eq. 2.5-9 (i.e., [0, 150 yr]) effectively becomes [100, 150 yr].

The set R_2 is used to show only the effects of cuttings removal. As a result, the only scenarios used in the definition of R_2 are of the form $S(\mathbf{n})$ and $S(\mathbf{I},\mathbf{n})$ shown in Eqs. 2.2-3 and 2.2-6. The probabilities $pS(\mathbf{n})$ and $pS(\mathbf{I},\mathbf{n})$ for these scenarios with a time-dependent rate term (i.e., $\lambda(t)$) in the Poisson model for drilling intrusions are defined in Eqs. 2.3-1 and 2.3-2, respectively, with the times t_i, i=0, 1, ..., 6, equal to

$$0, 150, 200, 500, 1500, 4500, 10{,}000 \text{ yr}. \tag{2.5-11}$$

Examples of the probabilities $pS(\mathbf{n})$ calculated with the rate term shown in Figure 2.5-1 are presented in Table 2.5-3. Further, the resultant probabilities for a constant-valued λ are illustrated in Table 2.5-4.

The scenario consequences $\mathbf{cS}_i$ for R_2 appearing in Eq. 2.5-8 are constructed as shown in Eqs. 2.4-10 and 2.4-12. As R_2 is used to show only the effects of cuttings removal to the accessible environment, the term $rGWl_{m(j)}$ corresponding to the groundwater release in Eqs. 2.4-10 and 2.4-12 is assumed to equal zero.

Table 2.5-3. Probabilities for Scenarios Involving Multiple Intrusions over 10,000 yr for the Time-Dependent λ Shown in Figure 2.5-1, 100 yr Administrative Control, and the Time Intervals [0, 150 yr], [150, 200 yr], [200, 500 yr], [500, 1500 yr], [1500, 4500 yr] and [4500, 10,000 yr]. The scenarios shown in this table are contained in the set R_2 defined in Eq. 2.5-8.

Scenario[a]	Prob with $\lambda \neq 0$[b]	Prob with $\lambda \to 0$[c]
	0 intrusions	
	(# Scenarios = 1)	
S(0,0,0,0,0,0)	8.703E-01	9.863E-01
Prob 0 intr[d]	8.703E-01	9.863E-01
Cum Prob[e]	8.703E-01	9.863E-01
	1 intrusion	
	(# Scenarios = 6)	
S(1,0,0,0,0,0)	1.572E-03	1.782E-03
S(0,1,0,0,0,0)	1.572E-03	1.782E-03
S(0,0,1,0,0,0)	4.601E-04	5.215E-04
S(0,0,0,1,0,0)	4.503E-03	5.103E-03
S(0,0,0,0,1,0)	3.009E-02	4.395E-03
S(0,0,0,0,0,1)	8.273E-02	0.000E+00
Prob 1 intr	1.209E-01	1.358E-02
Cum Prob	9.912E-01	9.999E-01
	2 intrusions	
	(# Scenarios = 21)	
S(2,0,0,0,0,0)	1.420E-06	1.609E-06
S(1,1,0,0,0,0)	2.840E-06	3.219E-06
S(1,0,1,0,0,0)	8.312E-07	9.420E-07
S(1,0,0,1,0,0)	8.134E-06	9.219E-06
S(1,0,0,0,1,0)	5.436E-05	7.940E-06
S(1,0,0,0,0,1)	1.495E-04	0.000E+00
S(0,2,0,0,0,0)	1.420E-06	1.609E-06
S(0,1,1,0,0,0)	8.312E-07	9.420E-07
S(0,1,0,1,0,0)	8.134E-06	9.219E-06
S(0,1,0,0,1,0)	5.436E-05	7.940E-06
S(0,1,0,0,0,1)	1.495E-04	0.000E+00
S(0,0,2,0,0,0)	1.216E-07	1.379E-07
S(0,0,1,1,0,0)	2.381E-06	2.698E-06
S(0,0,1,0,1,0)	1.591E-05	2.324E-06
S(0,0,1,0,0,1)	4.374E-05	0.000E+00
S(0,0,0,2,0,0)	1.165E-05	1.320E-05
S(0,0,0,1,1,0)	1.557E-04	2.274E-05
S(0,0,0,1,0,1)	4.281E-04	0.000E+00
S(0,0,0,0,2,0)	5.203E-04	9.794E-06
S(0,0,0,0,1,1)	2.861E-03	0.000E+00
S(0,0,0,0,0,2)	3.933E-03	0.000E+00
Prob 2 intr	8.403E-03	9.353E-05
Cum Prob	9.996E-01	1.000E+00
	3 intrusions	
	(# Scenarios = 56)	
S(3,0,0,0,0,0)	8.550E-10	9.690E-10
S(2,1,0,0,0,0)	2.565E-09	2.907E-09
S(2,0,1,0,0,0)	7.507E-10	8.509E-10
S(2,0,0,1,0,0)	7.347E-09	8.326E-09
S(2,0,0,0,1,0)	4.910E-08	7.172E-09
S(2,0,0,0,0,1)	1.350E-07	0.000E+00
S(1,2,0,0,0,0)	2.565E-09	2.907E-09
S(1,1,1,0,0,0)	1.501E-09	1.702E-09
S(1,1,0,1,0,0)	1.469E-08	1.665E-08
S(1,1,0,0,1,0)	9.820E-08	1.434E-08
S(1,1,0,0,0,1)	2.700E-07	0.000E+00
S(1,0,2,0,0,0)	2.197E-10	2.490E-10
S(1,0,1,1,0,0)	4.300E-09	4.874E-09
S(1,0,1,0,1,0)	2.874E-08	4.198E-09
S(1,0,1,0,0,1)	7.902E-08	0.000E+00
S(1,0,0,2,0,0)	2.104E-08	2.385E-08
S(1,0,0,1,1,0)	2.813E-07	4.108E-08
S(1,0,0,1,0,1)	7.733E-07	0.000E+00
S(1,0,0,0,2,0)	9.400E-07	1.769E-08
S(1,0,0,0,1,1)	5.168E-06	0.000E+00
S(1,0,0,0,0,2)	7.104E-06	0.000E+00
S(0,3,0,0,0,0)	8.550E-10	9.690E-10
S(0,2,1,0,0,0)	7.507E-10	8.509E-10
S(0,2,0,1,0,0)	7.347E-09	8.326E-09
S(0,2,0,0,1,0)	4.910E-08	7.172E-09
S(0,2,0,0,0,1)	1.350E-07	0.000E+00
S(0,1,2,0,0,0)	2.197E-10	2.490E-10
S(0,1,1,1,0,0)	4.300E-09	4.874E-09
S(0,1,1,0,1,0)	2.874E-08	4.198E-09
S(0,1,1,0,0,1)	7.902E-08	0.000E+00

[a] S(i,j,k,l,m,n) represents the scenario in which i,j,k,l,m, and n drilling intrusions occur in the time intervals [0, 150 yr], [150, 200 yr], [200, 500 yr], and [500, 1500 yr], [1500, 4500 yr], and [4500, 10,000 yr], respectively.

[b] Scenario probability calculated with $\lambda \neq 0$ over the time interval [100, 10,000 yr].

[c] Scenario probability calculated with $\lambda \neq 0$ over the time interval [100, 2000 yr] and $\lambda = 0$ over the time interval [2000, 10,000 yr].

[d] Probability of indicated number of intrusions.

[e] Cumulative probability for all scenarios.

Table 2.5-3. Probabilities for Scenarios Involving Multiple Intrusions over 10,000 yr for the Time-Dependent λ Shown in Figure 2.5-1, 100 yr Administrative Control, and the Time Intervals [0, 150 yr], [150, 200 yr], [200, 500 yr], [500, 1500 yr], [1500, 4500 yr] and [4500, 10,000 yr]. The scenarios shown in this table are contained in the set R_2 defined in Eq. 2.5-8. (concluded)

Scenario[a]	Prob with $\lambda \neq 0$[b]	Prob with $\lambda \rightarrow 0$[c]
S(0,1,0,2,0,0)	2.104E-08	2.385E-08
S(0,1,0,1,1,0)	2.813E-07	4.108E-08
S(0,1,0,1,0,1)	7.733E-07	0.000E+00
S(0,1,0,0,2,0)	9.400E-07	1.769E-08
S(0,1,0,0,1,1)	5.168E-06	0.000E+00
S(0,1,0,0,0,2)	7.104E-06	0.000E+00
S(0,0,3,0,0,0)	2.144E-11	2.430E-11
S(0,0,2,1,0,0)	6.293E-10	7.133E-10
S(0,0,2,0,1,0)	4.206E-09	6.143E-10
S(0,0,2,0,0,1)	1.156E-08	0.000E+00
S(0,0,1,2,0,0)	6.158E-09	6.980E-09
S(0,0,1,1,1,0)	8.232E-08	1.202E-08
S(0,0,1,1,0,1)	2.263E-07	0.000E+00
S(0,0,1,0,2,0)	2.751E-07	5.178E-09
S(0,0,1,0,1,1)	1.513E-06	0.000E+00
S(0,0,1,0,0,2)	2.079E-06	0.000E+00
S(0,0,0,3,0,0)	2.009E-08	2.277E-08
S(0,0,0,2,1,0)	4.028E-07	5.883E-08
S(0,0,0,2,0,1)	1.107E-06	0.000E+00
S(0,0,0,1,2,0)	2.692E-06	5.067E-08
S(0,0,0,1,1,1)	1.480E-05	0.000E+00
S(0,0,0,1,0,2)	2.035E-05	0.000E+00
S(0,0,0,0,3,0)	5.998E-06	1.455E-08
S(0,0,0,0,2,1)	4.947E-05	0.000E+00
S(0,0,0,0,1,2)	1.360E-04	0.000E+00
S(0,0,0,0,0,3)	1.246E-04	0.000E+00
Prob 3 intr[d]	3.892E-04	4.294E-07
Cum Prob[e]	1.000E+00	1.000E+00
	4 intrusions	
	(# Scenarios = 126)	
S(4,0,0,0,0,0)	3.861E-13	4.376E-13
S(3,1,0,0,0,0)	1.545E-12	1.751E-12
.	.	.
.	.	.
.	.	.
S(1,1,1,1,0,0)	7.769E-12	8.805E-12
.	.	.
.	.	.
.	.	.
S(0,0,0,0,1,3)	4.310E-06	0.000E+00
S(0,0,0,0,0,4)	2.962E-06	0.000E+00
Prob 4 intr	1.352E-05	1.478E-09
Cum Prob	1.000E+00	1.000E+00
	5 intrusions	
	(# Scenarios = 252)	
Prob 5 intr	3.758E-07	4.072E-12
Cum Prob	1.000E+00	1.000E+00
	6 intrusions	
	(# Scenarios = 462)	
Prob 6 intr	8.704E-09	9.346E-15
Cum Prob	1.000E+00	1.000E+00
	7 intrusions	
	(# Scenarios = 792)	
Prob 7 intr	1.728E-10	1.839E-17
Cum Prob	1.000E+00	1.000E+00
	8 intrusions	
	(# Scenarios = 1287)	
Prob 8 intr	3.002E-12	3.165E-20
Cum Prob	1.000E+00	1.000E+00
	9 intrusions	
	(# Scenarios = 2002)	
Prob 9 intr	4.635E-14	4.844E-23
Cum Prob	1.000E+00	1.000E+00
	10 intrusions	
	(# Scenarios = 3003)	
Prob 10 intr	6.441E-16	6.671E-26
Cum Prob	1.000E+00	1.000E+00

[a] S(i,j,k,l,m,n) represents the scenario in which i,j,k,l,m, and n drilling intrusions occur in the time intervals [0, 150 yr], [150, 200 yr], [200, 500 yr], and [500, 1500 yr], [1500, 4500 yr], and [4500, 10,000 yr], respectively.

[b] Scenario probability calculated with $\lambda \neq 0$ over the time interval [100, 10,000 yr].

[c] Scenario probability calculated with $\lambda \neq 0$ over the time interval [100, 2000 yr] and $\lambda = 0$ over the time interval [2000, 10,000 yr].

[d] Probability of indicated number of intrusions.

[e] Cumulative probability for all scenarios.

Table 2.5-4. Probabilities for Scenarios Involving Multiple Intrusions over 10,000 years for $\lambda = 3.78 \times 10^{-4}$ yr^{-1}, 100 yr Administrative Control, and the Time Intervals [0, 150 yr], [150, 200 yr], [200, 500 yr], [500, 1500 yr], [1500, 4500 yr] and [4500, 10,000 yr]. The scenarios shown in this table are contained in the set R_2 defined in Eq. 2.5-8, and $\lambda = 3.78 \times 10^{-4}$ yr^{-1} is the largest drilling rate considered in the 1992 WIPP PA.

Scenario[a]	Prob with $\lambda \neq 0$[b]	Prob with $\lambda \rightarrow 0$[c]
	0 intrusions	
	(# Scenarios = 1)	
S(0,0,0,0,0,0)	2.378E-02	4.879E-01
Prob 0 intr[d]	2.378E-02	4.879E-01
Cum Prob[e]	2.378E-02	4.879E-01
	1 intrusion	
	(# Scenarios = 6)	
S(1,0,0,0,0,0)	4.491E-04	9.214E-03
S(0,1,0,0,0,0)	4.491E-04	9.214E-03
S(0,0,1,0,0,0)	2.695E-03	5.528E-02
S(0,0,0,1,0,0)	8.982E-03	1.843E-01
S(0,0,0,0,1,0)	2.695E-02	9.214E-02
S(0,0,0,0,0,1)	4.940E-02	0.000E+00
Prob 1 intr	8.892E-02	3.501E-01
Cum Prob	1.127E-01	8.381E-01
	2 intrusions	
	(# Scenarios = 21)	
S(2,0,0,0,0,0)	4.240E-06	8.699E-05
S(1,1,0,0,0,0)	8.480E-06	1.740E-04
S(1,0,1,0,0,0)	5.088E-05	1.044E-03
S(1,0,0,1,0,0)	1.696E-04	3.480E-03
S(1,0,0,0,1,0)	5.088E-04	1.740E-03
S(1,0,0,0,0,1)	9.328E-04	0.000E+00
S(0,2,0,0,0,0)	4.240E-06	8.699E-05
S(0,1,1,0,0,0)	5.088E-05	1.044E-03
S(0,1,0,1,0,0)	1.696E-04	3.480E-03
S(0,1,0,0,1,0)	5.088E-04	1.740E-03
S(0,1,0,0,0,1)	9.328E-04	0.000E+00
S(0,0,2,0,0,0)	1.526E-04	3.132E-03
S(0,0,1,1,0,0)	1.018E-03	2.088E-02
S(0,0,1,0,1,0)	3.053E-03	1.044E-02
S(0,0,1,0,0,1)	5.597E-03	0.000E+00
S(0,0,0,2,0,0)	1.696E-03	3.480E-02
S(0,0,0,1,1,0)	1.018E-02	3.480E-02
S(0,0,0,1,0,1)	1.866E-02	0.000E+00
S(0,0,0,0,2,0)	1.526E-02	8.699E-03
S(0,0,0,0,1,1)	5.597E-02	0.000E+00
S(0,0,0,0,0,2)	5.130E-02	0.000E+00
Prob 2 intr	1.662E-01	1.256E-01
Cum Prob	2.789E-01	9.637E-01
	3 intrusions	
	(# Scenarios = 56)	
S(3,0,0,0,0,0)	2.669E-08	5.475E-07
S(2,1,0,0,0,0)	8.006E-08	1.643E-06
S(2,0,1,0,0,0)	4.804E-07	9.856E-06
S(2,0,0,1,0,0)	1.601E-06	3.285E-05
S(2,0,0,0,1,0)	4.804E-06	1.643E-05
S(2,0,0,0,0,1)	8.807E-06	0.000E+00
S(1,2,0,0,0,0)	8.006E-08	1.643E-06
S(1,1,1,0,0,0)	9.608E-07	1.971E-05
S(1,1,0,1,0,0)	3.203E-06	6.571E-05
S(1,1,0,0,1,0)	9.608E-06	3.285E-05
S(1,1,0,0,0,1)	1.761E-05	0.000E+00
S(1,0,2,0,0,0)	2.882E-06	5.913E-05
S(1,0,1,1,0,0)	1.922E-05	3.942E-04
S(1,0,1,0,1,0)	5.765E-05	1.971E-04
S(1,0,1,0,0,1)	1.057E-04	0.000E+00
S(1,0,0,2,0,0)	3.203E-05	6.571E-04
S(1,0,0,1,1,0)	1.922E-04	6.571E-04
S(1,0,0,1,0,1)	3.523E-04	0.000E+00
S(1,0,0,0,2,0)	2.882E-04	1.643E-04
S(1,0,0,0,1,1)	1.057E-03	0.000E+00
S(1,0,0,0,0,2)	9.688E-04	0.000E+00
S(0,3,0,0,0,0)	2.669E-08	5.475E-07
S(0,2,1,0,0,0)	4.804E-07	9.856E-06
S(0,2,0,1,0,0)	1.601E-06	3.285E-05
S(0,2,0,0,1,0)	4.804E-06	1.643E-05
S(0,2,0,0,0,1)	8.807E-06	0.000E+00
S(0,1,2,0,0,0)	2.882E-06	5.913E-05
S(0,1,1,1,0,0)	1.922E-05	3.942E-04
S(0,1,1,0,1,0)	5.765E-05	1.971E-04
S(0,1,1,0,0,1)	1.057E-04	0.000E+00
S(0,1,0,2,0,0)	3.203E-05	6.571E-04

[a] S(i,j,k,l,m,n) represents the scenario in which i,j,k,l,m, and n drilling intrusions occur in the time intervals [0, 150 yr], [150, 200 yr], [200, 500 yr], and [500, 1500 yr], [1500, 4500 yr], and [4500, 10,000 yr], respectively.

[b] Scenario probability calculated with $\lambda = 3.78 \times 10^{-4}$ yr^{-1} over the time interval [100, 10,000 yr].

[c] Scenario probability calculated with $\lambda = 3.78 \times 10^{-4}$ yr^{-1} over the time interval [100, 2000 yr] and $\lambda = 0$ over the time interval [2000, 10,000 yr].

[d] Probability of indicated number of intrusions.

[e] Cumulative probability for all scenarios.

Table 2.5-4. Probabilities for Scenarios Involving Multiple Intrusions over 10,000 years for $\lambda = 3.78 \times 10^{-4}$ yr^{-1}, 100 yr Administrative Control, and the Time Intervals [0, 150 yr], [150, 200 yr], [200, 500 yr], [500, 1500 yr], [1500, 4500 yr] and [4500, 10,000 yr]. The scenarios shown in this table are contained in the set R_2 defined in Eq. 2.5-8, and $\lambda = 3.78 \times 10^{-4}$ yr^{-1} is the largest drilling rate considered in the 1992 WIPP PA. (concluded)

Scenario[a]	Prob with $\lambda \neq 0$[b]	Prob with $\lambda \to 0$[c]
S(0,1,0,1,1,0)	1.922E-04	6.571E-04
S(0,1,0,1,0,1)	3.523E-04	0.000E+00
S(0,1,0,0,2,0)	2.882E-04	1.643E-04
S(0,1,0,0,1,1)	1.057E-03	0.000E+00
S(0,1,0,0,0,2)	9.688E-04	0.000E+00
S(0,0,3,0,0,0)	5.765E-06	1.183E-04
S(0,0,2,1,0,0)	5.765E-05	1.183E-03
S(0,0,2,0,1,0)	1.729E-04	5.913E-04
S(0,0,2,0,0,1)	3.170E-04	0.000E+00
S(0,0,1,2,0,0)	1.922E-04	3.942E-03
S(0,0,1,1,1,0)	1.153E-03	3.942E-03
S(0,0,1,1,0,1)	2.114E-03	0.000E+00
S(0,0,1,0,2,0)	1.729E-03	9.856E-04
S(0,0,1,0,1,1)	6.341E-03	0.000E+00
S(0,0,1,0,0,2)	5.813E-03	0.000E+00
S(0,0,0,3,0,0)	2.135E-04	4.380E-03
S(0,0,0,2,1,0)	1.922E-03	6.571E-03
S(0,0,0,2,0,1)	3.523E-03	0.000E+00
S(0,0,0,1,2,0)	5.765E-03	3.285E-03
S(0,0,0,1,1,1)	2.114E-02	0.000E+00
S(0,0,0,1,0,2)	1.938E-02	0.000E+00
S(0,0,0,0,3,0)	5.765E-03	5.475E-04
S(0,0,0,0,2,1)	3.170E-02	0.000E+00
S(0,0,0,0,1,2)	5.813E-02	0.000E+00
S(0,0,0,0,0,3)	3.552E-02	0.000E+00
Prob 3 intr	2.072E-01	3.004E-02
Cum Prob	4.861E-01	9.937E-01
	4 intrusions	
	(# Scenarios = 126)	
S(4,0,0,0,0,0)	1.260E-10	2.585E-09
S(3,1,0,0,0,0)	5.039E-10	1.034E-08
.	.	.
.	.	.
.	.	.
S(1,1,1,1,0,0)	3.628E-07	7.444E-06
.	.	.
.	.	.
.	.	.
S(0,0,0,0,1,3)	4.024E-02	0.000E+00
S(0,0,0,0,0,4)	1.845E-02	0.000E+00
Prob 4 intr	1.936E-01	5.390E-03
Cum Prob	6.797E-01	9.991E-01
	5 intrusions	
	(# Scenarios = 252)	
Prob 5 intr	1.448E-01	7.735E-04
Cum Prob	8.245E-01	9.999E-01
	6 intrusions	
	(# Scenarios = 462)	
Prob 6 intr	9.022E-02	9.250E-05
Cum Prob	9.147E-01	1.000E+00
	7 intrusions	
	(# Scenarios = 792)	
Prob 7 intr	4.819E-02	9.482E-06
Cum Prob	9.629E-01	1.000E+00
	8 intrusions	
	(# Scenarios = 1287)	
Prob 8 intr	2.252E-02	8.504E-07
Cum Prob	9.854E-01	1.000E+00
	9 intrusions	
	(# Scenarios = 2002)	
Prob 9 intr	9.356E-03	6.780E-08
Cum Prob	9.948E-01	1.000E+00
	10 intrusions	
	(# Scenarios = 3003)	
Prob 10 intr	3.498E-03	4.865E-09
Cum Prob	9.983E-01	1.000E+00

[a] S(i,j,k,l,m,n) represents the scenario in which i,j,k,l,m, and n drilling intrusions occur in the time intervals [0, 150 yr], [150, 200 yr], [200, 500 yr], and [500, 1500 yr], [1500, 4500 yr], and [4500, 10,000 yr], respectively.

[b] Scenario probability calculated with $\lambda = 3.78 \times 10^{-4}$ yr^{-1} over the time interval [100, 10,000 yr].

[c] Scenario probability calculated with $\lambda = 3.78 \times 10^{-4}$ yr^{-1} over the time interval [100, 2000 yr] and $\lambda = 0$ over the time interval [2000, 10,000 yr].

[d] Probability of indicated number of intrusions.

[e] Cumulative probability for all scenarios.

The sets R_1 and R_2 in Eqs. 2.5-1 and 2.5-8 provide two different summaries of the results of the WIPP performance assessment based on different partitioning of the sample space S shown in Eq. 2.2-1. These sets actually depend on both the partitioning of S into the scenarios S_i and the determination of the scenario probabilities pS_i and the scenario consequences $\mathbf{cS}_i$. Thus, a full specification of R_1 and R_2 would also contain subscripts indicating the manner in which the probabilities pS_i and the consequences $\mathbf{cS}_i$ are determined. To avoid the use of unnecessarily cumbersome notation, such subscripting is not employed in this presentation. However, the manner in which the pS_i and $\mathbf{cS}_i$ are defined for use with the risk representations R_1 and R_2 is indicated in Chapter 8 when analysis results are presented.

3. UNCERTAIN VARIABLES SELECTED FOR SAMPLING

The 1992 WIPP performance assessment selected 49 imprecisely known variables for consideration. These variables are listed in Table 3-1 and correspond to the elements x_j, j=1, 2, ..., nV = 49, of the vector **x** shown in Eq. 2.1-2. The distributions indicated in Table 3-1 and shown more explicitly in Figure 3-1 correspond to the distributions appearing in Eq. 2.1-4 and characterize subjective, or type B, uncertainty. The variables in Table 3-1 and the rationale for their distributions are discussed extensively in Volume 3 of this report, which can be consulted for more detailed information than is presented here.

Table 3-1. Variables Sampled in 1992 WIPP Performance Assessment (adapted from Tables 6.0-1, 6.0-2, and 6.0-3 of Volume 3 of this report)

Variable	Definition
BCBRSAT	Residual brine saturation for Salado Formation (S_{lr}) (dimensionless). Used in BRAGFLO. Range: 0.0 to 0.4. Median 0.2. Distribution: Uniform. Additional information: Section 2.3.1, Volume 3. Variable 13 in Latin hypercube sample (LHS).
BCEXP	Brooks and Corey pore-size distribution parameter for Salado Formation (λ) (dimensionless). Used in BRAGFLO. Range: 0.2 to 10. Median 0.7. Distribution: Piecewise uniform. Additional information: Same as BCBRSAT. Variable 11 in LHS.
BCFLG	Pointer variable (flag) for selection of characteristic curve for capillary behavior. Used in BRAGFLO. Range: {0, 1}. Distribution: 33% 0, 67% 1. Value of 0 selects van Genuchten-Parker model; value of 1 selects Brooks-Corey model. Additional information: Section 2.3.1, Volume 3. Variable 12 in LHS.
BCGSSAT	Brooks and Corey residual gas saturation for Salado Formation (S_{gr}) (dimensionless). Used in BRAGFLO. Range: 0.0 to 0.4. Median: 0.2. Distribution: Uniform. Additional information: Same as BCBRSAT. Variable 14 in LHS.
BHPERM	Borehole permeability (k) (m^2). Used in BRAGFLO. Range: 1×10^{-14} to 1×10^{-11}. Median: 3.16×10^{-12}. Distribution: Lognormal. Additional information: Freeze and Cherry, 1979, Table 2-2 (silty sand); Section 4.2.1 Volume 3. Variable 21 in LHS.
BPPRES	Initial pressure (p) of pressurized brine pocket in Castile Formation (Pa). Used in BRAGFLO. Range: 1.3×10^7 to 2.1×10^7. Median: 1.7×10^7. Distribution: Piecewise linear. Additional information: Popielak et al., 1983, p. H-52; Lappin et al., 1989, Table 3-19; Section 4.3.1, Volume 3. Variable 19 in LHS.

Table 3-1. Variables Sampled in 1992 WIPP Performance Assessment (adapted from Tables 6.0-1, 6.0-2, and 6.0-3 of Volume 3 of this report) (continued)

Variable	Definition
BPSTOR	Bulk storativity (S_b) of pressurized brine pocket in Castile Formation (m^3/Pa). Used in BRAGFLO. Range: 0.02 to 2. Median: 0.2. Distribution: Lognormal. Additional information: Section 4.3.1, Volume 3. Variable 20 in LHS.
BPAREAFR	Fraction of waste panel area underlain by a pressurized brine pocket (dimensionless). Used in CCDFPERM in calculation of probability of E1E2-type scenarios. Range: 0.24 to 0.568. Median: 0.40. Distribution: Piecewise Linear. Additional information: Section 5.1, Volume 3. Variable 24 in LHS.
BRSAT	Initial fluid (brine) saturation of waste (dimensionless). Used in BRAGFLO. Range: 0 to 0.14. Median: 0.07. Distribution: Uniform. Additional information: Section 3.4.3, Volume 3. Variable 1 in LHS.
CULCLIM	Recharge amplitude factor (A_m) for Culebra (dimensionless). Used in SECO-FLOW. Range: 1 to 1.07. Median: 1.035. Distribution: Uniform. Used in definition of time dependent boundary heads in Culebra, with the maximum head increasing from the estimated present-day head in the Culebra in the northern most element of the regional model domain for CULCLIM = 1 to the elevation of the Clayton Basin spill point (1007m) for CULCLIM = 1.07. Additional information: Section 6.4, of this Volume. Variable 32 in LHS is uniformly distributed on [0,1] and used to select value for CULCLIM by preprocessor to SECO-FLOW.
CULFRPOR	Fracture porosity (Θ_f) in Culebra (dimensionless). Used in SECO-FLOW and SECO-TRANSPORT. Range: 1×10^{-4} to 1×10^{-2}. Median: 1×10^{-3}. Distribution: Lognormal. Additional information: Tables 1-2 and E-6, Lappin et al., 1989; Section 2.6.2, Volume 3. Variable 33 in LHS.
CULFRSP	Fracture spacing (2B) in Culebra (m). Used in SECO-TRANSPORT. Range: 6×10^{-2} to 8. Median: 4×10^{-1}. Distribution: Piecewise uniform. Additional information: Beauheim et al., 1991b. Variable 34 in LHS.
CULCLYF	Clay filling fraction (b_c/b) in Culebra (dimensionless), where 2b is the fracture aperture and $2b_c$ is the total thickness of the clay lining in the fracture. Used in SECO-TRANSPORT. Range: 0 to 0.5. Median: 0. Distribution: $b_c/b=0$ has probability 0.5 and $b_c/b\neq0$ is uniformly distributed between 0 and 0.5. Additional information: Section 2.6.1, Volume 3. Variable 35 in LHS.
CULCLYP	Porosity of clay lining fractures in Culebra (dimensionless). Used in SECOTP. Range: 0.05 to 0.5. Median: 0.275. Distribution: Uniform. Additional information: Section 2.6.2, Volume 3. Variable 36 in LHS.

Table 3-1. Variables Sampled in 1992 WIPP Performance Assessment (adapted from Tables 6.0-1, 6.0-2, and 6.0-3 of Volume 3 of this report) (continued)

Variable	Definition
CULPOR	Matrix porosity (θ_m) in Culebra (dimensionless). Used in BRAGFLO and SECO-TRANSPORT. Range: 5.8×10^{-2} to 2.53×10^{-1}. Median: 1.39×10^{-1}. Distribution: Piecewise uniform. Additional information: Table 4.4, Kelley and Saulnier, 1990; Table E-8, Lappin et al., 1989; Section 2.6.2, Volume 3. Variable 43 in LHS.
CULTRFLD	Transmissivity field for Culebra. Seventy transmissivity fields consistent with available field data were constructed and ranked with respect to travel time to the accessible environment. CULTRFLD is a pointer variable used to select from these 70 fields, with travel time increasing monotonically with CULTRFLD. Used in STAFF2D and SECO-TRANSPORT. Range: 0 to 1. Median: 0.5. Distribution: Uniform. Additional information: Section 7.5, Volume 2; Section 2.6.3, Volume 3. Variable 31 in LHS.
DBDIAM	Drill bit diameter (m). Used in CUTTINGS and BRAGFLO. Range: 0.267 to 0.444. Median: 0.355. Distribution: Uniform. Additional information: Section 4.2.2, Volume 3. Variable 22 in LHS.
FKDAM	Fracture distribution coefficient (K_d) for Am in Culebra (m^3/ kg). Used in SECO-TRANSPORT. Range: 1×10^{-4} to 1×10^{3}. Median: 9.33×10^{1}. Distribution: Piecewise loguniform. Additional information: Section 2.6.4, Volume 3. Variable 37 in LHS.
FKDNP	Fracture distribution coefficient (K_d) for Np in Culebra (m^3/kg). Used in SECO-TRANSPORT. Range: 1×10^{-4} to 1×10^{3}. Median: 1. Distribution: Piecewise loguniform. Additional information: Section 2.6.4, Volume 3. Variable 38 in LHS.
FKDPU	Fracture distribution coefficient (K_d) for Pu in Culebra (m^3/kg). Used in SECO-TRANSPORT. Range: 1×10^{-4} to 1×10^{3}. Median: 2.04×10^{2}. Distribution: Piecewise loguniform. Additional information: Section 2.6.4, Volume 3. Variable 39 in LHS.
FKDRA	Fracture distribution coefficient (K_d) for Ra in Culebra (m^3/kg). Used in SECO-TRANSPORT. Range: 1×10^{-4} to 1×10^{2}. Median: 3.31×10^{-2}. Distribution: Piecewise loguniform. Additional information: Section 2.6.4, Volume 3. Variable 42 in LHS.
FKDTH	Fracture distribution coefficient (K_d) for Th in Culebra (m^3/kg). Used in SECO-TRANSPORT. Range: 1×10^{-4} to 1×10^{1}. Median: 1×10^{-1}. Distribution: Piecewise loguniform. Additional information: Section 2.6.4, Volume 3. Variable 40 in LHS.

Table 3-1. Variables Sampled in 1992 WIPP Performance Assessment (adapted from Tables 6.0-1, 6.0-2, and 6.0-3 of Volume 3 of this report) (continued)

Variable	Definition
FKDU	Fracture distribution coefficient (K_d) for U in Culebra (m^3/kg). Used in SECO-TRANSPORT. Range: 1×10^{-4} to 1. Median: 7.94×10^{-3}. Distribution: Piecewise loguniform. Additional information: Section 2.6.4, Volume 3. Variable 41 in LHS.
GRCORHF	Scale factor used in definition of gas generation rate for corrosion of steel under humid conditions (dimensionless). Actual gas generation rate is GRCORH = GRCORHF • GRCORI. Used in BRAGFLO. Range: 0 to 0.5. Median: 0.1. Distribution: Piecewise uniform. Additional information: Brush, 1991. Variable 3 in LHS.
GRCORI	Gas generation rate for corrosion of steel under inundated conditions (mol/m^2 surface area steel • s). Used in BRAGFLO. Range: 0 to 1.3×10^{-8}. Median: 6.3×10^{-9}. Distribution: Piecewise uniform. Additional information: Same as GRCORHF. Variable 2 in LHS.
GRMICHF	Scale factor used in definition of gas generation rate due to microbial degradation of cellulosics under humid conditions (mol/kg cellulosics • s). Actual gas generation rate is GRMICH = GRMICHF • GRMICI. Used in BRAGFLO. Range: 0 to 0.2. Median: 0.1. Distribution: Uniform. Additional information: Same as GRCORHF. Variable 6 in LHS.
GRMICI	Gas generation rate due to microbial degradation of cellulosics under inundated conditions (mol/kg cellulosics • s). Used in BRAGFLO. Range: 0 to 1.6×10^{-8}. Median: 3.2×10^{-9}. Distribution: Piecewise uniform. Additional information: Same as GRCORHF. Variable 5 in LHS.
LAMBDA	Pointer variable used to select rate term (λ or $\lambda(t)$, units: yr^{-1}) in Poisson model for drilling intrusions. Used in CCDFPERM. Range: 0 to 1. Median: 0.5. Distribution: Uniform. Additional information: Section 5.2, Volume 3. Variable 23 in LHS.
MBPERM	Permeability (k) in intact anhydrite marker beds in Salado Formation (m^2). Used in BRAGFLO. Range: 1×10^{-21} to 1×10^{-16}. Median: 5.0×10^{-20}. Distribution: Piecewise loguniform. Correlation: 0.3 rank correlation with SALPERM. Additional information: Section 2.4.2, Volume 3. Variable 15 in LHS.
MBPOR	Porosity (ϕ) in intact anhydrite marker beds in Salado Formation (dimensionless). Used in BRAGFLO. Range: 1×10^{-3} to 3×10^{-2}. Median: 1×10^{-2}. Distribution: Piecewise uniform. Additional information: Section 2.4.4, Volume 3. Variable 16 in LHS.

Table 3-1. Variables Sampled in 1992 WIPP Performance Assessment (adapted from Tables 6.0-1, 6.0-2, and 6.0-3 of Volume 3 of this report) (continued)

Variable	Definition
MBPRES	Far field pressure (p) in Salado Formation at the MB139 elevation. Used in BRAGFLO. Range: 1.2×10^{7} to 1.3×10^{7}. Median: 1.25×10^{7}. Distribution: Uniform. Additional information: Section 2.4.3, Volume 3. Variable 18 in LHS.
MKDAM	Matrix distribution coefficient (K_d) Am in Culebra (m^3/kg). Used in SECO-TRANSPORT. Range: 1×10^{-4} to 1×10^{2}. Median: 1.86×10^{-1}. Distribution: Piecewise loguniform. Additional information: Section 2.6.4, Volume 3. Variable 44 in LHS.
MKDNP	Matrix distribution coefficient (K_d) for Np in Culebra (m^3/kg). Used in SECO-TRANSPORT. Range: 1×10^{-4} to 1×10^{2}. Median: 4.78×10^{-2}. Distribution: Piecewise loguniform. Additional information: Section 2.6.4, Volume 3. Variable 45 in LHS.
MKDPU	Matrix distribution coefficient (K_d) for Pu in Culebra (m^3/kg). Used in SECO-TRANSPORT. Range: 1×10^{-4} to 1×10^{2}. Median: 2.61×10^{-1}. Distribution: Piecewise loguniform. Additional information: Section 2.6.4, Volume 3. Variable 46 in LHS.
MKDRA	Matrix distribution coefficient (K_d) for Ra in Culebra (m^3/kg). Used in SECO-TRANSPORT. Range: 1×10^{-4} to 1×10^{1}. Median: 1×10^{-2}. Distribution: Piecewise loguniform. Additional information: Section 2.6.4, Volume 3. Variable 49 in LHS.
MKDTH	Matrix distribution coefficient (K_d) for Th in Culebra (m^3/kg). Used in SECO-TRANSPORT. Range: 1×10^{-4} to 1. Median: 1×10^{-2}. Distribution: Piecewise loguniform. Additional information: Section 2.6.4, Volume 3. Variable 47 in LHS.
MKDU	Matrix distribution coefficient (K_d) for U in Culebra (m^3/kg). Used in SECO-TRANSPORT. Range: 1×10^{-4} to 1. Median: 2.88×10^{-2}. Distribution: Piecewise loguniform. Additional information: Section 2.6.4, Volume 3. Variable 48 in LHS.
SALPERM	Permeability (k) in intact halite component of Salado Formation (m^2). Used in BRAGFLO. Range: 1×10^{-24} to 1×10^{-19}. Median: 2×10^{-21}. Distribution: Piecewise loguniform. Correlation: 0.3 rank correlation with MBPERM. Additional information: Gorham et al., 1992; Howarth et al., 1991; Beauheim et al., 1991a; Section 2.3.5, Volume 3. Variable 10 in LHS.
SOLAM	Solubility of Am in brine (mol/ℓ). Used in PANEL. Range: 5×10^{-14} to 1.4. Median: 1×10^{-9}. Distribution: Piecewise loguniform. Additional information: Trauth et al., 1991; Section 3.3.5, Volume 3. Variable 25 in LHS.

Table 3-1. Variables Sampled in 1992 WIPP Performance Assessment (adapted from Tables 6.0-1, 6.0-2, and 6.0-3 of Volume 3 of this report) (continued)

Variable	Definition
SOLNP	Solubility of Np in brine (mol/ℓ). Used in PANEL. Range: 3×10^{-16} to 1.2×10^{-2}. Median: 1.0×10^{-7}. Distribution: Piecewise loguniform. Additional information: Same as SOLAM. Variable 26 in LHS.
SOLPU	Solubility of Pu in brine (mol/ℓ). Used in PANEL. Range: 2.5×10^{-17} to 5.5×10^{-4}. Median: 6×10^{-10}. Distribution: Piecewise loguniform. Additional information: Same as SOLAM. Variable 27 in LHS.
SOLRA	Solubility of Ra in brine (mol/ℓ). Used in PANEL. Range: 2 to 18.2. Median: 11. Distribution: Piecewise loguniform. Additional information: Same as SOLAM. Variable 28 in LHS.
SOLTH	Solubility of Th in brine (mol/ℓ). Used in PANEL. Range: 5.5×10^{-16} to 2.2×10^{-6}. Median: 1×10^{-10}. Distribution: Piecewise loguniform. Additional information: Same as SOLAM. Variable 29 in LHS.
SOLU	Solubility of U in brine (mol/ℓ). Used in PANEL. Range: 1×10^{-15} to 1. Median: 5.4×10^{-4}. Distribution: Piecewise loguniform. Additional information: Same as SOLAM. Variable 30 in LHS.
STOICCOR	Stoichiometric coefficient for corrosion of steel (dimensionless). Defines proportion of two different chemical reactions taking place during the corrosion process. Used in BRAGFLO. Range: 0 to 1. Median: 0.5. Distribution: Uniform. Additional information: Brush and Anderson, 1989. Variable 4 in LHS.
STOICMIC	Stoichiometric coefficient for microbial degradation of cellulosics (mol gas/mol CH_2O). Used in BRAGFLO. Range: 0 to 1.67. Median: 0.835. Distribution: Uniform. Additional information: Brush and Anderson, 1989. Variable 7 in LHS.
TZPORF	Scale factor used in definition of transition zone and disturbed rock zone porosity (ϕ_Z), with the transition zone and disturbed rock zone porosity defined by TZPOR = SALPOR + (0.06 - SALPOR)•TZPORF. Used in BRAGFLO. Range: 0 to 1. Median: 0.5. Distribution: Uniform. Additional information: Section 2.4.4, Volume 3. Variable 17 in LHS.
VMETAL	Fraction of total waste volume that is occupied by IDB (Integrated Data Base) metals and glass waste category (dimensionless). Used in BRAGFLO. Range: 0.276 to 0.476. Median: 0.376. Distribution: Normal. Additional information: Section 3.4.1, Volume 3. Variable 9 in LHS.

Table 3-1. Variables Sampled in 1992 WIPP Performance Assessment (adapted from Tables 6.0-1, 6.0-2, and 6.0-3 of Volume 3 of this report) (concluded)

Variable	Definition
VWOOD	Fraction of total waste volume that is occupied by IDB combustible waste category (dimensionless). Used in BRAGFLO. Range: 0.284 to 0.484. Median: 0.384. Distribution: Normal. Additional information: Section 3.4.1, Volume 3. Variable 8 in LHS.

As discussed in conjunction with Eq. 2.1-5, a Latin hypercube sample (McKay et al., 1979; Iman and Shortencarier, 1984) of size nK = 70 was generated from the variables listed in Table 3-1. The restricted pairing technique developed by Iman and Conover (1982) was used to induce the correlations between variables indicated in Table 3-1 and also to assure that the correlations between other variables were close to zero. The values used for each variable in the Latin hypercube sample are shown in Figure 3-1.

Once the sample indicated in Eq. 2.1-5 was generated from the variables in Table 3-1, the individual sample elements $\mathbf{x}_k$, k=1, ..., 70, were used in the generation of the risk results shown in Eq. 2.1-6. An overview of this process is provided in Sections 2.2, 2.3 and 2.4. In addition to many intermediate results, the final outcome of this process is a distribution of CCDFs of the form shown in Figure 2.1-2.

The analyses leading to the risk results shown in Eq. 2.1-6 were actually repeated a number of times with different modeling assumptions. The specific cases considered are listed in Table 3-2 (following Figure 3-1). Of the cases listed in Table 3-2, number 13, which is a dual-porosity transport model in the Culebra Dolomite with chemical sorption in both the dolomite matrix and clay-lined fractures, is believed by the WIPP performance assessment team to be the most credible and is presented as the best-estimate analysis in the 1992 WIPP performance assessment (see Section 2.2.4 of Volume 2 of this report). The other cases listed in Table 3-2 can be viewed as sensitivity studies that explore various perturbations on this best-estimate analysis.

In addition to the variation between the cases listed in Table 3-2, the sampling-based approach to the treatment of subjective uncertainty also produces uncertainty and sensitivity results for the individual cases. In Chapter 8, box plots and distributions of CCDFs are used to display the effect of subjective uncertainty on the cases listed in

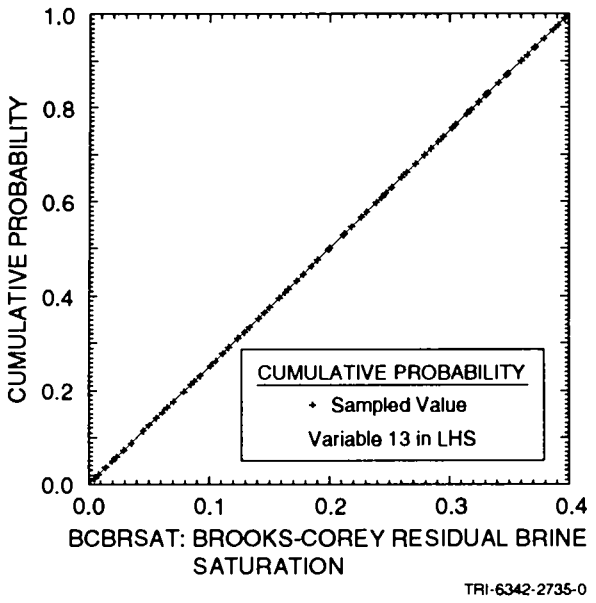

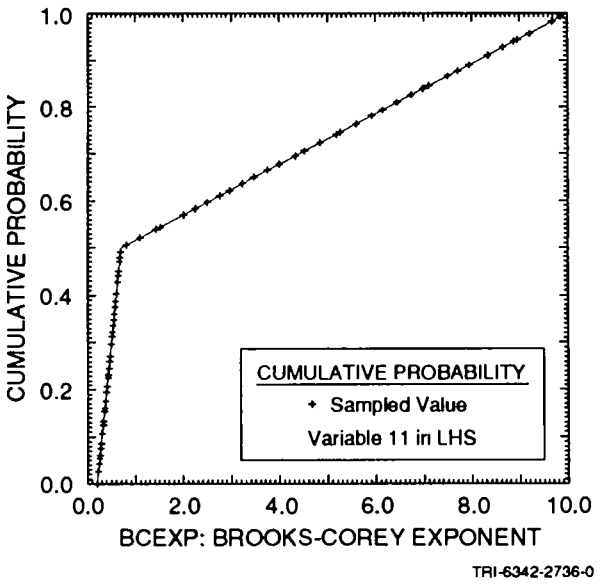

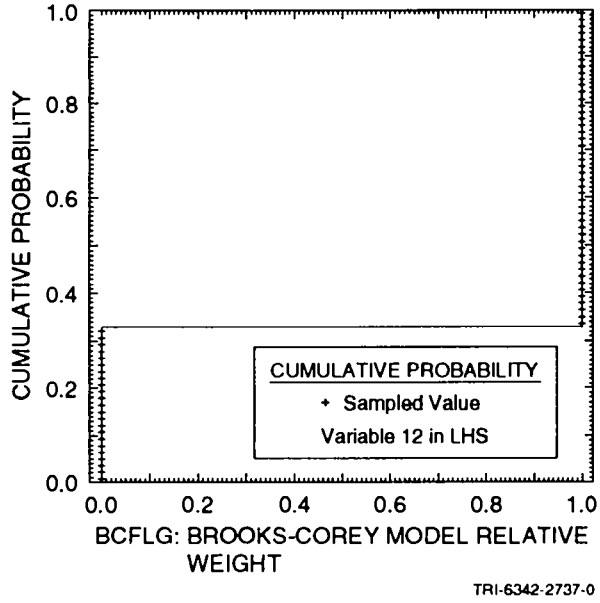

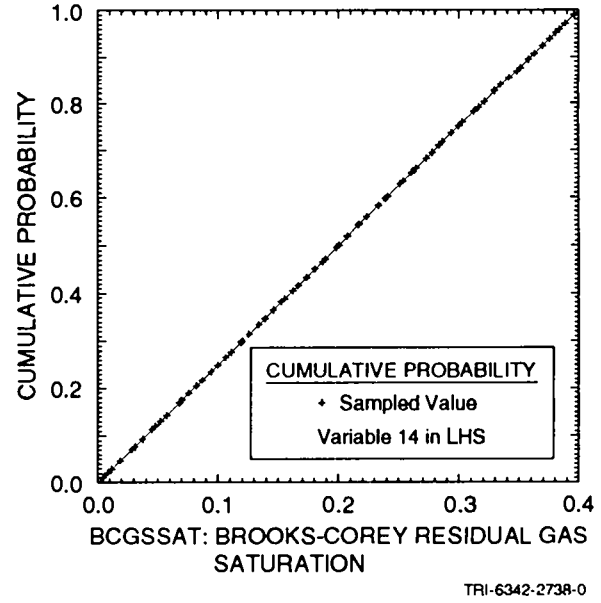

Figure 3-1. Distributions used for sampled variables in 1992 WIPP performance assessment.

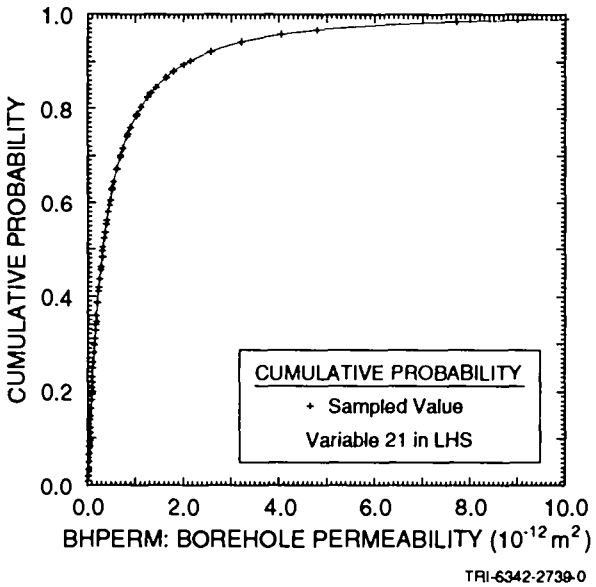

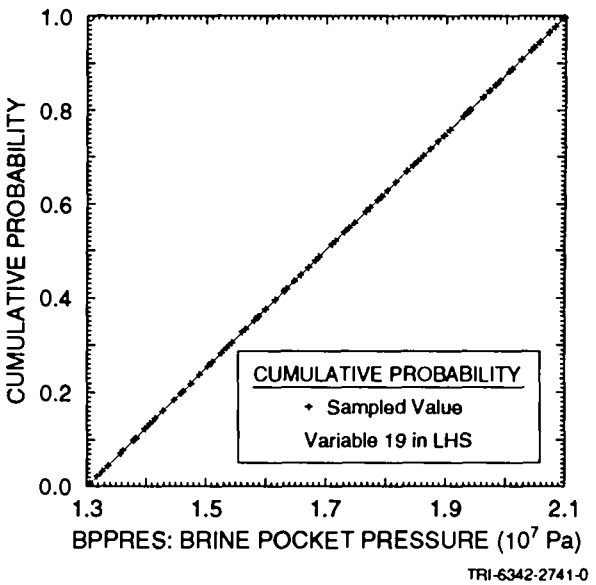

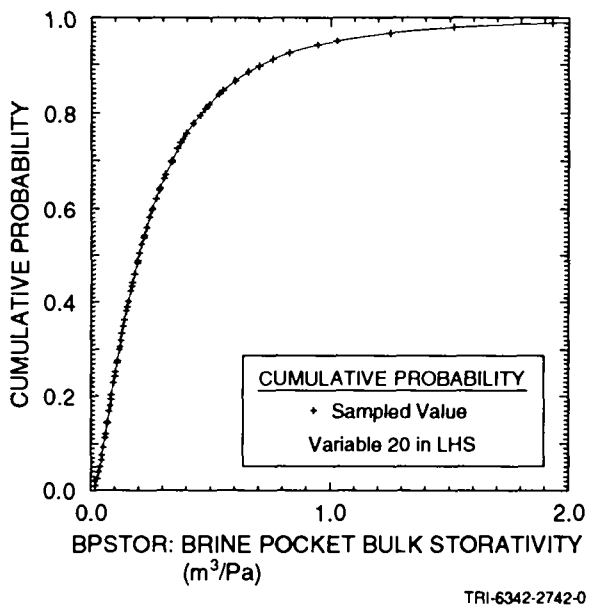

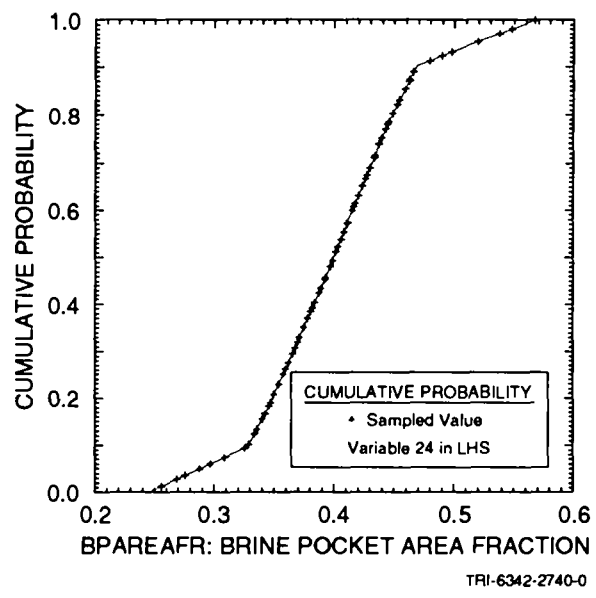

Figure 3-1. Distributions used for sampled variables in 1992 WIPP performance assessment. (continued)

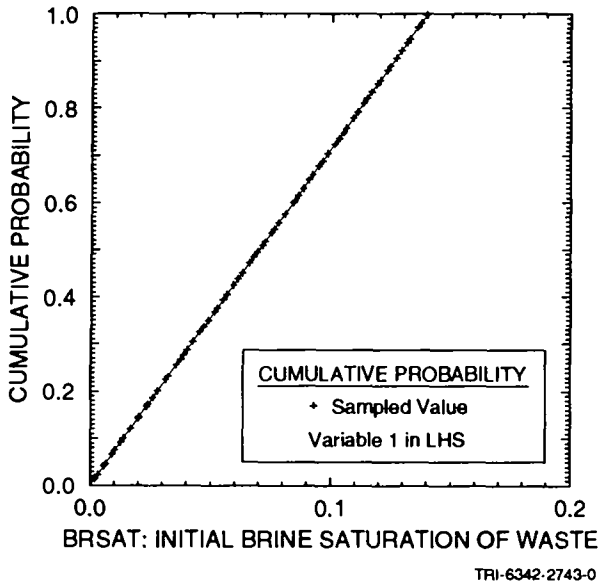

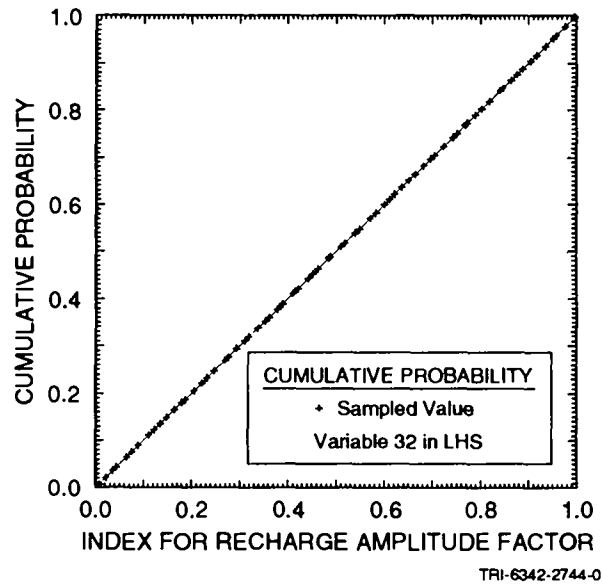

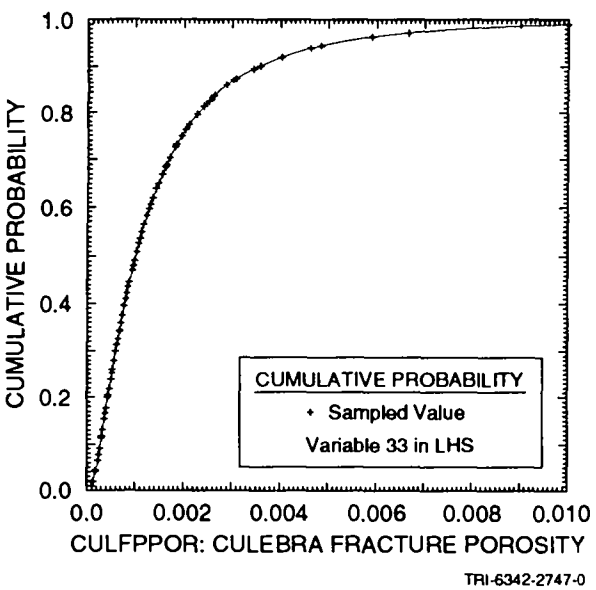

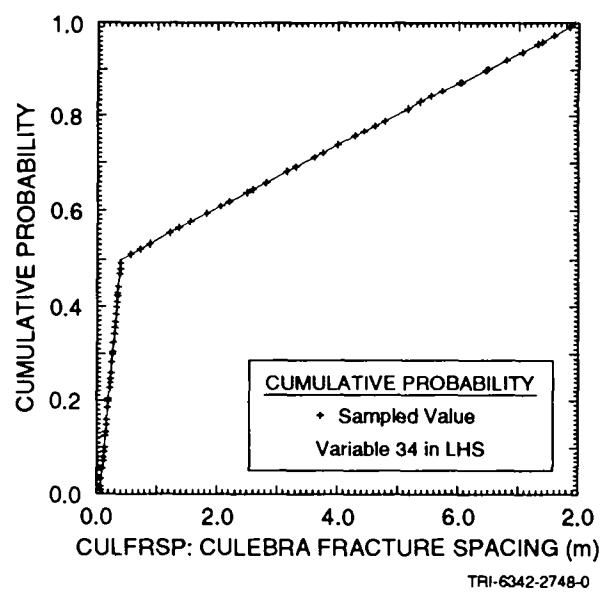

Figure 3-1. Distributions used for sampled variables in 1992 WIPP performance assessment. (continued)

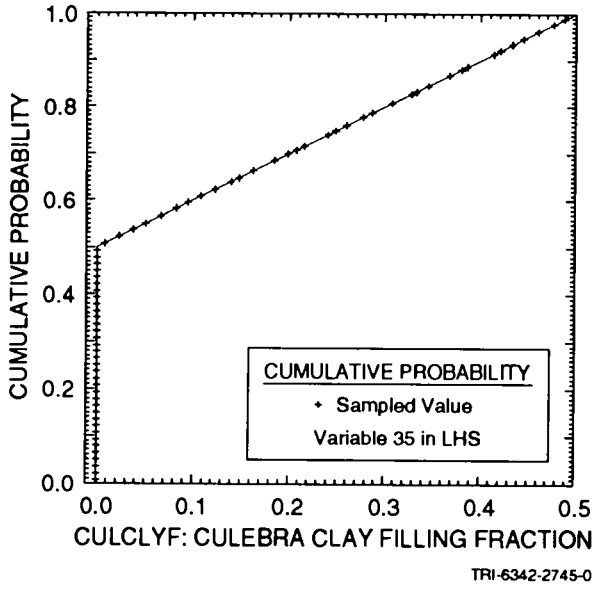

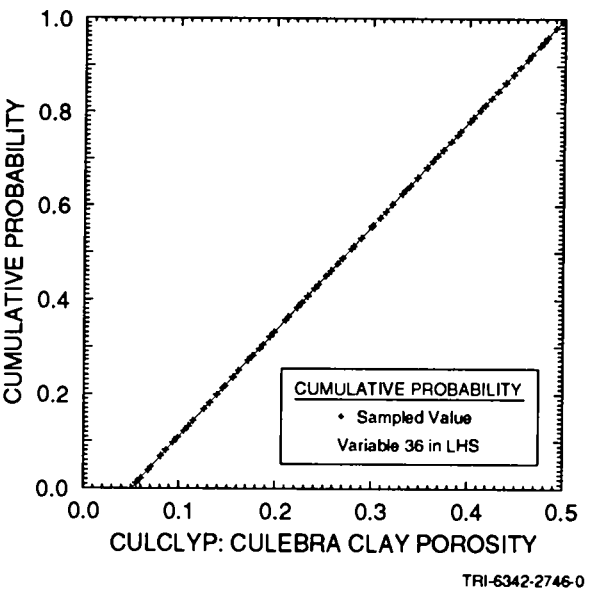

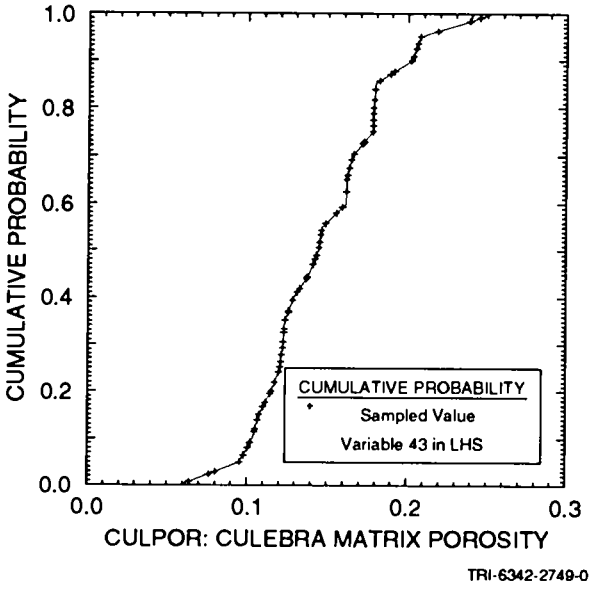

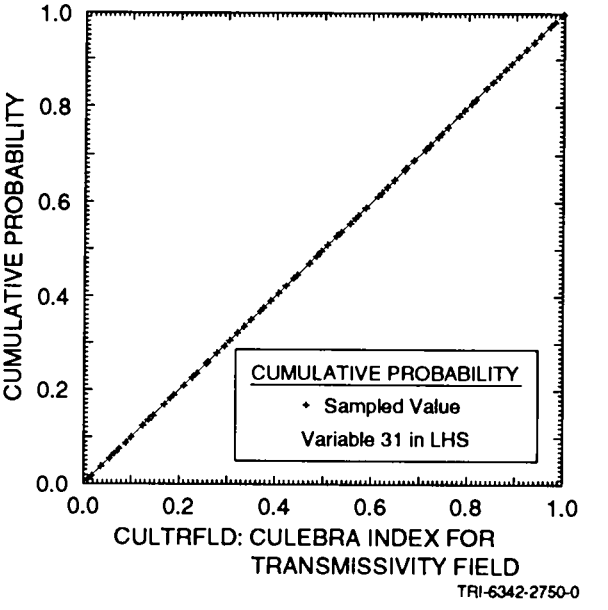

Figure 3-1. Distributions used for sampled variables in 1992 WIPP performance assessment. (continued)

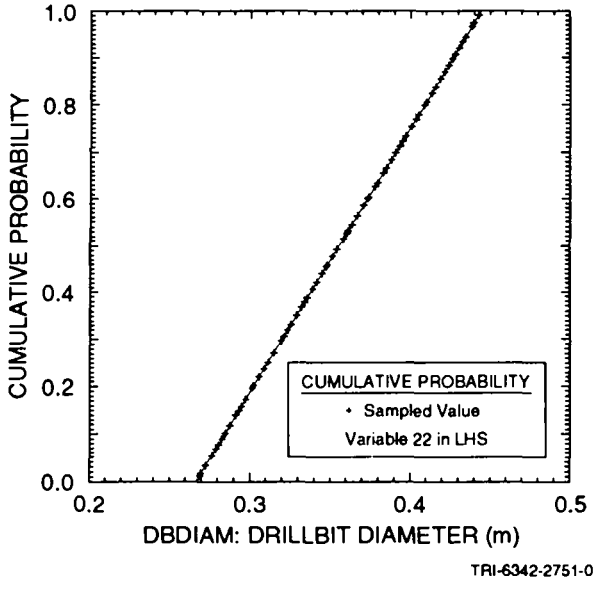

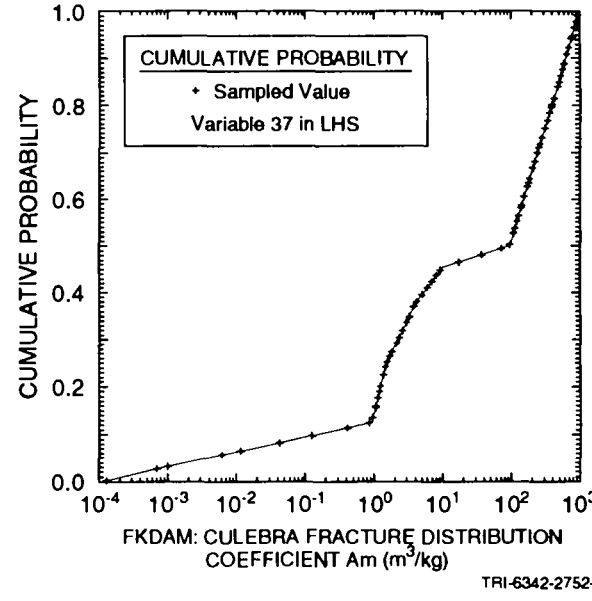

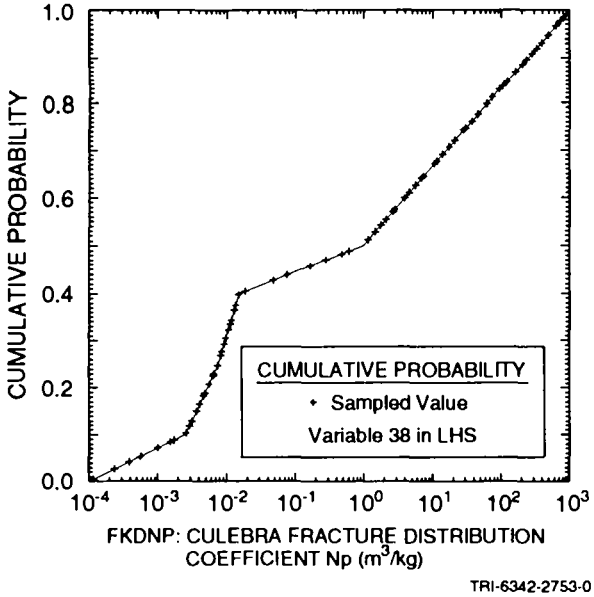

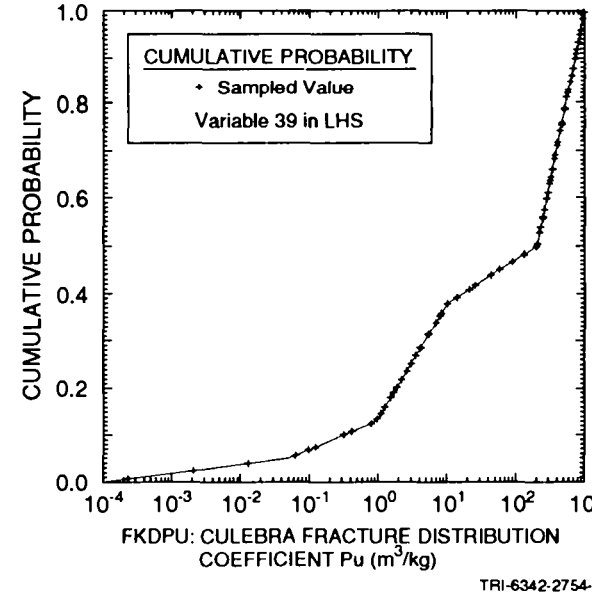

Figure 3-1. Distributions used for sampled variables in 1992 WIPP performance assessment. (continued)

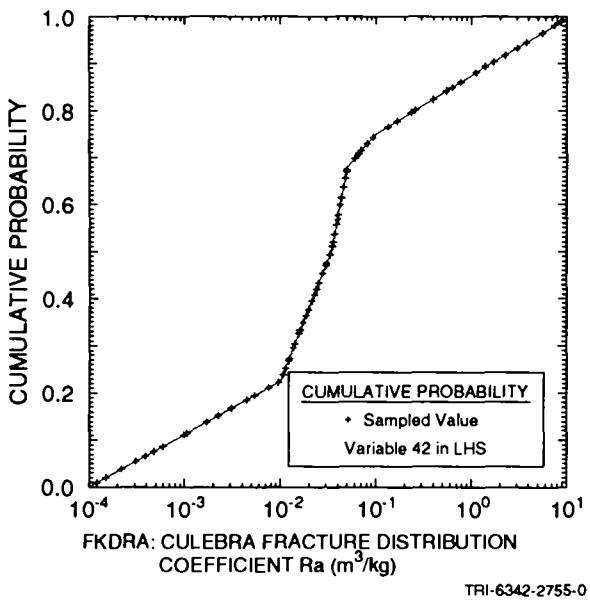

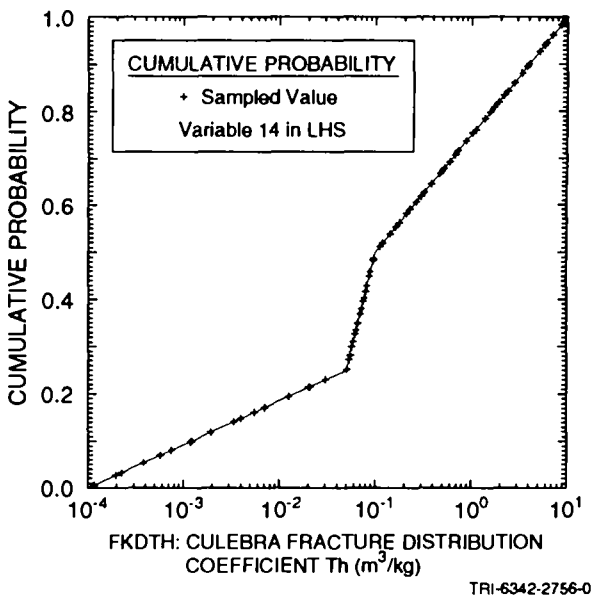

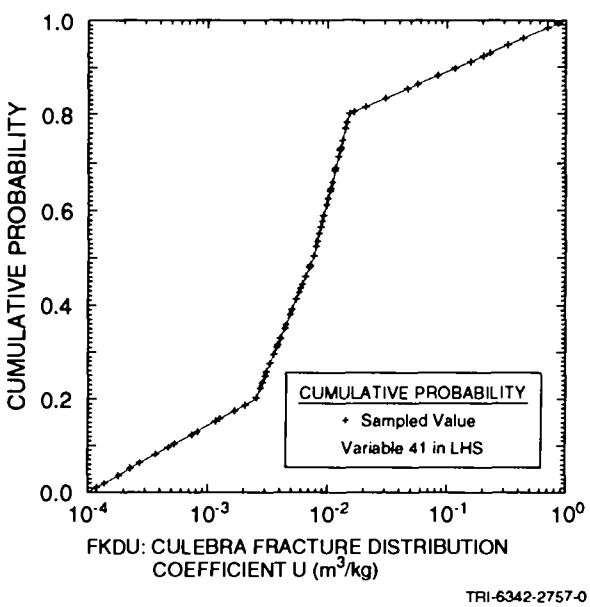

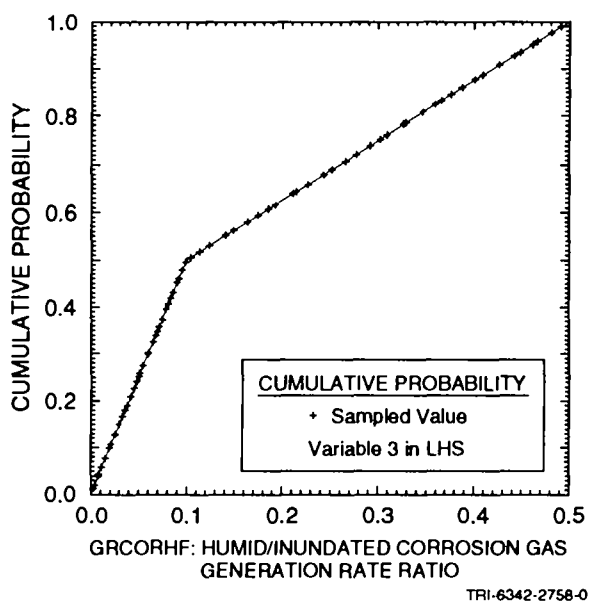

Figure 3-1. Distributions used for sampled variables in 1992 WIPP performance assessment. (continued)

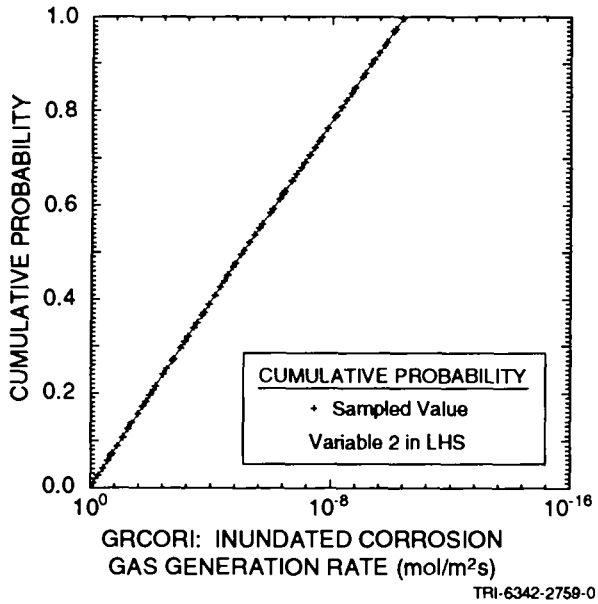

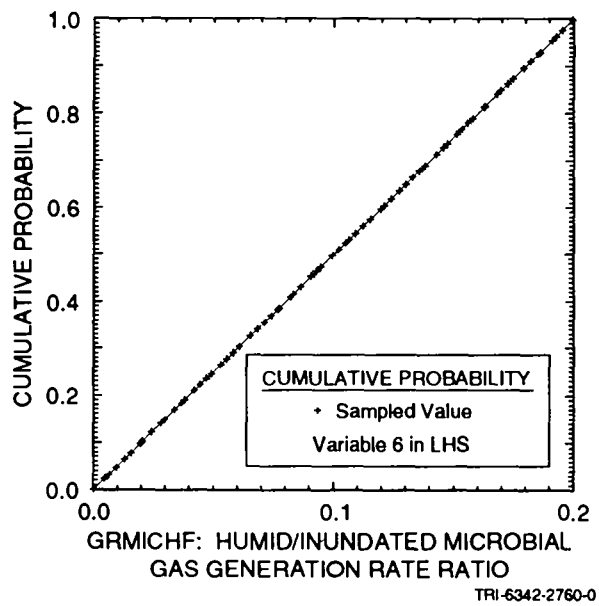

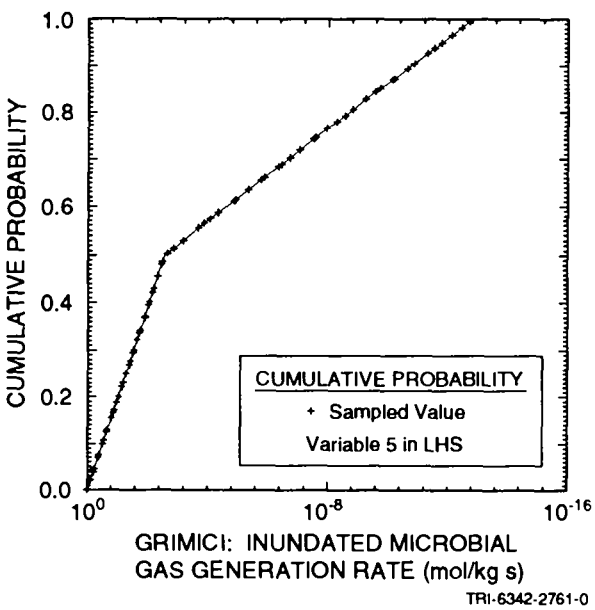

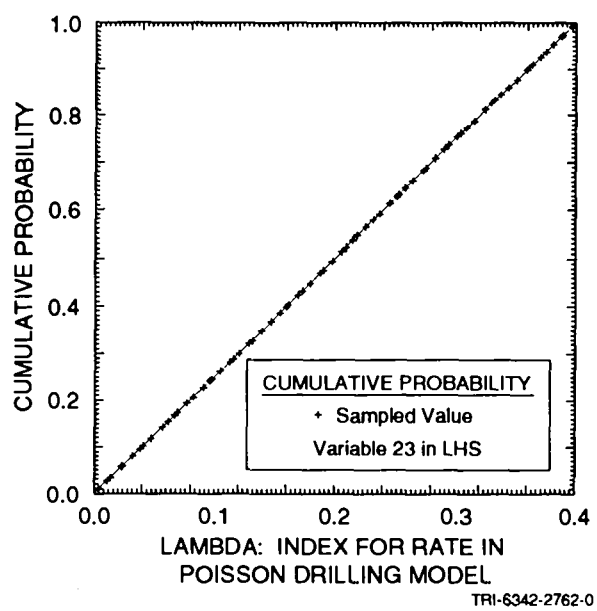

Figure 3-1. Distributions used for sampled variables in 1992 WIPP performance assessment. (continued)

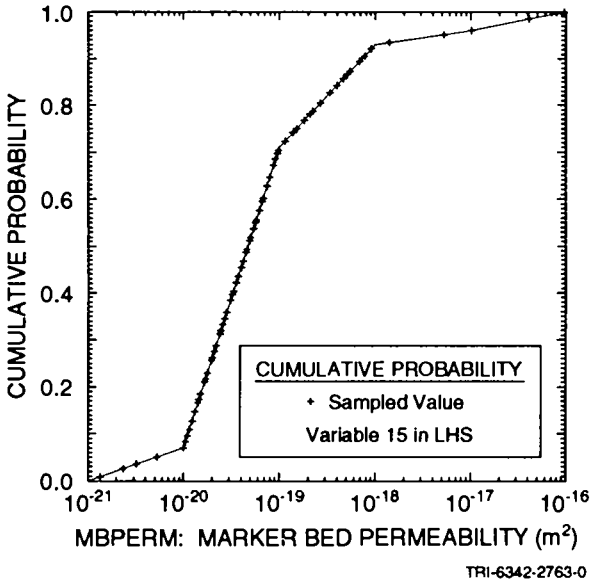

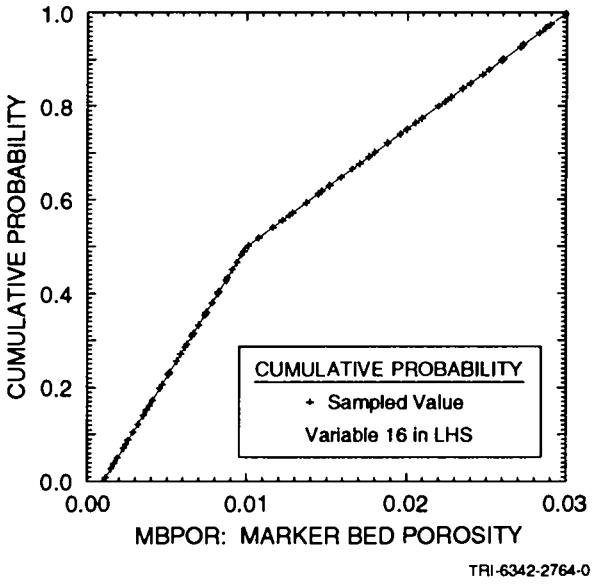

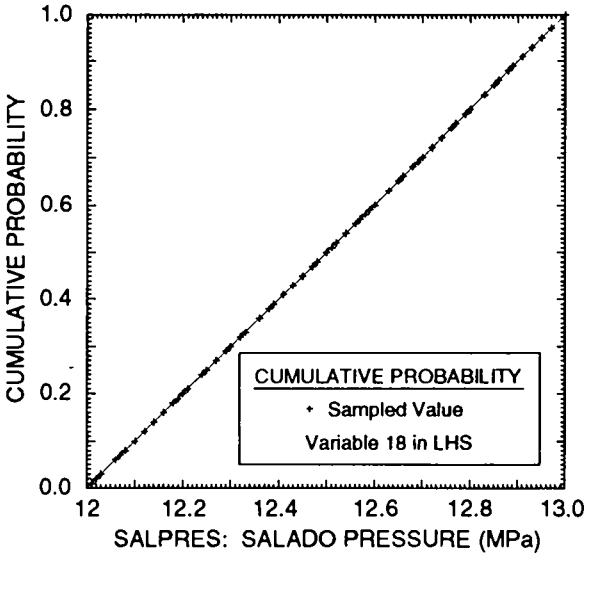

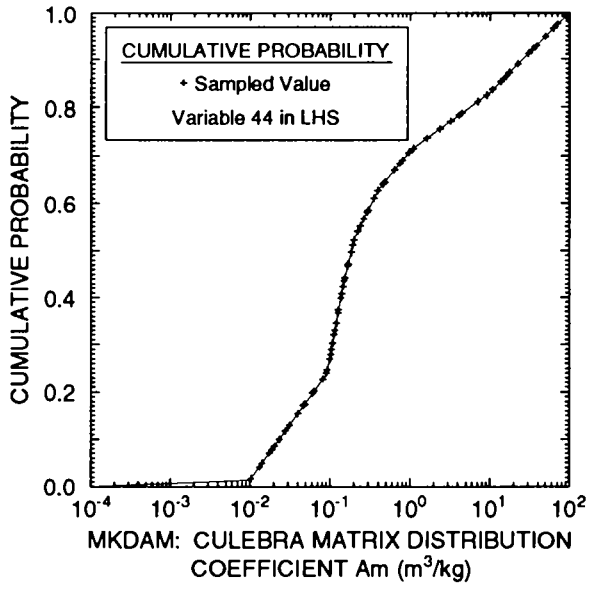

Figure 3-1. Distributions used for sampled variables in 1992 WIPP performance assessment. (continued)

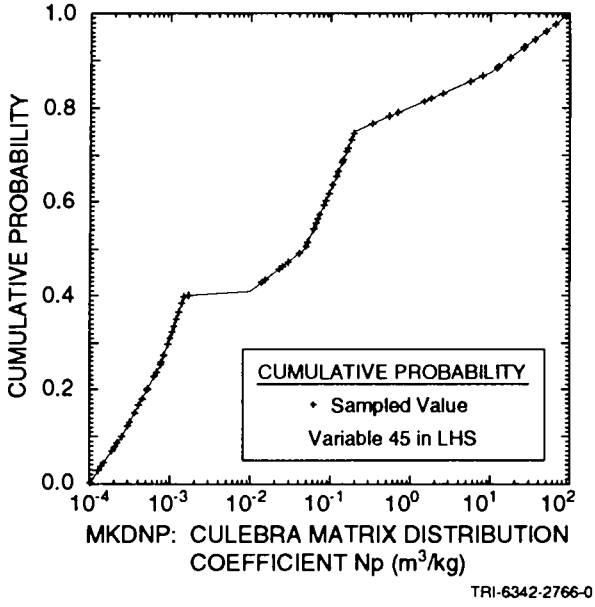

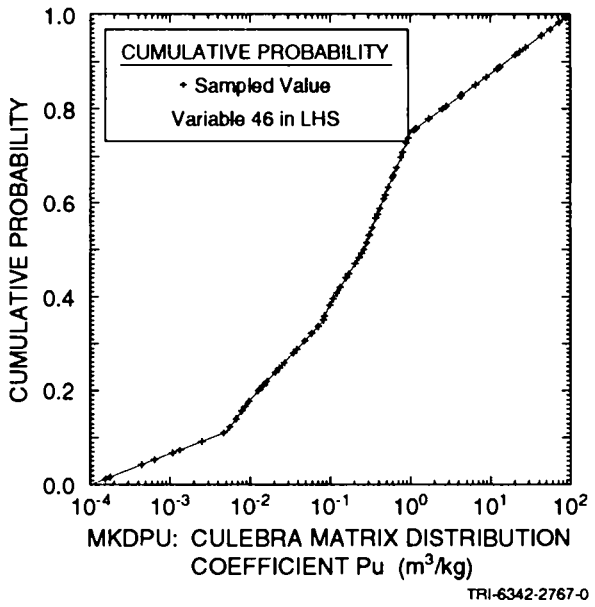

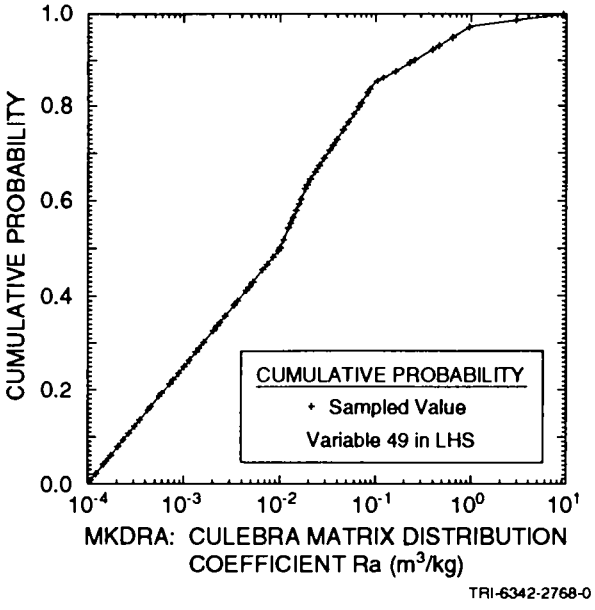

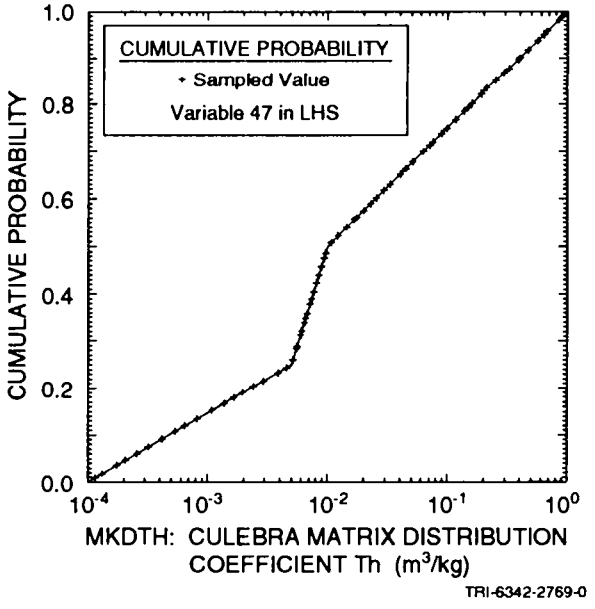

Figure 3-1. Distributions used for sampled variables in 1992 WIPP performance assessment. (continued)

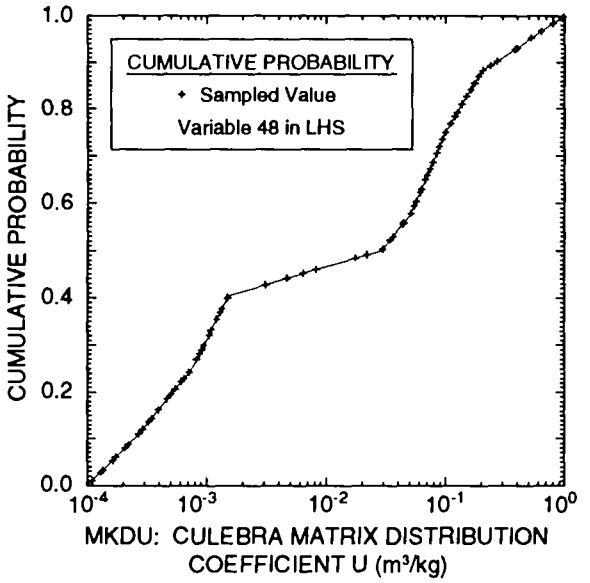

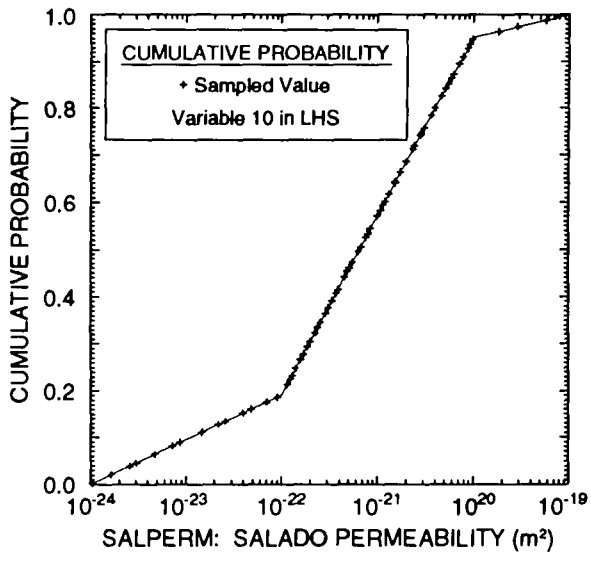

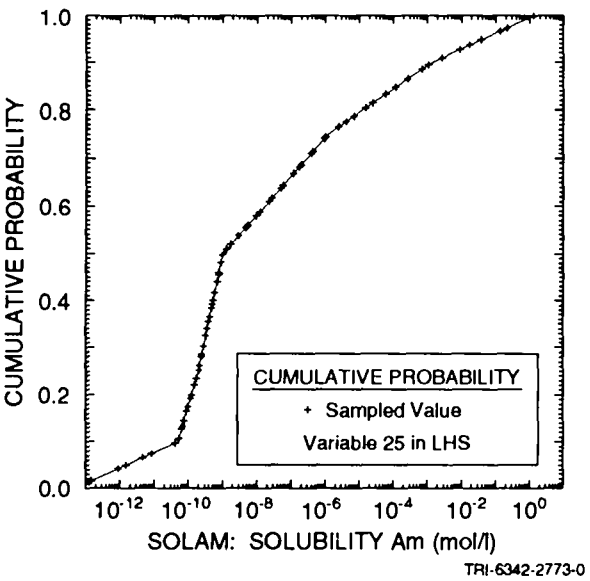

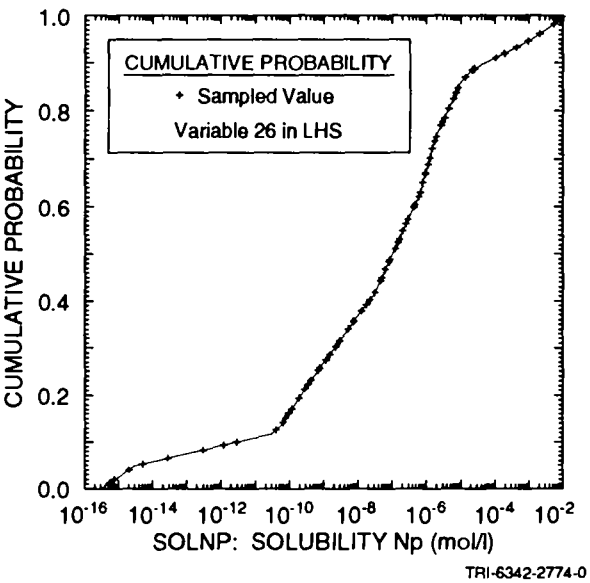

Figure 3-1. Distributions used for sampled variables in 1992 WIPP performance assessment. (continued)

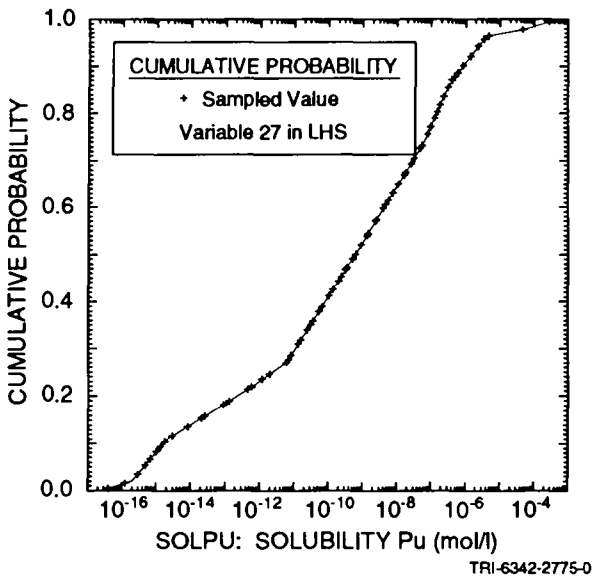

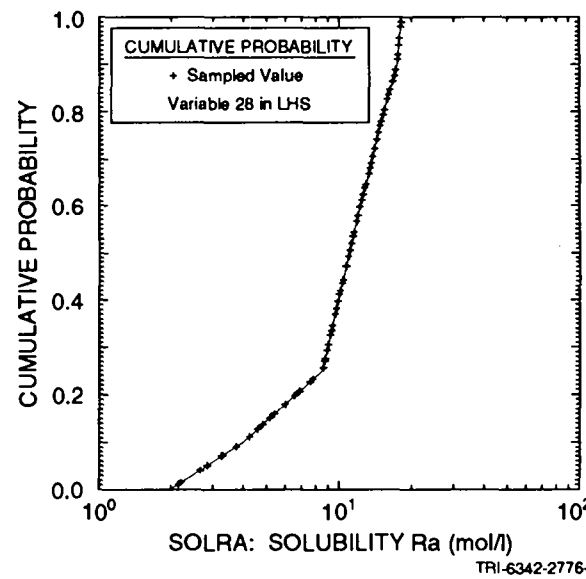

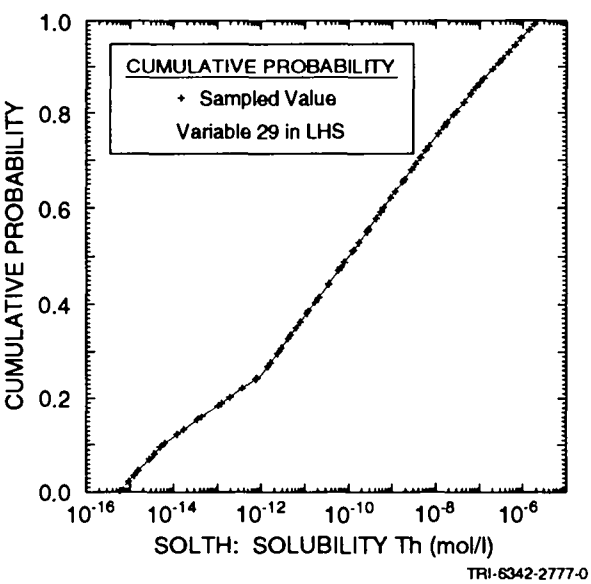

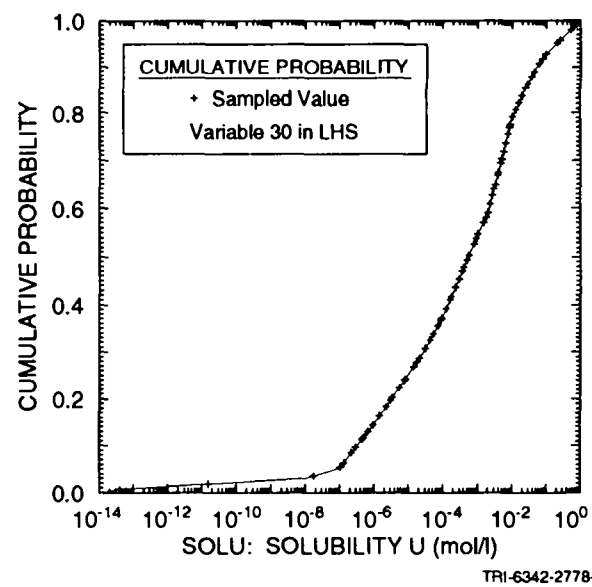

Figure 3-1. Distributions used for sampled variables in 1992 WIPP performance assessment. (continued)

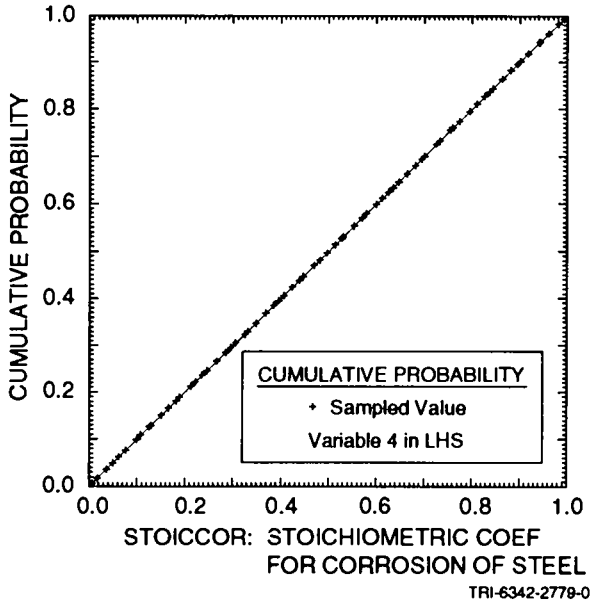

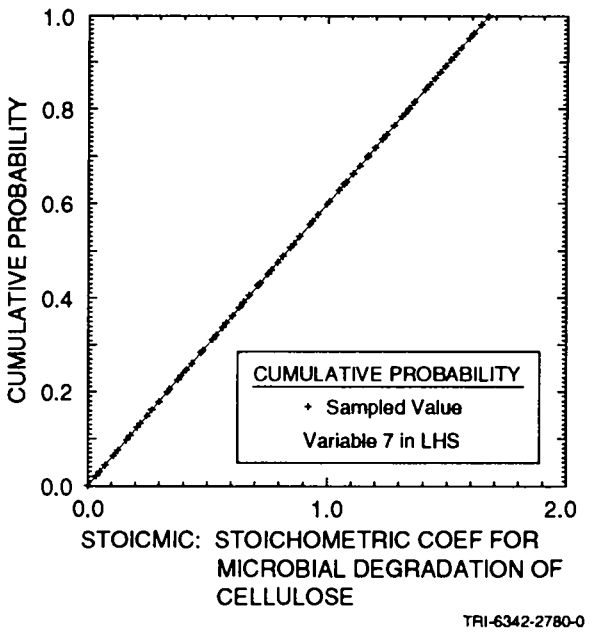

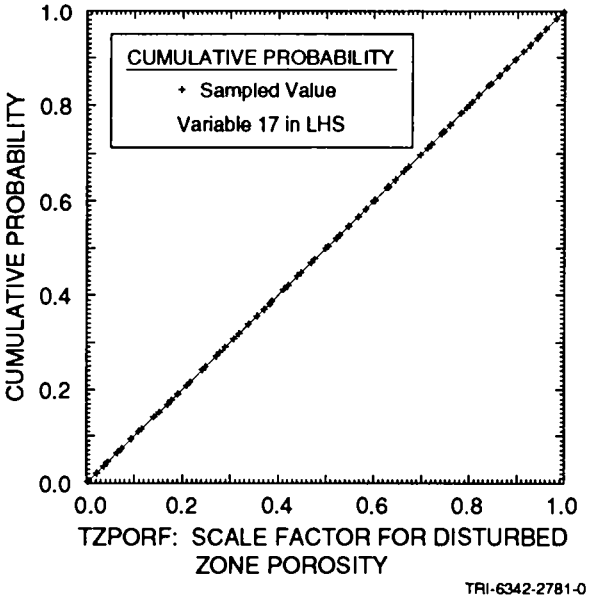

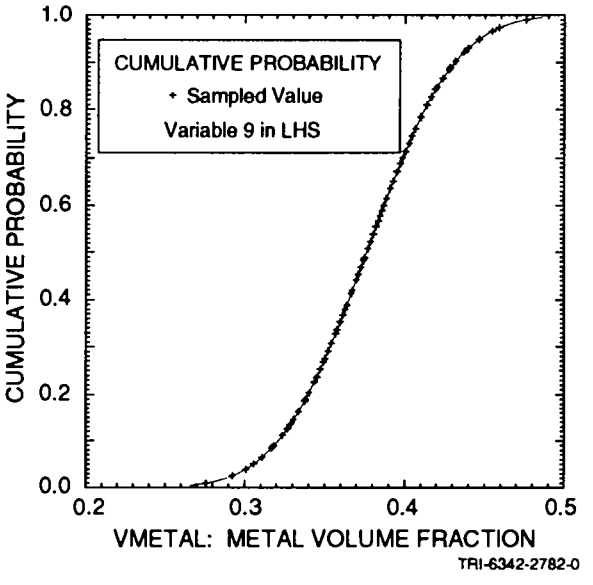

Figure 3-1. Distributions used for sampled variables in 1992 WIPP performance assessment. (continued)

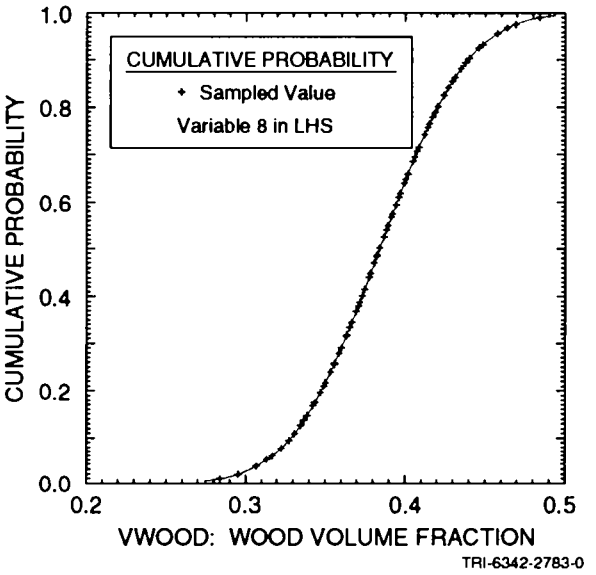

Figure 3-1. Distributions used for sampled variables in 1992 WIPP performance assessment. (continued)

Table 3-2. Further, the impact of individual variables are investigated with sensitivity analysis techniques based on scatterplots, regression analysis and partial correlation analysis. Scatterplots are also used to compare results obtained with the different analysis cases listed in Table 3-2.

Before concluding this chapter, it is perhaps worth emphasizing that the WIPP performance assessment uses two different experimental designs in the treatment of uncertainty. The division of the sample space S in Eq. 2.2-1 into the scenarios S_i indicated in Eq. 2.1-1, and more explicitly in Tables 2.5-1 through 2.5-4, is an experimental design based on importance sampling and is used to assure that the exceedance probabilities associated with the EPA release limits (i.e., 0.1 and 0.001) are approximately estimated (Helton and Iuzzolino, 1993). Such designs are used in analyses where it is important to include the effects of low probability, but possibly high consequence, occurrences. The generation of a Latin hypercube sample of size 70 from the 49 variables in Table 3-1 is a type of random design. Such designs, especially Latin hypercube sampling, are often used in uncertainty/sensitivity studies because of their efficient stratification across the range of each variable under consideration. Thus, the WIPP performance assessment is using an experimental design based on importance sampling to incorporate the effects of stochastic uncertainty and an experimental design based on Latin hypercube sampling to assess the effects of subjective uncertainty. In particular, the use of a Latin hypercube sample of size 70 to assess the effects of subjective uncertainty has no effect on the estimation of the 0.1 and 0.001 exceedance probabilities in the individual CCDFs used in comparison with the EPA release limits.

Additional information on the uncertainty and sensitivity analysis techniques in use is available elsewhere (Chapter 3 in Volume 2; Helton et al., 1991).

Table 3-2. Alternative Modeling Assumptions Considered in the 1992 WIPP Performance Assessment. "CUTTINGS" refers to direct releases at the ground surface during drilling. "GW TO ACC ENV" refers to releases at the subsurface boundary of the accessible environment due to groundwater transport in the Culebra Dolomite Member of the Rustler Formation.

	TYPE OF RELEASE	CUTTINGS	CHEMICAL RETARDATION	CLAY LINING IN FRACTURES	MATRIX DIFFUSION
1	CUTTINGS	+			
2	GW TO CULEBRA	-			
3	GW TO ACC ENV	-	-	-	-
4	GW TO ACC ENV	-	+	+	-
5	GW TO ACC ENV	-	+	-	+
6	GW TO ACC ENV	-	+	+	+
7	GW TO ACC ENV	-	-	+	-
8	GW TO ACC ENV	-	-	-	+
9	GW TO ACC ENV	-	-	+	+
10	CUTTINGS + GW TO ACC ENV	+	-	-	-
11	CUTTINGS + GW TO ACC ENV	+	+	+	-
12	CUTTINGS + GW TO ACC ENV	+	+	-	+
13	CUTTINGS + GW TO ACC ENV	+	+	+	+
14	CUTTINGS + GW TO ACC ENV	+	-	+	-
15	CUTTINGS + GW TO ACC ENV	+	-	-	+
16	CUTTINGS + GW TO ACC ENV	+	-	+	+

4. UNDISTURBED PERFORMANCE (REPOSITORY/SHAFT)

4.1 Model Geometry

For undisturbed performance of the repository/shaft system, BRAGFLO simulates two-phase flow[1] in a geometry very similar to that used in previous gas and brine migration analyses (Case 3 in WIPP PA Department, 1992) related to the Resource Conservation and Recovery Act (RCRA) (EPA, 1986). This model represents the three-dimensional repository (Figure 4.1-1) using a two-dimensional rectangular grid oriented vertically north-south through the disposal system (Figure 4.1-2). This grid preserves the initial excavated volume of various regions and their original excavated heights. Major assumptions made in the construction of this grid include:

- All waste is lumped into one region immediately south of the seals and backfill region. The volume of the waste-emplacement block equals the excavated volume of all the panels in the WIPP repository.

- The access and ventilation drifts are lumped into one region of high permeability immediately south of the shaft system. The volume of this region equals that of the original excavated volume of all of the drifts south of the Waste Shaft.

- The four shafts are consolidated into a single shaft at the location of the Waste Shaft. The volume and cross-sectional area of the consolidated shaft equals that of the four shafts. The single modeled shaft is divided vertically into two segments with a single seal in between. Thickness of the shaft seal is assumed to vary between 10 and 50 m.

- The experimental rooms are combined into a region directly north of the single shaft. The volume of this region equals that of all the excavated region north of the shafts.

---

1. The BRAGFLO computational model is described in detail in Appendix A in Volume 2 of this report, and in literature cited therein; a discussion of multiphase flow through porous media, which BRAGFLO models, is provided in Section 7.2 in Volume 2 of this report.

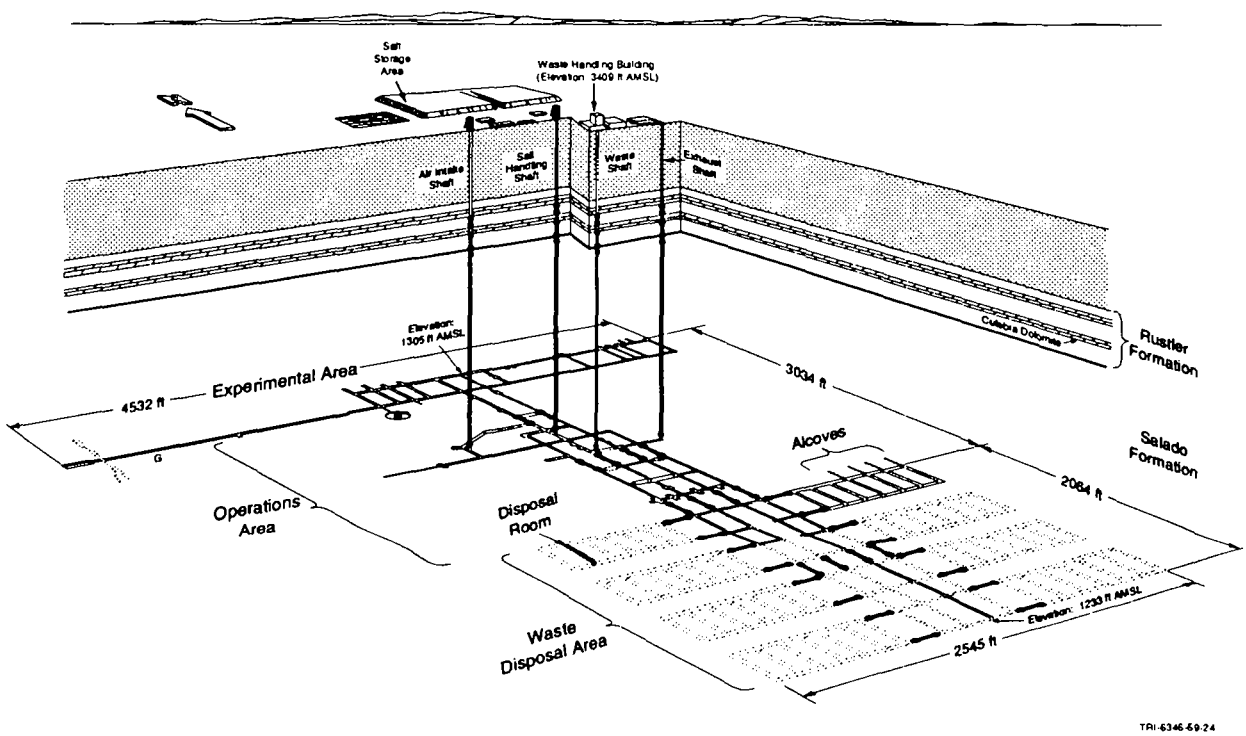

Figure 4.1-1. Proposed WIPP repository showing the 10 waste-disposal regions (panels) (after Waste Management Technology Department, 1987).

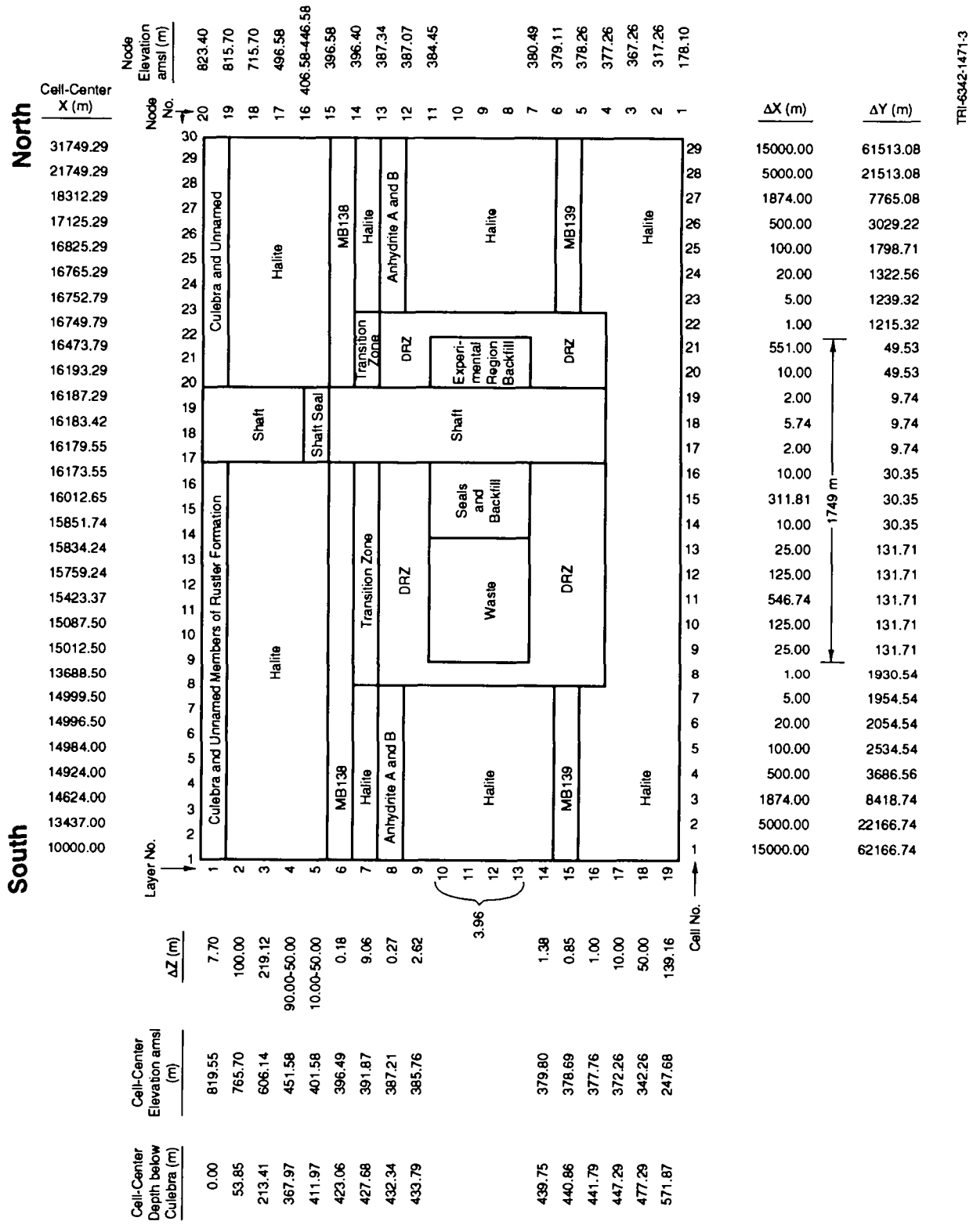

Cell-Center X (m)
31749.29
21749.29
18312.29
17125.29
16825.29
16765.29
16752.79
16749.79
16473.79
16193.29
16187.29
16183.42
16179.55
16173.55
16012.65
15851.74
15834.24
15759.24
15423.37
15087.50
15012.50
13688.50
14999.50
14996.50
14984.00
14924.00
14624.00
13437.00
10000.00

Node No.	Node Elevation amsl (m)
20	823.40
19	815.70
18	715.70
17	496.58
16	406.58-446.58
15	396.58
14	396.40
13	387.34
12	387.07
11	384.45
10	
9	
8	
7	380.49
6	379.11
5	378.26
4	377.26
3	367.26
2	317.26
1	178.10

Layer No.	Cell-Center Depth below Culebra (m)	Cell-Center Elevation amsl (m)	ΔZ (m)
1	0.00	819.55	7.70
2	53.85	765.70	100.00
3	213.41	606.14	219.12
4	367.97	451.58	90.00-50.00
5	411.97	401.58	10.00-50.00
6	423.06	396.49	0.18
7	427.68	391.87	9.06
8	432.34	387.21	0.27
9	433.79	385.76	2.62
10			3.96
11			
12			
13			
14	439.75	379.80	1.38
15	440.86	378.69	0.85
16	441.79	377.76	1.00
17	447.29	372.26	10.00
18	477.29	342.26	50.00
19	571.87	247.68	139.16

Cell No.	ΔX (m)	ΔY (m)
29	15000.00	61513.08
28	5000.00	21513.08
27	1874.00	7765.08
26	500.00	3029.22
25	100.00	1798.71
24	20.00	1322.56
23	5.00	1239.32
22	1.00	1215.32
21	551.00	49.53
20	10.00	49.53
19	2.00	9.74
18	5.74	9.74
17	2.00	9.74
16	10.00	30.35
15	311.81	30.35
14	10.00	30.35
13	25.00	131.71
12	125.00	131.71
11	546.74	131.71
10	125.00	131.71
9	25.00	131.71
8	1.00	1930.54
7	5.00	1954.54
6	20.00	2054.54
5	100.00	2534.54
4	500.00	3686.56
3	1874.00	8418.74
2	5000.00	22166.74
1	15000.00	62166.74

Figure 4.1-2. Plan view of the geometry of the two-dimensional vertical cross-section model used for modeling undisturbed performance of the repository/shaft system.

- Stratigraphic layers are assumed to be parallel and horizontal; the repository elevation actually follows the marker beds at the WIPP, which are slightly undulatory and dip less than 1 degree to the southeast. The elevation of the repository, excavated at a constant stratigraphic horizon, drops about 7 m between the Waste Shaft and the southernmost panel. The model does not include this change in elevation.

Figure 4.1-2 shows the model grid in the vertical (z), north-south (x) plane. The region extends vertically 645 m from the top of the Culebra Dolomite Member of the Rustler Formation to the bottom of the Salado Formation. The total north-south length is approximately 47 km. Stratigraphic units included in the model are the Culebra Dolomite, the intact halite of the Salado Formation, MB138, anhydrites A and B lumped into a single anhydrite layer, MB139, a disturbed rock zone (DRZ) surrounding the waste-emplacement and experimental areas, and a transition zone immediately above the DRZ that provides a potential pathway to MB138.

The width of the elements (the out-of-plane [y] dimension in Figure 4.1-2) varies significantly in the x direction, from as little as 9.74 m at the location of the shaft to as much as 62 km in the intact Salado Formation. The y dimension, however, does not vary vertically. For example, the Δy value for cell 20 (49.53 m), which is comparatively small because of the small excavated volume, remains the same regardless of the vertical (z) location specified by the node number. Figures 4.1-3 and 4.1-4 show a scaled plan view of the grid in the horizontal (x-y) plane containing the repository.

The out-of-plane grid block y dimension is included in the model only to allow for variable storage volumes in each block. Flow is not modeled in the y direction, and occurs only in the x and z directions (in the plane of Figure 4.1-2).

The y dimension at the ends of the mesh, south of the waste block and north of the experimental region backfill, increases in a cylindrical manner away from the model to simulate some of the three-dimensional behavior using a two-dimensional model. Close to the repository, flow paths will have complex orientations determined by the variable geometry of the excavations; fluid flow will be primarily horizontal and mostly through the anhydrite layers. Farther away from the repository, at a distance perhaps several times the maximum horizontal dimension of the repository (about 1.7 km), flow will be nearly radial. All flow is assumed to result from the disturbances introduced by the repository; i.e., there is no regional flow field that predates excavation of the repository. Flow to and from the repository in

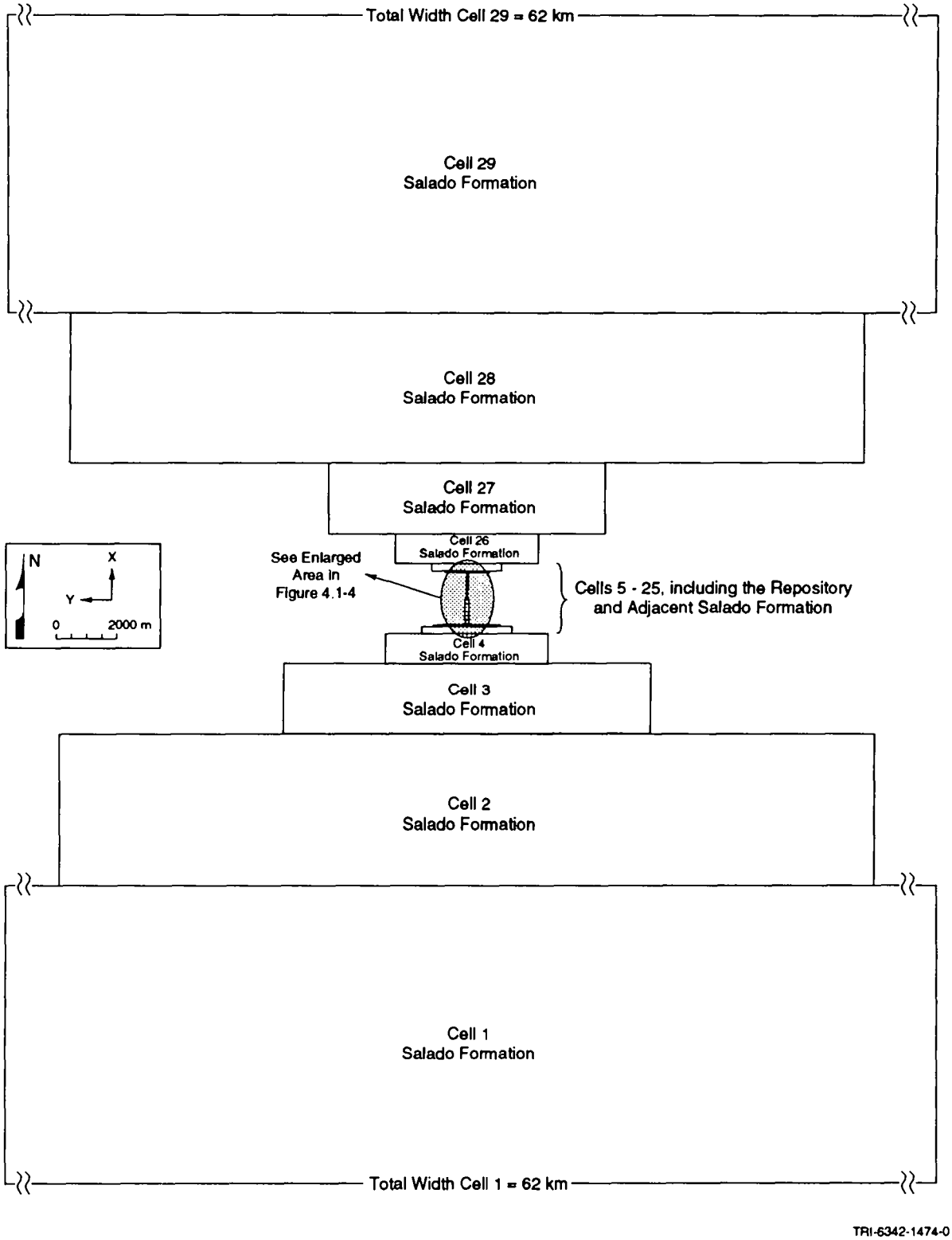

Figure 4.1-3. Scaled view of layer 12 of Figure 4.1-2. Cells representing the repository and its immediate vicinity are too small to plot individually at this scale.

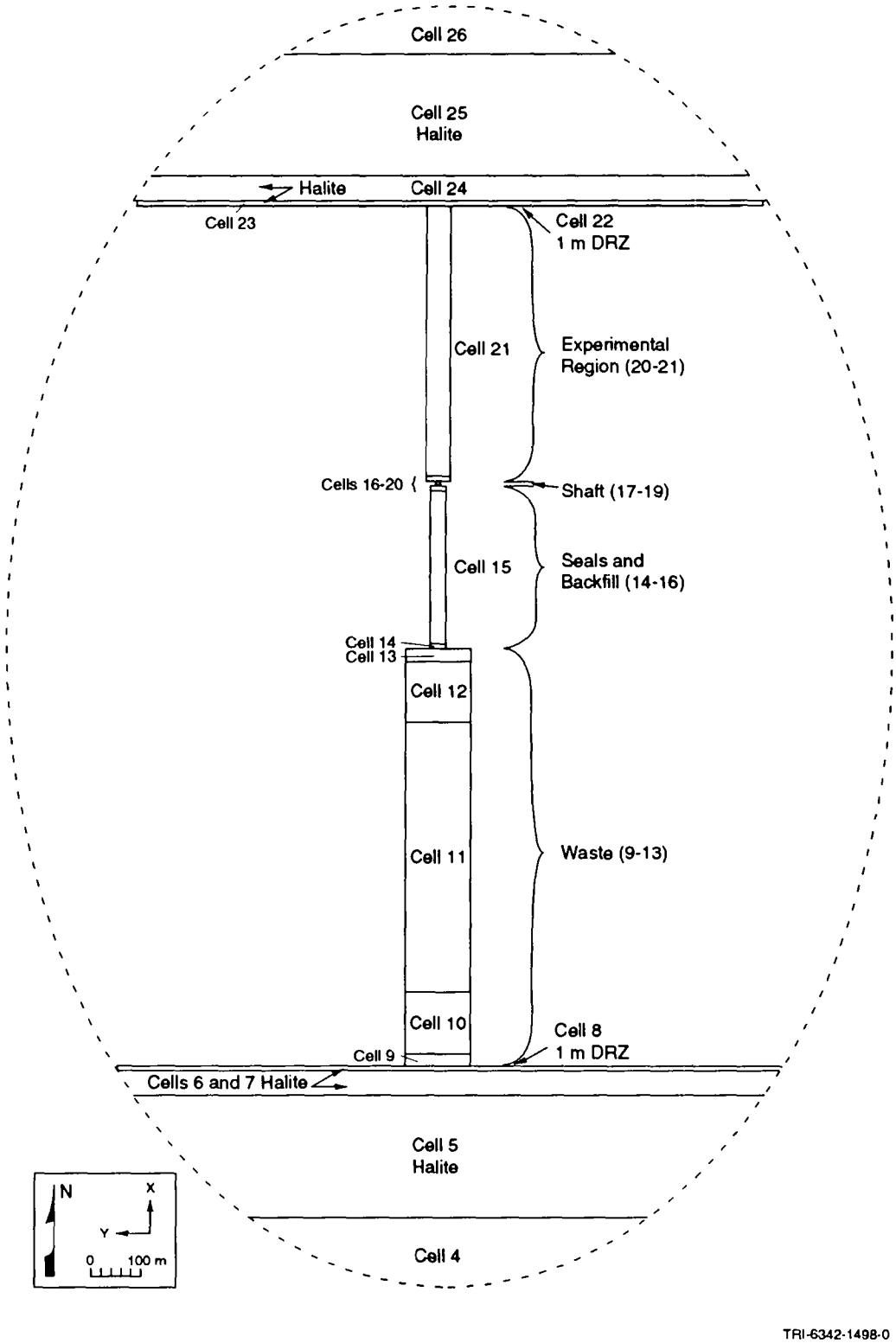

Figure 4.1-4. Enlargement of the central portion of Figure 4.1-3.

the surrounding region can be approximated with the two-dimensional model if the y dimension of the grid blocks increases away from the repository by a factor of approximately $2\pi r$, where r is the distance from the center of the grid (Voss, 1984).

In a strict sense, the $2\pi r$ relationship is valid only if it is applied to the entire mesh. Such a mesh represents a vertical cylinder that allows a two-dimensional model to simulate radial flow in a three-dimensional cylinder. In the mesh used for undisturbed performance of the repository/shaft system, only the north and south ends of the modeled regions are treated in this fashion, and the results are not expected to be precise in modeling all flow north and south of the repository/shaft system. However, as a first approximation, this procedure accounts for the radial increase in pore volume away from the central region. This radial increase in pore volume is important because brine and gas will not flow in only two dimensions (x and z) as they flow from (or towards) the repository. Rather, at a distance of a few kilometers from the repository (approximately the disposal-unit boundary), flow will be radial into (or from) an increasingly larger pore volume.

4.2 Material Properties

Material properties for undisturbed performance of the repository/shaft system are discussed in detail throughout Volume 3 of this report and are summarized in Chapter 6 of Volume 3. The following material properties that apply specifically to undisturbed performance of the repository/shaft system are discussed below in the indicated sections:

- permeability (Sections 4.1.2.1 and 4.1.2.4),
- porosity (Section 4.1.2.2),
- specific storage (Section 4.1.2.3),
- brine and gas saturations (Sections 4.1.2.4),
- capillary pressure (Section 4.1.2.4).

Radionuclide transport is not modeled for the undisturbed case because releases into the Culebra Dolomite Member of the Rustler Formation do not occur (see Section 4.4), and therefore, parameter values for radionuclide inventory and solubilities are not input for the undisturbed performance calculations.

4.2.1 Permeability

4.2.1.1 PERMEABILITY RANGES

Permeability values used for the undisturbed repository/shaft model are shown in Figure 4.2-1 and listed below in order of increasing permeability:

- Halite is assigned a range of permeability values from 1.0×10^{-24} to 1.0×10^{-19} m^2.
- The shaft seal is assigned a range from 3.3×10^{-21} to 3.3×10^{-20} m^2.
- Anhydrite interbeds (MB138, MB139, and anhydrite A and B) and the transition zone above the DRZ are assigned a range from 1.0×10^{-21} to 1.0×10^{-16} m^2.
- The DRZ, the upper and lower shaft, the seals and backfill for the waste storage rooms, and the backfill for the experimental region are assigned a value of 1.0×10^{-15} m^2.
- The Culebra is assigned a value of 2.1×10^{-14} m^2.
- The waste is assigned a value of 1.0×10^{-13} m^2.

The permeability range for the anhydrite interbeds (1.0×10^{-21} to 1.0×10^{-16} m^2) is larger than that estimated for undisturbed anhydrite, but does not explicitly take into account pressure dependent fracturing of these interbeds. Interbed fracturing as a result of gas pressurization is not modeled in the 1992 calculations. Implications of not modeling interbed fracturing are uncertain. The phenomenon will be modeled in future PAs.

4.2.1.2 CULEBRA PERMEABILITY

Culebra permeability above the repository/shaft system, which is an important material property primarily for the disturbed calculations, is explained in Section 5.1.2.2. Culebra permeability above the repository/shaft system for undisturbed conditions is determined in the same manner as for disturbed conditions.

4.2.2 Porosity

4.2.2.1 FIXED (TIME-INVARIANT) POROSITY

Assumed porosity values for materials in the undisturbed repository/shaft simulation that do not change with respect to time are listed below and shown in Figure 4.2-2:

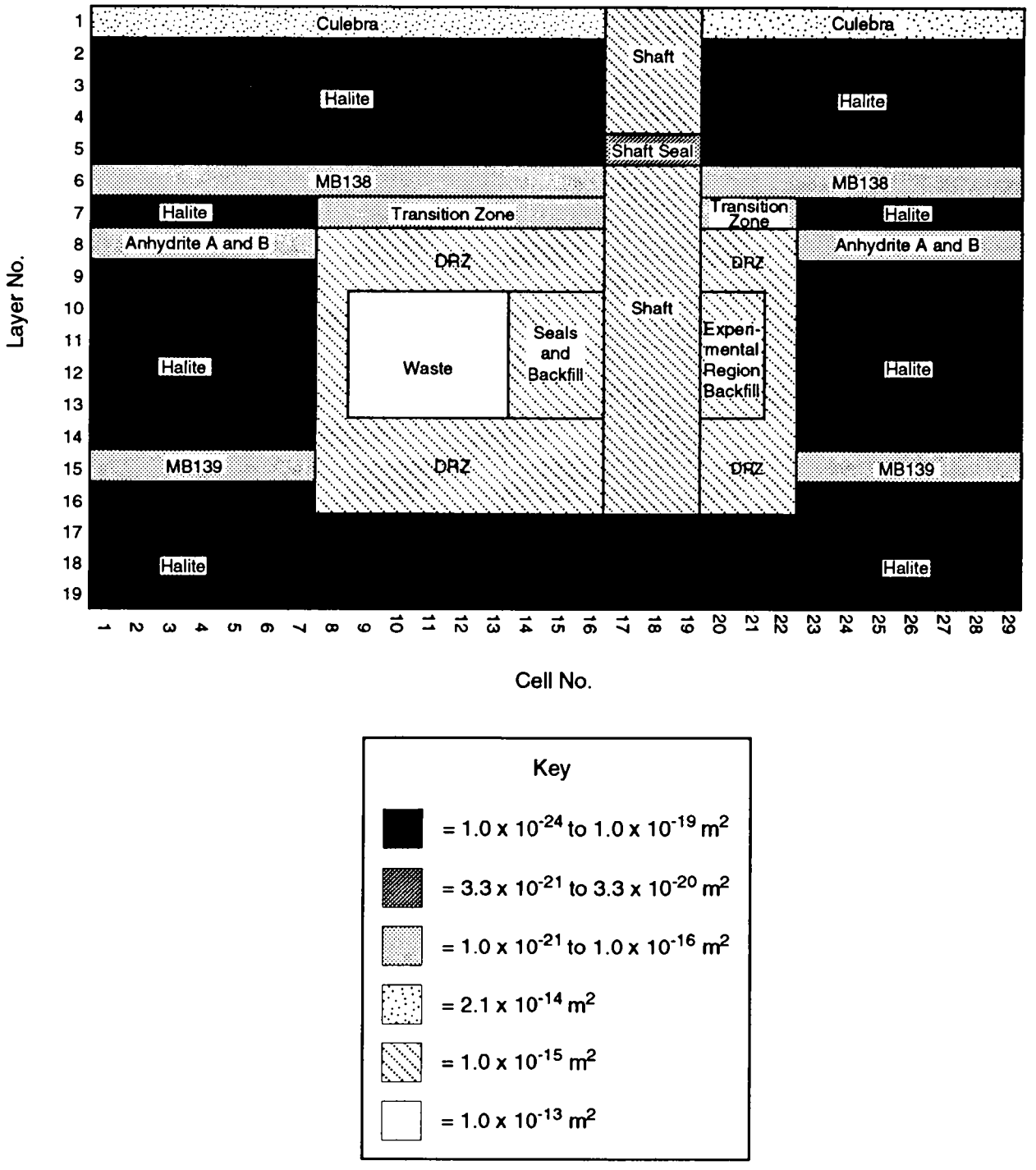

Figure 4.2-1. Permeability values for the undisturbed repository/shaft system.

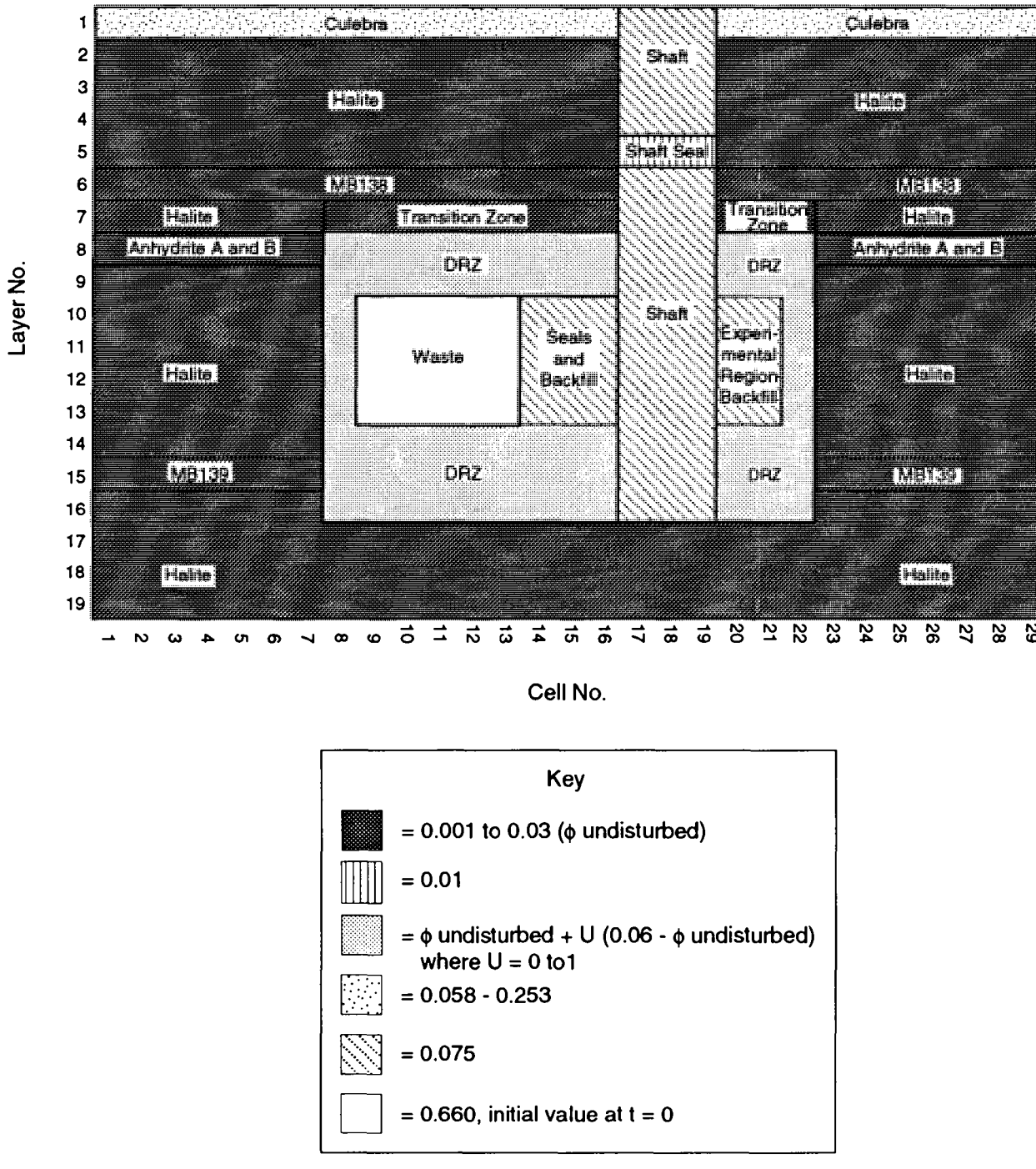

Figure 4.2-2. Time-invariant porosity values for the undisturbed repository/shaft system.

- Halite, the anhydrite interbeds, and the transition zone are assigned a range of porosity values from 0.001 to 0.03.

- The shaft seal is assigned a value of 0.01.

- A slightly higher range of porosity values is assigned to the DRZ. As is explained in Section 2.4.4 of Volume 3 of this report, the DRZ range is determined by the relationship

$$\phi_{disturbed} = \phi_{undisturbed} + U(0.06-\phi_{undisturbed}), \qquad (4.2\text{-}1)$$

where U is a number uniformly distributed between 0 and 1, and $\phi_{undisturbed}$ is the porosity range of the undisturbed halite (0.001 to 0.03). This relationship forces the DRZ porosity, $\phi_{disturbed}$, to fall within a range bounded by $\phi_{undisturbed}$ and 0.06, which is the maximum DRZ porosity considered (see WIPP PA Division 1991c, Section 2.3.7).

- A porosity value of 0.075 is assigned to the entire shaft (except the shaft seal) and the seals for the waste storage area, and the backfill for both the waste storage and experimental areas.

- The Culebra is assigned a range from 0.058 to 0.253.

- The waste prior to closure modeling is assigned a value of 0.660.

4.2.2.2 TIME-VARYING POROSITY

Background

In the 1991 and previous BRAGFLO simulations of the repository/shaft system (WIPP PA Division, 1991b; WIPP PA Department, 1992), porosity in the waste-emplacement panels was assumed to be constant in time. The effect of halite creep on waste-panel porosity was not accounted for. The porosities assigned to the waste panel for each of the 1991 realizations were determined in an external calculation (WIPP PA Division, 1991c). These porosities were calculated as the post-compaction pore volume required to store all of the waste-generated gas at lithostatic pressure in a brine-free repository. These "lithostatic equilibrium" porosities varied with sampled values for waste composition, gas-generation rates, and stoichiometry. Although these externally calculated porosities did not limit panel pressure to lithostatic, they may have overestimated the void volume available for gas for cases where the panel does not re-expand significantly beyond the closed state.

Another shortcoming of the 1991 approach was that the external calculation of porosities correlated porosity only to the theoretical gas-generation potential, which is the amount of gas that would be generated if all ferrous metal and cellulosic material was completely consumed (see Sections 1.4.1 and 3.3 of Volume 3 of this report for additional information about the gas-generation model). In some realizations, brine availability limits the amount of gas generated to less than the theoretical potential and not all ferrous metal or cellulose is consumed. Modeling studies using the finite element program SANCHO[2] for simulating quasistatic, large-deformation, inelastic response of two-dimensional solids indicate that low gas-generation rates result in more rapid closure and lower porosities at full compaction.

1992 Approach for Accounting for Time-Dependent Panel Porosity

The 1992 BRAGFLO calculations include a simple first attempt at accounting for time-dependent panel porosity. This time dependence is indirect in the sense that results from this application of SANCHO indicate that panel porosity varies with the amount of gas generated and the pore pressure in the waste area, each of which in turn varies with time.

The discussion that follows describes the implementation of the SANCHO halite deformation results in BRAGFLO for the 1992 PA calculations. The SANCHO results and data of importance for use in BRAGFLO, discussed in detail below, are

- moles of gas generated,
- time after sealing of repository,
- panel pressure, and
- panel porosity.

The porosity contours appearing in Figure 7-2 in Volume 2 of this report result from interpolation of the SANCHO results that describe the dependence of panel porosity on cumulative moles of gas produced and time after sealing. The direct (not interpolated) SANCHO porosity results are presented in Figure 4.2-3. "Noise" visible in the solutions are an artifact of the approach used

---

2. The SANCHO computational model is described by Stone et al., 1985, and summarized in Appendix B in Volume 2 of this report; a discussion of room closure, which SANCHO models, is provided in Section 7.3 in Volume 2 of this report. SANCHO is also discussed in Sections 1.4.1 and 1.4.7 of Volume 3 of this report.

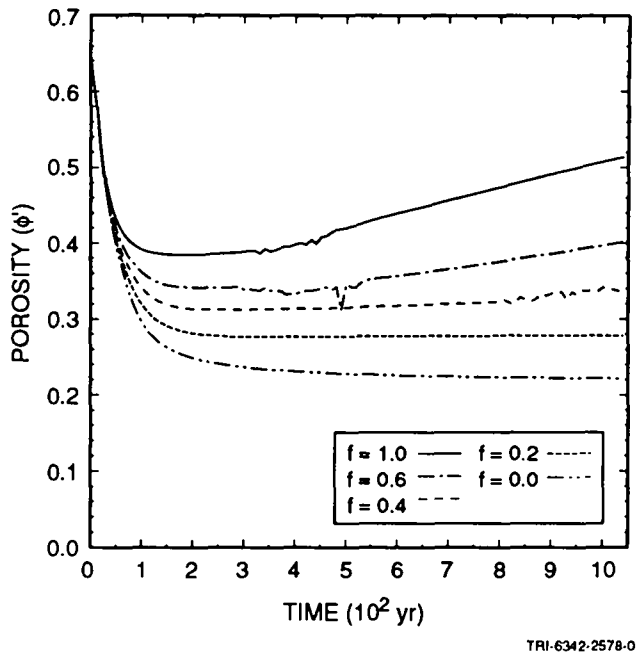

Figure 4.2-3. SANCHO results: porosity as a function of time for f=1.0, 0.6, 0.4 and 0.2; piecewise constant gas-generation rates; porosity based on SANCHO definition of porosity (ratio of void volume to instantaneous room volume); f is the fraction of the piecewise constant gas-generation rate and potential, where f=1.0 is defined as the sum of the corrosion rate (1 mole/drum-yr for 1050 yr) and the biodegradation rate (1 mole/drum-yr for 550 yr) (Brush, 1991; memorandum by Beraun and Davies in Appendix A of Volume 3 of this report).

to model separation at the surface between the waste/backfill and the overlying halite as pressure in the room exceeds lithostatic, and are not attributed to a physical process. This "noise" has been filtered out of the SANCHO solution prior to its use in BRAGFLO. Smoothed SANCHO results form the basis of accounting for the effect of halite creep on waste room porosity and are used within BRAGFLO.

The difference in definition of porosity by SANCHO and BRAGFLO requires further manipulation of the data presented in Figure 4.2-3. In SANCHO, as the halite creeps, the numerical mesh deforms; in BRAGFLO, the mesh dimensions are fixed with time. In the SANCHO room model, the porosity (ϕ' of Figure 4.2-3) is therefore defined as the ratio of the void volume to the current total volume of the panel. In BRAGFLO, the porosity (ϕ, Eq. 4.2-2) is therefore defined as the ratio of the void volume to the initial volume of the panel. If the mass and volume of the solids contained within the deforming panel does not change with time, the two differently defined porosities can be related by

$$\phi(t) = \phi'(t) \left[\frac{1-\phi'(t_o)}{1-\phi'(t)} \right] . \qquad (4.2\text{-}2)$$

A derivation of Eq. 4.2-2 is provided in Appendix B. The porosities as defined by SANCHO (Figure 4.2-3) are converted to porosity as defined by BRAGFLO by using Equation 4.2-2 and are presented in Figure 4.2-4.

Conceptual Modeling Differences Between SANCHO Room Model and BRAGFLO Panel/Repository Model

Because SANCHO and BRAGFLO simulate fundamentally different processes (large-scale quasistatic deformation of solids versus multi-phase fluid flow in nondeforming porous media), some differences have arisen in the conceptual models for the disposal system used in applications of the two codes. Differences between the SANCHO and BRAGFLO conceptualizations used in the 1992 PA that have important implications for the representation of time-varying porosity are as follows:

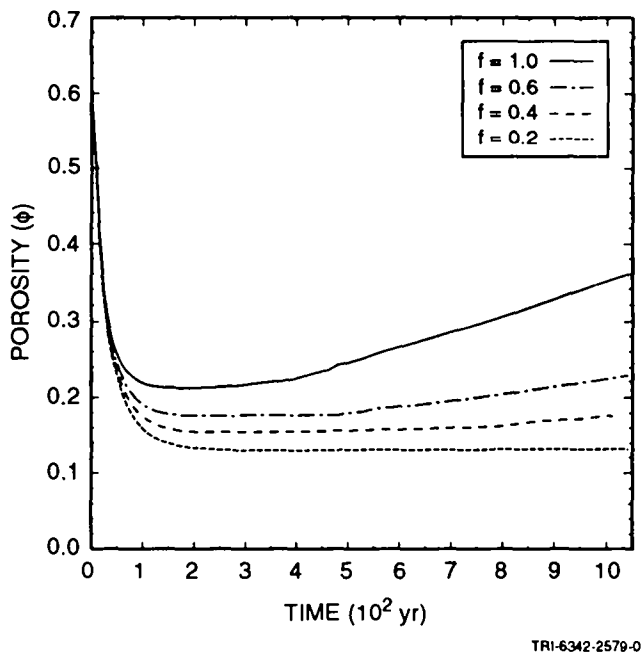

Figure 4.2-4. SANCHO results: porosity as a function of time for f=1.0, 0.6, 0.4, 0.2 and 0.1; piecewise constant gas-generation rates and potentials; porosity based on BRAGFLO definition of porosity (ratio of void volume to initial room volume); f is defined in Figure 4.2-3.

- This application of SANCHO models the behavior of a single room in an infinite array of rooms, simulating behavior of the middle rooms in a panel; BRAGFLO models the behavior of the entire repository for undisturbed conditions and an axisymmetric cylindrical-equivalent single panel for disturbed conditions.

- In the SANCHO room model, pressure and gas generation rates within the waste storage area are spatially uniform; in BRAGFLO, they vary spatially.

- In the SANCHO room model, the void space is completely occupied by waste-generated gas; in BRAGFLO, this space is occupied by two fluid phases, brine and gas.

- In the SANCHO room model, gas was not allowed to flow into or out of the waste area; in BRAGFLO, gas and brine flow into or out of the waste area.

- In the SANCHO room model, gas is generated at a constant rate for each reaction (corrosion and biodegradation) for fixed periods of time; in BRAGFLO, gas generation is not constant: it varies with degree of brine saturation in the waste area and continues until all of the corrodible metal and cellulose or brine are consumed.

- This application of the SANCHO room model simulates undisturbed repository performance for 2000 yr; these BRAGFLO simulations describe both undisturbed and disturbed performance for 10,000 yr.

Modeling Assumptions

The differences discussed above between the conceptual models used in the applications of the two codes led to difficulties in using the SANCHO porosity results in BRAGFLO. Specifically, the implementation of time-varying porosity in BRAGFLO for the 1992 PA required the following assumptions:

- Halite creep is assumed to affect the porosity of the waste storage area until the time of maximum repository pressure. Results were produced for cases in which pressure in the room increases from its initial level at various rates, dependent on gas-generation rates. Stress gradients between the host halite and the waste-filled room were not determined when waste-room pressure fell as gas escaped.

Rather than speculate on the halite response during decreasing waste-panel pore pressure, porosity in BRAGFLO is held constant at the value it has when pressure begins to fall. Porosity is maintained at this value unless and until pressure rises above its previous temporary maximum. This treatment of porosity may somewhat underestimate the degree of closure (overestimate porosity) by neglecting continuing creep closure. However, errors introduced by this treatment are believed to be small because reexpansion of the room is a relatively slow process compared to room closure/ consolidation, which is largely complete before pressures rise sufficiently to cause increases in porosity. Figure 4.2-4 indicates rather modest rates of increases in porosity after maximum consolidation, particularly at the lower gas-generation rates, compared to the dramatic decrease in porosity prior to maximum closure. As discussed in the following section, significant increases in waste-area porosity resulting from the reversal of creep closure require pressures in excess of lithostatic. As long as repository pore pressure is close to or below lithostatic, porosity in the waste panel is close to its fully compacted value. Limiting waste-panel porosity at this value somewhat limits the void volume available to store inflowing brine and generated gas.

- The effect of halite deformation on the porosity of material in a disposal room is assumed to be representative of the effect on the porosity of material in an excavated panel or the entire disposal region. It is recognized that the stress fields surrounding a single room do differ depending on where in the panel the room is located. The gross response of the halite resulting from the spatially varying deviatoric and room stress on porosity is assumed to be independent of the size or geometry of the WIPP excavation when implemented in BRAGFLO.

- In this application of SANCHO, pore pressure and gas-generation rate do not vary spatially within the waste-filled room. In BRAGFLO, pore pressure and gas-generation rate vary spatially throughout the waste-disposal region. Porosity in the panels is assumed to be spatially invariant in BRAGFLO despite spatial variations in pressure and gas-generation rate because the effective (representative) porosity is correlated to the effective panel pore pressure and gas-generation rate. This correlation is implemented by volume-averaging BRAGFLO pore pressures and gas-generation rates within the disposal region and using the average values to determine the porosity within the waste at any point in time.

- It is assumed that interpolation of the data in Figure 4.2-3 yields valid porosity results. The porosity surface (Figure 7-1 in Volume 2

of this report) and the data of Figure 4.2-3 were generated under specific constant rates of gas generation by corrosion and biodegradation and resulting pressure histories. It is assumed that all pressure and gas-generation histories that can be constructed within the bounds of the SANCHO results will yield valid predictions of the effect of halite deformation on waste-storage area porosity.

- Results of the SANCHO simulations indicate that room porosity varies with the gas-generation rate and the time. This is reasonable, because in this application of SANCHO, brine is assumed not to be present and gas cannot escape from the room. However, in BRAGFLO, where both brine and gas occupy void space and can flow into or out of the waste-storage area, the specification of time and gas-generation rate will not in general result in a unique porosity. The difficulty in using the porosity dependency from the no-flow, single-phase fluid system of SANCHO in the multiphase system of BRAGFLO is that Figure 4.2-4 fails to account for the change in pressure due to the flow of brine and gas into or out of the waste room. In addition, because this application of SANCHO did not include a brine phase, any effect the presence of brine in the waste area might have had on halite creep is not captured explicitly. If it is reasonable to assume that the halite responds in part to the degree of back pressure in the waste-storage area as well as the waste-storage area pore-pressure history, then it follows that the porosity associated with the no-flow single-phase system of SANCHO will differ from the porosity in the flowing two-phase system of BRAGFLO, at the same time following sealing and given the same gas-generation rate.

The results from the SANCHO room model strictly apply only to the case where the pore space in the waste-disposal room is occupied by gas and the gas remains in this volume. Additional SANCHO simulations are required to describe more adequately the deformation of the halite when the pore space in the waste area is occupied by both brine and gas and each phase is capable of flowing into or out of the waste. An improved way of dealing with these inconsistencies is planned for future performance assessments. As implemented for 1992, the use of SANCHO results in BRAGFLO are based on the following assumptions about the SANCHO modeling.

- Halite deformation can be correlated in part to pore-pressure history and is independent of the fluid that occupies the pore space.

- Halite deformation is independent of the amount of brine present in the pore space within the room.

- Porosity is parameterized in terms of the rate of gas generation and pore pressure, but not in terms of the amount of gas present in the pore space of the waste panel as calculated by BRAGFLO because gas may flow out of panel in BRAGFLO but is confined to the room in these SANCHO simulations.

The validity of these assumptions and their impact on repository performance are uncertain and still under evaluation. As a result, this extension of the SANCHO-calculated porosities into BRAGFLO should be viewed as an initial attempt to describe the effect of halite deformation on waste-storage area porosity for two-phase flow modeling.

The SANCHO results described in this section represent only a small portion of the types of calculations that have been addressed with this code. Although the closure inputs for the BRAGFLO calculations were derived assuming a single disposal room in an infinite array of rooms, calculations for a full panel of empty rooms are being completed by the Waste Isolation Pilot Plant (WIPP) Disposal Room Systems Department at Sandia National Laboratories (SNL). These calculations will be a first step in examination of the error introduced by using single room closure to approximate the response of larger portions of the repository. The results will be used to examine both porosity variations within a given room and porosity variations from room to room. Calculations for other two-dimensional representations of the repository or its components are equally feasible, depending on the required computer time. Computer time for WIPP closure solutions over hundreds of years is a pressing constraint on mechanical closure analyses because of the complex finite-element mesh that must be constructed to represent disposal room components.

A number of calculations with SANCHO also are being completed by the WIPP Disposal Room Systems Department at SNL to examine the consequences of a human intrusion on post-intrusion closure. Other studies will examine various features of the room model, including the effect of existing cracks in halite and interbeds on gas pressurization. The effect on closure caused by different waste forms will be examined. Although the current SANCHO calculations did not include any fluid flow, calculations are also being completed coupling the mechanical response of the room with single-phase brine flow, and this coupling will be further extended to two-phase fluid flow.

How SANCHO Pore Pressure Data Are Used

In SANCHO a unique pore-pressure history exists for each gas-generation rate. These pressure histories are presented in Figure 4.2-5. This

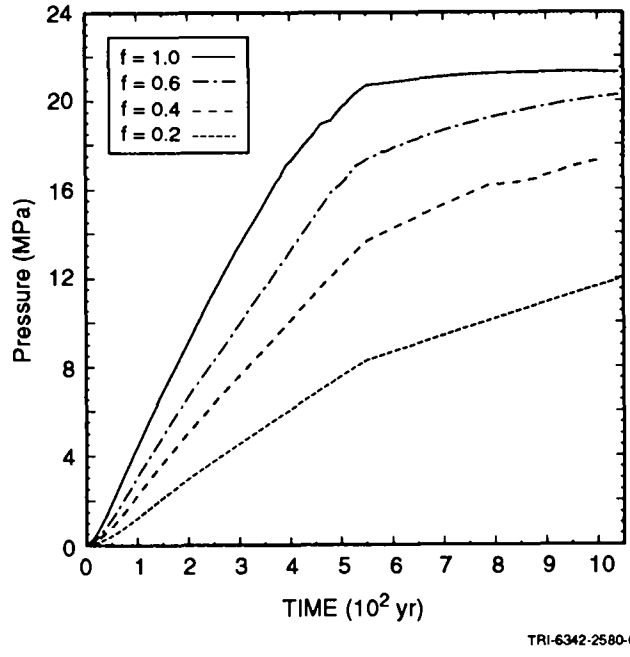

Figure 4.2-5. SANCHO results: pressure as a function of time for f=1.0, 0.6, 0.4 and 0.2; constant gas-generation rates for corrosion and biodegradation; f is defined in Figure 4.2-3.

relationship permits the unique determination of porosity given the gas-generation rate and the pore pressure instead of time, as is shown in Figure 4.2-6. In light of the assumptions mentioned above, the data presented in Figure 4.2-6 are used directly in BRAGFLO. The discussion that follows describes how the data in Figure 4.2-6 are used in the 1992 version of BRAGFLO.

First, the current fraction of gas potential is calculated by summing across all waste the cumulative moles of gas generated and normalizing this sum to the moles of gas that would have been generated under the baseline gas-generation conditions assumed in the SANCHO calculations. These conditions are

- for corrosion: 1 mole gas/(drum•yr) for 1050 yr, and
- for biodegradation: 1 mole gas/(drum•yr) for 550 yr.

To avoid extrapolation of data, this fraction is constrained to fall between a value of 1.0 and 0.1.

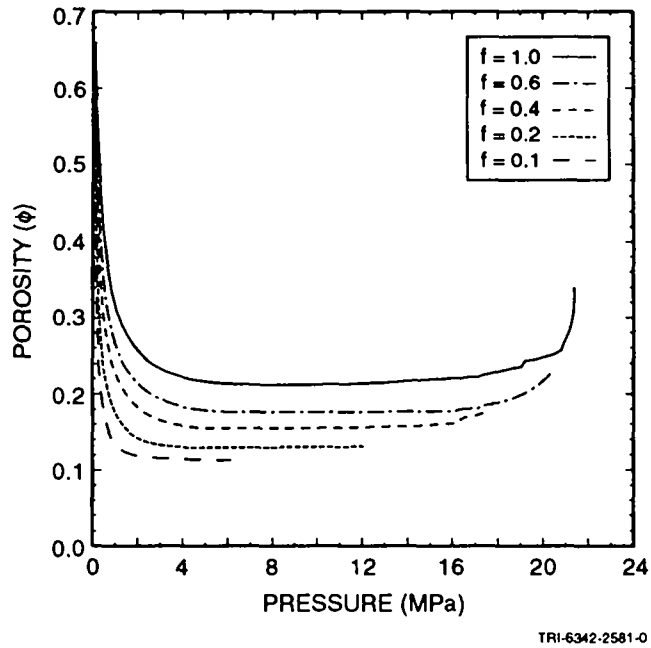

Figure 4.2-6. Modified SANCHO results as used in BRAGFLO: porosity as a function of pressure for constant gas-generation rates; porosity based on initial room brine; f is defined in Figure 4.2-3.

Second, the volume-averaged pore pressure in the waste area is calculated in BRAGFLO by

$$\bar{P} = \frac{\sum_{i=1}^{N} P_i V_i}{\sum_{i=1}^{N} V_i}, \qquad (4.2\text{-}3)$$

where the summation is over all waste grid blocks.

Third, the porosity associated with the BRAGFLO-calculated gas-generation rate fraction (f) and volume-averaged pressure is determined by linear interpolation of the data displayed in Figure 4.2-6. The gas-generation rate fraction is calculated by first accumulating the amount of gas generated in the waste over a given period of time, dividing by the length of time to give an average rate, and finally normalizing to the rates associated with f=1.0. These rates are given previously in this section and also in Figures 4.2-3 through 4.2-7. Some restrictions on the selection of the porosity are made to further avoid extrapolation of the data. These restrictions, depicted on Figure 4.2-7, are described below:

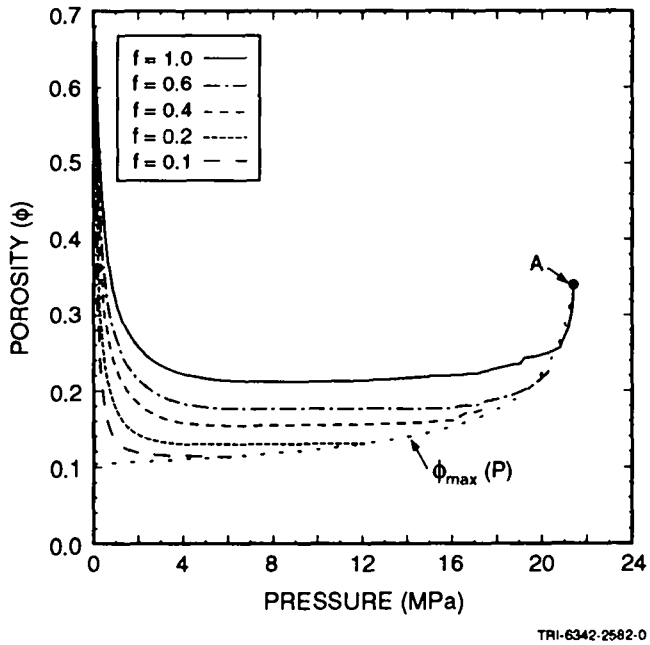

Figure 4.2-7. Limiting porosity, pressure, and gas generation in BRAGFLO implementation; f is as defined in Figure 4.2-3. Point A indicates maximum expanded porosity of waste (0.34), occurring at a pressure of 21.43 MPa.

- The maximum expanded porosity of the waste is limited to a value of 0.34, which occurs at a pore pressure of 21.4 MPa, at Point A in Figure 4.2-7.

- A bounding curve of porosity versus pore pressure, $\overline{P}$ (Pa), is constructed by connecting the points of maximum pressure for each of the gas-generation rate curves. The equation for this bounding curve is

$$\phi_{max} = 0.04991601 + \frac{0.2562233}{\sqrt{22.2 - (\overline{P})(1.0 \times 10^{-6})}} \quad , \qquad (4.2\text{-}4)$$

where $0.1 < \phi < 0.34$, $0 < P < 22$ MPa, and using the positive root.

If the pore pressure during a BRAGFLO simulation exceeds the maximum pressure associated with the current gas-generation fraction, then the dependence of porosity on pressure is restricted to this bounding curve.

- The curves are followed along the direction of low to high pressure only. The porosity results of SANCHO are generated only as waste pore pressure increases. The response of the halite to decreases in pore pressure is not simulated. This is not due to a limitation in SANCHO, but rather to scheduling constraints. Rather than speculate on a possible hysteresis effect, porosity is assumed to remain constant if waste pore pressure decreases and does not vary again until pressure exceeds the level at which it first began to decrease (Figure 4.2-8). If the direction path in which the data were generated is not preserved, physically unreal situations can result. For instance, consider the 10% base gas-generation curve at a pressure of 1 MPa (f = 0.1 on Figure 4.2-7). If the pressure were to decrease and the curve were followed, the porosity would actually increase even though pressure was well below lithostatic. Similarly, if the pressure were well above lithostatic and began to fall but still remained above lithostatic, the porosity from Figure 4.2-6 would decrease when in fact it would be expected still to increase but perhaps at a decreasing rate.

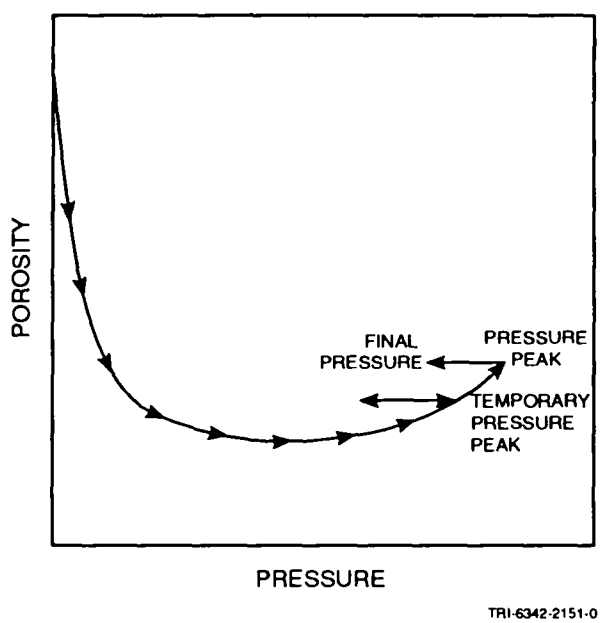

Figure 4.2-8. Hypothetical porosity/pressure path showing porosity treatment when pressure has a maximum.

Time-Step Considerations

Porosity is determined using the values of gas generation and pressure as outlined above at the beginning of a time step. In BRAGFLO, the initial values at a time step are converged values at the end of the previous time step. The porosity so determined is assumed to remain fixed across the current time step even though pressure and gas generation (via saturation) change during the intra-time iterations. The porosity is then updated at the start of the next time step. This explicit treatment of porosity is necessary because the more desirable implicit dating of porosity currently produces convergence difficulties for some of the input sets. In implicit dating, porosity would change with pressure and saturation during the intra-time-step iterations, and thus would change continuously across the time step rather than in step changes at the beginning of each time step, as in the explicit treatment. The more accurate implicit treatment is expected to be included in the 1993 PA BRAGFLO calculations.

4.2.3 Specific Storage

The mathematical relationship defining specific storage is

$$S_s = \rho g(\alpha + \phi\beta), \tag{4.2-5}$$

where S_s is specific storage (m^{-1}), ϕ is porosity, β is fluid compressibility (Pa^{-1}), and α is rock compressibility (Pa^{-1}). It is assumed that α is related to porosity change according to

$$\alpha = \frac{\partial \phi}{\partial p}, \tag{4.2-6}$$

where p is the fluid pressure in Pa.

BRAGFLO actually uses a modified rock compressibility, α',

$$\alpha' = \frac{1}{\phi}\frac{\partial \phi}{\partial p} = \frac{1}{\phi}\alpha. \tag{4.2-7}$$

Therefore, given the values for S_s, ρ, g, ϕ, and β, then α and α' can be computed. In the 1992 PA calculations, the following parameter values were used:

S_s = 1.0×10^{-6} m^{-1} (anhydrite)
S_s = 1.4×10^{-6} m^{-1} (halite)
ρ = 1230 kg/m^3
g = 9.79 m/s^2
ϕ = [0.001-0.03].

4.2.4 Relative Permeability [3] and Capillary Pressure[4]

In modeling two-phase phenomena, characteristic curves for surrogate materials using either the modified Brooks-Corey formulae (Equations 4.2-8 to 4.2-11) (Brooks and Corey, 1964) or the van Genuchten-Parker formulae (Equations 4.2-12 and 4.2-15) (van Genuchten, 1978; Parker et al., 1987) are used (see Section 2.3.1 of Volume 3 of this report). The Brooks-Corey relative permeability model is used for two-thirds of the calculations and the van Genuchten-Parker model is used for the remaining one-third of the calculations. An index parameter (0 or 1) is sampled with these probabilities, so that either one model or the other is used in any one realization. The rationale for treating model uncertainty (Brooks-Corey vs. van Genuchten-Parker) in this manner is discussed in the memorandum by Webb dated April 30, 1992, in Appendix A of Volume 3 of this report.

The modified Brooks-Corey relationships used are as follows:

Capillary pressure, P_c, is given by

$$P_c = \frac{P_t}{S_e^{1/\lambda}} \quad . \tag{4.2-8}$$

Threshold capillary pressure, P_t, is correlated to permeability (see Section 2.3.1 of Volume 3 of this report). S_e is the effective saturation in the modified Brooks-Corey model:

---

3. Relative permeability is a function of saturation of the phase of interest. It is a value between 0 and 1 that is multiplied by the absolute permeability to yield the effective permeability for that phase. Relative permeabilities are empirical fits of pressure drop and flow data to extensions of Darcy's law, and measurements taken at different degrees of saturation result in differing relative permeabilities (see Section 7.2 of Volume 2 and Section 2.3.1 of Volume 3 of this report).

4. Capillary pressure differences arise when immiscible phases exist simultaneously in a porous network (see Section 7.2 of Volume 2 and Section 2.3.1 of Volume 3 of this report).

$$S_e = \frac{S_l - S_{lr}}{1 - S_{gr} - S_{lr}} , \qquad (4.2\text{-}9)$$

where S_l is the liquid saturation, S_{gr} and S_{lr} are the residual gas saturation and residual liquid (brine) saturation, respectively, and λ is the pore size distribution parameter.

Relative permeability to liquid, $k_{r,l}$, and to gas, $k_{r,g}$, are given by

$$k_{r,l} = S_e^{(2+3\lambda)/\lambda} \qquad (4.2\text{-}10)$$

and

$$k_{r,g} = \left(1 - S_e\right)^2 \left(1 - S_e^{(2+\lambda)/\lambda}\right) . \qquad (4.2\text{-}11)$$

The capillary pressure relationship, Equation 4.2-8, is used throughout the entire saturation region ($0. \le S_l \le 1.$) even though, as discussed by Corey (1986), this relationship may not be appropriate at the higher liquid saturations when $S_e > 1.0$.

The relationship for the van Genuchten-Parker (van Genuchten, 1978; Parker et al., 1987) characteristic curves are as follows:

Capillary pressure is

$$P_c = P_o \left(S_e^{-1/m} - 1\right)^{1-m} , \qquad (4.2\text{-}12)$$

where $m = \lambda/(1+\lambda)$, and P_o is a capillary pressure constant discussed later.

Relative permeability is

$$k_{r,l} = S_e^{1/2}\left(1 - \left(1 - S_e^{1/m}\right)^m\right)^2 \qquad (4.2\text{-}13)$$

and

$$k_{r,g} = \left(1 - S_e\right)^{1/2} \left(1 - S_e^{1/m}\right)^{2m} , \qquad (4.2\text{-}14)$$

where the effective saturation, S_e, is now defined as

$$S_e = \frac{S_l - S_{lr}}{S_{ls} - S_{lr}} \qquad (4.2\text{-}15)$$

where S_{ls} is the maximum wetting phase saturation; a value of $S_{ls} = 1$ is used.

The same sampled values of relative permeability parameters are used for halite, anhydrite, the transition zone, and the DRZ. The waste, seals and backfill, experimental region, and all shaft sections use a fixed set of values and the Brooks-Corey model only. Residual brine and gas saturations range from 0.0 to 0.4. The Brooks-Corey pore-size distribution parameter, λ, ranges from 0.2 to 10.0. The van Genuchten-Parker parameter m is calculated from $m=\lambda/(1+\lambda)$ and ranges from 0.167 to 0.909. These parameter ranges are based on parameter values for surrogate materials, as discussed in Section 2.3.1 of Volume 3 of this report. These parameters have not yet been measured for WIPP materials.

The choice of the characteristic curve model has important implications on the expected behavior of multiphase flow in porous media. The most obvious effect stems from differences in the capillary pressure curve at high values of brine saturation. The Brooks-Corey model assumes an irreducible gas saturation, S_{gr}. When the gas saturation is below this residual value, the capillary pressure is assumed to remain at some fixed, non-zero value, known as the threshold capillary pressure. According to this model, in order for gas to penetrate a brine-filled pore, the gas pressure must first exceed this threshold value. This constraint effectively prohibits gas from flowing into a liquid-saturated medium until it overcomes this "barrier" to flow.

In the van Genuchten-Parker model, there is no residual gas saturation, and the capillary pressure is zero when the medium is fully brine saturated. Thus, there is no resistance to gas flow under fully brine-saturated conditions, and there is no "barrier" pressure to overcome. One incentive to using the van Genuchten-Parker model is to account in a simplistic way for the effects of fingering, which is the unstable displacement interface that occurs when a lower-viscosity fluid (gas) displaces a higher-viscosity fluid (brine). While this complex phenomenon cannot currently be modeled accurately by any method, its gross effects, such as unexpectedly rapid movement of gas, can be more closely approximated using a characteristic curve model such as the van Genuchten-Parker model that imposes no barrier to gas penetration into a brine-saturated medium. Conceptually, the van Genuchten-Parker model allows gas to migrate farther from the source (i.e., the waste) at a lower pressure than would occur under otherwise identical conditions using the Brooks-Corey model.

The characteristic curve model also affects brine flow, especially with the van Genuchten-Parker model when m is small (see Figure 4.2-9). Capillary pressures then rise steeply as the gas saturation increases from zero, and

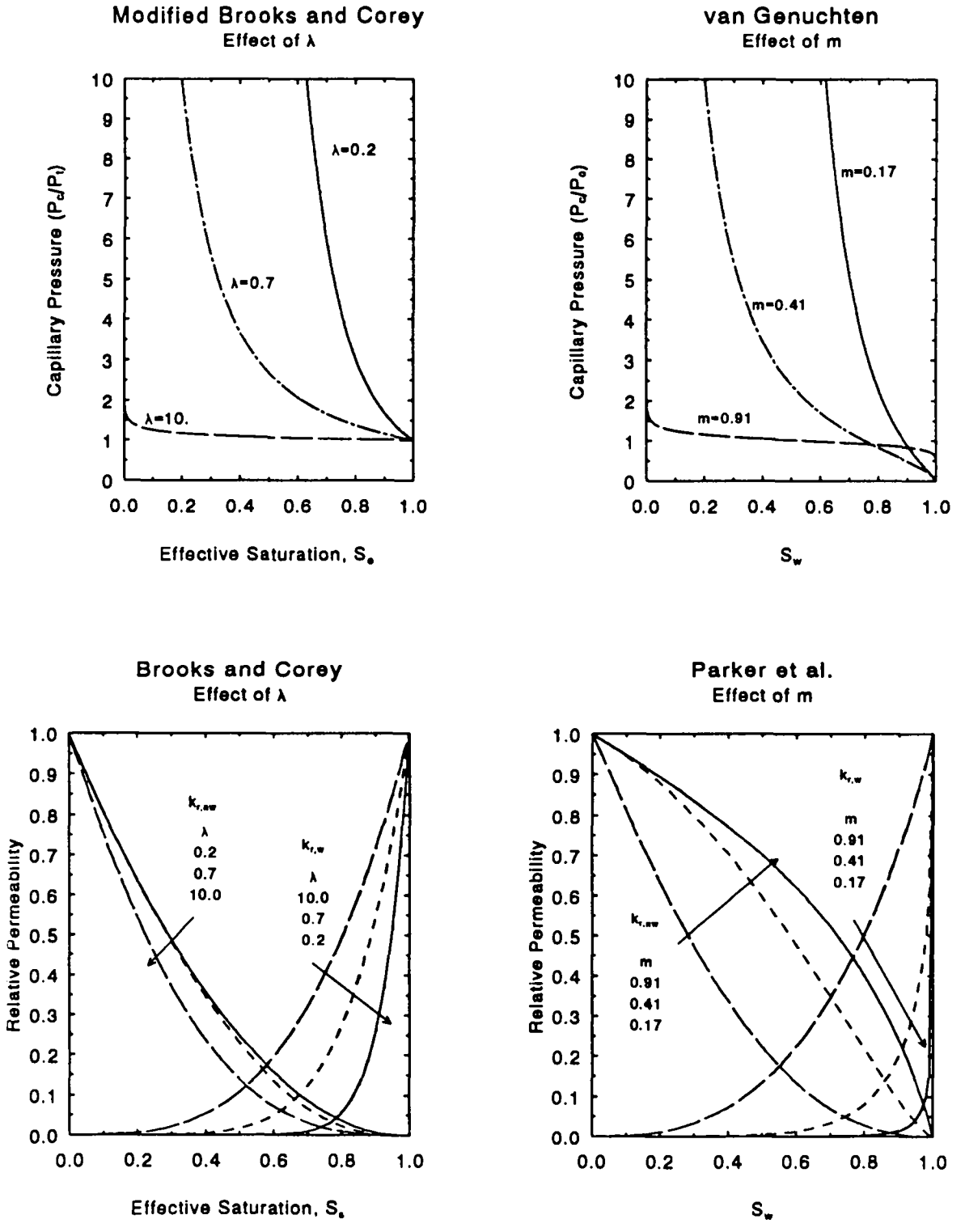

Figure 4.2-9. Capillary pressure and relative permeability functions (from memo from Webb to Anderson, 1992; in Appendix A of Volume 3).

the relative permeability curves are very steep at high brine saturations. Sampled values of m that are small effectively prevent brine from flowing when even a small amount of gas is present. With the Brooks-Corey model, even the smallest sampled values of λ have no inhibitory effect on brine flow until the gas saturation is below the residual value.

Threshold capillary pressures are determined from the correlation with permeability in all regions. The van Genuchten-Parker capillary pressure constant, p_o, is calculated by equating the capillary pressure from each of the two models at an effective saturation of 0.5, and solving the expression for Po. In the waste, in the DRZ, and in all excavated regions, capillary pressure is assumed to be zero. Zero capillary pressure for these regions is necessary because the capillary pressure curves are not defined for imbibition into a medium that has less than residual brine saturation. Any regions where the brine saturation starts out or may become less than residual (e.g., as a result of brine-consuming reactions that occur due to reactions in the waste region) were modeled with zero capillary pressure. However, if a maximum capillary pressure is specified and used at brine saturations less than residual, assuming zero capillary pressure is not necessary. Though this latter approach was not taken in the 1992 performance assessment it may be adopted for future calculations so that non-zero capillary pressure can be used without causing numerical problems when brine saturations below residual are encountered.

4.3 Initial and Boundary Conditions

A major difference between the 1992 and 1991 PA calculations for undisturbed conditions is in the treatment of initial conditions. The primary objective of taking a new approach in modeling initial conditions has been to establish a more realistic pressure distribution in the formations surrounding the waste at the time the repository will be sealed. This time is referred to here as time zero. The 1992 undisturbed calculations achieve more realistic time-zero conditions by varying the initial conditions in the repository over a 50-yr period immediately preceding time zero.

Before the 1992 calculations, it was always assumed that excavated regions were initially at atmospheric pressure with some arbitrary degree of brine saturation (various combinations of saturations were considered), while all other regions were fully brine saturated at hydrostatic pressure (relative to a sampled pressure at the level of MB139). These assumptions were unrealistic and produced results that may have been unrealistic for the following reasons:

- Brine in the DRZ above the waste could immediately drain down into the waste, presumably having been suspended there while the repository was excavated and filled. In many cases, brine from the DRZ was sufficient to corrode all ferrous metal in the waste, without any brine from the far field reaching the waste.

- The assumed pressure distribution imposed a large pressure gradient from the Salado halite to the shaft, which at time zero resulted in improbably large quantities of brine flowing from the halite into the shaft, despite the low permeability of the halite.

- The unrealistically high initial pressures surrounding the repository retarded migration of brine or gas from waste for much longer periods of time than could reasonably be expected, although the exact effect is unpredictable.

- Higher external pressures could raise the pressure in the waste more quickly, in part because of the higher pressure gradient near the waste, and in part because a faster influx of brine would cause gas generation by corrosion to occur more rapidly.

In reality, brine will seep in continually from the surrounding formations during the disposal phase of the WIPP. Water in the brine will evaporate into the well-ventilated atmosphere of the excavations or will be pumped out as standard mining practice if it accumulates anywhere. Thus, formations surrounding the excavations will be dewatered and depressurized while the panels are in use. Therefore, the initial conditions used in BRAGFLO now reflect the impact that the time between excavation and sealing of the panels will have on fluid saturations and pressures in the surrounding formations.

In 1992, the time between excavation and decommissioning is modeled explicitly, as detailed in Table 4.3-1. For the full repository, this phase is assumed to last 50 yr. The important features of conditions during this time are as follows:

- Except for the waste, the excavated regions, and the Culebra, the pressure distribution at 50 yr before time zero is hydrostatic relative to the pore pressure of MB139, which is sampled from a range of 12 to 13 MPa.

- Pressure at 50 yr before time zero in the waste and excavated regions is atmospheric, and the waste pressure is reset to this value at the end of the 50-yr period.

Table 4.3-1. Startup Procedure for Undisturbed Calculations

I. Don't allow brine inflow from the Culebra during initialization	1)	Set Culebra permeability to zero
II. Simulate the panels, seals, backfill, shaft, and experimental region as empty, newly excavated, gas-filled cavities	1)	Set initial porosity to 1.0
	2)	Set initial brine saturation to 0.0
	3)	Set initial pressure to 1 atm
	4)	Set residual brine and gas saturation to 0.0
	5)	Set permeability to 1.0×10^{-10} m^2
III. Simulate DRZ as initially pressurized, but partially fractured	1)	Set initial pressure to hydrostatic relative to sampled value of MB139 pore pressure
	2)	Set permeability to 1.0×10^{-17} m^2
	3)	Set initial porosity to volume average of sampled value of intact far field anhydrite and intact halite porosities (since DRZ has both)
	4)	Set initial brine saturation to 1.0
	5)	Set capillary pressure to 0.0 (so gas and brine pressures are same)
IV. Let the system equilibrate for 50 yr, the approximate time span between excavation and sealing of the repository	1)	Brine pressure in the excavation will increase slightly (~0.5%)
	2)	Brine will drain down from DRZ, approaching residual saturation
	3)	DRZ pressure will drop precipitously, approaching equal waste pressure
	4)	Let no creep closure occur
V. Instantly add the waste at 50 yr	1)	Reset waste pressure to 1 atm
	2)	Set brine saturation of waste to sampled "initial" brine saturation
	3)	Set waste residual brine and gas saturations to their sampled values
	4)	Set waste permeability to 1.0×10^{-13} m^2
	5)	Set waste porosity to "initial" value calculated from sampled values of volume fractions of metal and combustibles
	6)	Set reactant concentrations to "initial" values
VI. Adjust parameters for the DRZ and excavated regions	1)	Change porosity to final sampled values (except for creep closure and rock compressibility, simulating time-dependent porosity is beyond current modeling capability)
	2)	Adjust brine saturation so brine content of DRZ is unchanged; add gas to fill added pore volume
	3)	Reset DRZ and excavated region pressure to 1 atm
	4)	Reset brine saturation in excavated regions
	5)	Set DRZ permeability to 1.0×10^{-15} m^2 to account for fracturing
	6)	Set Culebra permeability to 2.1×10^{-14} m^2
VII. Resume calculation at 50 yr; this is the time normally called t=0	1)	Begin creep closure of repository
	2)	Allow gas generation to begin in waste
	3)	Pressures outside waste, DRZ, and excavated regions start from 50-yr values (t = 0)
VIII. Continue out to 10,050 yr, i.e., 10,000 yr past the time normally called t=0		

- Pressure in the Culebra at 50 yr before time zero is 1.053 MPa, and the far-field pressure is held at that value over the 10,050-yr calculation. (The Culebra has a fixed-pressure boundary condition, whereas the rest of the mesh uses a no-flow boundary condition.)

- The starting brine saturation is 1.0 everywhere except in the waste and other excavated regions, where the brine saturation starts at 0.0.

- At the end of the 50-yr period, the waste is assigned its sampled value of initial brine saturation, which ranges from 0.0 to 0.14.

The initial condition calculations themselves begin with initial conditions similar to those used in 1991; perhaps the greatest difference is simply in interpretation. What was called time zero in 1991 is now called -50 yr; this is the time of initial excavation. The performance calculations begin at time zero (50 yr after the initial condition calculation as started); this corresponds to the time of sealing of the repository.

During the initial conditions calculation, the permeability of the excavated regions is assumed to be very high (1×10^{-10} m^2), to simulate cavities. At the end of the 50-yr period, any brine that has flowed into the excavated regions is ignored, since it will have evaporated or will have been pumped out of the repository. The sampled initial brine saturation in the waste is introduced. Pressures in all the excavated regions are reset to atmospheric. Pressures there are generally barely above atmospheric (by a few hundred pascals) after the 50-yr emplacement period; they are reset to atmospheric to reestablish realistic conditions at time zero, since at the time of sealing, the excavated regions should be at atmospheric pressure. Except in the DRZ, pressures in all the surrounding formations, including the transition zone and the intact ahydrite interbeds, remain as they are at the end of the 50-yr period.

In the DRZ, at least the residual saturation of brine, and possibly more, will remain, the rest having drained into the excavated region that will later be filled with waste. At time zero, the brine remaining in the DRZ is left there; however, the porosity is assumed to change from the initial intact halite value to the final sampled DRZ porosity. This porosity change increases the void volume. In order to conserve the volume of brine in the DRZ, the additional void volume is assumed to be filled with gas. The pressures in the DRZ will typically be slightly above atmospheric at time zero. If the pressures were left at those values when additional gas is introduced at time zero, it could result in a gas-drive condition that would cause brine to be expelled suddenly from the DRZ into the waste at time zero. To prevent this unrealistic behavior, the pressure in the DRZ is also reset to atmospheric at time zero.

The previously excavated regions will contain no brine except for the initial brine brought in with the waste. The surrounding formations will be depressurized and dewatered to the extent expected after being exposed to ventilated air at atmospheric pressure for 50 yr. All surrounding formations are fully saturated with brine at time -50 yr. Generally, at time zero, they will still be fully brine-saturated (except for the DRZ). Except for the DRZ, brine saturation in surrounding formations is not modified to reflect a change in porosity at time zero.

The calculations proceed from this calculated initial condition for the 10,000-yr performance period. The most important effect of these more realistic initial condition is that less brine will flow into the excavated regions (including the waste), since the initial "surge" of brine that occurs upon excavation has been eliminated, and the pressure gradients in the immediate vicinity of excavations have been greatly reduced.

4.4 Results and Discussion (Undisturbed Performance)

General observations are described in this section that pertain to all of the calculations. Detailed statistical analyses that specific results relate to specific parameter values will be discussed in a later section.

The plots presented in this section show results as a function of time for all 70 realizations (vectors) on a single plot. These results enable trends to be easily observed if present. Although the plots are sometimes cluttered, they are useful for illuminating general behavior and allowing comparisons to be made among all of the realizations.

4.4.1 Repository Behavior

Pressures in the repository (Figure 4.4-1) invariably rise from the initial value of one atmosphere, primarily because of gas generation. The rise is not always monotonic. In many of the vectors, the pressure in the waste peaks relatively early, in 1000 to 2000 yr, then levels off at a slightly lower value. This leveling off may be the result of gas breaking through a lower-permeability barrier, such as the shaft seal, or it may occur simply as gas generation ceases. Either the reactants are fully consumed or no more brine can make its way into the waste to allow gas generation to continue. The peak pressure among all vectors was about 22 MPa. In the vectors in which the pressure peaked early, the peak was almost always greater than the far-field pore pressure, so even if gas did not break through any kind of barrier, the pressure would always tend to decrease. In a

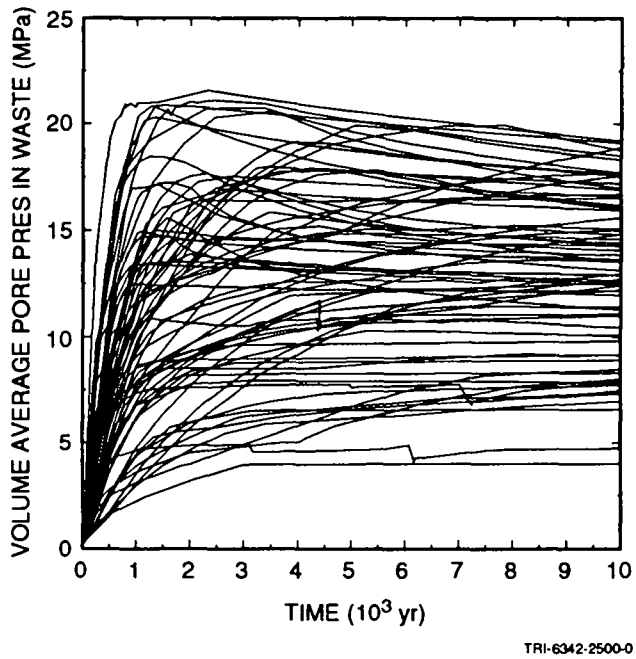

Figure 4.4-1. Volume average gas pressure in waste.

few vectors, the pressure rose continually over the 10,000-yr performance period, in some cases to pressures in excess of lithostatic (14.8 MPa), without ever peaking. This behavior is expected when the gas-generation rate is low, but the initial brine content of the waste is high enough to sustain reactions continuously without additional brine influx from outside the repository. At 10,000 yr, the range of pressures in the waste is very large, from 4 MPa to 19 MPa. For those realizations in which final pressures are at the lower end of the range, little gas has been generated and all of the surrounding formations have extremely low permeability, thereby preventing brine inflow from equalizing pressure with the far field. For those realizations in which pressures are at the upper end of the range, gas generation has been vigorous, resulting in pressures well above lithostatic.

Because of the implementation of the porosity surface (see Section 7.3 in Volume 2, of this report), pore volume (Figure 4.4-2) or porosity in the waste behaves similarly among all realizations. In all cases, the porosity drops from the initial value of 66% during the first few hundred years, as the repository creeps shut. The porosity reaches a minimum between 12% and 21%, depending on the rate at which the pressure in the repository increases, primarily as a result of gas generation. In the extreme case, in which the

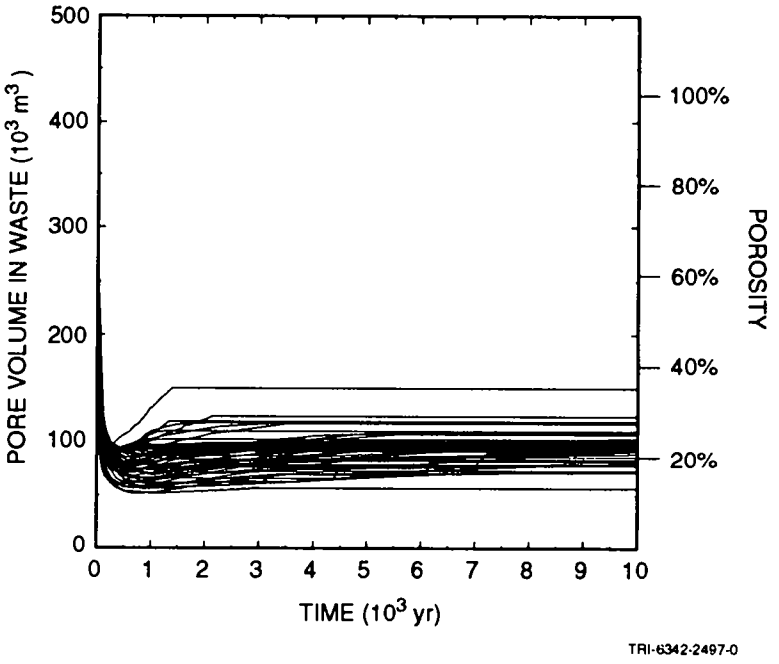

Figure 4.4-2. Pore volume in waste.

pressure rises rapidly to about 21 MPa, the repository reopens to a porosity of 34%, which is the maximum porosity resulting from reopening that is allowed in the current implementation of the porosity surface. Most vectors show much less expansion, generally to porosities of 15% to 21%. In the other extreme, pressures in the repository remain so low that almost no inflation occurs, and the porosity at 10,000 yr is still only 12.6%. Note that in the current model, porosity cannot decrease when pressure decreases. This explains why, after the initial expansion that typically occurs between 500 and 1500 yr, there is no decrease in pore volume, despite the fact that in many realizations pressures in the repository decrease after that. See Section 4.4.3 for further discussions of the effects of creep closure.

Although the average brine saturation in the waste varies greatly from vector to vector (Figure 4.4-3), the variations with time show nearly the same trends in all of the realizations. There is an initial period when the brine saturation increases rapidly, peaking in 500 to 1500 yr. This rise in brine saturation is a direct result of the rapid drop in porosity. As the pore volume decreases, gas, but not brine, is compressed, and as a result the brine saturation increases. During this same period, brine volume (or mass) generally decreases, as a result of consumption by corrosion (See

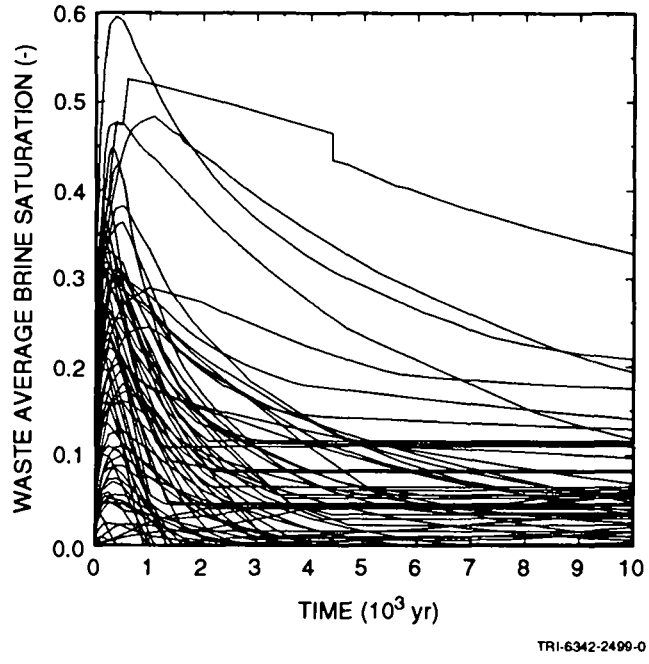

Figure 4.4-3. Waste average brine saturation.

Figure 4.4-4). Brine saturation increases initially in large part because porosity reduction resulting from creep closure occurs at a faster rate than brine consumption by corrosion. Once creep closure effectively ceases, in most cases within 500 yr, brine saturation is no longer influenced by porosity changes, although brine inflow causes brine saturation to continue to rise for as much as 1000 more years. Thereafter, the brine saturation generally decreases--rapidly at first, at a slower rate later--as brine is consumed by corrosion. Corrosion consumes as much as 29,000 m^3 of brine, as shown in Figure 4.4-5. Some brine may flow out of the waste; the maximum among the 70 realizations was 11,000 m^3 (Figure 4.4-6), but in 87% of the vectors, less than 2000 m^3 flows from the waste. Only in one vector is less than 2000 m^3 of brine consumed (Figure 4.4-5). Thus, in a general sense, most of the brine that disappears from the waste is consumed by reaction, rather than by outflow.

The rate and amount of gas generation varies greatly, as shown in Figure 4.4-7. Among the 70 realizations, the quantity of gas generated varies over more than an order magnitude, from 2 x 10^6 m^3 to 32 x 10^6 m^3 of hydrogen, at reference conditions (30°C, 1.01325 x 10^5 Pa). In almost all cases, gas generation ceases in less than 10,000 yr. (The curves in Figure 4.4-7 become flat at that point.) Apparently, gas generation as modeled ceases because

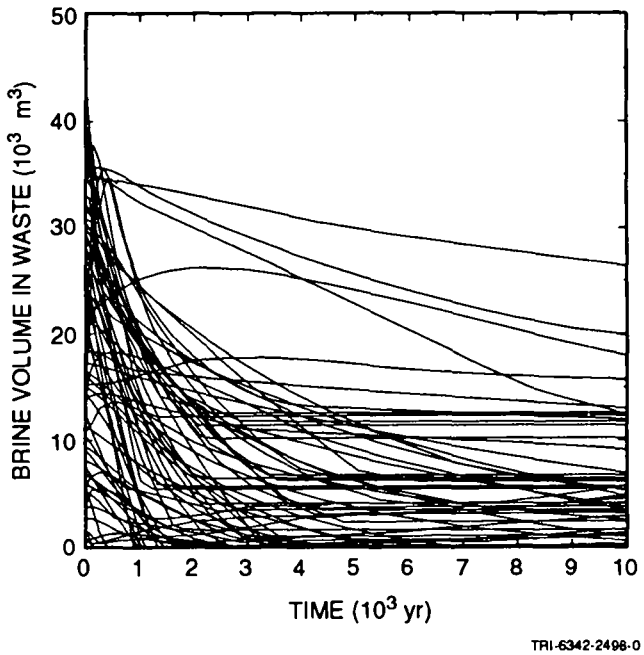

Figure 4.4-4. Brine volume in waste.

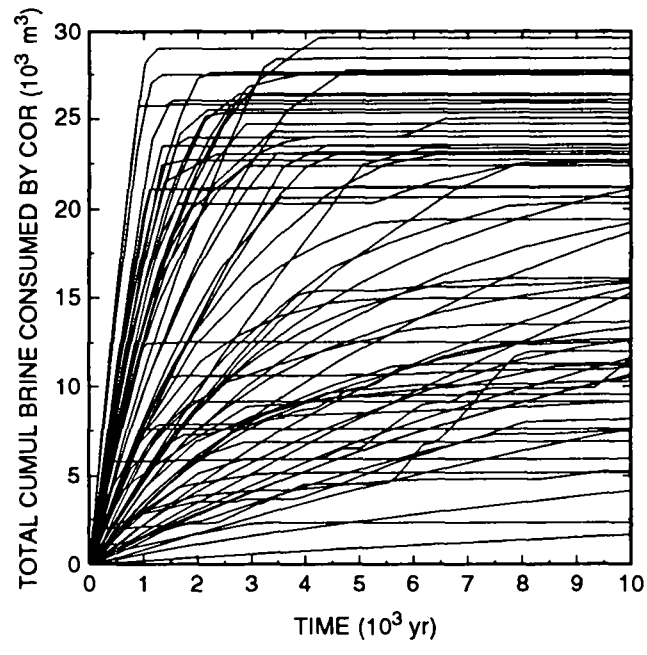

Figure 4.4-5. Total cumulative brine consumed by corrosion.

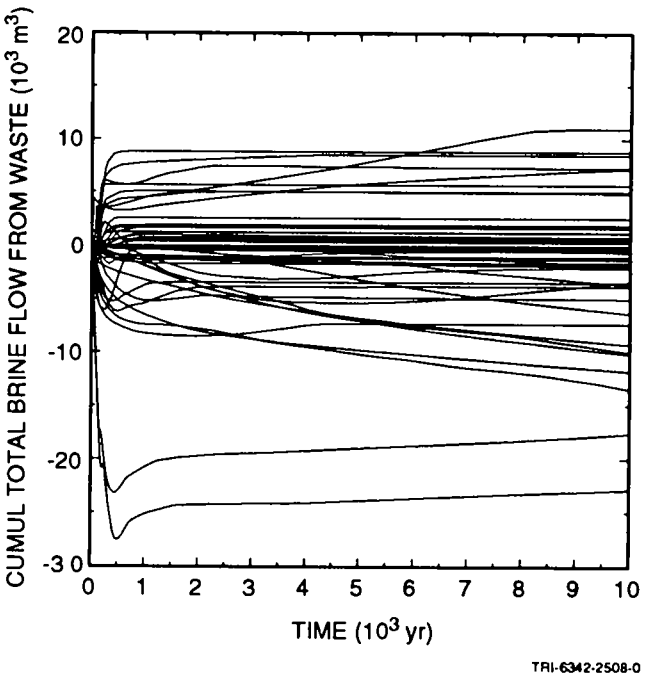

Figure 4.4-6. Cumulative net brine flow from waste.

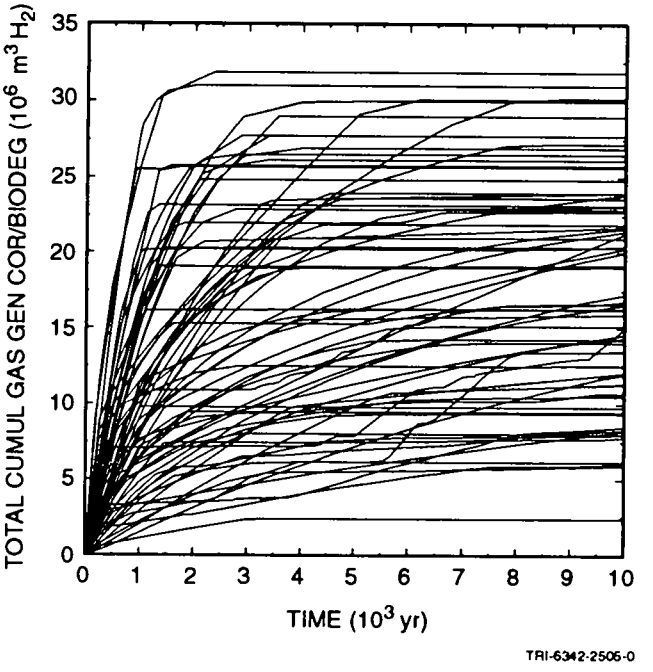

Figure 4.4-7. Total cumulative gas generated from corrosion and biodegradation.

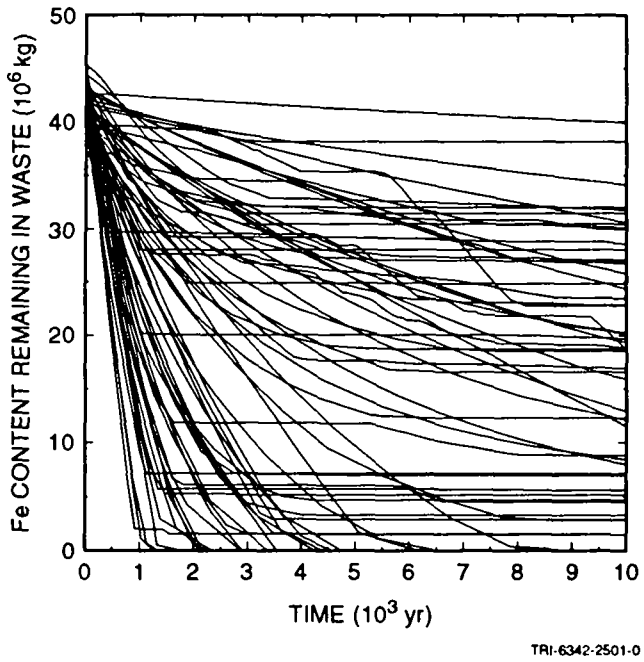

Figure 4.4-8. Iron content remaining in waste.

brine is no longer available for corrosion or biodegradation in those cells where iron and cellulosics remain. As shown in Figure 4.4-8, iron is still present in the waste in 53 of the 70 realizations after 10,000 yr, yet the rate of gas generation by corrosion (Figure 4.4-9) has decreased greatly from the rate at earlier times. Similarly, cellulose is still available in 17 realizations after 10,000 yr (see Figure 4.4-10) even though the biodegradation gas-generation rate has dropped nearly to zero for all realizations, as shown in Figure 4.4-11.

4.4.2 Conditions Outside of the Waste

As discussed in Volume 2, Section 4.2.3.1, the dominant pathways for contaminated brine flow from the waste to the accessible environment are: (1) along MB139 to the shaft and up the shaft to the Culebra; (2) through degraded drift and shaft seals to the shaft and up the shaft to the Culebra; and (3) along MB139 laterally outward toward the accessible environment. In addition, the anhydrite layers above the repository could provide a pathway for brine flow in the same manner as MB139.

Because BRAGFLO models only flow and does not simulate transport, it is difficult to state with certainty where contaminated brine has flowed.

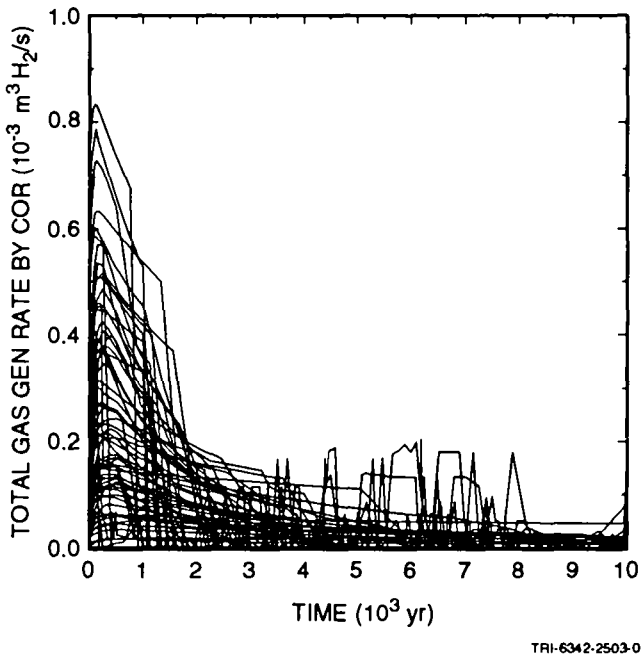

Figure 4.4-9. Rate of gas generation by corrosion.

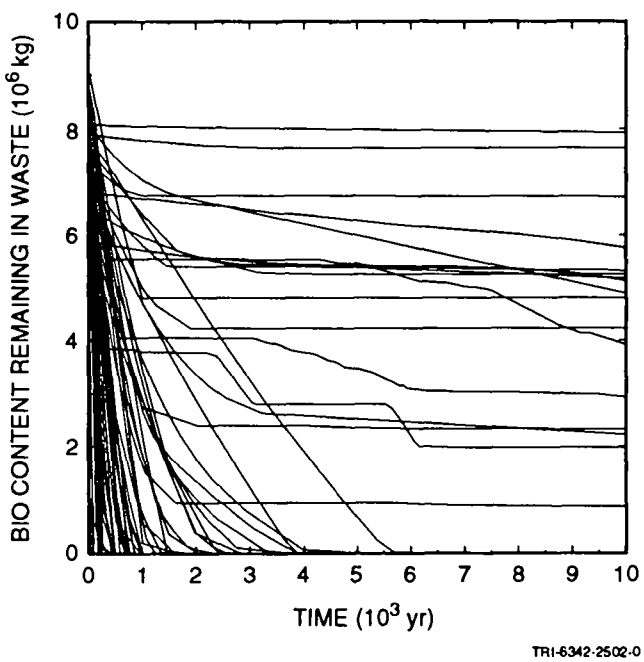

Figure 4.4-10. Biological content remaining in waste.

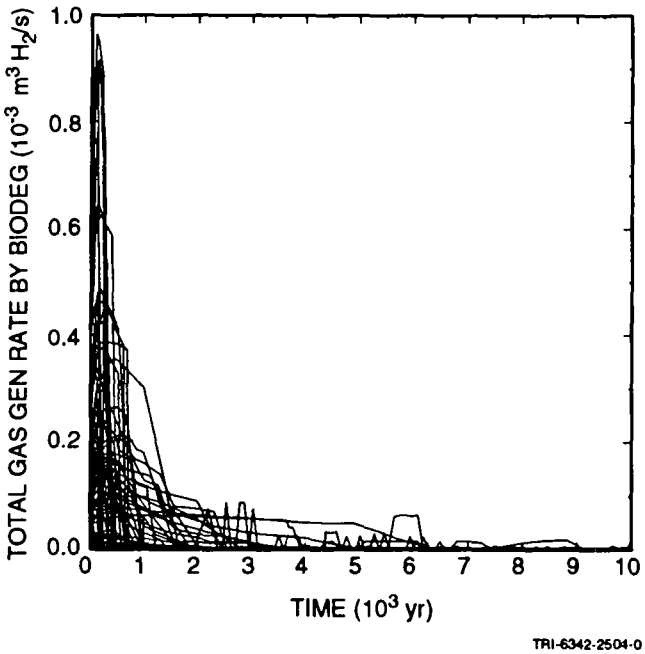

Figure 4.4-11. Rate of gas generation from biodegradation.

However, Figures 4.4-12 to 4.4-17 strongly suggest that no contaminated brine has flowed up the shaft. Figures 4.4-18 to 4.4-20 suggest that no contaminated brine has reached the accessible environment by way of lateral outward flow through the anhydrite layers or marker beds.

For contaminated brine to flow up the shaft, it must first flow either through the drift seals and backfill and into the shaft, or through the DRZ above and below the waste (see Figure 4.1-2). As Figure 4.4-12 shows, although some brine (less than 300 m^3) has flowed from the waste into the seals and backfill (in only four realizations), none has flowed from the seals and backfill into the shaft (Figure 4.4-13). In fact, as shown in Figure 4.4-13, for the assumptions used inthe 1992 PA, there was flow between these two regions in only two realizations, and it was <u>from</u> the shaft, rather than into the shaft. In more than 60 realizations, there was no flow between these two regions.

These results do not preclude the flow of contaminated brine from the waste through the DRZ and into the shaft. However, Figure 4.4-14 shows only a momentary (from the perspective of the 10,000-yr regulatory period) flow of brine from the DRZ into the shaft and in only two of the realizations. Brine

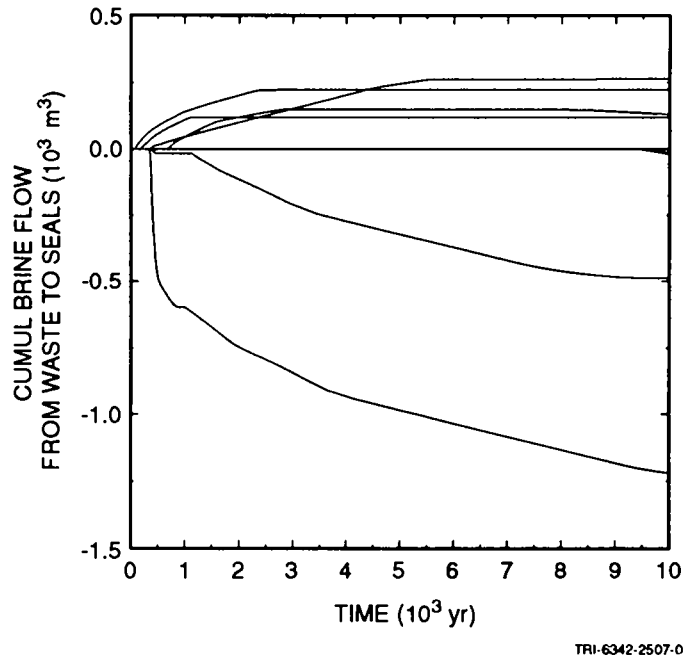

Figure 4.4-12. Cumulative brine flow from waste to seals.

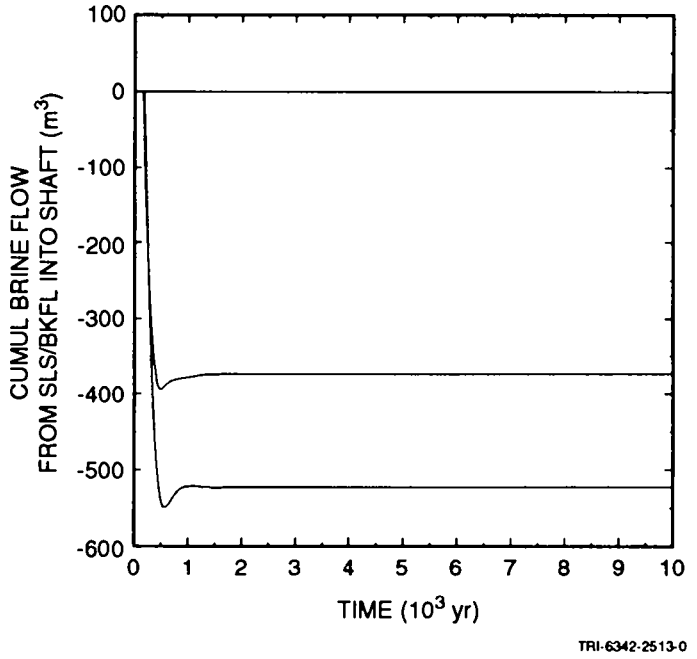

Figure 4.4-13. Cumulative brine flow from seals and backfill into shaft.

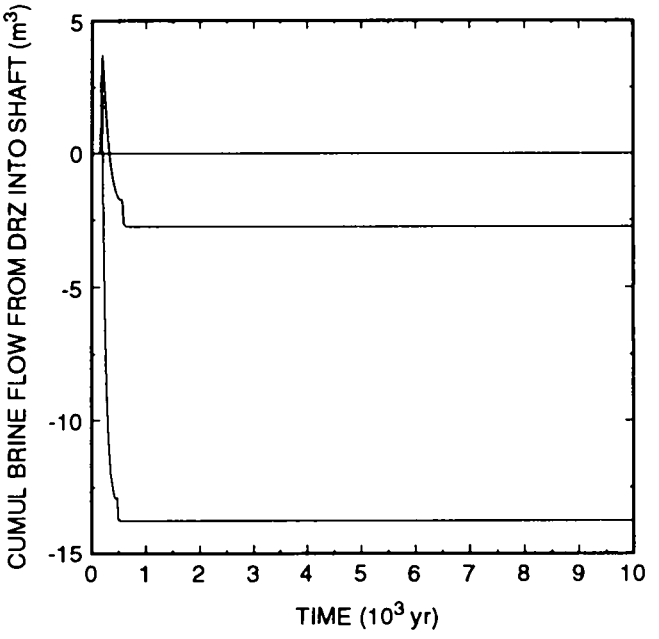

Figure 4.4-14. Cumulative flow from DRZ into shaft.

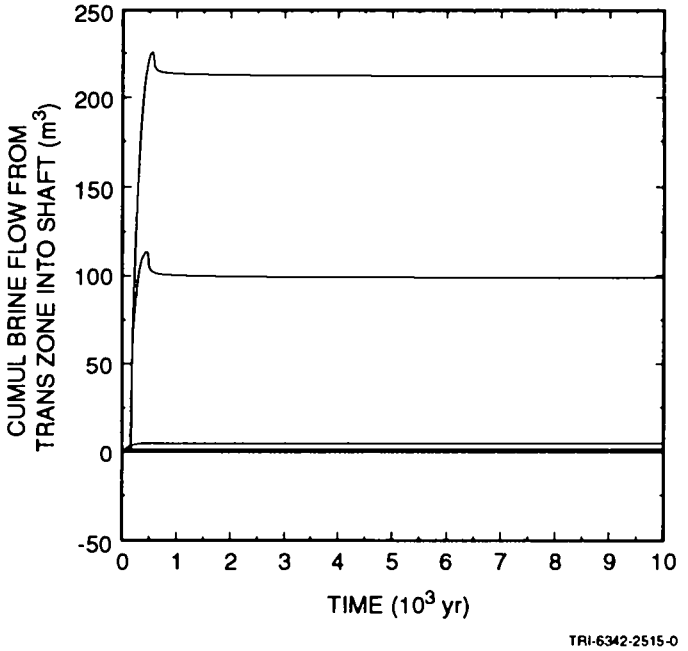

Figure 4.4-15. Cumulative brine flow from transition zone into shaft.

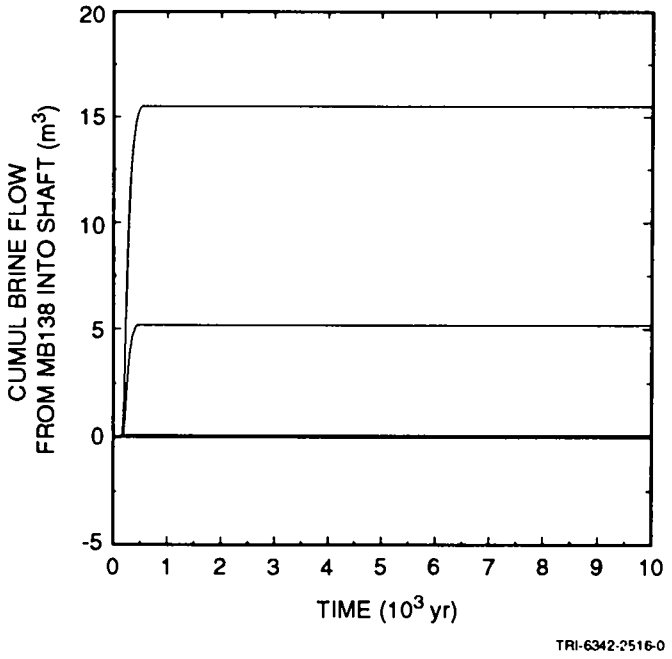

Figure 4.4-16. Cumulative brine flow from MB138 into shaft.

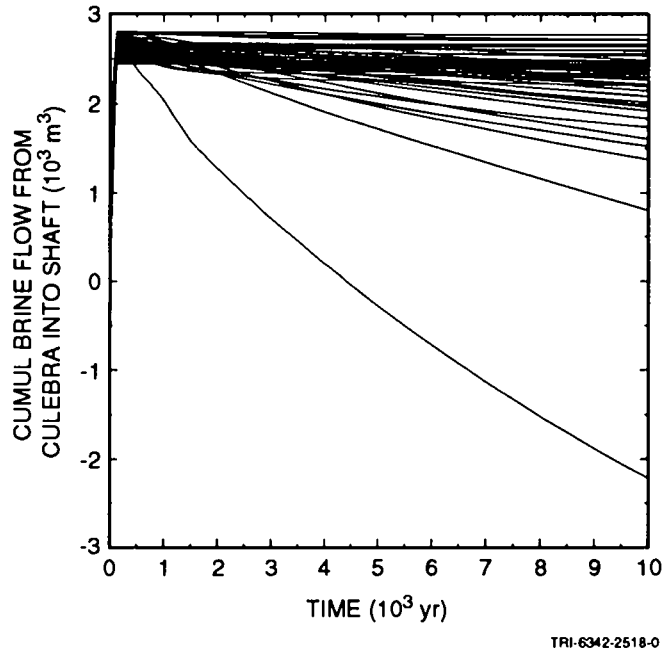

Figure 4.4-17. Cumulative brine flow from Culebra into shaft.

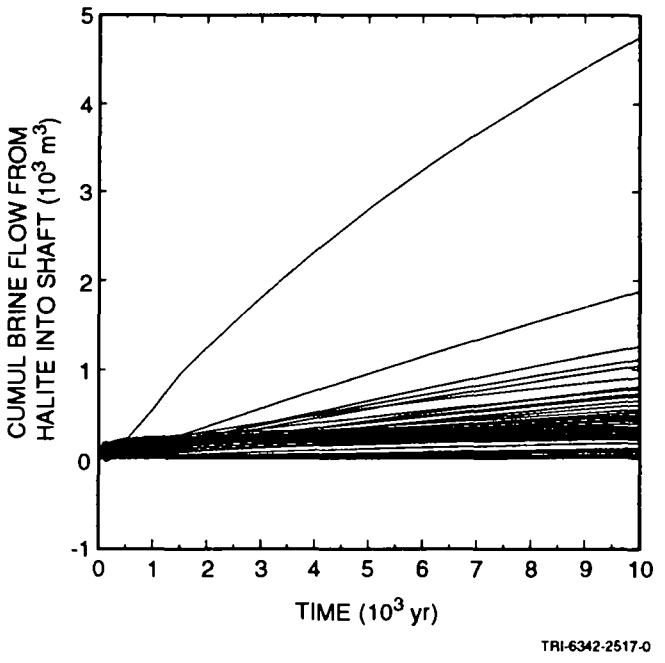

Figure 4.4-18. Cumulative brine flow from intact halite into the shaft.

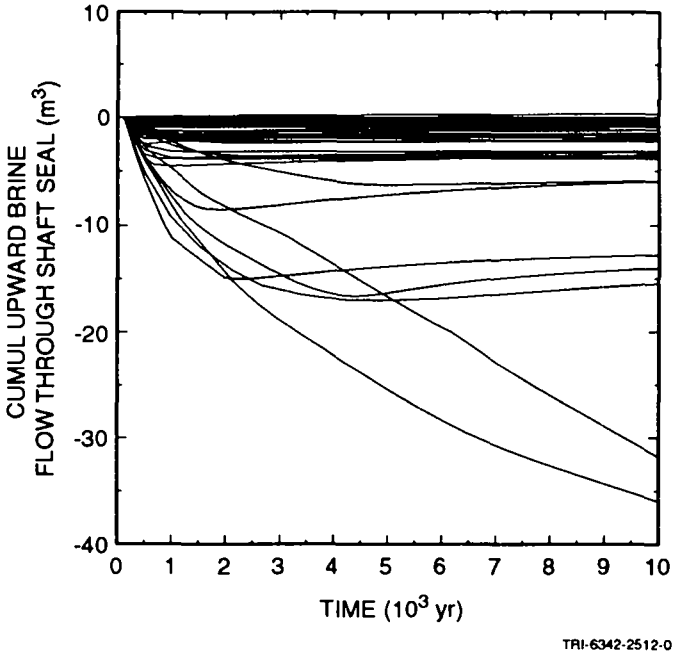

Figure 4.4-19. Cumulative brine flow upward through the shaft seal.

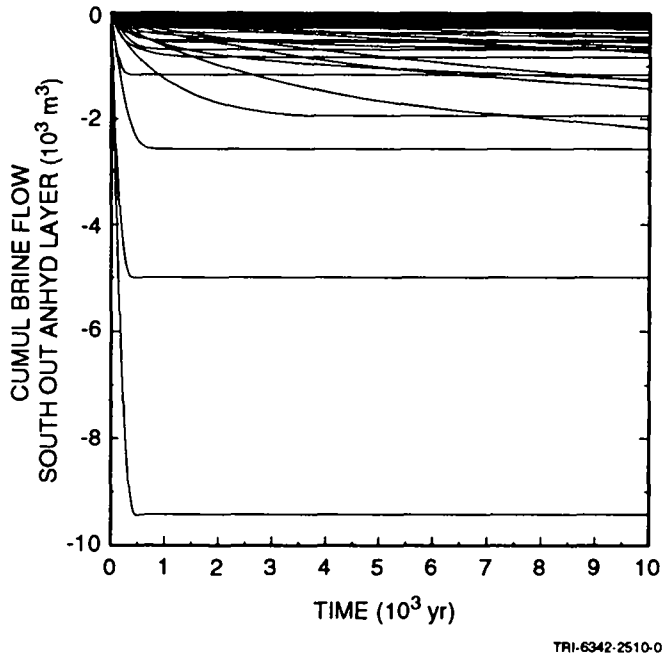

Figure 4.4-20. Cumulative brine flow south out of anhydrite layers A and B.

flow from the transition zone and MB138 into the shaft does occur in a few realizations (Figures 4.4-15 and 4.4-16), but it is unlikely that that brine has come from the waste, since these beds are several meters above the waste, and the waste is never fully saturated with brine (Figure 4.4-3). Figure 4.4-17 shows that there is a large net flow of brine from the Culebra into the shaft in all but one realization, and in that one realization, the brine flow comes from the halite, and not from the shaft seal (Figure 4.4-18). Finally, Figure 4.4-19 shows upward flow of brine through the shaft seal. In only one realization was there any pitive upward flow, and it amounted to only 0.26 m^3 of brine. In all other cases, there was either no flow through the seal, or there was flow downward. Thus, it appears highly unlikely that any brine originating in the waste could have flowed up and out of the shaft and into the Culebra.

In Figures 4.4-12 to 4.4-16, two realizations display behavior that is markedly different from all the rest. In these two realizations, the anhydrite permeability, a sampled parameter, is higher than in all the others, having values of 9.5×10^{-17} m^2 and 4.1×10^{-17} m^2. Apparently, this permeability is just high enough to allow sufficient influx of brine from the far field to flood the portion of the shaft below the shaft seal. Brine

flows into the shaft from MB138 and the transition zone and from the shaft into the seals, backfill region, and the DRZ. This occurs only in these two realizations. It does not occur in the realization having the next highest anhydrite permeability, 1.0×10^{-17} m^2, even though none of the other sampled parameters in this realization differs radically from the other two realizations. Evidently, the model is quite sensitive to anhydrite permeability when the permeability is greater than 1.0×10^{-17} m^2.

It is more difficult to establish that contaminated brine has not flowed laterally out the anhydrite layers beyond the WIPP boundaries without more detailed examination of the results, but an indirect argument can be made. First, note that since the likelihood of contaminated brine flowing into the shaft is negligible, it is even less likely that it could have flowed beyond the shaft to the north. (As Figure 4.1-2 shows, the shaft intersects all of the anhydrite layers, which are the only significant lateral flow paths.) As for the southern direction, Figure 4.4-20 shows that there was no brine flow south laterally out the anhydrite A and B layer. While there was some flow to the south out MB138 in some realizations (Figure 4.4-21), it is unlikely that this brine came from the waste. In order for contaminated brine to flow out the top of the waste, the repository must be saturated with brine, with the remaining gas at the residual gas saturation of 0.07. As Figure 4.4-3 showed, brine saturation never exceeded 60%, and was generally less than 40%. Therefore, contaminated brine flow out the top of the repository and laterally out MB138 is highly unlikely. In most realizations, there was a large flow of brine toward the repository through MB138. The only remaining possibility for lateral migration of contaminated brine is south out MB139. Among the nine realizations having a positive southward brine flow (Figure 4.4-22), the maximum cumulative southward flow was less than 1800 m^3. Assuming radial plug flow and a minimum porosity of 0.001, the farthest this amount of brine could have flowed south out MB139 is 626 m. In Figure 4.4-22, some of the curves (especially the bottom two) increase after passing through a minimum typically within the first 1000 yr. This indicates that even though the cumulative net brine flow is inward (toward the waste), there can still be a large outward flow of contaminated brine. In the worst case – the bottom curve - 6600 m^3 of brine flows out of the waste into MB139. However, in this particular realization, the porosity of MB139 is 0.0041 and the maximum gas saturation of MB139 is only 0.065, so the 6600 m^3 still flows out no farther than 626 m. (The distance of 626 m is the distance to the far end of the farthest grid block into which contaminated brine could have flowed.) In fact, this quantity of brine would not have flowed past the WIPP site boundary even with the minimum MB139 porosity of 0.001 and an improbable gas saturation throughout MB139 of 50%. Thus, it is unlikely that any contaminated brine could have flowed laterally beyond the WIPP site

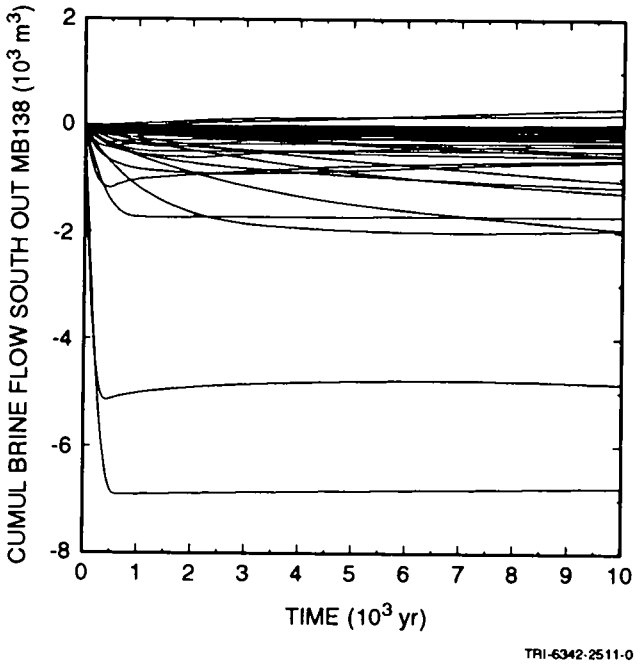

Figure 4.4-21. Cumulative brine flow south out of MB138.

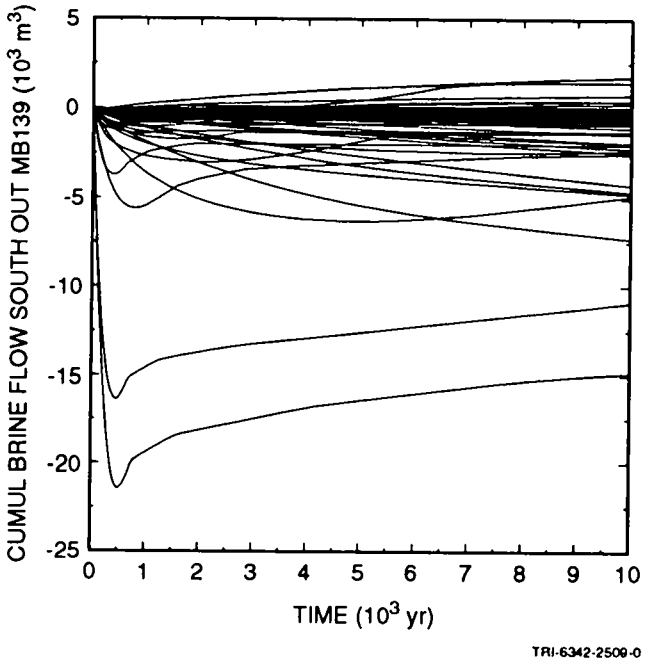

Figure 4.4-22. Cumulative brine flow south out of MB139.

boundaries (approximately 2400 m beyond the repository) in the undisturbed scenario.

4.4.3 Creep Closure Effects

The same set of 70 calculations that was described above was repeated with the only change being that creep closure of the waste was not allowed to take place dynamically. Instead, the porosity of the waste was held constant at a partially closed state (except for very small pressure-dependent compressibility effects). These calculations were done to determine what effect creep closure dynamics, as currently implemented, have on the results. These calculations will be referred to as "fixed-porosity" calculations to indicate that dynamic closure was not modeled, even though the repository is actually assumed to have crept to a final-state porosity.

The overall effect of modeling creep closure dynamically was minor. Pressures in the waste are generally higher without dynamic closure, but only because the fixed value of porosity is lower than the porosity calculated dynamically. Higher pressures result in gas flowing farther out the anhydrite layers. However, potentially contaminated brine still does not reach the disposal-unit boundary when a fixed porosity is used.

With creep closure modeled dynamically, the panel porosity was initially 66% and dropped as creep progressed, leveling off at 12% to 21%. In the fixed-porosity calculations, the waste panel porosity was initially 19%, which is the median final-state porosity of the waste. (See Table 3.4-1 in Volume 3 of this report.) The porosity was allowed to vary only as a result of the non-zero compressibility of the waste; because the value used for compressibility of the waste is very small (1.6×10^{-9} Pa^{-1}), the porosity increased only 1.1 percentage points even under the maximum pressures (Figure 4.4-23). This analysis helps to illustrate the significance of creep closure in assessing the performance of the WIPP. Although only the early time dynamics are accounted for in the current implementation, that is the period during which the greatest changes occur and during which transient effects of closure should have the greatest impact on the performance of the WIPP.

Pressure profiles from the fixed-porosity runs (Figure 4.4-24) are very similar to the calculations that include closure. The most apparent differences are in the peak pressures, which now are as high as 34 MPa, compared with 22 MPa with creep closure. Pressures are generally higher when the creep closure process is not modeled. This occurs because, as mentioned above, the porosity used in the fixed-porosity calculations is lower initially but the brine volume is the same, so with less pore volume in which

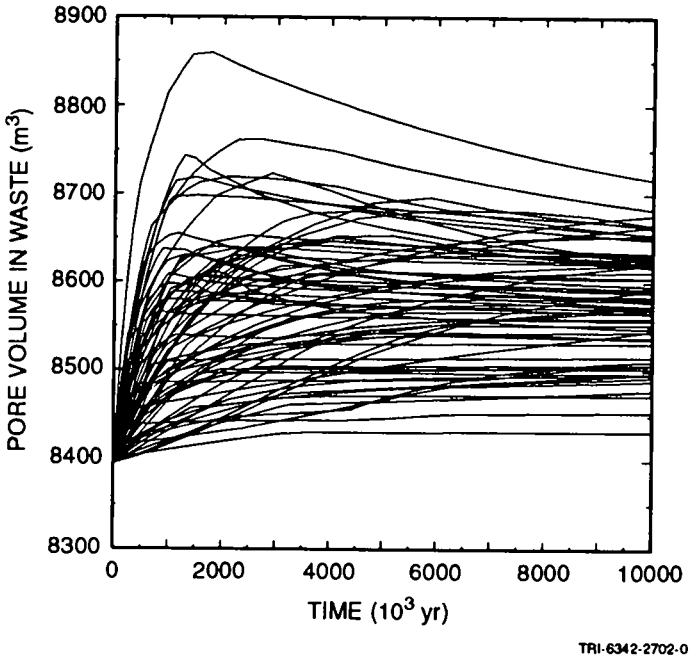

Figure 4.4-23. Waste porosity without creep closure.

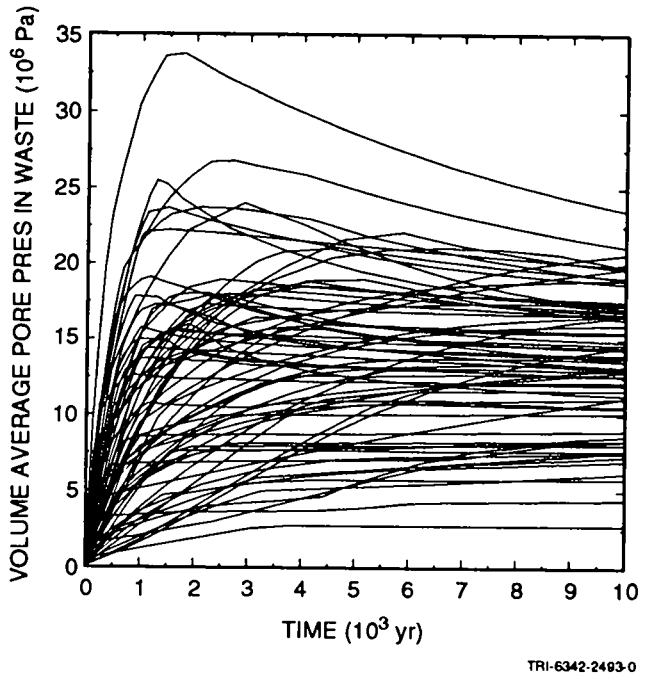

Figure 4.4-24. Panel pressure without creep closure.

to store the gas, pressures increase much more rapidly and go much higher, even though the amount of gas generated is roughly the same. Note that the pressure profiles and the pore volume profiles are identical in shape. The porosity is calculated as an exponential function of pressure, but because the compressibility is so low the function is essentially linear in pressure.

Most of the results from the BRAGFLO fixed-porosity calculations are nearly identical to the results that included creep closure dynamics. Compared with the 10,000-yr regulatory period, creep closure transients are brief; a nearly constant final closed state is reached in only a few hundred yr (as currently modeled). Most flow phenomena in the vicinity of the repository take place at very low rates because of the low permeabilities of the surrounding strata. Only the chemical reactions (corrosion and biodegradation) occur rapidly. The initial brine volume was the same (for a given realization) in both calculations, and the low inflow and outflow rates changed that volume little over the first few hundred years, so the extent of the reactions was largely unaffected by the different porosities in the two sets of calculations. Thus, profiles of the remaining iron and cellulose content of the waste (Figures 4.4-25 and 4.4-26), and the total cumulative gas generated (Figure 4.4-27), look very similar in both the closure and fixed-porosity calculations (Figures 4.4-8, 4.4-10, and 4.4-7, respectively). After a few hundred years, conditions in the fixed-porosity calculations are very close to those in the closure runs, because by then porosities in the creep closure calculations have reached stable values that range from about 13% to 25%, similar to those in the fixed-porosity calculations (19%). The exceptions are those few realizations in which the pressure rose rapidly and sufficiently high in the closure calculations to result in significant reinflation. In these, the stable final-state porosities are much higher (26% to 34%) than the porosities used in the fixed-porosity calculations, so pressures and other responses differed more substantially in the two sets of calculations.

Where the two calculations differed most was in the pressure-sensitive fluid-flow behavior, including gas flow out the Culebra, MB138, and the anhydrite A and B layer, and brine flow out MB139. Differences resulted from the lower average porosity in the fixed-porosity calculations, which produced higher pressures in the waste. The higher pressures forced gas farther out the gas flow paths, and pushed brine farther out MB139. However, the maximum volume of brine that flowed laterally out MB139 (3540 m^3) was still not enough to reach the accessible environment boundary, even if the porosity of MB139 had been 0.001 (the low end of the sampled range) in the realization producing the highest brine flow.

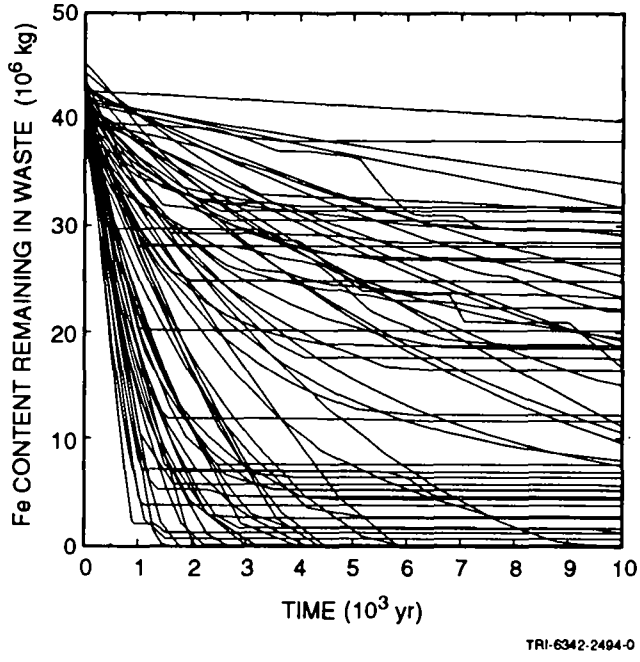

Figure 4.4-25. Iron content remaining in the waste without creep closure.

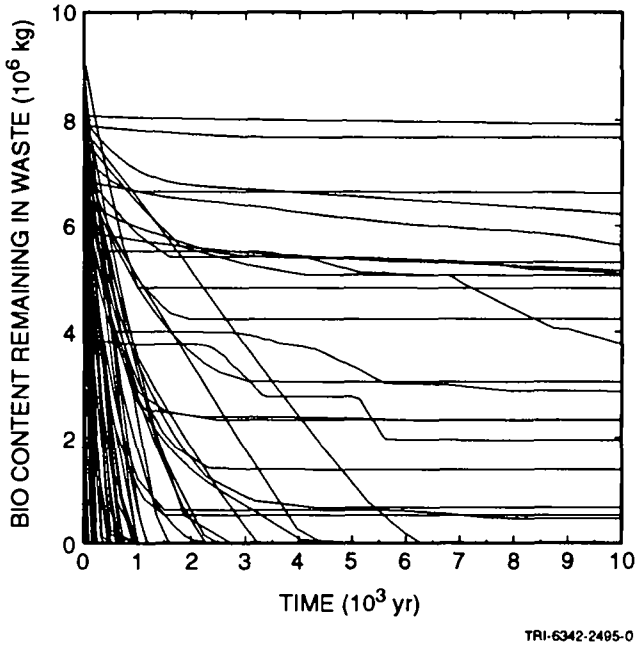

Figure 4.4-26. Cellulosic content remaining in the waste without creep closure.

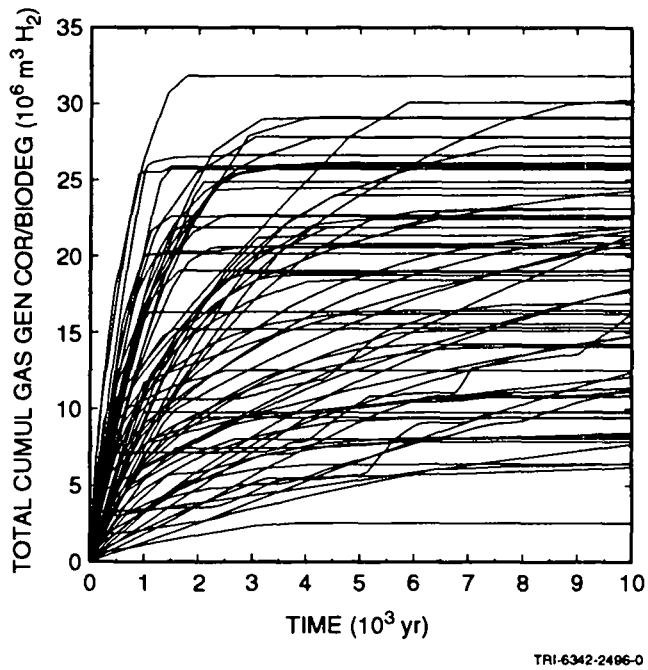

Figure 4.4-27. Total cumulative gas generated from corrosion and biodegradation, without creep closure.

4.4.4 Comparisons with 1991 Results

The 1992 undisturbed performance calculations can be compared with two earlier sets of calculations (WIPP PA Department, 1992), the first done on a single panel scale (similar to the 1992 disturbed performance calculations), and the second done on a full repository scale (similar to the 1992 undisturbed performance calculations).

The implementation of creep closure in the 1992 performance assessment resulted in significant differences in repository behavior, particularly in the pressure histories. Whereas peak pressures in the 1992 calculations are around 22 MPa, in the previous analyses they peaked at 17 MPa in the panel-scale calculations and 16 MPa in the full-repository (undisturbed) calculations. This resulted from the lower porosities obtained from creep closure. With creep closure, final waste porosities ranged from 13% to 34%. In the previous analyses without creep, closure porosities ranged from 33% to 60%. Waste pore volumes were nearly constant through time in all previous calculations, the only variation resulting from compressibility of the waste.

There was, however, no net effect on performance. Neither in previous analyses nor in the 1992 PA was there any release of contaminated brine to the accessible environment in the undisturbed scenario. This result could change when pressure-dependent fracturing of anhydrite interbeds is implemented in the model in 1993, because pressures exceeding lithostatic could cause greater migration through fractured marker beds. However, because of the high degree of nonlinearity in the model, it is impossible to predict with any certainty what effect fracturing will have until the calculations are performed.

5. DISTURBED PERFORMANCE

5.1 Repository/Shaft

5.1.1 Model Geometry

The model geometry for disturbed performance (i.e., scenarios in which the waste-disposal region is intruded by an exploratory borehole) of the repository/shaft system modeled by BRAGFLO[1] differs from that used for undisturbed performance (Section 4.1), and is based on a radial-panel approximation scaled to match the initial excavated volume of a single equivalent panel. The model uses axisymmetric geometry with the intruding borehole as the axis of symmetry (Figure 5.1-1) to represent one of the ten waste-disposal panels (labeled 1 through 10 in Figure 4.1-1) and the surrounding stratigraphy (also shown in Figure 4.1-1). Differences between this model geometry and the rectangular geometry used to simulate undisturbed performance reflect the different purposes of the two sets of analyses, and result in performance estimates from the two geometries that are not in all regards directly comparable.

Several assumptions are implicit in the axisymmetric model:

- As Figure 4.1-1 shows, the intruding borehole is located along the axis of symmetry of the cylindrically shaped equivalent panel. Strata directly above and below the panel are also represented by cylindrical elements. Strata adjacent to the panel are ring-shaped cylindrical elements surrounding the panel cylinder.

- The volume of the equivalent panel equals approximately one-tenth of the total storage volume of the repository. This smaller volume is based on the assumption that the panel seals will prevent fluid flow between each of the ten panels; therefore only one of the repository's ten panels is compromised by a borehole intrusion. The volume of this equivalent panel is assumed to equal the volume of one of the eight full-size waste-emplacement panels. The impact of allowing no flow between panels following human intrusion will be examined in future PAs.

---

1. The BRAGFLO computational model is described in Appendix A of Volume 2 of this report and in the literature cited therein. A discussion of multiphase flow through porous media, which BRAGFLO models, is provided in Section 7.2 in Volume 2 of this report.

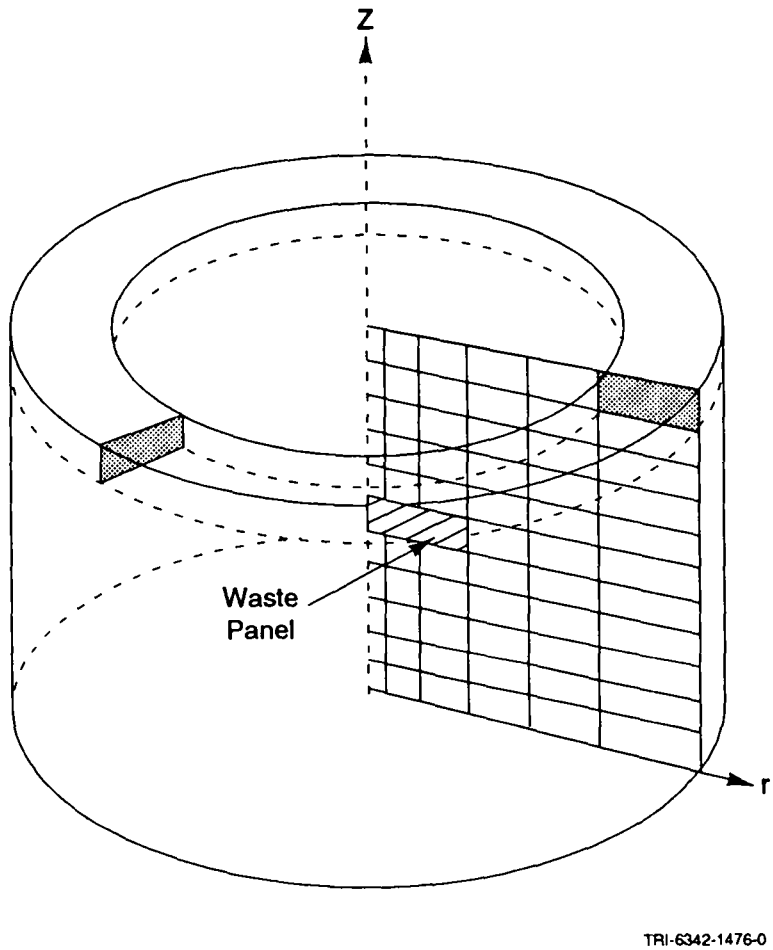

Figure 5.1-1. Schematic representation of the axisymmetric cylindrical model used for calculating disturbed performance of the repository/shaft system.

- Because flow of radionuclides up the exploratory borehole is the dominant radionuclide transport mechanism, radionuclide transport through the panel seals towards the existing shafts can be ignored. Therefore, the drift and shaft systems are omitted entirely from the model, and the mesh resolution is coarse in the strata surrounding the repository.

Figure 5.1-2 shows a vertical slice of the axisymmetric model. The region extends vertically 695 m from the top of the Culebra Dolomite Member of the Rustler Formation down to a hypothetical brine reservoir in the Castile Formation underlying the repository. The total radius is approximately 26 km. Stratigraphic units included in the model are the Culebra Dolomite, the intact halite of the Salado Formation, MB138, anhydrites A and B lumped into a single anhydrite layer, MB139, a disturbed rock zone (DRZ) surrounding the waste-storage area, and a transition zone above the DRZ overlying the waste-storage area.

5.1.2 Material Properties

Material properties for disturbed performance of the repository/shaft system are discussed in detail in Volume 3 of this report. The following material properties, which apply specifically to disturbed performance of the repository/shaft system, are discussed below in the following order:

- permeability,
- porosity,
- specific storage,
- relative permeability,
- brine and gas saturations,
- capillary pressure,
- Castile Formation brine reservoir pressure and storativity,
- radionuclide inventory, and
- radionuclide solubility.

All of the above material properties except radionuclide inventory and radionuclide solubility are used by BRAGFLO. These two material properties

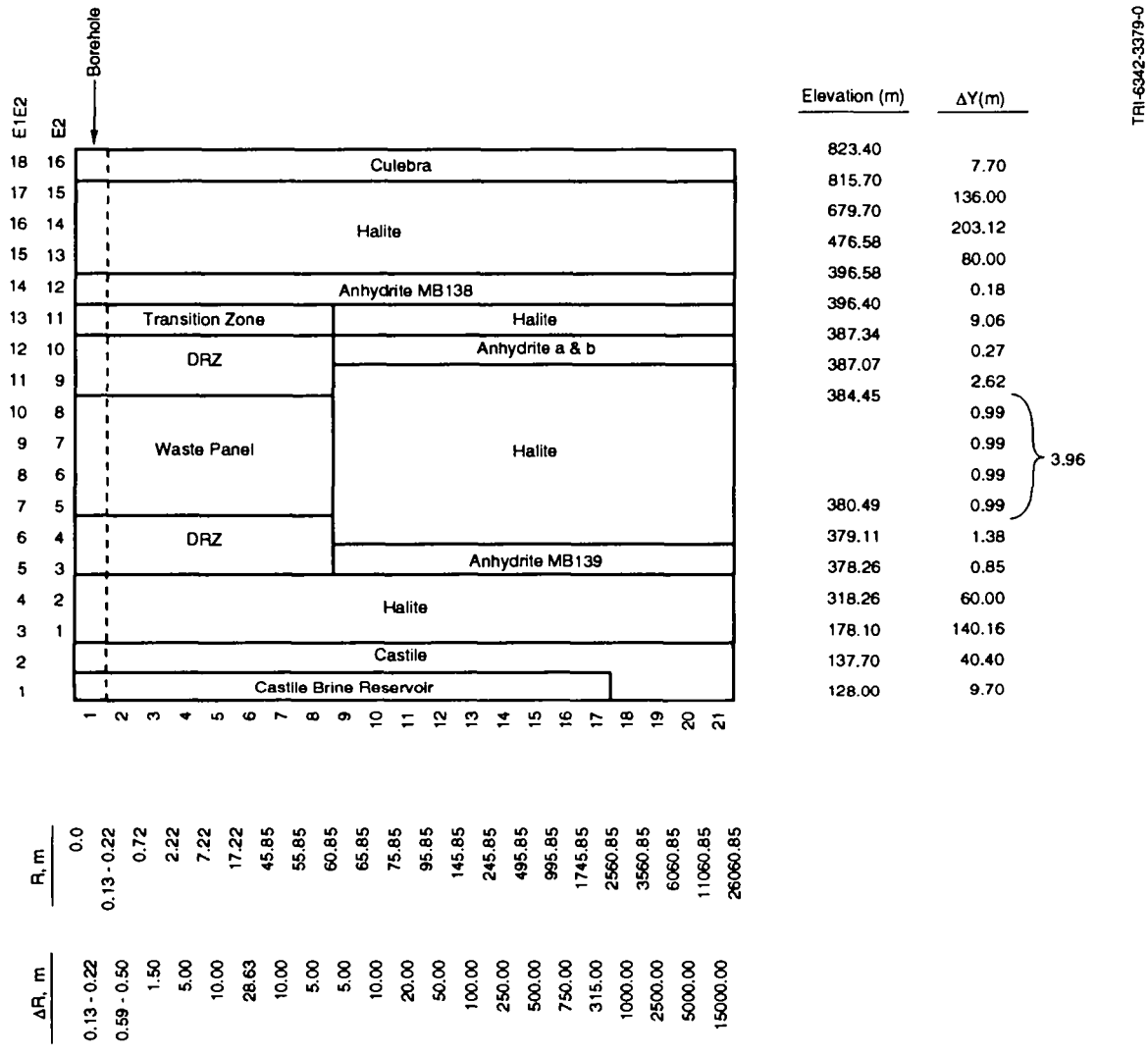

Figure 5.1-2. Geometry of the cylindrical equivalent panel model used for calculating disturbed performance of the repository/shaft system.

are input to the PANEL computational model, which is used to model radionuclide dissolution and mixing with brine flow up the intrusion borehole. PANEL is discussed further in Section 7.4 in Volume 2 of this report.

5.1.2.1 PERMEABILITY

Permeability Ranges

Assumed permeability values for the disturbed repository/shaft, shown in Figure 5.1-3, are listed below in order of increasing permeability

- Halite is assigned a range of permeability values from 1.0×10^{-24} to 1.0×10^{-19} m^2.
- The anhydrite interbeds (MB138, MB139, and anhydrite A and B) and the transition zone above the DRZ overlying the waste-disposal panel are assigned a range from 1.0×10^{-21} to 1.0×10^{-16} m^2.
- 1.0×10^{-15} m^2 is assigned to the DRZ.
- 2.1×10^{-14} m^2 is assigned to the Culebra.
- 1.0×10^{-13} m^2 is assigned to the waste.
- 1.0×10^{-11} m^2 is assigned to the Castile brine reservoir.

The Castile Formation (except for the brine reservoir) is assigned a permeability of zero. This is necessary to prevent the pressure in the brine reservoir from decaying before an intrusion occurs.

As discussed in Section 4.2.1, the permeability range for the anhydrite interbeds (1.0×10^{-21} to 1.0×10^{-16} m^2) is extended to reflect some increase in permeability associated with fracturing. The interbed fracturing process, however, is not modeled in the 1992 calculations.

Culebra Permeability

For each of the 70 transmissivity fields used in the 1992 PA analysis, an area-weighted hydraulic conductivity was computed for the repository/shaft calculations. The conductivity was estimated for a circular region 5 km in radius centered at the intrusion borehole location.[2]

2. For undisturbed calculations, this region is a 5-km-radius region centered about the waste storage area.

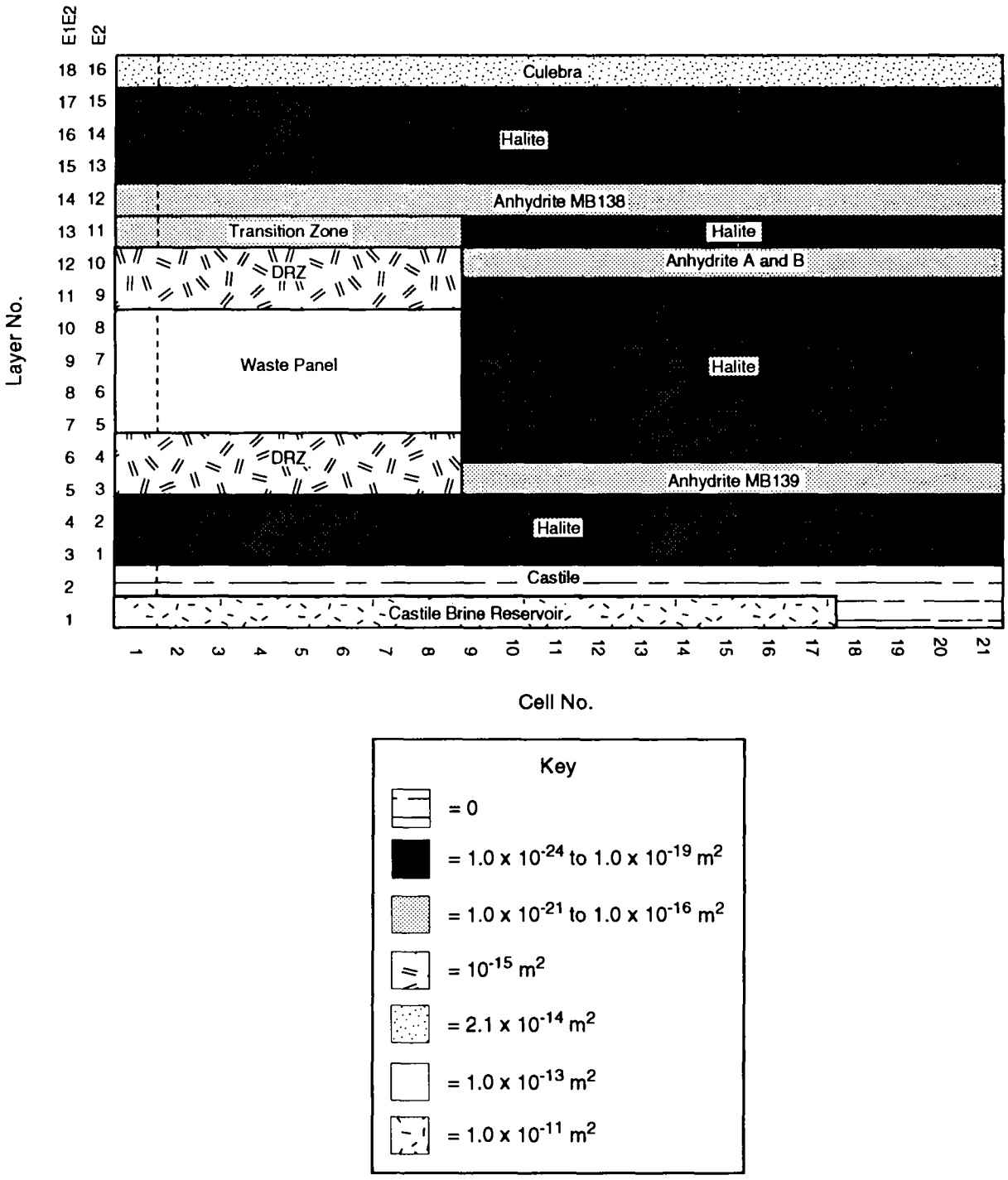

Figure 5.1-3. Permeability values for the disturbed repository/shaft system.

BRAGFLO uses intrinsic permeability (a property of the medium alone; usually referred to in this report simply as permeability) rather than hydraulic conductivity (which includes properties of the fluid) for the Culebra Dolomite above the repository. The relationship is given by

$$k = \frac{K\mu}{\rho g}, \qquad (5.1\text{-}1)$$

where k is intrinsic permeability (m^2), K is hydraulic conductivity (m/s), μ is fluid viscosity (Pa•s), ρ is fluid mass density (kg/m^3), and g is the gravitational constant (m/s^2). The median value of hydraulic conductivity was used and fluid properties for Culebra brine were obtained from the property data base. The following values were used:

$K = 2.24 \times 10^{-7}$ m/s,

$\mu = 0.001$ Pa•s,

$\rho = 1090$ kg/m^3, and

$g = 9.79$ m/s^2.

resulting in an intrinsic permeability, k, of 2.1×10^{-14} m^2.

5.1.2.2 POROSITY

Fixed (Time-Invariant) Porosity

Assumed porosity values for the disturbed repository/shaft that do not change in time, shown in Figure 5.1-4, are listed below:

- Halite, the anhydrite interbeds, and the transition zone are assigned a range of porosity values from 0.001 to 0.03.
- A slightly larger range of porosity values is assigned to the DRZ. As is explained in Section 2.4.4 of Volume 3 of this report, the DRZ range is determined by Equation 4.2-1 (Section 4.2.2.1)
- The waste prior to closure modeling is assigned a value of 0.660.

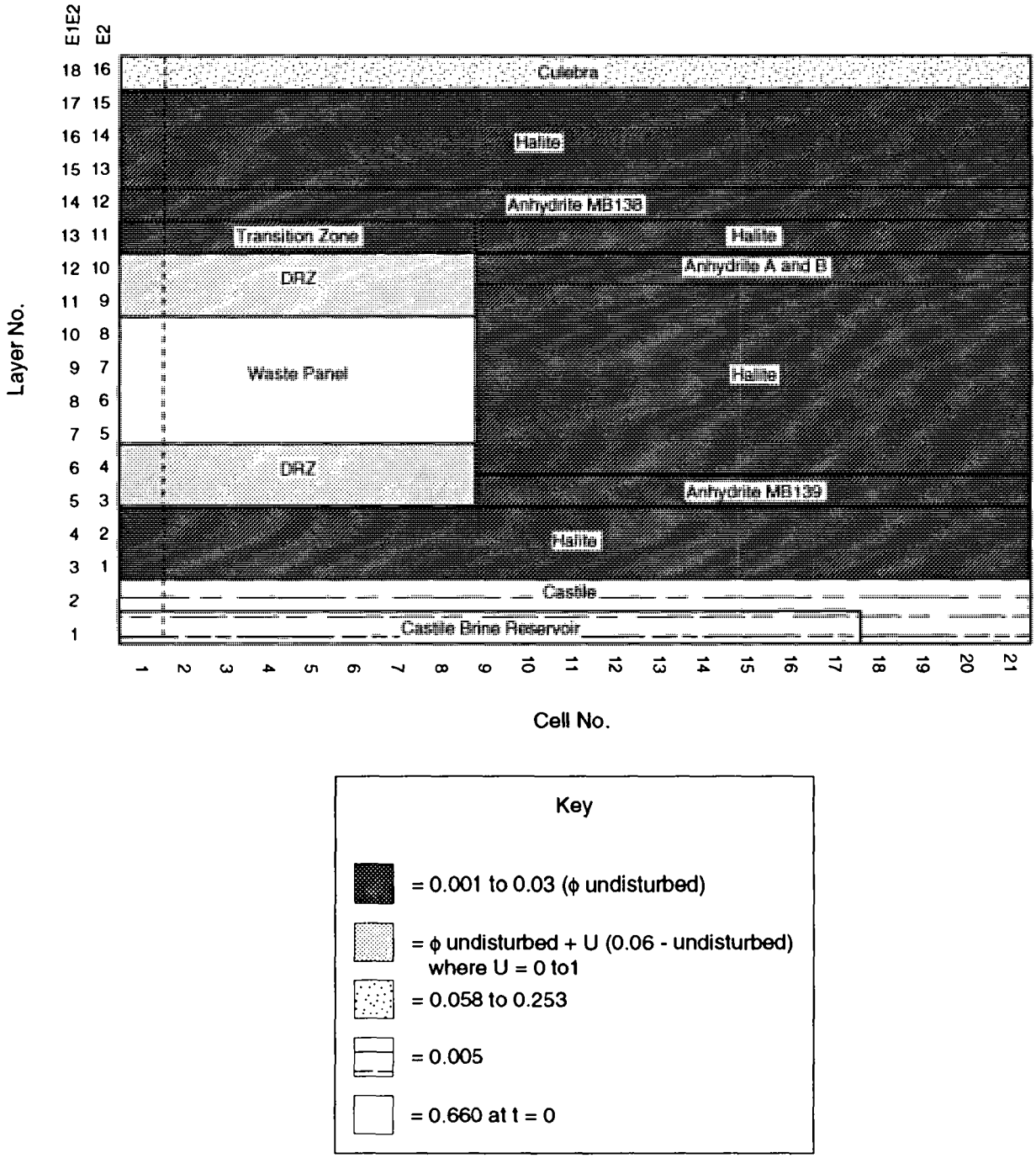

Figure 5.1-4. Porosity values for the disturbed repository/shaft system.

Variable (Time-Varying) Porosity

The 1992 calculations for the first time take into account time-varying changes in panel porosity caused by creep closure of the panel. Input is from the computer code SANCHO. The reader is referred to Section 4.2.2.2 for a complete discussion of how the SANCHO porosity results are incorporated into BRAGFLO. Observations applying specifically to the disturbed repository/shaft environment appear as footnotes to the text in Section 4.2.2.

5.1.2.3 SPECIFIC STORAGE

Specific storage values for the disturbed repository/shaft system are calculated based on the relations presented by Equations 4.2-5, 4.2-6, and 4.2-7 (Section 4.2.3).

5.1.2.4 RELATIVE PERMEABILITY[3] AND CAPILLARY PRESSURE[4]

In modeling two-phase phenomena, characteristic curves using either the Brooks-Corey formulae (Brooks and Corey, 1964) or the van Genuchten-Parker formulae (van Genuchten, 1978; Parker et al., 1987) are used (see Section 2.3.1 of Volume 3 of this report). The Brooks-Corey relative permeability model is used for two-thirds of the calculations and the van Genuchten-Parker model is used for the remaining one-third of the calculations. An index parameter (0 or 1) is sampled with these probabilities, so that either one model or the other is used in any one calculation.

Relative permeability parameters are varied and are the same for all materials except the waste and DRZ, which use a fixed set of values and the Brooks-Corey model. Residual brine and gas saturations range from 0.0 to

---

3. Relative permeability is a function of the saturation. It is a value between 0 and 1 that is multiplied by the absolute permeability to yield the effective permeability. Relative permeabilities are empirical fits of pressure drop and flow data to extensions of Darcy's law, and measurements taken at different degrees of saturation result in differing relative permeabilities (see Chapter 7 of Volume 2 and Section 2.3.1 of Volume 3 of this report).

4. Capillary pressure differences arise when the gas and brine phases flow simultaneously through a porous network (see Chapter 7 of Volume 2 and Section 2.3.1 of Volume 3 of this report).

0.4. The Brooks-Corey parameter, λ, ranges from 0.2 to 10.0. The van Genuchten-Parker parameter m is calculated from $m=\lambda/1+\lambda$. The choice of the characteristic curve model has important implications for the expected behavior of multiphase flow in porous media (see discussion in Section 4.2.4).

Threshold capillary pressures are determined from the correlation with permeability in all regions, as described in Section 2.3.1 of Volume 3 of this report. The van Genuchten-Parker capillary pressure constant, P_o, is calculated by equating the capillary pressure from each of the two models at an effective saturation of 0.5, and solving the expression for P_o. In the waste, in the DRZ, and in all excavated regions, the capillary pressure is assumed to be zero. In the 1992 performance assessment, zero capillary pressure for these regions is assumed because the capillary pressure curves are not defined for imbibition into a medium that has less than residual brine saturation. Any regions where the brine saturation starts out or may become less than residual (e.g., as a result of brine-consuming reactions) were modeled with zero capillary pressure. However, assuming zero capillary pressure may not be necessary in future calculations (see Section 4.2.4).

5.1.2.5 CASTILE BRINE RESERVOIR PRESSURE AND STORATIVITY

In disturbed performance of the repository/shaft system, an exploratory borehole can penetrate a pressurized brine pocket in the Castile Formation underlying the repository (see Section 4.3.3.2 in Volume 2 of this report). In order to calculate the effects of Castile brine flow through the waste following intrusion, brine pressure and storativity are required inputs. Initial pressure is assumed to range between 12.6 and 21.0 MPa; storativity is assumed to range between 0.2 and 2.0 m^3/Pa.

5.1.2.6 RADIONUCLIDE INVENTORY

Radionuclide inventory ranges for remote-handled (RH) and contact-handled (CH) waste vary by radioisotope. A complete list of ranges by isotope is provided in Table 3.3-1 of Volume 3 of this report.

5.1.2.7 RADIONUCLIDE SOLUBILITY

Radionuclide solubility varies by element. The lowest value is -16.5 log(molar) for plutonium and the highest value is 1.26 log(molar) for radium.

Complete information on radionuclide solubilities is provided in Section 3.3.5 of Volume 3 of this report.

5.1.3 Initial and Boundary Conditions

As with the calculations for undisturbed conditions, a major difference between the 1992 and 1991 PA calculations for disturbed conditions of the repository/shaft system is in the treatment of initial conditions (Section 4.3). The primary objective of taking a new approach in modeling the initial conditions has been to establish a more realistic pressure distribution in the formations surrounding the waste at the time the repository will be sealed. This time is referred to here as time zero. The 1992 calculations achieve more realistic time-zero initial conditions by varying the initial conditions in the repository over a 20-yr period immediately preceding time zero.

As explained in Section 4.3, it was previously assumed that excavated regions were initially at atmospheric pressure with some arbitrary degree of brine-saturation, while all other regions were fully brine-saturated at hydrostatic pressure. In reality, brine will seep in continually from the surrounding formations during the operational phase of the WIPP. Water in the brine will evaporate into the well-ventilated atmosphere of the excavations, or will be pumped out as a standard mining practice if it accumulates anywhere. Thus, formations surrounding the excavations will be partially dewatered and depressurized during the operation.

The operational phase for disturbed conditions is now modeled more explicitly, as detailed in Table 5.1-1. The important features of conditions during the operational phase are as follows:

- Because the disturbed-performance calculations are performed on a panel scale (Section 5.1.1), the operational phase is assumed to last 20 yr rather than the 50-yr period used for the repository-scale undisturbed calculations (Section 4.3). The 20-yr time period was chosen to incorporate some of the effects of other panels. While a single panel will not be likely to be open for 20 yr (except for the North and South Equivalent Panels), adjacent panels will be undergoing excavation or completing operations while each panel is being filled, and the formations surrounding a panel will be disturbed during operation.

- Except for the waste, the excavated regions, and the Culebra, the pressure distribution at 20 yr before time zero is hydrostatic

Table 5.1-1. Startup Procedure for Disturbed Calculations

I. Simulate the panel as an empty, newly excavated, gas-filled cavity	1) Set initial waste porosity to 1.0 2) Set initial waste brine saturation to 0.0 3) Set initial waste pressure to 1 atm 4) Set initial waste residual brine and gas saturation to 0.0 5) Set initial permeability to 1.0×10^{-10} m^2
II. Simulate DRZ as initially pressurized, but partially fractured	1) Set initial pressure to hydrostatic relative to sampled value of MB139 pore pressure 2) Set initial permeability to 1.0×10^{-17} m^2 3) Set initial porosity to volume average of sampled value of intact far field anhydrite and intact halite porosities (since DRZ has both) 4) Set initial brine saturation to 1.0 5) Set capillary pressure to 0.0 (so gas and brine pressures are same)
III. Let the system equilibrate for 20 yr, the approximate time span between excavation and sealing of the repository	1) Waste pressure will increase slightly (~-0.5%) 2) Brine will drain down from DRZ, leaving residual saturation 3) DRZ pressure will drop precipitously, to equal waste pressure 4) Let no creep closure occur
IV. Instantly add the waste at 20 yr	1) Reset waste pressure to 1 atm 2) Set brine saturation of waste to sampled "initial" brine saturation 3) Set waste residual brine and gas saturations to their sampled values 4) Set waste permeability to 1.0×10^{-13} m^2 5) Set waste porosity to "initial" value calculated from sampled values of volume fractions of metal and combustibles 6) Set reactant concentrations to "initial" values
V. Adjust parameters for the DRZ and Culebra	1) Change porosity to final sampled values (except for the creep closure and rock compressibility, simulating time-dependent porosity is beyond current modeling capability) 2) Adjust brine saturation so brine content of DRZ is unchanged; add gas to fill added pore volume 3) Reset DRZ pressure to 1 atm 4) Set DRZ permeability to 1.0×10^{-15} m^2 to account for fracturing
VI. Resume calculation at 20 yr, this is the time normally called t=0	1) Begin creep closure 2) Allow gas generation to begin 3) Pressures outside waste and DRZ start from 20- yr values
VII. Continue out to 10,020 yr, i.e., 10,000 yr past the time normally called t=0	

relative to the pore pressure of MB139, for which a sampled range of 12 to 13 MPa is used.

- Pressure at 20 yr before time zero in the waste and excavated regions is atmospheric, and the waste pressure is reset to this value at the end of the 20-yr period.

- Pressure in the Culebra at 20 yr before time zero is 1.053 MPa, and the far-field pressure is held at that value over the 10,020-yr calculation. (The Culebra has a fixed-pressure boundary condition, whereas the rest of the mesh uses a no-flow boundary condition.)

- The starting brine saturation will be 1.0 everywhere except in the waste panel (there are no other excavated regions in disturbed scenarios except maybe the borehole, but it doesn't exist until 1000 yr have elapsed), where the brine saturation starts at 0.0.

- At the end of the 20-yr operational period, the waste is emplaced instantaneously and assigned its sampled value of initial brine saturation, which will range from 0.0 to 0.14.

The initial-condition calculations themselves begin with initial conditions similar to those used in 1991; perhaps the greatest difference is simply in interpretation. What was called time zero last year is now called -20 yr; this is the time of initial excavation. The performance calculations begin at time zero (20 yr after the initial-condition calculation has started); this corresponds to the time of sealing of the repository.

For the initial-conditions calculation, the permeability of the excavated regions is assumed to be very high (1×10^{-10} m^2) to simulate cavities. At the end of the 20-yr operational period, any brine that has flowed into the excavated regions is ignored, since it will have evaporated or will have been pumped out of the repository. The sampled initial liquid saturation in the waste is introduced. Pressures in all the excavated regions are reset to atmospheric. Pressures there will generally be barely above atmospheric (by a few hundred pascals); they are reset to atmospheric to reestablish realistic conditions at time zero, since at the time of sealing, the excavated regions should really be at atmospheric pressure. With the exception of the DRZ pressures in all the surrounding formations, including the transition zone and the anhydrite interbeds, remain as they are at the end of the 20 yr.

In the DRZ, at least the residual saturation of brine, and possibly more, will remain, the rest having drained into the excavated region that will later be filled with waste. At time zero, porosity is assumed to change from

the initial intact halite value to the final sampled DRZ porosity. This porosity change increases the void volume. In order to conserve the volume of brine in the DRZ, the additional void volume is assumed to be filled with gas. The pressures in the DRZ will typically be slightly above atmospheric at time zero. If the pressures were left at those values when additional gas is introduced at time zero, it could result in a gas-drive condition that would cause brine to be expelled suddenly from the DRZ into the waste at time zero. To prevent this unrealistic behavior, the pressure in the DRZ is also reset to atmospheric at time zero.

The previously excavated regions will contain no brine except for the initial liquid brought in with the waste. The surrounding formations will be depressurized and dewatered to the extent expected after being exposed to ventilated air at atmospheric pressure for 20 yr. All surrounding formations are fully saturated with brine at time -20 yr. Generally, at time zero, they will still be fully brine-saturated (except for the DRZ). Except for the DRZ, the brine saturation in surrounding formations is not modified due to a change in porosity at time zero.

The calculations proceed from this calculated initial condition for the 10,000-yr performance period. The most important effect of these more realistic initial conditions is that less brine will flow into the excavated regions (including the waste), since the initial "surge" of brine that occurs upon excavation has been eliminated, and the pressure gradients in the immediate vicinity of excavations have been greatly reduced.

5.2 Results and Discussion (Disturbed Performance)

As with the results of the undisturbed performance calculations, some general descriptions of the results for disturbed performance calculations are provided here. Plots showing the time dependence of various results include all 70 realizations (vectors), which allows trends to be observed and gross behavior comparisons to be made among all the vectors. Scenarios analyzed (E2 and E1E2) are defined in Section 2.2 of this volume and described in more detail in Section 4.2.3.2 of Volume 2 of this report.

5.2.1 E2 Scenario

5.2.1.1 WASTE PANEL BEHAVIOR

The time dependence of pressures in the waste panel is shown in Figure 5.2-1 for all 70 realizations. In only two of the vectors does the peak

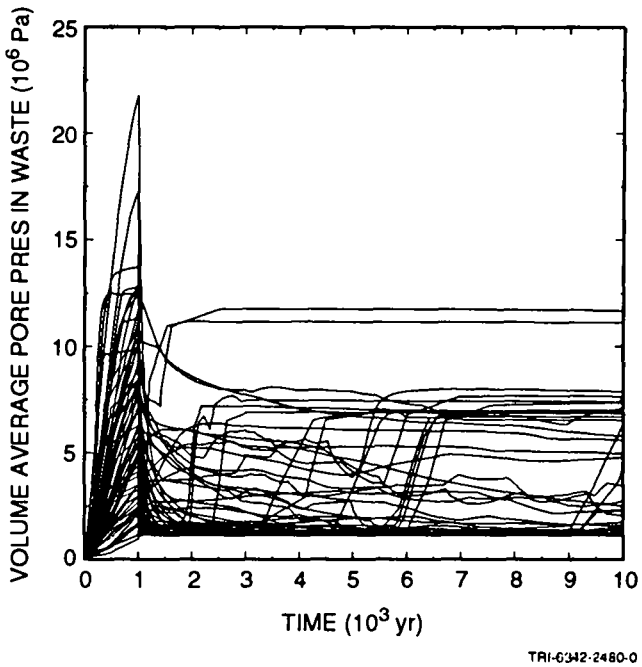

Figure 5.2-1. E2 scenario, intrusion at 1000 yr: volume average gas pressure in waste.

pressure exceed lithostatic (~14.8 MPa), probably as a result of rapid gas-generation rates and high initial brine content in the waste.

At the time of human intrusion, 1000 yr, the waste panel pressure in all of the vectors drops precipitously (except for two cases in which the pressure was so low that intrusion had no immediate effect). After intrusion, two general types of behavior can be seen. The more common response is for the pressure to continue to decrease after the intrusion. The other response is for the pressure to rise again relatively rapidly following a period of low or slowly decreasing pressure. The time lag between intrusion and repressurization lasts from 500 to over 8000 yr. During this time, gas that has filled the panel is driven up the intrusion borehole as brine flows into the waste through the anhydrite layers (principally MB139). Once the panel is filled with brine (except for residual gas and, in some cases, large trapped bubbles), brine begins to flow up the borehole, eventually filling the borehole to the Culebra. Once the borehole is filled with brine, the pressure in the waste reaches hydrostatic relative to the Culebra pressure, and then levels off. Pressure fluctuations can be seen in the pressure profiles in Figure 5.2-1 with a rapid buildup in pressure as the borehole fills with brine followed by the pressure leveling off at hydrostatic, approximately 7 MPa. There are two realizations in which

the pressure levels off at much higher values. It is not clear why in these two realizations, the pressures level off at such high values. The only parameter that distinguishes these two from the other 68 is that they have the highest sampled anhydrite permeabilities, which would have provided good communication to the higher far-field pressures. In these two vectors, there are no other extreme values among all other parameters that were sampled. However, vectors having similarly high anhydrite permeabilities did not result in final pressures intermediate between the two high ones (>11.1 MPa) and all the rest (<7.8 MPa). This may be a case where the model is extremely sensitive to certain combinations of sampled parameters, and the sampling was not sufficiently detailed in the range of parameters over which the model is most sensitive.

Panel porosities follow the same trends as seen in the undisturbed performance calculations. From the initial waste porosity of 66%, the porosity drops rapidly, bottoming out at 12% to 21% in 300 to 1000 yr. All vectors behave quite similarly, since the creep closure process, as currently modeled, does not allow much deviation from a median closure rate. Only vector 59 shows a different response; in this case, very high pressures were obtained as a result of high gas-generation rates before the human intrusion occurred, and the panel inflated to the maximum allowed porosity, 34%. None of the other vectors indicated sufficient pressure before the intrusion to cause inflation. As Figure 4.2-7 shows, the pressure in the waste must reach at least 6 MPa at low gas-generation rates and as high as 18 MPa at high gas-generation rates before expansion of the panel is noticeable. After intrusion occurs, creep closure is no longer allowed; only compressibility of the waste affects the porosity, and that effect can barely be detected in the plots of waste pore volume (Figure 5.2-2). Thus, the porosity is nearly constant after intrusion.

5.2.1.2 BOREHOLE INTRUSION EFFECTS

In 14 of the 70 realizations, brine from the waste flowed up the borehole into the Culebra. The maximum cumulative brine flow from the waste was 16,300 m^3. As Figure 5.2-3 shows, a group of five vectors has substantial flows up the borehole over the 10,000-yr performance period (ranging from 7200 m^3 to 16,300 m^3); another group of nine vectors had much lower flows (from 800 m^3 to 2600 m^3). Judging from the pressure profiles (Figure 5.2-1) there were two more vectors in which brine flow occurred into the borehole, but which had no release to the Culebra within 10,000 yr. In all of the other vectors, the panel did not fill with brine, and therefore there was no release up the borehole. In most of these cases, the permeability of the surrounding formations was simply too low to allow enough brine to flow in to fill the panel.

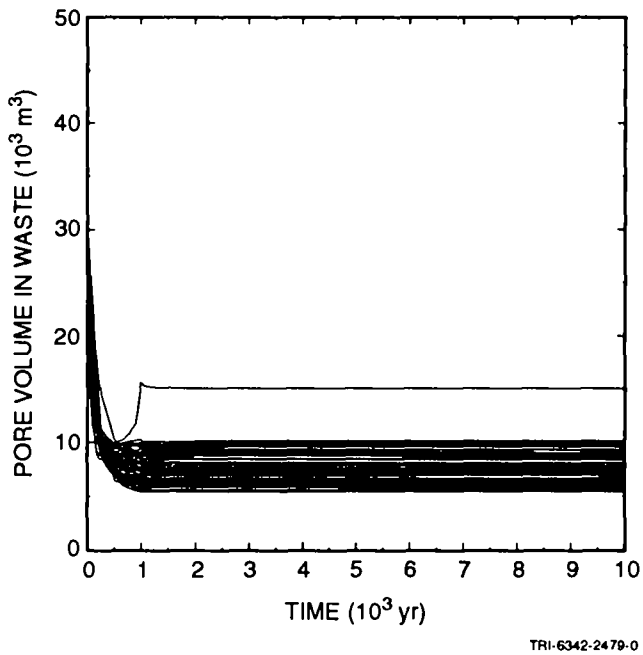

Figure 5.2-2. E2 scenario, intrusion at 1000 yr: pore volume in waste.

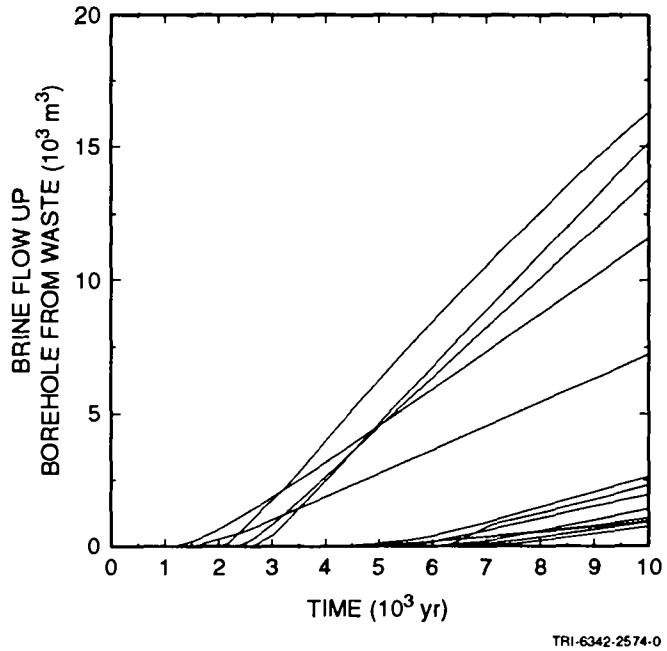

Figure 5.2-3. E2 scenario, intrusion at 1000 yr: cumulative brine flow up borehole.

5.2.1.3 FLOW IN ANHYDRITE LAYERS

It is hypothetically possible for contaminated brine to flow out one of the anhydrite layers to beyond the WIPP boundaries. This possibility cannot be ruled out completely based upon these BRAGFLO simulations alone, since specific particles within the brine have not been tracked. However, it can be shown to be highly unlikely given the assumptions of these calculations using information on the amount of brine flow from the panel. Figures 5.2-4 and 5.2-5 show cumulative brine flow from and toward the panel, respectively, in MB138. The greatest outflow was only 120 m^3, which is not enough to fill the pore space in MB138 between the panel and the WIPP boundary. The quantity of brine that flowed toward the panel in MB138 varied from zero to 8000 m^3. Given the low probability of contaminated brine even reaching MB138, which lies nearly 12 m above the panel, it appears to be unlikely that contaminated brine can flow out as far as the WIPP boundary. Similarly, Figure 5.2-6 shows that almost no brine flows out the anhydrite A and B layer, while as much as 12,000 m^3 may flow in (Figure 5.2-7). The most likely conduit for contaminated brine flow from the waste is MB139. Figure 5.2-8 shows that in one case 2500 m^3 of brine flowed out MB139 from the waste panel. Without tracking particles, it cannot be stated with complete certainty that contaminated brine has not flowed out MB139 to the WIPP boundary. However, if the porosity is as low as can be expected, 0.001, this brine would travel only 935 m radially from the panel, well short of the WIPP boundaries. Note that MB139 is the major conduit for brine inflow; as much as 38,000 m^3 of brine flowed into the waste via MB139 in these calculations (Figure 5.2-9). Based on these calculations, the only probable release conduit from the waste is up the borehole. Some contaminated brine may migrate outward along the marker beds, but not enough to constitute a release to the accessible environment. This assumes that the anhydrite layers do not fracture as the pressure in the waste increases and radial flow occurs along a uniform front. The effects of fracturing will be accounted for in the 1993 PA calculations.

5.2.1.4 EFFECTS OF CREEP CLOSURE

The same set of 70 realizations described above was repeated with the only change being that creep closure of the waste was not allowed to take place. The objective was to determine what effect creep closure, as currently implemented, has on the results. With creep closure, the panel porosity was initially 66% and dropped to 12% to 21%. In the calculations without dynamic creep closure, the waste-panel porosity was initially 19%, which is the median final-state porosity of the waste. (See Table 3.4-1 in Volume 3 of this report.) The porosity was allowed to vary only as a result of the non-zero compressibility of the waste; because the value used for

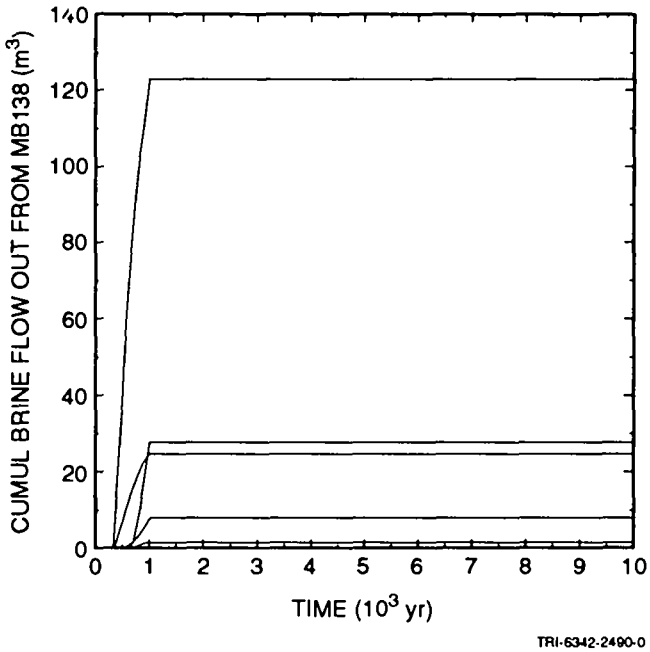

Figure 5.2-4. E2 scenario, intrusion at 1000 yr: cumulative brine flow out MB138.

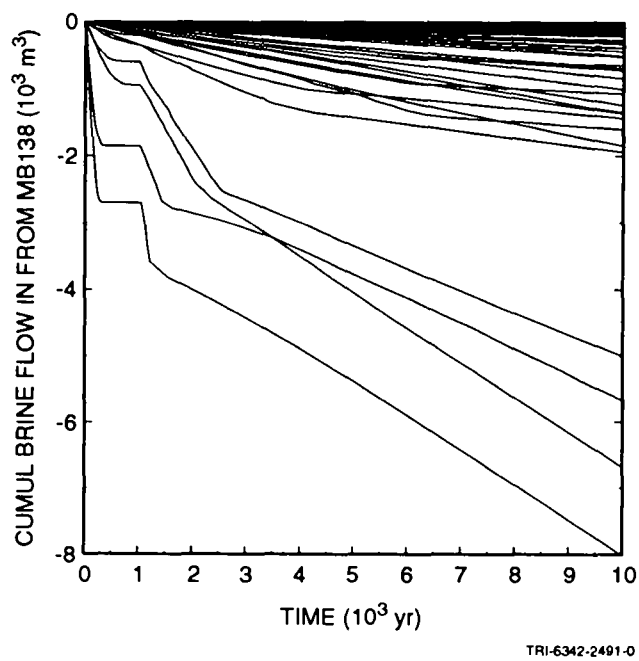

Figure 5.2-5. E2 scenario, intrusion at 1000 yr: cumulative brine flow in from MB138.

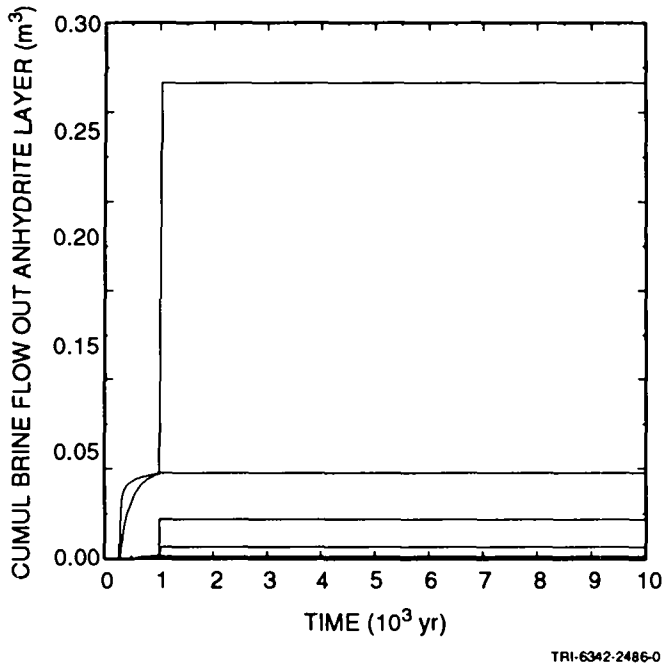

Figure 5.2-6. E2 scenario, intrusion at 1000 yr: cumulative brine flow out anhydrite layers A and B.

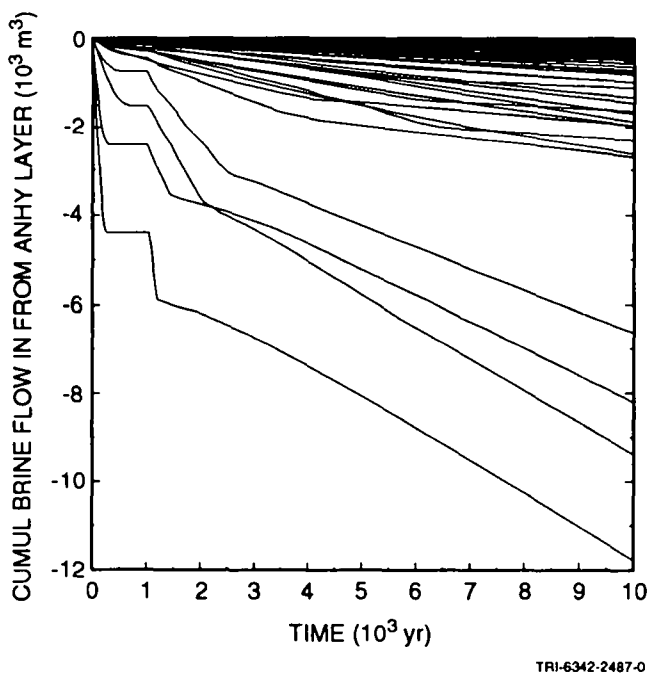

Figure 5.2-7. E2 scenario, intrusion at 1000 yr: cumulative brine flow in from anhydrite layers A and B.

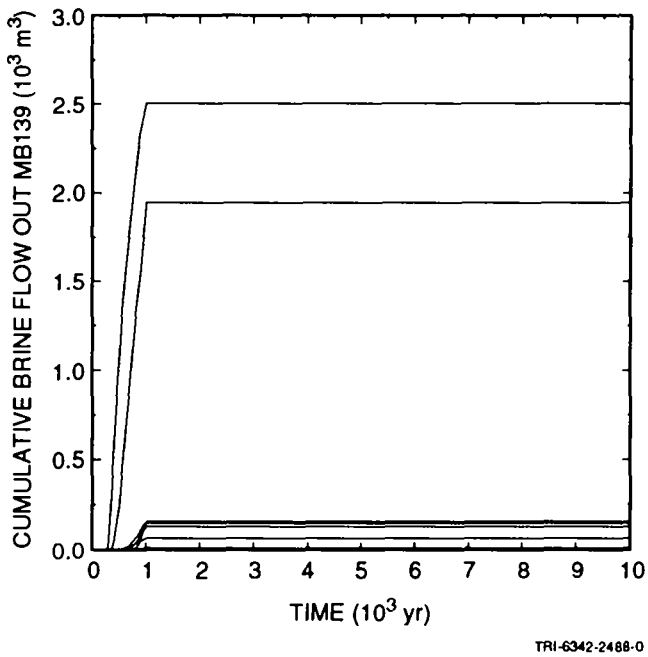

Figure 5.2-8. E2 scenario, intrusion at 1000 yr: cumulative brine flow out MB139.

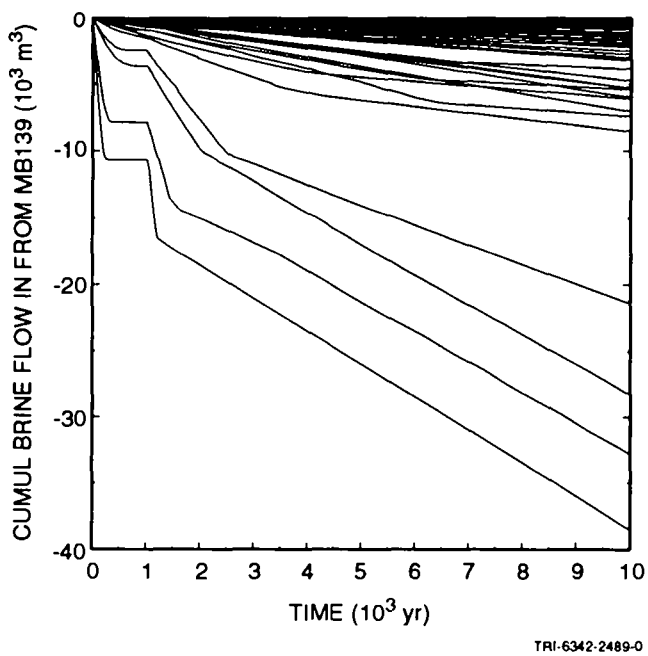

Figure 5.2-9. E2 scenario, intrusion at 1000 yr: cumulative brine flow in from MB139.

compressibility of the waste is very small (1.6×10^{-9} Pa^{-1}), the porosity varied less than 1.2% even under high pressures (Figure 5.2-10). These simulations are therefore referred to as the "fixed-porosity" case. This analysis illustrates the significance of creep closure, to the limit of current modeling assumptions, in assessing the performance of the WIPP. Although only the early time dynamics are accounted for in the current implementation, it is during that time period when the greatest changes occur, so it should be the period during which closure should have a major impact on the performance of the WIPP.

Overall, dynamically modeling creep closure results in only minor differences compared with using a fixed porosity. Transient behavior prior to the intrusion, such as pressure in the repository, may be very different. However, after 10,000 yr, total gas production is nearly identical, and the release of contaminated brine to the Culebra averages about 1% less with dynamic creep closure. Comparisons of results are complicated because the two sets of calculations must start with different initial conditions. The closure calculations start with 66% porosity and a sampled initial brine saturation in the waste, which translates into a certain initial brine volume. Because the rate and volume of gas production is strongly dependent on the initial brine volume, the fixed-porosity calculations were initialized with this same brine volume, rather than the same brine saturation. However, because the pore volume in the fixed-porosity calculations is initially much lower, the pressure in the waste rises more rapidly and much higher, even to unrealistic values. The alternative would be to start with the same initial brine saturation, but then the initial brine volume would be less, so pressures would rise much more slowly, and much less gas would be produced.

As expected, pressure profiles from the fixed-porosity runs (Figure 5.2-11) show some major differences prior to human intrusion. The most obvious differences are in the peak pressures, which now are as high as 38 MPa, compared with 22 MPa with creep closure. Pressures are generally higher without dynamic closure until the intrusion occurs. This results, as mentioned above, because the porosity used in the fixed-porosity calculations is lower initially while the brine volume is the same. With less pore volume in which to store the gas, pressures increase more rapidly and go higher, even though the amount generated is roughly the same.

Following intrusion, the waste pressures are very similar in both the dynamic closure and fixed-porosity results, since by then the porosities are of similar magnitude, much of the brine that is initially present has been consumed, and the gas has been vented to the same low-pressure sink (the

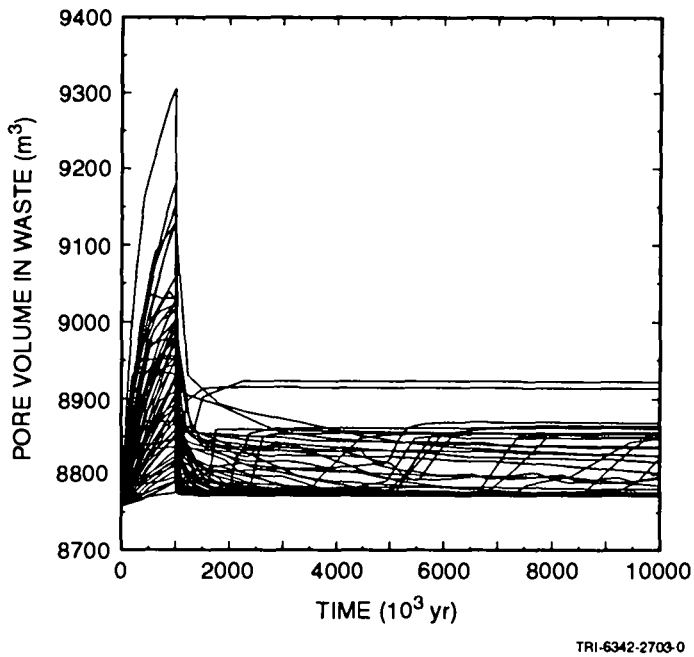

Figure 5.2-10. E2 scenario, intrusion at 1000 yr, no dynamic creep closure: waste porosity.

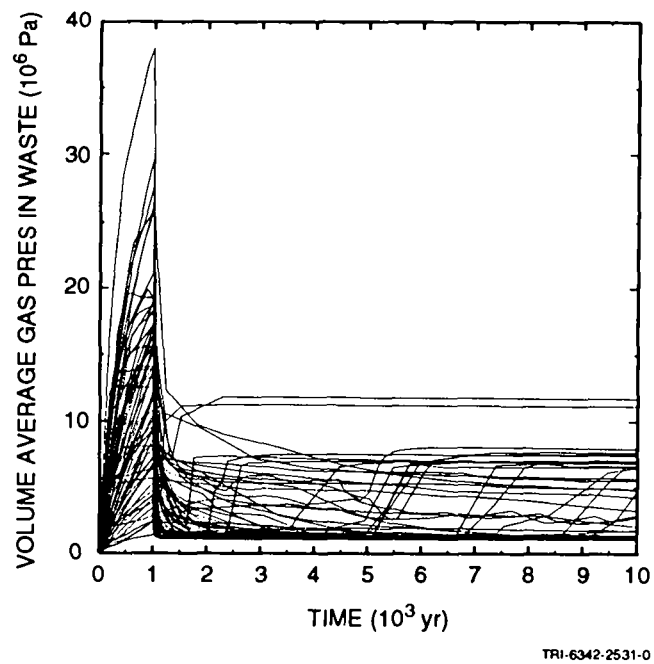

Figure 5.2-11. E2 scenario, intrusion at 1000 yr, no dynamic creep closure: panel pressure.

Culebra). Comparison of plots of the remaining iron and cellulose content for the fixed-porosity runs with those for the runs that include dynamic creep closure reveals a greater extent of reaction early on in the fixed porosity set that seemed to affect about a third of the realizations (Figure 5.2-12). However, except for lowering those particular curves, the general shape of most of the plots is quite similar. This further illustrates that the behavior in the two sets of runs differs little after intrusion.

Plots of the total cumulative gas generated show some distinct differences (Figure 5.2-13), especially in the rate of gas generation (i.e., the slopes of the curves). However, after 10,000 yr, the amount of gas that has been produced is approximately the same in both the dynamic closure and fixed-porosity calculations. The fixed-porosity calculations started with higher brine saturation. Since the gas generation rate is dependent on the brine saturation, the rate is higher initially in the fixed-porosity runs. The initial reactant concentrations are the same in both calculations, as is the initial brine volume in the waste. Thus, the total gas produced is nearly the same with and without dynamic closure.

The maximum amount of brine that flowed up the borehole is slightly less with dynamic closure (Figure 5.2-14). The largest cumulative brine flow up the borehole in the calculations with closure was 16,300 m^3; in the fixed-porosity calculations, it was 17,800 m^3. Among the nonzero flows, the average cumulative flow was 5490 m^3 in the dynamic closure calculations and 4850 m^3 in the fixed-porosity runs. In the dynamic closure calculations, 14 of the 70 vectors showed some positive flow of brine to the Culebra; in the fixed-porosity calculations, 16 vectors had some positive cumulative flow, although two of those amounted to less than 20 m^3. Among the other 14 fixed-porosity nonzero-flow vectors, the average cumulative flow was 5540 m^3, slightly more than the closure average. The net effect of including dynamic creep closure as it is currently implemented, therefore, is to decrease slightly the estimated release of contaminated brine to the Culebra, although the difference is very small, averaging less than 1%.

5.2.1.5 COMPARISONS WITH THE 1991 PA RESULTS

It is useful to compare the 1992 disturbed performance calculations with those from the 1991 performance assessment. Significant changes since 1991 include some parameter value changes (in most cases, only the range of sampled values changed; there was still some overlap in the parameter ranges), and the inclusion of creep closure in 1992. In the 1991 performance

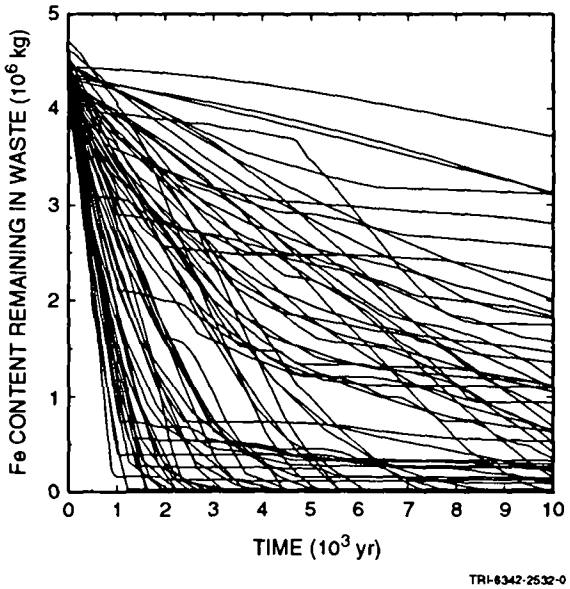

(a)

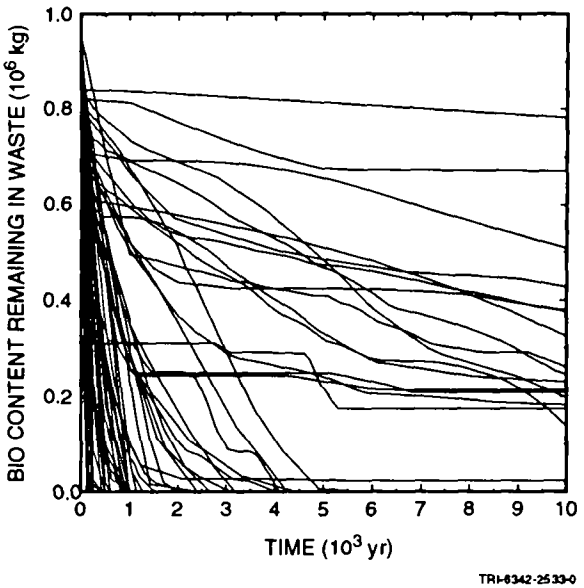

(b)

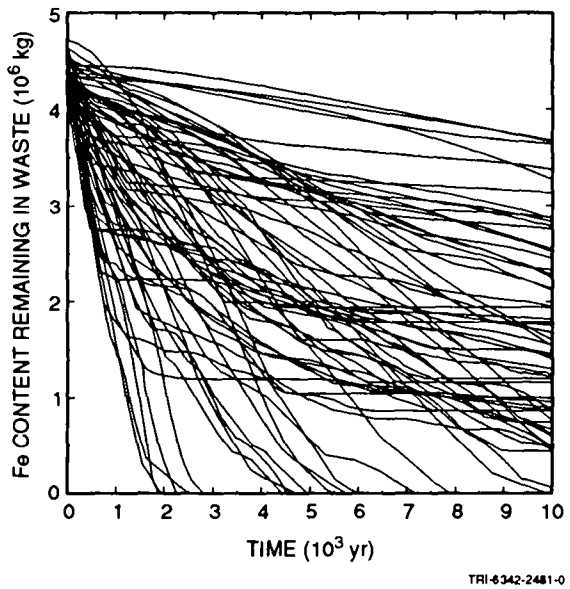

(c)

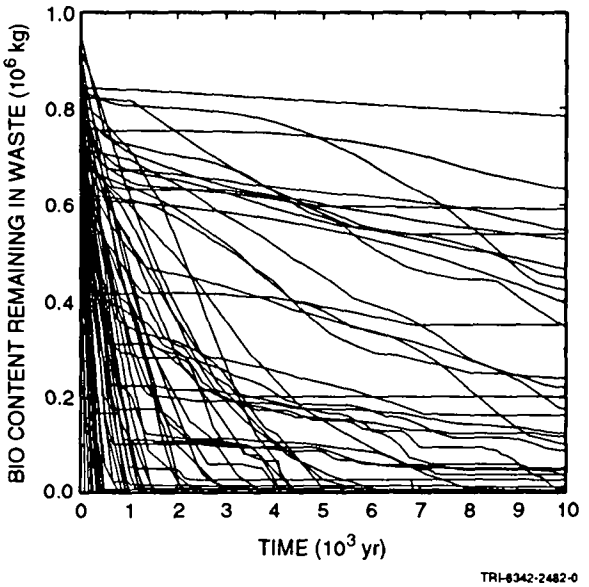

(d)

Figure 5.2-12. E2 scenario, intrusion at 1000 yr: iron and cellulosic content remaining with fixed porosity (5.2-12a and 5.2-12b) and with dynamic creep closure (5.2-12c and 5.2-12d).

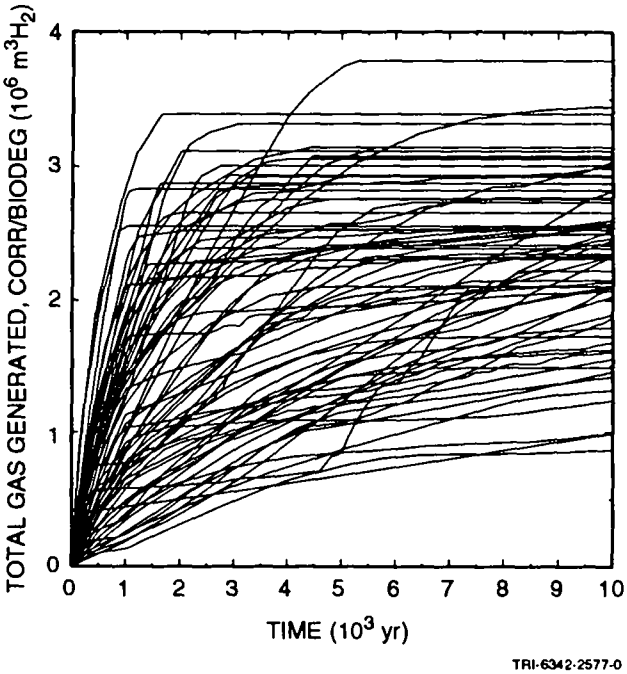

(a)

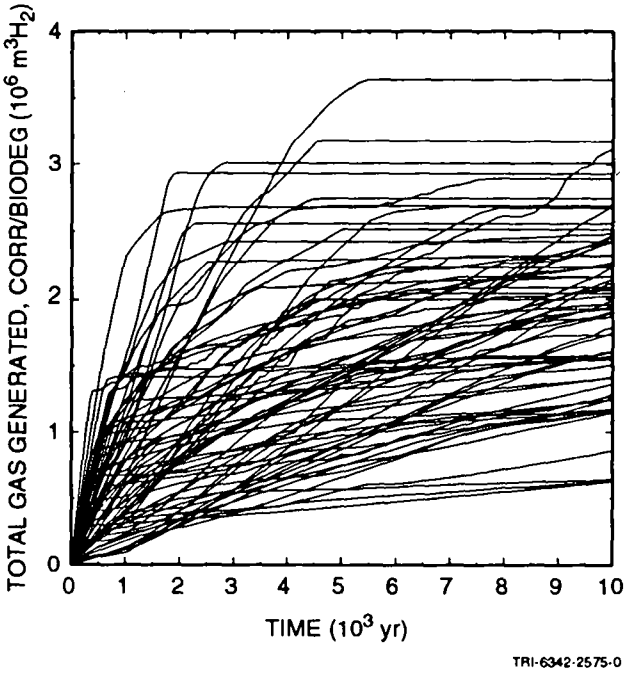

(b)

Figure 5.2-13. E2 scenario, intrusion at 1000 yr: total cumulative gas generated by corrosion and microbial degradation with fixed porosity (Figure 5.2-13a) and with dynamic creep closure (Figure 5.2-13b).

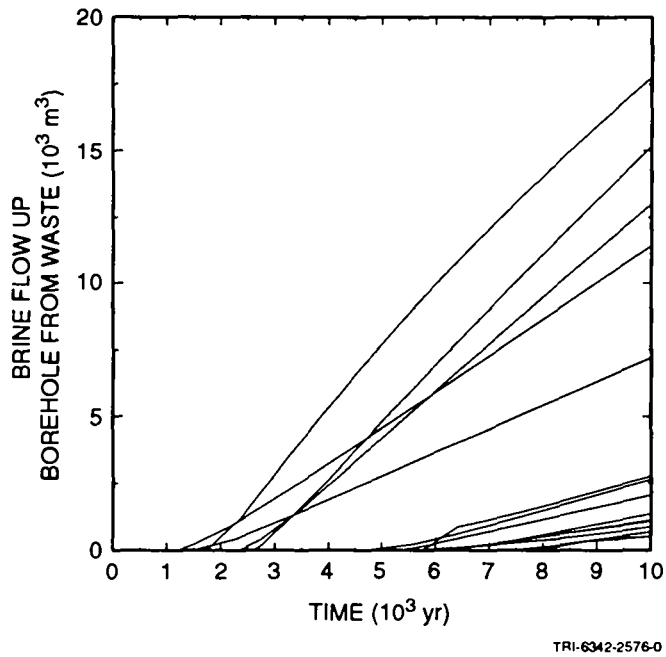

(a)

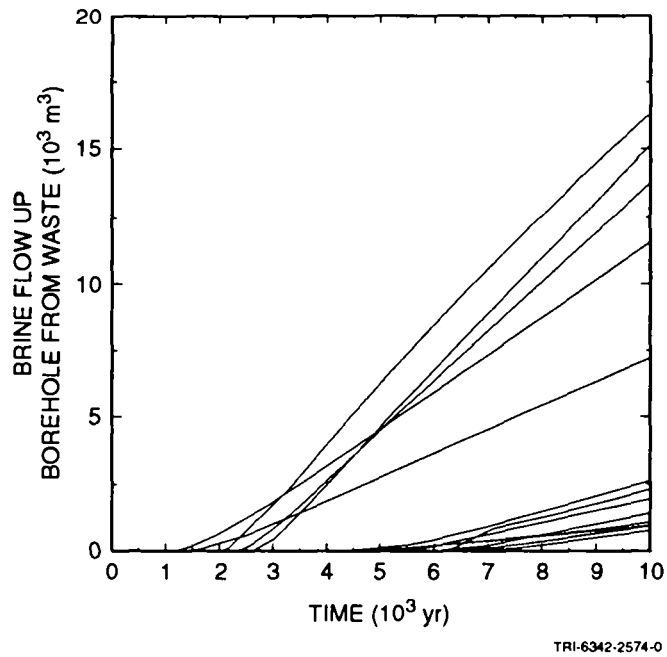

(b)

Figure 5.2-14. E2 scenario, intrusion at 1000 yr: cumulative brine flow up the borehole with fixed porosity (Figure 5.2-14a) and with dynamic creep closure (Figure 5.2-14b).

assessment, in the E2 scenario with an intrusion at 1000 years, there were 17 instances of brine release up the borehole among the 60 vectors, or 28%. In the 1992 performance assessment, 14 of 70 vectors resulted in borehole releases, or 20%. The more detailed analyses described later in this report indicate what parameter changes or conceptual model changes produced this small difference in the number of releases. In 1991, the maximum release in an E2 scenario was about 45,000 m^3; in 1992 it is 16,300 m^3. Both volumes are small relative to brine releases from the E1E2 scenario (Section 5.2.2).

The maximum pressure observed in the 1992 performance assessment, 22 MPa, is higher than that obtained in 1991, when the maximum was less than 17 MPa. However, peak pressures in excess of lithostatic were seen in only two vectors in 1992; except for those two, the highest pressures seen were about 13 MPa. And except for the two vectors in which the pressure remained at 11 to 12 MPa for most of the 10,000 yr, the pressures in the waste settled into a range from 1 to 7 MPa. In the 1991 performance assessment, more than 10% of the vectors maintained pressures higher than 7 MPa. Under "normal" circumstances, if the borehole fills with brine, the waste pressure should level off at around 7 MPa, which is hydrostatic relative to the Culebra, where the pressure is modeled as constant at 1.05 MPa. When pressures remain in excess of 7 MPa, the waste is either over-pressured with gas, or it is in excellent communication with the far field, where fluid pressures may exceed hydrostatic.

5.2.2 E1E2 Scenario

5.2.2.1 WASTE PANEL BEHAVIOR

The time dependence of pressures in the waste panel is shown in Figure 5.2-15. Up to the time of intrusion, 1000 yr, the behavior is identical to that in the E2 scenario. In only two vectors does the pressure rise above lithostatic. In most cases, the pressure rises steadily, at widely varying rates, until the intrusion occurs. From that point on, the behavior differs greatly from the E2 scenario. In the majority of vectors, the pressure undergoes some rapid transients immediately following the intrusion. In some cases, there is a sudden depressurization when the intrusion borehole connects the pressurized panel with the lower-pressure Culebra. In other instances, the pressure in the waste is still low at the time of intrusion, and it increases suddenly when the borehole connects the panel with the pressurized Castile brine reservoir. In most of the runs, a relatively steady pressure is attained fairly quickly at a value intermediate between the pressure in the Castile and in the Culebra. These pressures range from about 7.5 MPa to 13.7 MPa. In about one-third of the vectors,

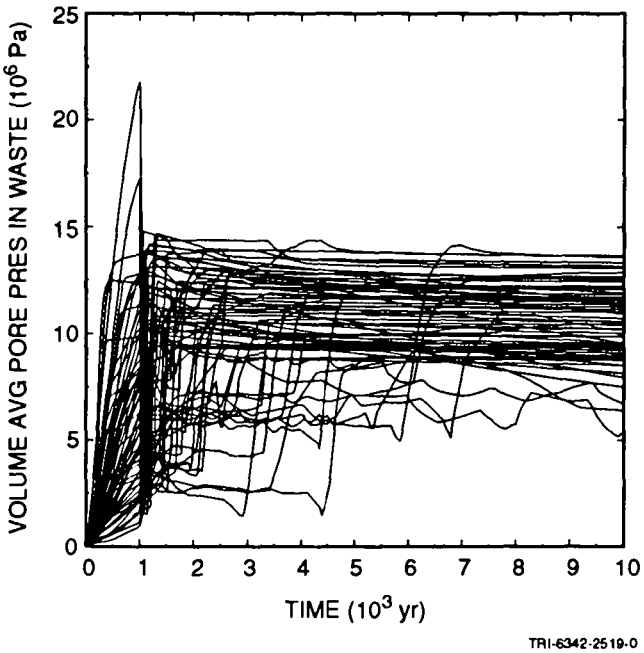

Figure 5.2-15. E1E2 scenario, intrusion at 1000 yr: panel pressure.

there is a time lag between the intrusion and attainment of this steady pressure. During this period, panel pressure is not yet strongly influenced by the Castile pressure because of low borehole permeability, small borehole diameter, or sufficient gas generation in the waste to retard flow of brine up the borehole. Whatever the cause, it takes anywhere from a few hundred to several thousand years for good communication to be established between the Castile and the Culebra, which will occur once the borehole becomes completely filled with brine from the Castile to the Culebra. A few vectors show erratic pressure behavior over the full 10,000 yr. This behavior results from borehole permeabilities that are too low to keep the waste panel filled with Castile brine. Pressures in the waste in these realizations fluctuate as some brine starts to flow up the borehole from the waste, but then is displaced as gas generation consumes brine and newly generated gas refills the borehole. Given sufficient time (perhaps tens of thousands to hundreds of thousands of years), these pressures would eventually level out at hydrostatic pressure relative to the Culebra, after all gas generation ceases and brine from the far field refills the panel.

Because creep closure is not modeled after the intrusion occurs, the waste porosities in the E1E2 scenario are nearly identical to those in the E2 scenario. The only differences result from different pressure histories after the intrusion, which affects porosity because the waste is still

assumed to be compressible. However, the effects on porosity are insignificant.

5.2.2.2 BOREHOLE INTRUSION EFFECTS

In all but two realizations, brine flows up the intrusion borehole from the waste (Figure 5.2-16). Cumulative nonzero brine flows at 10,000 yr range from 156 to 9.8 x 10^5 m^3. There is a strong correlation between borehole permeability and cumulative brine flow up the borehole. The three vectors with the highest brine flows also have the highest sampled borehole permeabilities. It is assumed that all of this brine is contaminated with radionuclides from the waste. As currently modeled, most of this brine would flow directly from the Castile to the Culebra with little mixing with the waste unless mixing was assumed. However, the E1E2 scenario involves lateral flow through the waste, rather than simply vertical flow through the waste, so all of the brine flowing up the borehole is assumed to flow through the waste. (Calculation of radionuclide releases, using PANEL [see Table 2.4-1], involves elemental solubility and radionuclide inventory, in addition to brine flow rate.)

The amount of brine that flows through the waste is large compared to the E2 scenario; the maximum cumulative flow is a factor of 60 higher. This

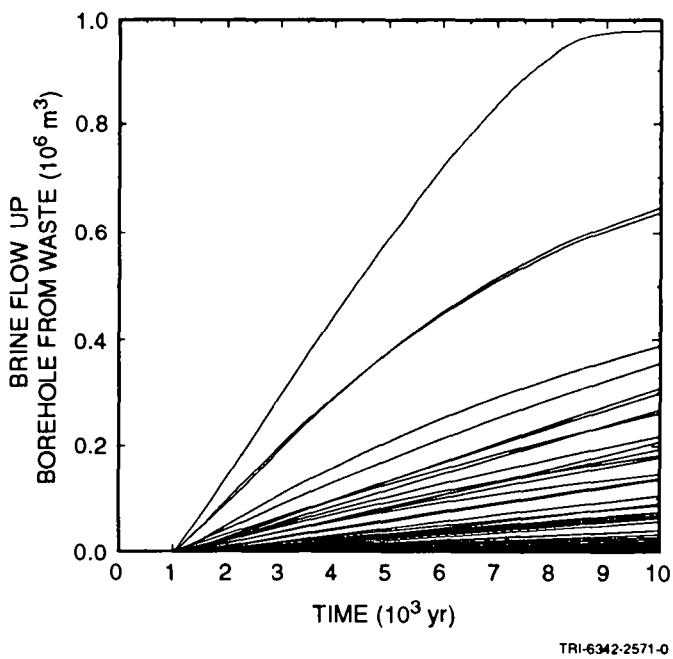

Figure 5.2-16. E1E2 scenario, intrusion at 1000 yr: cumulative brine flow up the borehole.

has a major effect on corrosion and biodegradation. The ready availability of brine results in all of the iron content in the waste being consumed in all but five realizations, and all of the cellulose being consumed in all but two realizations (Figures 5.2-17 and 5.2-18). Compare this with the E2 scenario, in which the only brine available had to flow in from the far field through the relatively impermeable (compared to the intrusion borehole) anhydrite layers. In the E2 scenario, iron remained in the waste after 10,000 yr in 55 of the vectors (Figure 5.2-17) and cellulose was unreacted in 30 vectors (Figure 5.2-18).

The effect of this greater consumption of degradable materials in the waste is to generate more gas. Whereas the maximum cumulative gas generated in the E1E2 scenario is nearly identical to that in the E2 scenario (3.60×10^6 m^3 H_2 at reference conditions vs. 3.64×10^6 m^3), the average cumulative gas generated was 2.6×10^6 m^3, compared with 2.0×10^6 m^3 in the E2 scenario. Most vectors in the E1E2 scenario resulted in 1.4×10^6 m^3 to 3.3×10^6 m^3 H_2 (Figure 5.2-19), compared to a lower and broader range of 0.6×10^6 m^3 to 3.1×10^6 m^3 for the E2 scenario (Figure 5.2-19b). However, because of the much higher brine flow rates in the E1E2 scenario, the higher gas-generation rates and volumes affected the release of brine up the borehole less than in the E2 scenario, in which the presence of gas tended more to interfere with the flow of brine.

5.2.2.3 BRINE FLOW IN ANHYDRITE LAYERS

The behavior of the anhydrite layers in the E1E2 scenario is essentially identical to the E2 scenario. Only in four vectors was there any net outward flow of brine from the waste panel, and the maximum amounted to only 68 m^3. In all other vectors, the net cumulative flows were inward (Figures 5.2-20), and ranged up to 36,000 m^3. The bulk of the flow (typically 65%), came in from MB139; about 20% came in through anhydrite A and B, and the remainder (about 15%) came through MB138. In considering possible lateral flow of contaminated brine to the accessible environment, it may be more useful to look at absolute outward flows, rather than net flows, since brine that has flowed outward may leave adsorbed contaminants even after the flow has been reversed. In this case, there were four vectors in which there was no outward flow at all. The maximum cumulative outward flow in any of the anhydrite layers was 2500 m^3 in MB139 (Figure 5.2-21). Even at the minimum porosity of 0.001, under the present modeling assumptions this brine could have traveled out MB139 no more than 500 m. So, as with the E2 scenario, it is improbable that contaminated brine can reach the accessible environment (2500 m from the panel) by means of lateral flow through the anhydrite layers, assuming again that these layers do not fracture as the pressure in

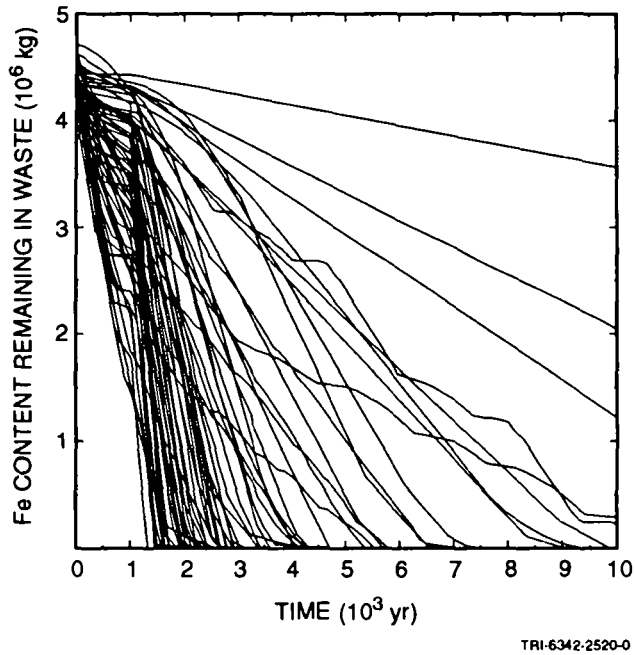

Figure 5.2-17. E1E2 scenario, intrusion at 1000 yr: iron remaining in waste.

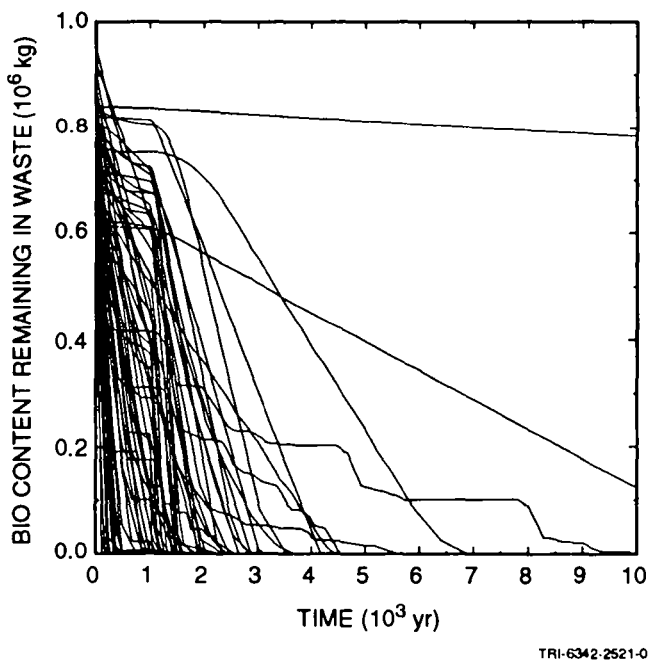

Figure 5.2-18. E1E2 scenario, intrusion at 1000 yr: cellulosics remaining in waste.

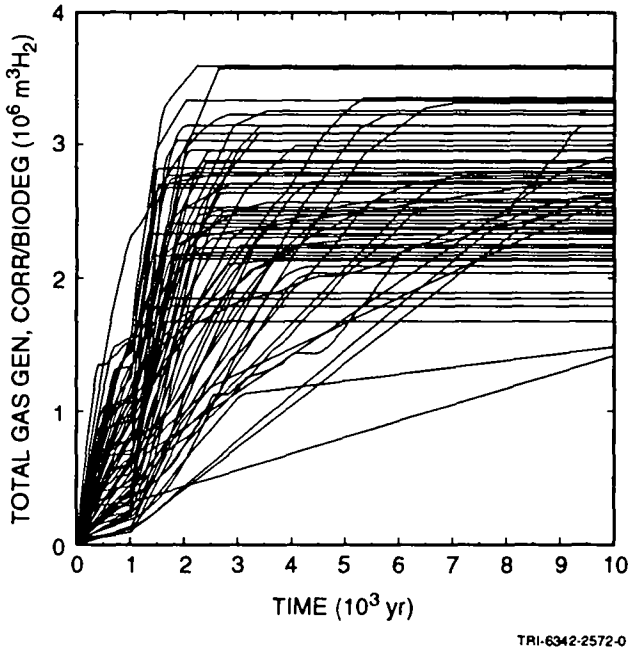

Figure 5.2-19. E1E2 scenario, intrusion at 1000 yr: total cumulative gas generated by corrosion and microbial biodegradation.

the waste increases. (However, note that the pressure in the waste exceeded lithostatic in only two of the vectors, so it is difficult to determine how much impact fracturing may have on radionuclide releases resulting from the E1E2 scenario. Fracturing of anhydrite layers will be included in next year's PA calculations.)

5.2.2.4 EFFECTS OF CREEP CLOSURE

The comments made above on the results of the E2 scenario calculations apply to E1E2 scenario almost without change. In the fixed-porosity calculations, the pressures reach similarly unrealistically high values, up to 38 MPa (Figure 5.2-22). The reasons are the same: The initial pore volume has been decreased as the initial porosity was reduced from 66% in the closure calculations to 19% in the fixed porosity calculations, while initial brine volume, rather than brine saturation, was conserved. Gas was produced at roughly the same rate, but with less storage volume in the panel, the pressure rose more rapidly. As a result of this pressure increase, the porosity increased, but only slightly (to a maximum of 20.2% at the maximum peak pressure). Unlike the E2 scenario, however, most of the reactants (iron and cellulose) are consumed within 10,000 yr in the E1E2 scenario, regardless of how the waste porosity is modeled, so the cumulative gas volume

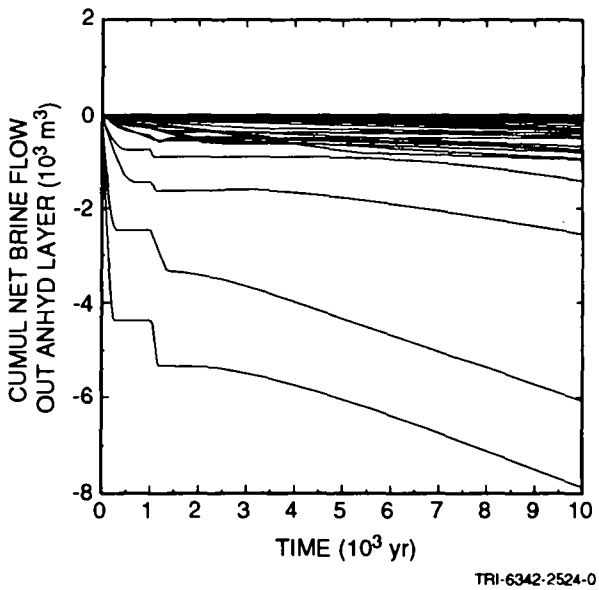

(a)

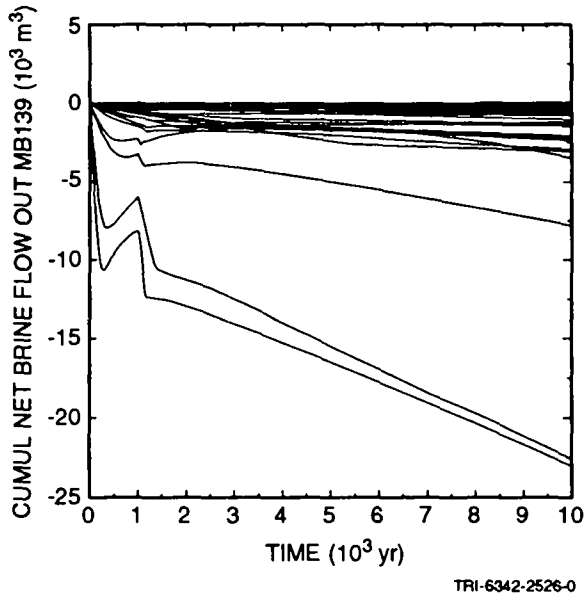

(b)

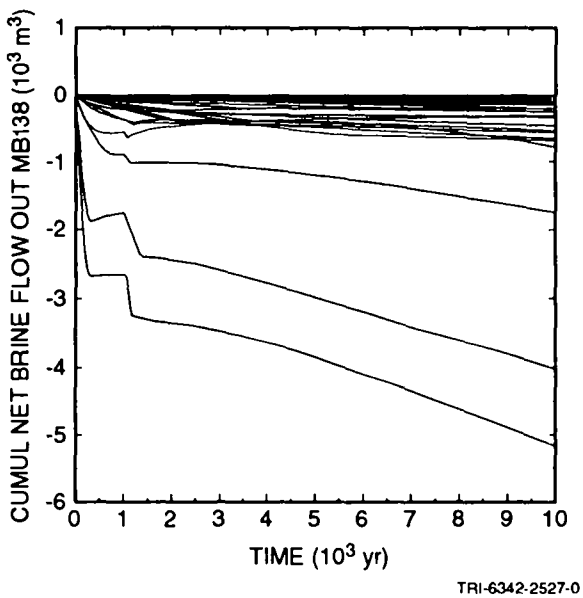

(c)

Figure 5.2-20. E1E2 scenario, intrusion at 1000 yr: cumulative net brine flow out anhydrite A and B (Figure 5.2-20a), MB139 (Figure 5.2-20b), and MB138 (Figure 5.2-20c).

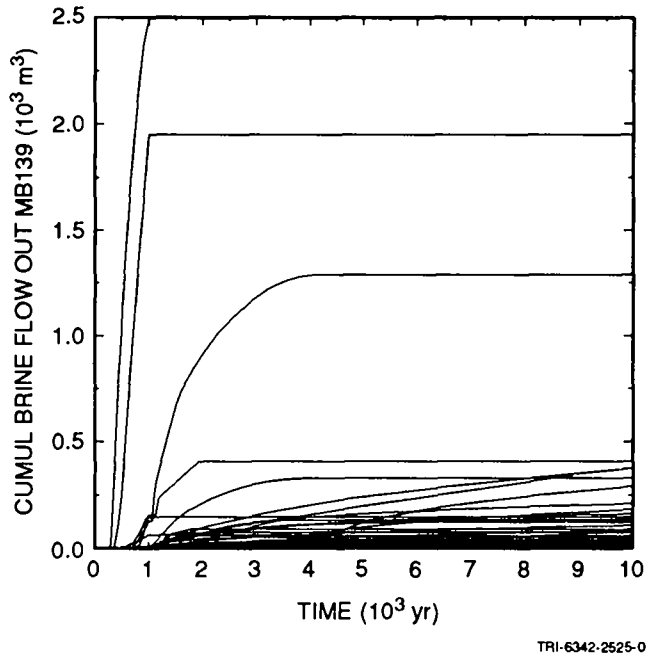

Figure 5.2-21. E1E2 scenario, intrusion at 1000 yr: cumulative absolute brine flow out MB139.

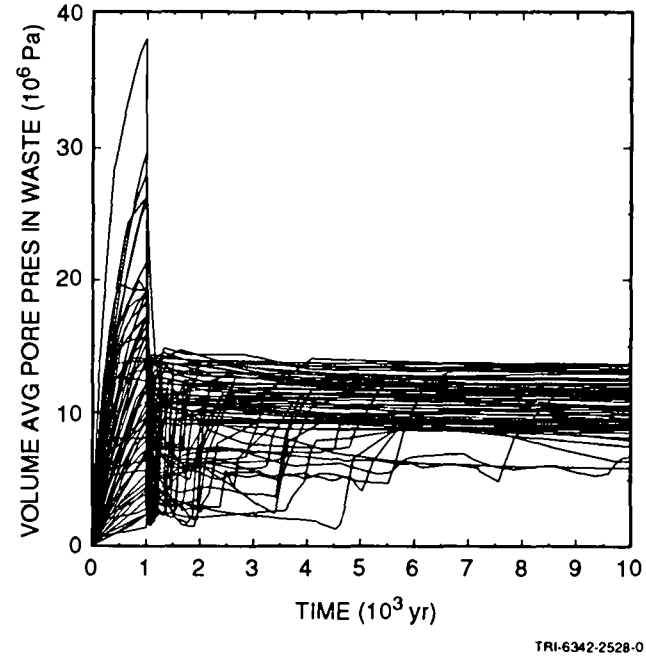

Figure 5.2-22. E1E2 scenario, intrusion at 1000 yr: pressure in waste, without dynamic creep closure.

generated differs very little in the fixed-porosity calculations from the calculations with dynamic creep closure.

The fixed-porosity calculations resulted in cumulative brine flows up the borehole that were nearly identical to those from the closure calculations (Figures 5.2-16 and 5.2-23). Whereas the maximum cumulative flow in the closure calculations was 9.79×10^5 m^3, it was 9.77×10^5 m^3 in the fixed porosity calculations. The average flow in the closure calculations was 9.71×10^4 m^3 and 9.70×10^4 m^3 in the fixed porosity calculations. In both sets of runs there were only two vectors that produced zero brine flow to the Culebra. Despite some major effects on transient behavior (such as waste pressures), the current dynamic creep closure model has no net effect on the performance assessment compared with the fixed-porosity model.

5.2.2.5 COMPARISON WITH THE 1991 PA RESULTS

The maximum cumulative release of contaminated brine to the Culebra is higher than in the 1991 performance assessment: 1.24×10^6 m^3, compared with 6.75×10^5 m^3 in the 1991 performance assessment. This can be attributed almost entirely to the borehole permeabilities used in those particular vectors. As long as pressure in the Castile is high enough to drive brine all the way to the Culebra, and borehole permeability is high, then cumulative flows to the Culebra are proportional to borehole permeability. This observation reflects the dominant role that borehole permeability plays in controlling flows in an E1E2 intrusion. Confirmation of that observation is provided by the following results: The ratio of the maximum flow in the 1992 performance assessment to the maximum flow in the 1991 performance assessment is 1.84; the ratio of the borehole permeability in the 1992 vector with maximum flow (1.0×10^{-11} m^2) to the borehole permeability in the 1991 vector with maximum flow (5.5×10^{-12} m^2) is 1.82. Under these conditions (high borehole permeability and sufficiently high Castile pressure), none of the other sampled parameters has much impact on releases to the Culebra. However, when the borehole permeability is not high, other parameters come into play. This is apparent when one considers that the average cumulative flow to the Culebra calculated in the 1992 performance assessment is 126,000 m^3, whereas the average obtained last year was 70,400 m^3, even though the ranges of borehole permeabilities and diameters and Castile pressures that were sampled were the same in 1992 as in 1991.

In the 1992 performance assessment, only two of the 70 realizations resulted in zero flow to the Culebra. In the 1991 performance assessment, there were also only two realizations (out of 60) with zero flow. In both the 1991 and 1992 calculations, E1E2 intrusions almost always result in releases to the Culebra.

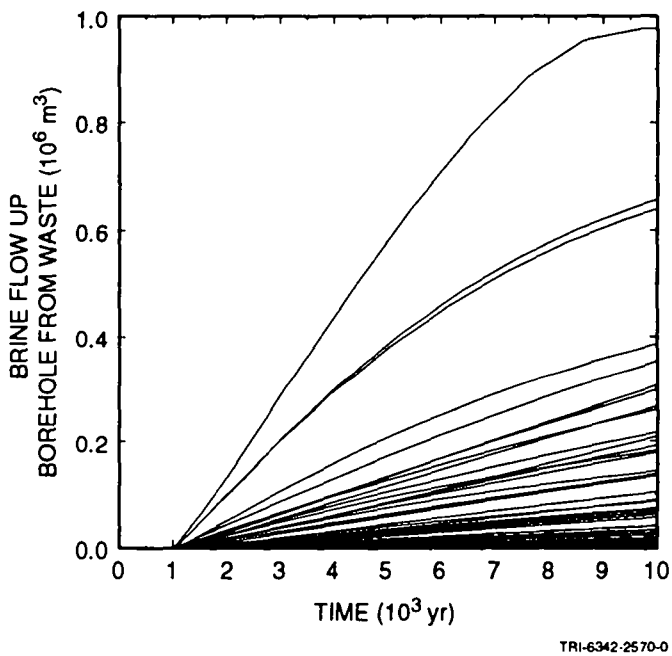

Figure 5.2-23. E1E2 scenario, intrusion at 1000 yr: cumulative brine flow up borehole without dynamic creep closure.

6. DISTURBED PERFORMANCE: CULEBRA GROUNDWATER FLOW AND TRANSPORT

This chapter describes the implementation of the 1992 PA model for groundwater flow and radionuclide transport in the Culebra Dolomite Member of the Rustler Formation. The computer codes used are SECO-FLOW for groundwater flow and SECO-TRANSPORT for radionuclide transport. Both codes are described in Chapter 7 and Appendix C of Volume 2 of this report. Flow is calculated in seventy different transmissivity fields that are described in Chapter 7 and Appendix D of Volume 2 of this report and by LaVenue and RamaRao (1992).

6.1 Conceptual Model

The conceptual model for flow in the Culebra Dolomite Member of the Rustler Formation is essentially unchanged from that used in the 1990 and 1991 PA (Bertram-Howery et al., 1990; WIPP PA Division, 1991b, Section 6.1). As discussed in Chapter 7 of Volume 2 of this report, conceptual models for transport have been modified to allow a more complete representation of the possible affect of clay linings in fractures on both physical and chemical retardation. Geologic and hydrologic information supporting the flow and transport models are described in Chapter 2 of Volume 2 of this report. Major aspects of the models are as follows.

- **Single-porosity Darcian flow.** Results of hydrologic tests on wells completed in the Culebra are consistent with the response of a heterogeneous medium obeying Darcy's law (Jones et al., 1992). Results of some well tests indicate dual-porosity response during the early part of the tests (Beauheim, 1987; Jones et al., 1992). This is interpreted to be caused by disequilibrium between pressure in coextensive fracture and matrix porosity sets. Because the time of pressure equilibration between the porosity sets is much smaller than the time scale of processes considered in the human-intrusion scenario, the Culebra is modeled as a heterogeneous single-porosity medium for the purpose of fluid-flow calculations. (Dual-porosity effects on transport are considered, however, as discussed below.)

- **Two-dimensional flow.** Most hydrologic test wells in the Culebra are completed across the entire vertical extent of the unit. Parameters derived from tests on these wells are therefore composite or average values over the vertical extent of the member. Although flow is known to be localized to particular elevations within the Culebra at several wells (Mercer and Orr, 1979), there is insufficient information to

characterize vertical variability of hydrologic properties within the Culebra. A vertically integrated two-dimensional model has therefore been adopted.

- **No flow through upper and lower boundaries.** Potentiometric differences between the Culebra and other members of the Rustler Formation suggest that vertical flow between the members is extremely slow over the WIPP and in much of the surrounding study area (Beauheim, 1987; Brinster, 1991). The present conceptual model includes impermeable upper and lower boundaries on the Culebra. The validity of the assumption that leakage between the Culebra and the over- and underlying units can be neglected is uncertain, and the importance of possible vertical flux will be examined when information is available from regional three-dimensional hydrologic modeling being conducted by the SNL Fluid Flow and Transport Department.

- **Flow in Nash Draw parallel to the axis of the draw.** Nash Draw is believed to be a major sub-surface drain for the Rustler Formation west of the WIPP (Davies, 1989; Brinster, 1991). Groundwater flow in the draw is therefore assumed to parallel the topographic axis of the draw.

- **Pressure equilibrium and flow prior to WIPP construction.** Time constants of pressure changes due to compression of the fluid and matrix are small compared to time constants of fluid density changes, transmissivity changes, or other transient processes affecting pressure. For any subdomain of the Culebra, and in the absence of fluid sources or sinks within the subdomain, the Culebra pressure is assumed to be currently in equilibrium with pressures around the boundary of the subdomain.

- **Future flow-field transients induced by external changes.** The future state of the Culebra flow field is assumed to differ from the present state through regional climate change. Climate change is assumed to affect recharge and discharge rates external to the model domain, and therefore to influence flow within the model domain through a change in boundary pressures (memorandum by Swift in WIPP PA Division, 1991c; WIPP PA Division, 1991b; Swift, 1993).

- **Transport decoupled from flow.** In the human intrusion scenario, one or more boreholes create a long-term connection between the repository and the Culebra. Hydrologic properties of the borehole limit potential fluid discharge to the Culebra to approximately 80 m^3/yr. This rate of fluid injection is assumed to have no impact on the prevailing Culebra flow field (Reeves et al., 1991). Fluid injected from the repository

is also assumed to have no effect on Culebra fluid density. Estimation of the Culebra flow field and estimation of radionuclide transport through this flow field are, therefore, considered as separate problems.

- **Dual-porosity transport.** Matrix and fracture porosities that are coextensive and communicating can result in local disequilibrium between radionuclide concentrations between the fracture and matrix (Jones et al., 1992). The time constant associated with this disequilibrium is determined by the rate of exchange of radionuclides between the porosity sets and the radionuclide storage capacity of the fracture and matrix. Because this equilibration time may be significant in comparison to the time scale of source-term concentration change, a dual-porosity transport model has been adopted. The 1992 conceptual model for dual-porosity transport differs from that used in 1991 in that porosity of the clay linings within fracture is modeled explicitly, and diffusion may occur in both the clay linings and the dolomite matrix (see Section 7.6 of Volume 2 of this report). Alternative conceptual models are examined with and without clay linings and dolomite matrix porosity (see Section 5.1 of Volume 1 of this report and Chapter 8 of this volume). Available information is insufficient to confirm or refute these alternative conceptual models at this time. Proposed tracer tests may provide additional information to support a choice of transport model (Beauheim and Davies, 1992).

- **Linear equilibrium sorption of radionuclides.** In addition to hydrodynamic processes, radionuclide concentrations in Culebra groundwater are assumed to be affected by geochemical interactions with the host rock. Reversible sorption is assumed to be the only mechanism on interaction of the radionuclides with the rock (Trauth et al., 1992). Sorption is further assumed to follow a linear Freundlich isotherm, with different coefficients describing sorption on the dolomite matrix and the clay linings in fractures. Chemical retardation of radionuclides by sorption is believed realistic, but, by agreement between the DOE and the State of New Mexico, cannot be considered in a final compliance evaluation unless supported by experimental data (US DOE and the State of New Mexico, 1981, as modified). Experimental programs are in progress or planned to reduce these uncertainties, including laboratory-scale radioactive tracer tests in core samples (US DOE, 1992, and references cited therein) and nonradioactive tracer tests between well locations in the Culebra (Beauheim and Davies, 1992).

6.2 Model Geometry

6.2.1 Regional Domain

The regional domain (Figure 6.2-1) is 25 x 30 km, with the long axis oriented 38 degrees east of north. The grid (Figure 6.2-2) consists of 50 x 57 x 1 (x,y,z) blocks and has varying spacing in the x-y plane, reflecting the spatial distribution of transmissivity data from wells. Grid spacing is finer in the central portion of the model in the vicinity of H-3, H-11, WIPP-13, and the shafts. Grid-block dimensions range from 50 m near the center of the site to approximately 2800 m at the model boundary. The vertical dimension of the grid is 7.7 m, and is the mean thickness of the Culebra Dolomite Member of the Rustler Formation in the WIPP area (LaVenue et al., 1988).

The rotated orientation of the grid and the location of a model boundary along the axis of Nash Draw were chosen to take advantage of the draw as a natural no-flow symmetry boundary. Locations and orientations of the regional model boundaries are the same as those used in the 1991 PA (WIPP PA Division, 1991b).

6.2.2 Local Domain

The 5.75 x 6.625 km local domain (Figure 6.2-1) is oriented with its long dimension north-south, and the grid (Figure 6.2-2) consists of 46 x 53 x 1 (x,y,z) blocks, each of which is 125 x 125 m. The vertical thickness of the blocks is 7.7 m, and is the same as the thickness of the regional grid. The intrusion borehole is assumed to intersect the Culebra directly over the center of the disposal region (see the following Section 6.2.3 for a discussion of the location of this point). The local grid is positioned to place the intrusion borehole at a grid-block center. Fluid flow and mass transport in the local domain are solved using regional head solutions as input boundary conditions.

6.2.3 Location of the Intrusion Borehole

The location of the intrusion borehole in the local domain is held constant in all 70 realizations at a point directly above the center of the waste-disposal region. Specifically, the intersection of the intrusion borehole and the Culebra is located above the center of the central pillar separating the southern and northern equivalent panels (panels 9 and 10 on Figure 4.1-1). See Figure 3.1.2 in Volume 3 of this volume for a scale drawing providing coordinates for this point.

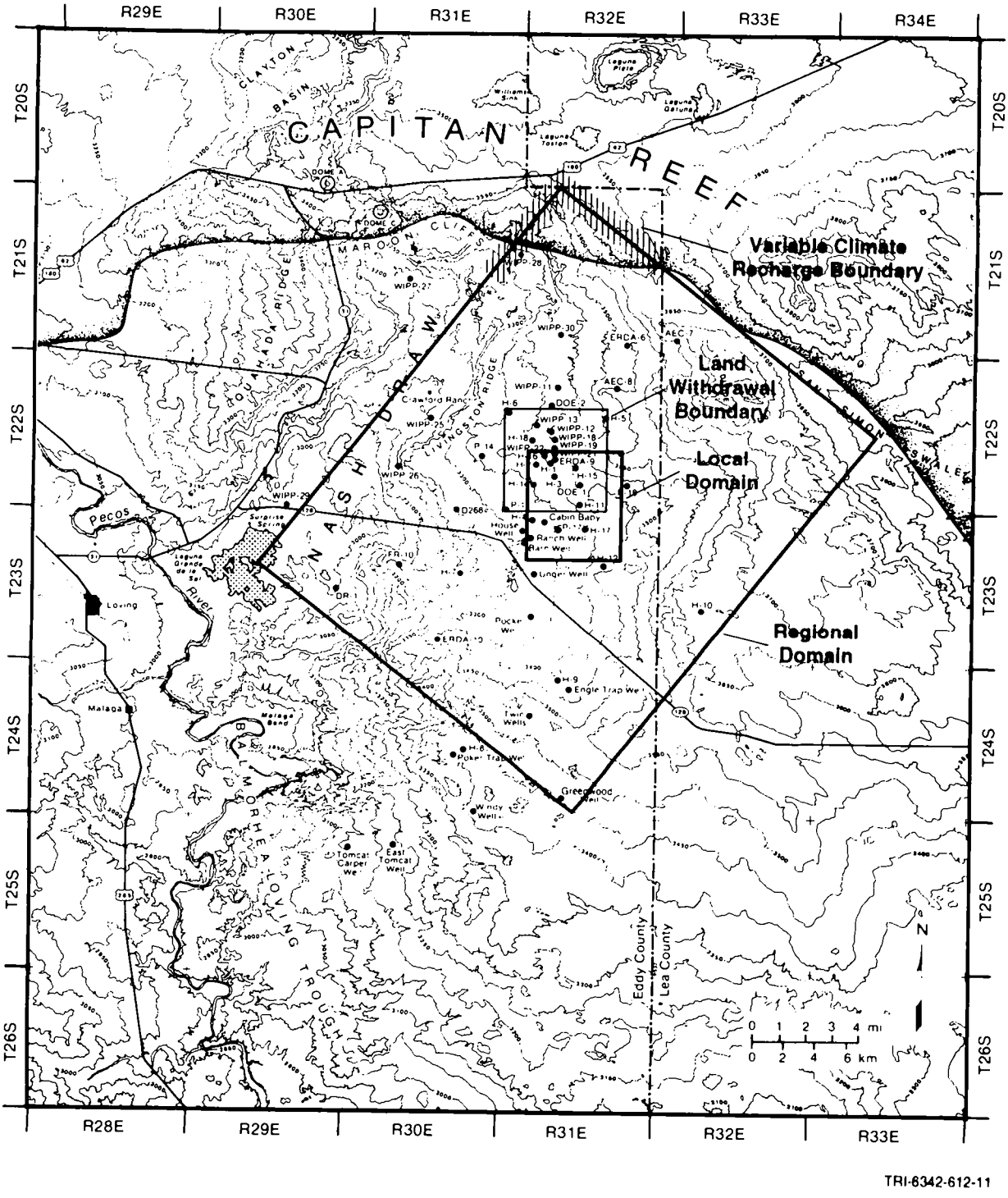

Figure 6.2-1. Regional and local domains for groundwater flow and transport calculations.

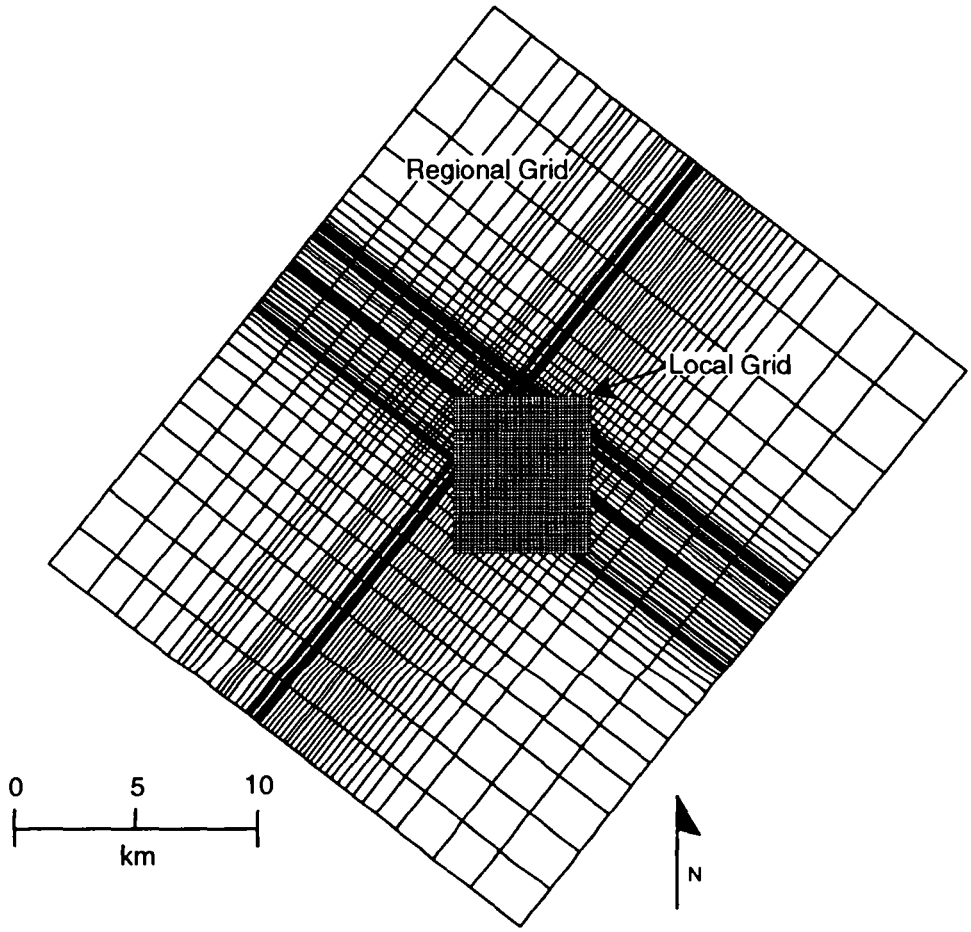

TRI-6342-2680-0

Figure 6.2-2. Grids for regional and local domains for groundwater flow and transport calculations.

The choice of a fixed location for the intrusion borehole is an assumption made for convenience in defining computational scenarios and determining scenario probabilities (WIPP PA Division, 1991b, Chapter 2). Spatial variability of future drilling events is assumed to be uniform, and the straight-line distance between the center of the waste-disposal region and the subsurface boundary of the accessible environment is therefore the mean distance between an intrusion and a regulatory release point. As discussed in the following paragraphs, this distance is approximately 2.4 km. Based on the planned dimensions of the waste-disposal region (Figure 3.1.2 in Volume 3 of this report), the actual straight-line distance from a randomly-located intrusion borehole to the accessible environment boundary may be as much as approximately 315 m more or less than this mean distance. As shown in Section 6.8.3 of this report, modeled flow does not occur along straight lines, and transport distances are therefore somewhat greater than the minimum distance.

The shortest horizontal distance from waste to the accessible environment is a straight line south from any of the southern panels to the WIPP land-withdrawal boundary at the southern edge of either sections 32 or 33, T22S, R31E (Figure 6.2-3). Based on the surveyed location of the southern end of the South Drift (WEC, 1988) and the north-south dimensions of sections 29 and 32, T22S, R31E, as scaled from the Los Medaños 7.5 minute topographic quadrangle (USGS, 1985a), this distance is estimated to be 2414 m (7916 ft). Possible sources of error in this estimate are as follows:

- Gonzales (1989) noted that the WIPP survey coordinates for the northeast corner of section 29, T22S, R31E give a location about 12 m south of that indicated by the USGS coordinates for the same point. Gonzales (1989) concluded that the WIPP survey was more reliable, and the distance reported here is based on WIPP survey coordinates.

- Accuracy in scaling from the topographic map is estimated to be ± 10 m.

- No estimate is made here of the accuracy of either the WIPP survey or the topographic map.

- No estimate is made of the precision with which future excavations will match present design.

- Possible horizontal emplacement of remote-handled transuranic (RH-TRU waste) in the southern walls of the southern panels is not included in this estimate.

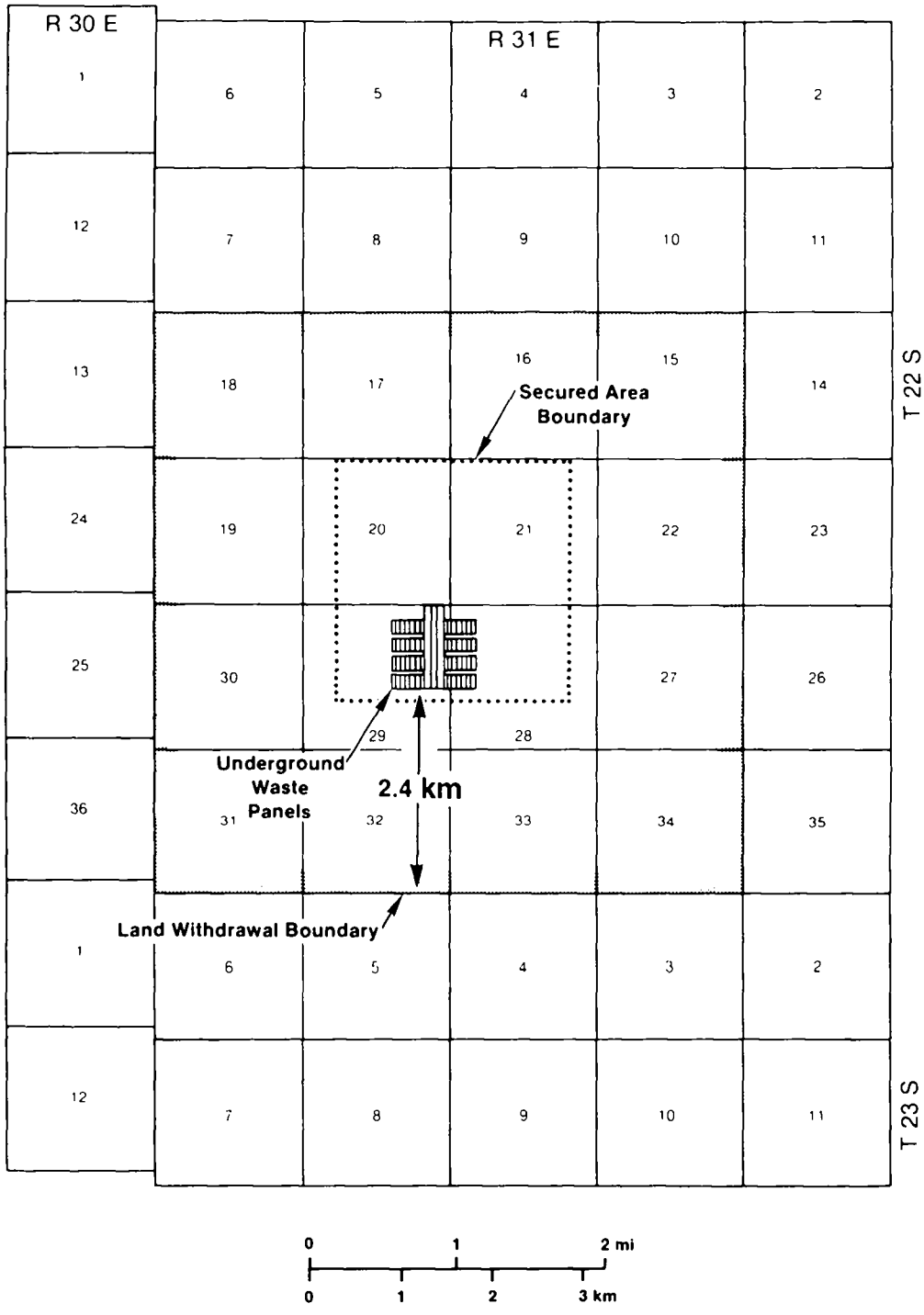

Figure 6.2-3. Position of the waste-emplacement panels relative to the WIPP boundaries and surveyed section lines (US DOE, 1989).

6.3. Material Properties

The most important hydrologic property used in modeling the flow and transport pathways is the transmissivity of the Culebra. In the 1992 PA, 70 groundwater transmissivity fields (presented in Appendix C of Volume 3 of this report) were generated using a multiple-realization technique to account for spatial variability of the transmissivity field within the Culebra (LaVenue and RamaRao, 1992; see also Section 6.8 of this volume and Section 7.5 of Volume 2 of this report). Each of the 70 realizations in the 1992 PA used a different transmissivity field and a corresponding different flow solution. All other hydrologic parameters were held constant, at values described in Volume 3 of this report. The only sampled parameter affecting flow within the transmissivity fields was the climate factor, discussed in the following section. Sampled parameters affecting radionuclide transport are described in Chapter 3 of this volume, and include distribution coefficients for each radionuclide, fracture porosity and spacing, matrix porosity, the fraction of fracture openings lined with clay, and the porosity of the clay linings.

6.4 Boundary and Initial Conditions

Three different types of boundary conditions were used for the regional domain: no-flow, time-dependent head, and fixed head. Locations in which these boundary conditions were applied are shown in Figure 6.4-1. As previously noted (Section 6.2.1), a no-flow boundary was used along a portion of the northwest side of the domain, coinciding with the axis of Nash Draw beginning 4.0 km NE of the origin of the domain at its western corner and continuing to 18.595 km NE. No-flow boundaries were also assigned to the NE portion of the domain, from 30 km NE, 17.3 km SE to 27.240 km NE, 25 km SE. These northeastern no-flow boundary segments correspond to a region of low permeability in the Culebra (see Chapter 2 of Volume 2 of this report).

Time-dependent heads were used to simulate possible effects of climatically varying recharge (see Sections 6.4.1 and 6.4.2, following), and were assigned to a 21.505 km "recharge strip" surrounding the northern apex of the regional domain. Specifically, time-dependent heads were used along the northwestern boundary between 18.595 km NE, 0 km SE and 30 km NE, 0 km SE, and along the northeastern boundary from 30 km NE, 0 km SE to 30 km NE, 10 km SE. Heads within this strip were prescribed as a function of a sinusoidal climate function applied to the initial calibrated heads derived from the steady-state solution for each transmissivity field (see Sections 6.4.1 and 6.4.2).

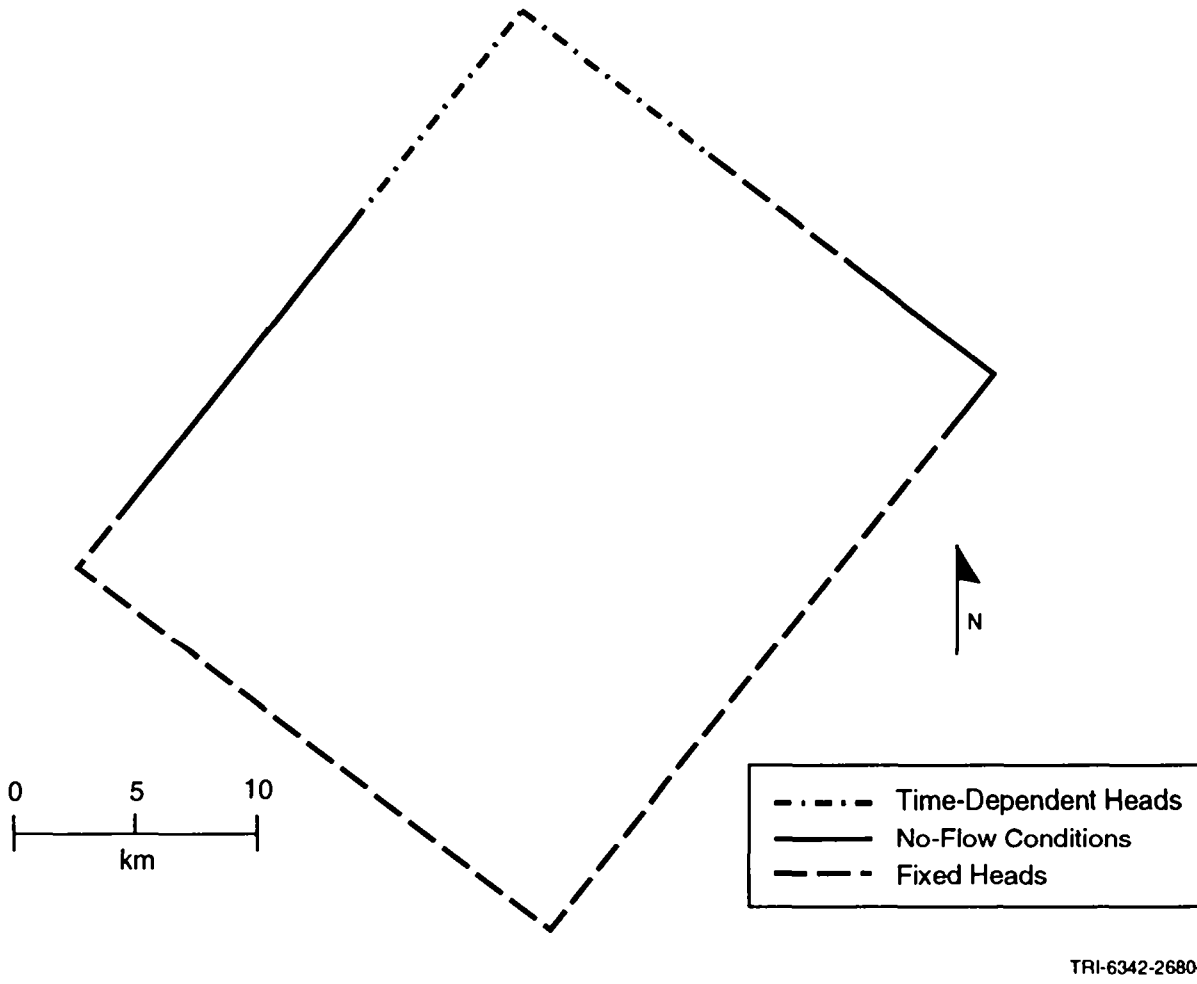

Figure 6.4-1. Boundary conditions for regional domain.

All other boundary conditions were fixed (time-invariant) heads based on the steady-state solution for each transmissivity field (see Section 6.8.2), and therefore were different for each realization.

As with the fixed boundary heads, initial heads within the regional domain were determined from the steady-state solution for each transmissivity field. No vertical flow (i.e., leakage) was allowed within the model domain. Possible effects of leakage into or out of the Culebra will be examined in future PAs when a three-dimensional model for regional groundwater flow is available.

As previously noted, boundary and initial conditions for the local domain were determined by the solution of flow in the regional domain. Because the the local grid elements do not exactly overlay the regional grid elements, SECO-FLOW interpolates boundary conditions for the local grid.

6.4.1 Climatic Variability

As discussed in more detail in Swift (1993) and Section 2.2.3.2 of Volume 2 of this report, climate in southeastern New Mexico is likely to be wetter than that of the present at some times during the next 10,000 yr. The timing of future climatic changes is unknown, but the wettest plausible climate during the next 10,000 yr is expected to be no wetter than that of the late Pleistocene (20,000 yr ago), which was approximately twice as wet as that of the present (Swift, 1993).

The effect of climatic changes on regional boundary conditions cannot be modeled directly because of uncertainty in the location of present and future recharge and uncertainty in the hydrologic properties affecting the flow path from the recharge area to the regional domain boundary. Climatic effects are instead approximated indirectly using information about hydrologic conditions during past climatic conditions. Geologic evidence (Bachman, 1985, p. 20-21) indicates that at some time or times during the Pleistocene the water table was sufficiently high to sustain springs along the east margin of Nash Draw and a lake in Clayton Basin north of Nash Draw (see Figure 6.2-1). Rustler Formation outcrops in Clayton Basin have been identified as a possible recharge area for groundwater in the Culebra at the WIPP (Mercer, 1983), and the 1992 PA therefore uses the highest possible lake elevation in Clayton Basin as a maximum boundary head condition that could result from climatic change. The present elevation of the Clayton Basin spill point (1007 m, in section 11, T20S,R29E [USGS, 1885b]) is assumed to be the maximum possible lake elevation. This elevation is used as the maximum head elevation at the northern apex of the regional model domain, reached during future wet climates. Heads elsewhere along the

"recharge strip" are scaled upward during wet climates proportional to the amount head at the apex is raised.

The choice of the elevation of the Clayton Basin spill point as the maximum head value represents a change from the 1991 PA, in which maximum heads were allowed to rise to the ground surface (1030 m), scaled according to the same climate function. The change was made to improve consistency with the confined-aquifer conceptual model.

Scaling of heads along the recharge strip is based on the calibrated initial heads for each transmissivity field, a "climate factor" (CULCLIM in Chapter 3 of this volume) derived from a sampled index parameter, and the following sinusoidal function (Swift, 1991, memorandum in Appendix A of WIPP PA Division, 1991c).

$$\frac{h_f(t)}{h_p} = \frac{3A + 1}{4} - \frac{A - 1}{2}\left(\cos \Theta t + \frac{1}{2}\cos \Phi t - \sin \frac{1}{2} \Phi t\right) \qquad (6.4\text{-}1)$$

defines time-dependent heads in the Culebra, where

$h_f(t)$ = head (m) in Culebra at time t (s),
h_p = estimate of present-day boundary head in Culebra (e.g., 880 m),
A = recharge amplitude factor (dimensionless) for Culebra (i.e., CULCLIM),
Θ = frequency (Hz) for Pleistocene glaciations: 1.7×10^{-12} Hz (5.4×10^{-5} yr^{-1}),
Φ = frequency (Hz) for second-order climatic fluctuations: 1.0×10^{-10} Hz (3.2×10^{-3} yr^{-1}),

and

t = time (s), with t=0 corresponding to decommissioning of the WIPP.

This function is not used to predict future climates, but rather is designed to provide a simple way to examine the influence of possible climatic changes during the next 10,000 yr. The periodicity of the function is based on approximately 30,000 yr of paleoclimatic data from southeastern New Mexico and the surrounding region and the global record of Pleistocene glaciations (Swift, 1993). The glacial frequency term Θ produces a maximum value of the function $h_f(t)$ at 60,000 yr, and has little effect during the regulatory period. Most of the introduced variability results from second-

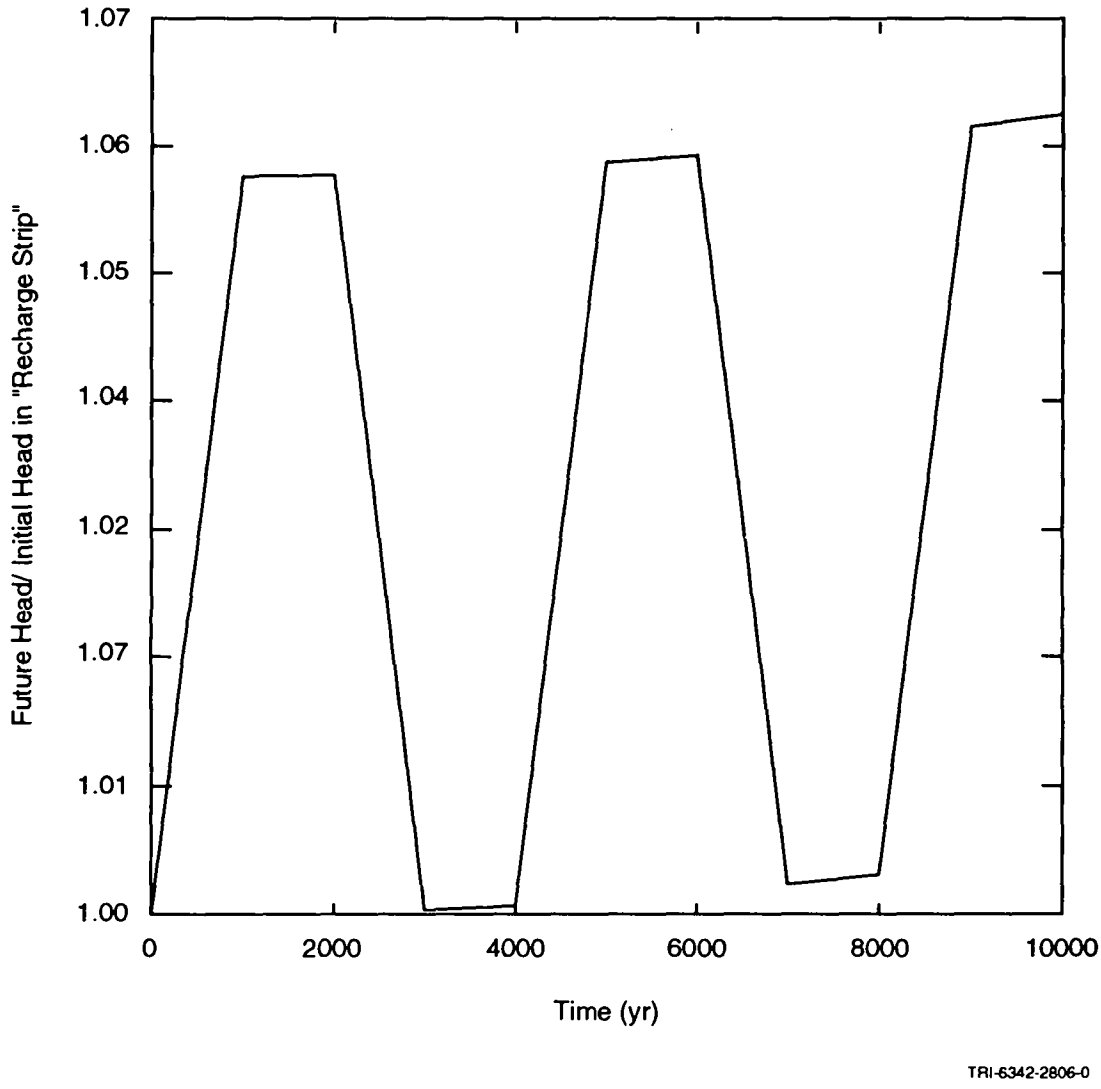

Figure 6.4-2. 10,000-yr history of climate function, evaluated at 1000-yr time steps for the maximum value of CULCLIM.

order fluctuations controlled by the higher-frequency term Φ. This variability corresponds to the frequency of nonglacial climatic fluctuations observed in both late Pleistocene and Holocene paleoclimatic data. The chosen value for Φ results in a sinusoidal curve with three peaks in 10,000 years. Figure 6.4-2 illustrates the function as applied in the 1992 SECO-FLOW calculations, with values calculated only at the 1000 yr time steps.

6.4.2 Time-Dependant Boundary Heads

The recharge amplitude factor CULCLIM used in Equation 6.4-1 is a dimensionless scaling factor that varies uniformly between 1.07 and 1.00, and is derived from a sampled climate index variable that varies uniformly between 0 and 1 (see Section 4.4 of Volume 3 of this report). At 1500 yr (not simulated by the 1000 yr time steps), a maximum value of 1.07 for CULCLIM results in the maximum head in the grid block at the northern apex of the regional domain to rise from its initial elevation of 942.5 m (LaVenue and RamaRao, 1992) to the elevation of the spill point of Clayton Basin, 1007 m. Heads in other grid blocks within the "recharge strip" are scaled using the same value for CULCLIM, and may therefore reach a maximum elevation somewhat higher or lower than the head in the northernmost block, depending on their initial elevations. At its minimum value (1.00), CULCLIM results in no change in boundary heads throughout the 10,000 years. Intermediate values of CULCLIM result in intermediate increases in boundary heads. For all values of CULCLIM greater than 1.00, the maximum head elevation occurs at the final, 10,000 yr climatic peak. Heads in earlier peaks are slightly less, because of the effect of the glacial term in the climate function.

6.5 Effect of Climatic Change on Groundwater Flow

The effects of climatically varying heads along the "recharge strip" is different in each of the 70 realizations, because each realization uses a different transmissivity field (Section 6.8). Changes in groundwater flow are discussed here for two realizations that contained the largest sampled value for the climate index factor and an intermediate value. The largest sampled value for the climate index factor, 0.9966, occurred in realization 11 and resulted in a value for CULCLIM of 1.068. The calculated head field for this realization is displayed for time zero (initial conditions) (Figure 6.5-1a) and for 10,000 yr (Figure 6.5-1b). Vector representations of the specific discharge (i.e., volume of fluid moving through a unit area in a unit time) are shown for the corresponding velocity fields in Figures 6.5-1c and 6.5-1d. Similar plots are shown in Figure 6.5-2 for realization 20, which contained a sampled value for the climate index factor of 0.4519,

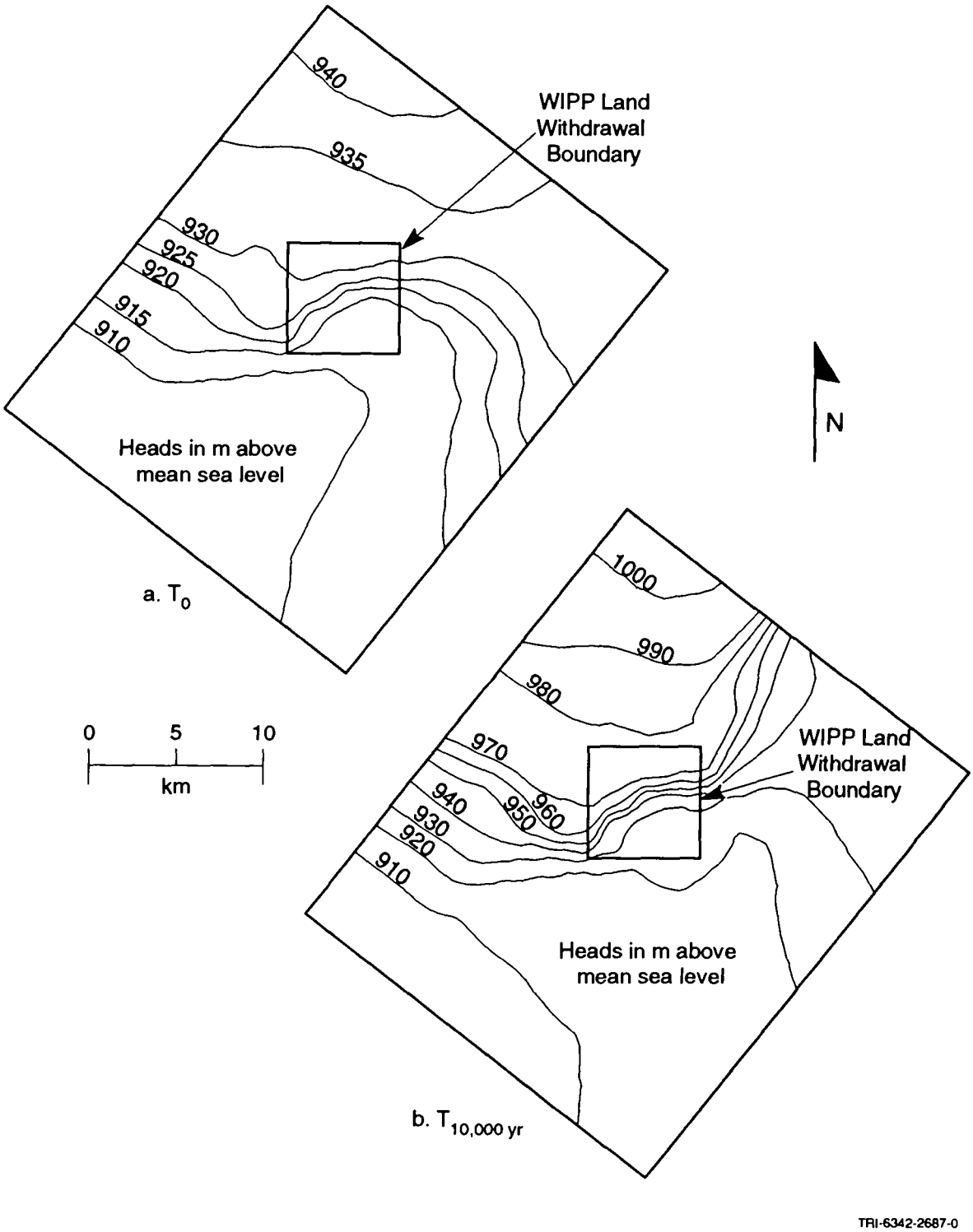

Figure 6.5-1. Head (Figures 6.5-1a,b) and specific discharge (Figures 6.5-1c,d) plots for the SECO-FLOW regional domain for realization 11 at time zero and 10,000 yr. This realization contains the largest value for CULCLIM.

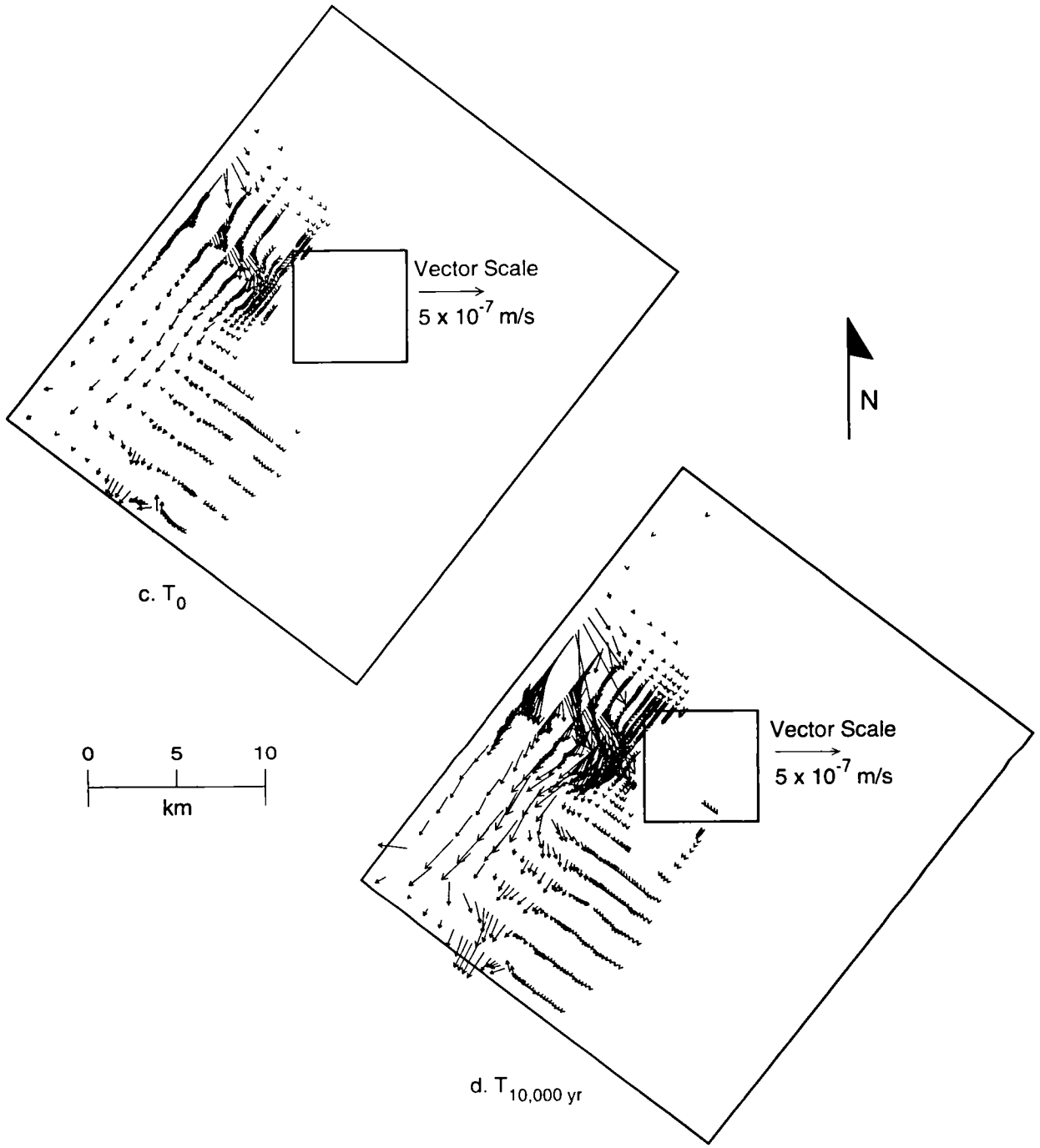

Figure 6.5-1. Head (Figures 6.5-1a,b) and specific discharge (Figures 6.5-1c,d) plots for the SECO-FLOW regional domain for realization 11 at time zero and 10,000 yr. This realization contains the largest value for CULCLIM. (continued)

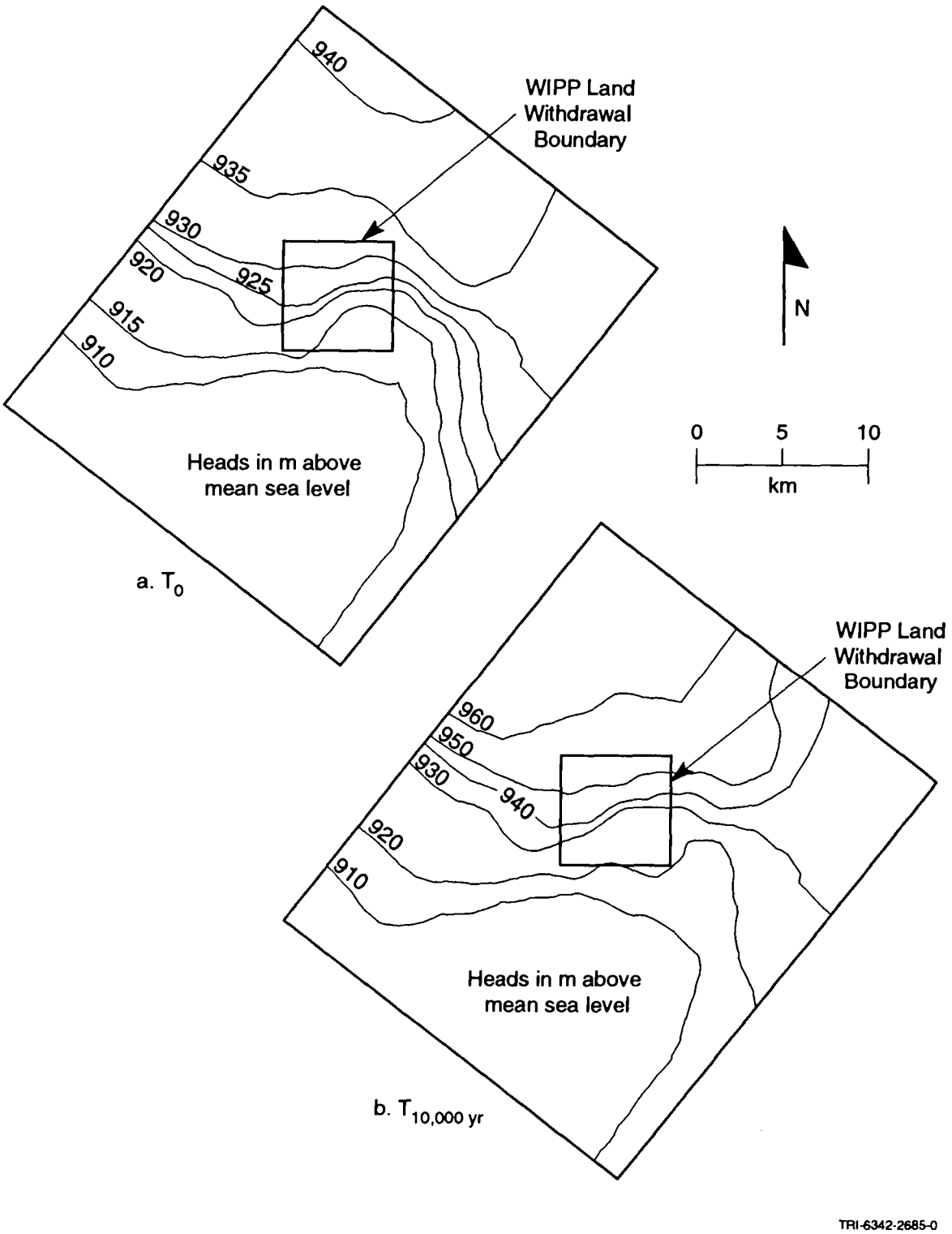

Figure 6.5-2. Head (Figures 6.5-2a,b) and specific discharge (Figures 6.5-2c,d) plots for the SECO-FLOW regional domain for realization 20 at time zero and 10,000 yr. This realization contains an intermediate value for CULCLIM.

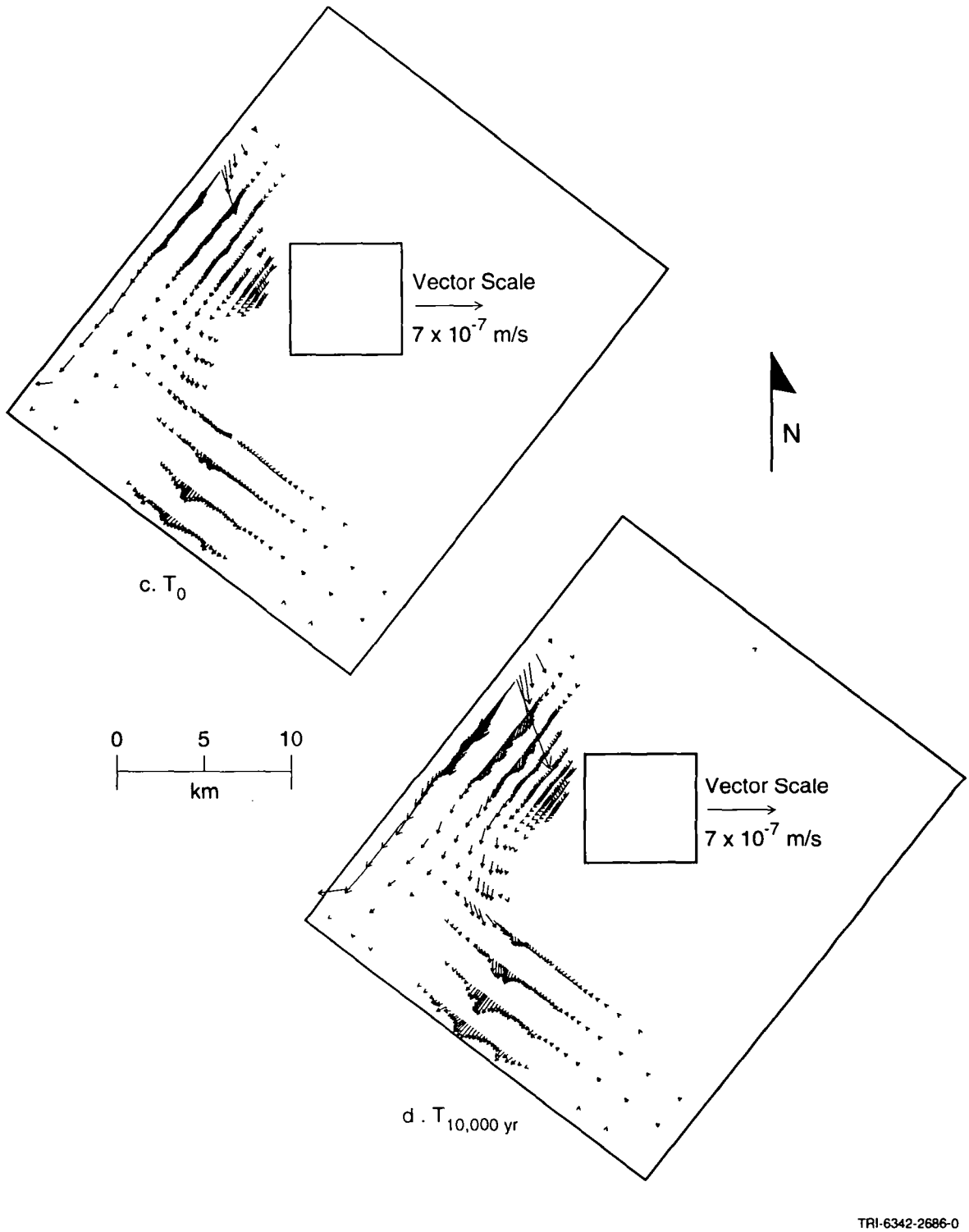

Figure 6.5-2. Head (Figures 6.5-2a,b) and specific discharge (Figures 6.5-2c,d) plots for the SECO-FLOW regional domain for realization 20 at time zero and 10,000 yr. This realization contains an intermediate value for CULCLIM. (continued)

resulting in a value for CULCLIM of 1.031. Examination of these figures shows that the largest increases in head occur in the northern and northwestern portion of the regional domain, and that most of the increase in groundwater flow occurs in and near Nash Draw. Some increase in groundwater flow is observed within the land-withdrawal boundary. CULCLIM does not, however, appear as an important parameter in stepwise linear regression analyses (see Chapter 8), and subsurface releases of radionuclides are not sensitive to climatic variation of heads along the modeled "recharge strip."

6.6 Flow and Transport Model Coupling

Radionuclide transport was modeled on the same computational grid used for the local flow calculations. Flow fields generated from the first time step by SECO-FLOW were used as the initial and boundary conditions by SECO-TRANSPORT. The transient SECO-FLOW flow fields from subsequent time steps, starting at 1000 yr, were used for solute transport modeling. Radionuclide release from the repository to the Culebra was from a single, time-dependent source term located above the center of the waste-disposal region. Density and volume of liquid injected into the Culebra was assumed to be negligible relative to the total flow within the aquifer. Source-term flux was therefore disregarded, and did not affect flux in the flow fields. Volume and density affects of injecting brine into the Culebra will be examined in future PAs.

SECO-FLOW solves the time-dependent partial differential equation for hydraulic head for a heterogeneous, isotropic aquifer, and provides the specific discharge (volume of fluid moving through a unit area in a unit time) for each grid element. Heterogeneity is introduced through each spatially-varying transmissivity field. SECO-TRANSPORT models radionuclide transport in a fractured medium under a variety of assumptions (see Section 7.6 of Volume 2 of this report). The fluid is transported in fracture porosity only, and not in the matrix porosity of the dolomite or clay fracture linings. Matrix porosity affects diffusion into and storage in the matrix. Therefore, dividing the specific discharge by fracture porosity to obtain pore-water velocity within the fractures can result in relatively fast travel times to the accessible environment boundary if other processes (e.g., matrix diffusion and sorption) are not effective in retarding radionuclide transport. However, if matrix diffusion and/or sorption are effective in retarding radionuclide transport, travel times may be orders of magnitude longer.

6.7 Coupling the Repository/Shaft and Culebra Models

Radionuclide releases into the Culebra were modeled for E2- and E1E2-type intrusions (see Section 4.4.2.4 of Volume 2 of this report). Solute concentration and rate of discharge was dependent on parametrically described geochemical and physical processes and interactions. The code PANEL (see Section 7.4 of Volume 2 of this report) calculated the solute concentration and pulse length. Sampled parameters affecting these processes were used in both PANEL and BRAGFLO, and each realization therefore had a specific suite of source files which consisted of a source term having varying pulse lengths and concentrations for each radionuclide. The source files, from PANEL and located on a separate CAMDAT data base, were imported and attached to the local velocity flow fields by the SECO-TRANSPORT preprocessor for the transport calculations.

6.8 Transmissivity Fields

The synthetic transmissivity fields generated by LaVenue and RamaRao (1992) represent an improvement over the fields used in 1991 (WIPP PA Division, 1991b), in that they more accurately characterize the uncertainty due to spatial variability in aquifer properties, and, therefore, result in better characterization of uncertainty in groundwater flow. A discussion of the 1992 transmissivity field results, extracted from LaVenue and RamaRao (1992), follows.

6.8.1 Ensemble Mean Transmissivities

Each of the 70 fields were calibrated to steady-state and transient head data using conditionally simulated (CS) fields (presented in Appendix C of Volume 3 of this report) composed of an underlying kriged field to which different conditional random error fields were added. Thus, each of the calibrated CS transmissivity fields has a different spatial distribution of transmissivities. For example, in some cases there is a broad zone of higher transmissivity that extends from the DOE-1 borehole west to H-14 (see Figure 6.2-1 for borehole locations). In other cases, the high-transmissivity zone has a narrow, tortuous and in some instances, discontinuous nature.

An ensemble mean calculation was performed across the realizations to determine the average transmissivity value at each grid block. The resulting ensemble transmissivity field (Figure 6.8-1) has features which are very similar to the 1990 kriged transmissivity field that was used as

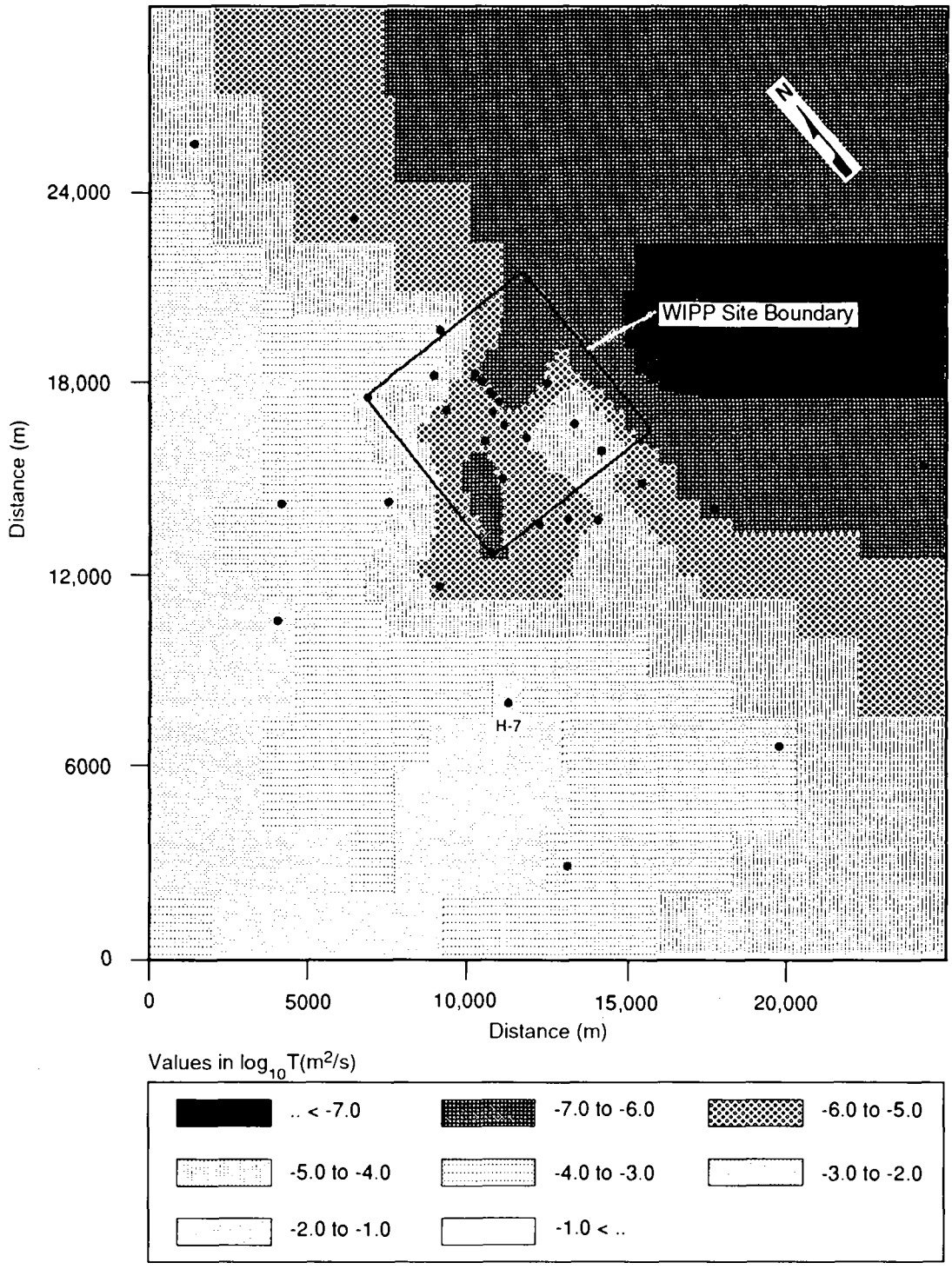

Figure 6.8-1. Ensemble transmissivity field resulting from a mean calculation performed across the realizations.

the basis for generating the transmissivity fields for the 1991 PA calculations. Outside the land-withdrawal area, the re-entry of high transmissivities from the Nash Draw area occurs south of the WIPP near the H-7 borehole in both the 1990 results and in the ensemble mean field. The high-transmissivity zone within the land-withdrawal boundary, as represented in the ensemble mean field (Figure 6.8-2), extends northward from the P-17 borehole where it narrowly lies between the P-17 and H-17 boreholes. Once crossing the southern land-withdrawal boundary, the high-transmissivity zone widens significantly extending westward to the H-3 borehole. The eastern extent terminates approximately 100 m east of the H-11 and DOE-1 boreholes. The nature of the high-transmissivity zone as determined in the 1990 study (Figure 6.8-3) is quite similar to the ensemble mean field with a narrow width toward the southern land-withdrawal boundary, which widens in both the east and west directions as it extends northward toward the H-15 borehole.

6.8.2 Ensemble Steady-State Head Differences

A root-mean squared error (RMSE) between calculated and observed steady-state heads was calculated in order to summarize the fit of each realization to the steady-state data. The RMSE values at each of the boreholes that had steady-state observed head data were then summed within each simulation to obtain an average RMSE. A histogram of the average RMSE value for each of the 70 simulations (Figure 6.8-4) depicts a mean RMSE value within the simulations between 2.0 and 5.0 m. Uncertainty in the steady-state heads is approximately 1.5 m. The simulation with the worst steady-state head fit is shown to have an average RMSE value between 6.5 and 7.5 m. This particular realization illustrates a situation in which the difference field (added to the kriged field during the CS process) significantly reduced the ability of the code to calibrate the field to steady-state conditions within 50 calibration steps. This situation occurs when the initial CS field generated has features that produce significantly high initial-head differences. The code then has to add more pilot points to modify the CS field to bring the head field into agreement with the observed data than may be necessary for an initial CS field which produces initial head differences that are low. Because a fixed number of pilot points were specified for calibrating to the steady-state data, some fields had smaller RMSE values than others.

RMSE values were also calculated to determine average head differences over the ensemble of realizations at each borehole location. Figure 6.8-5

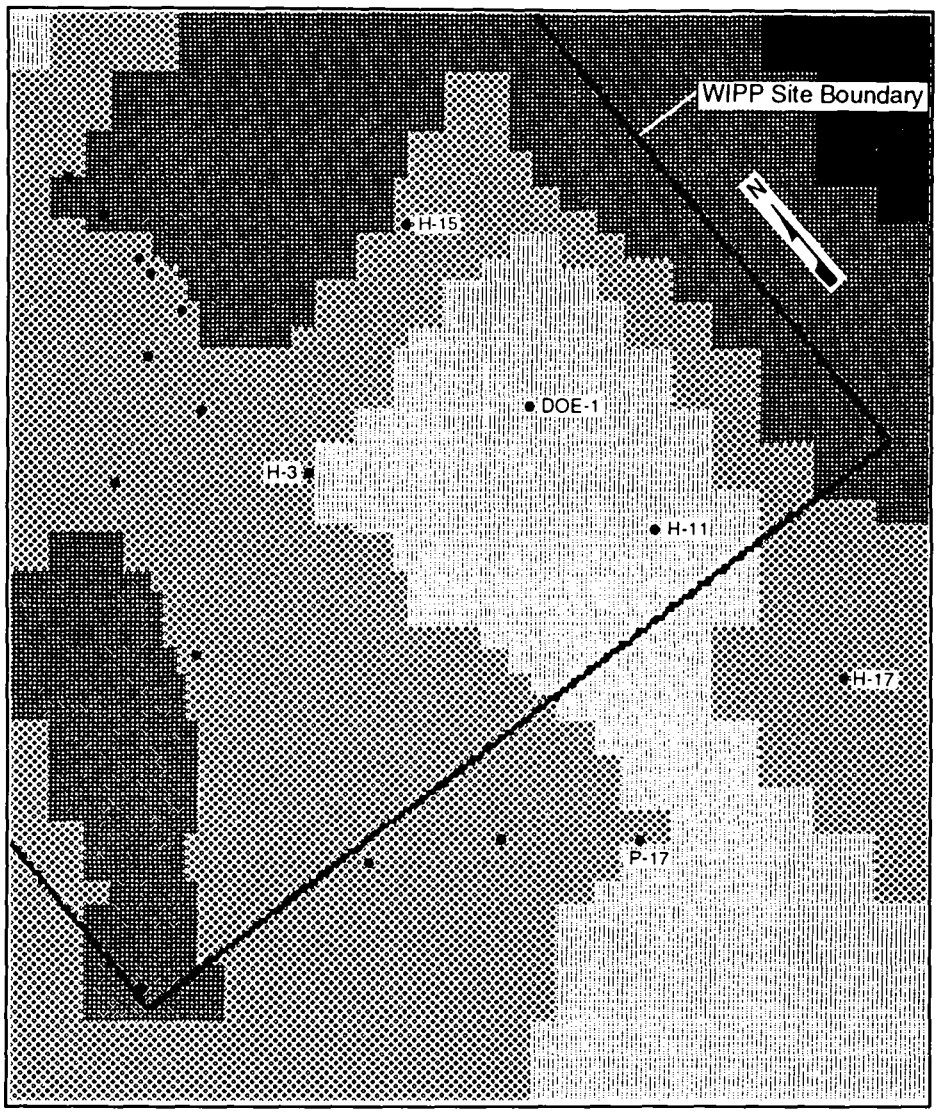

Figure 6.8-2. Ensemble transmissivity field in the vicinity of the southern land-withdrawal boundary.

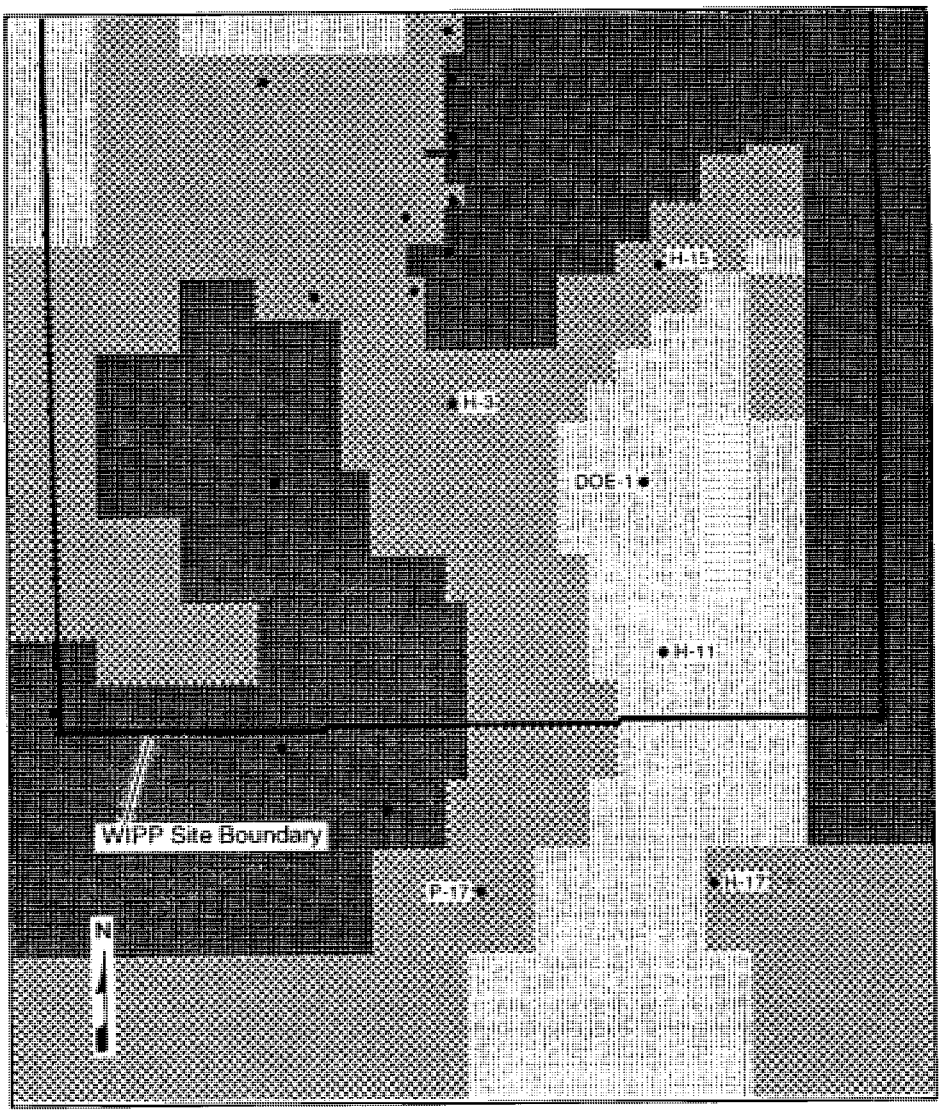

Figure 6.8-3. Calibrated transmissivities in the vicinity of southern land-withdrawal boundary.

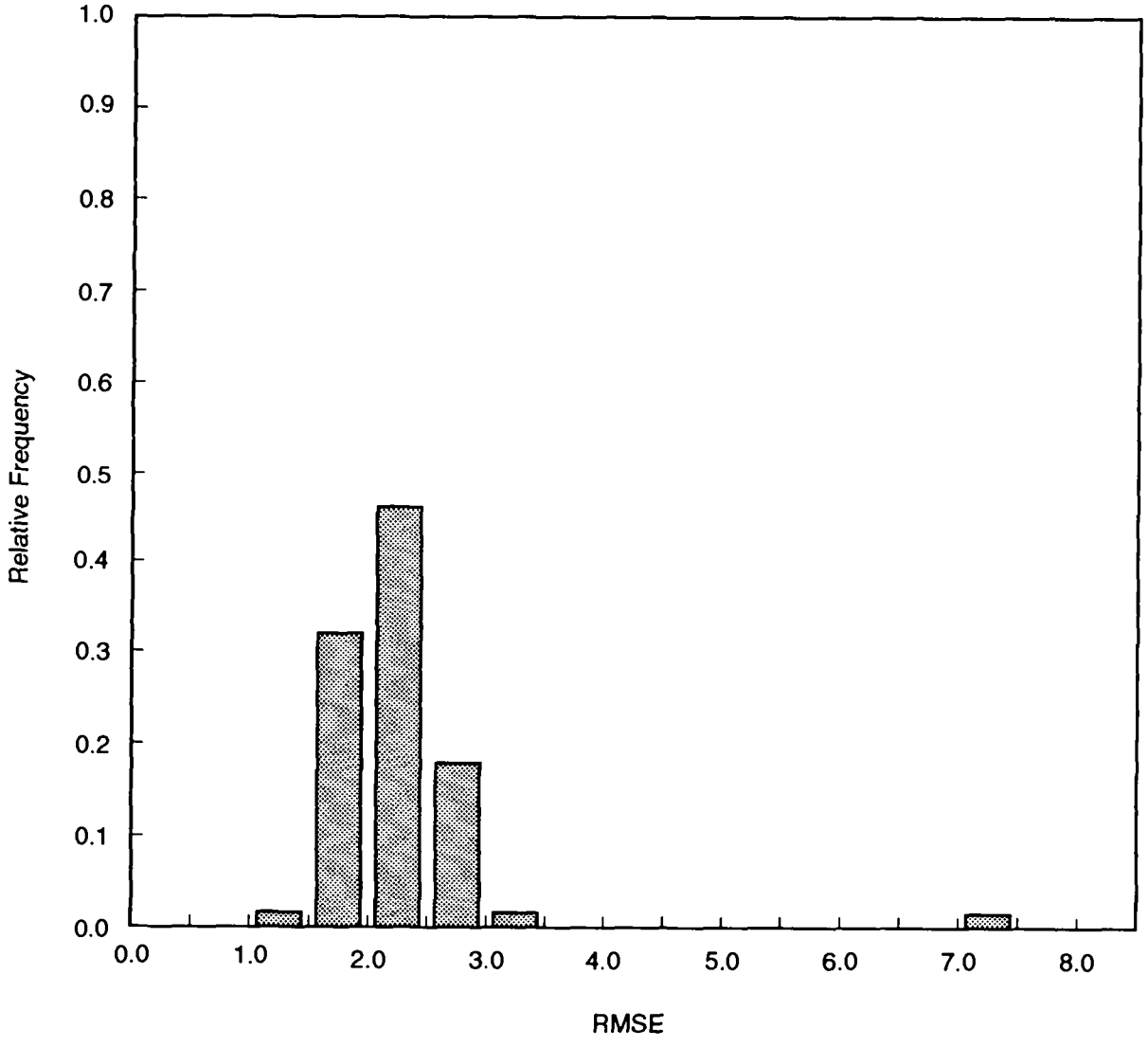

Figure 6.8-4. Histogram of the average RMSE value for each of the 70 simulations.

contains a contour surface of the RMSE values over the model domain. The maximum average difference between the calculated and observed data occurs at the H-7 borehole where the RMSE value is -4.3 m. (Note: The sign of the RMSE was assigned after evaluating the ensemble differences.) The head differences in the southern portion of the regional domain and the central portion of the land-withdrawal area also have negative signs with average values ranging between -0.7 m and -2.8 m. The regions that have positive head differences occur in the area immediately adjacent to the H-11 borehole and in the area between the P-14 and WIPP-26 boreholes. The average head differences in these regions are less than 2.0 m. The difference at the H-17 borehole is the highest with a positive value of 3.4 m.

The average head differences illustrated in Figure 6.8-5 indicate that the boundary conditions specified along the southern and western boundaries are not consistent with the observed heads. Several iterations were made to the boundary conditions prior to beginning the calibration exercise. The iterations were necessary due to the difficulty in matching the H-7, USGS-1, and H-9 observed heads while properly fitting the heads in the rest of the model domain. The difficulty arises from the existence of the no-flow region along the Nash Draw axis and the extremely flat hydraulic gradients in the southern area. If the specified heads are increased along the southern boundary to fit H-7 and USGS-1, the southern boundary converts from a discharge boundary to a recharge boundary. However, the Pecos River, and the Malaga Bend region in particular, has been determined to behave as a discharge region for regional flux from the Rustler (Mercer, 1983). While no absolute conclusions may be made yet concerning the direction of groundwater flow in the southern portion of the regional domain, the results determined in this study have indicated that there is an inconsistency between the observed heads in this area if regional groundwater flow is to the south. This may indicate a groundwater divide occurs between the H-9 borehole and the H-8 borehole south of the model domain.

6.8.3 Ensemble Groundwater Travel Times

The groundwater travel time from a point above the center of the waste-disposal region (Section 6.2.3) to the land-withdrawal boundary was calculated for each of the calibrated CS fields. This groundwater travel time is not the same as the radionuclide transport travel times calculated by SECO-TRANSPORT, which are used as input to the CCDF calculations. The purpose of the groundwater-travel-time calculations described here is to characterize the transmissivity fields, not to predict transport of radionuclides. These travel times were calculated assuming advection of groundwater through a single-porosity medium without fracture flow--i.e.,

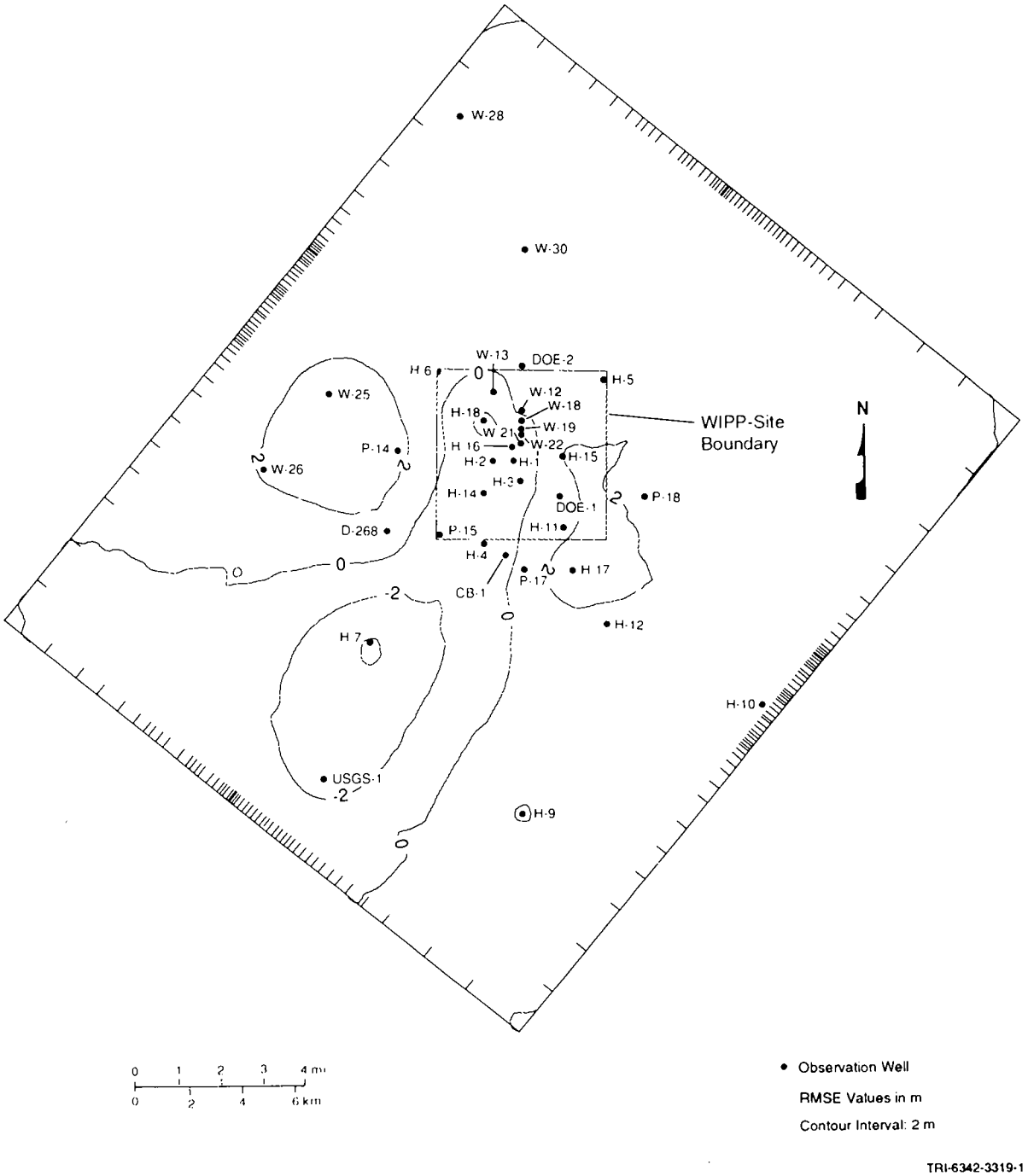

Figure 6.8-5. Contour surface of the RMSE values over the model domain.

total porosity was equal to a matrix porosity of 0.16. Travel times are therefore substantially longer than those calculated assuming transport in fractures, with an average fracture porosity of 0.001.

Matrix travel-time distributions are displayed as a cumulative distribution function (CDF) that represents the probability of various travel times occurring (Figure 6.8-6). This CDF shows, for example, that 90% of the travel times were longer than 12,000 yr, 50% of the travel times were longer than 18,000 yr, and 10% of the travel times were longer than 27,000 yr. The histogram shown in Figure 6.8-7 also conveys the narrow distribution of groundwater travel times.

The travel paths that correspond to the travel times contained in the CDF are illustrated in Figure 6.8-8. Most of the travel paths follow a southeasterly direction until reaching the DOE-1 vicinity at which point the paths travel directly south to the land-withdrawal boundary. A few paths travel directly south from the starting point while several others have an east-southeasterly direction prior to moving south toward the land-withdrawal boundary. The travel paths are indicative of the southerly groundwater-flow direction observed today. Should significant changes occur in the future in the direction of the hydraulic gradient, travel paths would also change.

Assuming the numerical model used to simulate a system properly accounts for the physics and scale of the problem of interest, the uncertainty of model results should decrease as the data set to which the model is conditioned increases. Conditioning a transmissivity field used in a model to observed steady-state pressure data reduces uncertainty in the transmissivity estimates away from the observed locations. Conditioning to transient-pressure data further reduces uncertainty in the transmissivity estimates between pressure-measurement locations due to the increase in information regarding the transmissivity between these two locations. The reduction in the uncertainty of the travel time due to the conditioning of the Culebra model to the transient pressure data base is illustrated in Figure 6.8-9 where the CDF of travel times determined from the transient-calibrated model (referred to herein as the TCDF) and the CDF determined from the steady-state calibrated model (referred to herein as the SCDF) are shown. The CDF of the steady-state model was calculated by removing all the pilot points added during transient calibration from the input data sets of each of the realizations.

As illustrated in Figure 6.8-9, the SCDF has a much broader range of travel times than the TCDF. The minimum values between the two are approximately the same; however, the median and maximum travel times are

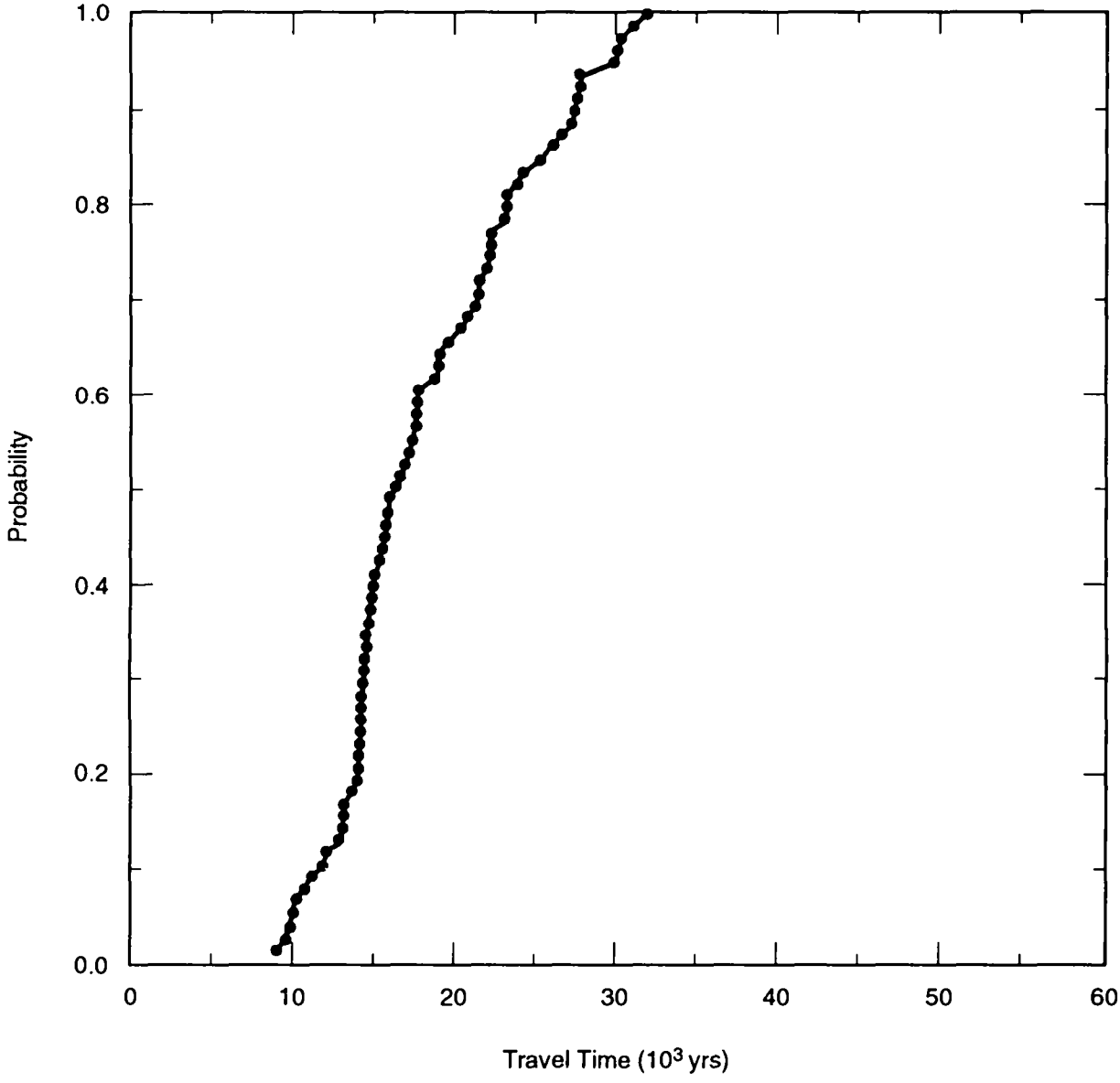

Figure 6.8-6. Travel time cumulative distribution function (CDF) determined from the 70 calibrated fields (assuming matrix porosity of 16%).

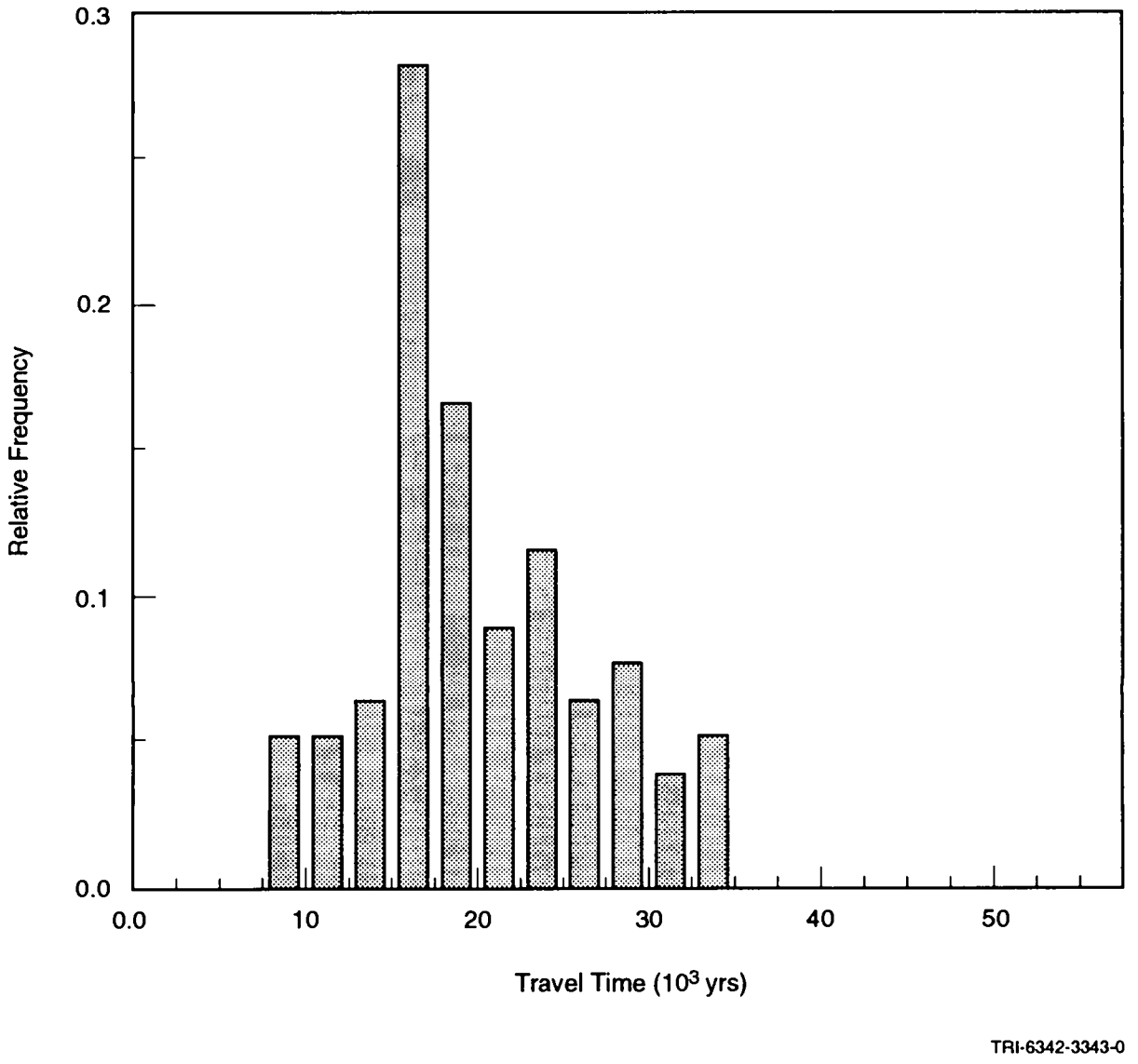

Figure 6.8-7. Histogram of travel times from ensemble of transient calibrated fields.

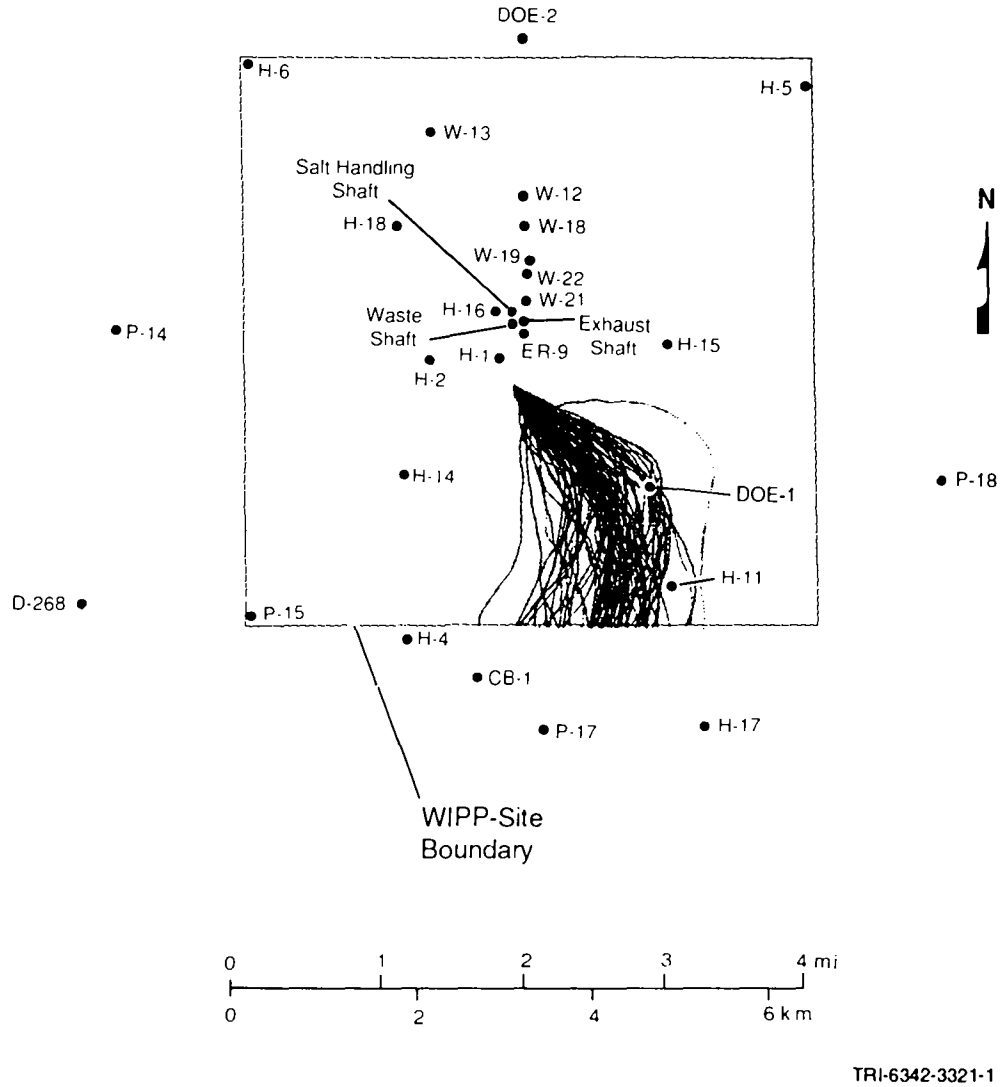

Figure 6.8-8. Travel paths that correspond to the travel times contained in the cumulative distribution function (CDF) shown in Figure 6.8-4.

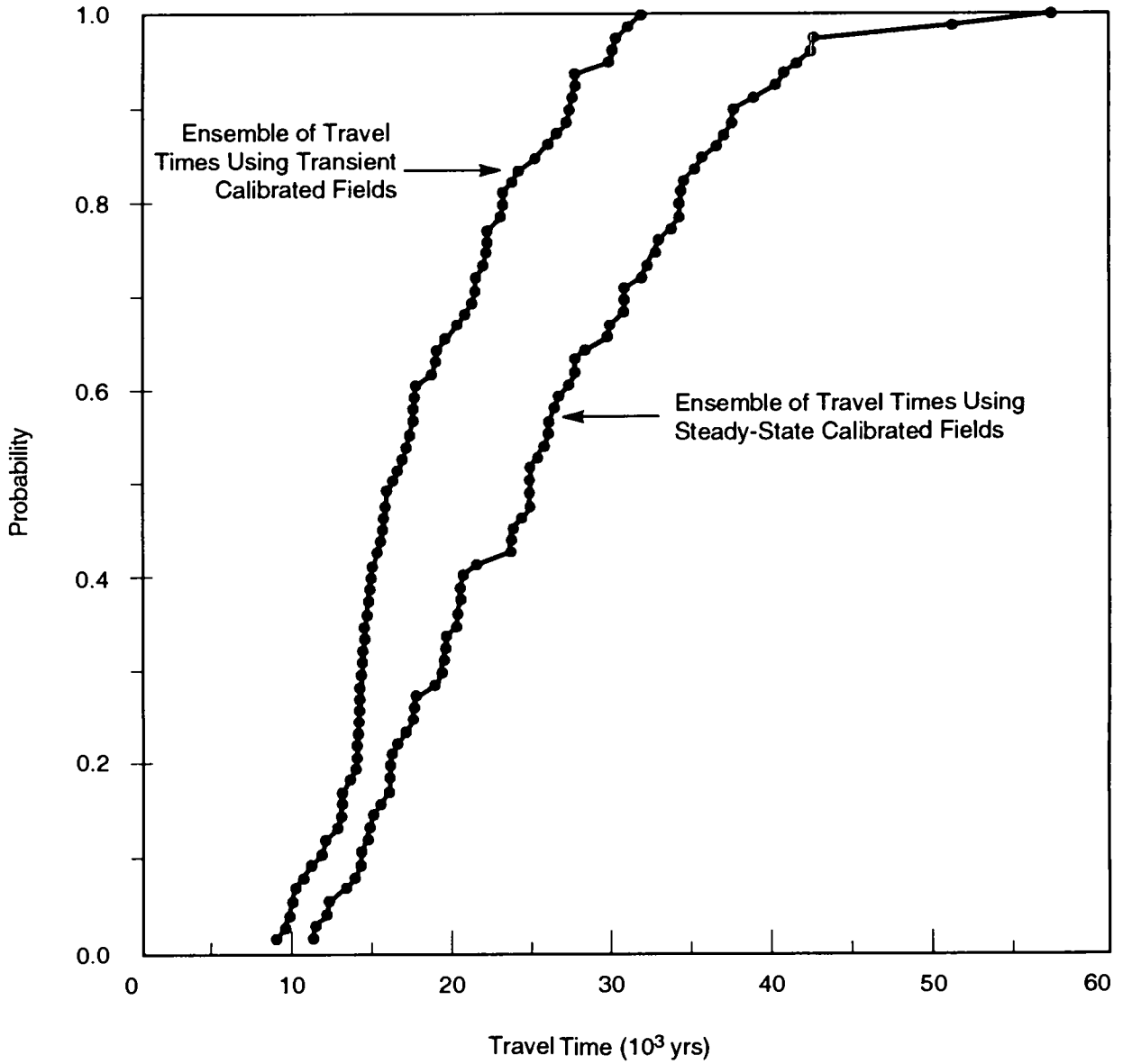

Figure 6.8-9. Cumulative distribution function (CDF) of travel times determined from the transient-calibrated model (TCDF) and the CDF determined from the steady-state calibrated model (SCDF).

quite different. As mentioned above, 50% of the travel times in the TCDF were greater than 18,000 yr and 10% were greater than 27,000 yr. In the SCDF, 50% of the travel times are greater than 25,000 yr and 10% are greater than 37,500 yr. The maximum travel times for the steady-state and transient-calibrated fields are 57,000 yr and 33,000 yr, respectively. The histogram of travel times using only the steady-state calculated models also illustrates this point (Figure 6.8-10).

Thus, the calibration to the transient-pressure data has significantly reduced the magnitude and range of observed travel times. The extension of the high-transmissivity zone toward the H-15 borehole and the subsequent effect the extension has upon the reduction in travel distance from the starting point (above the center of the waste-disposal region) to a region of higher transmissivities has reduced the uncertainty in the travel times. The reduction in uncertainty occurs, as stated above, because of the modifications to the CS transmissivity fields in the southeastern region of the land-withdrawal area, which are necessary to match the observed transient pressures in this region.

For comparison purposes, the travel paths that correspond to the travel times contained in the SCDF are illustrated in Figure 6.8-11. Like the travel paths shown in Figure 6.8-8, most of the travel paths follow a southeasterly direction until reaching the DOE-1 vicinity at which time the paths travel directly south to the land-withdrawal boundary. A few more paths traveldirectly south from the starting point while several others have an east-southeasterly direction prior to moving south toward the land-withdrawal boundary. In general though, the distribution of paths seems very similar to those illustrated in Figure 6.8-8.

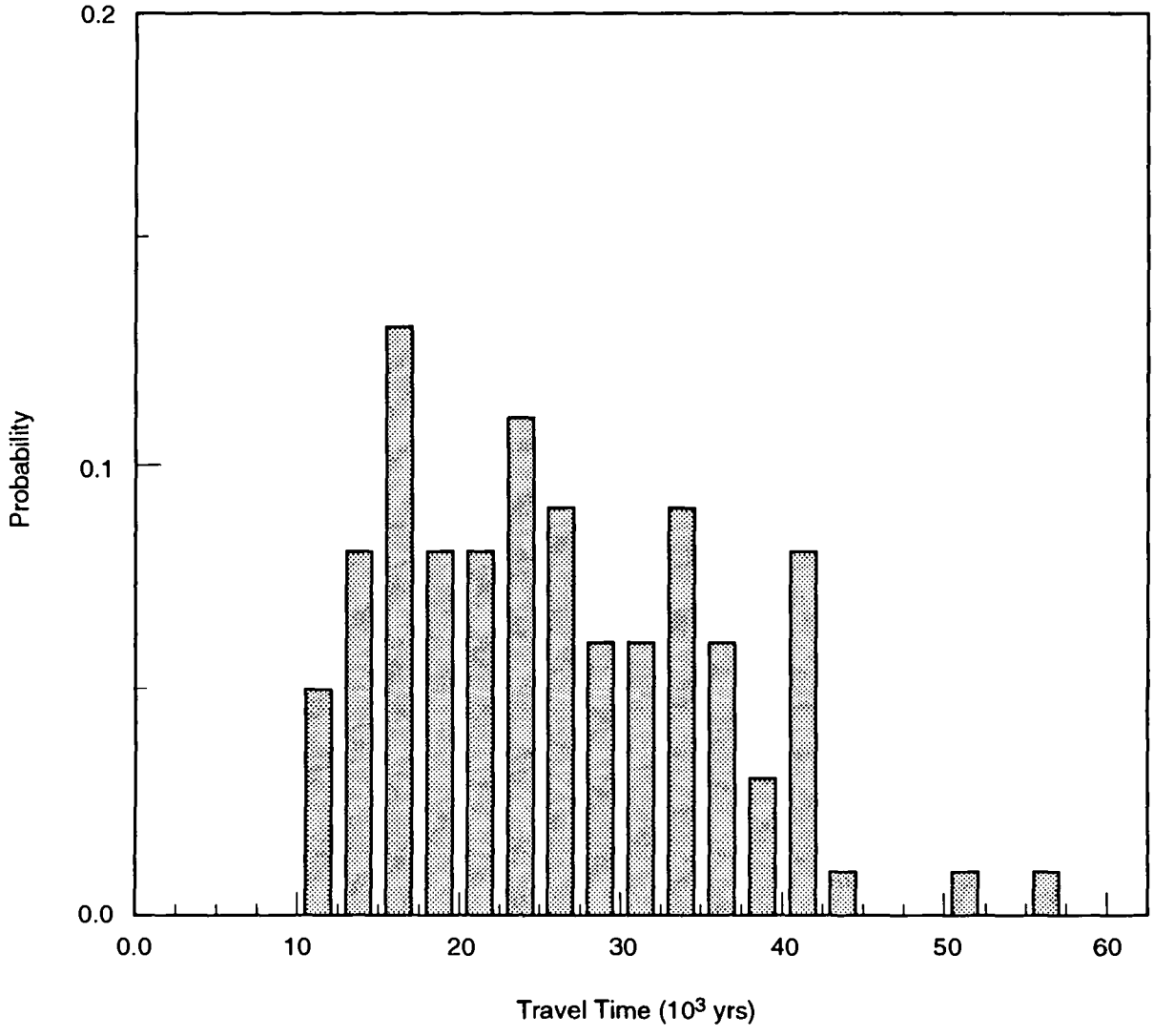

Figure 6.8-10. Histogram of travel times from ensemble of fields calibrated only to steady-state head data.

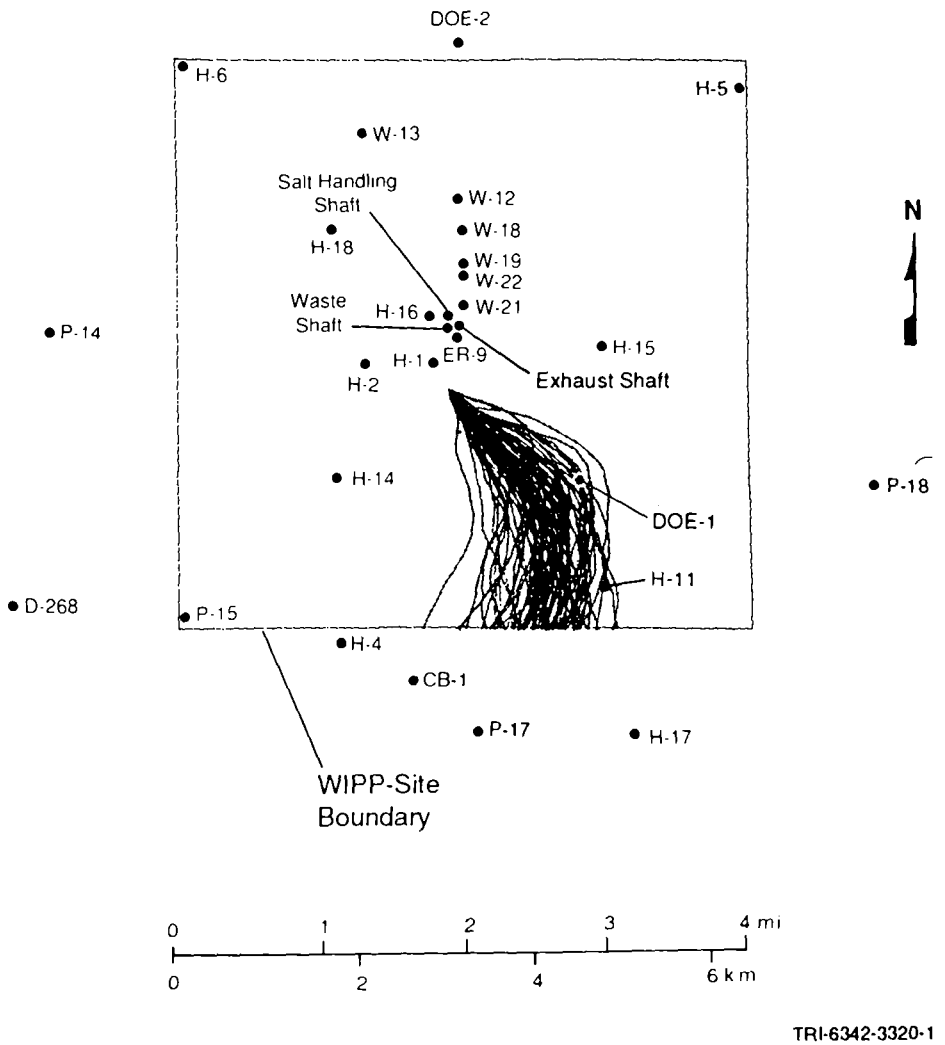

Figure 6.8-11. Travel paths associated with ensemble of transmissivity fields calibrated only to steady-state head data.

7. DISTURBED PERFORMANCE: DIRECT RELEASES TO THE GROUND SURFACE DURING DRILLING

This chapter describes the implementation of the 1992 PA model CUTTINGS for calculating the quantity of radionuclides removed directly to the surface due to an intrusion event. Only exploratory drilling for hydrocarbons is considered. Present-day rotary drilling methods are assumed to persist throughout the regulatory period. Cuttings are estimated based on the drill-bit diameter which is a sampled variable with a CDF constructed from past drilling history in the Delaware Basin (Section 4.4.2 of Volume 3 of this report). Cavings, comprised of waste material eroded from the borehole wall by drilling fluid, are also removed to the surface with the cuttings. The amount of cavings removed depends on the assumption that erosion occurs when the calculated drilling fluid shear stress exceeds the effective shear strength of the consolidated waste, as estimated from analogue data (Table 3.4.1 of Volume 3 of this report). The quantity of waste material spalled from the borehole wall when the drill bit penetrates a gas-pressurized waste panel has not been included because this mechanism is not yet sufficiently understood. Modeling and laboratory work are presently investigating this phenomenon. When constant λs are used, the assumption that present-day drilling technology and practice persists for 10,000 yr is consistent with the philosophy that the risk to future generations should be equally weighted with that to the present generation. The assumptions concerning future levels of technology made by the Futures Panel (memorandum by Hora in Appendix A of Volume 3 of this report) and used for constructing time-varying λs, however, indicate a lower risk to future generations that is not wholly consistent with this philosophy. The volume of waste brought to the ground surface will depend upon the physical properties of the compacted, decomposed wastes, the drilling procedures used, and the pore pressures encountered. Because of radioactive decay, the radioactivity of the removed waste (in curies) will also depend upon the time of intrusion.

7.1 Current Drilling Practices

In standard rotary drilling, a cutting bit attached to a series of hollow drill collars and drill pipes is rotated at a fixed angular velocity and is directed to cut downward through the underlying strata. To remove the drill cuttings, a fluid is pumped down the drill pipe, through and around the drill bit, and up to the surface within the annulus formed by the drillpipe and the borehole wall (Figure 7.1-1). In addition to the removal of cuttings, the drilling fluid (mud) serves to cool and clean the bit, reduce drilling friction, maintain borehole stability, prevent the inflow of

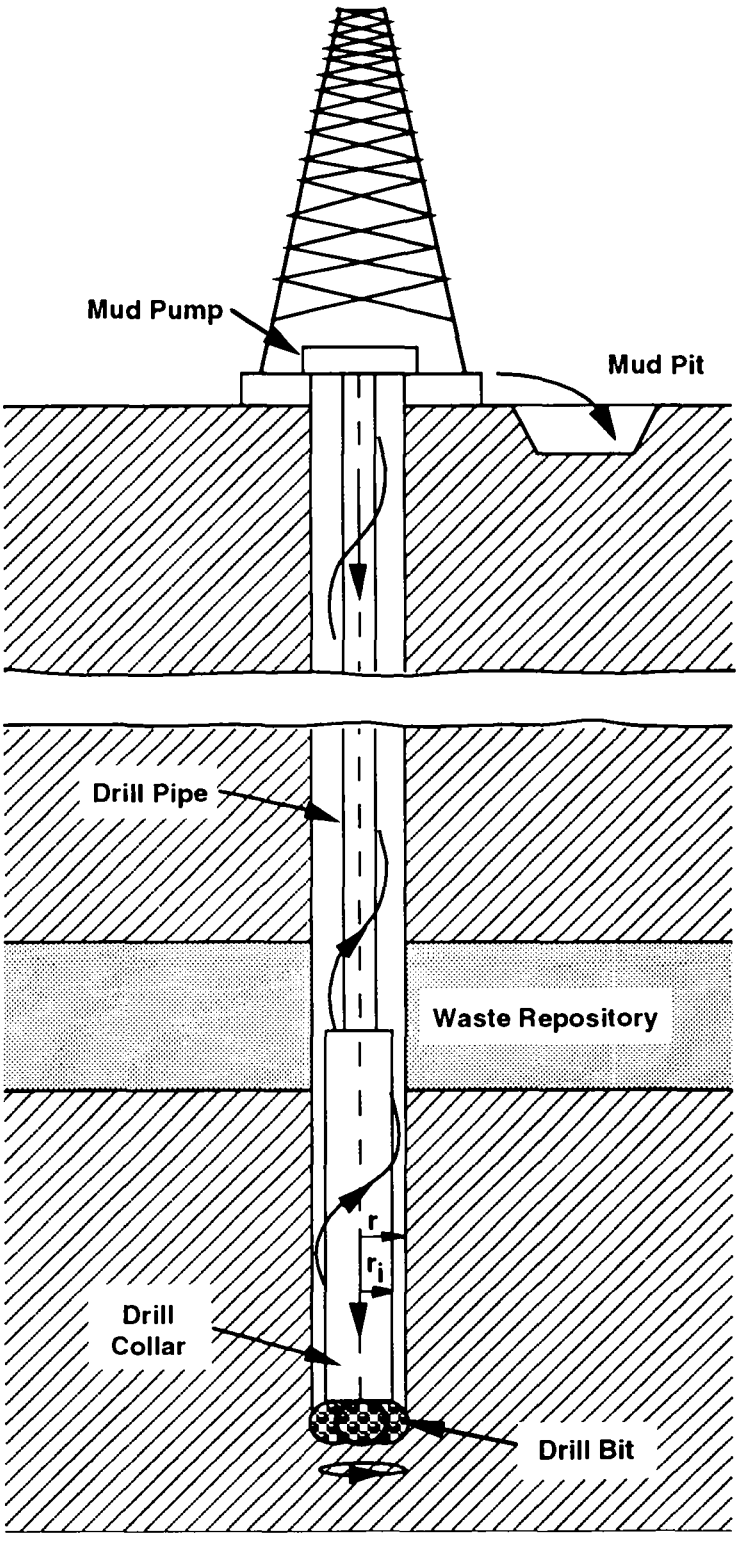

Figure 7.1-1. Rotary drilling.

unwanted fluids from permeable formations, and form a thin, low-permeability barrier on the surface of penetrated formations. When drilling through salt, a saturated brine is often used as the drilling fluid to prevent excessive erosion of the borehole wall through dissolution (Berglund, 1990; Pace, 1990). For a gauge borehole, the volume of cuttings removed and transported to the surface is equal to the product of the drill-bit area and the drill depth. Thus, to estimate the total volume of waste removed due to the cutting action of the drill-bit, it is only necessary to know the compacted repository height and the drill-bit area. The cuttings volume calculated in this manner is a lower bound to the total quantity of waste removed by drilling.

After passing through the drill bit, the drilling fluid flows up the annulus formed by the borehole wall and the drill collar (or drill pipe). In the annulus, the motion of the drilling fluid has both a vertical and rotational component, the latter caused by the rotating drill string. Depending on fluid properties, annulus geometry, and flow rates, the fluid flow within the annulus may be smooth and laminar or turbulent.

7.2 Mechanisms for Waste Removal

There are at least two mechanisms that can be identified as contributing to the removal of waste to the accessible environment over and above that transported by the direct cutting of a gauge borehole. The first is the erosion of the borehole wall caused by the action of the upward-flowing drilling fluid within the annulus. This eroded material is referred to as cavings. The second arises from the effect on the waste of waste-generated gas escaping to the lower-pressure borehole. Material released by this mechanism is referred to as spallings. Both of these phenomena and models for them are discussed in detail by Berglund (1992). In the case of erosion, Berglund (1992) has developed a quantitative model that is based on an effective shear strength for erosion of the compacted, decomposed waste. In the absence of specific experimental data, waste removal from the borehole wall into the drilling fluid due to gas flow is much more difficult to address. For this latter mechanism, Berglund (1992) discusses the general phenomenology, but no quantitative model is available.

7.2.1 Mechanism I: Erosion within the Borehole Annulus

Although a number of factors exist that may influence borehole erosion, Berglund (1992) identifies the effects of fluid shear acting on the borehole wall and the character of the fluid flow (laminar or turbulent) as the most important. To consider these effects, it is necessary to know the threshold

fluid shear stress acting on the borehole wall that will initiate erosion. This "effective" borehole shear strength for erosion must be determined by experiment and may be different for laminar and turbulent flow. In Berglund's (1992) analysis, it is assumed that borehole erosion is caused primarily by the magnitude of the fluid shear stress acting on the borehole wall. Other effects are generally ignored, except insofar as they may influence the experimentally determined effective shear strength for erosion of the repository material.

In the annulus formed by the collars or drill pipe and the borehole wall, the flow of the drilling fluid has both a vertical and rotational component. Within this helical flow pattern, shear stresses are generated by the relative motion of adjacent fluid regions and by the action of the fluid on the borehole wall. It is assumed that if the fluid shear stress at the wall exceeds the effective shear strength for erosion of the wall material (caked drilling fluid or compacted repository wastes), erosion of the wall material will occur, increasing the diameter of the bored hole. The eroded material will then be passed to the surface in the flowing drilling fluid.

Flow in the annulus between the drill pipe and borehole wall is usually laminar (Darley and Gray, 1988). Adjacent to the collars (Figure 1-1), however, the flow may be either laminar or turbulent as a consequence of the larger collar diameter and resulting higher mud velocities (Berglund, 1990; Pace, 1990). For laminar flow, the analysis lends itself to classical solution methods. Turbulent flow, where the flow is assumed to be axial with no rotational component, requires a more approximate approach. For both cases, erosion is assumed to be axisymmetric. The following discussion of these two cases is taken from Berglund (1992).

7.2.1.1 LAMINAR FLOW

Below Reynolds numbers[1] of about 2100 for Newtonian fluids and 2400 for some non-Newtonian fluids (Walker, 1976), experiments have shown that the flow of a fluid in a circular pipe or annulus is well behaved and can be

---

1. The Reynolds number (R_e) is defined as

$$R_e = \frac{\overline{\rho} V D_e}{\overline{\eta}} \qquad (7.2\text{-}1)$$

where D_e is the equivalent hydraulic diameter, $\overline{\rho}$ is the drill fluid density, V is the average fluid velocity, and $\overline{\eta}$ is the average fluid viscosity.

described using a well-defined relationship between the velocity field and the fluid shear stress. This type of flow is called laminar.

Some of the early work on laminar helical flow of a non-Newtonian fluid in an annulus was performed by Coleman and Noll (1959), and Fredrickson (1960). The laminar helical flow solution procedure used in the CUTTINGS code is, for the most part, an adaptation of methods described in a paper by Savins and Wallick (1966).

One of the principal difficulties in solving for the shear stresses within a helically flowing drilling fluid is the shear-rate dependence of the fluid viscosity. This non-Newtonian fluid behavior necessitates choosing a functional form for the variation of viscosity with shear rate for the fluid. There are several functional forms for the viscosity of drilling fluids that can be assumed. For example, in the oil and gas industry, the Bingham and power law models are often used to approximate the shear rate dependence of the fluid viscosity. An alternative form is that chosen by Oldroyd (1958) and used in the analysis by Savins and Wallick (1966). Oldroyd assumed that the viscosity varied according to the functional relation

$$\eta = \eta_o \left[\frac{1+\sigma_2 \Gamma^2}{1+\sigma_1 \Gamma^2} \right] , \qquad (7.2\text{-}2)$$

where σ_1 and σ_2 are constants, η_o is the limiting viscosity at zero rate of shear and Γ is the shear rate. The viscous shear stress is described by $\tau = \eta\Gamma$.

Using the Oldroyd viscosity, Eq. 7.2-2, the viscous shear stress can be illustrated graphically as in Figure 7.2-2. This is a rate softening (pseudoplastic) model that has an initial slope of η_o and a limiting slope of η_∞ for large shear rates, where η_∞ (defined as $\eta_o(\sigma_2/\sigma_1)$) is the limiting viscosity at infinite rate of shear.

The Oldroyd model cannot account for drilling fluids that exhibit a yield stress. However, above a shear rate of zero, parameters can be chosen so that the model can be made to approximate the pseudoplastic rate response of many drilling fluids (see Figure 7.2-1).

Savins and Wallick (1966), expanding on the work of Coleman and Noll (1959) and Fredrickson (1960), showed that the solution for laminar helical flow of a non-Newtonian fluid in an annulus could be written in terms of three nonlinear integral equations.

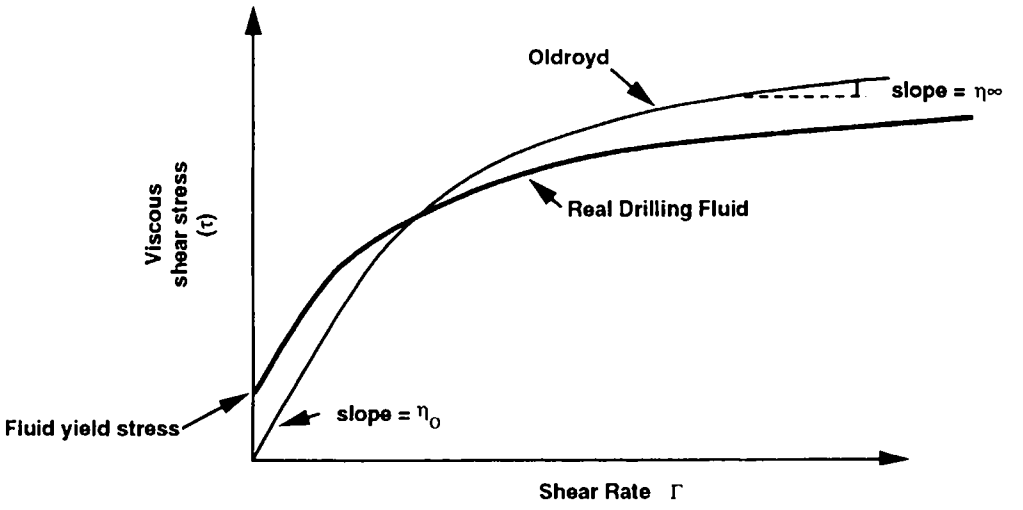

Figure 7.2-1. Viscous shear stress for Oldroyd and real drilling fluids.

These three nonlinear integral equations must be solved numerically (Berglund, 1992). A Fortran computer CUTTINGS code was written to perform the necessary computations for a solution to the problem of laminar helical flow in an annulus. This code was partially verified by comparing its results against those published by Savins and Wallick (1966).

For the specific case of borehole erosion, once a solution to the three integral equations is found, the shear stress in the fluid at the wall can be calculated. By changing the outer radius of the hole, the fluid shear stress can be forced to equal the repository effective shear strength for erosion. The required outer hole radius is determined by iteration as shown in Figure 7.2-2.

The effective shear strength for erosion equals the threshold value of fluid shear stress required to sustain general erosion at the borehole wall. Partheniades and Paaswell (1970), in discussing investigations on the erosion of seabed sediments and in channels, have noted that this effective soil shear strength is not related to the soil shear strength as normally

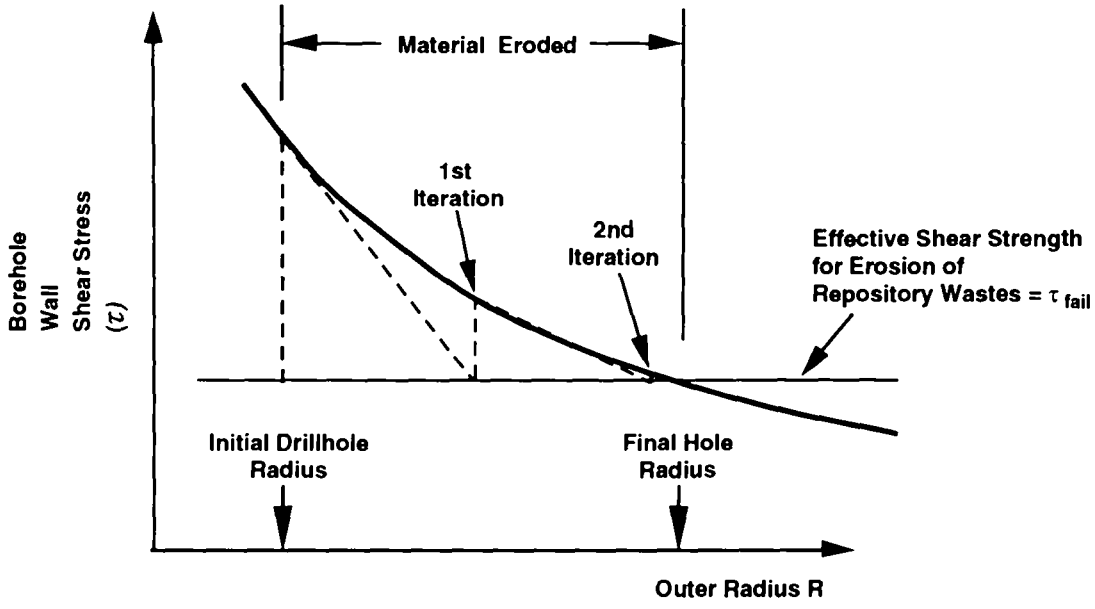

Figure 7.2-2. Iteration procedure for finding the final hole radius.

determined from conventional soil tests. The effective shear strength for erosion based on seabed data, as determined by Partheniades and Paaswell (1970), is on the order of 1 to 5 Pa and is thus smaller by several orders of magnitude than the macroscopic soil shear strength.

7.2.1.2 TURBULENT FLOW

For Newtonian fluids with Reynolds numbers greater than about 2100, flow in a circular pipe or annulus starts to become more or less random in character, which makes orderly mathematical analysis of the flow difficult, if not impossible. With increasing Reynolds numbers, this random behavior increases until, at a Reynolds number of about 3000, the flow becomes fully turbulent. In fully turbulent flow, momentum effects dominate and the fluid viscosity is no longer important in characterizing pressure losses.

For Newtonian fluids, the value to use for the viscosity is clear because the viscosity is constant for all rates of shear. Non-Newtonian fluids exhibit a changing viscosity with shear rate and present a special problem in calculating R_e. For fluids that exhibit a limiting viscosity at high rates of shear (such as the Bingham model and in our case the Oldroyd

model), it has been suggested (Broc, 1982) that the limiting viscosity ($\bar{\eta} = \eta_\infty$) be used in calculating the Reynolds number.

The Reynolds number for an Oldroyd fluid in an annulus can then be written as (Broc, 1982)

$$R_e = \frac{0.8165 D \bar{V} \rho}{\bar{\eta}} , \qquad (7.2\text{-}3)$$

where the hydraulic diameter is expressed as $D = 2(r - r_i)$, where r is the radius of the drill bit and r_i is the radius of the drill collar (see Figure 7.1-1).

The most important influence viscosity has on the calculation of pressure losses in fully turbulent flow of non-Newtonian fluids appears to be in the calculation of the Reynolds number. A far more important parameter is the surface roughness past which the fluid must flow. As previously noted, the Reynolds number, however, does have a role in determining the onset of turbulence; for Newtonian fluids this critical number R_{ec} is about 2100. For non-Newtonian, rate-thinning fluids, R_{ec} tends to be greater than 2100 but less than 2400 (Walker, 1976). For our purposes, a value of 2100 will be used to represent R_{ec} for the Oldroyd fluid model. Because turbulent flow is more effective in generating fluid shear stresses at the borehole wall, this assumption is conservative.

A transition region exists beyond R_{ec} before the development of fully turbulent flow. In this regime, the flow has the character of both laminar and turbulent flow. However, because pressure losses increase rapidly in turbulent flow and affect borehole shear stresses more severely, it will be assumed that beyond R_{ec} the flow is fully turbulent.

Turbulent flow is very complex and, thus, to characterize the turbulent flow regime, the great bulk of analysis has concentrated on empirical procedures. For axial flow in an annulus, the pressure loss under turbulent conditions can be approximated by (Broc, 1982)

$$\Delta P = \frac{2 f L \bar{\rho} \bar{V}^2}{(0.8165) D} , \qquad (7.2\text{-}4)$$

where f is the coefficient of pressure head loss (Fanning friction factor) and L is the borehole length.

If the shear stress due to the flowing fluid is assumed to be uniformly distributed on the inner and outer surfaces of the annulus, it can be easily

shown using Eq. 7.2-4 that the shear stress is related to the average fluid velocity through the relation

$$\tau = \frac{f\overline{\rho V^2}}{2(0.8165)} \quad , \tag{7.2-5}$$

The Fanning friction factor is empirically related to the Reynolds number and relative roughness by the equation (Whittaker, 1985)

$$\frac{1}{\sqrt{f}} = -4\log_{10}\left(\frac{\varepsilon}{3.72D} + \frac{1.255}{Re\sqrt{f}}\right) \quad , \tag{7.2-6}$$

where ε/D is the relative roughness. For circular pipes, D in this equation represents the inside diameter and ε is the absolute roughness or the average depth of pipe wall irregularities. In the absence of a similar equation for flow in an annulus, it will be assumed that this equation also applies here, where D is the hydraulic diameter as defined earlier and ε is the absolute roughness of the waste-borehole interface.

Using a relative roughness and a calculated Reynolds number, a Fanning friction factor can be determined by iteratively solving Eq. 7.2-5. The value of the shear stress acting on the borehole wall can then be determined from Eq. 7.2-4. Using an iterative procedure similar to that for the laminar flow problem (Figure 7.2-2), the fluid shear stress can be forced to equal the repository shear strength for erosion (τ_{fail}) to obtain the final eroded borehole radius.

In the actual solution sequence employed in CUTTINGS, the Reynolds number is calculated first to determine which solution regime (laminar or turbulent) should be initiated. For Reynolds numbers initially less than R_{ec}, the code calculates the flow as laminar. Any increase in diameter of the borehole calculated during the laminar calculation will cause the Reynolds number to decrease as a result of a velocity decrease, ensuring that the calculation remains laminar. If the initial Reynolds number is greater than R_{ec}, the turbulent formulation is used to calculate borehole erosion. When the turbulent calculation is complete, a check is again made to determine whether the Reynolds number still exceeds R_{ec}. If it does not, the laminar calculation is performed starting with a "critical" borehole radius. The critical borehole radius corresponds to a Reynolds number of R_{ec} and is given by

$$R_{crit} = \frac{\overline{\rho}Q}{1286\pi\eta_{\infty}} - R_i, \tag{7.2-7}$$

7.2.1.3 EROSION CALCULATIONS

The equations governing erosion based on laminar and turbulent flow were combined into a single Fortran computer code called CUTTINGS. Using appropriately selected input based on the physical properties of the waste and other drilling parameters, this code calculates the final eroded diameter of the borehole that passes through the waste. The drilling parameters chosen must reflect data typical of that valid near the WIPP repository. Berglund (1992) provides a discussion of suitable parameter values and model sensitivity to uncertainty in those parameters. Drill bit diameter (DBDIAM) is the most important parameter, and is the only parameter used with the CUTTINGS code that is sampled in the 1992 PA. Values for other model parameters are given in Berglund (1992) and Chapter 4 of Volume 3 of this report.

7.2.2 Mechanism II: Waste-Gas-Induced Borehole Spall

The storage, compaction, and brine-induced corrosive degradation of transuranic waste is not directly analogous to any known phenomenon that has occurred in nature. However, considerable information exists in the literature on the exploration for and production of fossil fuels and the problems encountered during these activities. The failure, sloughing, or spalling of borehole walls is a common occurrence in oil and gas drilling and can be caused by a number of different mechanisms, including an encounter with a geopressurized formation. Available literature, summarized by Berglund (1992), supports the need to study the potential for gas-induced spall in waste. The problem is complex, involving the flow of gas in a moving waste matrix, changing stress states, changing porosity and permeability of the waste, waste failure, and, when the waste interacts with the drill bit, turbulent mixing of the three phases – solid waste, drilling fluid, and gas. Berglund (1992) describes simplifying assumptions and modeling approaches that could be used for the WIPP PA. Spalling has not been included in the 1992 PA, and implementation of any of the available models will require additional information about the material properties of decomposed and compacted wastes. Tests are planned to provide this information (US DOE, 1990, in revision). Until such information is available, estimates of releases due to spalling are speculative. Berglund (1992) concludes, however, that "it does not appear unreasonable that volumes of waste several times greater than the lower bound volume [bit area times waste thickness] could eventually reach the ground surface" as a result of spalling. The volumes of waste removed as cavings in the 1991 and 1992 PAs are also several times greater than cuttings volumes. As shown in

Section 5.1 of Volume 1 and Section 8.5 of this volume, the cuttings releases (including cavings but not yet including spallings) control the location of the CCDF (and therefore regulatory compliance) if retardation by either matrix diffusion or sorption occurs in the Culebra Dolomite Member of the Rustler Formation.

7.3 Radionuclide Inventory Available for Removal

Figure 7.3-1 shows the EPA-normalized inventory of the repository, radionuclide by radionuclide, as a function of time (based on the most recent Integrated Data Base [IDB; US DOE, 1991] as reported in the memorandum by Peterson in Appendix A of Volume 3). Time-dependent inventories are shown to 10^4 yr, which is the end of the regulatory period specified by 40 CFR 191B. All radionuclides shown in Figure 7.3-1 are included in the estimation for cuttings release in the 1992 PA. Radionuclides whose normalized inventories never exceed 10^{-2} during 10^4 yr cannot result in releases greater than 10^{-2}, and are not considered in analyses of subsurface transport for 40 CFR 191B.

Figure 7.3-1a shows that the normalized inventories of Pu-239, Pu-240, Am-241, U-233, U-234, Np-237, Th-229, Th-230, and Ra-226 all exceed 10^{-2} during the 10^4-yr period. Figure 7.3-1b shows an additional radionuclide with normalized inventory exceeding 10^{-2}, Pu-238, which is significant only early in the regulatory period. PA modeling for 1991 examined subsurface transport to the accessible environment of 7 of these radionuclides (Pu-239, Pu-240, Am-241, U-233, U-234, Np-237, and Th-230) (WIPP PA Division, 1991c, Section 6.5.2.10). Subsurface transport of two of the remaining radionuclides is modeled in 1992, Th-229 and Ra-226. Transport of Pu-238 in the Culebra will not be modeled because of its short half-life (87.7 yr). Pb-210, which reaches an EPA-normalized inventory of 10^{-2} at late times approaching 10^5 yr, may be considered for subsurface transport in future dose calculations as a daughter product created in the Culebra. Groundwater transport of Pb-210 is not modeled here because of its low inventory at 10^4 yr and short half-life (22.3 yr), and consequent low impact on 40 CFR 191B compliance. Transport of both Pu-238 and Pb-210 in brine brought directly to the ground surface following intrusion (not yet included in performance assessments) also has the potential to contribute to doses.

Table 7.3-1 lists the initial inventory of waste used in the 1992 calculations, Table 7.3-2 lists the decay chains used for transport calculations in the Culebra Dolomite, and Table 7.3-3 lists the activity levels considered in the estimation of cuttings releases.

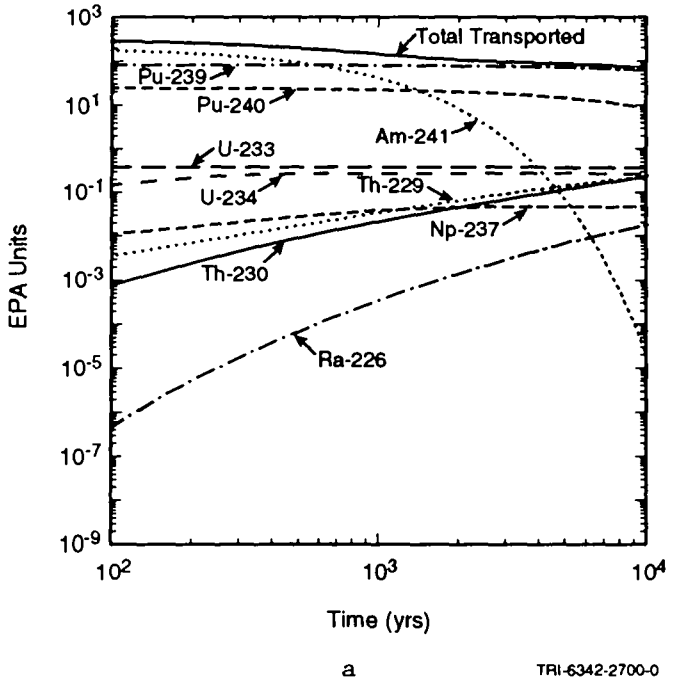

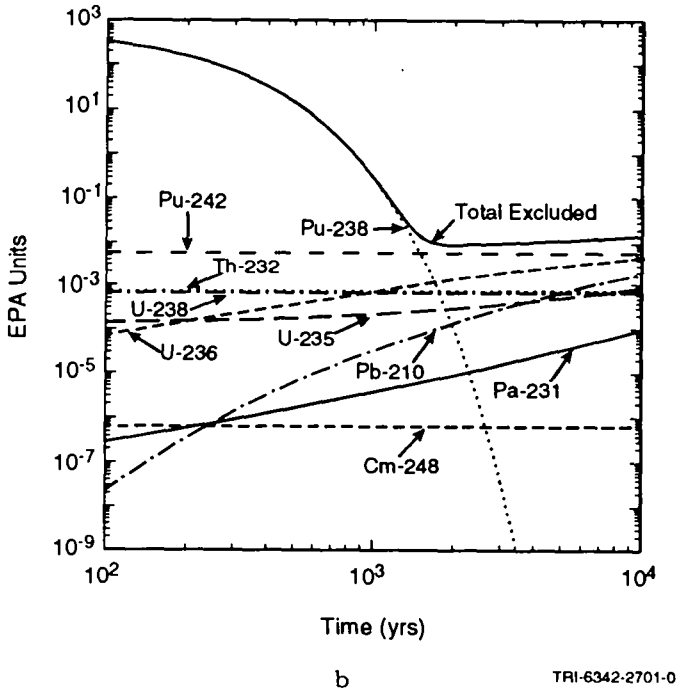

Figure 7.3-1. Decay histories expressed in EPA units (i.e., the normalized units used in showing compliance with 40 CFR 191) for the present IDB inventory for a single waste panel. The total WIPP inventory used in the 1992 PA is ten times the values shown in this figure. Figure 7.3-1a shows radionuclides included in groundwater transport calculations. Figure 7.3-1b shows radionuclides not included in groundwater transport because of low inventory or short half-life. All radionuclides shown are included in estimates of cuttings releases.

The cuttings releases used in the 1992 WIPP performance assessment were calculated with the program CUTTINGS for waste of average activity level. Then, the releases for activity levels 1 through 5 shown in Table 7.3-3 were obtained by multiplying the average activity level releases by scale factors of the form

$$SF_{i\ell} = AL_{i\ell}/AL_i, \tag{7.3-1}$$

where

$AL_{i\ell}$ = projected radioactivity (Ci/m^2) contained in waste of activity level ℓ at time i, where 1 ~ 125 yr, 2 ~ 175 yr, 3 ~ 350 yr, 4 ~ 1000 yr, 5 ~ 3000 yr, and 6 ~ 7250 yr,

and

AL_i = projected radioactivity (Ci/m^2) contained in waste of average activity at time i.

For example, the scale factor

$$SF_{24} = 184.01/7.9658 = 23.100 \tag{7.3-2}$$

is used to convert from a release of average activity at 3000 yr to a release of activity level 4 at 3000 yr.

Table 7.3-1. Potentially Important Radionuclides Associated with Initial Contact-Handled Waste Inventory Used in Calculations for Cuttings Removal and Release to Culebra Dolomite (from memorandum by Peterson in Appendix A of Volume 3)

Radionuclide	$t_{1/2}$(yr)	Curies
Pu-238	8.77×10^{1}	3.06×10^{6}
Pu-239	2.41×10^{4}	3.35×10^{5}
Pu-240	6.53×10^{3}	1.00×10^{5}
Pu-242	3.76×10^{5}	2.35×10^{1}
U-233	1.59×10^{5}	1.53×10^{3}
U-234	2.44×10^{5}	0
U-236	2.34×10^{7}	0
Am-241	4.32×10^{2}	7.14×10^{5}
Np-237	2.14×10^{6}	2.08×10^{1}
Th-229	7.43×10^{3}	0
Th-230	7.70×10^{4}	0
Ra-226	1.60×10^{3}	0

Table 7.3-2. Simplified Radionuclide Decay Chains Used for Transport Calculations in the Culebra Dolomite (from Figure 3.3.1 of Volume 3 of this report)

(1) Pu-240

(2) Am-241 → Np-237 → U-233 → Th-229

(3) U-234 → Th-230 → Ra-226

(4) Pu-239

Table 7.3-3. Projected Activity Levels (Ci/m^2) in the WIPP Due to Waste that is Currently Stored and May Be Shipped to the WIPP (based on Memorandum by Peterson in Appendix A of Volume 3 of this report)

Activity Level	Type[a]	Probability[b]	Time (yr) 0	125	175	350	1000	3000	7250
1	CH[c]	0.3968	2.7578	0.7994	0.6468	0.3884	0.2078	0.1387	0.1156
2	CH	0.3572	27.578	7.9941	6.4683	3.8844	2.0782	1.3867	1.1559
3	CH	0.1259	275.78	79.941	64.683	38.844	20.782	13.867	11.559
4	CH	0.0060	2757.8	799.41	646.83	388.44	207.82	138.67	115.59
5	RH[d]	0.1141	124.70	7.7110	3.3430	1.1180	0.8210	0.7080	0.6280
Average for CH Waste:			70.145	20.333	16.452	9.8800	5.2860	3.5270	2.9400

a CH designates contact-handled waste; RH designates remotely-handled waste

b Probability that a randomly placed borehole through the waste panels will intersect waste of activity level ℓ, $\ell = 1,2,3,4,5$.

c CH activity levels based on 111,520 m^2 total surface area

d RH activity levels based on 14,360 m^2 total surface area

8. UNCERTAINTY AND SENSITIVITY ANALYSIS RESULTS

8.1 Scenario Probability

As indicated in Section 2.3, drilling intrusions into the repository are assumed to follow a Poisson process in the 1992 WIPP performance assessment. Both stationary (i.e., constant λ) and nonstationary (i.e., time-dependent λ) processes are considered. The rate term in these processes is treated as being uncertain; the sampled variable LAMBDA in Table 3-1 is used to identify the λ used for each sample element. For the stationary case, the actual λ used in the analysis is assumed to be uniformly distributed on the interval $[0, 3.78 \times 10^{-4}\ \text{yr}^{-1}]$. For the nonstationary case, the $\lambda(t)$'s used in the analysis were developed in an expert review process (memorandum by Hora, Appendix A, pp. A-69 to A-99, of Volume 3) and are listed in Appendix D of Volume 3.

This section contains two illustrations of the uncertainty in scenario probability. Probabilities for the scenarios

$$S(0,0),\ S(1,0),\ \ldots,\ S(6,0) \tag{8.1-1}$$

used in conjunction with the risk representation R_1 defined in Eq. 2.5-1 are shown in Figure 8.1-1. Figure 8.1-1 shows scenario probabilities determined with both constant λ's and time-dependent λ's. As a reminder, the risk representation R_1 uses time intervals of [0, 2000 yr] and [2000, 10,000 yr] as indicated in Eq. 2.5-2. For both the constant and time-dependent cases, the individual λ's are assumed to equal 0 yr^{-1} after 2000 yr. The actual formulas used to calculate the probabilities are given in Eqs. 2.5-4 and 2.5-6. As examination of Figure 8.1-1 shows, scenario probability decreases rapidly with increasing number of drilling intrusions. Further, the use of the time-dependent λ's results in considerably lower scenario probabilities for scenarios involving drilling intrusions than the use of constant λ's.

Probabilities for the scenarios

$$S(0,0,0,0,0,0), S(1,0,0,0,0,0), S(0,1,0,0,0,0), \ldots, S(0,0,0,0,0,1) \tag{8.1-2}$$

used in conjunction with the risk representation R_2 defined in Eq. 2.5-8 are shown in Figure 8.1-2. Figure 8.1-2 shows scenario probabilities determined with both constant λ's and time-dependent λ's. As a reminder, the risk representation R_2 uses time intervals of [0, 150 yr], [150, 200 yr],

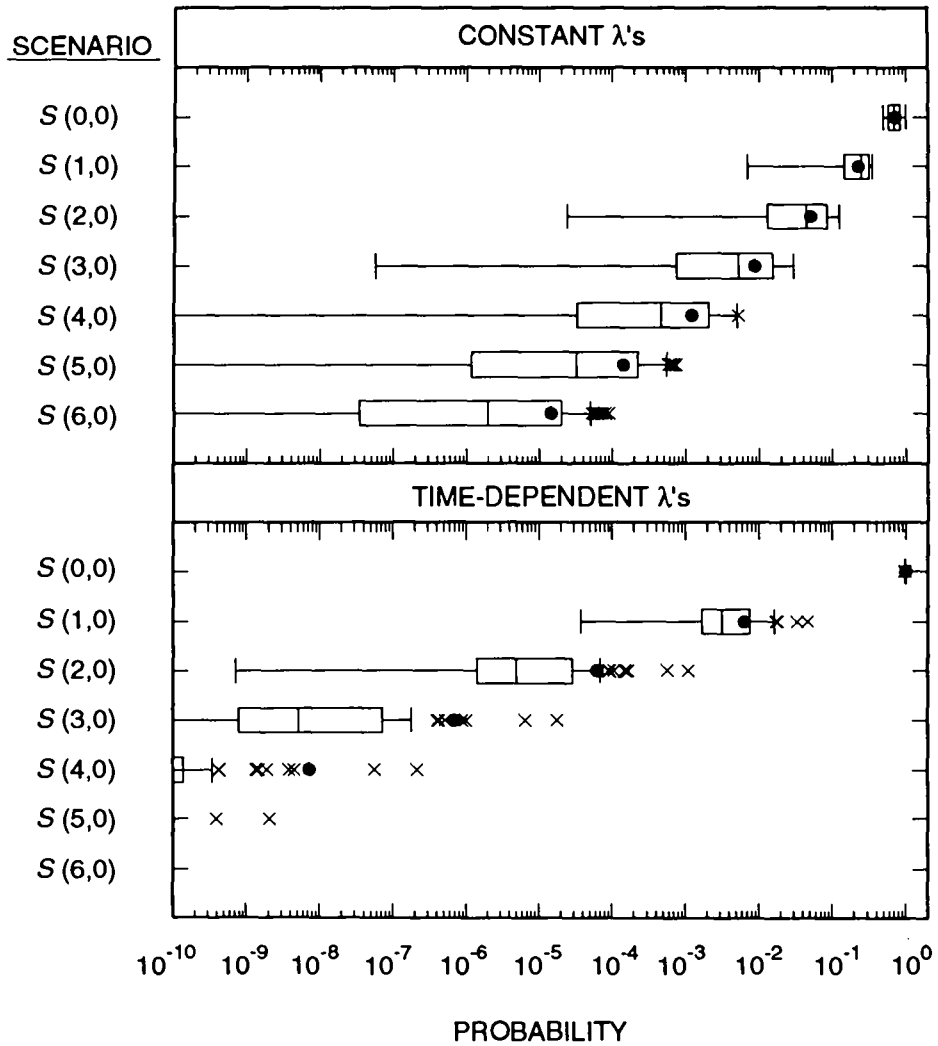

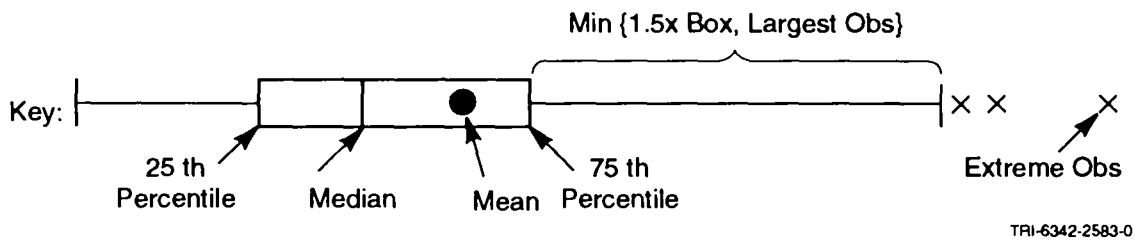

Figure 8.1-1. Uncertainty in probability of scenarios $S(0,0)$, $S(1,0)$, ..., $S(6,0)$ used in conjunction with the risk representation R_1 defined in Eq. 2.5-1 with an assumed 100 yr period of administrative control in which drilling intrusions cannot occur.

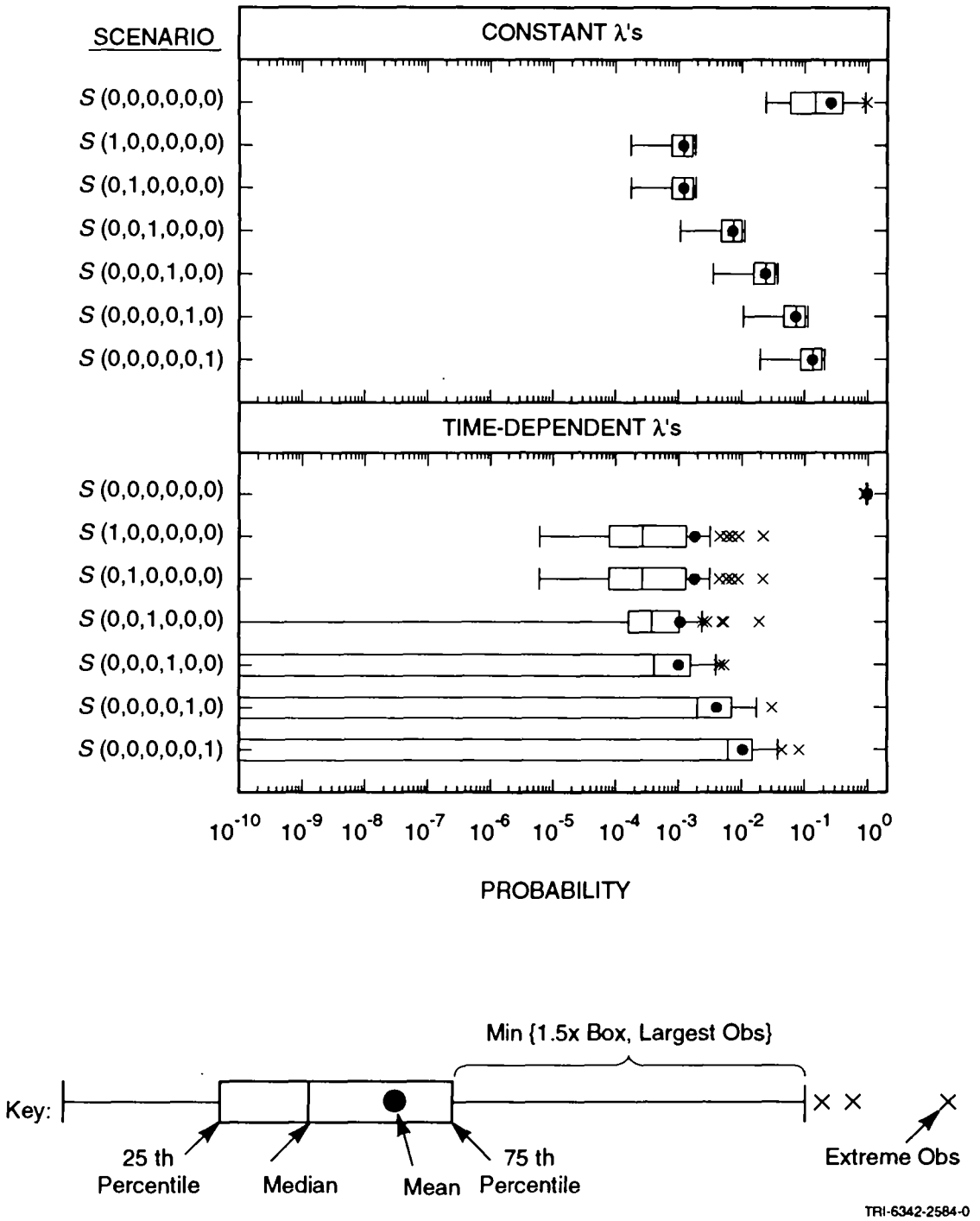

Figure 8.1-2. Uncertainty in probability of scenarios $S(0,0,0,0,0,0)$, $S(1,0,0,0,0,0)$, $S(0,1,0,0,0,0)$, ... , $S(0,0,0,0,0,1)$ used in conjunction with the risk representation R_2 defined in Eq. 2.5-8 with an assumed 100 yr period of administrative control in which drilling intrusions cannot occur.

[200, 500 yr], [500, 1500 yr], [1500, 4500 yr] and [4500, 10,000 yr] as indicated in Eq. 2.5-9. The formula used to calculate the probabilities is given in Eq. 2.3-1 and specializes to

$$pS(\mathbf{n}) = \left\{ \prod_{i=1}^{nT} [\lambda(t_i - t_{i-1})]^{n(i)}/n(i)! \right\} \exp[-\lambda(t_{nT} - t_0)] \qquad (8.1\text{-}3)$$

for the constant λ case. The differences in probability between scenarios in Figure 8.1-2 result from the use of unequal time intervals in scenario definition.

The probabilities in Figure 8.1-2 are for exactly 1 intrusion over 10,000 yr, with that intrusion occurring in a specified time interval. As indicated in Tables 2.5-3 and 2.5-4, many different combinations of drilling intrusion times are used in the definition of the risk representation R_2 given in Eq. 2.5-8. Because of the large number of scenarios involved, box plots of the form shown in Figure 8.1-2 cannot be presented for all scenarios contained in R_2. However, due to the effects of radioactive decay, the cuttings releases for a scenario are often dominated by the time at which the first drilling intrusion occurs. For this reason, it is useful to examine the probability of drilling intrusions in specified time intervals regardless of the drilling intrusions that may occur in subsequent time intervals. Specifically, Figure 8.1-3 presents probabilities for the scenarios

$$S(\geq 1,\geq 0,\geq 0,\geq 0,\geq 0,\geq 0),\ S(0,\geq 1,\geq 0,\geq 0,\geq 0,\geq 0),\ S(0,0,\geq 1,\geq 0,\geq 0,\geq 0),$$
$$S(0,0,0,\geq 1,\geq 0,\geq 0),\ S(0,0,0,0,\geq 1,\geq 0),\ S(0,0,0,0,0,\geq 1), \qquad (8.1\text{-}4)$$

where the notation $\geq n(i)$ in expressions of the form

$$S(\geq n(1),\ \geq n(2),\ \geq n(3),\ \geq n(4),\ \geq n(5),\ \geq n(6)) \qquad (8.1\text{-}5)$$

indicates that the number of drilling intrusions in the i^{th} time interval (i.e., $[t_{i-1}, t_i]$) equals or exceeds n(i). For example, the scenario $S(0,\geq 1,\geq 0,\geq 0,\geq 0,\geq 0)$ appearing in Eq. 8.1-4 consists of all time histories contained in the sample space S defined in Eq. 2.2-1 in which 0 drilling intrusions occur in the time interval [0, 150 yr], 1 or more drilling intrusions occur in the time interval [150, 200 yr], and 0 or more drilling intrusions occur in each of the time intervals [200, 500 yr], [500, 1500 yr], [1500, 4500 yr], and [4500, 10,000 yr]. The defining formulas for the scenario probabilities in Figure 8.1-3 are given in Table 8.1-1. The box plots in Figure 8.1-3 are displaying the uncertainty in the probability that the first drilling intrusion occurs in each of the time intervals used in the definition of the risk representation R_2. As shown in Section 8.2, the size of the cuttings removal release decreases with time.

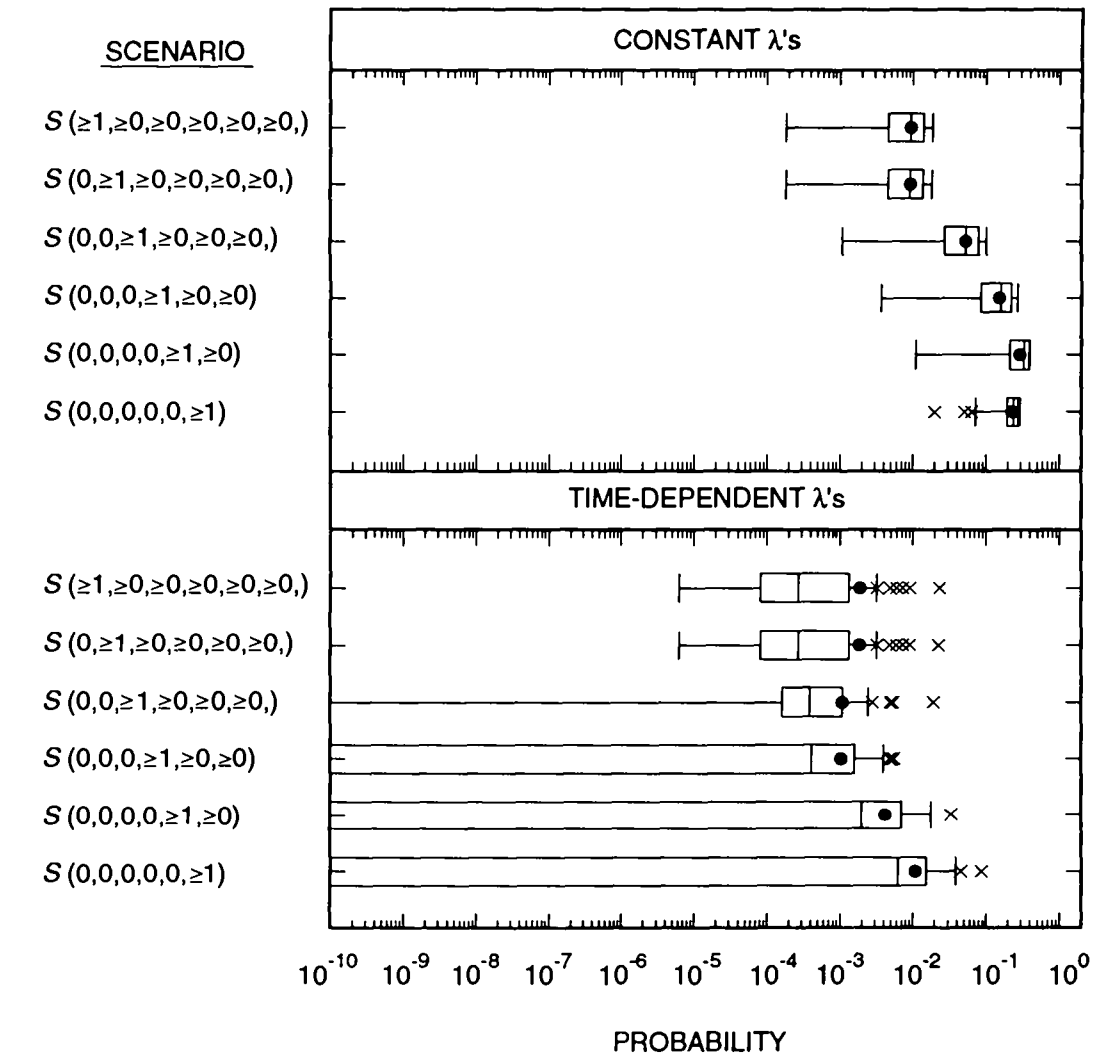

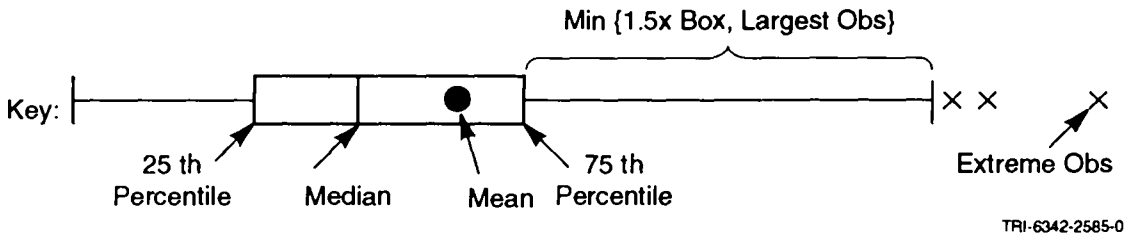

Figure 8.1-3. Uncertainty in probabilities of scenarios $S(\geq 1,\geq 0,\geq 0,\geq 0,\geq 0,\geq 0)$, $S(0,\geq 1,\geq 0,\geq 0,\geq 0,\geq 0)$, ..., $S(0,0,0,0,0,\geq 1)$ associated with risk representation R_2 defined in Eq. 2.5-8 with an assumed 100 yr period of administrative control in which drilling intrusions cannot occur.

Table 8.1-1. Probability of Scenarios $S(\geq 1,\geq 0,\geq 0,\geq 0,\geq 0)$, $S(0,\geq 1,\geq 0,\geq 0,\geq 0)$, ..., $S(0,0,0,0,0,\geq 1)$ Associated with the Risk Representation R_2 Defined in Eq. 2.5-8.

$$pS(\geq 1,\geq 0,\geq 0,\geq 0,\geq 0,\geq 0)$$

$$= \sum_{i=1}^{\infty} \sum_{j=0}^{\infty} \sum_{k=0}^{\infty} \sum_{l=0}^{\infty} \sum_{m=0}^{\infty} \sum_{n=0}^{\infty} pS(i,j,k,l,m,n)$$

$$= 1 - \exp\left[-\int_{t_0}^{t_1} \lambda(t)dt\right]$$

$$pS(0,\geq 1,\geq 0,\geq 0,\geq 0,\geq 0)$$

$$= \sum_{j=1}^{\infty} \sum_{k=0}^{\infty} \sum_{l=0}^{\infty} \sum_{m=0}^{\infty} \sum_{n=0}^{\infty} pS(0,j,k,l,m,n)$$

$$= \left\{\exp\left[-\int_{t_0}^{t_1} \lambda(t)dt\right]\right\} \left\{1-\exp\left[-\int_{t_1}^{t_2} \lambda(t)dt\right]\right\}$$

$$pS(0,0,\geq 1,\geq 0,\geq 0,\geq 0)$$

$$= \sum_{k=1}^{\infty} \sum_{l=0}^{\infty} \sum_{m=0}^{\infty} \sum_{n=0}^{\infty} pS(0,0,k,l,m,n)$$

$$= \left\{\exp\left[-\int_{t_0}^{t_2} \lambda(t)dt\right]\right\} \left\{1-\exp\left[-\int_{t_2}^{t_3} \lambda(t)dt\right]\right\}$$

$$\bullet$$

$$\bullet$$

$$\bullet$$

$$pS(0,0,0,0,0,\geq 1)$$

$$= \sum_{n=1}^{\infty} pS(0,0,0,0,0,n)$$

$$= \left\{\exp\left[-\int_{t_0}^{t_5} \lambda(t)dt\right]\right\} \left\{1-\exp\left[-\int_{t_5}^{t_6} \lambda(t)dt\right]\right\}$$

8.2 Cuttings Removal

The risk representation R_2 defined in Eq. 2.5-8 is used to display the effects of cuttings removal. The releases associated with single intrusions into waste of average activity at different times are summarized in Figure 8.2-1. As discussed in Section 7.3, the releases shown in Figure 8.2-1 are then scaled to determine the releases associated with intrusions into waste of different activity levels. Further, as discussed in Section 2.4, the releases in Figure 8.2-1 are also used in the construction of the cuttings releases assigned to scenarios that involve more than one drilling intrusion.

The cuttings releases shown in Figure 8.2-1 are initially (i.e., at 100 yr) centered around approximately 3.2×10^{-2} EPA release units. The size of the release then decreases due to radioactive decay, with release being reduced to values centered around 5.5×10^{-3} EPA release units by 3000 yr. An additional reduction to about 4×10^{-3} EPA release units occurs by 10,000 yr.

The isotopes associated with the releases at 100 yr and 1000 yr are shown in Figure 8.2-2. The release at 100 yr is dominated by Pu-238, with additional contributions from Am-241, Pu-239 and Pu-240. Due to the short half-life of Pu-238 (i.e., 88 yr), the dominant contributor to the cuttings release at 1000 yr is Pu-239, with additional contributions from Am-241 and Pu-240. Due to the 432 yr half-life of Am-241, the cuttings releases at later times are dominated by Pu-239, with a small contribution from Pu-240.

The only sampled variable that affects cuttings removal is DBDIAM (drillbit diameter). As shown in Figure 4.3-1 of Helton et al. (1992), an almost linear relationship exists between DBDIAM and the cuttings release to the accessible environment. The relationship is actually quadratic. However, due to the range of values for drillbit diameter under consideration (i.e., 0.267-0.444 m), the relationship is close to being linear.

For a given set of analysis input, the risk representation R_2 defined in Eq. 2.5-8 leads to a single CCDF for cuttings removal to the accessible environment. The 1992 WIPP performance assessment considered two imprecisely known variables that affected the CCDF for cuttings removal: drillbit diameter (DBDIAM) and the rate term in the Poisson model for drilling intrusions (LAMBDA). As discussed in Section 2.1, the uncertainty in these variables leads to a distribution of CCDFs. Actually, two cases were considered: constant rate terms and time-dependent rate terms. The

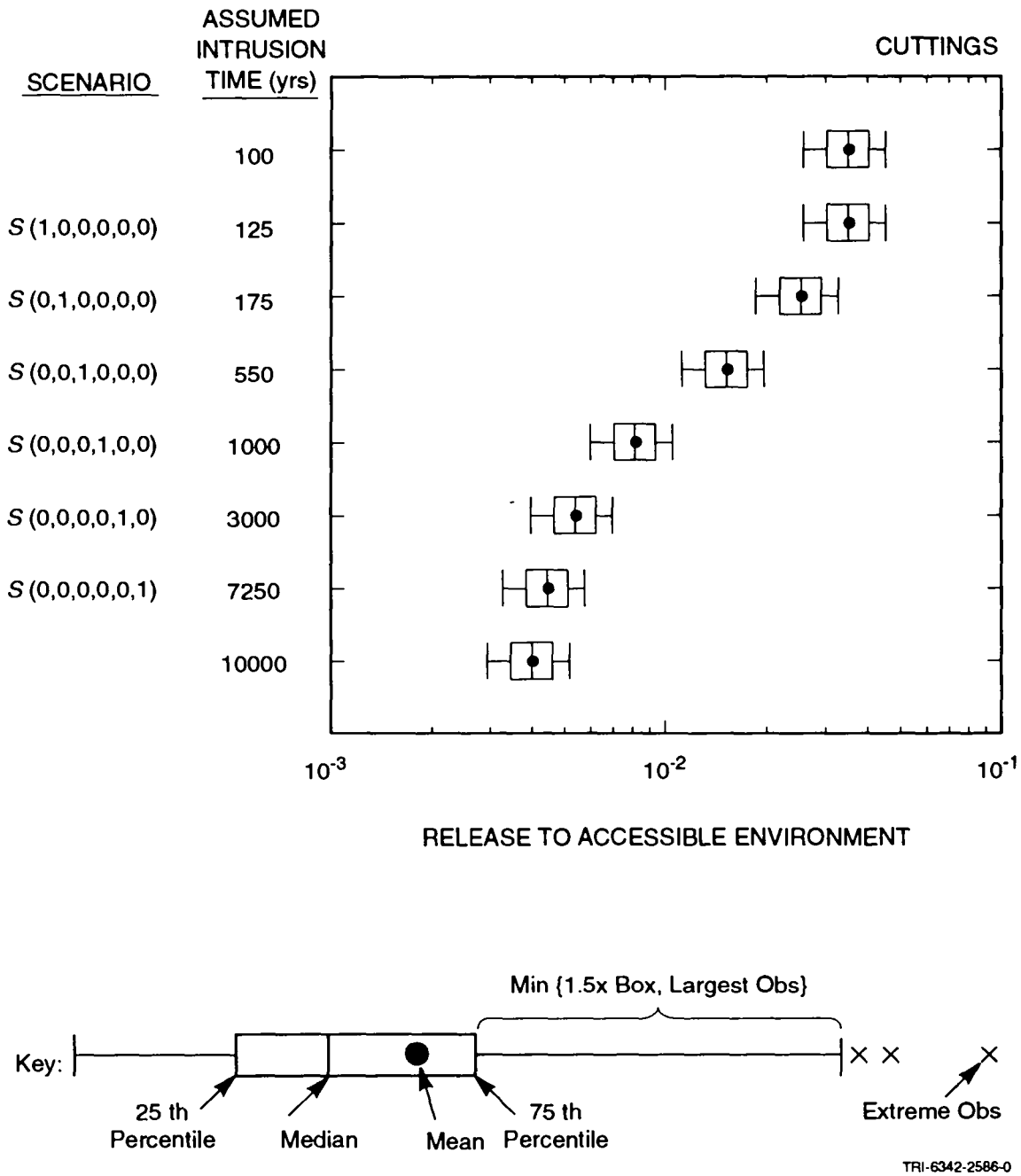

Figure 8.2-1. Total normalized release to the accessible environment due to cuttings removal from waste of average activity level.

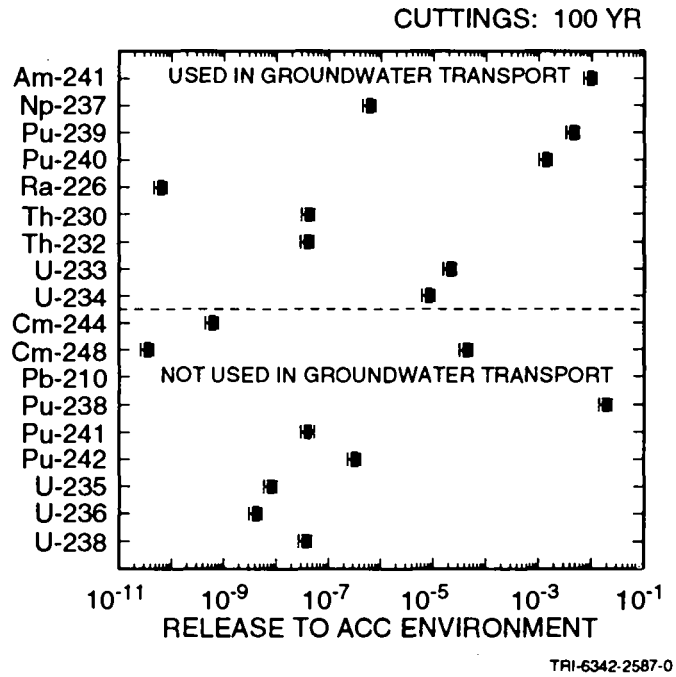

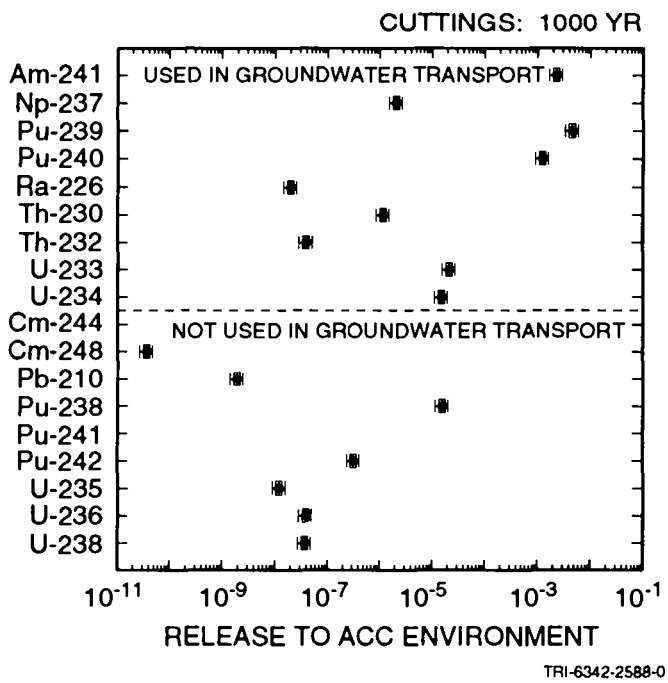

Figure 8.2-2. Normalized releases to the accessible environment for individual isotopes for cuttings removal resulting from a single borehole intersecting waste of average activity level at 100 yr and 1000 yr.

distributions of CCDFs that result for these two cases are shown in the two left frames of Figure 8.2-3; summaries based on mean and percentile curves are shown in the two right frames. Due to the use of a sample of size 70 in the 1992 WIPP performance assessment, the individual plots in Figure 8.2-3 are based on 70 CCDFs.

As examination of Figure 8.2-3 shows, the CCDFs for cuttings removal fall substantially below the EPA release limits. Further, the CCDFs constructed with the time-dependent rate terms obtained through an expert-review process fall below the CCDFs constructed with constant rate terms. As a reminder, the constant rate terms were obtained by generating a uniformly-distributed sample from the interval $[0, 3.75 \times 10^{-4}\ yr^{-1}]$, where $3.75 \times 10^{-4}\ yr^{-1}$ corresponds to the maximum drilling rate of 30 boreholes/km^2/10,000 yr specified by the EPA.

The variability in the CCDFs shown in Figure 8.2-3 is due primarily to uncertainty in the rate term in the Poisson model for drilling intrusions (i.e., in the function $\lambda(t)$ appearing in Eq. 2.3-1), with a small additional contribution from drillbit diameter (DBDIAM). Sensitivity analyses based on partial correlation analysis or regression analysis produce results similar to those shown in Figures 4.6-1 and 4.6-2 of Helton et al. (1992). In particular, there is a strong positive correlation between exceedance probability and the rate term in the Poisson model for drilling intrusions (LAMBDA), and a positive but less strong correlation between exceedance probability and drillbit diameter.

The steps appearing in the individual CCDFs in Figure 8.2-3 result from the discretization of the waste into five activity levels for the calculation of cuttings removal. The use of more activity levels would cause these steps to be eliminated but would not significantly alter the distributions of CCDFs for cuttings removal. Additional discussion of this pattern is provided in conjunction with Figure 4.6-3 of Helton et al. (1992).

8.3 Release to Culebra

Due to constraints imposed by computational cost, the 1992 WIPP performance assessment performed groundwater transport calculations only for intrusions occurring at 1000 yr. As discussed in Section 2.4 and in more detail in Chapters 4 and 5, the first step in these calculations is the use of the BRAGFLO model to determine time-dependent releases into the Culebra Dolomite. The integrated (i.e., total) values for these releases over 10,000 yr are summarized in Figure 8.3-1 for scenarios $S(1,0)$ and $S^{+-}(2,0)$, which

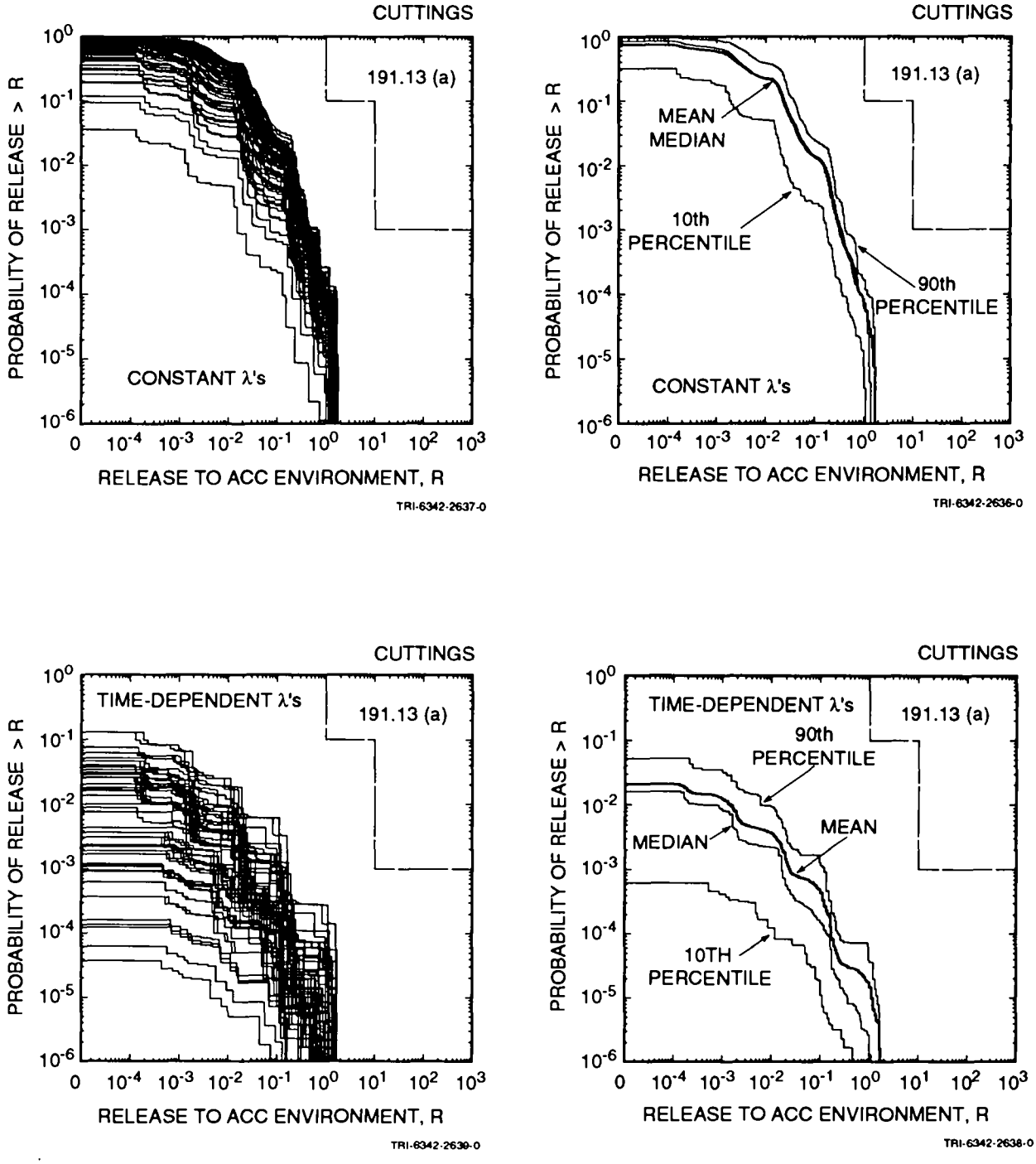

Figure 8.2-3. Distribution of CCDFs for normalized release to the accessible environment over 10,000 yr for cuttings removal constructed for the risk representation R_2 defined in Eq. 2.5-8 with constant (upper two frames) and time-dependent (lower two frames) rate terms in the Poisson model for drilling intrusions.

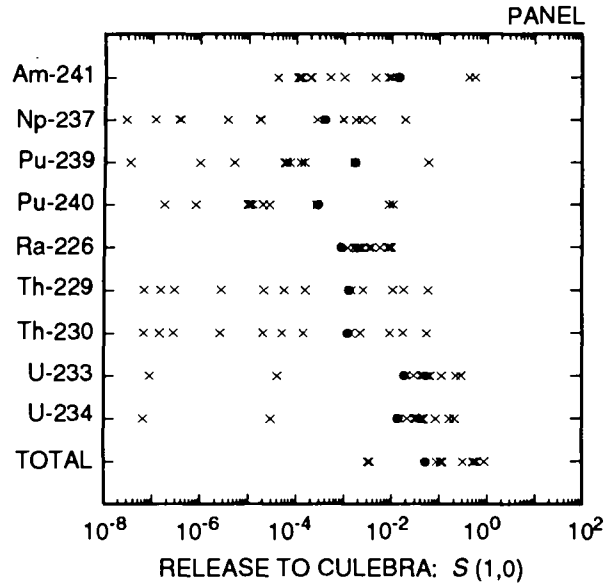

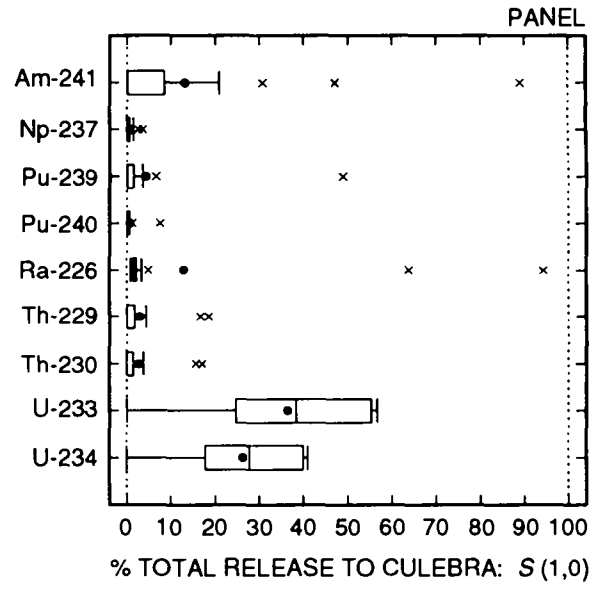

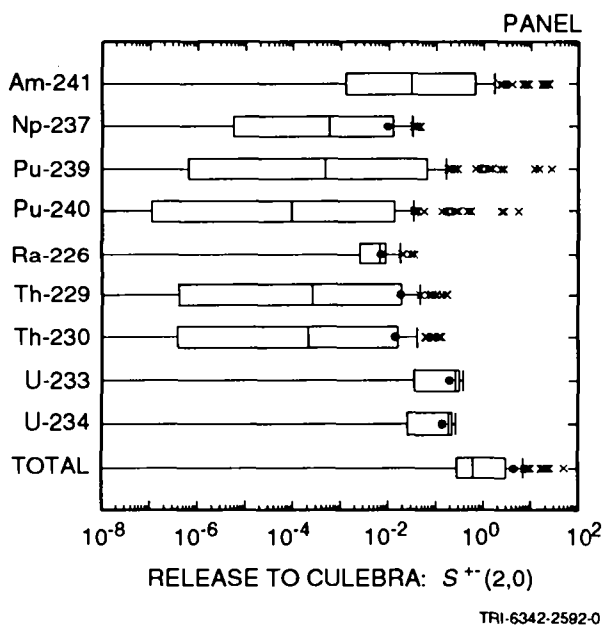

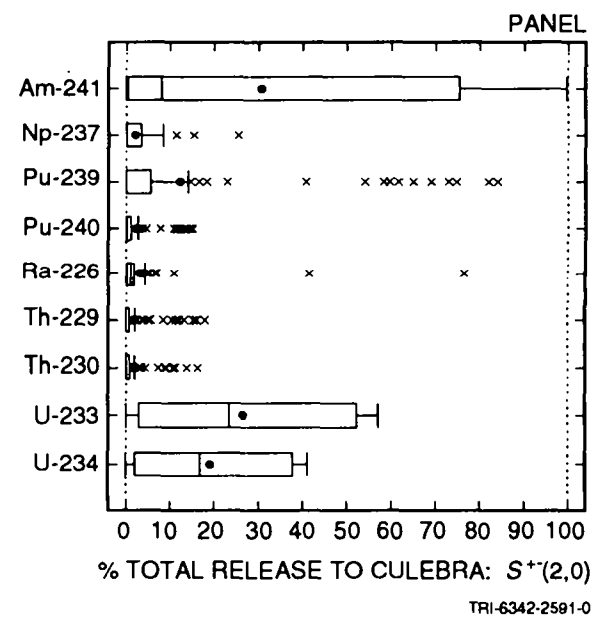

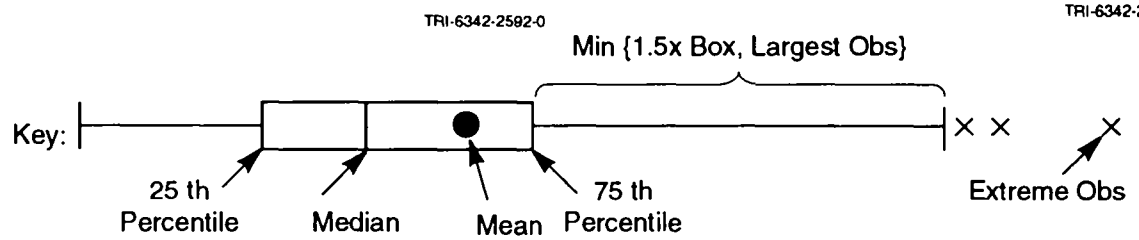

Figure 8.3-1. Normalized releases to the Culebra Dolomite over 10,000 yr due to groundwater transport for scenarios $S(1,0)$ and $S^{+-}(2,0)$ used in conjunction with the risk representation R_1 defined in Eq. 2.5-1 with intrusion occurring at 1000 yr.

are used in conjunction with the risk representation R_1 defined in Eq. 2.5-1 to develop CCDFs for normalized release to the accessible environment due to groundwater transport.

Only 14 of the 70 sample elements used in the analysis resulted in nonzero releases to the Culebra for scenario $S(1,0)$. Thus, the individual box plots in Figure 8.3-1 for scenario $S(1,0)$ are based on a maximum of 14 nonzero normalized releases. The total normalized release to the Culebra for scenario $S(1,0)$ is always less than 1, with the total release being dominated by U-233, U-234 and Am-241. As shown by the scatterplot in Figure 8.3-2, zero releases to the Culebra tend to be associated with the smaller values for Salado halite permeability (SALPERM). This pattern occurs because the repository fails to fill with brine for small values of SALPERM, with the result that there is no brine flow, and hence no radionuclide transport, up an intruding borehole.

In contrast to scenario $S(1,0)$, only two sample elements resulted in no release to the Culebra for scenario $S^{+-}(2,0)$. As examination of Figure 8.3-1 shows, half the sample elements have total normalized releases to the Culebra that exceed 0.6 EPA release units. Further, 9 sample elements have total normalized releases that exceed 10. As for scenario $S(1,0)$, the total release tends to be dominated by Am-241, U-233 and U-234, with Pu-239 also making a large contribution to the total release for some sample elements. The larger brine flows associated with scenario $S^{+-}(2,0)$ permit radionuclides with short half-lives to be transported out of the repository before they are lost due to radioactive decay. Because of this, Am-241 is a larger contributor to the total release for scenario $S^{+-}(2,0)$ than it is for scenario $S(1,0)$.

As shown in Table 8.3-1, stepwise regression analysis can be used to investigate which of the sampled variables listed in Table 3.1 dominate the uncertainty in the releases to the Culebra summarized in Figure 8.3-1 for scenario $S^{+-}(2,0)$. The results contained in Table 8.3-1 and other similar presentations in this report were calculated with the STEPWISE program (Iman et al., 1980) with rank-transformed data (Iman and Conover, 1979). The rationale for using rank-transformed data is that this transform enables the analysis to identify the extent to which variables tend to increase and decrease together, which is typically the question of interest in a sensitivity analysis. Further, use of the rank transform avoids some of the technical problems associated with other transforms (e.g., appropriately weighting outliers and the treatment of zeros).

For Am-241, the uncertainty in the integrated release to the Culebra is dominated by BHPERM (borehole permeability) and SOLAM (solubility for Am),

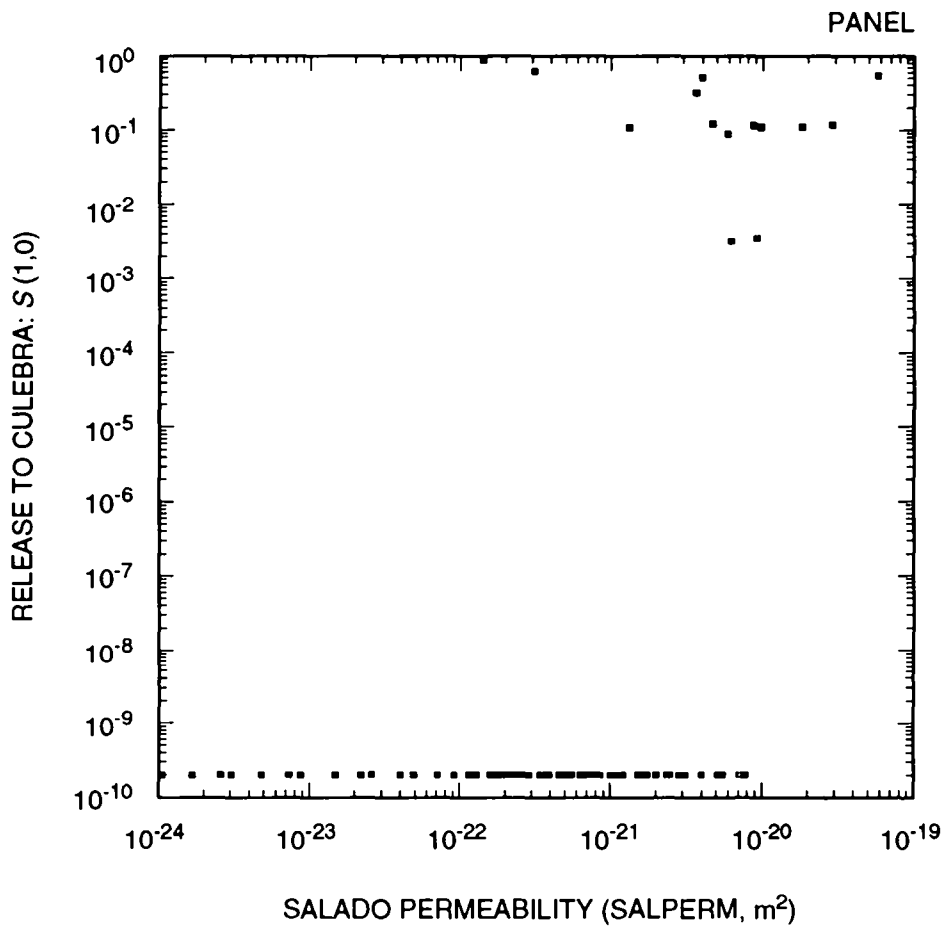

Figure 8.3-2. Scatterplot for total normalized release to the Culebra Dolomite over 10,000 yr versus Salado Permeability (SALPERM) for scenario $S(1,0)$ with intrusion occurring at 1000 yr.

Table 8.3-1. Stepwise Regression Analyses with Rank-Transformed Data for Integrated Release to the Culebra Dolomite over 10,000 yr for Scenario S^{+-}(2,0) with Intrusion Occurring 1000 yr after Repository Closure.

	Variable[a]	R^{2b}	Variable	R^2	Variable	R^2	Variable	R^2
Step[c]	Am-241		Np-237		Pu-239		Pu-240	
1	BHPERM	0.42(+)	SOLNP	0.75(+)	SOLPU	0.86(+)	SOLPU	0.86(+)
2	SOLAM	0.81(+)	BHPERM	0.90(+)	BHPERM	0.94(+)	BHPERM	0.94(+)
3	DBDIAM	0.83(+)			DBDIAM	0.95(+)	DBDIAM	0.95(+)
Step	Ra-226		Th-229		Th-230		U-233	
1	BHPERM	0.21(+)	SOLTH	0.77(+)	SOLTH	0.77(+)	BHPERM	0.41(+)
2	SOLTH	0.33(-)	BHPERM	0.89(+)	BHPERM	0.88(+)	SOLU	0.60(+)
Step	U-234		Total					
1	BHPERM	0.41(+)	BHPERM	0.48(+)				
2	SOLU	0.60(+)	SOLAM	0.60(+)				

[a]Variables listed in order of selection in regression analysis
[b]Cumulative R^2 value with entry of each variable into regression model, with "+" and "-" indicating positive and negative regression coefficients, respectively
[c]Steps in stepwise regression analysis

with the release tending to increase as each of these variables increases. These positive effects result because increasing BHPERM reduces resistance to flow up the boreholes and increasing SOLAM increases the amount of Am-241 that can be dissolved in brine. The regression model with BHPERM and SOLAM can account for 81% (i.e., R^2 = 0.81) of the variability in the Am-241 release to the Culebra. The release patterns that result in the selection of BHPERM and SOLAM in the regression analysis for Am-241 summarized in Table 8.3-1 are shown in Figure 8.3-3 for both log-transformed and rank-transformed data. The flattening associated with large values of SOLAM is due to inventory limits; as shown in Figure 7.3-1, the amount of Am-241 in one waste panel at 1000 yr is approximately 40 EPA release units. The regression analysis for Am-241 in Table 8.3-1 also indicates a small positive effect for DBDIAM (drillbit diameter), which results because increasing DBDIAM increases the diameter of the intruding boreholes and thus produces a larger area through which brine flow can take place.

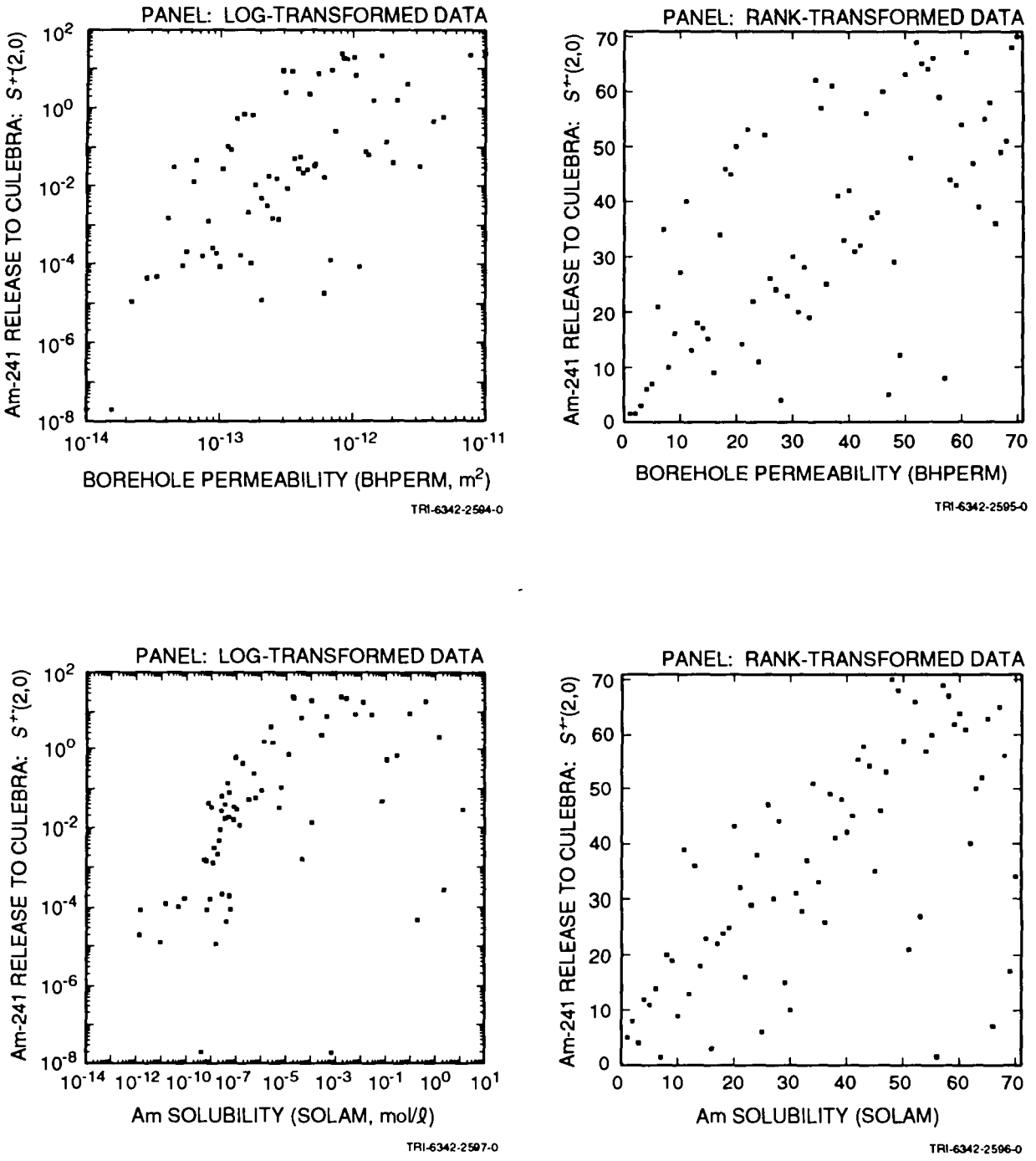

Figure 8.3-3. Scatterplots with log-transformed and rank-transformed data for normalized release of Am-241 to the Culebra Dolomite over 10,000 yr for variables BHPERM (borehole permeability) and SOLAM (solubility of Am) and scenario $S^{+-}(2,0)$ with intrusion occurring 1000 yr after repository closure.

The radionuclides Np-237, Pu-239, Pu-240, Th-229 and Th-230 show release patterns similar to those shown by Am-241, although the solubility limits (i.e., SOLNP, SOLPU, SOLTH) tend to be more important than borehole permeability (BHPERM). In the analysis for Am-241, solubility and borehole permeability were of approximately equal importance. This difference in importance for BHPERM results from the relatively short half-life of Am-241 (i.e., 432 yr), which makes reduced flow rates up an intruding borehole more important for Am-241 than for Np-237, Pu-239, Pu-240, Th-229 and Th-230 due to loss resulting from radioactive decay. As an example, the scatterplot for Pu-239 release to the Culebra versus SOLPU in Figure 8.3-4 shows less spread than the corresponding scatterplot for Am-241 in Figure 8.3-3. Also, the scatterplot for Pu-239 in Figure 8.3-4 does not suggest the presence of any effects due to inventory limitations as is the case for Am-241 in Figure 8.3-3.

The regression analysis for Ra-226 summarized in Table 8.3-1 is not very successful, with two variables selected and an R^2 value of only 0.33. In particular, the analysis indicates that the release of Ra-226 to the Culebra tends to increase as BHPERM (borehole permeability) increases and tends to decrease as SOLTH (solubility of Th) increases. The patterns that give rise to these selections are shown in the scatterplots in Figure 8.3-5 with both log-transformed and rank-transformed data. The positive effect indicated for BHPERM in Table 8.3-1 and Figure 8.3-5 results because increasing BHPERM increases brine flow out the intruding boreholes, and the negative effect indicated for SOLTH results because increasing SOLTH increases the amount of Th-230 removed from the waste panel and thus decreases the amount of Ra-226 that will be produced within the panel by radioactive decay. The solubility limit for radium (SOLRA) is assigned a high range of values (i.e., 2 to 18.2 mol/L). As a result, all available Ra-226 goes into solution, and thus SOLRA does not show up as an important variable in the regression analysis for Ra-226 release to the Culebra. As examination of the box plots for Ra-226 in Figure 8.3-1 and the range of Ra-226 releases on the coordinates in Figure 8.3-5 shows, the high values for SOLRA result in a smaller range of release values for Ra-226 than is the case for the other isotopes considered in this study due to a complete removal of the available Ra-226.

The scatterplots in Figure 8.3-5 suggest that a regression analysis with log-transformed data may indicate a stronger relationship between Ra-226 release to the Culebra and the variables BHPERM (borehole permeability) and SOLTH (solubility of Th) than was observed with rank-transformed data. The two sample elements with zero release to the Culebra were dropped from the analysis and the remaining 68 sample elements were used in a regression analysis with log-transformed data. This produced the regression model

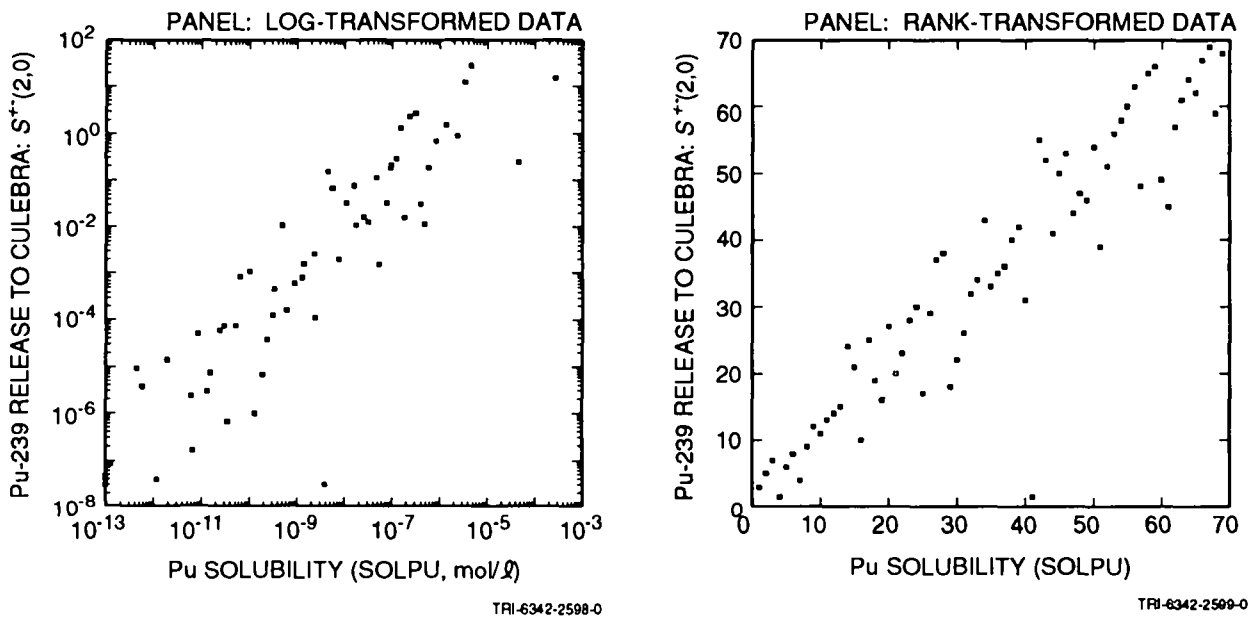

Figure 8.3-4. Scatterplots with log-transformed and rank-transformed data for normalized release of Pu-239 to the Culebra Dolomite over 10,000 yr versus plutonium solubility (SOLPU) for scenario $S^{+-}(2,0)$ with intrusion occurring 1000 yr after repository closure.

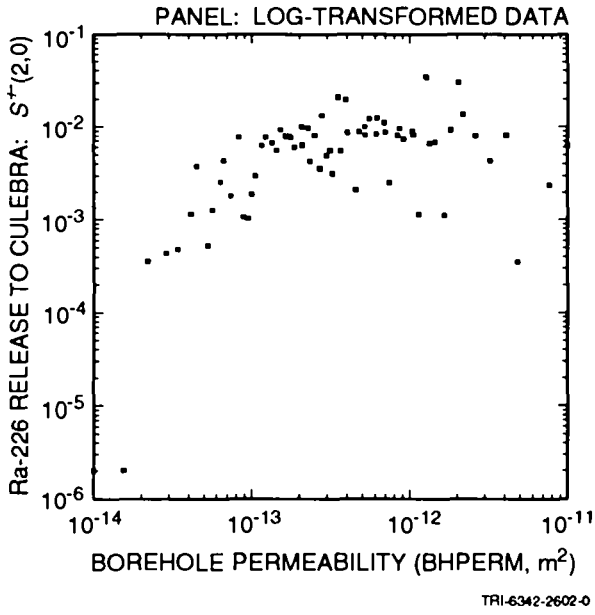

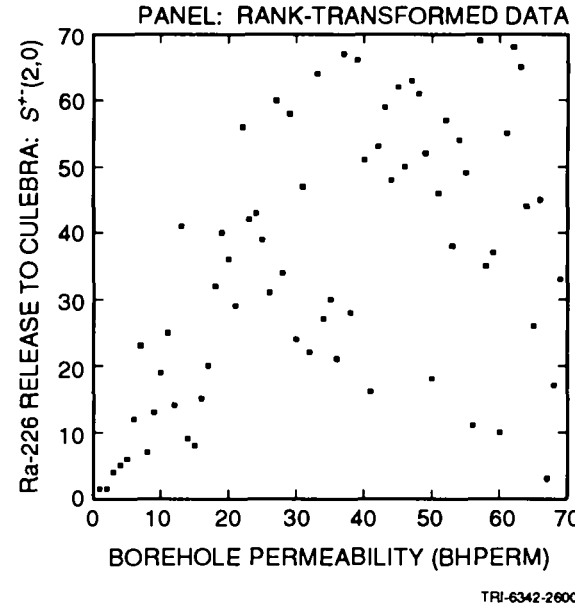

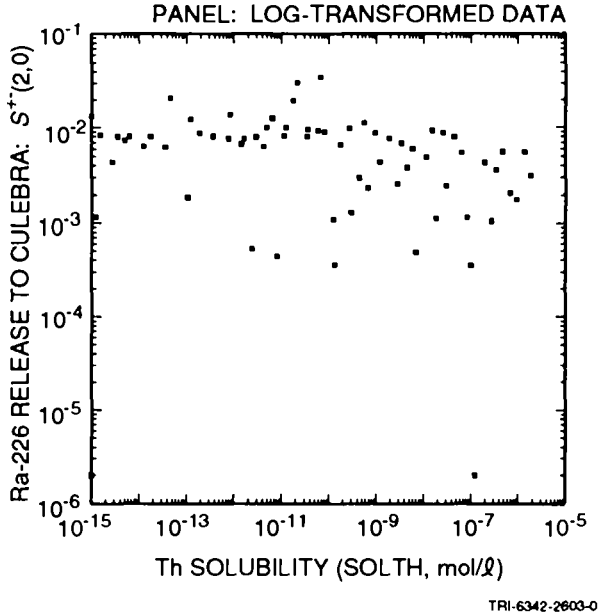

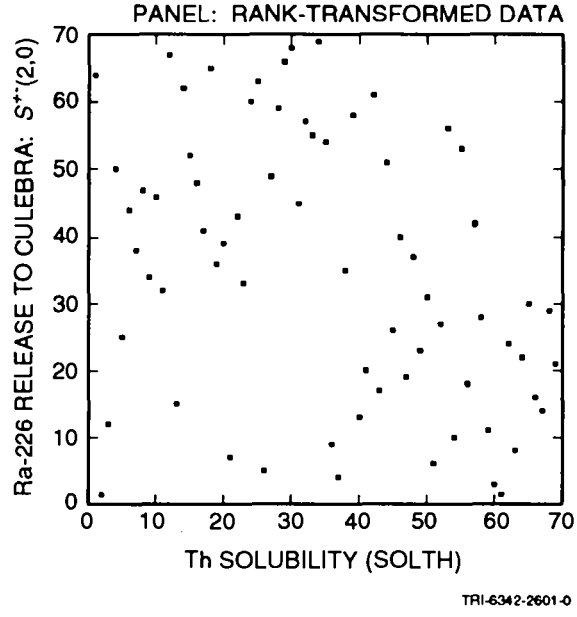

Figure 8.3-5. Scatterplots with log-transformed and rank-transformed data for normalized release of Ra-226 to the Culebra Dolomite over 10,000 yr for variables BHPERM (borehole permeability) and SOLTH (solubility of Th) and scenario $S^{+-}(2,0)$ with intrusion occurring 1000 yr after repository closure.

$$\log y = 0.762 + 0.289 \log \text{BHPERM} - 0.052 \log \text{SOLTH}, \quad R^2 = 0.24 \qquad (8.3\text{-}1)$$

where y is the normalized release of Ra-226 to the Culebra. Thus, the use of log-transformed data does not improve the regression results for Ra-226 (i.e., R^2 = 0.33 with rank-transformed data and R^2 = 0.24 with log-transformed data).

The regression analyses for U-233 and U-234 summarized in Table 8.3-1 produce similar results, with release tending to increase as BHPERM (borehole permeability) and SOLU (solubility for U) increase. However, the regressions with these two variables have R^2 values of only 0.60. Scatterplots for U-233 release to the Culebra versus BHPERM and SOLU are shown in Figure 8.3-6. The lines of approximately equal releases across the tops of these scatterplots correspond to the U-233 inventory in a single waste panel (i.e., approximately 0.4 EPA release units as shown in Figure 7.3-1). A similar pattern also occurs in the corresponding scatterplots for U-234. Thus, the larger values for both BHPERM and SOLU result in a complete removal of U-233 and U-234 from the waste panel, which creates a pattern that is not well-captured by the regression techniques in use. Similar behavior was also observed for U-233 and U-234 in the 1991 WIPP performance assessment (e.g., see Helton et al., 1992, Figures 4.5-2 and 5.1-6).

The last regression analysis summarized in Table 8.3-1 is for the total normalized release to the Culebra. This analysis indicates that the total release tends to increase as each of BHPERM (borehole permeability) and SOLAM (solubility for Am) increases. The regression model with these two variables has an R^2 value of 0.60, which is not particularly good. As shown in Figure 8.3-1, U-233 and U-234 are important contributors to total release. Thus, the low R^2 value in the regression analysis for total release is due in part to the inventory-related patterns shown in Figure 8.3-6 for U-233 and similar patterns for U-234.

The radionuclide releases to the Culebra analyzed in Table 8.3-1 result from brine flow up the two intruding boreholes associated with scenario S^{+-} (2,0). These flows are summarized in Figure 5.2-16. The uncertainty in the cumulative brine flow to the Culebra shown in Figure 5.2-16 results from the uncertainty in the following 21 variables contained in Table 3-1: BHPERM, BPPRES, BPSTOR, BRSAT, BCBRSAT, BCEXP, BCFLG, BCGSSAT, DBDIAM, GRCORHF, GRCORI, GRMICHF, GRMICI, MBPERM, MBPOR, SALPERM, SALPRES, STOICCOR, STOICMIC, VMETAL AND VWOOD. The PCCSRC program (Iman et al., 1985) can be used to determine which of the sampled variables dominates the uncertainty in the cumulative brine flows shown in Figure 5.2-16. In particular, PCCSRC can be used to calculate the partial rank correlation coefficients (PRCCs) between the cumulative brine flow appearing above fixed times on the abcissa

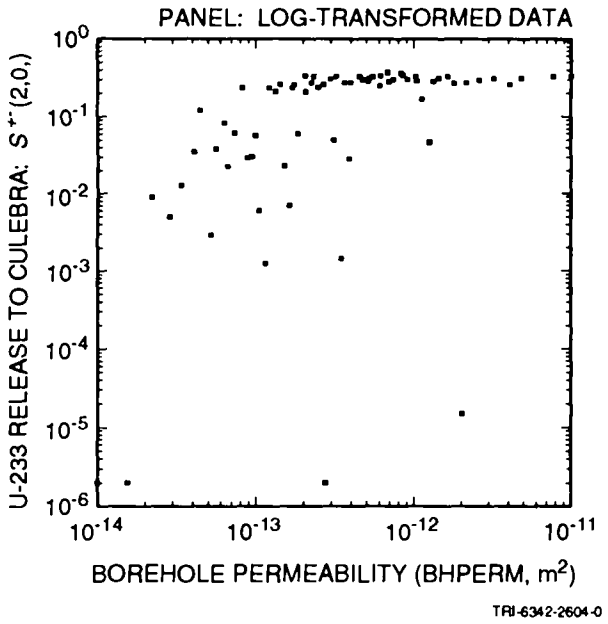

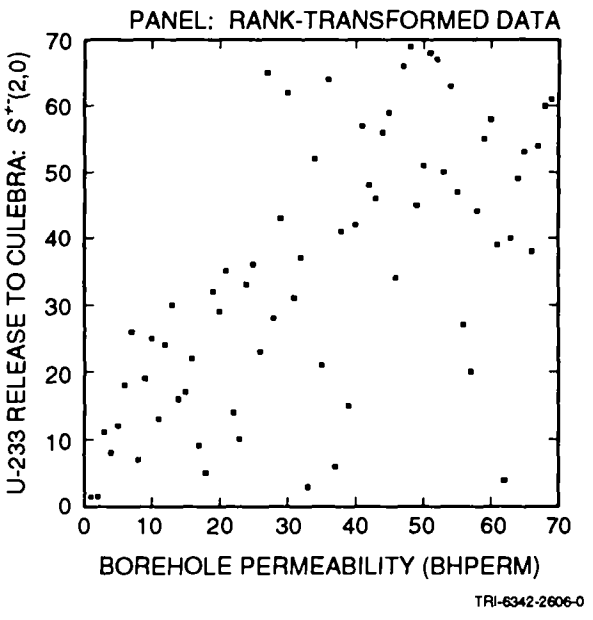

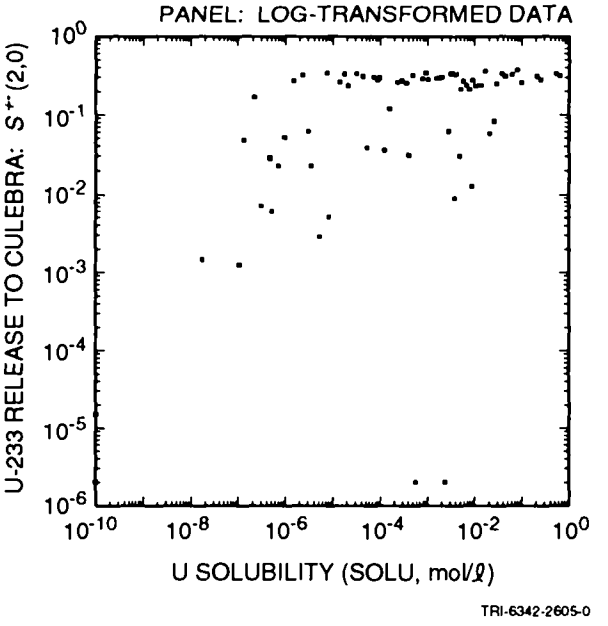

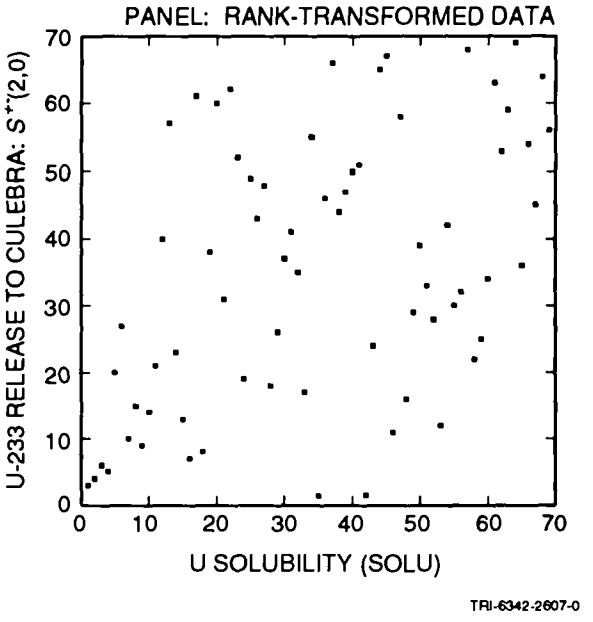

Figure 8.3-6. Scatterplots with log-transformed data and rank-transformed data for normalized release of U-233 to the Culebra Dolomite over 10,000 yr for variables BHPERM (borehole permeability) and SOLU (solubility of U) for scenario $S^{+-}(2,0)$ with intrusion occurring 1000 yr after repository closure.

and the previously indicated variables in Table 3-1. The values for these PRCCs can be plotted above the corresponding times and then connected to form continuous curves. As shown in Figure 8.3-7, the most important variables identified in this analysis are BHPERM (borehole permeability), DBDIAM (drillbit diameter) and BPPRES (brine pocket pressure), with cumulative brine flow tending to increase as each of these variables increases. These positive effects result because increasing BHPERM reduces the resistance to brine flow in the intruding boreholes, increasing DBDIAM increases the diameter of the intruding boreholes, and increasing BPPRES increases brine pressure within the waste panel. A small negative effect is also indicated for GRCORI (gas-generation rate for corrosion of steel under inundated conditions) between 1500 and 3000 yr, although GRCORI appears to have little or no effect on cumulative brine flow at later times. This pattern probably results from the effect of GRCORI in reducing the amount of brine in the waste at the assumed intrusion time of 1000 yr, with the result that more brine is required to enter the repository before flow up the boreholes can commence than might be the case otherwise. As indicated by PRCCs of approximately one, BHPERM is the most important variable with respect to the uncertainty in brine flow.

Stepwise regression analysis can also be used to investigate brine flow out of a waste panel through the intruding boreholes associated with scenario $S^{+-}(2,0)$. In particular, a stepwise regression analysis for cumulative brine flow over 10,000 yr (i.e., for the cumulative brine flows appearing above 10,000 yr in Figure 5.2-16 is presented in Table 8.3-2. As previously indicated by the PRCCs in Figure 8.3-7, BHPERM (borehole permeability) is the dominant variable with an R^2 value of 0.94. Further, the addition of DBDIAM (drillbit diameter), BPPRES (brine pocket pressure) and BPSTOR (brine pocket storativity) results in a regression model with an R^2 value of 0.99. These results indicate that brine flow is dominated by variables affecting borehole properties (BHPERM, DBDIAM), with small additional effects coming from variables that define brine pocket properties (BPPRES, BPSTOR). The relationship between BHPERM and cumulative brine flow is shown in the scatterplot in Figure 8.3-8.

For a given set of analysis input, the risk representation R_1 defined in Eq. 2.5-1 leads to a single CCDF for release to the Culebra. The 1992 WIPP performance assessment considered the following 29 imprecisely known variables defined in Table 3-1 that affect the CCDF for release to the Culebra: BHPERM, BPPRES, BPSTOR, BPAREAFR, BRSAT, BCBRSAT, BCEXP, BCFLG, BCGSSAT, DBDIAM, GRCORHF, GRCORI, GRMICHF, GRMICI, LAMBDA, MBPERM, MBPOR, SALPERM, SALPRES, SOLAM, SOLNP, SOLPU, SOLRA, SOLTH, SOLU, STOICCOR, STOICMIC, VMETAL and VWOOD. As discussed in Section 2.1, the uncertainty in

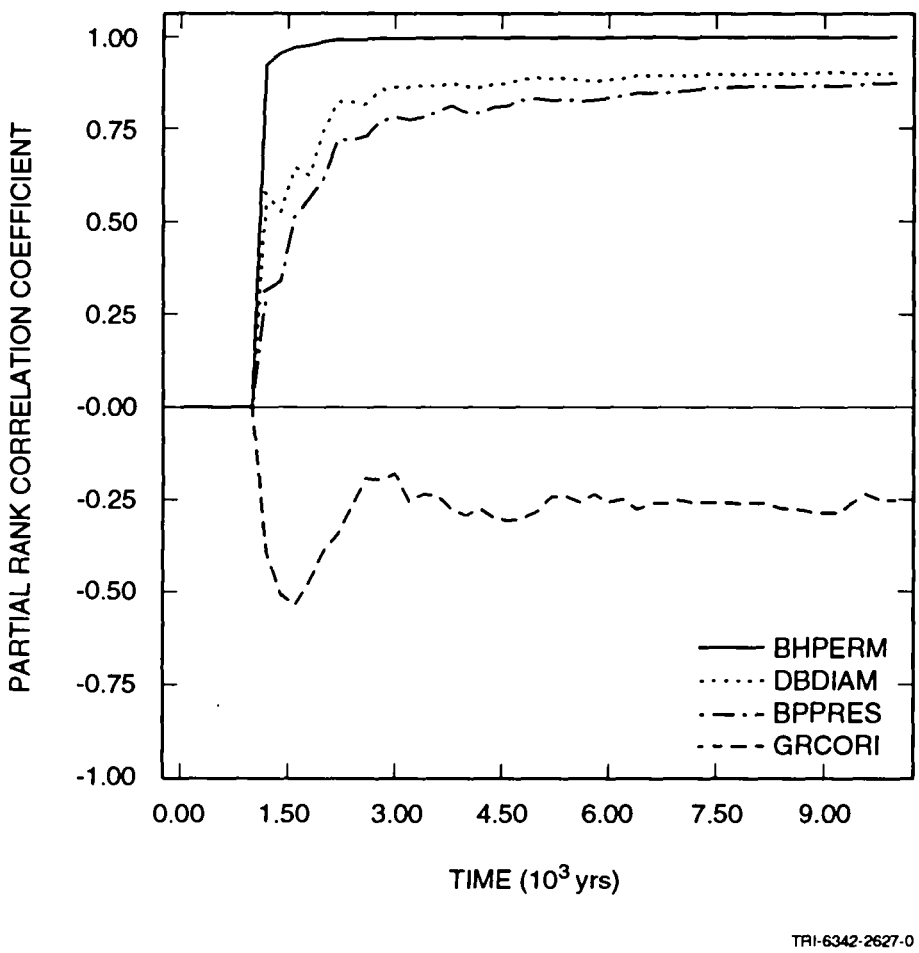

Figure 8.3-7. Partial rank correlation coefficients for cumulative flow of brine into a borehole over 10,000 yr for scenario $S^{+-}(2,0)$ with intrusion occurring at 1000 yr.

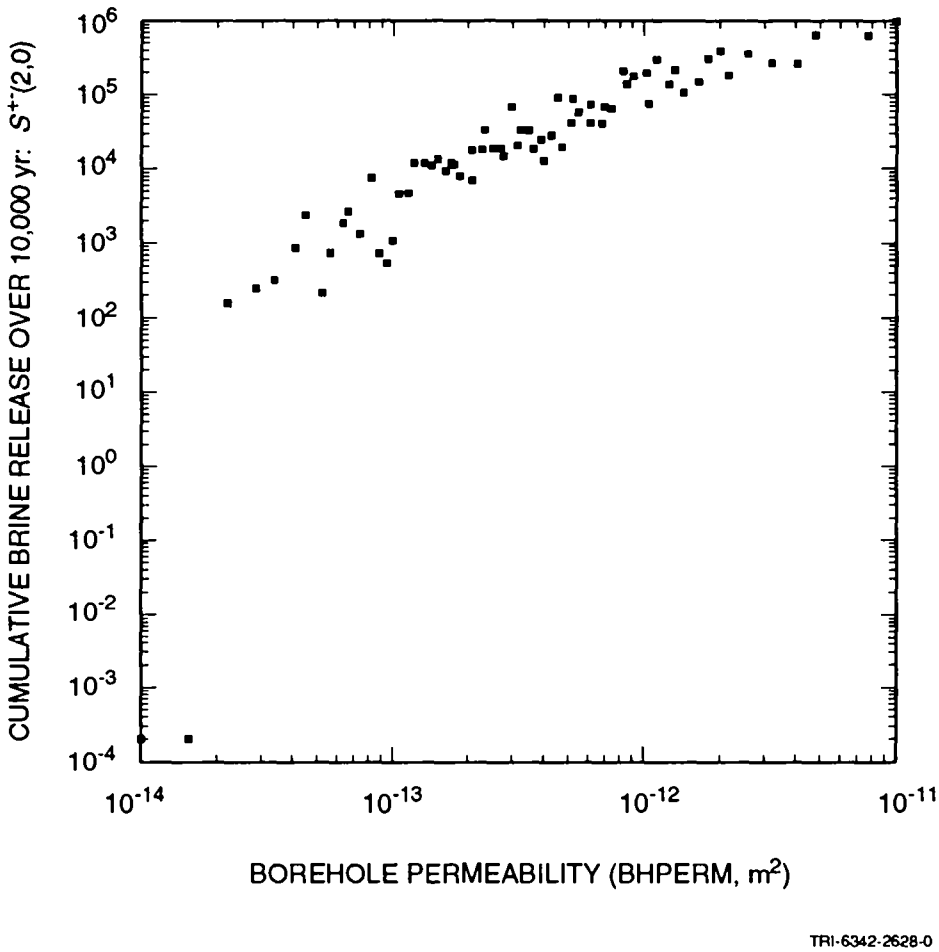

Figure 8.3-8 Scatterplot for borehole permeability (BHPERM, m^2) and volume of brine (m^3) released into a borehole over 10,000 yr for Scenario $S^{+-}(2,0)$ with intrusion occurring at 1,000 yr.

Table 8.3-2 Stepwise Regression Analysis with Rank-Transformed Data for Cumulative Flow of Brine into a Borehole Over 10,000 yr for Scenario S^{+-}(2,0) with Intrusion at 1,000 years.

Steps[a]	Variable[b]	R^2 [c]
1	BHPERM	0.94 (+)
2	DBDIAM	0.97 (+)
3	BPPRES	0.99 (+)
4	BPSTOR	0.99 (+)

[a]Steps in stepwise regression analysis
[b]Variables listed in order of selection in regression analysis
[c]Cumulative R^2 value with entry of each variable into regression model, with "+" and "-" indicating positive and negative regression coefficients, respectively

these variables leads to a distribution of CCDFs. As previously noted in the discussion of cuttings releases, two cases were considered in the analysis for the rate term (i.e., λ) in the Poisson model for drilling intrusions: constant rate terms and time-dependent rate terms. The distribution of CCDFs that result for these two cases are shown in the two left frames of Figure 8.3-9; further, summaries based on mean and percentile curves are shown in the two right frames. Because a sample size of 70 is used in the 1992 WIPP performance assessment, the individual plots in Figure 8.3-9 are based on 70 CCDFs.

As examination of the upper two frames in Figure 8.3-9 shows, the use of constant-valued rate terms in the Poisson model for drilling intrusions results in most CCDFs falling below the EPA release limits. Further, the mean and percentile curves also fall beneath the EPA release limits, although both the mean and 90^{th} percentile curves come close to intercepting the release limit at the (10, 0.001) point. As shown in the two lower frames in Figure 8.3-9, the use of time-dependent rate terms in the Poisson model for drilling intrusions produces CCDFs that are shifted down from those obtained with constant-valued rate terms. In particular, the mean and 90^{th} percentile curves obtained with time-dependent rate terms fall approximately two orders of magnitude below the corresponding curves obtained with constant-valued rate terms. Due to the skewed nature of the distributions shown in Figure 8.3-9 and other similar figures, it is possible for parts of the mean curve to be located above the 90^{th} percentile curve. Such behavior occurs when a distribution has a few very large values and many small values.

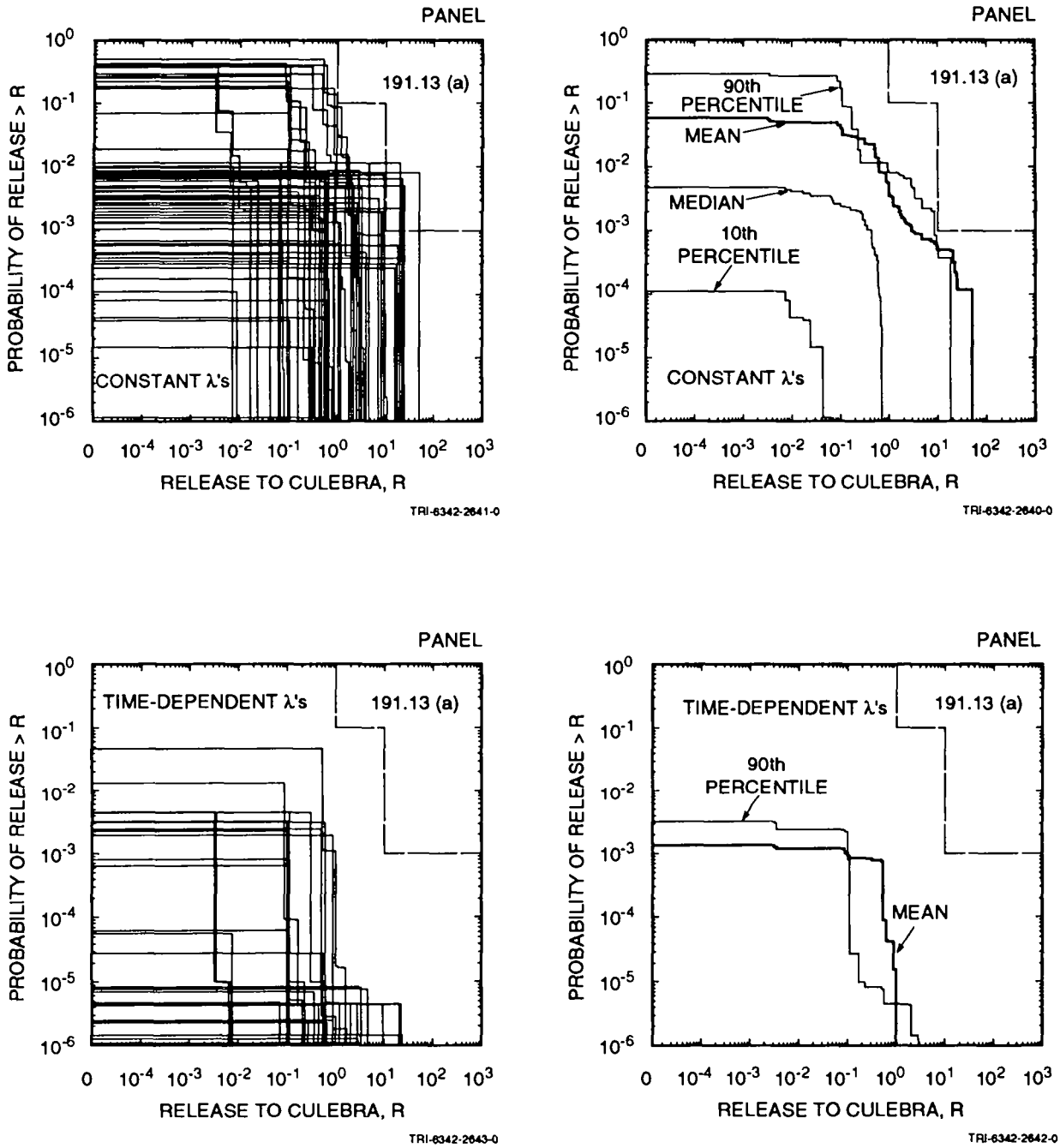

Figure 8.3-9. Distribution of CCDFs for normalized release to the Culebra Dolomite over 10,000 yr constructed for the risk representation R_1 defined in Eq. 2.5-1 with constant (upper two frames) and time-dependent (lower two frames) rate terms in the Poisson model for drilling intrusions. As the release under consideration is to the Culebra, the CCDFs shown in this figure are not the CCDFs used for comparison with the bounds given in 40 CFR 191, Subpart B.

As discussed in conjunction with Figure 8.3-7, the PCCSRC program (Iman et al., 1985) can be used to determine which of the sampled variables dominates the uncertainty in the CCDFs shown in the upper left frame of Figure 8.3-9. In particular, PCCSRC can be used to calculate PRCCs between the exceedance probabilities appearing above fixed release values on the abcissa and the variables in Table 3.1. The values for these PRCCs can be plotted above the corresponding release values and then connected to form continuous curves. As shown in Figure 8.3-10, the three most important variables identified in this analysis were LAMBDA (rate constant in Poisson model for drilling intrusions), BHPERM (borehole permeability), and SOLAM (solubility for Am). No other variables were identified as having a substantial effect on the indicated distribution of CCDFs. The variable LAMBDA defines the probability of having one or more drilling intrusions and hence controls the initial horizontal section of the CCDFs. The variables BHPERM and SOLAM control the size of releases and hence determine how far the individual CCDFs extend to the right before they drop to the abcissa.

The two lower plots in Figure 8.3-9 were generated with the same releases to the Culebra as the upper two plots but with time-dependent rather than constant rate terms in the Poisson model for drilling intrusions. Thus, the downward shift of the CCDFs associated with the two lower frames is indicative of the impact of the time-dependent rate terms developed in an expert review process as part of the WIPP performance assessment (Hora et al., 1991; memorandum by Hora in Appendix A, pp. A-69 to A-99, in Volume 3 of this report).

8.4 Groundwater Transport to Accessible Environment

As indicated in Table 8.4-1, seven alternative modeling assumptions for radionuclide transport in the Culebra were evaluated. Transport results without chemical retardation are presented in Sections 8.4.1 and 8.4.5 and transport results with chemical retardation are presented in Sections 8.4.2, 8.4.3 and 8.4.4. The results in Section 8.4.1 are for no chemical retardation, no clay lining in fractures and no matrix diffusion, with the result that releases to the Culebra are transported unimpeded to the accessible environment. This is believed to be the most conservative set of assumptions for modeling radionuclide transport in the Culebra. Several variants on the assumption of no chemical retardation are presented in Section 8.4.5. The most important of these variants assumes diffusion into the Dolomite matrix and thus illustrates the effect of physical retardation (i.e., retardation in the Dolomite matrix) in the absence of chemical retardation. The analyses in Sections 8.4.2, 8.4.3 and 8.4.4 with chemical retardation illustrate the effects of assuming fracture only (i.e., no matrix

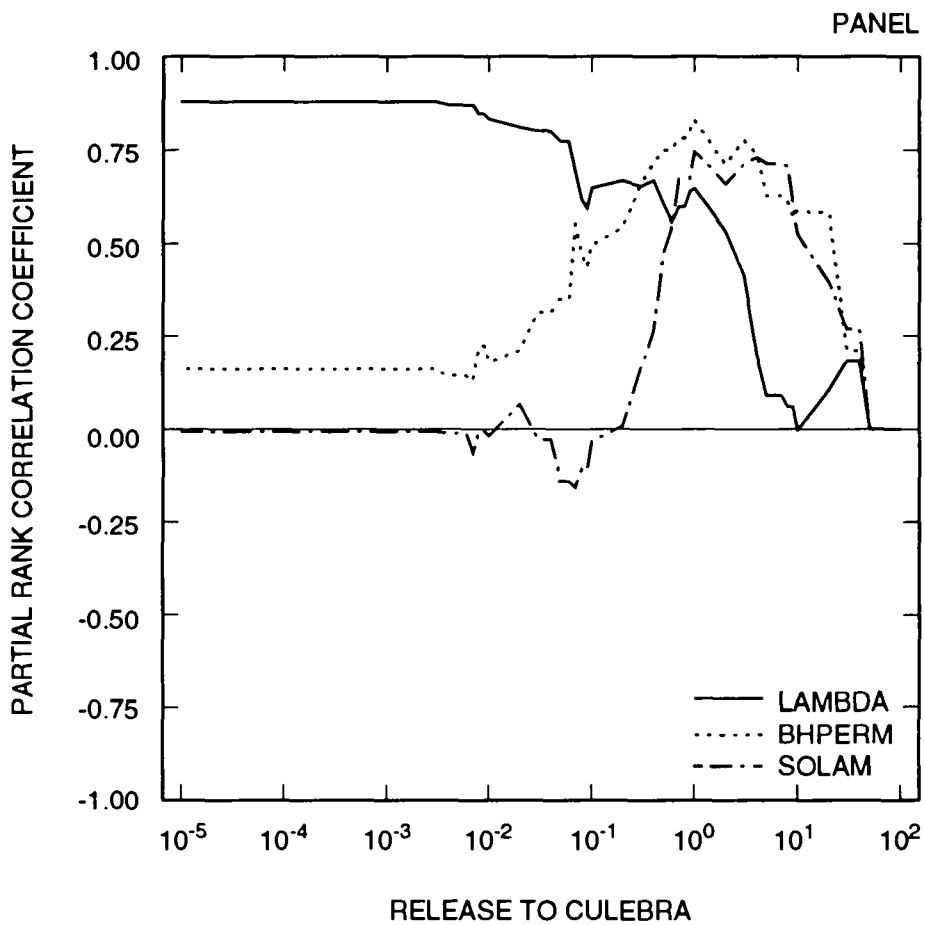

Figure 8.3-10. Partial rank correlation coefficients for exceedance probabilites associated with individual CCDFs in Figure 8.3-9 for release to the Culebra Dolomite with constant rate terms in the Poisson model for drilling intrusions.

Table 8.4-1. Alternative Modeling Assumptions for Radionuclide Transport in the Culebra Dolomite.

Section	Chemical Retardation	Clay Lining in Fractures	Matrix Diffusion	Comment
8.4.1	-	-	-	No chemical sorption and no movement to dolomite matrix. Illustrates most conservative modeling assumptions.
8.4.2	+	+	-	Chemical sorption in fractures only and no movement of dolomite matrix. Illustrates transport in fractures only.
8.4.3	+	-	+	Chemical sorption in dolomite matrix only.
8.4.4	+	+	+	Chemical sorption in fractures and dolomite matrix. Believed to be most realistic case.
8.4.5	-	+	-	No chemical sorption and no movement to dolomite matrix.
8.4.5	-	-	+	No chemical sorption with movement to dolomite matrix. Illustrates physical retardation in dolomite matrix.
8.4.5	-	+	+	No chemical sorption with movement to dolomite matrix.

diffusion) and dual porosity (i.e., diffusion into the dolomite matrix) transport. The case in Section 8.4.4 with chemical retardation in both the fractures and the dolomite matrix is believed by the WIPP performance assessment project to be the most appropriate model for radionuclide transport in the Culebra.

8.4.1 No Chemical Retardation, No Clay in Fractures, No Matrix Diffusion

This section presents results calculated with the assumptions that all fluid flow within the Culebra takes place in fractures, no clay is present in the fractures, and no chemical retardation occurs within the fractures. Thus, radionuclides released into the Culebra are transported unimpeded to the accessible environment. As shown by the scatterplot in Figure 8.4-1, these assumptions result in the releases to the accessible environment being essentially identical to the releases to the Culebra. Thus, the discussions in Section 8.3 for release to the Culebra also apply to release to the accessible environment for no chemical retardation and no matrix diffusion. In particular, the distribution of CCDFs for release to the accessible environment due to groundwater transport with no chemical retardation, no clay and no matrix diffusion are visually indistinguishable from those appearing in Figure 8.3-9 for release to the Culebra.

8.4.2 Chemical Retardation, Clay-Lined Fractures, No Matrix Diffusion

This section presents results calculated with the assumptions that all fluid flow within the Culebra takes place in fractures and that these fractures are lined with clay that can sorb radionuclides. The variable CULCLYF (clay-filling fraction in Culebra) determines the total thickness of the clay lining in fractures in the Culebra Dolomite. As indicated in Table 3-1 and Figure 3-1, this variable was assigned a distribution in the 1992 WIPP performance assessment that implies with a certain degree of belief (i.e., 0.5) that no fractures in the Culebra have a clay lining. As the purpose of this section is specifically to investigate the effects of clay-lined fractures, only calculations performed for the 35 sample elements that have a non-zero value for CULCLYF will be considered. The calculations performed for the 35 sample elements in which CULCLYF = 0 produce results identical to the results obtained for these sample elements in the calculations for Section 8.4.1.

The scatterplot in Figure 8.4-2 provides a comparison of releases to the accessible environment calculated with and without a clay lining in the fractures. The significance of the presence of a clay lining is that

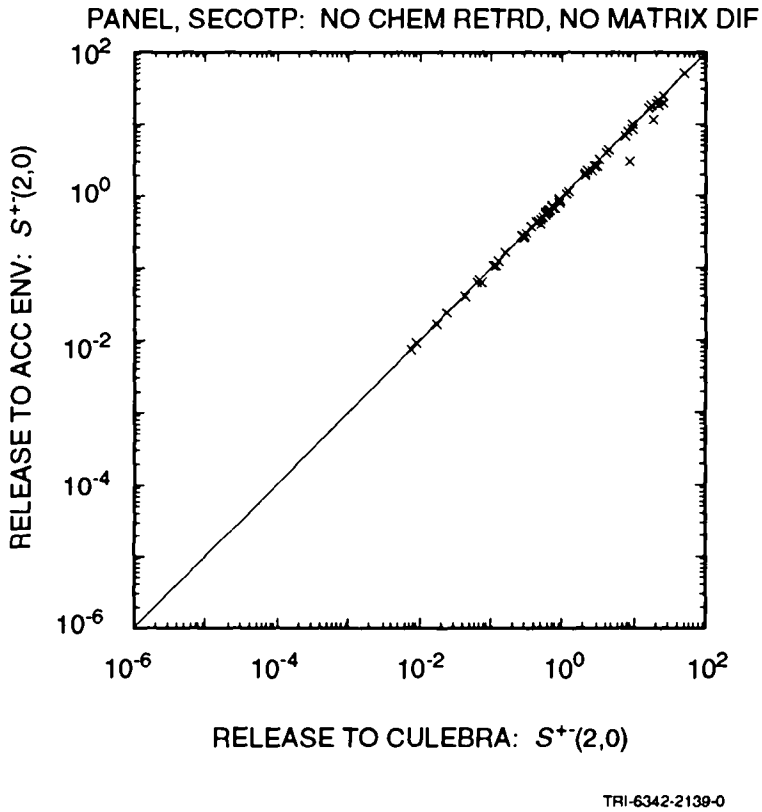

Figure 8.4-1. Scatterplot for total normalized release to Culebra over 10,000 yr versus total normalized release to the accessible environment due to groundwater transport with no chemical retardation and no matrix diffusion for scenario $S^{+-}(2,0)$ used in conjunction with the risk representation R_1 defined in Eq. 2.5-1 with intrusion occurring at 1000 yr after repository closure.

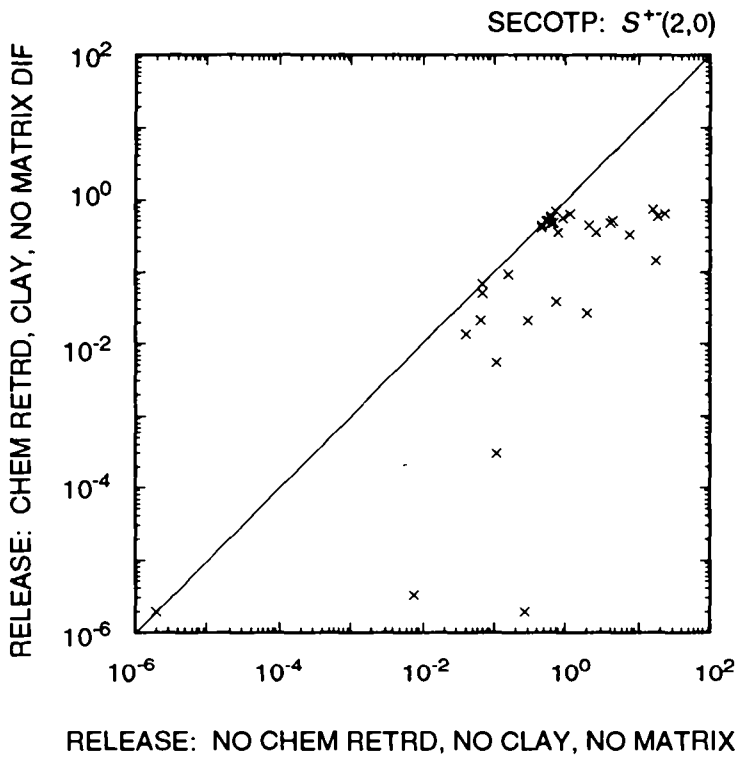

Figure 8.4-2. Scatterplot for total normalized release to the accessible environment over 10,000 yr due to groundwater transport with no chemical retardation and no matrix diffusion versus total normalized release to the accessible environment over 10,000 yr due to groundwater transport with chemical retardation, clay-lined fractures and no matrix diffusion for scenario $S^{+-}(2,0)$ used in conjunction with the risk representation R_1 defined in Eq. 2.5-1 with intrusion occurring 1000 yr after repository closure.

chemical retardation takes place in the presence of clay-lined fractures but is assumed not to take place in the absence of a clay lining in the fractures. As indicated in the preceding paragraph, this scatterplot is based on the 35 sample elements for which CULCLYF $\neq$ 0. The large number of points falling below the diagonal line in Figure 8.4-2 indicate that the presence of a clay lining in fractures has the potential to reduce releases from those that would be obtained without a clay lining. This reduction is due to radionuclide sorption.

As shown by the box plots in Figure 8.4-3, the releases to the accessible environment for this case are dominated by U-234 and U-233, with additional contributions from Np-237, Th-230 and Th-229. In contrast, the corresponding release to the accessible environment in the absence of clay-lined fractures is dominated by Am-241, with lesser contributions from Pu-239, U-233 and U-234 (i.e., see Figure 8.3-1 and discussion in Section 8.4.1).

As indicated by the scatterplot in Figure 8.4-4 for U-233, the entire uranium release to the Culebra is transported to the accessible environment over the 10,000-yr period under consideration for most sample elements. A more extensive reduction between release to the Culebra and release to the accessible environment is shown by the scatterplot for Np-237. This difference in behavior results from the fracture distribution coefficients (FKDU and FKDNP) assigned to uranium and neptunium, which have median values of 0.001 and 1 m^3/kg, respectively. The points in Figure 8.4-4 that indicate that the Np-237 release to the accessible environment exceeds the Np-237 release to the Culebra result from the decay of Am-241 to Np-237 within the Culebra. As shown by the scatterplot in Figure 8.4-5, the releases of Np-237 to the accessible environment are zero for values of FKDNP above 0.1 m^3/kg. The higher fracture distribution coefficients assigned to americium and plutonium result in essentially no Am-241, Pu-239 and Pu-240 being transported to the accessible environment. Radium and thorium display patterns intermediate to those displayed by uranium and neptunium.

As shown in Figure 8.4-6, the CCDFs for release to the accessible environment generated for groundwater transport with chemical retardation, clay-lined fractures, no matrix diffusion and constant rate terms in the Poisson model for drilling intrusions fall below the EPA release limits. Further, these CCDFs are shifted down and to the left when time-dependent rate terms are used.

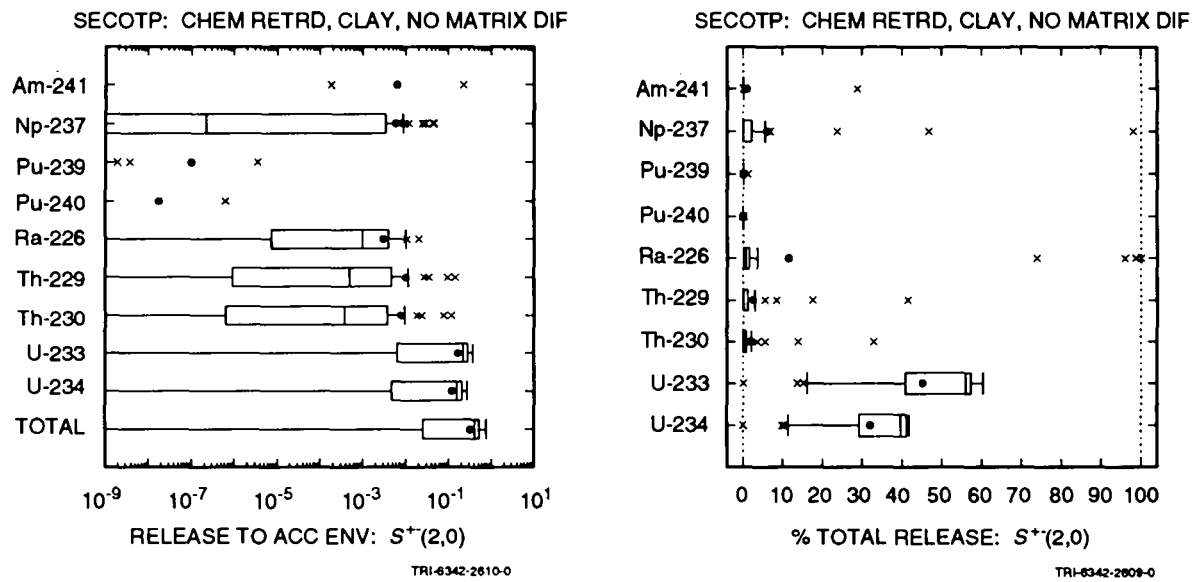

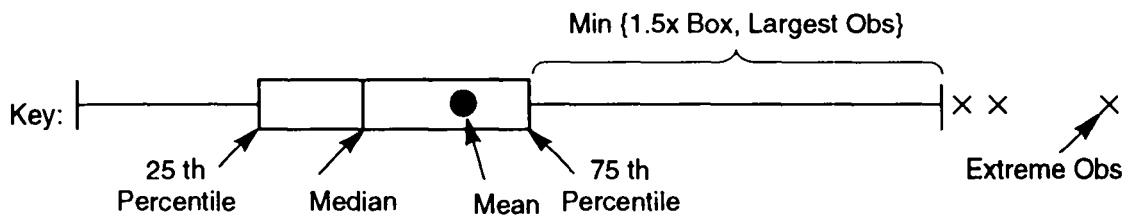

Figure 8.4-3. Normalized releases to the accessible environment over 10,000 yr due to groundwater transport with chemical retardation, clay lining in fractures and no matrix diffusion for scenario $S^{+-}(2,0)$ used in conjunction with the risk representation R_1 defined in Eq. 2.5-1 with intrusion occurring 1000 yr after repository closure.

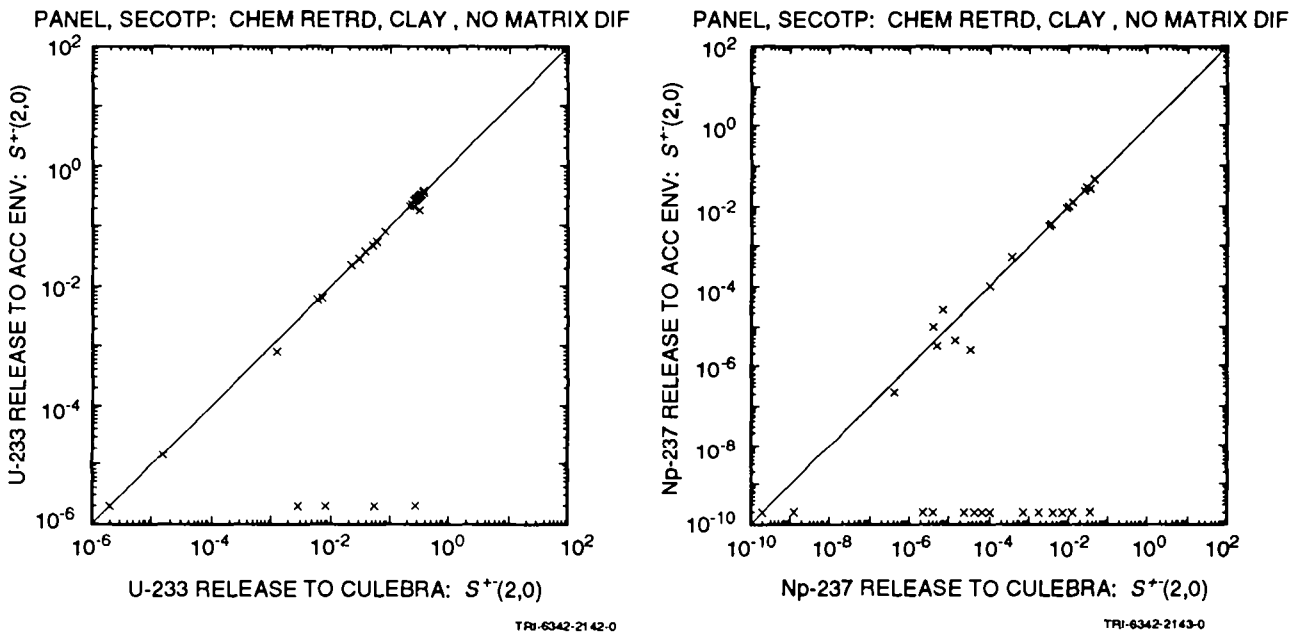

Figure 8.4-4. Scatterplots for total normalized release to the Culebra over 10,000 yr versus total normalized release to the accessible environment over 10,000 yr due to groundwater transport with chemical retardation, clay-lined fractures and no matrix diffusion for U-233 and Np-237 for scenario $S^{+-}(2,0)$ used in conjunction with the risk representation R_1 defined in Eq. 2.5-1 with intrusion occurring 1000 yr after closure.

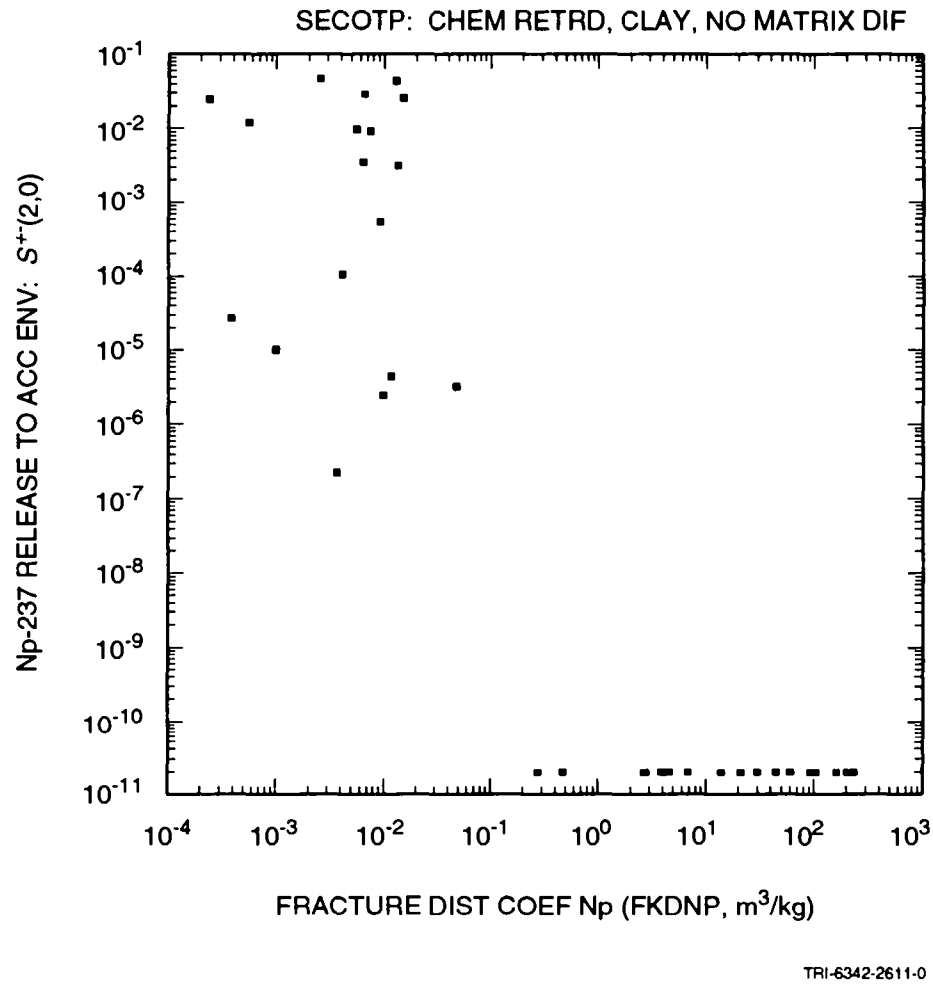

Figure 8.4-5. Scatterplot for normalized release of Np-237 to the accessible environment over 10,000 yr due to groundwater transport with chemical retardation, clay-lined fractures and no matrix diffusion versus FKDNP (fracture distribution coefficient for Np) for scenario $S^{+-}(2,0)$ used in conjunction with the risk representation R_1 defined in Eq. 2.5-1 with intrusion occurring 1000 yr after repository closure.

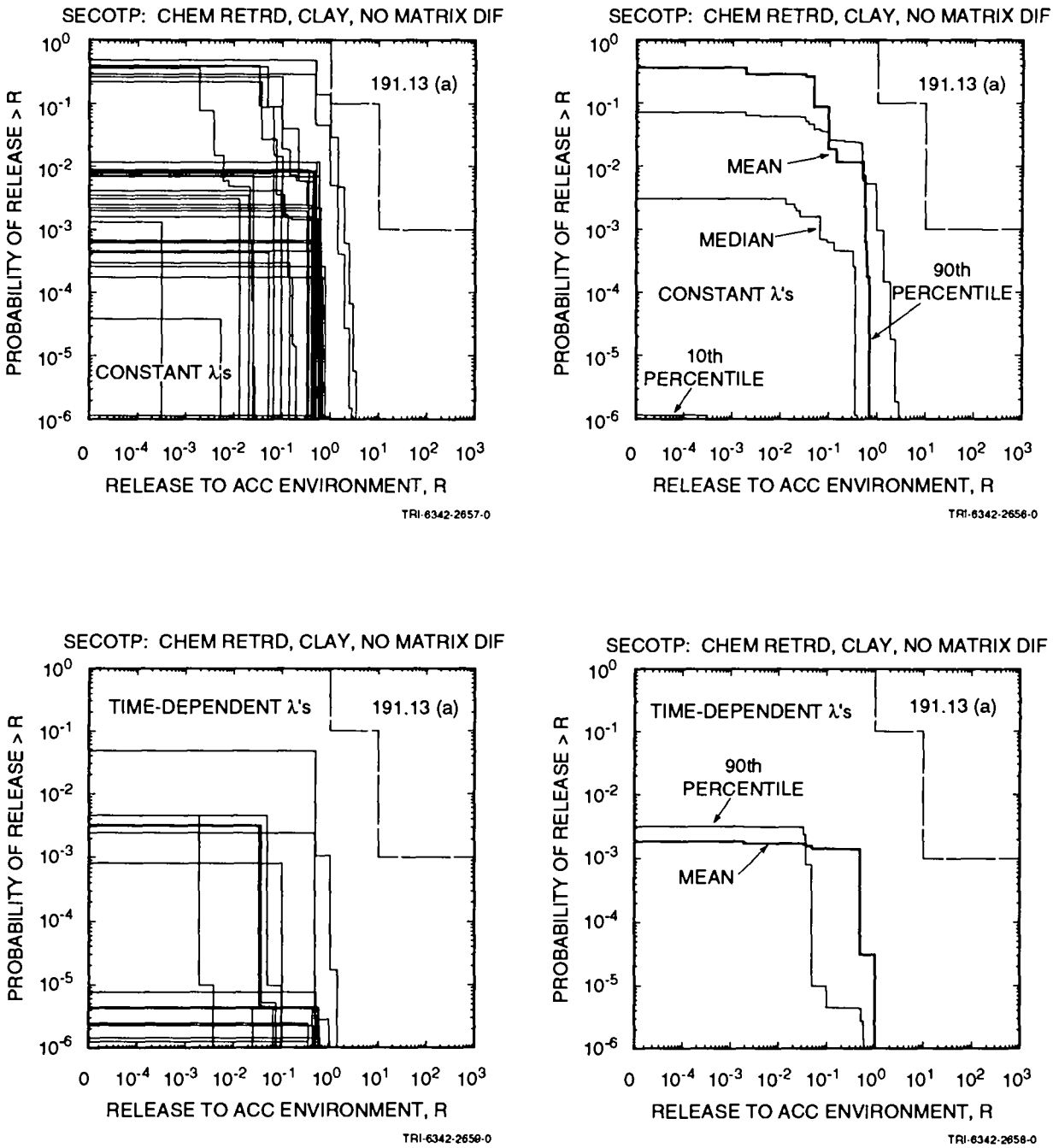

Figure 8.4-6. Distribution of CCDFs for normalized release to the accessible environment over 10,000 yr due to groundwater transport with chemical retardation, clay-lined fractures and no matrix diffusion for risk representation R_1 defined in Eq. 2.5-1 with constant (upper two frames) and time-dependent (lower two frames) rate terms in the Poisson model for drilling intrusions.

8.4.3 Chemical Retardation, No Clay Lining in Fractures, Matrix Diffusion

This section presents results calculated with the assumptions that diffusion occurs into the dolomite matrix, chemical retardation occurs in the dolomite matrix, and no clay lining is present in the fractures. Due to the absence of a clay lining, no chemical retardation occurs in the fractures. As shown by the scatterplot in Figure 8.4-7 for scenario $S^{+-}(2,0)$, these assumptions result in releases to the accessible environment that are substantially less than the releases to the Culebra. Specifically, only 21 sample elements result in releases to the accessible environment that exceed 1×10^{-10} EPA release units and the largest release is approximately 0.1 EPA release units. As shown by the box plots in Figure 8.4-8, the nonzero releases to the accessible environment tend to be dominated by U-233, U-234, Th-229, Th-230 and Ra-226, although all the releases tend to be small (i.e., less than 0.1 EPA release units).

As indicated by the two scatterplots in Figure 8.4-9 for U-233, release to the accessible environment is controlled primarily by processes associated with the dolomite matrix. In particular, the left scatterplot indicates that U-233 releases occur only for values of MKDU (matrix distribution coefficient for U) that are less than approximately 10^{-3} m^3/kg, and the right scatterplot indicates that releases occur only for values of CULFRSP (Culebra fracture spacing) that exceed 1 m. Increasing CULFRSP decreases the number of fractures and thus also decreases the total surface area through which diffusion can take place from the fractures to the dolomite matrix. As a result, the nonzero releases associated with the larger values of CULFRSP result from decreased diffusion into the dolomite matrix. The effect of distribution coefficients is element specific but increasing surface area for diffusion affects all elements. As shown in Figure 8.4-10, the occurrence of nonzero releases to the accessible environment is strongly associated with the larger values for CULFRSP.

The CCDFs for release to the accessible environment due to groundwater transport with diffusion into the dolomite matrix, chemical retardation in the dolomite matrix, and no clay lining in the fractures are presented in Figure 8.4-11. As examination of this figure shows, the indicated assumptions lead to CCDFs that are significantly below the EPA release limits. Indeed, only 8 out a possible 70 CCDFs appear in the upper left frame when constant rate terms are used, and only 1 out of a possible 70 CCDFs appear in the lower right frame when time-dependent rate terms are

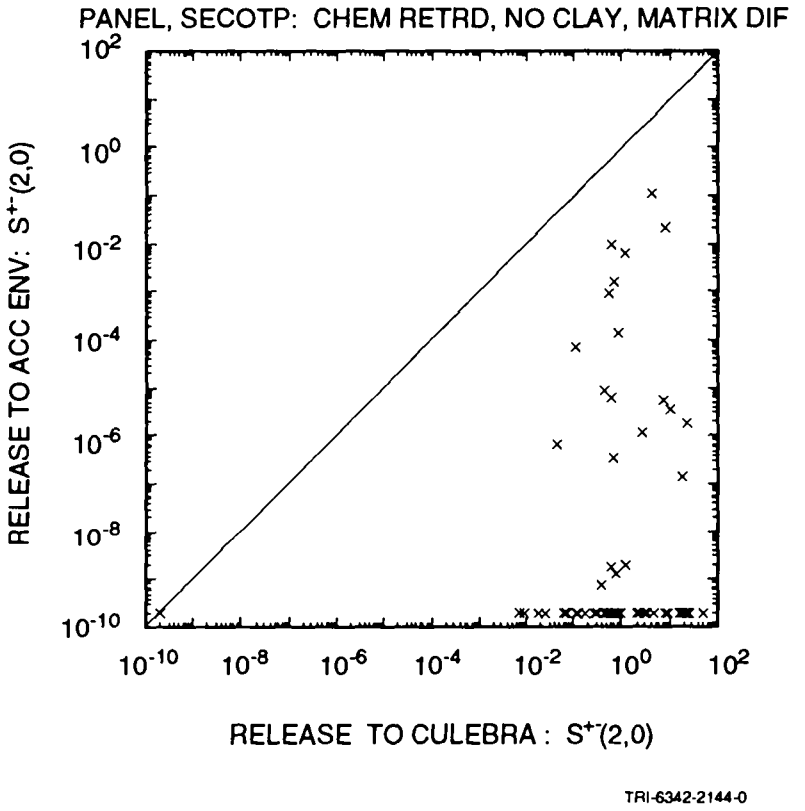

Figure 8.4-7. Scatterplot for total normalized release to Culebra over 10,000 yr versus total normalized release to accessible environment over 10,000 yr due to groundwater transport with chemical retardation, no clay lining in fractures and matrix diffusion for scenario $S^{+-}(2,0)$ used in conjunction with the risk representation R_1 defined in Eq. 2.5-1 with intrusion occurring at 1000 yr.

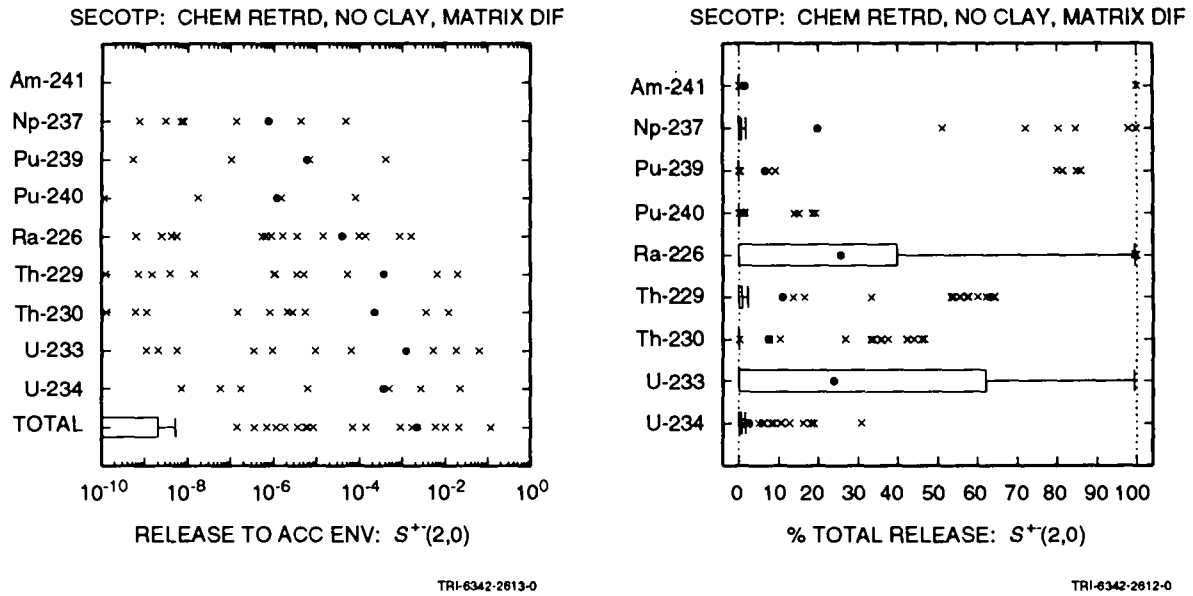

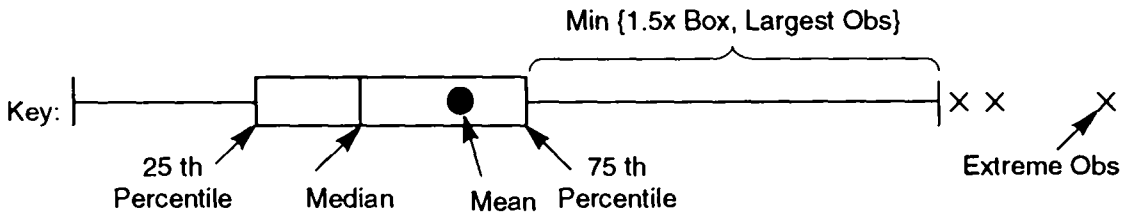

Figure 8.4-8. Normalized releases to accessible environment over 10,000 yr due to groundwater transport with chemical retardation, no clay lining in fractures and matrix diffusion for scenario $S^{+-}(2,0)$ used in conjunction with the risk representation R_1 defined in Eq. 2.5-1 with intrusion occurring at 1000 yr after repository closure.

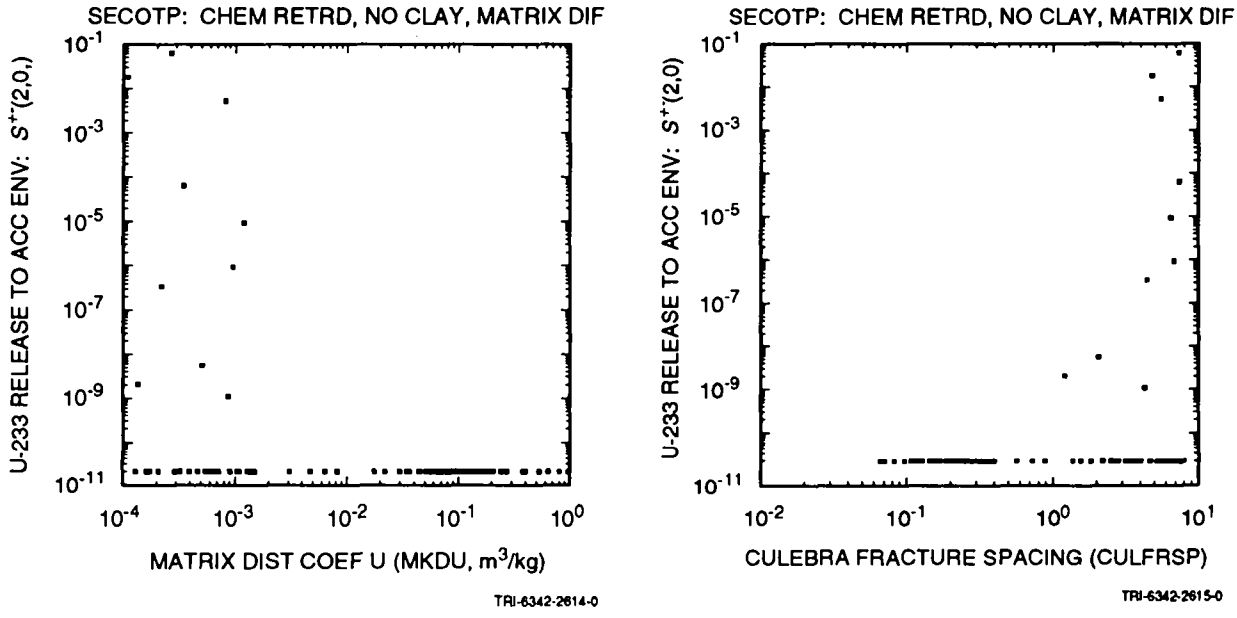

Figure 8.4-9. Scatterplots for normalized release of U-233 to the accessible environment over 10,000 yr due to groundwater transport with chemical retardation, no clay lining in fractures and matrix diffusion versus variables MKDU (matrix distribution coefficient for U) and CULFRSP (Culebra fracture spacing) for scenario $S^{+-}(2,0)$ used in conjunction with the risk representation R_1 defined in Eq. 2.5-1 with intrusion occurring 1000 yr after repository closure.

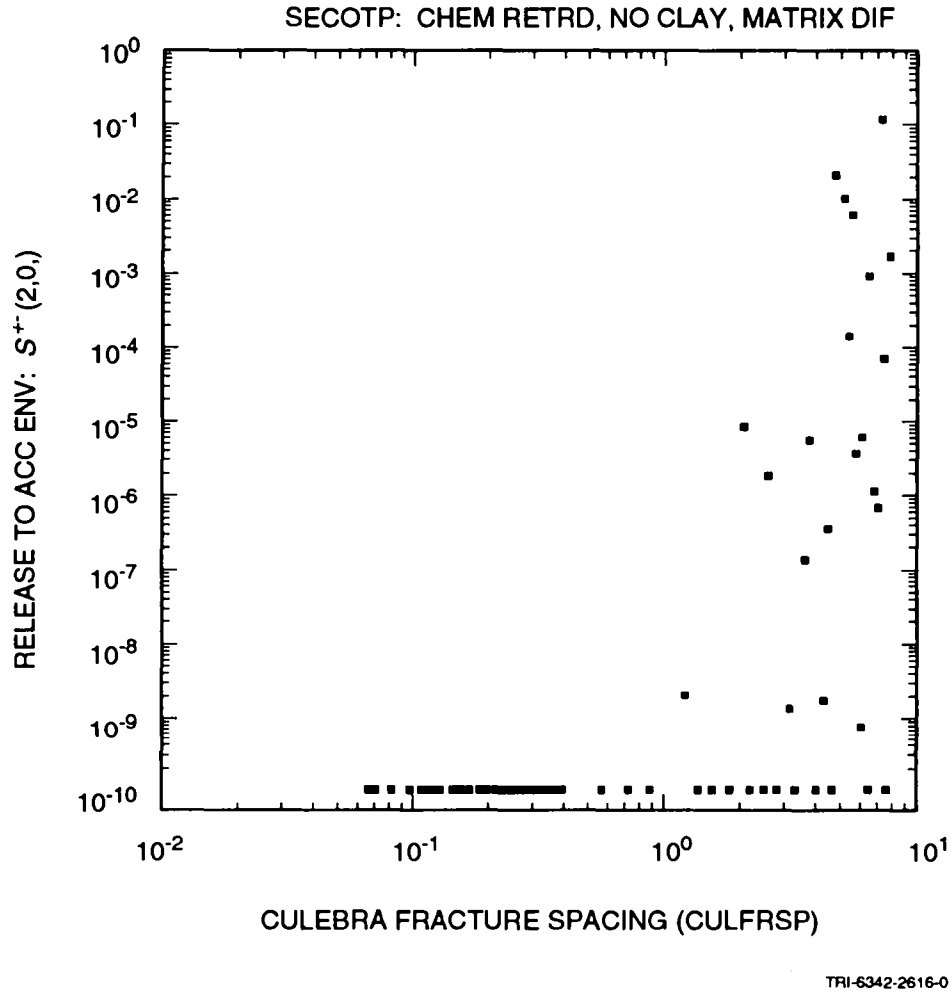

Figure 8.4-10. Scatterplot for total normalized release to the accessible environment over 10,000 yr due to groundwater transport with chemical retardation, no clay lining in fractures and matrix diffusion versus CULFRSP (Culebra fracture spacing) for scenario $S^{+-}(2,0)$ used in conjunction with the risk representation R_1 defined in Eq. 2.5-1 with intrusion occurring 1000 yr after repository closure.

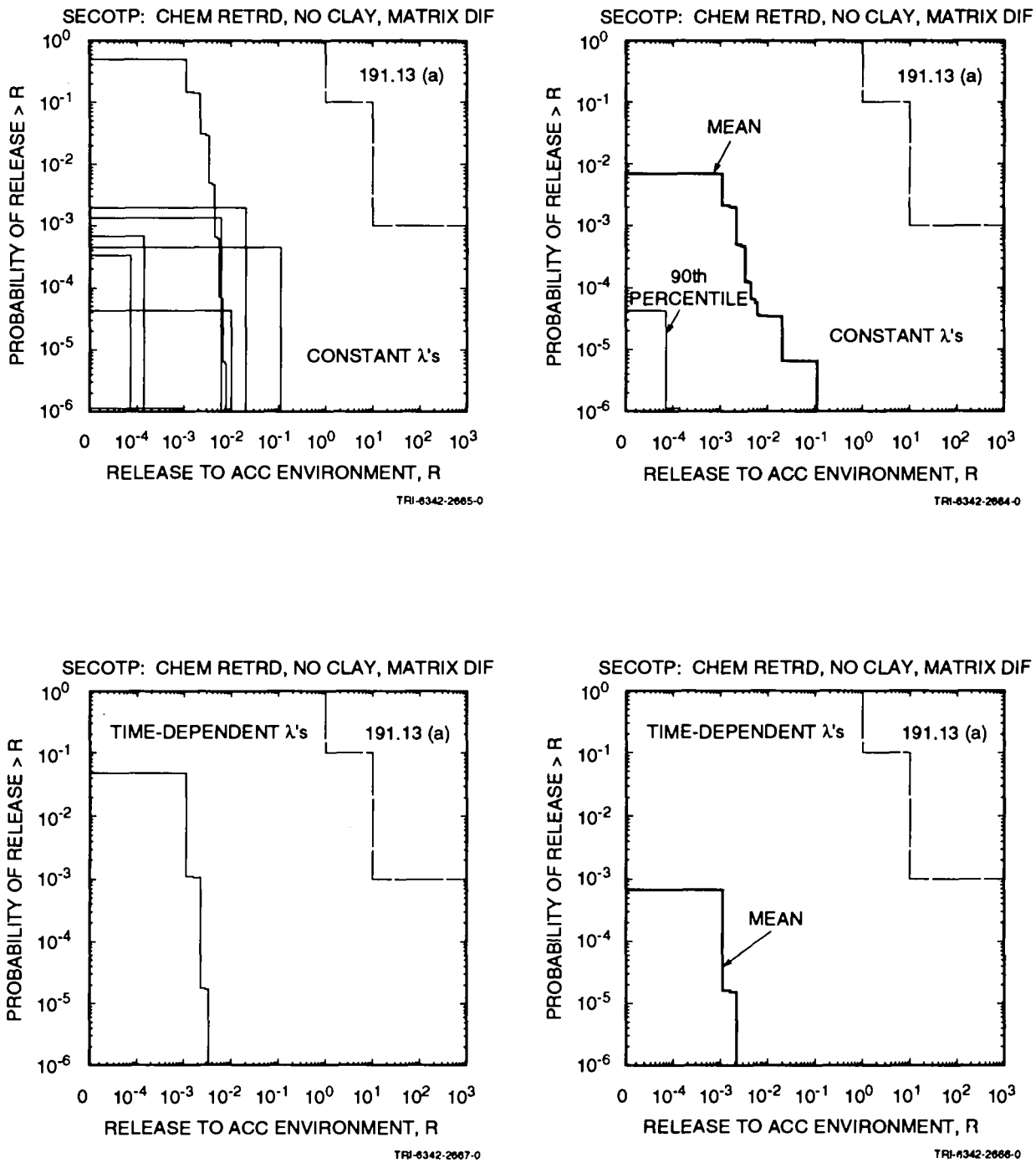

Figure 8.4-11. Distribution of CCDFs for normalized release to the accessible environment over 10,000 yr due to groundwater transport with chemical retardation, no clay lining in fractures and matrix diffusion constructed for the risk representation R_1 defined in Eq. 2.5-1 with constant (upper two frames) and time-dependent (lower two frames) rate terms in the Poisson model for drilling intrusions.

used. As a reminder, only 21 sample elements produce releases to the accessible environment that exceed 1 x 10^{-10} EPA release units for scenario $S^{+-}(2,0)$, and only 14 sample elements produce nonzero releases to the Culebra for scenario $S(1,0)$, with these releases being smaller than the corresponding releases for scenario $S^{+-}(2,0)$.

8.4.4 Chemical Retardation, Clay Lining in Fractures, Matrix Diffusion

This section presents results calculated with the assumptions that diffusion occurs into the dolomite matrix, clay-lined fractures are present, and sorption takes place in both the dolomite matrix and the clay lining of the fractures. As discussed in Section 8.4.2, only half the sample elements used in the 1992 WIPP performance assessment have clay-lined fractures. Therefore, the results presented in this section involve only the 35 sample elements that have clay-lined fractures (i.e., those sample elements for which CULCLYF≠0). At present, the WIPP performance assessment project believes this is the most appropriate set of assumptions to use for radionuclide transport in the Culebra.

As a reminder, only 21 out of 70 sample elements result in releases to the accessible environment that exceed 1 x 10^{-10} EPA release units for chemical retardation, no clay lining in fractures and matrix diffusion. Thus, approximately two-thirds of the sample elements produce no release to the accessible environment in the absence of clay-lined fractures. As shown by the scatterplot in Figure 8.4-12, the releases calculated with clay-lined fractures tend to equal or exceed the releases calculated without clay-lined fractures. This pattern probably results because the clay lining of the fractures slows diffusion into the dolomite matrix. However, it should be recognized that this comparison is based on only 9 nonzero releases to the accessible environment out of a total of 35 sample elements that have clay-lined fractures.

As 26 of the 35 sample elements with clay-lined fractures result in no releases to the accessible environment for scenario $S^{+-}(2,0)$, most of the resultant CCDFs for comparison with the EPA release limits are degenerate. The few nonzero CCDFs that do result are shown in Figure 8.4-13. As comparison of Figures 8.4-11 and 8.4-13 shows, the presence of matrix diffusion in conjunction with chemical retardation results in releases that fall substantially below the EPA release limits regardless of whether or not a clay lining is present in the fractures.

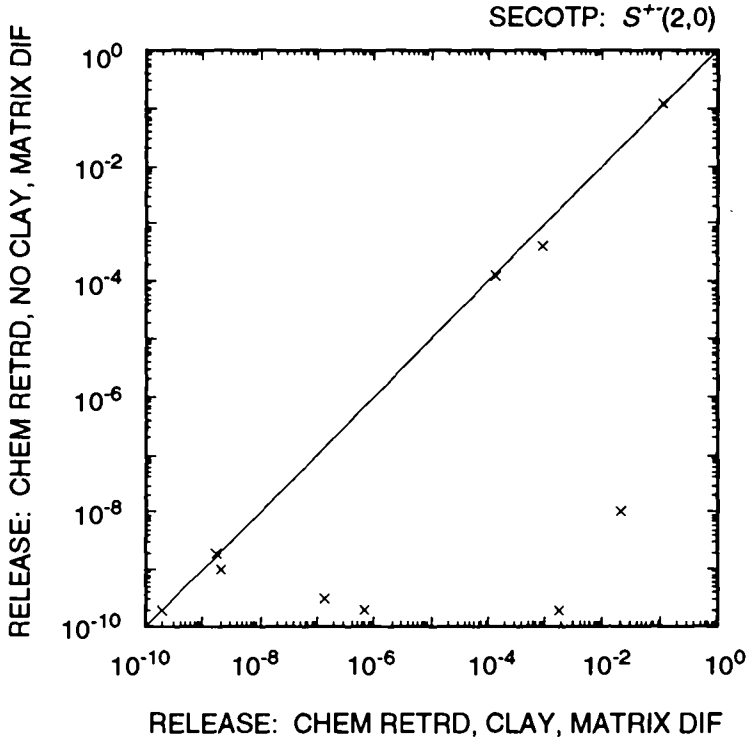

Figure 8.4-12. Scatterplot for total normalized release to the accessible environment over 10,000 yr due to groundwater transport with chemical retardation, no clay-lined fractures and matrix diffusion versus total normalized release to the accessible environment over 10,000 yr due to groundwater transport with chemical retardation, clay-lined fractures and matrix diffusion for scenario $S^{+-}(2,0)$ used in conjunction with the risk representation R_1 defined in Eq. 2.5-1 with intrusion occurring 1000 yr after repository closure.

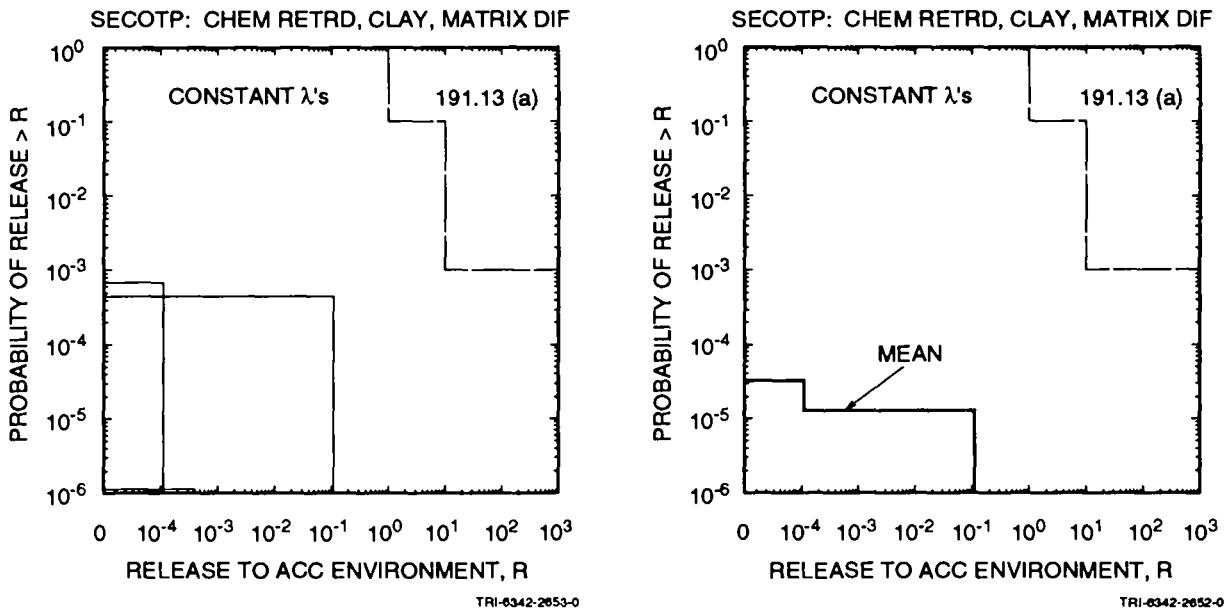

Figure 8.4-13. Distribution of CCDFs for normalized release to the accessible environment over 10,000 yr due to groundwater transport with chemical retardation, clay-lined fractures and matrix diffusion for risk representation R_1 defined in Eq. 2.5-1 with constant terms in the Poisson model for drilling intrusions. The use of time-dependent rate terms in the Poisson model results in all CCDFs being outside the plotting limits in use. The plots in this figure are based on 35 sample elements rather than 70 sample elements as in Figure 8.4-1 and other similar figures.

8.4.5 No Chemical Retardation

Calculations without chemical retardation were performed for three additional sets of assumptions: (1) clay-lined fractures and no matrix diffusion, (2) no clay lining in fractures and matrix diffusion, and (3) clay-lined fractures and matrix diffusion. The releases to the accessible environment for Assumption (1) were essentially identical to the results obtained for release to the Culebra (Section 8.3) and for release to the accessible environment with no chemical retardation, no clay lining in fractures and no matrix diffusion (Section 8.4.1). The releases to the accessible environment for Assumptions (2) and (3) were similar to each other. Further, as shown in Figure 8.4-14, the releases for Assumptions (2) and (3) were larger than the corresponding releases obtained with chemical retardation and matrix diffusion (Sections 8.4.3 and 8.4.4) and, as shown in Figure 8.4-15, often smaller than the releases obtained with chemical retardation and no matrix diffusion (Section 8.4.2).

The releases of the individual radionuclides to the accessible environment due to groundwater transport with no chemical retardation, no clay lining in fractures and matrix diffusion are summarized in Figure 8.4-16. As examination of this figure shows, the total release is dominated by Pu-239, with additional contributions from Am-241 and U-233. The corresponding results for chemical retardation, no clay-lining in fractures and matrix diffusion appear in Figure 8.4-8, while the results for chemical retardation, clay-lined fractures and no matrix diffusion appear in Figure 8.4-3. As comparison with Figures 8.4-3 and 8.4-8 shows, the removal of chemical retardation increases the importance of Pu-239 in the release to the accessible environment.

Because of the large number of zero releases, no regression-based sensitivity analyses were presented for groundwater transport to the accessible environment with chemical retardation. However, such analyses have the potential to be more revealing for the transport results in the absence of chemical retardation due to the occurrence of a larger number of nonzero releases. The results of such analyses for no chemical retardation, no clay lining in fractures and matrix diffusion are presented in Table 8.4-1. As examination of Table 8.4-1 shows, the variable with the largest influence on release to the accessible environment is CULFRSP (Culebra fracture spacing), with release tending to increase as CULFRSP increases. This positive effect results because increasing CULFRSP reduces the surface area over which diffusion into the dolomite matrix can take place. Positive effects are also indicated for BHPERM (borehole permeability) and the solubilities of individual elements (i.e., SOLAM, SOLNP, SOLPU, SOLTH, SOLU). Increasing BHPERM decreases resistance to brine flow up an intruding

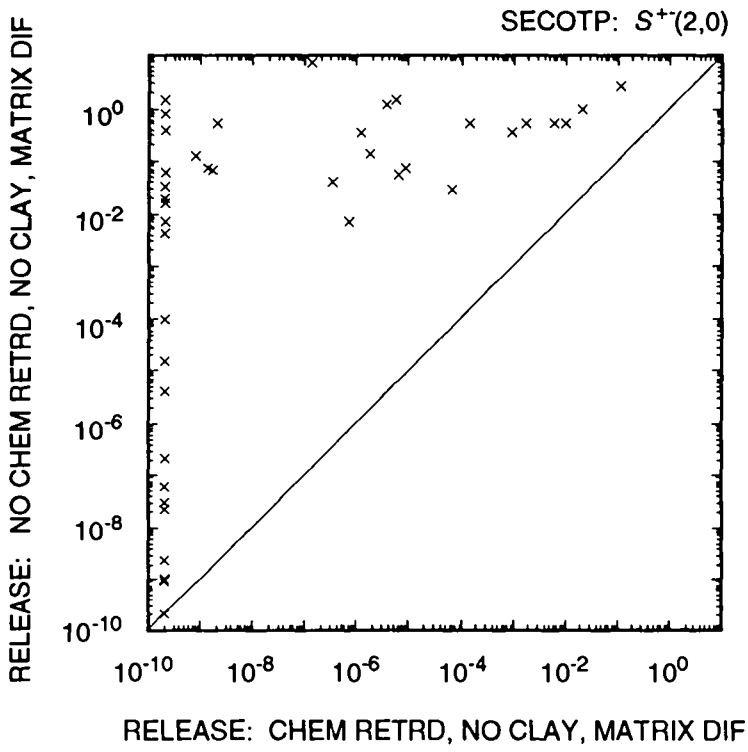

Figure 8.4-14. Scatterplot for total normalized release to the accessible environment over 10,000 yr with and without chemical retardation for groundwater transport with matrix diffusion and no clay lining in fractures for scenario $S^{+-}(2,0)$ used in conjunction with the risk representation R_1 defined in Eq. 2.5-1 with intrusion occurring 1000 yr after repository closure.

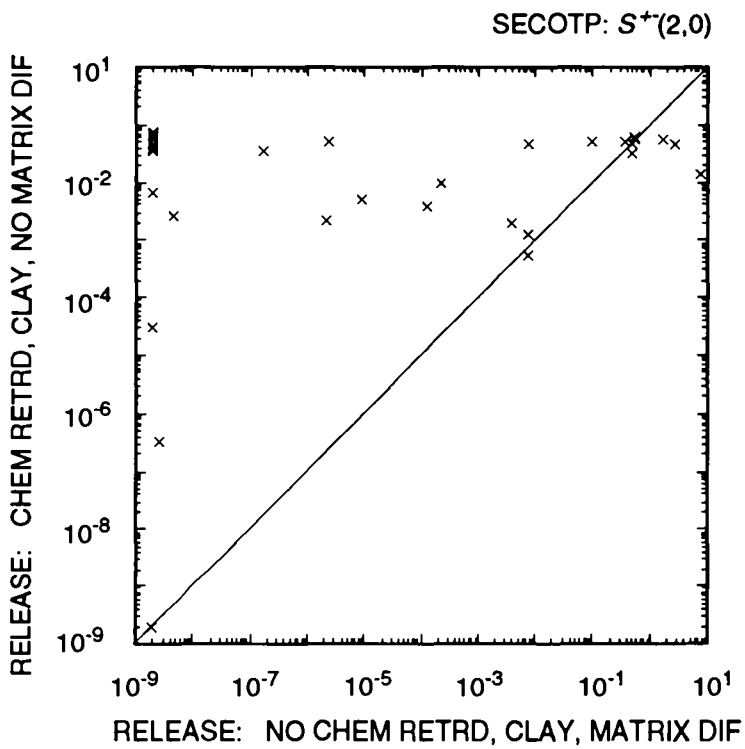

Figure 8.4-15. Scatterplot for total normalized release to the accessible environment over 10,000 yr due to groundwater transport with no chemical retardation, clay-lined fractures and matrix diffusion versus total normalized release to the accessible environment over 10,000 yr due to groundwater transport with chemical retardation, clay-lined fractures and no matrix diffusion for scenario $S^{+-}(2,0)$ used in conjunction with the risk representation R_1 defined in Eq. 2.5-1 with intrusion occurring 1000 yr after repository closure.

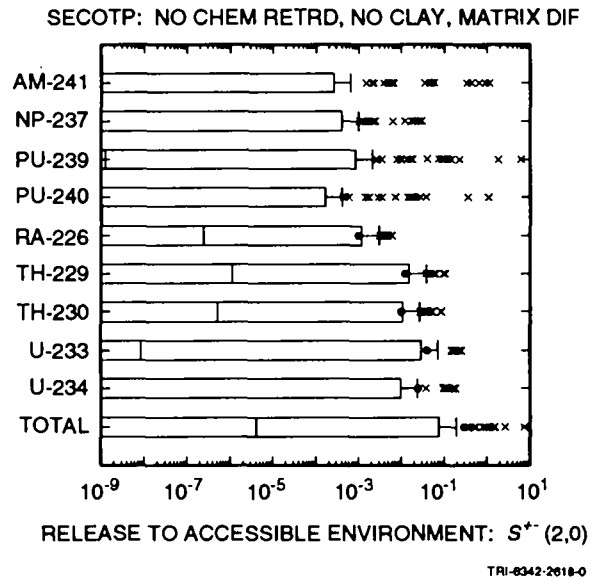

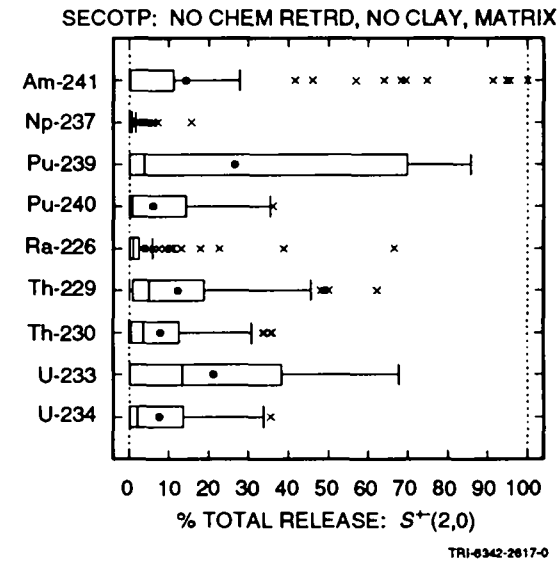

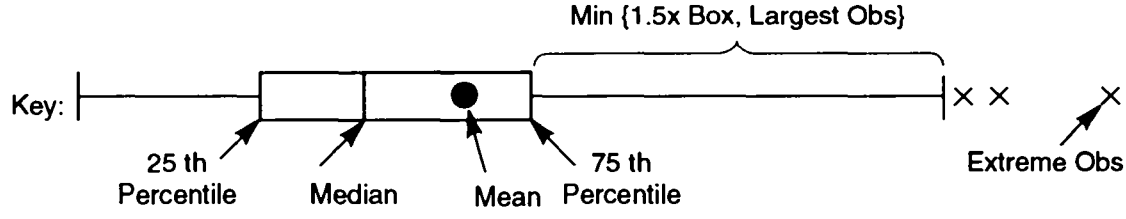

Figure 8.4-16. Normalized releases to accessible environment over 10,000 yr due to groundwater transport with no chemical retardation, no clay lining in fractures and matrix diffusion for scenario $S^{+-}(2,0)$ used in conjunction with the risk representation R_1 defined in Eq. 2.5-1 with intrusion occurring at 1000 yr after repository closure.

Table 8.4-1. Stepwise Regression Analyses with Rank-Transformed Data for Integrated Release to the Accessible Environment over 10,000 yr due to Groundwater Transport with No Chemical Retardation, No Clay Lining in Fractures and Matrix Diffusion for Scenario S^{+-}(2,0) with Intrusion Occurring 1000 yr after Repository Closure.

	Variable[a]	R^{2b}	Variable	R^2	Variable	R^2	Variable	R^2
Step[c]	Am-241		Np-237		Pu-239		Pu-240	
1	CULFRSP	0.54(+)	CULFRSP	0.56(+)	CULFRSP	0.42(+)	CULFRSP	0.42(+)
2	BHPERM	0.64(+)	BHPERM	0.64(+)	SOLPU	0.64(+)	SOLPU	0.64(+)
3	SOLAM	0.70(+)	SOLNP	0.68(+)	BHPERM	0.71(+)	BHPERM	0.71(+)
4	CULPOR	0.74 (-)			CULTRFLD	0.74 (-)	CULTRFLD	0.74 (-)
Step	Ra-226		Th-229		Th-230		U-233	
1	CULFRSP	0.60(+)	CULFRSP	0.53(+)	CULFRSP	0.54(+)	CULFRSP	0.57(+)
2	BHPERM	0.69(+)	BHPERM	0.63(+)	BHPERM	0.64(+)	BHPERM	0.67(+)
3	CULPOR	0.72 (-)	SOLTH	0.68(+)	SOLTH	0.69(+)	SOLU	0.70(+)
4	CULTRFLD	0.74 (-)						
Step	U-234		Total					
1	CULFRSP	0.58(+)	CULFRSP	0.58(+)				
2	BHPERM	0.68(+)	BHPERM	0.68(+)				
3			CULTRFLD	0.72 (-)				
4			SOLPU	0.74(+)				

[a]Variables listed in order of selection in regression analysis

[b]Cumulative R^2 value with entry of each variable into regression model, with "+" and "-" indicating positive and negative regression coefficients, respectively

[c]Steps in stepwise regression analysis

borehole, and increasing the solubilities increases the amount of dissolved radionuclides that can be transported by a given volume of brine. Small negative effects are indicated for CULPOR (matrix porosity in Culebra) and CULTRFLD (transmissivity field for Culebra). Increasing CULPOR increases the amount of radionuclide that can be held in the dolomite matrix and thus tends to decrease release. The variable CULTRFLD is actually the travel time to the accessible environment for the individual transmissivity fields used in the analysis. Thus, increasing CULTRFLD increases the amount of time required to transport a radionuclide from its release point into the Culebra to the accessible environment, which in turn tends to decrease the amount of a radionuclide that can be transported to the accessible environment over 10,000 yr.

Examination of scatterplots often provides an additional perspective on regression-based sensitivity analysis results of the form presented in Table 8.4-1. The regression analyses in Table 8.4-1 consistently identify CULFRSP (Culebra fracture spacing) and BHPERM (borehole permeability) as being important variables, with CULFRSP being the first variable selected in every analysis. As an example, scatterplots for CULFRSP and BHPERM for the release of Am-241 to the accessible environment are presented in Figure 8.4-17. Consistent with the regression results in Table 8.4-1, a stronger positive relationship between release to the accessible environment and CULFRSP can be seen in Figure 8.4-17 than between release to the accessible environment and BHPERM.

The analyses for Pu-239 and Pu-240 in Table 8.4-1 differ from the analyses for the other radionuclides in that solubility of plutonium (SOLPU) is indicated as being more important for release to the accessible environment than is solubility for the other elements (i.e., SOLAM, SOLNP, SOLRA, SOLTH, SOLU). To a great extent, this importance results from the very large range of values (i.e., 2.5×10^{-17} to 5.5×10^{-4} mol/ℓ) assigned to SOLPU. As shown in Figure 8.4-18, there is an interplay between the effects of CULFRSP (Culebra fracture spacing) and SOLPU. In particular, the value assigned to CULFRSP is a major determinant of whether or not a release to the accessible environment will occur. However, given that there is a release, the size of this release tends to increase as SOLPU increases.

Distributions of CCDFs for release to the accessible environment generated for groundwater transport with no chemical retardation, no clay lining in fractures and matrix diffusion are shown in Figure 8.4-19. The upper two frames show results for constant rate terms in the Poisson model for drilling intrusion, and the lower two frames show results for time-dependent rate terms. As already suggested by the comparison in Figure 8.4-14, the assumptions of no chemical retardation and matrix diffusion lead

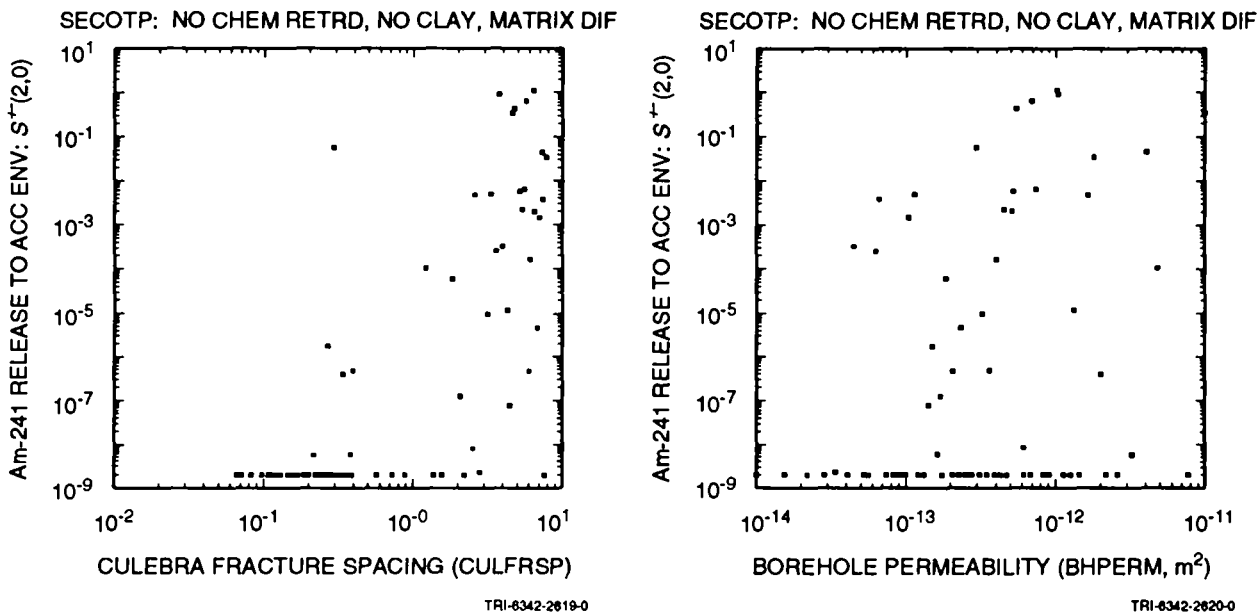

Figure 8.4-17. Scatterplots for normalized release of Am-241 to the accessible environment over 10,000 yr due to groundwater transport with no chemical retardation, no clay lining in fractures and matrix diffusion versus variables CULFRSP (Culebra fracture spacing) and BHPERM (borehole permeability) for scenario $S^{+-}(2,0)$ used in conjunction with the risk representation R_1 defined in Eq. 2.5-1 with intrusion occurring 1000 yr after repository closure.

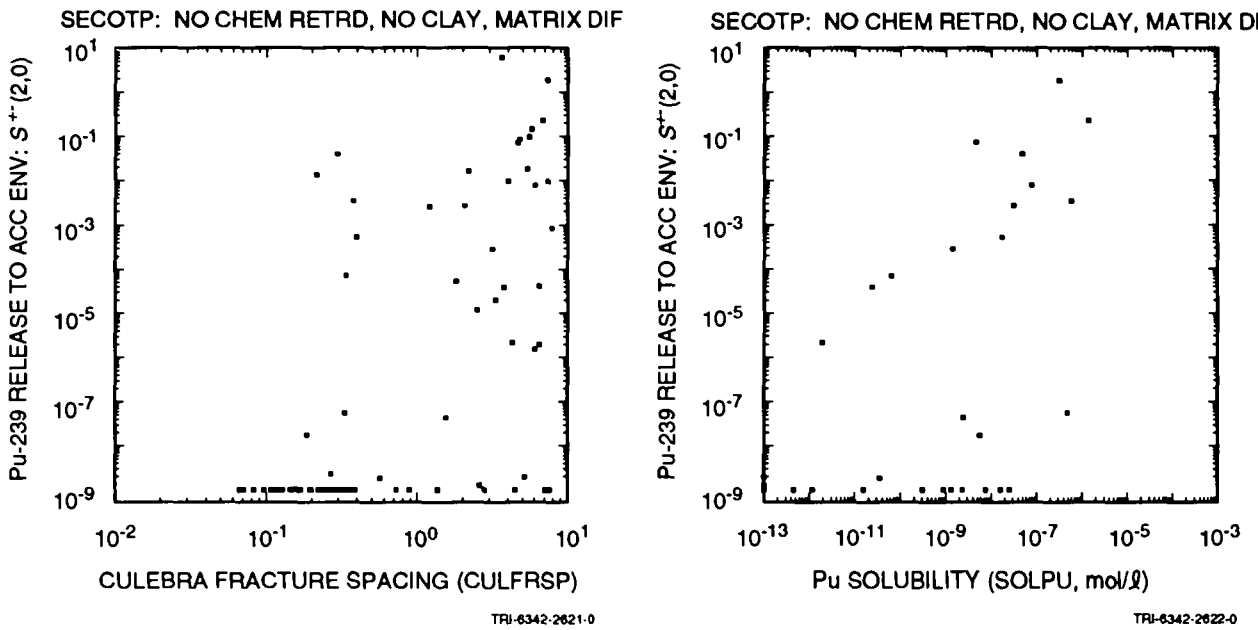

Figure 8.4-18. Scatterplots for normalized release of Pu-239 to the accessible environment over 10,000 yr due to groundwater transport with no chemical retardation, no clay lining in fractures and matrix diffusion versus variables CULFRSP (Culebra fracture spacing) and SOLPU (solubility of plutonium) for scenario $S^{+-}(2,0)$ used in conjunction with the risk representation R_1 defined in Eq. 2.5-1 with intrusion occurring 1000 yr after repository closure.

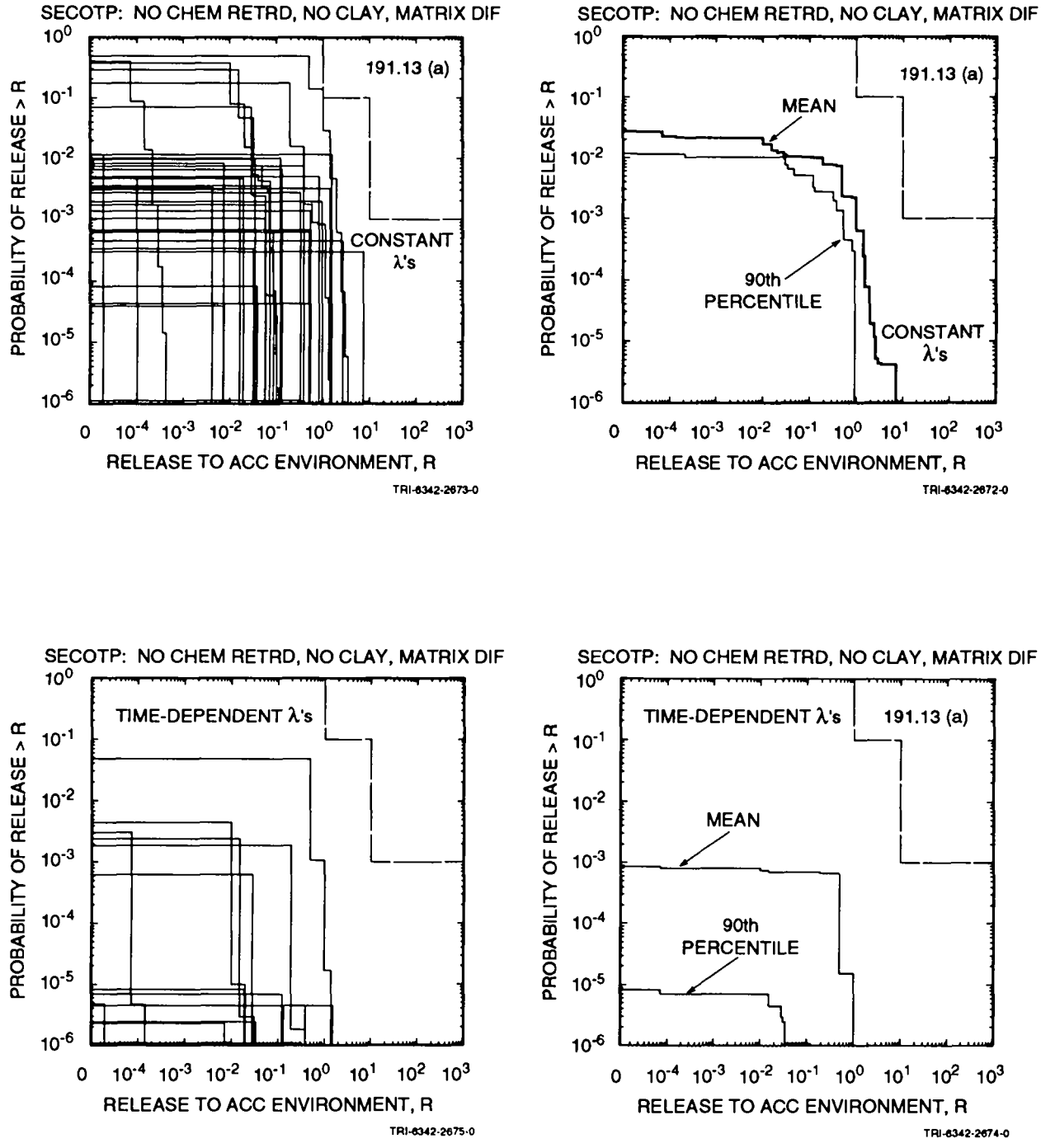

Figure 8.4-19. Distribution of CCDFs for normalized release to the accessible environment over 10,000 yr due to groundwater transport with no chemical retardation, no clay lining in fractures and matrix diffusion constructed for the risk representation R_1 defined in Eq. 2.5-1 with constant (upper two frames) and time-dependent (lower two frames) rate terms in the Poisson model for drilling intrusions.

to CCDFs that are closer to the EPA release limits than the CCDFs in Figure 8.4-11 obtained with chemical retardation and matrix diffusion. Further, as suggested by the comparison in Figure 8.4-15, the assumptions of no chemical retardation and matrix diffusion leads to a distribution that is similar to the one obtained with chemical retardation, clay-lined fractures and no matrix diffusion, although the assumption of matrix diffusion produces more small releases.

8.5 Total Release to Accessible Environment

As shown in Eqs. 2.4-10 through 2.4-14, the total release to the accessible environment is obtained by combining a release due to cuttings removal and a release due to groundwater transport. Summaries of this total release, and the cuttings removal and groundwater transport components from which it is constructed, are given in Figures 8.5-1 and 8.5-2 for scenarios $S(1,0)$ and $S^{+-}(2,0)$ used in conjunction with the risk representation R_1 defined in Eq. 2.5-1 and the various alternative modeling assumptions considered in the 1992 WIPP performance assessment.

For scenario $S(1,0)$, only 14 out of the 70 sample elements result in a release to the Culebra. Further, most of these releases (i.e., 11 out of 14) fall between 0.1 and 1 EPA release units. This narrow range of nonzero releases results from an almost complete removal of U-233 and U-234 from the waste (i.e., see Figures 8.3-1 and 7-4). As a result, the releases for the alternative modeling assumptions shown in Figure 8.5-1 for scenario $S(1,0)$ tend to be dominated by the cuttings release component, although in a few sample elements the groundwater transport release does exceed the cuttings release.

For scenario $S^{+-}(2,0)$, 68 out of the 70 sample elements result in releases to the Culebra. Further, most (i.e., 58 out of 68) exceed 0.1 EPA release units. As a result, scenario $S^{+-}(2,0)$ provides a more revealing comparison of releases than scenario $S(1,0)$. Each of the alternative modeling assumptions without matrix diffusion produces releases that are dominated by the groundwater transport component. In contrast, the release is almost completely dominated by the cuttings component when chemical retardation and matrix diffusion are assumed. For no chemical retardation and matrix diffusion, both the groundwater component and the cuttings component are important contributors to the total release.

Due to the large number of nonzero releases to the Culebra that result for scenario $S^{+-}(2,0)$, Figure 8.5-2 also provides a convenient

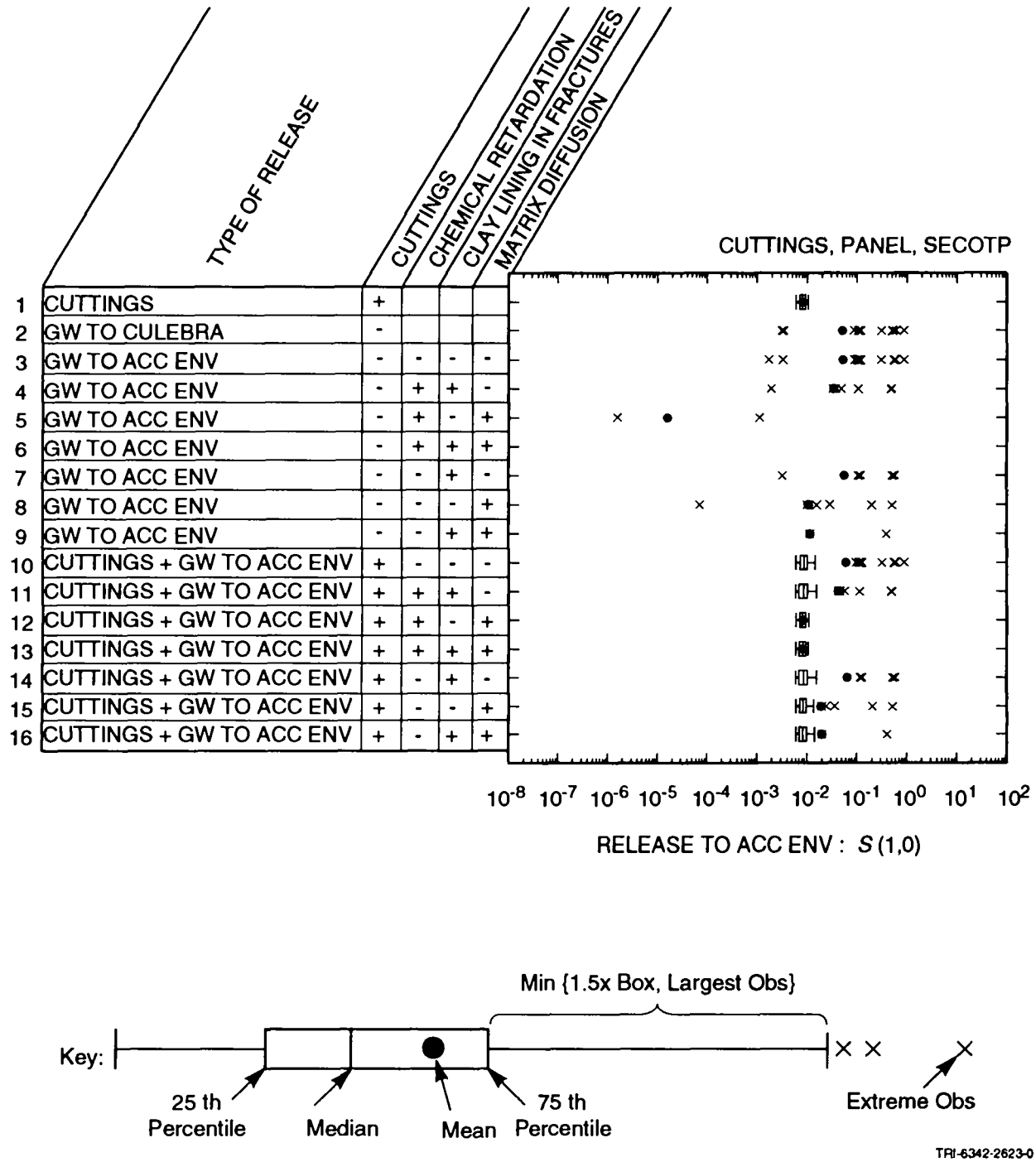

Figure 8.5-1. Summary of total normalized releases to the accessible environment over 10,000 yr for scenario $S(1,0)$ used in conjunction with the risk representation R_1 defined in Eq. 2.5-1 with intrusion occurring 1000 yr after repository closure. Box plots for results without a clay lining in fractures in the Culebra Dolomite are generated with 70 observations; box plots for results with a clay lining are generated with 35 observations (i.e., the observations in which CULCLYF=0 have been dropped).

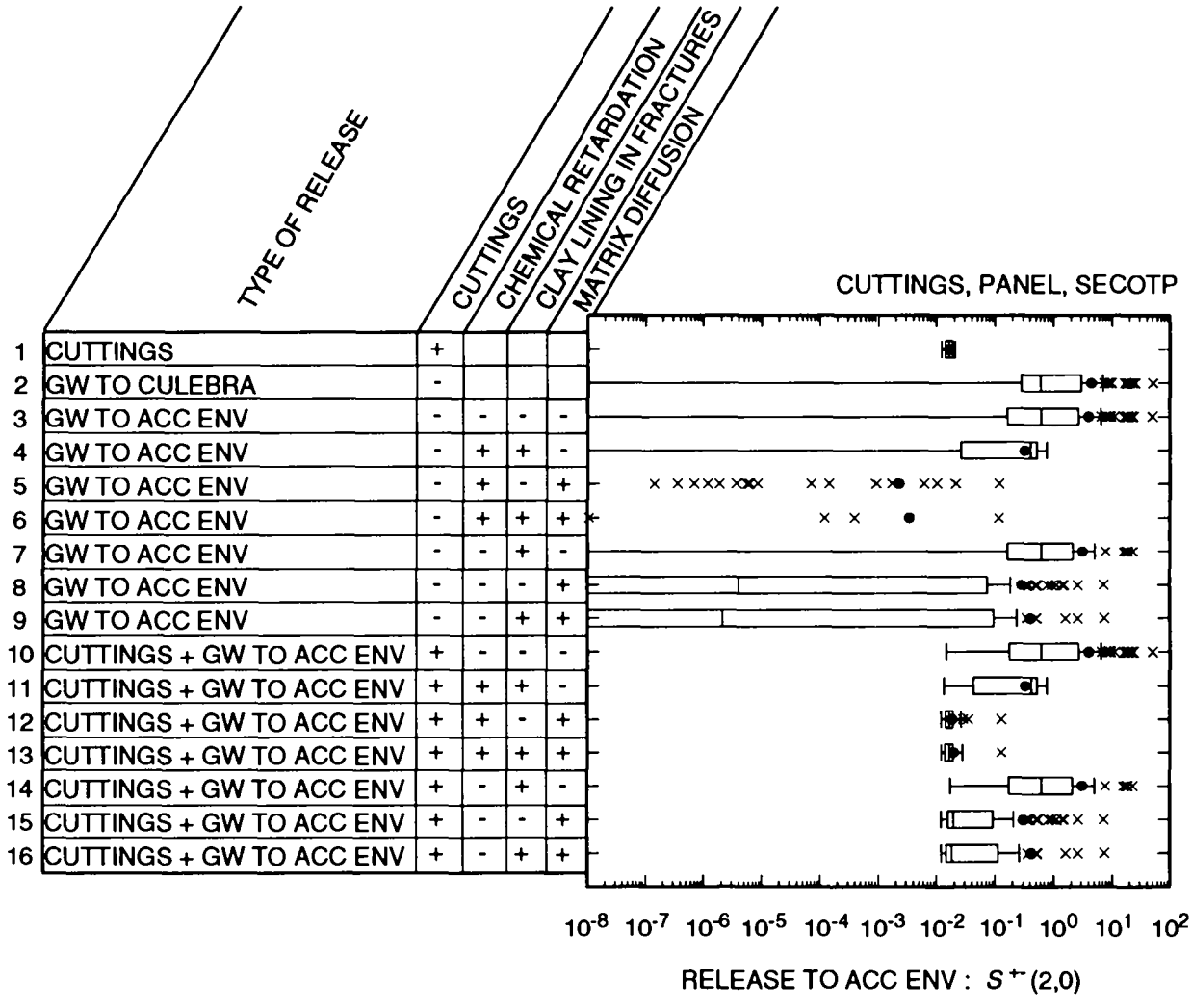

Figure 8.5-2. Summary of total normalized releases to the accessible environment over 10,000 yr for scenario $S^{+-}(2,0)$ used in conjunction with the risk representation R_1 defined in Eq. 2.5-1 with intrusion occurring 1000 yr after repository closure. Box plots for results without a clay lining in fractures in the Culebra Dolomite are generated with 70 observations; box plots for results with a clay lining are generated with 35 observations (i.e., the observations in which CULCLYF=0 have been dropped).

comparison of the effects of the alternative modeling assumptions. In particular, no chemical retardation and no matrix diffusion produce releases to the accessible environment that are essentially identical to the release to the Culebra. The assumption of chemical retardation and no matrix diffusion lowers the releases to the accessible environment somewhat and has a noticeable effect on reducing the largest releases. Further, the assumption of chemical retardation and matrix diffusion leads to very small releases, with most releases being less than 1×10^{-8} EPA release units. The assumption of matrix diffusion in conjunction with no chemical retardation produces releases that are generally larger than those obtained with chemical retardation and matrix diffusion and smaller than those obtained with chemical retardation and no matrix diffusion, although the largest releases for matrix diffusion in conjunction with no chemical retardation exceed the largest releases for chemical retardation and no matrix diffusion.

The CCDFs constructed in the 1992 WIPP performance assessment for comparison with the EPA release limits are based on releases for each scenario that include both groundwater transport and cuttings removal components. As suggested by the results in Figures 8.5-1 and 8.5-2, the CCDFs for a particular set of modeling assumptions are often dominated by either the cuttings release or the groundwater release.

Before presenting CCDFs for total releases due to both cuttings removal and groundwater transport, it is useful to review the cuttings removal results presented in Section 8.2. In particular, the CCDFs for cuttings removal presented in Figure 8.2-3 were constructed for the risk representation R_2 defined in Eq. 2.5-8. This representation uses the six time intervals in Eq. 2.5-9 in the definition of scenarios. Due to computational constraints, the CCDFs presented in Sections 8.4 and 8.5 for releases due to groundwater transport are constructed for the risk representation R_1 defined in Eq. 2.5-1, which uses the two time intervals in Eq. 2.5-2. Further, the rate term λ in the Poisson model for drilling intrusion is assumed to equal 0 yr^{-1} after 2000 yr in the calculation of scenario probabilities for R_1. In contrast, no such constraint is placed on the λ's in the determination of scenario probabilities for R_2, although some of the time-dependent λ's obtained in the expert review process do go to zero before 10,000 yr (see Appendix D in Volume 3).

The CCDFs for total release (i.e., cuttings removal and groundwater transport) presented in this section use the risk representation R_1 defined in Eq. 2.5-1. To facilitate comparisons between groundwater releases, cuttings releases and total releases, CCDFs are presented in Figure 8.5-3 for the cuttings release to the accessible environment constructed for R_1 with

the rate term λ in the Poisson model for drilling intrusions equal to 0 yr^{-1} after 2000 yr. The corresponding results for the risk representation R_2 defined in Eq. 2.5-8 with no restrictions on λ are presented in Figure 8.2-3. As the more explicit comparison in Figure 8.5-4 shows, use of the risk representation R_1 with constant λ's produces mean and 90th percentile curves for cuttings removal that are shifted down and to the left by factors of approximately 3 or less from the corresponding curves obtained with the risk representation R_2; similar shifts also occur for time-dependent λ's.

The CCDFs for total release to the accessible environment with no chemical retardation, no clay lining in fractures and no matrix diffusion are presented in Figure 8.5-5. For comparison, the associated releases due to cuttings removal only and groundwater transport only appear in Figures 8.5-3 and 8.3-9, respectively. As a reminder, the CCDFs for release to the Culebra shown in Figure 8.3-9 are essentially identical to the CCDFs for release to the accessible environment for groundwater transport with no chemical retardation, no clay lining in fractures and no matrix diffusion (see Section 8.4.1). As comparison with Figure 8.5-3 shows, the larger releases to the accessible environment associated with the CCDFs in Figure 8.5-5 are due to groundwater transport. However, because of the zero releases associated with scenarios of the form $S(1,0)$, $S(2,0)$, ... for many sample elements, large parts of many CCDFs are still dominated by the cuttings release. This effect can be seen in the similarity of parts of the CCDF plots on the left side of Figure 8.5-5 to the corresponding plots in Figure 8.5-3. Although the inclusion of groundwater transport releases does cause a shift to the right of the cuttings removal only CCDFs in Figure 8.5-3, most CCDFs still fall below the EPA release limits for constant rate terms in the Poisson model for drilling intrusion, and all CCDFs fall considerably below the EPA release limits for time-dependent rate terms.

The removal of the assumption that the rate term in the Poisson model for drilling intrusions is equal to 0 yr^{-1} after 2000 yr would cause the CCDFs in Figure 8.5-5 and other similar figures in this section to be shifted up and to the right. However, as the comparisons in Figure 8.5-4 show, these shifts would probably not move the CCDFs up or to the right by more than a factor of 3. The shifts in the CCDFs for groundwater transport are anticipated to be similar to those for cuttings removal because the scenario probabilities are undergoing the same change. Thus, although the use of the risk representation R_1, defined in Eq. 2.5-1, does produce lower risk results than the representation R_2, defined in Eq. 2.5-8, results obtained with R_1 do provide insights in comparisons with the EPA release limits.

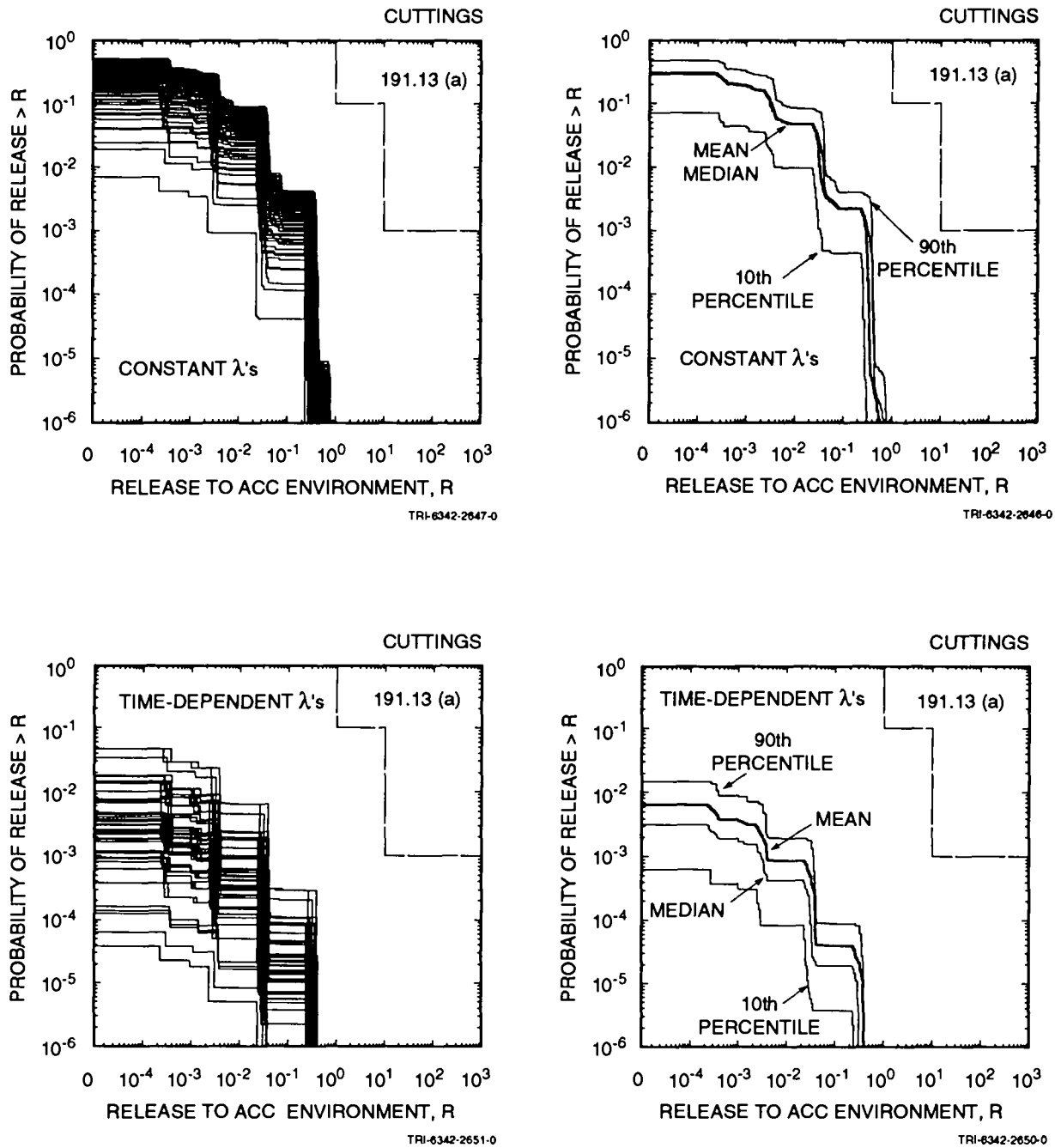

Figure 8.5-3. Distribution of CCDFs for normalized release to the accessible environment over 10,000 yr for cuttings removal constructed with the risk representation R_1 defined in Eq. 2.5-1 with constant (upper two frames) and time-dependent (lower two frames) rate terms in the Poisson model for drilling intrusions.

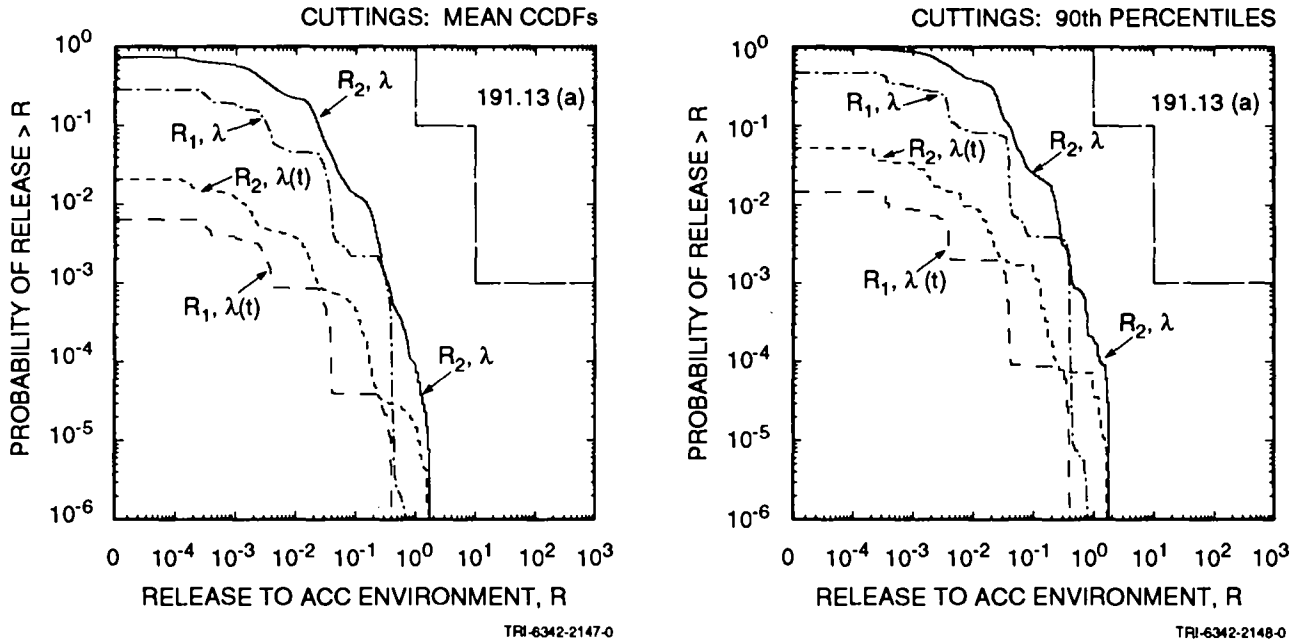

Figure 8.5-4. Comparison of mean and 90th percentile curves for cuttings removal over 10,000 yr obtained for risk representations R_1 (Eq. 2.5-1) and R_2 (Eq. 2.5-8) with constant (λ) and time-dependent ($\lambda(t)$) rate terms in the Poisson model for drilling intrusion.

The CCDFs for total release to the accessible environment with chemical retardation, clay-lined fractures and no matrix diffusion are presented in Figure 8.5-6. As discussed in Section 8.4.2, these CCDFs are based on 35 sample elements. As shown by the box plots in Figures 8.5-1 and 8.5-2, this analysis alternative produces releases to the accessible environment that are somewhat smaller than the corresponding releases to the Culebra. Further, when releases to the Culebra occur, they are often larger than the corresponding cuttings release for waste of average activity level. However, as is the case for all of the alternative analyses, most sample elements (i.e., 56 out of 70) result in no release to the Culebra for scenarios of the form $S(1,0)$, $S(2,0)$, ... The overall result is that the CCDFs in Figure 8.5-6 tend to fall somewhat farther to the right than the CCDFs for cuttings removal only in Figure 8.5-3 and yet display much of the structure present in Figure 8.5-3 for CCDFs based on cuttings removal only. The mean and 90th percentile curves in Figure 8.5-6 constructed with constant values

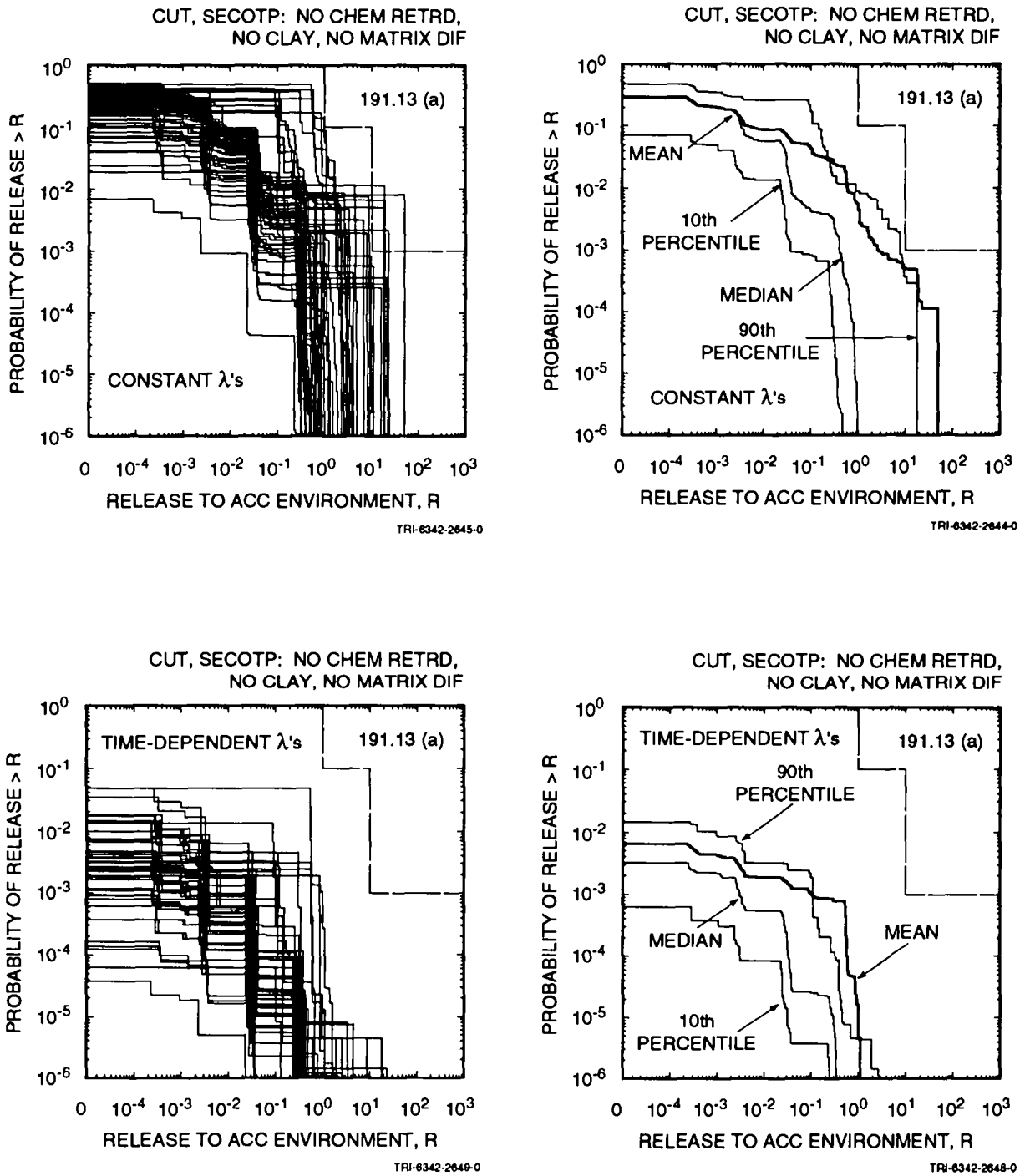

Figure 8.5-5. Distribution of CCDFs for normalized release to the accessible environment over 10,000 yr due to cuttings removal and groundwater transport with no chemical retardation, no clay lining in fractures and no matrix diffusion for risk representation R_1 defined in Eq. 2.5-1 with constant (upper two frames) and time-dependent (lower two frames) rate terms in the Poisson model for drilling intrusions.

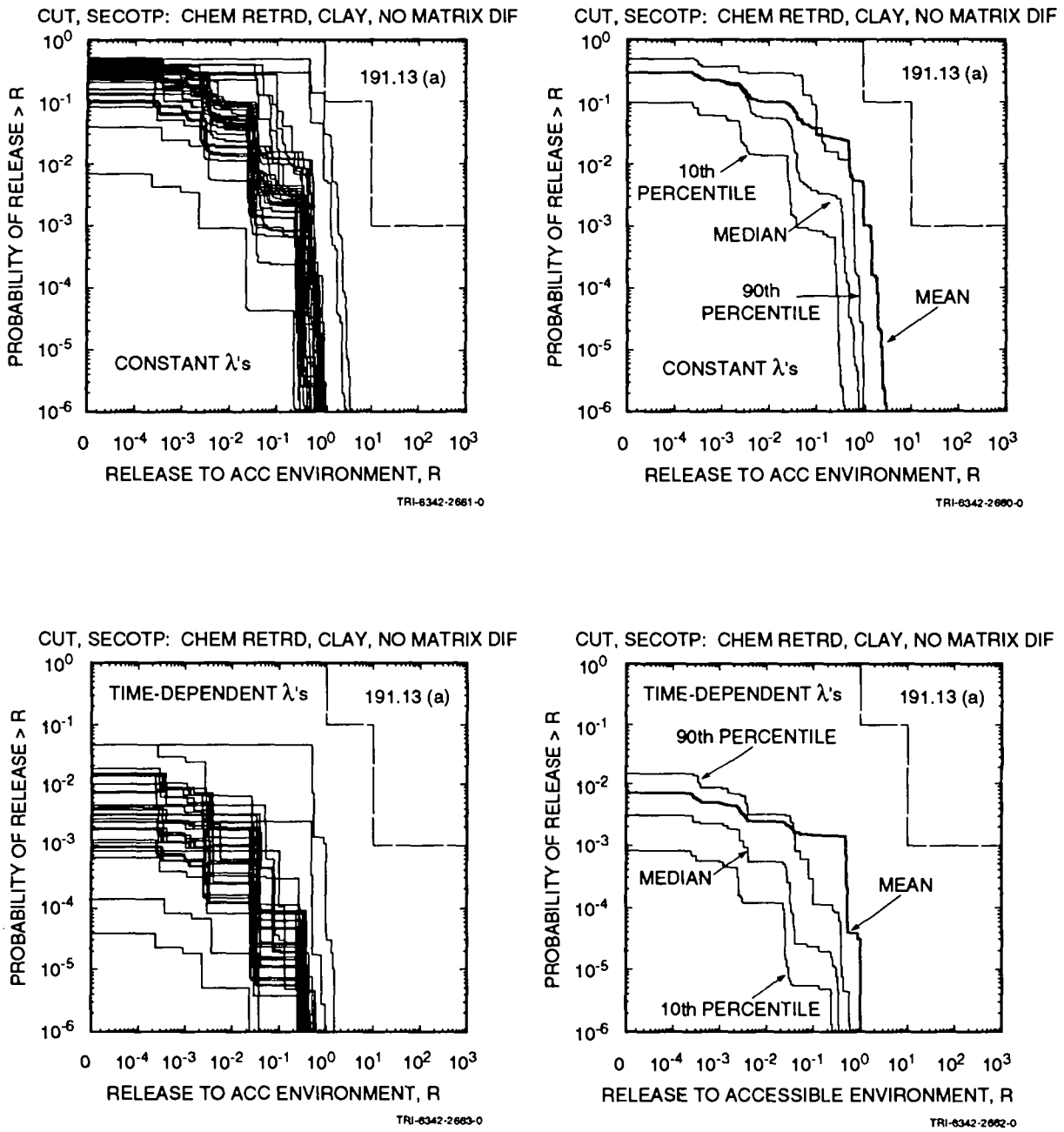

Figure 8.5-6. Distribution of CCDFs for normalized release to the accessible environment over 10,000 yr due to cuttings removal and groundwater transport with chemical retardation, clay-lined fractures and no matrix diffusion for risk representation R_1 defined in Eq. 2.5-1 with constant (upper two frames) and time-dependent (lower two frames) rate terms in the Poisson model for drilling intrusions.

for the rate constant λ in the Poisson model for drilling intrusions fall substantially below the EPA release limits. Further, as is the case throughout this analysis, the use of the time-dependent λ's produces CCDFs that are farther from the EPA release limits than those obtained with the constant λ's. As comparison with the results in Figure 8.5-5 for groundwater transport with no chemical retardation, no clay lining in fractures and no matrix diffusion shows, the addition of chemical retardation causes a noticeable shift of the CCDFs away from the EPA release limits.

The CCDFs for total release to the accessible environment with chemical retardation, no clay lining in fractures and matrix diffusion are presented in Figure 8.5-7. As suggested by the very small releases shown in Figures 8.5-1 and 8.5-2 for this analysis alternative, the CCDFs in Figure 8.5-7 for total release are essentially identical to the CCDFs in Figure 8.5-3 for cuttings removal only. Although not shown, the CCDFs for total release to the accessible environment with chemical retardation, clay-lined fractures and matrix diffusion are also essentially identical to the CCDFs for cuttings removal only in Figure 8.5-3.

The CCDFs for total release to the accessible environment with no chemical retardation, no clay lining in fractures and matrix diffusion are presented in Figure 8.5-8. As shown in Figures 8.5-1 and 8.5-2, most releases due to groundwater transport for this analysis alternative are less than the corresponding releases due to cuttings removal, although there are some sample elements for which the groundwater release exceeds the cuttings removal release. The result is that the CCDFs in Figure 8.5-8 for total release are similar to the CCDFs in Figure 8.5-3 for cuttings removal only, with a few CCDFs for total release being shifted closer to the EPA release limits than the corresponding CCDFs for cuttings removal only.

As shown in Figures 8.5-1 and 8.5-2, releases to the accessible environment due to groundwater transport calculated with and without a clay lining in fractures in conjunction with no chemical retardation and matrix diffusion are similar. The box plot in Figure 8.5-2 for groundwater transport with no chemical retardation, no clay lining in fractures and matrix diffusion appears to have more extreme values than the corresponding plot for results obtained with clay-lined fractures. This difference is due to the use of 35 and 70 sample elements, respectively, to generate the box plots for the cases with and without clay-lined fractures. As comparison of the box plots shows, similar mean, median and 75th percentile values are obtained for releases calculated with and without clay-lined fractures. As a result, the CCDFs for total release to the accessible environment with no chemical retardation, clay-lined fractures and matrix diffusion are essentially the same as the CCDFs in Figure 8.5-8 for total release to the accessible environment with no chemical retardation, no clay lining in fractures and matrix diffusion, and thus are not shown.

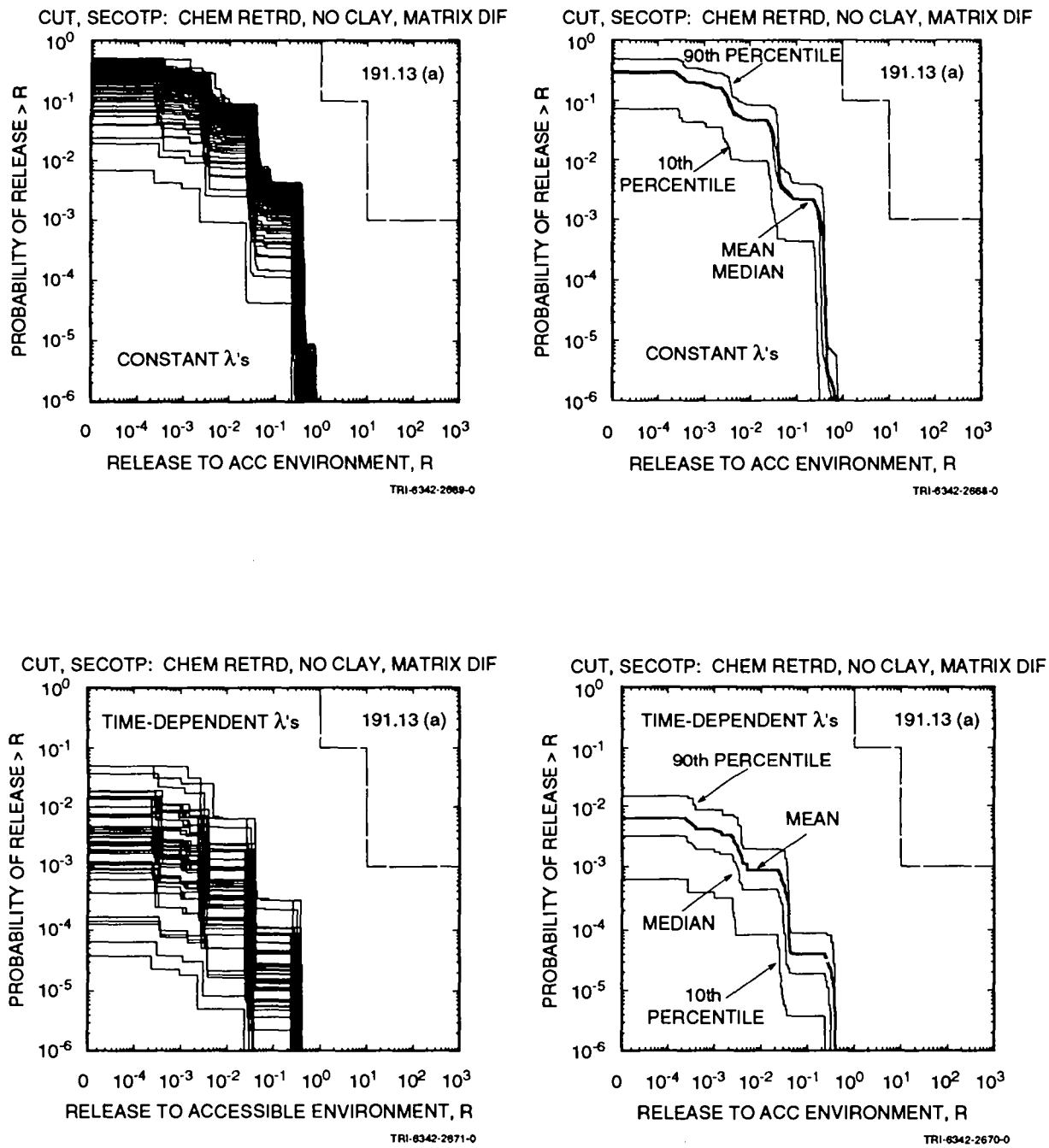

Figure 8.5-7. Distribution of CCDFs for normalized release to the accessible environment over 10,000 yr due to cuttings removal and groundwater transport with chemical retardation, no clay lining in fractures and matrix diffusion for risk representation R_1 defined in Eq. 2.5-1 with constant (upper two frames) and time-dependent (lower two frames) rate terms in the Poisson model for drilling intrusions.

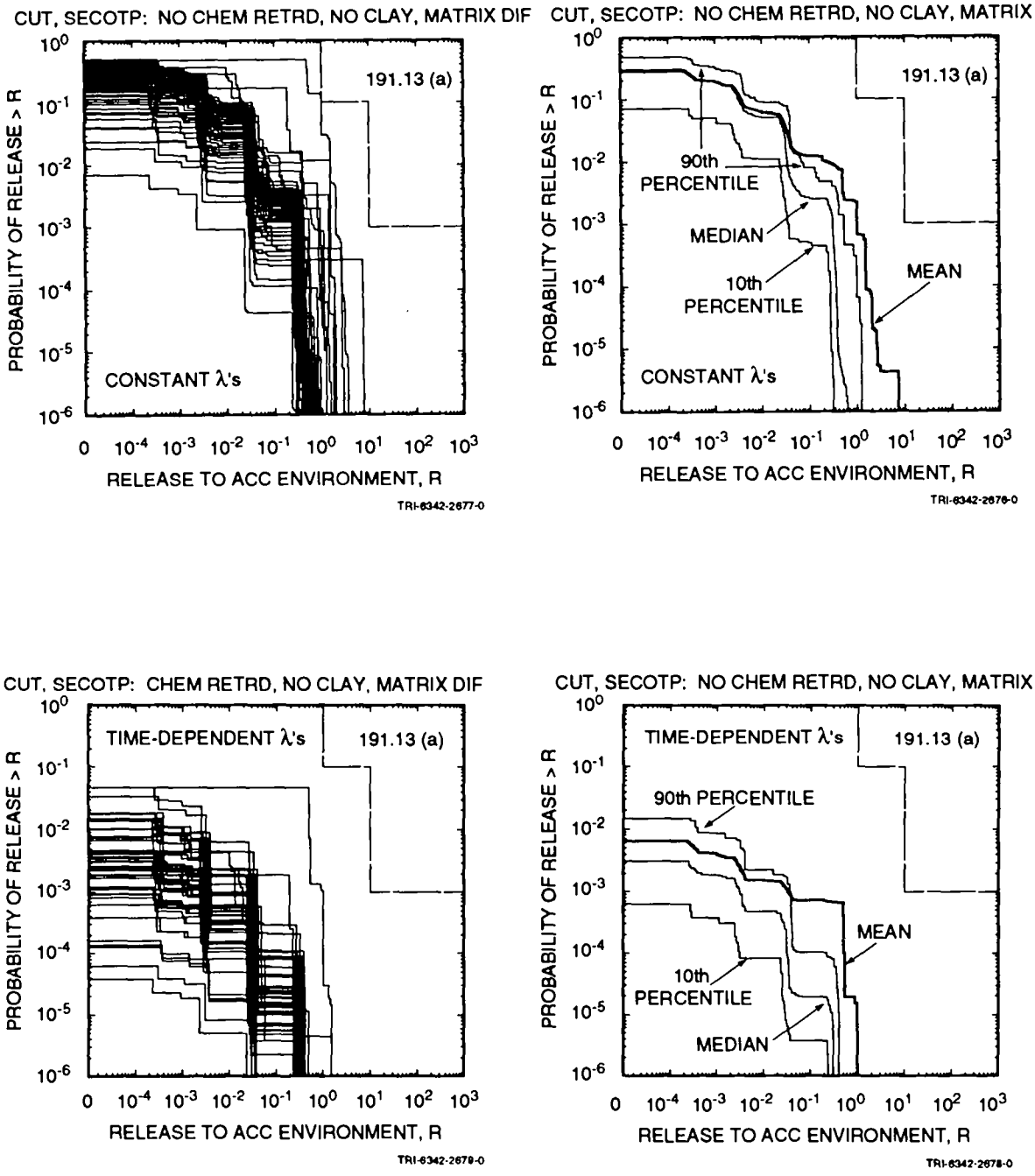

Figure 8.5-8. Distribution of CCDFs for normalized release to the accessible environment over 10,000 yr due to cuttings removal and groundwater transport with no chemical retardation, no clay lining in fractures and matrix diffusion for risk representation R_1 defined in Eq. 2.5-1 with constant (upper two frames) and time-dependent (lower two frames) rate terms in the Poisson model for drilling intrusions.

9. DISCUSSION

As described in Volumes 1 and 2 of this report, major modeling improvements have been made since the 1991 preliminary comparison with 40 CFR 191 (WIPP PA Division, 1991a, 1991b, 1991c). These improvements include the following: coupling creep closure of the repository to gas generation and two-phase flow; accounting for spatial variability in the transmissivity fields of the Culebra Dolomite Member of the Rustler Formation in a way that each field reproduces exactly measured transmissivity data at well locations and is also calibrated to steady-state and transient-pump data; more accurately simulating radionuclide transport in the Culebra; and accounting for the effects of passive marker systems through time-varying drilling intensities within the Poisson model for calculating intrusion probabilities. As described in Volumes 2 and 3 of this report, other improvements have been made throughout the modeling system and data base. Improvements remain to be made in many areas, including the following: modeling of possible pressure-dependent fracturing of anhydrite interbeds in the Salado Formation; modeling of three-dimensional groundwater flow in the Rustler Formation including the effects of subsidence of potash mine excavations; incorporating effects of plug degradation in intrusion boreholes; understanding and modeling spalling phenomena; modeling of gas-generation processes; acquiring experimental data for actinide solubilities and retardations; and determining the most appropriate conceptual model for radionuclide transport in the Culebra.

Consideration of alternative models for the probability of human intrusion and radionuclide transport in the Culebra provides insights into the relative impacts on performance of specific components of the natural and engineered barrier system and institutional controls at the Waste Isolation Pilot Plant (WIPP). Resulting CCDFs, grouped into major barrier effects, are presented in Figure 9-1.

The uppermost CCDF in Figure 9-1, labeled (1) and calculated without any transport in the Culebra and with constant rate term λ, represents an estimate of the performance of the disposal system with no contribution from the natural barrier provided by retardation in the Culebra and no contribution from the potential institutional barrier that could be provided by passive markers, as required by the Assurance Requirements (§ 191.14c). For the modeling system and data base used in 1992, the mean CCDF for this case lies below the EPA limits.

The CCDF in Figure 9-1 labeled (2) represents an estimate of the performance of the disposal system if physical retardation by diffusion into

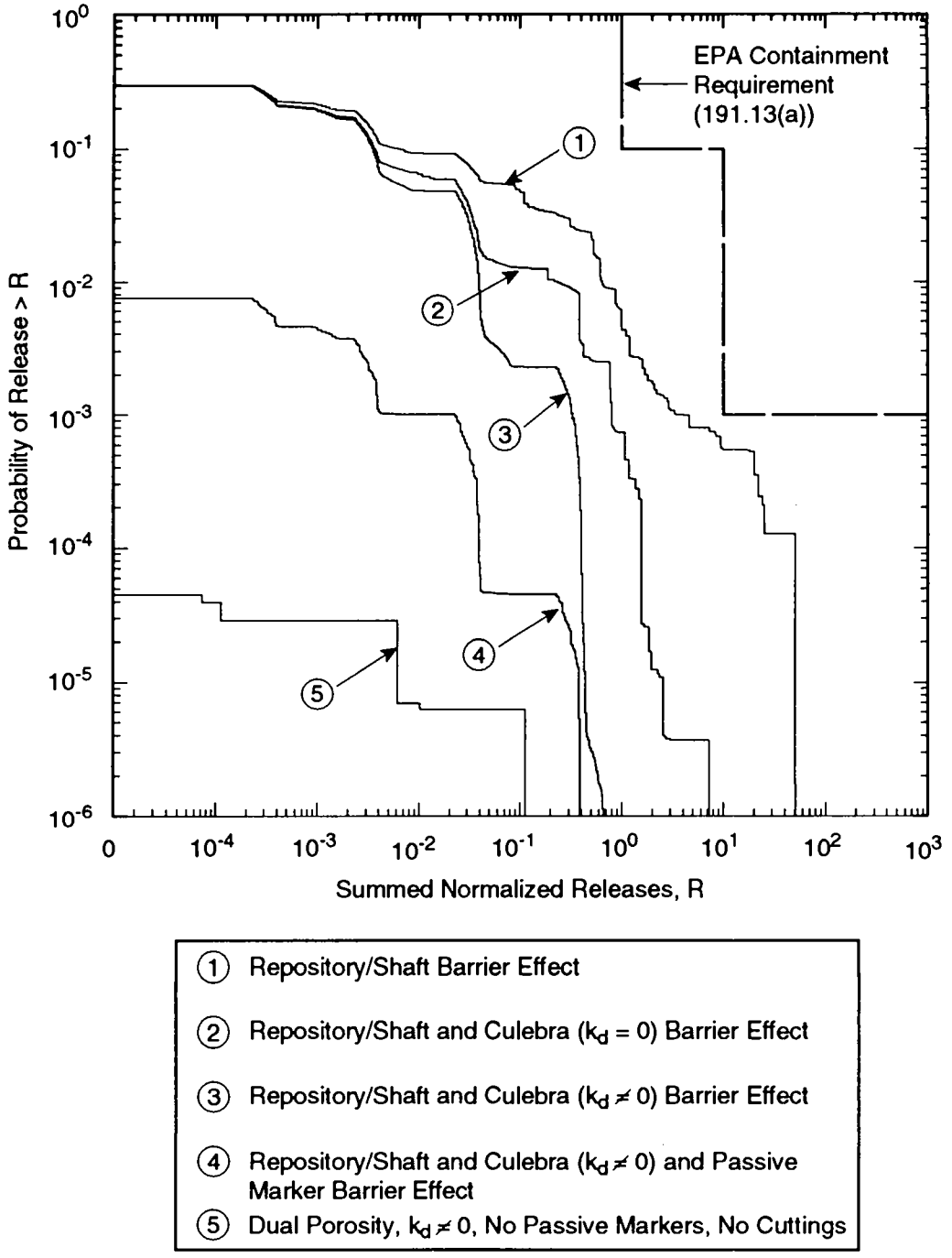

Figure 9-1. A comparison of mean CCDFs by barrier effect. CCDFs are constructed using releases from intrusions occurring at 1000 yr. CCDFs display the impact of including specific components of the engineered, natural, and institutional barrier systems as shown.

the pore volume of the Culebra is included as a part of the natural barrier system. The area between the first and second CCDFs is a measure of the potential regulatory impact of including physical retardation. Similarly, the next CCDF in Figure 9-1, labeled (3), represents an estimate of performance of the disposal system if both physical and chemical retardation in the Culebra are included in the natural barrier system. Because the location of this CCDF is determined entirely by cuttings releases, it represents the largest possible shift to the left because of including the barrier effect of non-Salado units.

The CCDF in Figure 9-1 labeled (5) represents an estimate of the performance of the disposal system only considering subsurface releases to the accessible environment, i.e., cuttings are not included. These subsurface releases plus cuttings releases result in the previous CCDF, labeled (3). Comparison of these two CCDFs shows the importance of cuttings releases in the CCDF labeled with (3) representing the combined barrier effect of sorption and physical retardation.

The CCDF in Figure 9-1 labeled (4) shows the effect of including expert judgment on the efficacy of passive markers in reducing the probability of human intrusion. This final CCDF (number 4) in Figure 9-1, also determined entirely by cuttings releases, was calculated using what the WIPP PA Department believes at this time to be the most realistic conceptual model for the disposal system, based on models and data available in 1992. As indicated previously, results are preliminary, and none of the curves shown in Figure 9-1 are believed sufficiently defensible for use in a final compliance evaluation.

The CCDFs in Figure 9-1 represent a barrier-effect display of the status of WIPP PA with respect to the Containment Requirements (§ 191.13). The barrier effects are represented by "total" (cuttings plus subsurface) CCDFs for the repository/shaft barrier labeled (1); the zero-sorption, physical retardation barrier effect of the Culebra labeled (2); the nonzero sorption, physical retardation barrier effect of the Culebra labeled (3); and the passive-marker-barrier effect CCDF labeled (4). Other important displays are CCDFs for cuttings alone [coincident with (3)] and subsurface releases alone (5). Important parameters for each of these cases will now be discussed barrier by barrier in the context of a possible approach to defending a closure decision for compliance.

Cuttings are a part of each CCDF that represents a viable comparison with the Containment Requirements. As seen in Figure 8.2-2, the important radionuclides contributing to releases in excess of 10^{-2} that would have any chance of contributing to the CCDF near the limit $(1, 10^{-1})$ and $(10, 10^{-3})$ are Pu-238, Am-241, and Pu-239. The important parameter that dominates virtually

all of the variability up to EPA Sums of 10^{-1} is the drilling intensity. Clearly, if no intrusion occurs, there are no cuttings releases.

The repository/shaft barrier-effect, mean CCDF (1) lies close to but below the regulatory criterion of (10, 10^{-3}). From Figure 8.3-1, it is evident that the important radionuclides (EPA Sums greater than 10^{-2}) are, in descending order, Am-241, Pu-239, Pu-240, U-233, U-234, Th-229, Th-230, Np-237, and Ra-226. Comparison with Figure 7.3-1 shows that this list includes all radionuclides in the inventory that have not decayed below 10^{-2} by the 1000-yr intrusion time except Pu-238. Regression analyses (Table 8.3-1) indicated that the important parameters are intrusion borehole permeability, radionuclide solubilities, and Salado halite and anhydrite permeabilities (correlated at 0.8). If intrusion occurs, the permeability of the borehole fill is the most important parameter affecting releases because it is a direct determinant of the quantity of brine released. The assumptions about the range and distribution of this parameter are determined by regulatory guidance. After assumptions about the intrusion event, the next most important parameters are related to how much brine flows through the waste and the solubility of radionuclides in that brine. With the present conceptual model for the Salado and its interbeds, the permeabilities of these units determine brine inflow and outflow. In fact, Figure 8.3-2 shows a threshold of permeability (10^{-22} m^2) below which brine inflow will not occur in sufficient amount to result in any release to the Culebra. The scatterplot emphasizes the importance of this parameter, and is the reason for placing halite and anhydrite permeabilities equal to solubilities in importance. If brine flows through the waste and borehole to the Culebra, then radionuclide solubilities determine the quantity of radionuclides released. Note that drill-bit diameter is the next most important parameter in the regression analysis, but only accounts for a very small amount of the variability in releases.

Table 9-1 shows the important parameters and radionuclides for only the repository/shaft barrier. These results are based on 68/70 nonzero releases for E1E2-type scenarios and 14/70 nonzero releases for E1- and E2-type scenarios. The family of CCDFs (Figure 8.3-9) that gave rise to the mean CCDF as a summary measure contained 6/70 sample elements resulting in CCDFs above the regulatory limit and resulting in the 90th-percentile curve falling just below the (10,10^{-3}) limit. Therefore, defending a compliance decision would be strongly influenced by the list of parameters in Table 9-1. Note that of the five parameters listed, only one parameter, solubility, can be changed by action taken within the repository. Only one parameter (permeabilities of halite and anhydrite) can be reduced in uncertainty with continued in-situ investigation. Three parameters are determined by regulatory guidance. Further, the list of important radionuclides requiring

Table 9-1. Important Radionuclides and Parameters for the Repository/Shaft Barrier

Radionuclides	Parameters
Am-241	Drilling Intensity
Pu-239, Pu-240	Intrusion Borehole Permeability
U-233, U-234	Salado (Marker Bed) Permeabilities
Th-229, Th-230	Radionuclide Solubilities
Np-237, Ra-226	Drill-Bit Diameter

solubility estimates has not changed from last year's guidance (Memorandum by Marietta and Nowak in Appendix D of this volume) to the solubility/leachate experimental program.

The next barrier-effect CCDF, labeled (2), represents only physical retardation or zero sorption in the Culebra as specified in the Consultation and Cooperation Agreement (US DOE and State of New Mexico, 1981, as modified) in the absence of in-situ measurements. Inspection of Figure 8.4-16 shows a change in important radionuclides from the repository/shaft barrier-effect CCDF. Am-241 and Pu-238 have dropped in importance because of increased travel times in the Culebra and their subsequent decay. The same radionuclides, Pu-239, Pu-240, Am-241, U-233, U-234, Th-229, Th-230, and Np-237, are released at amounts greater than EPA Sums of 10^{-2} for a few sample elements, but with lower values. All sample elements show Ra-226 below 10^{-2}, and Pu-239, Pu-240, and Am-241 have exchanged positions. Because physical retardation in the Culebra now represents the last retardation effect in the system, parameters related to this effect move to the top of the list resulting from the regression analysis (see Table 9-2). Thus, Culebra fracture spacing accounts for most of the variability in releases, followed closely by intrusion borehole permeability. Radionuclide solubility accounts for less variability. The effect of Culebra transmissivity fields and Culebra porosity accounts for a small amount of the variability.

The next barrier-effect CCDF, labeled (3), represents the full Culebra barrier effect with both physical retardation and sorption. Inspection of Figure 8.4-8 shows another change in important radionuclides from the previous two barrier-effect CCDFs. Am and Pu do not appear because they have been sorbed within the land-withdrawal boundary in the Culebra. Only U-233, U-234, Th-229, and Th-230 are released for a few sample elements at amounts greater, but only slightly greater, than EPA Sums of 10^{-2}. Parameters related to sorption comprise the list resulting from the regression analysis. Thus, Culebra fracture spacing and matrix K_ds are the only parameters

Table 9-2. Important Radionuclides and Parameters for the Culebra

Radionuclides	Parameters
Pu-239, Pu-240	Culebra Fracture Spacing
Am-241	Intrusion Borehole Permeability
U-233, U-234	Radionuclide Solubilities
Th-229, Th-230	Culebra Transmissivity Fields
Np-237	Culebra Porosity

selected during the regression analysis. Because only a few nonzero releases occur, very little variability can be accounted for. Further, the list of important radionuclides requiring retardation estimates has not changed from the last year's guidance to the tracer-column experimental program (Memorandum by Marietta and Gelbard in Appendix D of this volume).

Now the problem is how to summarize the results of the above barrier-by-barrier analyses in a list of important parameters. Compiling such a list is a subjective process that assumes a strategy for building a defensible PA, and it must rely on setting priorities to reach a closure decision on compliance. This list of important parameters by barrier effect is assembled in the following sense. Conditional on the present analysis, the repository/shaft CCDF falls below the criteria with a level of confidence of 90%. Therefore, increasing the defensibility of the assumptions that were involved in constructing the repository/shaft barrier-effect CCDF should get highest priority for building defensibility of the overall PA. Only some of these assumptions can actually be impacted by additional investigations and/or programmatic decisions, whereas the others are impacted by regulatory guidance.

Next, the Culebra barrier effect provides an additional margin of safety. This margin of safety is important in providing an additional shift of the CCDF to the compliance side of the criteria. Because the repository/shaft case is already essentially in compliance, this additional safety margin of the Culebra should assume a lower priority in compiling the summary list. However, no matter how well the Culebra and other non-Salado units are characterized, the resulting CCDFs will never fall to the right of the repository/shaft case or to the left of the cuttings-only case. This represents a spread in uncertainty over about two orders of magnitude with respect to normalized release. Of course, reduction of uncertainty within the repository, such as that associated with actinide solubilities, will shrink this spread because cuttings will not be affected by such a reduction. Cuttings-only CCDFs could, in fact, move to the right slightly with the

inclusion of spalled material from the waste. Thus, for defending a closure decision, a small spread in uncertainty exists that could be affected by additional characterization of non-Salado units.

The separate issue of assessing long-term safety of the repository from a health-effects point of view requires additional consideration. Because the subsurface-to-stock-well-to-cow-to-human pathway, is the important exposure pathway (conditional on an assumption that present-day conditions persist), the shift from zero-sorption to nonzero-sorption cases is important. Defending this shift between zero-sorption and nonzero-sorption CCDFs is analogous to defending a shift in overall, long-term safety of the repository of about four orders of magnitude. Even though the CCDF labeled (3) is the one that should be compared to the regulatory criteria, the CCDF labeled (5) can lead to a site-specific measure of long-term safety in terms of human risk.

Next, the passive-marker barrier effect provides a second additional margin of safety with respect to both compliance with 40 CFR 191 and site-specific, long-term safety (health effects), representing a shift of another two orders of magnitude.

Taking the above barrier-by-barrier reasoning into account, the regression, partial correlation, and scatterplot sensitivity analysis results are compiled into the list of important parameters in Table 9-3. Parameters in the first three categories are those for which reductions in uncertainty have the potential to affect the location of the mean CCDF near the compliance criteria. Conditional on the present modeling assumptions and parameter-value distributions, long-term disposal-system performance with regard to 40 CFR 191 is not sensitive to uncertainty in parameters included in the "Less Important" category. Defensibility of a compliance decision will require, however, that uncertainties assigned to all parameters, including those identified as less important, adequately capture reality. Specifically, wherever practical, site-specific information should be collected to verify with sufficient confidence that reality lies within the assigned range and distribution for each parameter.

With respect to 40 CFR 191, improvements to be made in either the next or following PA are expected to have the following effects on these results. (1) The addition of pressure-dependent fracturing in anhydrite interbeds of the Salado Formation: No effect on the shape of the CCDF near the criteria because brine flow into a borehole for high-consequence sample elements will not be impacted. (2) Modeling of three-dimensional groundwater flow innon-Salado units: The inclusion of vertical flow and effects on vertical flow because of climate variability and subsidence events may create changes in the list of important parameters for the natural-barrier system. However,

Table 9-3. Importance of Sampled Parameters with Respect to 40 CFR 191B. Results apply only to disturbed performance of the repository (human intrusion), and are conditional on modeling assumptions, the choice of parameters sampled, and the assumed parameter-value distributions. Comparable results for 40 CFR 268.6 (undisturbed performance) can be found in Volume 5 of this report.

Parameter Name	Parameter Description
Critically Important Parameters (listed in order of importance)	
LAMBDA	Drilling intensity
BHPERM	Intrusion borehole permeability
Very Important Parameters (listed in order of importance)	
SALPERM	Salado halite permeability
MBPERM	Salado anhydrite permeability
SOLx	Radionuclide solubilities (6, x = AM,NP,PU, RA,TH,U)
CULFRSP	Culebra fracture spacing
MKDx	Matrix K_ds (6, x = AM,NP,PU,RA,TH,U)
Important Parameters (listed in order of importance)	
CULTRFLD	Culebra transmissivity fields
CULPOR	Culebra matrix porosity
Less Important Parameters (listed in alphabetical order)	
BCBRSAT	Residual brine saturation in Salado Fm.
BCEXP	Brooks-Corey relative permeability model exponent
BCFLG	Brooks-Corey/van Genuchten-Parker pointer
BCGSSAT	Brooks-Corey residual gas saturation for Salado Fm.
BPPRES	Castile brine pressure
BPSTOR	Castile brine reservoir storativity
BPAREAFR	Castile brine reservoir area fraction
BRSAT	Initial brine saturation in waste
CULCLIM	Climatic recharge factor
CULFRPOR	Culebra fracture porosity
CULCLYF	Culebra fracture clay filling fraction
CULCLYP	Culebra fracture clay filling porosity
FKDx	Fracture K_ds (6, x = AM,NP,PU,RA,TH,U)
GRCORHF	Corrosion gas-generation rate factor, humid conditions

Table 9-3. Importance of Sampled Parameters with Respect to 40 CFR 191B. Results apply only to disturbed performance of the repository (human intrusion), and are conditional on modeling assumptions, the choice of parameters sampled, and the assumed parameter-value distributions. Comparable results for 40 CFR 268.6 (undisturbed performance) can be found in Volume 5 of this report (concluded).

Parameter Name	Parameter Description
GRCORI	Corrosion gas-generation rate, inundated conditions
GRMICHF	Biodegradation gas-generation rate factor, humid conditions
GRMICI	Biodegradation gas-generation rate, inundated conditions
MBPOR	Salado anhydrite porosity
MBPRES	Far-field pressure in Salado Fm.
STOICCOR	Corrosion stoichiometric coefficient
STOICMIC	Biodegradation stoichiometric coefficient
TZPORF	Transition Zone and DRZ porosity factor
VMETAL	Volume fraction of metals and glass in waste
VWOOD	Volume fraction of combustibles in waste

the resulting CCDFs will always lie between the repository/shaft barrier-effect CCDF (number 1 in Figure 9-1) and the cuttings-only CCDF (number 3). (3) Modeling of gas-generation processes: This model is primarily a RCRA issue, and gas-generation model parameters have little importance in the regression analyses for 40 CFR 191. For the Containment Requirements, the important issue is whether gas is generated or not because gas generation diminishes brine and radionuclide releases. Once some gas generation occurs, the uncertainty associated with the gas-generation model is relatively unimportant compared to other system parameters listed in Table 9-3. (4) Actinide source-term modeling: Inspection of Table 9-3 shows that radionuclide solubilities are the parameters affecting the repository/shaft barrier that are ranked in the first two categories, and that can most readily be impacted by programmatic decisions and an experimental program. Based on the present wide range of uncertainty in the PA data base for solubilities, more project effort here has the potential for improving the compliance picture by shifting the CCDF labeled (1) to the left in Figure 9-1. (5) Addition of releases because of spalling of waste material into an intruding borehole: The mechanism for this phenomenon is poorly understood. Preliminary estimates indicate that cuttings releases could be increased significantly (Berglund, 1992). If the experimental program corroborates this estimate, the CCDF labeled

(3) will shift to the right slightly. This shift would not significantly impact the compliance picture, but as these improvements in the PA system move CCDFs (1) and (3) closer together, the range of uncertainty that can be impacted by further work in the Culebra and non-Salado units shrinks. (6) Addition of plug degradation in the intrusion boreholes: Allowing plugs to degrade to essentially borehole-fill properties should result in two effects. The probability of E1E2-type flow paths will diminish, and flow directly to the surface may occur. The latter effect cannot result in a shift of the CCDF past the repository/shaft barrier-effect CCDF because calculating EPA Sums at the discharge point in the Culebra is equivalent with transporting directly to the surface. (7) The use of time-varying drilling intensities: The above discussion of uncertainty and sensitivity analyses relied primarily on the use of time-invariant drilling intensities, within the Poisson model that have been used for calculating scenario probabilities. The constant rate term is a sampled parameter that has a different value, constant for 10,000 yr, for each sample element, whereas the time-dependant rate term is a different function of time for each sample element. The time-dependant rate term incorporates the deterrent effect and estimated efficacy of possible passive marker systems for future societies of different levels of technology. The passive-marker barrier effect does not depend on the Culebra (or non-Salado) barrier effect and can be used equally well with the repository/shaft, barrier-effect CCDF or the cuttings-only CCDF to provide additional safety margins. In any case, a shift of about two orders of magnitude is indicated. Again, defense of the PA and compliance assessment should be based on defending the repository/shaft barrier-effect CCDF (number 1) and determining the potential contribution of the natural barrier system (displayed here as the region between CCDFs 1 and 3). In addition, passive marker systems could provide a convincing and effective margin of safety without requiring extensive reduction of uncertainty in the natural-barrier system.

10. REFERENCES

Bachman, G.O. 1985. *Assessment of Near-Surface Dissolution At and Near the Waste Isolation Pilot Plant (WIPP), Southeastern New Mexico.* SAND84-7178. Albuquerque, NM: Sandia National Laboratories.

Beauheim, R.L. 1987. *Interpretations of Single-Well Hydraulic Tests Conducted At and Near The Waste Isolation Pilot Plant (WIPP) Site, 1983-1987.* SAND87-0039. Albuquerque, NM: Sandia National Laboratories.

Beauheim, R.L., and P.B. Davies. 1992. "Experimental Plan for Tracer Testing in the Culebra Dolomite at the WIPP Site." Revision A. Albuquerque, NM: Sandia National Laboratories.

Beauheim, R.L., G.J. Saulnier, Jr., and J.D. Avis. 1991a. *Interpretation of Brine-Permeability Tests of the Salado Formation at the Waste Isolation Pilot Plant Site: First Interim Report.* SAND90-0083. Albuquerque, NM: Sandia National Laboratories.

Beauheim, R.L., T.F. Corbet, P.B. Davies, and J.F. Pickens. 1991b. "Appendix A: Recommendations for the 1991 Performance Assessment Calculations on Parameter Uncertainty and Model Implementation for Culebra Transport Under Undisturbed and Brine-Reservoir-Breach Conditions," *Preliminary Comparison with 40 CFR Part 191, Subpart B for the Waste Isolation Pilot Plant, December 1991. Volume 3: Reference Data.* WIPP Performance Assessment Division. Eds. R.P. Rechard, A.C. Peterson, J.D. Schreiber, H.J. Iuzzolino, M.S. Tierney, and J.S. Sandha. SAND91-0893/3. Albuquerque, NM: Sandia National Laboratories. A-7 through A-18.

Berglund, J.W. 1990. Appendix A: "Letter 1a: Bar Graphs Representing Range of Values for Drilling Operations Near WIPP Site," *Data Used in Preliminary Performance Assessment of the Waste Isolation Pilot Plant (1990).* R.P. Rechard, H.J. Iuzzolino, and J.S. Sandha. SAND89-2408. Albuquerque, NM: Sandia National Laboratories. A-157 through A-164.

Berglund, J.W. 1992. *Mechanisms Governing the Direct Removal of Wastes from the Waste Isolation Pilot Plant Repository Caused by Exploratory Drilling.* SAND92-7295. Albuquerque, NM: Sandia National Laboratories.

Bertram-Howery, S.G., M.G. Marietta, D.R. Anderson, K.F. Brinster, L.S. Gomez, R.V. Guzowski, and R.P. Rechard. 1989. *Draft Forecast of the Final Report for the Comparison to 40 CFR Part 191, Subpart B, for the Waste Isolation Pilot Plant.* SAND88-1452. Albuquerque, NM: Sandia National Laboratories.

Bertram-Howery, S.G., M.G. Marietta, R.P. Rechard, P.N. Swift, D.R. Anderson, B.L. Baker, J.E. Bean, Jr., W. Beyeler, K.F. Brinster, R.V. Guzowski, J.C. Helton, R.D. McCurley, D.K. Rudeen, J.D. Schreiber, and P. Vaughn. 1990. *Preliminary Comparison with 40 CFR Part 191, Subpart B for the Waste Isolation Pilot Plant, December 1990.* SAND90-2347. Albuquerque, NM: Sandia National Laboratories.

Brinster, K.F. 1991. *Preliminary Geohydrologic Conceptual Model of the Los Medaños Region Near the Waste Isolation Pilot Plant for the Purpose of Performance Assessment.* SAND89-7147. Albuquerque, NM: Sandia National Laboratories.

Broc, R., ed. 1982. *Drilling Mud and Cement Slurry Rheology Manual.* Houston, TX: Gulf Publishing Company.

Brooks, R.H., and A.T. Corey. 1964. *Hydraulic Properties of Porous Media.* Hydrology Paper No. 3. Fort Collins, CO: Civil Engineering Department, Colorado State University.

Brush, L.H. 1991. "Appendix A: Current Estimates of Gas Production Rates, Gas Production Potentials, and Expected Chemical Conditions Relevant to Radionuclide Chemistry for the Long-Term WIPP Performance Assessment," *Preliminary Comparison with 40 CFR Part 191, Subpart B for the Waste Isolation Pilot Plant, December 1991. Volume 3: Reference Data.* WIPP Performance Assessment Division. Eds. R.P. Rechard, A.C. Peterson, J.D. Schreiber, H.J. Iuzzolino, M.S. Tierney, and J.S. Sandha. SAND91-0893/3. Albuquerque, NM: Sandia National Laboratories. A-25 through A-36.

Brush, L.H., and D.R. Anderson. 1989. "A.1: Drum (Metal) Corrosion, Microbial Decomposition of Cellulose, Reactions Between Drum-Corrosion Products and Microbially Generated Gases, Reactions on WIPP Gas and Water Budgets," *Systems Analysis, Long-Term Radionuclide Transport, and Dose Assessments, Waste Isolation Pilot Plant (WIPP), Southeastern New Mexico; March 1989.* Eds. A.R. Lappin, R.L. Hunter, D.P. Garber, and P.B. Davies. SAND89-0462. Albuquerque, NM: Sandia National Laboratories. A-3 through A-30.

Coleman, B.D., and W. Noll. 1959. "Helical Flow of General Fluids," *Journal of Applied Physics.* Vol. 30, no. 10, 1508-1515.

Corey, A.T. 1986. *Mechanics of Immiscible Fluids in Porous Media.* Littleton, CO: Water Resources Publications.

Cranwell, R.M., R.V. Guzowski, J.E. Campbell, and N.R. Ortiz. 1990. *Risk Methodology for Geologic Disposal of Radioactive Waste: Scenario Selection Procedure.* NUREG/CR-1667, SAND80-1429. Albuquerque, NM: Sandia National Laboratories.

Darley, H.C.H., and G.R. Gray. 1988. *Composition and Properties of Drilling and Completion Fluids.* Houston, TX: Gulf Publishing Company. 243.

Davies, P.B. 1989. *Variable-Density Ground-Water Flow and Paleohydrology in the Waste Isolation Pilot Plant (WIPP) Region, Southeastern New Mexico*. Open-File Report 88-490. Albuquerque, NM: US Geological Survey.

EPA (Environmental Protection Agency). 1985. "40 CFR Part 191: Environmental Standards for the Management and Disposal of Spent Nuclear Fuel, High-Level and Transuranic Radioactive Wastes; Final Rule," *Federal Register*. Vol. 50, no. 182, 38066-38089.

EPA (Environmental Protection Agency). 1986. "40 CFR Part 268: Land Disposal Restrictions," as amended and published in the most recent *Code of Federal Regulations*. Washington, DC: Office of the Federal Register, National Archives and Records Administration.

Fredrickson, A.G. 1960. "Helical Flow of an Annular Mass of Visco-Elastic Fluid," *Chemical Engineering Science*. Vol. 11, no. 3, 252-259.

Freeze, R.A., and J.A. Cherry. 1979. *Groundwater*. Englewood Cliffs, NJ: Prentice-Hall, Inc.

Gonzales, M.M. 1989. *Compilation and Comparison of Test-Hole Location Surveys in the Vicinity of the Waste Isolation Pilot Plant Site*. SAND88-1065. Albuquerque, NM: Sandia National Laboratories.

Gorham, E., R. Beauheim, P. Davies, S. Howarth, and S. Webb. 1992. "Appendix A: Recommendations to PA on Salado Formation Intrinsic Permeability and Pore Pressure for 40 CFR 191 Subpart B Calculations," *Preliminary Performance Assessment for the Waste Isolation Pilot Plant, December 1992. Volume 3: Model Parameters*. Sandia WIPP Project. SAND92-0700/3. Albuquerque, NM: Sandia National Laboratories. A-47 through A-67.

Helton, J.C. 1993a. "Drilling Intrusion Probabilities for Use in Performance Assessment for Radioactive Waste Disposal," *Reliability Engineering and System Safety*. Vol. 40, no. 3, 259-275.

Helton, J.C. 1993b. "Risk, Uncertainty in Risk, and the EPA Release Limits for Radioactive Waste Disposal," *Nuclear Technology*. Vol. 101, no. 1, 18-39.

Helton, J.C., and R.J. Breeding. 1993. "Calculation of Reactor Accident Safety Goals," *Reliability Engineering and System Safety*. Vol. 39, no. 2, 129-158.

Helton, J.C., and H.J. Iuzzolino. 1993. "Construction of Complementary Cumulative Distribution Functions for Comparison with the EPA Release Limits for Radioactive Waste Disposal," *Reliability Engineering and System Safety*. Vol. 40, no. 3, 277-293.

Helton, J.C., J.W. Garner, R.D. McCurley, and D.K. Rudeen. 1991. *Sensitivity Analysis Techniques and Results for Performance Assessment at the Waste Isolation Pilot Plant*. SAND90-7103. Albuquerque, NM: Sandia National Laboratories.

Helton, J.C., J.W. Garner, R.P. Rechard, D.K. Rudeen, and P.N. Swift. 1992. *Preliminary Comparison with 40 CFR Part 191, Subpart B for the Waste Isolation Pilot Plant, December 1991—Volume 4: Uncertainty and Sensitivity Analysis Results*. SAND91-0893/4. Albuquerque, NM: Sandia National Laboratories.

Hora, S.C., D. von Winterfeldt, and K.M. Trauth. 1991. *Expert Judgment on Inadvertent Human Intrusion into the Waste Isolation Pilot Plant*. SAND90-3063. Albuquerque, NM: Sandia National Laboratories.

Howarth, S.M., E.W. Peterson, P.L. Lagus, K-H. Lie, S.J. Finley, and E.J. Nowak. 1991. "Interpretation of In-Situ Pressure and Flow Measurements of the Salado Formation at the Waste Isolation Pilot Plant," *1991 Joint Rocky Mountain Regional Meeting, Society of Petroleum Engineers and Low Permeability Reservoirs Symposium, Denver, CO, April 15-17, 1991*. SPE-21840; SAND90-2334C. Richardson, TX: Society of Petroleum Engineers.

Huyakorn, P.S., H.O. White, Jr., and S. Panday. 1991. *STAFF2D, Version 3.1, A Two-Dimensional Finite Element Code for Simulating Fluid Flow and Transport of Radionuclides in Fractured Porous Media with Water Table Boundary Conditions*. Herndon, VA: HydroGeoLogic, Inc. (Copy on file in the Waste Management and Transportation Library, Sandia National Laboratories, Albuquerque, NM.)

IAEA (International Atomic Energy Agency). 1989. *Evaluating the Reliability of Predictions Made Using Environmental Transfer Models*. Safety Series Report No. 100. Vienna, Austria: International Atomic Energy Agency.

Iman, R.L., and W.J. Conover. 1979. "The Use of the Rank Transform in Regression," *Technometrics*. Vol. 21, no. 4, 499-509.

Iman, R.L., and W.J. Conover. 1982. "A Distribution-Free Approach to Inducing Rank Correlation Among Input Variables," *Communications in Statistics: Simulation and Computation*. Vol. B11, no. 3, 311-334.

Iman, R.L., and M.J. Shortencarier. 1984. *A FORTRAN 77 Program and User's Guide for the Generation of Latin Hypercube and Random Samples for Use with Computer Models*. NUREG/CR-3624, SAND83-2365. Albuquerque, NM: Sandia National Laboratories.

Iman, R.L., J.M. Davenport, E.L. Frost, and M.J. Shortencarier. 1980. *Stepwise Regression with PRESS and Rank Regression (Program User's Guide)*. SAND79-1472. Albuquerque, NM: Sandia National Laboratories.

Iman, R.L., M.J. Shortencarier, and J.D. Johnson. 1985. *A FORTRAN 77 Program and User's Guide for the Calculation of Partial Correlation and Standardized Regression Coefficients*. NUREG/CR-4122, SAND85-0044. Albuquerque, NM: Sandia National Laboratories.

Jones, T.L., V.A. Kelley, J.F. Pickens, D.T. Upton, R.L. Beauheim, and P.B. Davies. 1992. *Integration of Interpretation Results of Tracer Tests Performed in the Culebra Dolomite at the Waste Isolation Pilot Plant Site*. SAND92-1579. Albuquerque, NM: Sandia National Laboratories.

Kaplan, S., and B.J. Garrick. 1981. "On the Quantitative Definition of Risk," *Risk Analysis*. Vol. 1, no. 1, 11-27.

Kelley, V.A., and G.J. Saulnier, Jr. 1990. *Core Analyses for Selected Samples from the Culebra Dolomite at the Waste Isolation Pilot Plant Site*. SAND90-7011. Albuquerque, NM: Sandia National Laboratories.

Lappin, A.R., R.L. Hunter, D.P. Garber, P.B. Davies, R.L. Beauheim, D.J. Borns, L.H. Brush, B.M. Butcher, T. Cauffman, M.S.Y. Chu, L.S. Gomez, R.V. Guzowski, H.J. Iuzzolino, V. Kelley, S.J. Lambert, M.G. Marietta, J.W. Mercer, E.J. Nowak, J. Pickens, R.P. Rechard, M. Reeves, K.L. Robinson, and M.D. Siegel. 1989. *Systems Analysis, Long-Term Radionuclide Transport, and Dose Assessments, Waste Isolation Pilot Plant (WIPP), Southeastern New Mexico; March 1989*. SAND89-0462. Albuquerque, NM: Sandia National Laboratories.

LaVenue, A.M., and B.S. RamaRao. 1992. *A Modeling Approach To Address Spatial Variability within the Culebra Dolomite Transmissivity Field*. SAND92-7306. Albuquerque, NM: Sandia National Laboratories.

LaVenue, A.M., A. Haug, and V.A. Kelley. 1988. *Numerical Simulation of Ground-Water Flow in the Culebra Dolomite at the Waste Isolation Pilot Plant (WIPP) Site: Second Interim Report*. SAND88-7002. Albuquerque, NM: Sandia National Laboratories.

Leigh, C.D., B.M. Thompson, J.E. Campbell, D.E. Longsine, R.A. Kennedy, and B.A. Napier. 1993. *User's Guide for GENII-S: A Code for Statistical and Deterministic Simulations of Radiation Doses to Humans from Radionuclides in the Environment*. SAND91-0561. Albuquerque, NM: Sandia National Laboratories.

Marietta, M.G., S.G. Bertram-Howery, D.R. Anderson, K.F. Brinster, R.V. Guzowski, H. Iuzzolino, and R.P. Rechard. 1989. *Performance Assessment Methodology Demonstration: Methodology Development for Evaluating Compliance with EPA 40 CFR 191, Subpart B, for the Waste Isolation Pilot Plant*. SAND89-2027. Albuquerque, NM: Sandia National Laboratories.

McKay, M.D., R.J. Beckman, and W.J. Conover. 1979. "A Comparison of Three Methods for Selecting Values of Input Variables in the Analysis of Output from a Computer Code," *Technometrics*. Vol. 21, no. 2, 239-245.

Mercer, J.W. 1983. *Geohydrology of the Proposed Waste Isolation Pilot Plant Site, Los Medaños Area, Southeastern New Mexico.* Water-Resources Investigations Report 83-4016. Albuquerque, NM: US Geological Survey.

Mercer, J.W., and B.R. Orr. 1979. *Interim Data Report on the Geohydrology of the Proposed Waste Isolation Pilot Plant Site, Southeast New Mexico.* US Geological Survey Water-Resources Investigations 79-98. Albuquerque, NM: US Geological Survey.

Oldroyd, J.G. 1958. "Non-Newtonian Effects in Steady Motion of Some Idealized Elastico-Viscous Liquids," *Proceedings of the Royal Society of London.* Series A, Vol. 245, no. 1241, 278-297.

Pace, B.O. 1990. Appendix A: "Letter 1b: Changes to Bar Graphs," *Data Used in Preliminary Performance Assessment of the Waste Isolation Pilot Plant (1990).* R.P. Rechard, H. Iuzzolino, and J.S. Sandha. SAND89-2408. Albuquerque, NM: Sandia National Laboratories. A-165 through A-170.

Parker, J.C., R.J. Lenhard, and T. Kuppusamy. 1987. "A Parametric Model for Constitutive Properties Governing Multiphase Flow in Porous Media," *Water Resources Research.* Vol. 23, no. 4, 618-624.

Parry, G.W. 1988. "On the Meaning of Probability in Probabilistic Safety Assessment," *Reliability Engineering and System Safety.* Vol. 23, no. 4, 309-314.

Partheniades, E., and R.E. Paaswell. 1970. "Erodibility of Channels with Cohesive Boundary," *Journal of the Hydraulics Division, Proceedings of the American Society of Civil Engineers.* Vol. 96, no. HY3, 755-771.

Paté-Cornell, M.E. 1986. "Probability and Uncertainty in Nuclear Safety Decisions," *Nuclear Engineering and Design.* Vol. 93, nos. 2-3, 319-327.

Popielak, R.S., R.L. Beauheim, S.R. Black, W.E. Coons, C.T. Ellingson, and R.L. Olsen. 1983. *Brine Reservoirs in the Castile Formation, Waste Isolation Pilot Plant (WIPP) Project, Southeastern New Mexico.* TME-3153. Carlsbad, NM: US Department of Energy.

Rechard, R.P., H. Iuzzolino, and J.S. Sandha. 1990. *Data Used in Preliminary Performance Assessment of the Waste Isolation Pilot Plant (1990).* SAND89-2408. Albuquerque, NM: Sandia National Laboratories.

Reeves, M., G.A. Freeze, V.A. Kelley, J.F. Pickens, D.T. Upton, and P.B. Davies. 1991. *Regional Double-Porosity Solute Transport in the Culebra Dolomite Under Brine-Reservoir-Breach Release Conditions: An Analysis of Parameter Sensitivity and Importance.* SAND89-7069. Albuquerque, NM: Sandia National Laboratories.

Savins, J.G., and G.C. Wallick. 1966. "Viscosity Profiles, Discharge Rates, Pressures, and Torques for a Rheologically Complex Fluid in a Helical Flow," *A.I.Ch.E. Journal*. Vol. 12, no. 2, 357-363.

Stone, C.M., R.D. Krieg, and Z.E. Beisinger. 1985. *SANCHO: A Finite Element Computer Program for the Quasistatic, Large Deformation, Inelastic Response of Two-Dimensional Solids*. SAND84-2618. Albuquerque, NM: Sandia National Laboratories.

Swift, P.N. 1991. Appendix A: "Climate and Recharge Variability Parameters for the 1991 WIPP PA Calculations," *Preliminary Comparison with 40 CFR Part 191, Subpart B for the Waste Isolation Pilot Plant, December 1991. Volume 3: Reference Data*. WIPP Performance Assessment Division. Eds. R.P. Rechard, A.C. Peterson, J.D. Schreiber, H.J. Iuzzolino, M.S. Tierney, and J.S. Sandha. SAND91-0893/3. Albuquerque, NM: Sandia National Laboratories. A-107 through A-121.

Swift, P.N. 1993. "Long-Term Climate Variability at the Waste Isolation Pilot Plant, Southeastern New Mexico, USA," *Environmental Management*. SAND91-7055. Vol. 17, no. 1, 83-97.

Tierney, M.S. 1990. *Constructing Probability Distributions of Uncertain Variables in Models of the Performance of the Waste Isolation Pilot Plant: The 1990 Performance Simulations*. SAND90-2510. Albuquerque, NM: Sandia National Laboratories.

Trauth, K.M., S.C. Hora, R.P. Rechard, and D.R. Anderson. 1992. *The Use of Expert Judgment to Quantify Uncertainty in Solubility and Sorption Parameters for Waste Isolation Pilot Plant Performance Assessment*. SAND92-0479. Albuquerque, NM: Sandia National Laboratories.

US DOE (Department of Energy). 1989. *Waste Isolation Pilot Plant Compliance Strategy for 40 CFR Part 191, March 17, 1989*. DOE-WIPP 86-013. Carlsbad, NM: WIPP Project Office.

US DOE (Department of Energy). 1990. *WIPP Test Phase Plan: Performance Assessment*. DOE/WIPP 89-011, Rev. 0. Carlsbad, NM: US Department of Energy, Waste Isolation Pilot Plant.

US DOE (Department of Energy). 1991. *Integrated Data Base for 1991: U.S. Spent Fuel and Radioactive Waste Inventories, Projections, and Characteristics*. DOE/RW-0006, Rev. 7. Oak Ridge, TN: Oak Ridge National Laboratory.

US DOE (Department of Energy). 1992. *WIPP Test Phase Activities in Support of Critical Performance Assessment Information Needs (40 CFR 191, Subpart B)*. Washington, DC: US Department of Energy. Attachment I.

US DOE (Department of Energy) and State of New Mexico. 1981, as modified. "Agreement for Consultation and Cooperation" on WIPP by the State of New Mexico and US Department of Energy, modified 11/30/84, 8/4/87, and 4/18/88.

USGS (United States Geological Survey). 1985a. *Los Medaños Quadrangle, New Mexico-Eddy Co.* 7.5 Minute Series (Topographic). Provisional Edition. Reston, VA: US Geological Survey. (Copy on file in the Waste Management and Transportation Library, Sandia National Laboratories, Albuquerque, NM.)

USGS (United States Geological Survey). 1985b. *Illinois Camp SE Quandrangle, New Mexico-Eddy Co.* 7.5 Minute Series (Topographic). Provisional Edition. Reston, VA: US Geological Survey. (Copy on file in the Waste Management and Transportation Library, Sandia National Laboratories, Albuquerque, NM.)

van Genuchten, R. 1978. *Calculating the Unsaturated Hydraulic Conductivity with a New Closed-Form Analytical Model.* Research Report 78-WR-08. Princeton, NJ: Princeton University, Department of Civil Engineering.

Vesely, W.E., and D.M. Rasmuson. 1984. "Uncertainties in Nuclear Probabilistic Risk Analyses," *Risk Analysis.* Vol. 4, no. 4, 313-322.

Voss, C.I. 1984. *SUTRA (Saturated-Unsaturated Transport): A Finite-Element Simulation Model for Saturated-Unsaturated, Fluid-Density-Dependent Ground-Water Flow with Energy Transport or Chemically-Reactive Single-Species Solute Transport.* Water-Resources Investigations Report 84-4369. Reston, VA: US Geological Survey.

Walker, R.E. 1976. "Hydraulic Limits Are Set by Flow Restrictions," *Oil and Gas Journal.* Vol. 74, no. 40, 86-90.

Waste Management Technology Department. 1987. *The Scientific Program at the Waste Isolation Pilot Plant.* SAND85-1699. Albuquerque, NM: Sandia National Laboratories.

WEC (Westinghouse Electric Corporation). 1988. *WIPP Underground Mine Plan, Bulkhead Locations and Numbers.* Drawing 54-W-012-W, Rev. A. Carlsbad, NM: Westinghouse Waste Isolation Division. (Copy on file in the Waste Management and Transportation Library, Sandia National Laboratories, Albuquerque, NM.)

Whittaker, A., ed. 1985. *Theory and Application of Drilling Fluid Hydraulics.* Boston, MA: International Human Resources Development Corporation.

WIPP PA (Performance Assessment) Department. 1992. *Long-Term Gas and Brine Migration at the Waste Isolation Pilot Plant: Preliminary Sensitivity Analyses for Post-Closure 40 CFR 268 (RCRA), May 1992.* SAND92-1933. Albuquerque, NM: Sandia National Laboratories.

WIPP PA (Performance Assessment) Department. 1993. *Preliminary Comparison with 40 CFR Part 191, Subpart B for the Waste Isolation Pilot Plant, December 1991. Volume 6: Guidance to the WIPP Project from the December 1991 Performance Assessment*. SAND91-0893/6. Albuquerque, NM: Sandia National Laboratories. (draft)

WIPP PA (Performance Assessment) Division. 1991a. *Preliminary Comparison with 40 CFR Part 191, Subpart B for the Waste Isolation Pilot Plant, December 1991. Volume 1: Methodology and Results*. SAND91-0893/1. Albuquerque, NM: Sandia National Laboratories.

WIPP PA (Performance Assessment) Division. 1991b. *Preliminary Comparison with 40 CFR Part 191, Subpart B for the Waste Isolation Pilot Plant, December 1991. Volume 2: Probability and Consequence Modeling*. SAND91-0893/2. Albuquerque, NM: Sandia National Laboratories.

WIPP PA (Performance Assessment) Division. 1991c. *Preliminary Comparison with 40 CFR Part 191, Subpart B for the Waste Isolation Pilot Plant, December 1991. Volume 3: Reference Data*. Eds. R.P. Rechard, A.C. Peterson, J.D. Schreiber, H.J. Iuzzolino, M.S. Tierney, and J.S. Sandha. SAND91-0893/3. Albuquerque, NM: Sandia National Laboratories.

APPENDIX A: VERIFICATION OF THE SECO-TRANSPORT CODE

Verification of the SECO-TRANSPORT Code

Kambiz Salari

April 2, 1993

Contents

1 SECO-TRANSPORT Code

1.1 Transport Model

The code predicts solute transport in fractured porous media using the dual-porosity approach. It allows for radioactive decay and generation of daughter products. In addition, the matrix block equation can model both the matrix material and the clay lining.

For the fracture-with-matrix block system, transport in the fracture is produced by the combined effect of convection and hydrodynamic dispersion, while transport in the matrix block is dominated by molecular diffusion. Two sets of governing equations are used to describe the concentration in the fracture and matrix block.

The equation for the transport of kth radionuclide component in the fracture (N species) can be written

$k = 1, \ldots, N$:

$$\begin{aligned} \nabla \cdot [\mathbf{D}\nabla C_k - \mathbf{V}C_k] &= \phi R_k \frac{\partial C_k}{\partial t} + \phi R_k \lambda_k C_k - \phi R_{k-1}\lambda_{k-1} C_{k-1} \\ &\quad -Q\tilde{C}_k - \Gamma_k \end{aligned} \tag{1}$$

where the dependent variables are C_k, the concentration of the kth radionuclide. For $k = 1$, the term involving C_{k-1} is omitted. Physical parameters include $\mathbf{D}(\mathbf{x}, t)$, a 2×2 hydrodynamic dispersion tensor (velocity-dependent); $\mathbf{V}(\mathbf{x}, t)$, the Darcy velocity, $\phi(\mathbf{x})$; the fracture porosity; R_k, the retardation coefficient; λ_k, the species decay constant; and $\tilde{C}_k$, the concentration of the kth injected radionuclide. The well injection rate is Q. Detailed physical descriptions of these terms can be found in [1, 2].

The N fracture equations are linear and sequentially-coupled. A general Robin boundary condition is assumed

$$\alpha C_k + \beta \frac{\partial C_k}{\partial n} = \gamma \tag{2}$$

on a planar rectangular domain Ω. For various choice of α, β, and γ, one may obtain Dirichlet, Neumann, or Cauchy boundary conditions on different portions of the boundary. For example, the commonly used flux boundary condition is

$$\mathbf{V}C_k - \mathbf{D}\nabla C_k = \mathbf{V}f(t) \tag{3}$$

where f is a known function.

The flow-field $\mathbf{V}$ is assumed to be independent of the solute concentration. In practice, the flow-field is obtained from the SECO-FLOW code [6].

Since the dual-continuum model [3, 4, 5] includes the exchange of mass between the matrix block and the fracture, it is necessary to solve a transport equation in the matrix block. Assuming that there is no fluid flow, the equation for the concentration of the kth species, is given (for a slab block model) by

$$\frac{\partial}{\partial \chi}(D' \frac{\partial C'_k}{\partial \chi}) = \phi' R'_k \frac{\partial C'_k}{\partial t} + \phi' R'_k \lambda_k C'_k - \phi' R'_{k-1} \lambda_{k-1} C'_{k-1} \tag{4}$$

where χ is the coordinate originating from the symmetry line of the matrix block, the prime is denoting matrix block, D' is the coefficient of the molecular diffusion, and the remaining symbols have the same meaning as those in the equation for fracture transport (Eq. 1).

The equations for the fracture and the matrix block are coupled through the mass transfer term Γ_k which is given by

$$\Gamma_k = -\frac{2}{b}(D' \frac{\partial C'_k}{\partial \chi}|_{\chi=0}) \tag{5}$$

where b is the fracture aperture.

For a typical matrix slab of thickness b', the initial and boundary conditions are given by

$$C'_k(\chi, t=0) = C'^0_k \tag{6}$$

$$D' \frac{\partial C'_k}{\partial \chi}(0,t) = 0 \tag{7}$$

$$C'_k(b',t) = C_k - \zeta D' \frac{\partial C'_k}{\partial \chi} \tag{8}$$

where ζ is a parameter characterizing the resistance of the thin skin adjacent to the fracture. This parameter is defined as $\zeta = b_s/D_s$, where b_s and D_s are the skin thickness and the skin diffusion coefficient, respectively.

1.2 Numerical Discretization, Algorithm

1.2.1 Fracture Equation

Equation (1) has been transformed into stretched Cartesian coordinates

$$t = \tau, \tag{9}$$

$$x = x(\xi), \tag{10}$$

$$y = y(\eta) \tag{11}$$

where metric transformations are $\xi_x = Jy_\eta$, $\eta_y = Jx_\xi$, and $J = \xi_x\eta_y$. The transformed equation, with further algebraic manipulations, was put into a strong conservation form [7, 8]. This is done to ensure mass conservation, which is essential here. The transformed equation is given by

$$\begin{aligned}\phi R_k\frac{\partial}{\partial t}(\hat{C}_k) + \frac{\partial}{\partial\xi}(\hat{E}) + \frac{\partial}{\partial\eta}(\hat{F}) &= \frac{\partial}{\partial\xi}(\hat{E}_{v1}) + \frac{\partial}{\partial\xi}(\hat{E}_{v2}) \\ &+ \frac{\partial}{\partial\eta}(\hat{F}_{v1}) + \frac{\partial}{\partial\eta}(\hat{F}_{v2}) \\ &+ \phi R_k\lambda_k\hat{C}_k + \phi R_{k-1}\lambda_{k-1}\hat{C}_{k-1} \\ &+ \hat{Q} + \hat{\Gamma}\end{aligned} \tag{12}$$

where

$$\hat{C}_k = \frac{C_k}{J}, \tag{13}$$

$$\hat{E} = \xi_x u\hat{C}_k, \tag{14}$$

$$\hat{F} = \eta_y v\hat{C}_k, \tag{15}$$

$$\hat{E}_{v1} = \frac{\xi_x^2 D_{11}}{J}\frac{\partial\hat{C}_k}{\partial\xi}, \tag{16}$$

$$\hat{E}_{v2} = \frac{\xi_x\eta_y D_{12}}{J}\frac{\partial\hat{C}_k}{\partial\eta}, \tag{17}$$

$$\hat{F}_{v1} = \frac{\xi_x\eta_y D_{21}}{J}\frac{\partial\hat{C}_k}{\partial\xi}, \tag{18}$$

$$\hat{F}_{v2} = \frac{\eta_y^2 D_{22}}{J}\frac{\partial\hat{C}_k}{\partial\eta}, \tag{19}$$

$$\hat{Q} = \frac{Q\tilde{C}_k}{J}, \tag{20}$$

$$\hat{\Gamma} = \frac{\Gamma}{J}. \tag{21}$$

Equation (12) is solved using an implicit Approximate Factorization procedure [9]. The convective terms are modeled by TVD [10] and the remaining terms by central differencing. A general two-level implicit finite volume scheme, in delta form [9], can be written as

$$\phi R_k \triangle \hat{C}_k^n = \frac{\theta \triangle t}{1+\varphi}(\phi R_k \triangle \hat{C}_k^n)_t + \frac{\triangle t}{1+\varphi}(\phi R_k \hat{C}_k^n)_t + \frac{\varphi}{1+\varphi}(\phi R_k \triangle \hat{C}_k^{n-1}) \tag{22}$$

where

$$\triangle \hat{C}_k^n = \hat{C}_k^{n+1} - \hat{C}_k^n$$

The $\triangle \hat{C}_k^n$ can be thought of as a correction to advance the solution to a new time-level (n+1). The time difference equation (22), with appropriate choice of the parameters θ and φ, produces many two- and three-level implicit schemes as shown in Table 1. Applying equation (22) to equation (12) we have

$$\begin{aligned}
\phi R_k \triangle \hat{C}_k^n &= \frac{\theta \triangle t}{1+\varphi}[-(\triangle \hat{E}^n)_\xi - (\triangle \hat{F}^n)_\eta + (\triangle \hat{E}_{v1}^n)_\xi + (\triangle \hat{F}_{v2}^n)_\eta \\
&\qquad -\phi R_k \lambda_k \triangle \hat{C}_k^n] \\
&+ \frac{\theta \triangle t}{1+\varphi}[(\triangle \hat{E}_{v2}^{n-1})_\xi + (\triangle \hat{F}_{v1}^{n-1})_\eta] \\
&+ \frac{\triangle t}{1+\varphi}[-\hat{E}_\xi^n - \hat{F}_\eta^n + (\hat{E}_{v1}^n)_\xi + (\hat{E}_{v2}^n)_\xi + (\hat{F}_{v1}^n)_\eta + (\hat{F}_{v2}^n)_\eta \\
&\qquad -\phi R_k \lambda_k \hat{C}_k^n + \phi R_{k-1} \lambda_{k-1} \hat{C}_{k-1}^n + \hat{Q}^n + \hat{\Gamma}^n] \\
&+ \frac{\varphi}{1+\varphi}[\phi R_k \triangle \hat{C}_k^{n-1}]
\end{aligned} \tag{23}$$

The cross derivative terms are time-lagged to facilitate the factorization of the right-hand-side operator. The error introduced by lagging these terms can be corrected through an intra-time step iteration. This procedure has been employed here.

The convective terms are modeled using the following TVD flux which we have developed for staggered meshes. The flux is a combination of upwind and centered schemes.

$$\begin{aligned}
\hat{E}_{j-\frac{1}{2},k}^n &= \frac{1}{2}(1 - \Phi_{j-\frac{1}{2},k})[(C_{j,k}^n + C_{j-1,k}^n)u_{j-\frac{1}{2},k}^n - (C_{j,k}^n - C_{j-1,k}^n) \mid u_{j-\frac{1}{2},k}^n \mid] \\
&\quad + \frac{1}{2}\Phi_{j-\frac{1}{2},k}(\hat{C}_{j,k}^n + \hat{C}_{j-1,k}^n)(\tilde{\xi}_x^n)_{j-\frac{1}{2},k} u_{j-\frac{1}{2},k}^n
\end{aligned} \tag{24}$$

Table 1: Partial list of schemes available

θ	φ	Schemes	Truncation error
1	0	Euler, implicit	O($\triangle t$)
$\frac{1}{2}$	0	Trapezoidal, implicit	O($\triangle t^2$)
1	$\frac{1}{2}$	3-point-backward, implicit	O($\triangle t^2$)

where

$$(\tilde{\xi}_x^n)_{j-\frac{1}{2},k} = \frac{2(\xi_x)_{j,k}(\xi_x)_{j-1,k}}{(\xi_x)_{j,k} + (\xi_x)_{j-1,k}}$$

The function Φ is called a limiter function. There are a number of limiter functions available ranging from very compressive (Roe superbee) to very dissipative (minmod) [10].

After the explicit portion (RHS) of equation (23) has been evaluated, the solution at the new time level is obtained through the following sequence

$$(I + \alpha_x L_{xx})\triangle \bar{C}_{j,k} = RHS, \tag{25}$$

$$(I + \alpha_y L_{yy})\triangle \hat{C}_{j,k} = \triangle \bar{C}_{j,k}, \tag{26}$$

$$\hat{C}_{j,k}^{n+1} = \hat{C}_{j,k}^{n} + \triangle \hat{C}_{j,k}^{n} \tag{27}$$

where I is an identity matrix and L_{xx}, L_{yy} are the x and y operators, respectively. The first sweep in either the x or y direction produces intermediate results, denoted by $\bar{C}_{j,k}$. The second sweep uses the intermediate results to complete the cycle. The order of the sweep can be symmetrized by alternating the direction. After both sweeps are complete, the solution is updated.

The boundary conditions (Dirichlet, Neumann, and Robin) are all implicitly implemented in the 1-D operator in both directions. This ensures the second-order accuracy of the scheme. The implicit construction of boundary conditions requires an intermediate boundary condition for the initial sweep. The intermediate boundary condition is subtle, and is evaluated by applying either the x or y operator, depending on the boundary, to

the equation of the ghost cell. The stencils of these operators will be different near the boundaries.

This algorithm uses a finite-volume mesh where fluxes are evaluated at cell faces and concentrations at cell centers.

1.2.2 Matrix Block Equation

Using a similar procedure oulined for the fracture equation (1), equation (4) is first mapped to a computational space

$$\phi' R'_k \frac{\partial \hat{C}'_k}{\partial t} = \frac{\partial \hat{F}'_v}{\partial \xi} - \phi' R'_k \lambda_k \hat{C}'_k + \phi' R'_{k-1} \lambda_{k-1} \hat{C}'_{k-1} \tag{28}$$

where

$$\hat{C}'_k = \frac{C'_k}{J} \tag{29}$$

$$\hat{F}'_v = D' \xi_x \frac{\partial C'_k}{\partial \xi} \tag{30}$$

Then, the above equation is discretized using the general implicit finite volume scheme, in a delta form given by equation 22.

$$\begin{aligned} \phi' R'_k \triangle \hat{C}'^n_k &= \frac{\theta \triangle t}{1+\varphi}[(\triangle \hat{F}'^n_v)_\xi - \phi' R'_k \lambda_k \hat{C}'^n_k] \\ &+ \frac{\triangle t}{1+\varphi}[(\hat{F}'^n)_\xi - \phi' R'_k \lambda_k \hat{C}'^n_k + \phi' R'_{k-1} \lambda_{k-1} \hat{C}'^n_{k-1}] \\ &+ \frac{\varphi}{1+\varphi}[\phi' R'_k \triangle \hat{C}'^{n-1}_k] \end{aligned} \tag{31}$$

where

$$(\hat{F}'^n_v)_{j-\frac{1}{2}} = D'_{j-\frac{1}{2}} (\xi_x)_{j-\frac{1}{2}} (C'^n_j - C'^n_{j-1}) \tag{32}$$

$$(\triangle \hat{F}'^n_v)_{j-\frac{1}{2}} = D'_{j-\frac{1}{2}} (\xi_x)_{j-\frac{1}{2}} [J_j \triangle \hat{C}'^n_j - J_{j-1} \triangle \hat{C}'^n_{j-1}] \tag{33}$$

Equation (31) is solved using a tridiagonal inversion with implicit boundary conditions.

1.2.3 Fracture-Matrix Coupling

The equations for the fracture and the matrix block are coupled through a mass transfer term Γ_k. This term is proportional to the gradient of the solute concentration in a matrix

block at their interface. A simple approach to couple these equations is to time lag the Γ term or, in other words, treat the coupling term explicitly. Our experience with the matrix block equation has shown if the molecular diffusion coefficient is high, if there exists a clay lining, or if there is high resolution at the interface, the solution for the coupled system would be unstable. To make the coupling more robust, the equations must be coupled in a fully implicit manner. A procedure outlined in reference [1] was adapted and modified to work with the approximate factorization and delta formulation of the transport equation. This new procedure would couple the equations implicitly and has shown to be quite robust.

Even with implicit coupling, a problem can arise if the characteristic time for the matrix block, i.e., the time in which the solution in the matrix would approximately reach steady state, is much smaller than the time step used to advance the fracture solution. In such a case, the coupling term Γ can exhibit an oscillatory behavior in time which is not physical. To avoid such a behavior the fracture time step must resolve or be smaller than the characteristic time of the matrix block.

1.3 Improvements / Issues

The present code uses a TVD scheme with three-level time differencing and directional splitting to improve accuracy and execution time. The code is second-order accurate both in time and space. Problems with moderately-high Peclet number would greatly benefit from this scheme by avoiding spurious oscillations commonly associated with the central differencing schemes. The long time-scales of the problems to which the code is to be applied dictate the use of fully-implicit algorithms.

The flow field is computed by the SECO-flow code. It is important to note that the convergence tolerance on the flow must be smaller in magnitude than the *source* for the transport calculation. Lack of proper iterative convergence in the flow calculation can show up as a source term in the transport calculation due to its conservation formulation and in some cases can lead to instabilities.

In practice the computational boundaries for transport and the flow are not the same.

This difference in the location of the far-field boundaries can pose a difficult problem (unbounded source) for the transport calculation. The SECO-transport code can eliminate this difficulty by automatically assigning the boundary conditions using the flow field.

The code is capable of computing the history of integrated discharge around any number of defined closed boundaries within the computational mesh.

2 Analytic Solutions & Convergence Test

2.1 Fracture Transport

The code, which has been developed based on the scheme described in the algorithm section (section 1.2), is verified for temporal and spatial accuracy using the following unsteady equation and its solution, with $\mathbf{V} = u\mathbf{i}$.

$$C_t + uC_x = \alpha_L u C_{xx} + \alpha_T u C_{yy} - g(x, y, t), \tag{34}$$

where

$$g(x, y, t) = (x - ut)^2 + y^2, \tag{35}$$

and $0 < x < 1$, $0 < y < 1$. The initial condition is given by

$$C(x, y, 0) = \frac{1}{12u}\left[\frac{x^4}{\alpha_L} + \frac{y^4}{\alpha_T}\right]. \tag{36}$$

The exact solution to equation (34) is

$$C(x, y, t) = \frac{1}{12u}\left[\frac{(x - ut)^4}{\alpha_L} + \frac{y^4}{\alpha_T}\right]. \tag{37}$$

Since the computational domain is finite, the Dirichlet boundary conditions are time dependent and may be obtained from the exact solution.

Table 2 presents the computed solution to equation (34) at time=$25sec$, for four different grid sizes and time steps. The magnitude of coefficients are $u = 0.1m/s$, $\alpha_L = 1.0m$, $\alpha_T = 0.1m$. By examining the ratio of Root Mean Square (RMS) of errors, it is evident that the overall solution is second-order accurate in time and space.

Table 2: Convergence results, uniform grid

Size	$\triangle x$	$\triangle t$	RMS	RMS ratio
20x20	.05	.25	7.697E-3	
40x40	.025	.125	1.954E-3	3.94
80x80	.0125	.0625	4.921E-4	3.97
160x160	.00625	.03125	1.234E-4	3.99

To illustrate the advantages of this algorithm, we have chosen to solve a two-dimensional convection-dispersion problem for which we have an exact solution [11]. The medium is assumed to be homogeneous and isotropic with unidirectional steady state flow. The initial solute concentration is zero. At a certain time, a strip-type source with a finite length (2a) along the y-axis is introduced. For detailed information regarding this problem see Reference [11]. In our test problems, the solute concentration at the source remains constant with time.

The solution is obtained for two cases. A uniform grid 80x80 where $0 < x < 200m$, $-100 < y < 100m$ and Van Leer MUSCL limiter [10] are used for both cases. Case 1: low mesh Peclet number, $Pe = 2$, $u = 1.0m/s$, $\alpha_L = 0.5m$, $\alpha_T = 0.1m$, $\lambda = 0.0$, and $a = 50$. Figures 1a and 1b present the numerical solution and the absolute error at time=$100sec$, respectively. The maximum error is 6.1E-2 and is located in the vicinity of the discontinuity on the boundary and RMS=6.389E-3. Figures 2a and 2b show the same calculation using implicit upwind differencing. The latter computations serve as a representative solution computed by the majority of existing codes. The maximum error is .1847 and is located around the front as one would expect and the RMS=5.111E-2. The maximum error is about three times and the RMS about 8 times larger than TVD solution. Case 2: moderately high mesh Peclet number, $Pe = 10$, $u = 1.0$, $\alpha_L = \alpha_T = 0.1$, and $a = 50$. Figure 3 shows solute concentration computed using TVD at Time=100. Figure 4 presents the same calculation using upwinding. The difference between the two solutions is dramatic. As expected, the TVD scheme retained a sharp front as opposed

to a very diffused front generated by the implicit upwind differencing. Unfortunately, we encountered numerical difficulties in computing the exact solution at Peclet numbers higher than 4; hence, we have no comparison to exact solution. However, if Case 1 is any indication, the error introduced by implicit upwinding should be much higher than was observed in the previous case.

As we have shown above, the TVD scheme in conjunction with second-order time discretization is more accurate in tracking sharp changes in solute concentration even for low-Peclet number cases.

2.2 Dual Porosity Transport

To verify both fracture and the matrix finite volume discretization as a system and the coupling procedure, we have chosen a dual porosity problem in one dimension with the analytical solution given by Tang [12]. The fracture equation is

$$\frac{\partial c}{\partial t} + \frac{v}{R}\frac{\partial c}{\partial z} - \frac{D}{R}\frac{\partial^2 c}{\partial z^2} + \lambda c - \frac{\theta D'}{bR}\frac{\partial c'}{\partial x}|_{x=b} = 0 \tag{38}$$

where $0 \leq z < \infty$. The initial and boundary conditions are

$$c(0,t) = 0 \tag{39}$$

$$c(\infty,t) = 0 \tag{40}$$

$$c(z,0) = 0 \tag{41}$$

The matrix equation is given by

$$\frac{\partial c'}{\partial t} - \frac{D'}{R'}\frac{\partial^2 c'}{\partial x^2} + \lambda c' = 0 \tag{42}$$

where $b \leq x < \infty$. The initial and boundary conditions are

$$c'(b,z,t) = c(z,t) \tag{43}$$

$$c'(\infty,z,t) = 0 \tag{44}$$

$$c'(x,z,0) = 0 \tag{45}$$

for further explanation of the problem and the definition of parameters and the analytical solution see reference [12].

The test problem is set up by defining the required parameters as follows. Fracture length, $x_0 = 10m$, fracture spacing $2.4m$. *Fracture properties:* aperture, $b = 10^{-4}m$, seepage velocity, $V = 0.01m/d$, longitudinal dispersivity, $\alpha_L = 0.50m$, molecular diffusion coefficient, $D = 1.382 \times 10^{-4}m^2/d$, and fracture porosity, $\phi_f = 0.42 \times 10^{-4}$. *Matrix properties:* matrix porosity, $\phi' = 0.01$, and matrix diffusion coefficient, $D' = 1.382 \times 10^{-7}m^2/d$. *Radionuclide properties:* decay constant, $\lambda = 0.154 \times 10^{-3} 1/d$, and retardation factor, $R = R' = 1$. *Initial condition:* $c(x,0) = c'(x,z,0) = 0$. The boundary conditions are

$$c(0,t) = 1 \tag{46}$$

$$\frac{\partial c}{\partial x}(x,0,t) = c(x,t) \tag{47}$$

$$c'(x,0,t) = c(x,t) \tag{48}$$

$$\frac{\partial c'}{\partial x}(x,z_0,t) = 0 \tag{49}$$

Fracture length is discretized using 80 stretched cells and 15 stretched cells was used for the matrix block. The calculation was stopped at time equal to 100 days to test both spatial and temporal accuracy of the computed solution. Figures 5 and 6 present the comparison of the fracture and matrix solution to the analytical solution, respectively. The computed solution in both regions seems to be quite accurate which also verifies the accuray of the coupling procedure. Further mesh refinement in both fracture and the matrix block reproduced the same results.

Unfortunately, proper grid convergence test is not possible since in the above transport problem the size of the matrix block is infinite whereas in computation we have a finite matrix block length.

3 Convergence Test on PA Problems

To verify the code on a realistic problem (excluding extreme cases), we will use one of the 1992 PA calculations [14].

3.1 Fracture Transport

For grid convergence test on fracture transport we have chosen vector 2 (E1E2 scenario). This vector has moderate parameters, such as, fracture aperture and realistic fracture travel time with climate from the source to the far field boundary of 72 years

Since we do not have an exact solution for vector 2, to check the convergence of the solution on different grids we rely on contours of the solution for judging convergence. We will use three different grid sizes, 46×53, 93×107, and 187×215. For each grid size three different time steps are used, $\triangle t = 10, 5$, and 2.5 years, for time convergence.

Figure 7 shows temporal behavior of the source function over 10,000 years. Figures 8a,8c, and 8e present the contours of solute concentrations on the first grid at t=10,000 years for three different time steps, respectively. The time resolution for this mesh is quite adequate since there is hardly any change between contour plots. Figures 8b,8d, and 8f present breakthrough curves, with each plot presenting integrated discharges through three closed boundaries. As is the case for solute concentrations, there are no massive changes in the solution as the time accuracy of the computation is increased. Figures 9 and 10 show similar plot for grids number 2 and 3. As we refine the grid, the plume becomes narrower and the concentration front becomes sharper. This is due to improved effectiveness of the TVD algorithm.

These sequences of grid and time steps clearly show that we have resolved this problem adequately.

3.2 Dual-Porosity Transport

For a dual-porosity transport calculation vector 52 (E1E2 scenario) is a realistic example, which has no extremes in its parameters, for grid convergence test. Some of the parameters are calculation time, 10,000 years; fracture travel time with climate, 219 years; and matrix characteristic time, 8076 years.

We will use the same grid sizes as in the fracture transport case, However, vector 52 has different time scales for both fracture and the matrix block, and requires different time steps, with $\triangle t = 2, 1$, and 0.66 years.

Figure 11 shows temporal behavior of the source function over 10,000 years. Figures 12a,12c, and 12e present the solute concentration on the first grid at t=10,000 years for different time steps, respectively. Similar to the fracture calculation, the time resolution is satisfactory. Figures 12b,12d, and 12f present breakthrough curves. Again, there are no massive changes in the solution as the time accuracy of the computation is increased. Figures 13 and 14 show a similar plot for grids number 2 and 3. As the grid becomes finer the concentration front becomes sharper as we have observed in the fracture calculation. Figure 12c show some discharge on the side boundary where on the finer meshes there are no discharges. This points out that the first grid is not resolving the solution well. However, the other grids seem to be adequate.

3.3 Recommendations for Input Parameters

As our grid convergence test on fracture and fracture-matrix calculations have shown, the coarse grid (46×53), which has been used for the 1992 PA caculations, is not adequate in both cases. This grid was not dense enough to properly resolve the gradients in the solution. However, the time-step sizes have all resolved the time scales in both cases adequately.

4 Improvements

A three-dimensional version of the SECO-TRANSPORT code in stretched cartesian coordinates will be available for the next PA cycle. Other improvements will be general coordinate transformation in both two and three dimensions in conjunction with solution adaptivity. Also, more benchmark tests; for example, the Sudicky problem [13] for which an analytical solution exists for a dual-porosity assumption with a specified finite matrix block length.

References

[1] Huyakorn, P.S. and Pinder, G.F. *Computational Methods in Subsurface Flow*, Academic Press, New York, 1983.

[2] Bear, J. and Bachmat, Y. *Introduction to Modeling of Transport Phenomena in Porous Media*, Kluwer Academic Publishers, Dordrecht, Netherlands, 1990.

[3] Streltsova-Adams, T.D. 'Well Hydraulics in Heterogeneous Aquifer Formations' *Advances in Hydroscience*, Vol. 11, (Ed., Chow, V.T.), pp. 357-423, Academic Press, New York, 1978.

[4] Huyakorn, P.S., Lester, B.H., and Mercer, J.W. 'An Efficient Finite Element Technique for Modeling Transport in Fractured Porous Media: Single Species Transport' *Water Res. Res.*, Vol. 19, No. 3, pp. 841 - 854, 1983.

[5] Huyakorn, P.S., Lester, B.H., and Mercer, J.W. 'An Efficient Finite Element Technique for Modeling Transport in Fractured Porous Media: Nuclide Decay Chain Transport' *Water Res. Res.*, Vol. 19, No. 5, pp. 1286-1296, 1983.

[6] Roache, P.J., Knupp, P.M., Steinberg, S., and Blaine, R.L. 'Experience with Benchmark Test Cases for Groundwater Flow' in ASME FED Vol. 93 (Ed. Celik, I. and Freitas, C.J.), *Benchmark Test Cases for Computational Fluid Dynamics*, 1990.

[7] Pulliam, T.H. 'Efficient Solution Methods for the Navier-Stokes Equations', *Lecture Notes for the Von Karman Institute for Fluid Dynamics Lecture Series*, Brusses, Belgium, 1986.

[8] Steinberg, S., and Roache, P.J. '*Discretizing Symmetric Operators in General Coordinates*', to appear.

[9] Fletcher, C.A.J. *Computational Techniques for Fluid Dynamics*, Volumes I and II, Springer-Verlag, 1988.

[10] Yee, H.C. 'Construction of Explicit and Implicit Symmetric TVD Schemes and Their Applications' *J. Comp. Phys.*, Vol. 68, pp. 151-179, 1987.

[11] Javandel, I., Doughty, C., and Tsang, C.F. *Groundwater Transport: Handbook of Mathematical Models*, American Geophysical Union, Washington, D.C. , 1984.

[12] Tang, D.H., Frind, E.O., and Sudicky, E.A. 'Contaminant Transport in Fractured Porous Media: Analytical Solution for a Single Fracture' *Water Resources Research*, Vol. 17, No. 3, pp. 555-564, 1981.

[13] Sudicky, E.A., and Frind, E.O. 'Contaminant Transport in Fractured Porous Media: Analytical Solutions for a System of Parallel Fractures' *Water Resources Research*, Vol. 18, No. 6, pp. 1634-1642, 1982.

[14] Proper ref. for appendix in volume 4

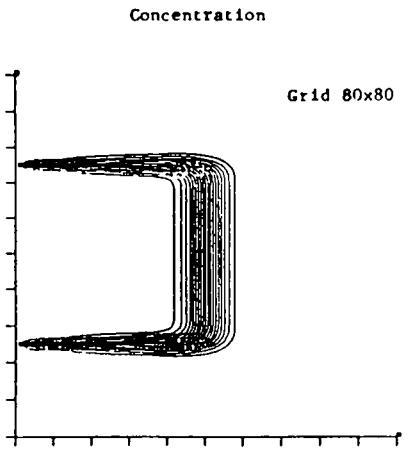

Figure 1a. TVD scheme, MUSCL limiter, Pe = 2.

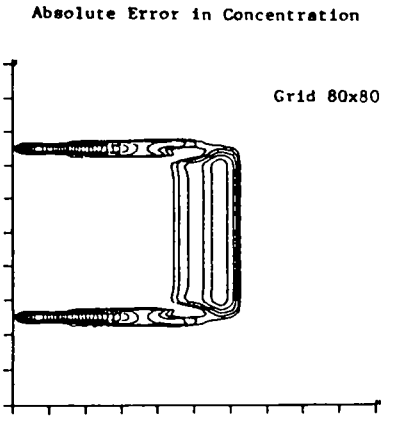

Figure 1b. TVD scheme, MUSCL limiter, Pe = 2.

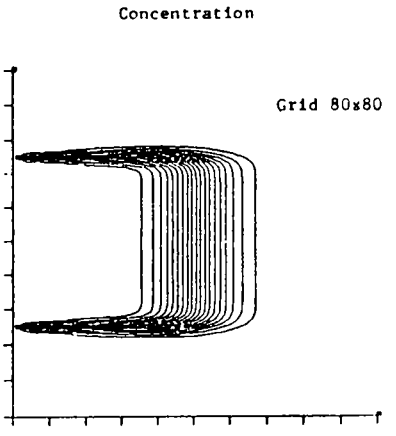

Figure 2a. Upwind, Pe = 2.

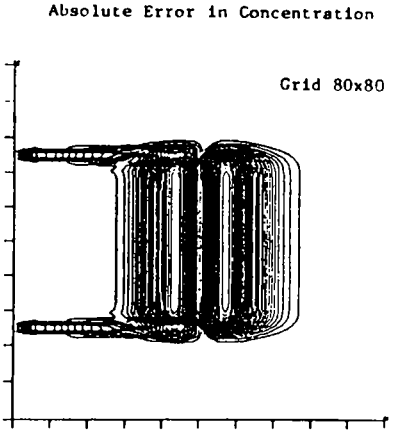

Figure 2b. Upwind, Pe = 2.

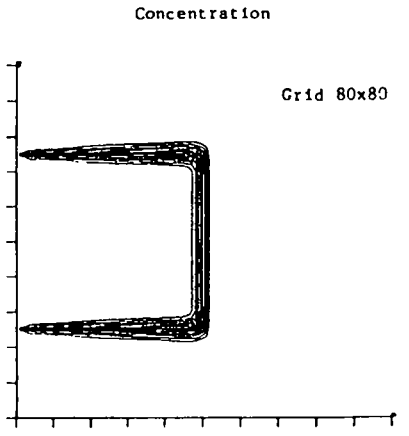

Figure 3. TVD scheme, MUSCL limiter, Pe = 10.

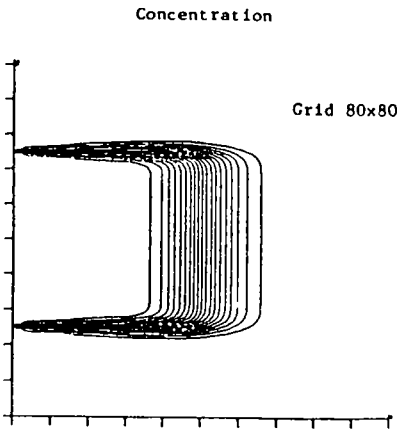

Figure 4. Upwind, Pe = 10.

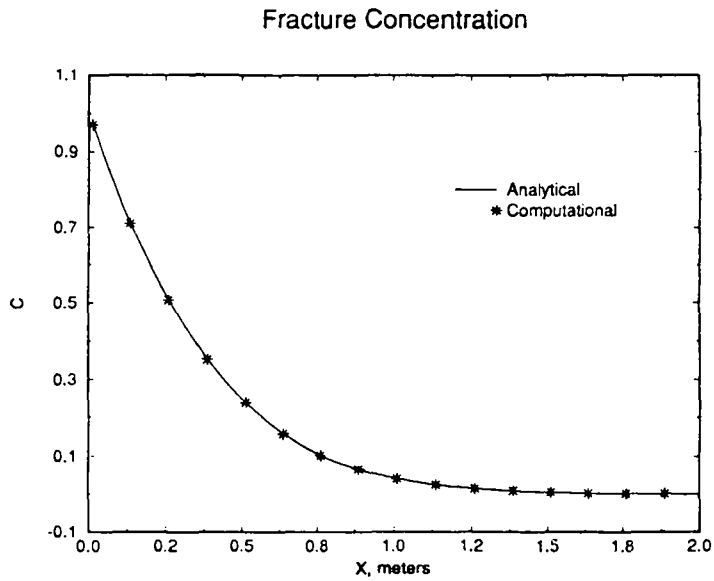

Figure 5

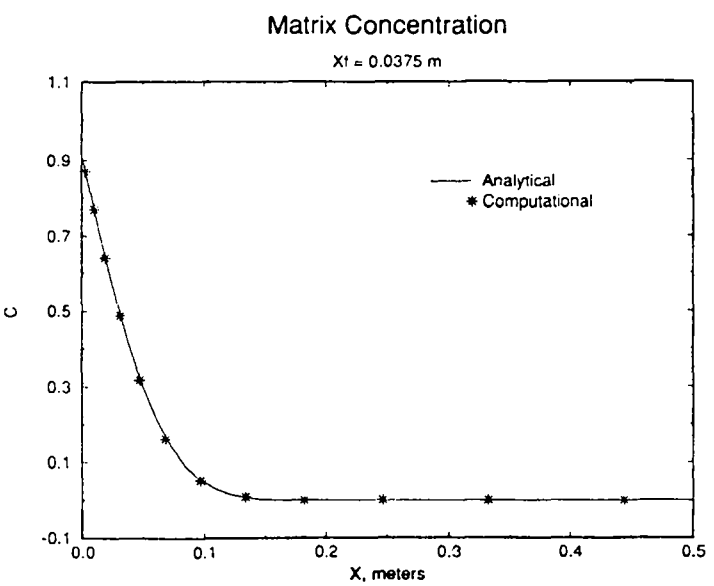

Figure 6

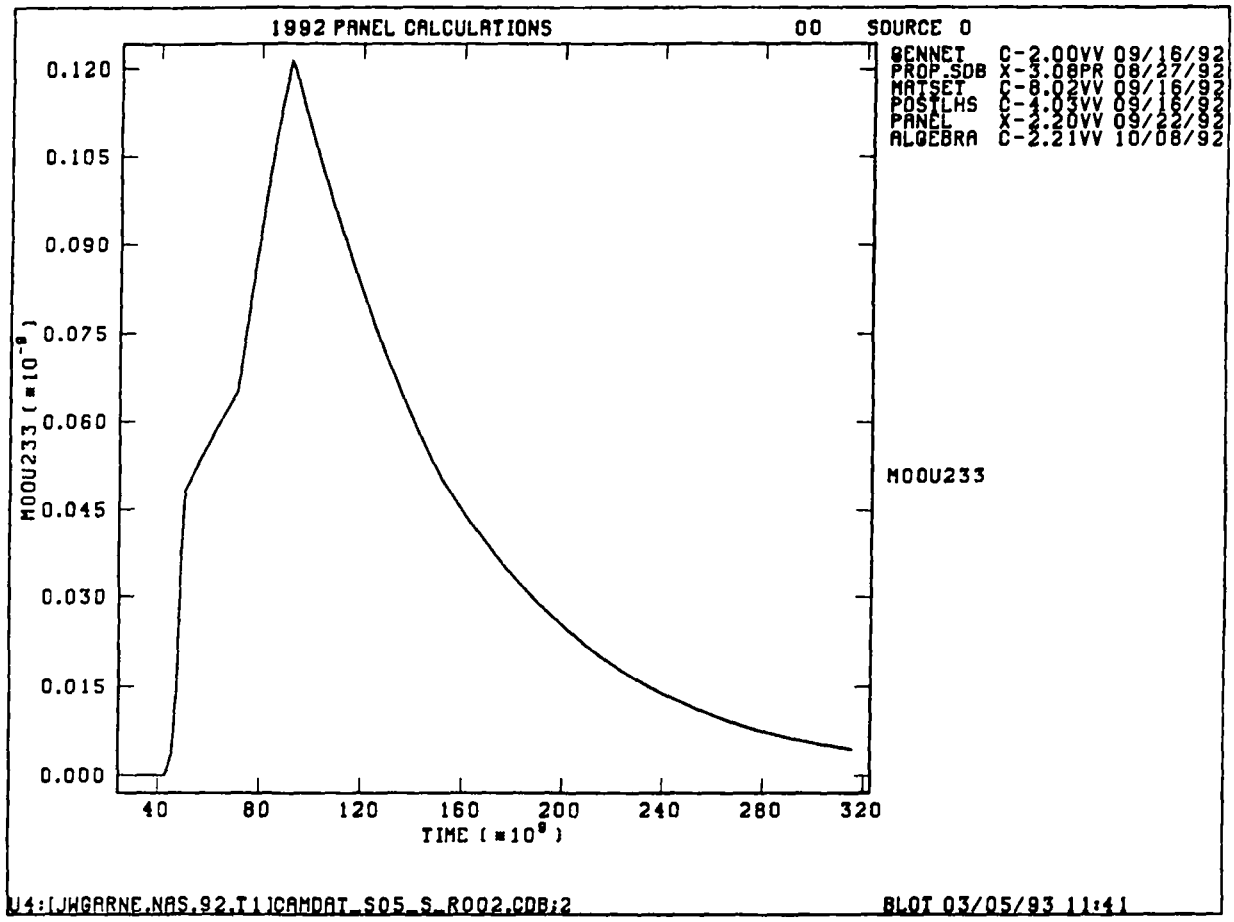
1992 PANEL CALCULATIONS
00 SOURCE 0
GENNET C-2.00VV 09/16/92
PROP.SDB X-3.08PR 08/27/92
MATSET C-8.02VV 09/16/92
POSTLHS C-4.03VV 09/16/92
PANEL X-2.20VV 09/22/92
ALGEBRA C-2.21VV 10/08/92
M00U233
M00U233 (*10^-6)
0.120
0.105
0.090
0.075
0.060
0.045
0.030
0.015
0.000
40
80
120
160
200
240
280
320
TIME (*10^6)
U4:[JWGARNE.NAS.92.T1]CAMDAT_S05_S_R002.CDB;2
PLOT 03/05/93 11:41

Figure 7

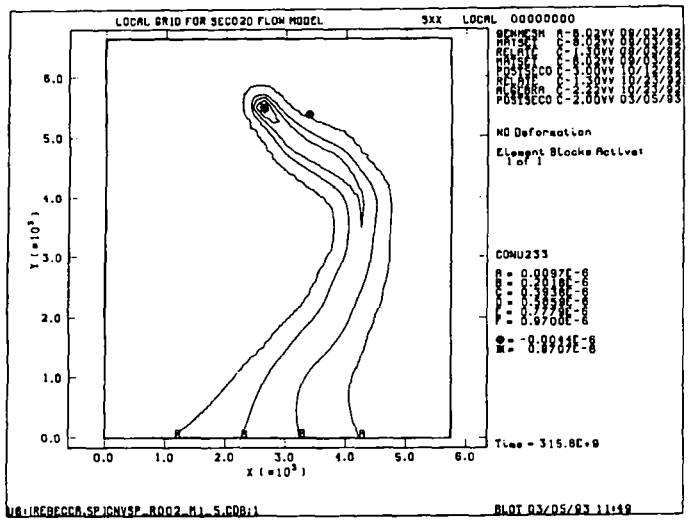

(a)

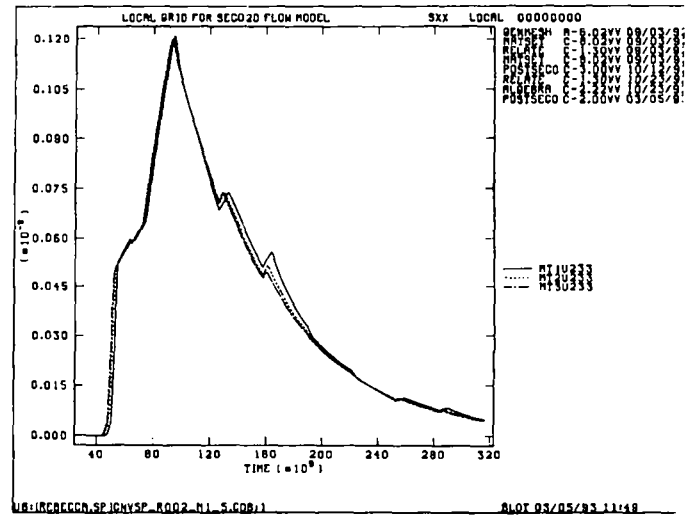

(b)

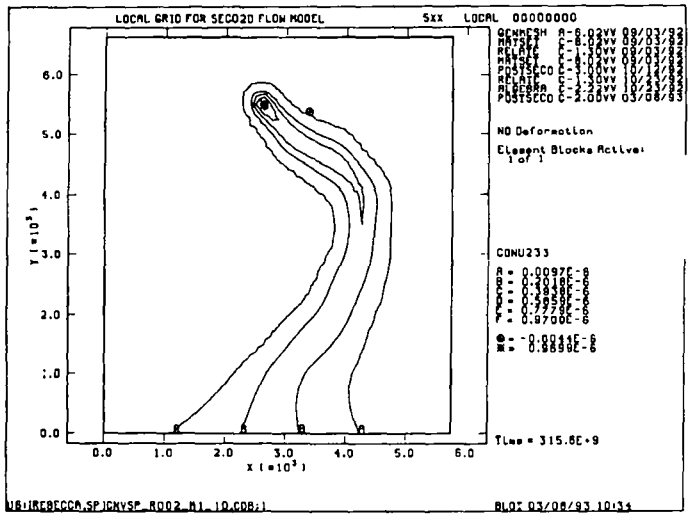

(c)

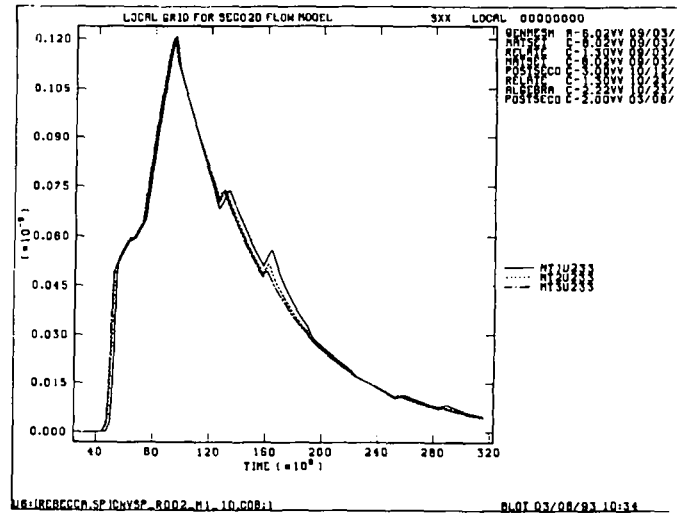

(d)

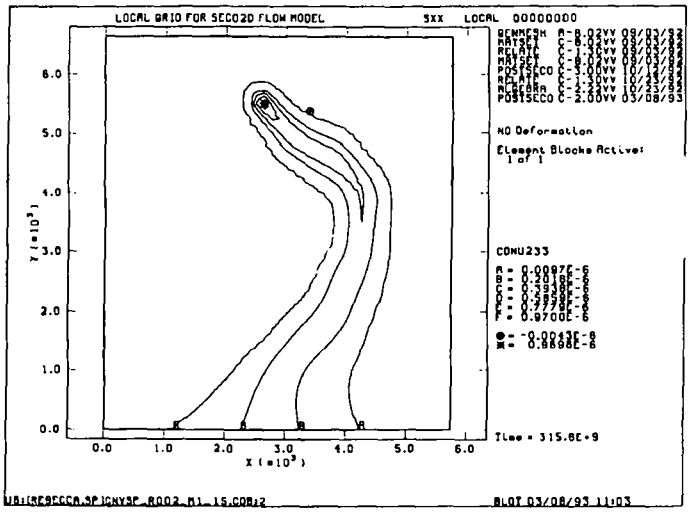

(e)

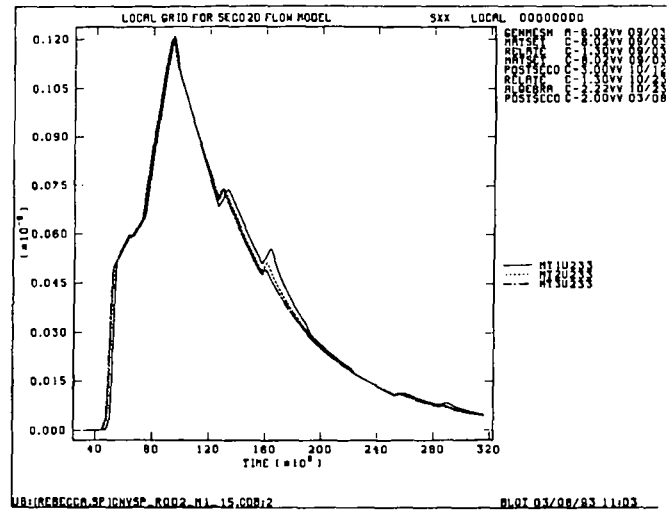

(f)

Figure 8

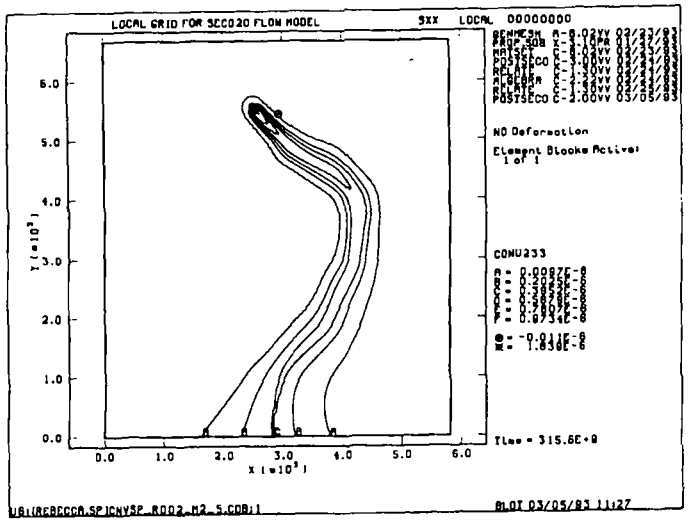

(a)

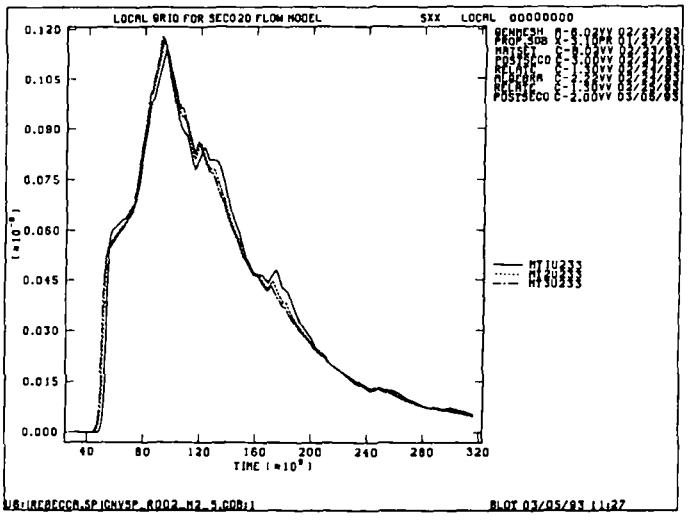

(b)

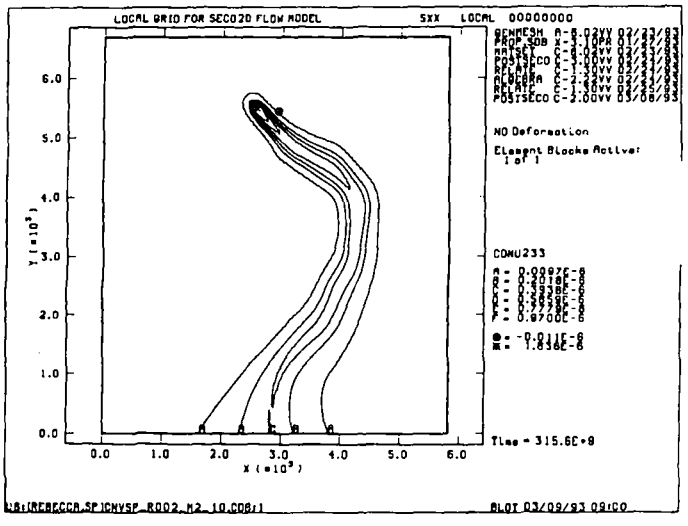

(c)

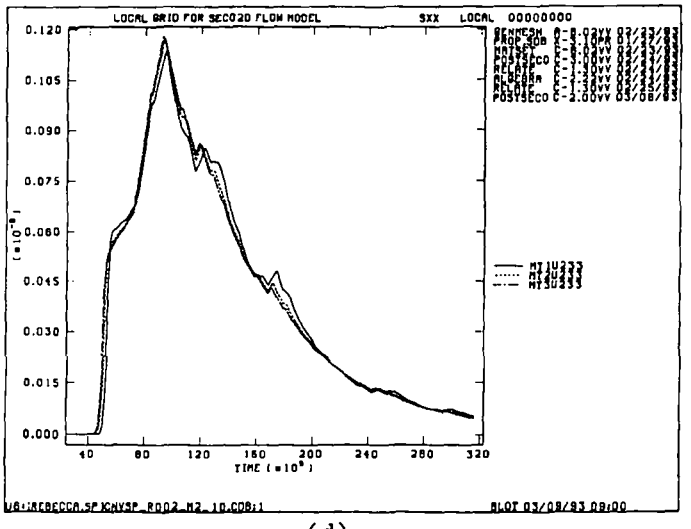

(d)

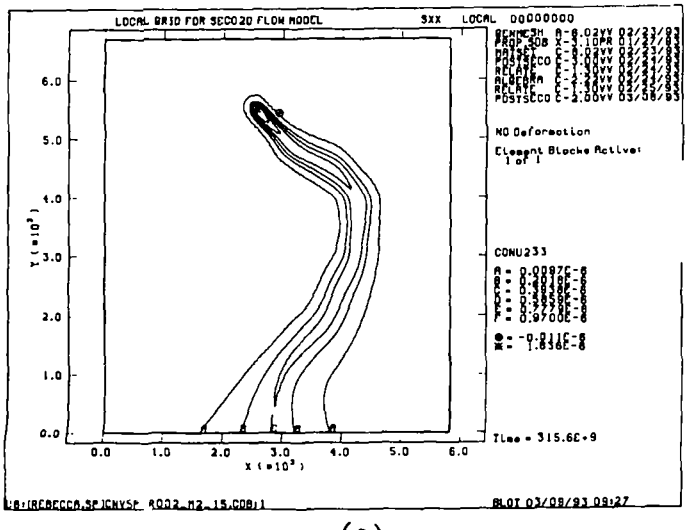

(e)

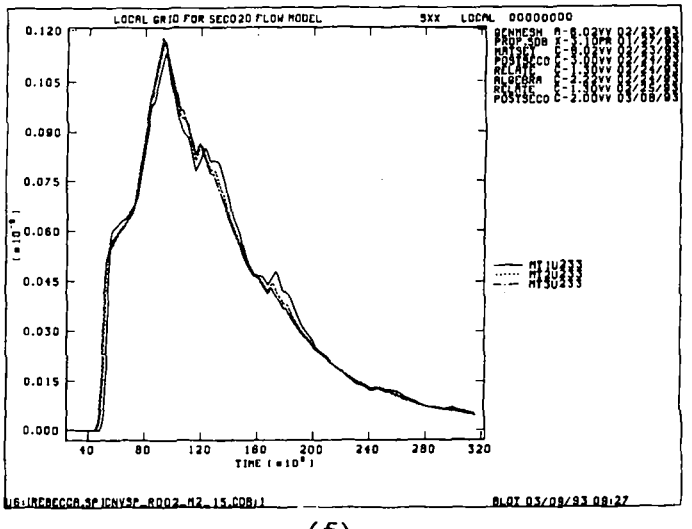

(f)

Figure 9

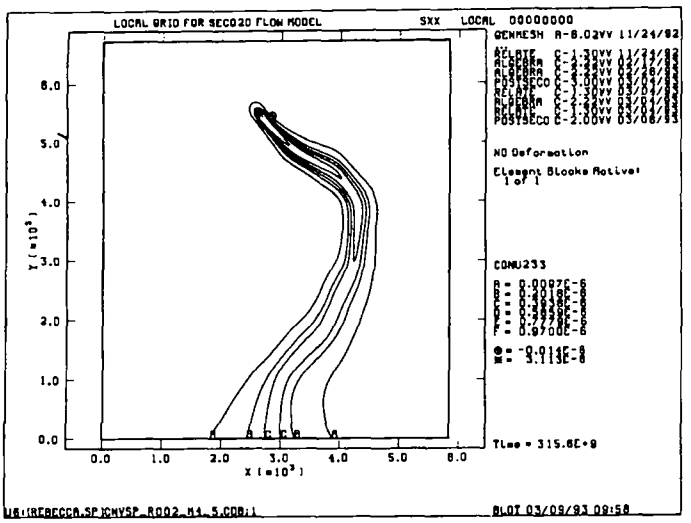

(a)

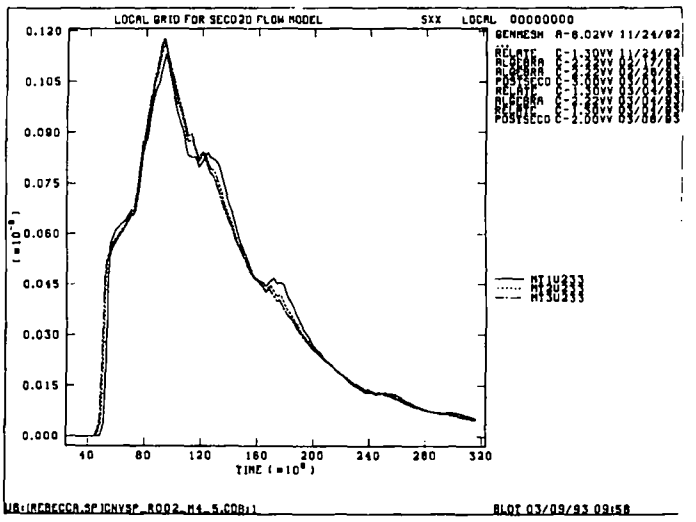

(b)

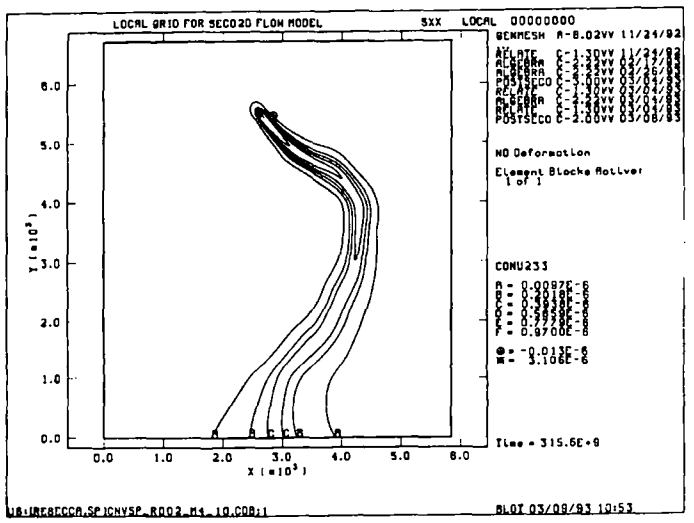

(c)

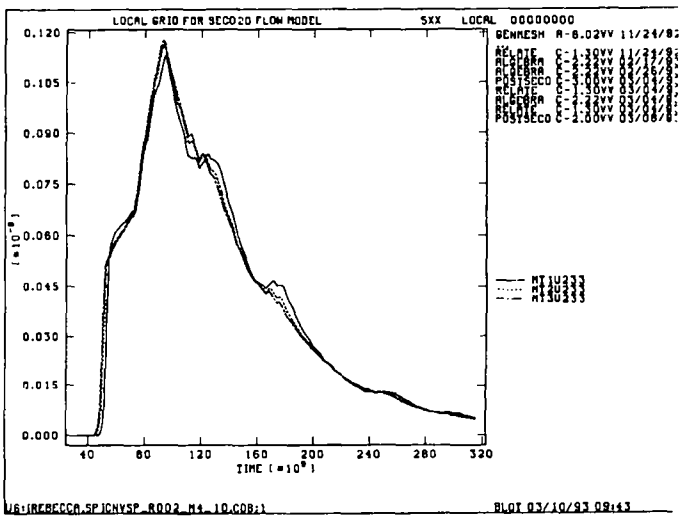

(d)

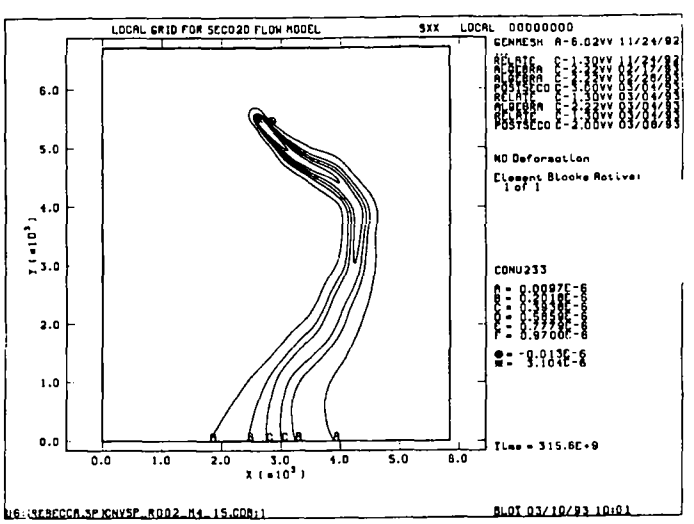

(e)

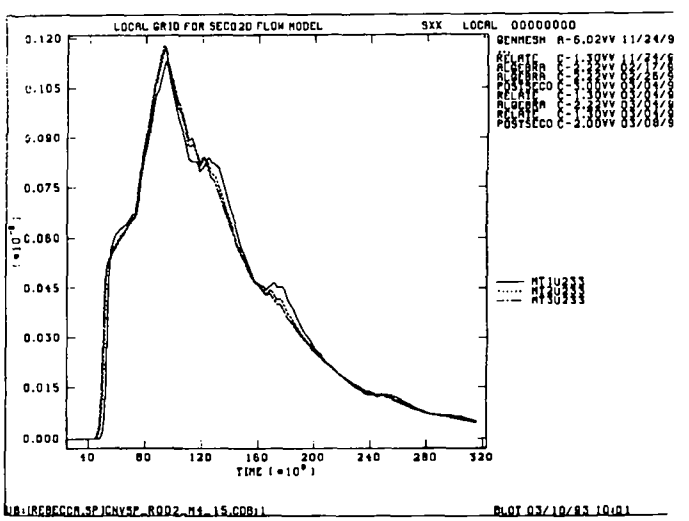

(f)

Figure 10

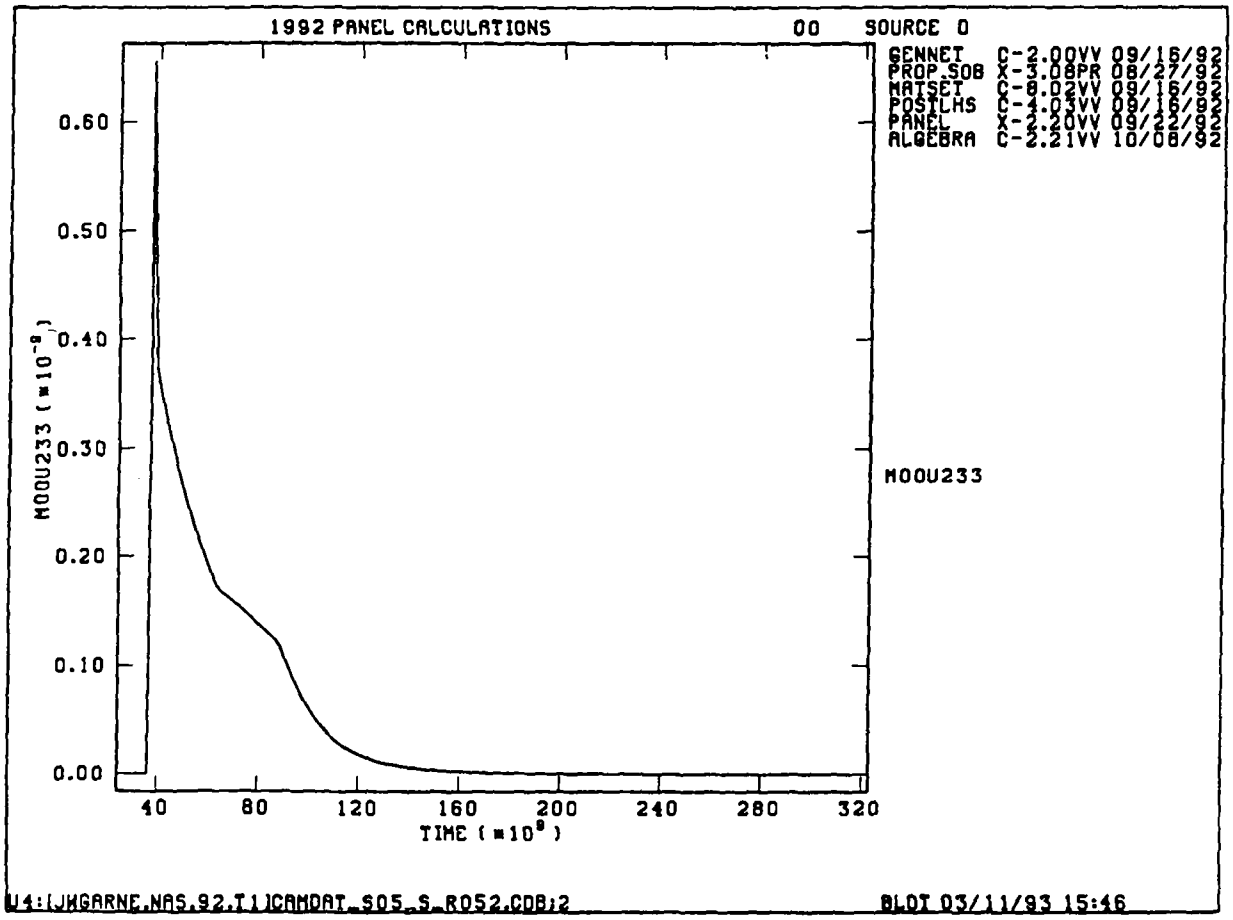
1992 PANEL CALCULATIONS
00
SOURCE 0
GENNET C-2.00VV 09/16/92
PROP.SOB X-3.08PR 08/27/92
MATSET C-8.02VV 09/16/92
POSTLHS C-4.03VV 09/16/92
PANEL X-2.20VV 09/22/92
ALGEBRA C-2.21VV 10/08/92
MOOU233
MOOU233 (*10^-9)
0.60
0.50
0.40
0.30
0.20
0.10
0.00
40
80
120
160
200
240
280
320
TIME (*10^9)
U4:[JHGARNE.NAS.92.T1]CAMDAT_S05_S_R052.CDB;2
PLOT 03/11/93 15:46

Figure 11

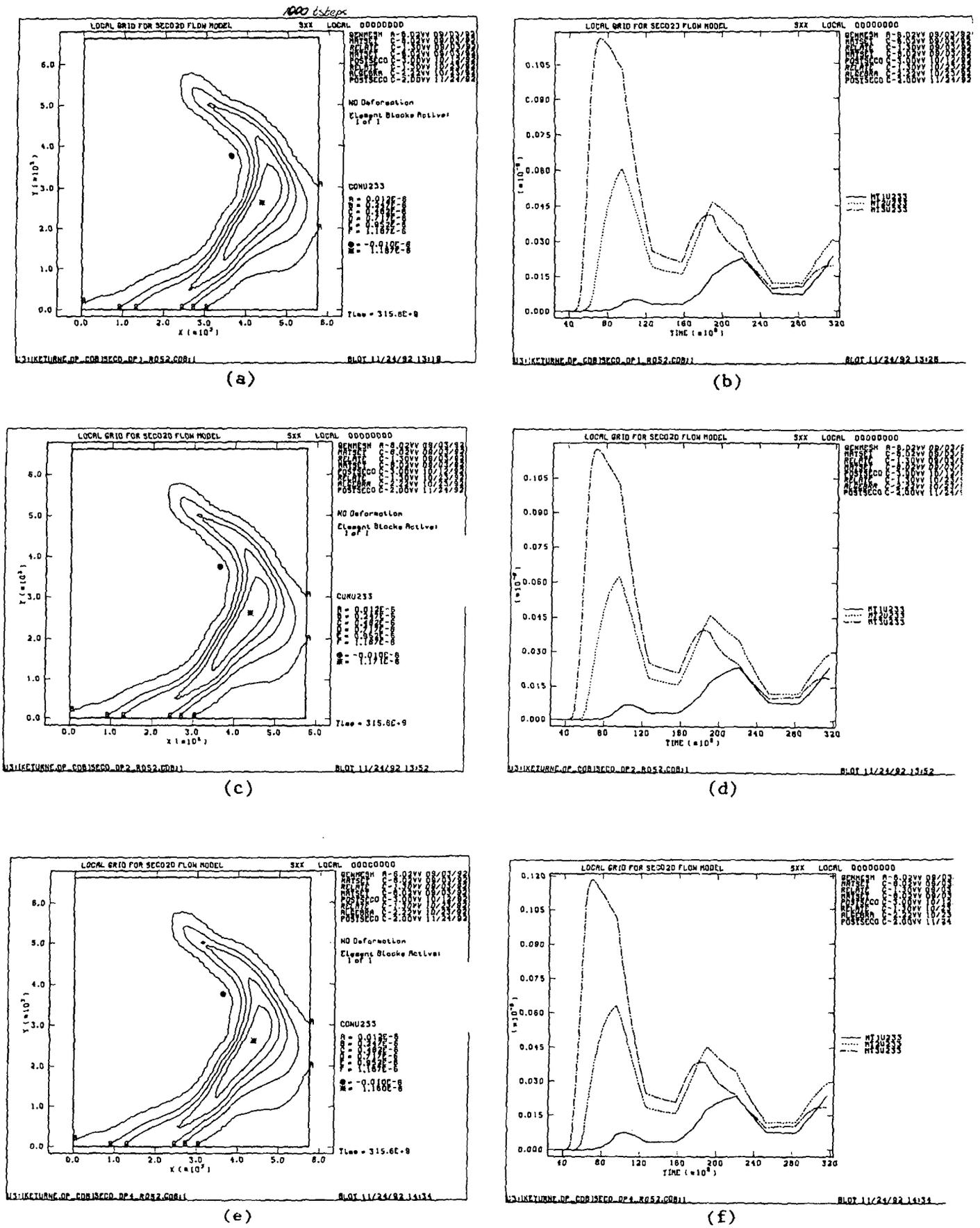
1000 tsteps
LOCAL GRID FOR SECO3D FLOW MODEL
SXX LOCAL 00000000
NO Deformation
CONU233
TLee = 315.8E+9
X (*10³)
Y (*10³)
TIME (*10⁸)
(a)
(b)
(c)
(d)
(e)
(f)

Figure 12

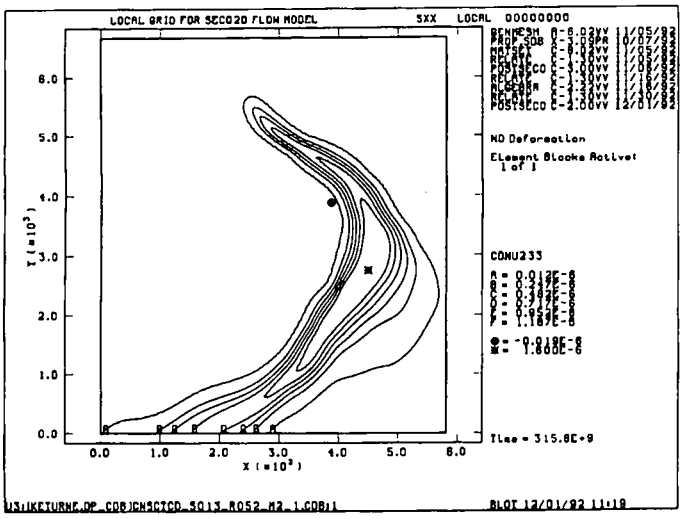

(a)

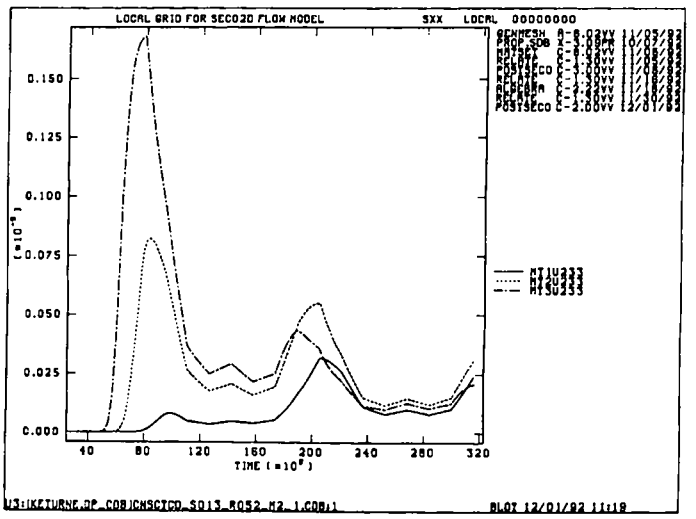

(b)

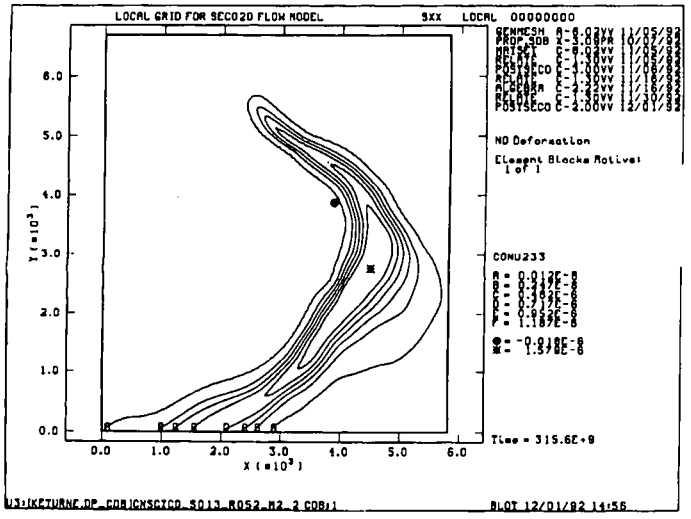

(c)

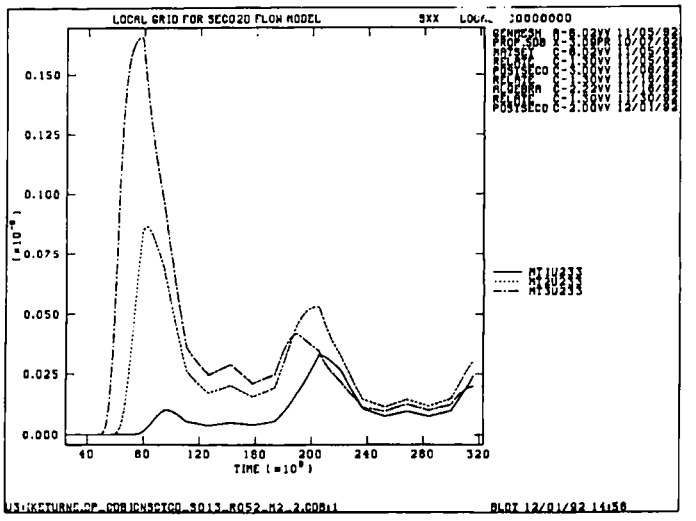

(d)

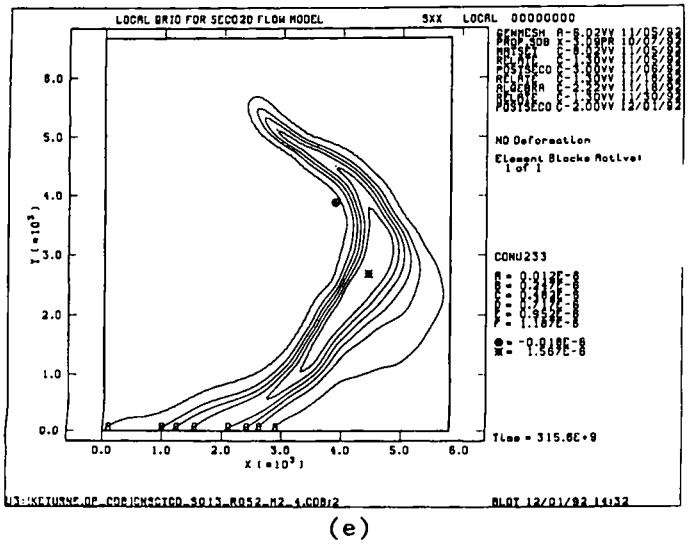

(e)

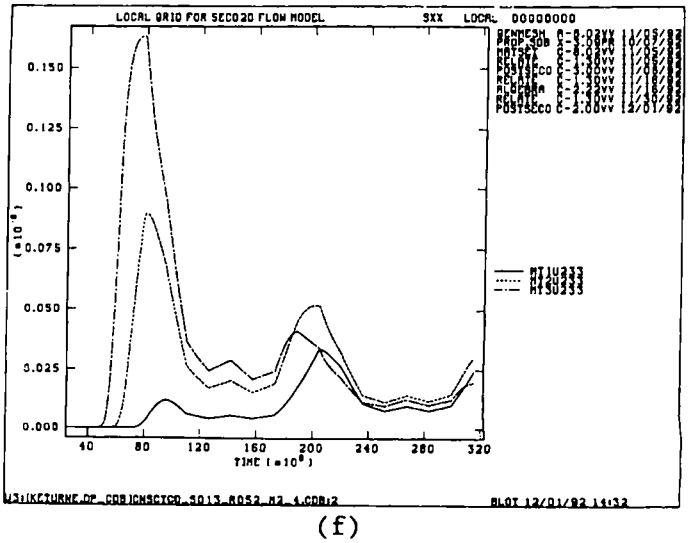

(f)

Figure 13

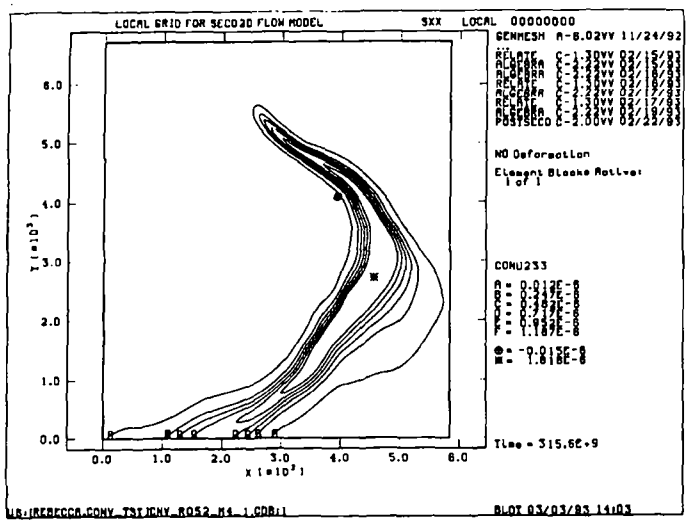

(a)

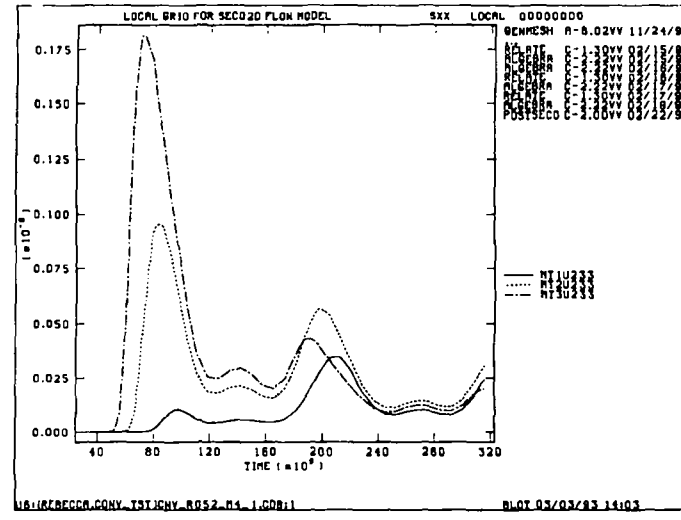

(b)

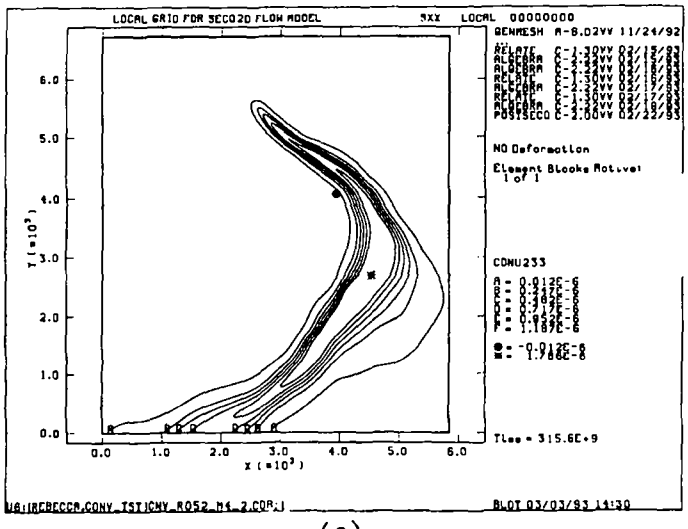

(c)

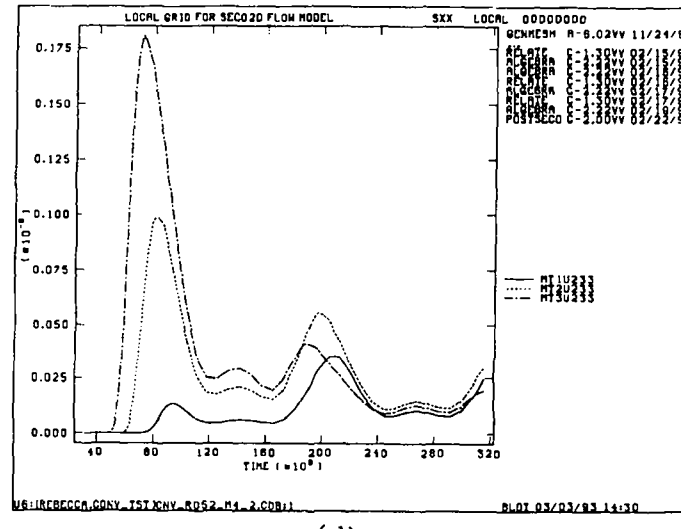

(d)

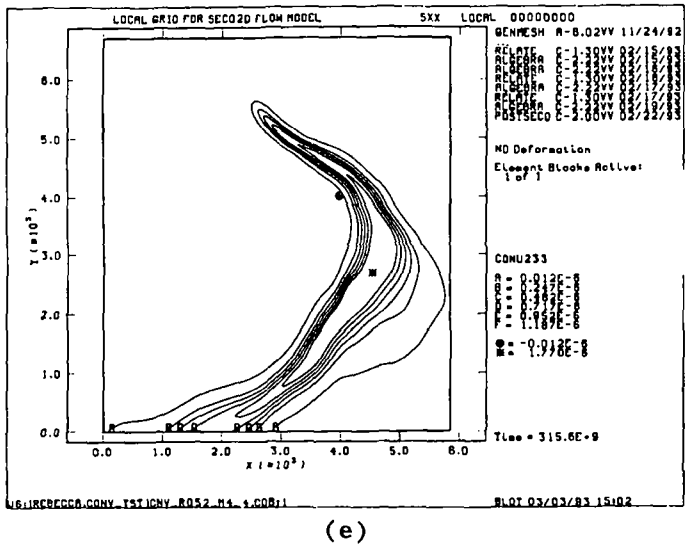

(e)

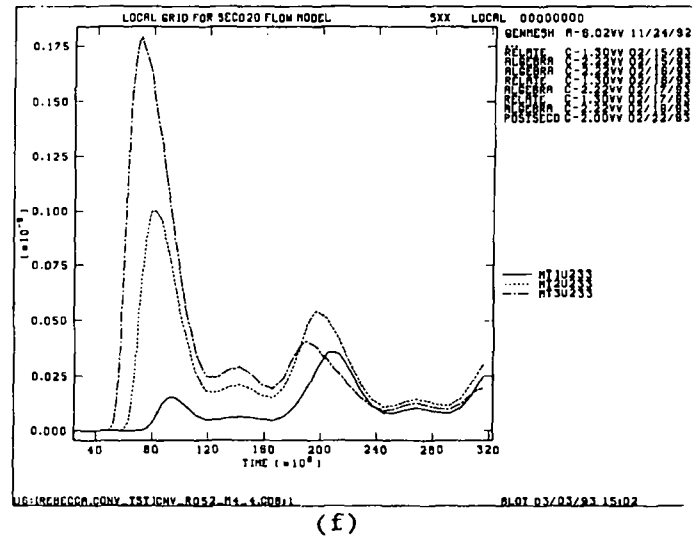

(f)

Figure 14

APPENDIX B: ASSUMPTIONS AND DERIVATION OF EQUATION 4.2-2 RELATING SANCHO POROSITY TO BRAGFLO POROSITY

APPENDIX B: ASSUMPTIONS AND DERIVATION OF EQUATION 4.2-2 RELATING SANCHO POROSITY TO BRAGFLO POROSITY

Inherent in Equation 4.2-2 is that the compressibility of halite is small compared to the compressibility of the gas that occupies the voids within the waste panel. Making this assumption permits the conclusion that the mass and volume occupied by the solid (waste and backfill) within the moving boundary defining the time variant dimensions of the waste panel remains constant. The volume of solids within the waste panel, at any time, is the same as the volume of solids that are present initially in the waste panel prior to compaction (Equation B-1).

$$V_s\ (t=0) = V_s(t) \tag{B-1}$$

where

V_s = volume of solids within the boundaries defining the waste panel.

Figure B-1 depicts the waste panel in two states, the top figure, a, depicts the waste panel initially, at t=0, while the bottom figure, b, depicts the waste-panel after some consolidation, at time t. While the figure implies compaction of the waste panel by movement of the upper boundary or roof, this is for convenience only; movement of the other boundaries may also participate in the compaction process.

The porosity, ϕ', of the waste panel is defined, at any time, as the ratio of the void volume (V_v) to the total volume, V_t, where V_t is the sum of the void volume and solid volume, Equations B-2 and B-3, respectively,

$$\phi'(t) = \frac{V_v\ (t)}{V_t\ (t)} \tag{B-2}$$

and

$$V_t(t) = V_v(t) + V_s(t). \tag{B-3}$$

Substitution of Equation B-3 into Equation B-2 allows the solid volume to be expressed in terms of porosity and total panel volume, Equation B-4,

$$V_s = (1 - \phi')\ V_t. \tag{B-4}$$

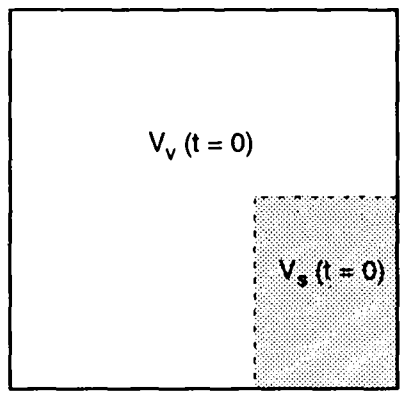

a) Waste-panel at initial state.

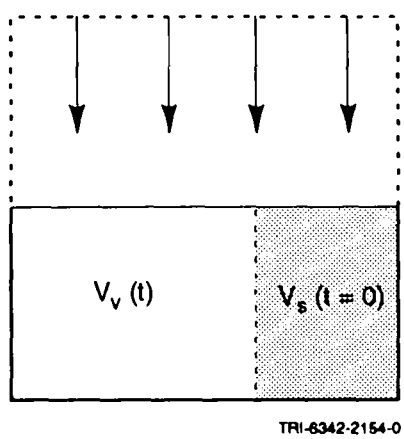

b) Waste-panel at compacted state.

Figure B-1. Waste-Panel at two states of compaction, showing volume of voids (V_V) and volume of solids (V_S).

Applying Equation B-4 at time, t=0, and at an arbitrary time, t, and using the equality of Equation B-1, after some rearrangement yields Equation B-5,

$$\frac{1 - \phi'(t=0)}{1 - \phi'(t)} = \frac{V_t(t)}{V_t(t=0)} \quad . \tag{B-5}$$

Now, define an alternate porosity, ϕ, as the ratio of the void volume at any given time to the total initial volume of the waste panel prior to compaction, Equation B-6,

$$\phi(t) = \frac{V_v(t)}{V_t(t=0)} \quad . \tag{B-6}$$

It is desired to relate ϕ and ϕ' in a way that conserves void volume. This can be done by determining the porosity associated with the waste panel of initial dimensions and volume that is equivalent to the void volume of the compacted and collapsed representation of the waste panel. Combining Equations B-2 and B-6 and solving for $\phi(t)$ yields the desired result, Equation B-7,

$$\phi(t) = \frac{\phi'(t)\, V_t(t)}{V_t(t=0)} \quad . \tag{B-7}$$

Equation B-8, reproduced as Equation 4.2-2, is obtained by substituting the left hand side of B-5 for the ratio, $V_t(t)/V_t(t=0)$ in Equation B-7,

$$\phi(t) = \phi'(t) \left[\frac{1 - \phi'(t=0)}{1 - \phi'(t)} \right] \quad . \tag{B-8}$$

Equation B-8 relates ϕ to only ϕ' at a given value of time and is used to transform the porosities resulting from the Segrangian treatment of the numerical mesh in SANCHO to the Eulerian treatment in BRAGFLO, while conserving void volume.

APPENDIX C: LHS SAMPLES AND CALCULATED NORMALIZED RELEASES

Contents For Appendix C

Tables

APPENDIX C: LHS SAMPLES AND CALCULATED NORMALIZED RELEASES

This appendix contains the 70 sample elements for each of the 49 parameters varied and sampled by LHS and summaries of EPA-normalized radionuclide releases to the 2.9-km, accessible environment boundary south of the WIPP for the E1 and E1E2 scenarios with an intrusion at 1000 yr. Releases are given for simulations assuming a dual porosity model with chemical retardation for transport in the Culebra Dolomite Member of the Rustler Formation.

This appendix also contains the summaries of release to the accessible environment from initially drilling into the repository and bringing up cuttings from one average activity of CH waste and one average activity of RH waste. (The CH waste activity is subsequently multiplied by a factor to account for the four CH activity levels. This modified activity along with the probability of actually hitting these various CH activity levels is used when constructing the CCDF). Cuttings were calculated for six different intrusion times. Releases are the same for the E1, E2 or E1E2 scenarios, and different scenarios are accounted for by the CCDFPERM program.

The output tables were created by the CCDFCALC computer code from output databases created by SECO-TRANSPORT and CUTTINGS and are the input to the CCDFPERM program which calculates the final CCDF.

Table C-1 lists the 49 parameters sampled and the distribution type used.

Table C-1. Numerical ID and Distributions of 49 Sampled Parameters In December 1992 WIPP PA Calculations

Parameter	Range		Distribution
1 Initial Brine Saturation of Waste (BRSAT)	0.	0.14	Uniform
2 Inundated Corrosion Gas Generation Rate (mol/m^2•s) (GRCORI)	0.	1.3E-08	Cumulative
3 Humid/Inundated Corrosion Gas Generation Rate Ratio (GRCORHF)	0.	0.5	Cumulative
4 Stoichiometric For Corrosion of Steel (STOICCOR)	0.	1.	Uniform
5 Inundated Microbial Gas Generation Rate (mol/kg•s) (GRMICI)	0.	1.6E-08	Cumulative
6 Humid/Inundated Microbial Gas Generation Rate Ratio (GRMICHF)	0.	0.2	Uniform
7 Stoichiometric Coef For Biodegradation of Cellulose (STOICMIC)	0.	1.67	Uniform
8 Wood Volume Fraction (VWOOD)	0.284	0.484	Normal
9 Metal Volume Fraction (VMETAL)	0.276	0.476	Normal
10 Log Salado Permeability (m^2) (SALPERM)	-24.	-19.	Cumulative
11 Brooks-Corey Exponent (BCEXP)	0.2	10.	Cumulative
12 Brooks-Corey Model Relative Weight (BCFLG)	0.	1.	Delta
13 Brooks-Corey Residual Brine Saturation (BCBRSAT)	0.	0.4	Uniform
14 Brooks-Corey Residual Gas Saturation (BCGSSAT)	0.	0.4	Uniform
15 Log Marker Bed Permeability (m^2) (MBPERM)	-21.	-16.	Cumulative
16 Marker Bed Porosity (MBPOR)	0.001	0.03	Cumulative
17 Scale Factor For Disturbed Zone Porosity (TZPORF)	0.	1.	Uniform
18 Salado Pressure (Pa) (MBPRES)	1.2E+07	1.3E+07	Uniform
19 Brine Pocket Pressure (Pa) (BPPRES)	1.3E+07	2.1E+07	Uniform

Table C-1. Numerical ID and Distributions of 49 Sampled Parameters In December 1992 WIPP PA Calculations (Continued)

	Parameter	Range		Distribution
20	Brine Pocket Bulk Storativity (m^3/Pa) (BPSTOR)	0.02	2.	Lognormal
21	Borehole Permeability (m^2) (BHPERM)	1.0E-14	1.0E-11	Lognormal
22	Drillbit Diameter (m) (DBDIAM)	0.2667	0.4445	Uniform
23	Index for Rate in Poisson Drilling Model (LAMBDA)	0.	1.	Uniform
24	Brine Pocket Area Fraction (BPAREAFR)	0.24479	0.56771	Cumulative
25	Log Solubility Am (mol/l) (SOLAM)	-13.3	0.15	Cumulative
26	Log Solubility Np (mol/l) (SOLNP)	-15.52	-1.92	Cumulative
27	Log Solubility Pu (mol/l) (SOLPU)	-16.6	-3.26	Cumulative
28	Log Solubility Ra (mol/l) (SOLRA)	0.3	1.26	Cumulative
29	Log Solubility Th (mol/l) (SOLTH)	-15.26	-5.66	Cumulative
30	Log Solubility U (mol/l) (SOLU)	-15.	0.	Cumulative
31	Culebra Index for Transmissivity Field (CULTRFLD)	0.	1.	Uniform
32	Index for Recharge Amplitude Factor (CULCLIM)	0.	1.	Uniform
33	Culebra Fracture Porosity (CULFRPOR)	0.0001	0.01	Lognormal
34	Culebra Fracture Spacing (m) (CULFRSP)	0.06	8.	Cumulative
35	Culebra Clay Filling Fraction (CULCLYF)	0.	0.5	Cumulative
36	Culebra Clay Porosity (CULCLYP)	0.05	0.5	Uniform
37	Log Culebra Fracture Dist Coef Am (m^3/kg) (FKDAM)	-4.	3.	Cumulative
38	Log Culebra Fracture Dist Coef Np (m^3/kg) (FKDNP)	-4.	3.	Cumulative
39	Log Culebra Fracture Dist Coef Pu (m^3/kg) (FKDPU)	-4.	3.	Cumulative
40	Log Culebra Fracture Dist Coef Th (m^3/kg) (FKDTH)	-4.	1.	Cumulative
41	Log Culebra Fracture Dist Coef U (m^3/kg) (FKDU)	-4.	0.	Cumulative
42	Log Culebra Fracture Dist Coef Ra (m^3/kg) (FKDRA)	-4.	2.	Cumulative
43	Culebra Matrix Porosity (CULPOR)	.058056	0.2525	Data
44	Log Culebra Matrix Dist Coef Am (m^3/kg) (MKDAM)	-4.	2.	Cumulative
45	Log Culebra Matrix Dist Coef Np (m^3/kg) (MKDNP)	-4.	2.	Cumulative
46	Log Culebra Matrix Dist Coef Pu (m^3/kg) (MKDPU)	-4.	2.	Cumulative
47	Log Culebra Matrix Dist Coef Th (m^3/kg) (MKDTH)	-4.	0.	Cumulative
48	Log Culebra Matrix Dist Coef U (m^3/kg) (MKDU)	-4.	0.	Cumulative
49	Log Culebra Matrix Dist Coef Ra (m^3/kg) (MKDRA)	-4.	1.	Cumulative

Table C-2 lists the Latin Hypercube sampled (LHS) values for each of the 49 parameters.

Table C-2. Seventy Values Sampled by LHS for 49 Parameters that Were Varied in December 1992 PA Calculations

Material Parameter RUN NO.	BRSAT X(1)	GRCORI X(2)	GRCORHF X(3)	STOICCOR X(4)	GRMICI X(5)	GRMICHF X(6)	STOICMIC X(7)	VWOOD X(8)	VMETAL X(9)	SALPERM X(10)
1	4.023E-02	1.570E-09	1.238E-01	4.810E-01	1.154E-08	8.629E-02	7.677E-01	3.601E-01	3.741E-01	-2.044E+01
2	1.269E-01	3.730E-09	2.775E-01	2.119E-01	1.588E-08	1.696E-01	1.264E-01	4.242E-01	3.910E-01	-2.001E+01
3	8.612E-02	8.501E-10	7.155E-02	4.965E-02	3.585E-09	1.532E-01	7.179E-04	3.914E-01	3.452E-01	-2.088E+01
4	3.242E-02	1.013E-08	8.783E-03	4.382E-01	9.379E-09	4.926E-02	2.213E-01	3.425E-01	4.137E-01	-2.082E+01
5	1.149E-01	3.321E-10	1.539E-02	6.945E-01	1.195E-08	5.316E-02	4.741E-01	3.808E-01	3.928E-01	-2.154E+01
6	1.373E-01	1.176E-08	3.287E-01	6.461E-01	3.979E-09	9.957E-02	1.322E+00	4.637E-01	4.465E-01	-2.314E+01

Table C-2. Seventy Values Sampled by LHS for 49 Parameters that Were Varied in December 1992 PA Calculations (Continued)

Material Parameter RUN NO.	BRSAT X(1)	GRCORI X(2)	GRCORHF X(3)	STOICCOR X(4)	GRMICI X(5)	GRMICHF X(6)	STOICMIC X(7)	VWOOD X(8)	VMETAL X(9)	SALPERM X(10)
7	1.395E-01	1.041E-08	3.263E-01	6.245E-01	1.421E-09	1.238E-01	4.816E-01	3.225E-01	3.987E-01	-2.194E+01
8	8.068E-02	6.341E-09	4.805E-01	7.551E-01	7.905E-09	4.721E-02	5.214E-01	3.502E-01	3.437E-01	-2.131E+01
9	5.937E-02	1.715E-09	3.813E-02	3.057E-01	8.037E-09	5.041E-05	1.425E+00	4.689E-01	4.191E-01	-2.332E+01
10	7.619E-02	8.712E-09	2.143E-01	7.950E-01	6.070E-09	1.297E-02	1.229E+00	3.587E-01	3.578E-01	-2.040E+01
11	1.202E-01	9.067E-09	2.269E-01	6.636E-03	2.159E-09	1.064E-01	3.519E-02	3.065E-01	4.027E-01	-2.011E+01
12	8.396E-02	1.127E-08	9.043E-02	4.057E-01	3.123E-09	6.075E-02	1.490E+00	3.632E-01	3.785E-01	-2.004E+01
13	3.577E-02	4.420E-09	2.111E-01	9.610E-01	6.352E-10	1.559E-01	7.945E-01	3.733E-01	4.369E-01	-2.306E+01
14	1.272E-02	1.138E-08	3.582E-02	1.254E-01	2.820E-10	1.745E-01	3.435E-01	4.060E-01	3.886E-01	-2.215E+01
15	1.315E-01	2.155E-09	3.880E-01	3.308E-01	8.800E-09	8.200E-02	1.339E+00	4.120E-01	3.523E-01	-2.352E+01
16	4.263E-02	5.910E-09	4.610E-01	3.478E-01	1.216E-08	1.580E-01	1.667E+00	3.436E-01	3.820E-01	-2.070E+01
17	5.151E-02	2.705E-09	1.751E-01	9.018E-01	7.343E-09	4.462E-02	9.611E-01	4.016E-01	3.183E-01	-2.189E+01
18	6.297E-02	5.140E-10	3.003E-02	2.212E-01	1.285E-09	1.021E-01	1.446E+00	3.556E-01	3.845E-01	-2.117E+01
19	5.652E-02	8.036E-09	4.058E-03	3.615E-02	1.413E-08	2.054E-02	5.646E-01	4.048E-01	3.375E-01	-2.240E+01
20	3.744E-02	5.687E-09	2.713E-03	1.508E-01	5.405E-09	4.216E-02	1.606E+00	3.995E-01	4.760E-01	-1.974E+01
21	1.046E-02	1.095E-08	3.090E-01	1.887E-01	1.268E-08	6.836E-02	1.108E+00	3.841E-01	3.952E-01	-1.954E+01
22	7.499E-02	1.962E-09	5.486E-02	6.810E-01	2.061E-09	1.300E-01	9.990E-01	4.185E-01	3.697E-01	-2.026E+01
23	8.469E-02	7.970E-09	4.012E-01	7.260E-01	2.704E-09	1.680E-01	3.339E-01	4.075E-01	4.277E-01	-2.126E+01
24	7.128E-02	4.287E-09	2.143E-02	5.270E-01	2.922E-09	1.995E-01	8.854E-01	3.275E-01	3.802E-01	-2.092E+01
25	7.809E-02	7.428E-09	9.208E-02	5.991E-01	3.319E-09	1.195E-01	5.792E-01	3.560E-01	2.760E-01	-2.015E+01
26	1.014E-01	1.164E-08	1.136E-01	5.786E-01	4.518E-10	4.783E-03	7.210E-01	4.269E-01	3.382E-01	-2.076E+01
27	2.606E-02	1.061E-08	1.638E-01	2.359E-01	1.602E-09	1.821E-01	6.518E-01	4.840E-01	3.869E-01	-2.129E+01
28	2.351E-02	6.576E-09	5.147E-02	5.697E-01	5.082E-09	7.677E-02	4.355E-01	3.970E-01	3.748E-01	-2.134E+01
29	6.911E-02	1.295E-08	8.140E-02	9.815E-01	2.366E-09	1.852E-01	5.370E-01	3.868E-01	3.236E-01	-2.063E+01
30	8.819E-02	1.196E-08	4.481E-01	5.139E-01	1.556E-08	9.290E-02	7.124E-01	4.171E-01	4.237E-01	-2.110E+01
31	1.292E-01	6.995E-09	4.523E-02	9.431E-01	6.670E-09	7.725E-02	3.767E-01	3.943E-01	3.568E-01	-2.147E+01
32	5.255E-02	1.368E-10	7.907E-02	3.954E-01	7.986E-10	1.859E-01	1.553E+00	4.151E-01	4.101E-01	-2.021E+01
33	9.849E-02	3.385E-09	2.919E-01	4.463E-01	1.200E-09	1.427E-01	2.698E-01	4.349E-01	3.108E-01	-2.100E+01
34	9.053E-02	1.081E-08	7.457E-02	8.960E-01	7.207E-09	9.077E-02	1.079E+00	3.784E-01	4.395E-01	-2.162E+01
35	2.035E-02	4.618E-09	6.518E-02	8.269E-01	1.067E-08	1.631E-01	1.468E+00	3.823E-01	3.402E-01	-2.051E+01
36	7.227E-02	9.288E-09	3.464E-01	6.634E-01	9.881E-10	1.971E-02	1.277E+00	3.922E-01	3.170E-01	-2.180E+01
37	3.864E-02	7.111E-09	3.316E-02	6.227E-02	6.134E-09	9.403E-03	4.126E-01	3.894E-01	3.058E-01	-2.107E+01
38	4.888E-02	1.119E-09	9.576E-02	7.598E-01	4.617E-09	6.536E-02	1.049E+00	4.085E-01	4.099E-01	-2.029E+01
39	1.031E-01	3.905E-09	2.661E-01	8.822E-01	1.884E-09	2.835E-02	1.532E+00	3.717E-01	4.067E-01	-2.112E+01
40	4.701E-02	1.228E-08	7.826E-03	6.342E-01	1.442E-08	1.152E-01	8.155E-01	4.003E-01	3.834E-01	-2.259E+01
41	1.689E-02	3.028E-09	3.656E-01	8.111E-01	9.466E-09	2.958E-02	2.491E-01	3.775E-01	4.046E-01	-2.023E+01
42	1.994E-02	1.218E-08	3.757E-01	1.081E-01	2.577E-09	1.627E-01	1.199E+00	3.388E-01	3.639E-01	-2.120E+01
43	3.326E-03	5.150E-09	1.927E-01	8.371E-01	1.101E-08	1.090E-01	1.782E-01	4.140E-01	3.627E-01	-2.061E+01
44	1.359E-01	9.052E-10	1.171E-02	4.237E-01	6.858E-10	3.679E-02	6.056E-01	3.635E-01	3.725E-01	-2.040E+01
45	1.326E-01	7.140E-10	4.905E-01	7.660E-02	2.197E-09	1.121E-01	7.530E-01	3.748E-01	3.710E-01	-2.054E+01
46	9.242E-03	3.435E-09	3.021E-01	1.721E-02	4.856E-09	1.792E-01	1.245E+00	3.667E-01	3.543E-01	-2.398E+01
47	1.167E-01	1.019E-08	6.963E-02	2.849E-01	2.386E-09	1.724E-01	9.291E-01	4.484E-01	3.285E-01	-1.924E+01
48	1.406E-02	2.606E-09	4.659E-01	8.438E-01	1.769E-09	6.468E-03	8.594E-01	3.471E-01	3.267E-01	-2.055E+01
49	9.471E-02	9.572E-09	6.801E-02	7.736E-01	2.535E-09	1.910E-01	1.588E+00	3.309E-01	4.285E-01	-2.170E+01
50	3.147E-02	1.265E-08	6.036E-02	2.953E-01	1.106E-09	2.437E-02	2.987E-01	3.884E-01	3.672E-01	-2.173E+01
51	6.122E-02	5.379E-09	2.432E-01	7.003E-01	1.180E-11	1.356E-01	1.407E+00	4.295E-01	3.614E-01	-2.006E+01
52	2.412E-02	3.170E-09	2.522E-01	7.324E-01	3.087E-09	1.577E-02	1.628E-01	2.953E-01	4.004E-01	-2.070E+01

Table C-2. Seventy Values Sampled by LHS for 49 Parameters that Were Varied in December 1992 PA Calculations (Continued)

Material Parameter RUN NO.	BRSAT X(1)	GRCORI X(2)	GRCORHF X(3)	STOICCOR X(4)	GRMICI X(5)	GRMICHF X(6)	STOICMIC X(7)	VWOOD X(8)	VMETAL X(9)	SALPERM X(10)
53	1.190E-01	1.257E-08	8.368E-02	4.961E-01	1.480E-09	3.382E-02	6.351E-01	3.825E-01	4.589E-01	-2.033E+01
54	1.048E-01	4.903E-09	8.608E-02	9.416E-01	1.032E-08	1.952E-01	1.009E+00	4.310E-01	2.923E-01	-2.143E+01
55	6.768E-02	5.538E-09	4.791E-02	1.810E-01	1.717E-09	1.272E-01	9.388E-01	4.399E-01	3.493E-01	-2.185E+01
56	6.598E-02	6.245E-09	2.555E-02	8.643E-01	2.762E-09	1.049E-01	3.921E-01	2.840E-01	3.337E-01	-2.378E+01
57	1.244E-01	8.522E-09	1.496E-01	5.302E-01	1.922E-09	7.123E-02	1.071E+00	3.493E-01	3.502E-01	-2.141E+01
58	9.213E-02	7.530E-09	1.041E-01	9.933E-02	1.514E-08	1.209E-01	1.167E+00	3.654E-01	3.306E-01	-2.266E+01
59	1.232E-01	8.353E-09	3.593E-01	2.458E-01	1.274E-08	7.395E-02	1.512E+00	3.961E-01	3.769E-01	-2.283E+01
60	1.061E-01	4.043E-09	5.023E-02	1.658E-01	1.330E-08	1.378E-01	1.171E+00	3.709E-01	3.951E-01	-2.204E+01
61	1.108E-01	9.816E-09	2.580E-02	5.530E-01	8.393E-09	9.473E-02	1.637E+00	3.369E-01	3.007E-01	-2.097E+01
62	1.090E-01	5.998E-09	5.971E-02	2.666E-01	1.377E-10	3.802E-02	1.361E+00	3.136E-01	3.665E-01	-2.191E+01
63	4.544E-02	6.794E-09	9.919E-02	6.120E-01	2.423E-10	1.513E-01	1.073E-01	4.460E-01	3.857E-01	-2.151E+01
64	5.499E-02	4.681E-09	1.980E-02	9.927E-01	1.357E-08	1.455E-01	6.761E-01	4.375E-01	3.473E-01	-2.177E+01
65	2.810E-02	2.293E-09	1.413E-01	9.178E-01	9.936E-09	8.331E-02	5.036E-02	3.535E-01	4.544E-01	-2.081E+01
66	9.633E-02	8.857E-09	4.421E-01	1.287E-01	2.928E-09	5.813E-02	2.075E-01	4.576E-01	4.164E-01	-2.231E+01
67	5.864E-03	9.458E-09	1.858E-01	3.687E-01	8.269E-10	1.328E-01	1.136E+00	3.695E-01	3.597E-01	-2.094E+01
68	1.134E-01	2.460E-09	4.183E-02	4.695E-01	1.067E-09	1.927E-01	7.354E-02	3.347E-01	4.317E-01	-2.165E+01
69	6.604E-03	7.825E-09	4.264E-01	3.850E-01	1.472E-08	1.471E-01	8.473E-01	3.170E-01	4.200E-01	-2.159E+01
70	1.904E-03	1.351E-09	4.095E-01	3.248E-01	4.814E-10	5.544E-02	1.310E+00	4.204E-01	3.972E-01	-2.359E+01

Material Parameter RUN NO.	BCEXP X(11)	BCFLG X(12)	BCBRSAT X(13)	BCGSSAT X(14)	MBPERM X(15)	MBPOR X(16)	TZPORF X(17)	MBPRES X(18)	BPPRES X(19)	BPSTOR X(20)
1	9.679E+00	0.000E+00	8.789E-02	2.330E-01	-1.785E+01	2.866E-02	2.165E-02	1.202E+07	1.543E+07	1.947E-01
2	4.966E-01	1.000E+00	1.457E-01	1.259E-01	-1.977E+01	6.990E-03	4.764E-01	1.300E+07	1.458E+07	3.996E-01
3	6.790E-01	1.000E+00	1.849E-01	2.166E-01	-1.804E+01	2.897E-02	7.123E-01	1.260E+07	1.561E+07	1.364E-01
4	5.182E+00	1.000E+00	1.726E-01	1.890E-01	-1.930E+01	5.613E-03	9.978E-01	1.201E+07	1.511E+07	9.468E-01
5	4.071E-01	1.000E+00	1.988E-01	1.459E-01	-1.994E+01	2.056E-02	6.428E-02	1.233E+07	1.600E+07	1.657E-01
6	6.142E+00	0.000E+00	3.317E-01	4.793E-02	-1.982E+01	1.375E-02	9.602E-01	1.256E+07	2.082E+07	3.368E-01
7	1.099E+00	0.000E+00	3.543E-02	1.622E-01	-1.975E+01	2.593E-02	2.709E-01	1.245E+07	1.407E+07	2.578E-01
8	6.448E+00	1.000E+00	3.866E-01	2.852E-02	-1.874E+01	3.185E-03	5.669E-01	1.250E+07	1.874E+07	1.565E-01
9	4.261E-01	1.000E+00	3.408E-01	1.869E-01	-1.991E+01	2.727E-02	4.401E-01	1.230E+07	1.306E+07	1.483E-01
10	1.517E+00	1.000E+00	7.900E-02	3.481E-01	-1.728E+01	9.677E-03	2.896E-01	1.238E+07	1.972E+07	8.469E-02
11	5.125E-01	0.000E+00	2.717E-01	2.003E-01	-1.988E+01	2.573E-03	6.303E-01	1.227E+07	2.010E+07	8.790E-02
12	7.496E+00	1.000E+00	1.410E-01	2.862E-01	-1.865E+01	9.827E-03	5.472E-01	1.236E+07	2.097E+07	8.068E-02
13	2.249E+00	1.000E+00	3.650E-01	2.937E-01	-1.931E+01	1.661E-02	7.349E-02	1.277E+07	1.845E+07	7.603E-01
14	3.062E-01	1.000E+00	8.366E-03	1.736E-01	-2.000E+01	1.960E-02	4.472E-01	1.272E+07	1.683E+07	4.436E-02
15	4.462E-01	0.000E+00	2.310E-01	3.835E-01	-1.968E+01	1.159E-03	8.622E-01	1.279E+07	1.535E+07	4.805E-02
16	5.359E-01	1.000E+00	3.789E-01	2.172E-01	-1.829E+01	5.870E-03	7.594E-01	1.220E+07	1.357E+07	2.458E-01
17	5.919E+00	0.000E+00	1.113E-01	3.806E-01	-1.924E+01	2.395E-02	8.442E-01	1.297E+07	1.803E+07	1.258E-01
18	5.873E-01	0.000E+00	2.947E-01	8.612E-03	-1.918E+01	6.137E-03	3.866E-01	1.248E+07	2.042E+07	1.308E-01
19	2.005E+00	1.000E+00	1.164E-01	1.667E-01	-1.934E+01	6.255E-03	7.942E-01	1.286E+07	2.047E+07	3.845E-01
20	6.709E-01	1.000E+00	1.294E-01	3.211E-01	-1.935E+01	1.707E-02	7.418E-01	1.295E+07	1.817E+07	3.349E-01
21	2.259E-01	0.000E+00	1.977E-02	2.233E-01	-1.894E+01	2.350E-02	2.158E-01	1.207E+07	1.961E+07	1.515E-01
22	1.434E+00	1.000E+00	2.183E-01	1.871E-02	-1.913E+01	2.603E-02	7.201E-01	1.216E+07	1.990E+07	1.931E+00
23	7.099E+00	1.000E+00	2.388E-01	4.523E-02	-1.945E+01	2.992E-02	8.192E-01	1.210E+07	1.929E+07	1.816E-01

Table C-2. Seventy Values Sampled by LHS for 49 Parameters that Were Varied in December 1992 PA Calculations (Continued)

Material Parameter RUN NO.	BCEXP X(11)	BCFLG X(12)	BCBRSAT X(13)	BCGSSAT X(14)	MBPERM X(15)	MBPOR X(16)	TZPORF X(17)	MBPRES X(18)	BPPRES X(19)	BPSTOR X(20)
24	4.327E-01	1.000E+00	6.127E-02	2.643E-01	-1.921E+01	1.471E-02	1.909E-01	1.243E+07	2.006E+07	3.497E-02
25	2.761E+00	1.000E+00	3.051E-01	9.990E-02	-1.949E+01	2.472E-02	8.779E-01	1.214E+07	1.379E+07	5.503E-01
26	5.266E+00	1.000E+00	2.470E-01	6.806E-02	-1.962E+01	1.882E-02	8.054E-01	1.252E+07	1.490E+07	3.907E-02
27	8.333E+00	1.000E+00	2.128E-01	7.573E-02	-1.966E+01	2.274E-03	4.993E-01	1.268E+07	1.773E+07	8.291E-01
28	7.946E+00	0.000E+00	3.474E-01	1.527E-01	-1.971E+01	2.883E-03	2.091E-01	1.219E+07	1.793E+07	2.722E-01
29	6.041E-01	1.000E+00	3.304E-01	3.578E-01	-1.951E+01	1.268E-02	1.152E-01	1.277E+07	1.382E+07	1.189E-01
30	2.004E-01	0.000E+00	1.405E-02	1.553E-01	-1.913E+01	8.791E-03	9.132E-01	1.221E+07	1.566E+07	3.610E-01
31	3.316E-01	1.000E+00	2.113E-01	2.405E-01	-2.049E+01	1.765E-02	3.827E-01	1.212E+07	1.887E+07	5.362E-02
32	8.880E+00	1.000E+00	3.143E-01	3.755E-01	-1.998E+01	2.093E-02	9.418E-01	1.257E+07	1.428E+07	7.034E-02
33	5.220E-01	1.000E+00	1.053E-01	3.419E-01	-1.833E+01	6.664E-03	9.820E-01	1.206E+07	1.853E+07	1.092E-01
34	8.652E+00	0.000E+00	2.515E-01	3.628E-01	-1.991E+01	9.103E-03	5.828E-01	1.224E+07	1.398E+07	2.319E-01
35	3.947E-01	1.000E+00	2.907E-01	1.339E-01	-1.955E+01	2.423E-03	7.825E-01	1.218E+07	1.786E+07	6.246E-02
36	2.750E-01	1.000E+00	3.709E-01	3.696E-01	-1.970E+01	2.712E-02	6.279E-01	1.241E+07	2.056E+07	2.884E-01
37	6.978E+00	1.000E+00	2.265E-01	3.079E-02	-1.959E+01	5.096E-03	5.286E-01	1.270E+07	1.767E+07	9.572E-02
38	2.964E+00	1.000E+00	1.781E-01	3.962E-01	-1.882E+01	1.894E-03	6.447E-01	1.243E+07	1.447E+07	1.412E-01
39	2.606E-01	1.000E+00	1.633E-01	3.724E-02	-1.925E+01	1.009E-02	6.724E-01	1.283E+07	1.635E+07	2.122E-01
40	2.416E-01	1.000E+00	2.434E-01	1.110E-01	-1.868E+01	2.276E-02	1.097E-01	1.254E+07	1.504E+07	7.721E-02
41	5.749E-01	1.000E+00	1.334E-01	1.065E-01	-1.840E+01	1.802E-02	1.518E-01	1.251E+07	1.475E+07	2.549E-01
42	5.484E-01	0.000E+00	3.964E-01	3.350E-01	-2.063E+01	2.199E-02	4.115E-01	1.274E+07	1.581E+07	7.030E-01
43	4.000E+00	0.000E+00	3.907E-01	1.204E-01	-1.857E+01	5.179E-03	4.205E-01	1.227E+07	1.588E+07	6.006E-02
44	3.605E-01	0.000E+00	2.598E-01	5.735E-02	-1.927E+01	3.901E-03	2.482E-01	1.208E+07	1.462E+07	6.582E-01
45	3.239E-01	1.000E+00	1.583E-01	9.419E-02	-1.901E+01	9.387E-03	2.787E-01	1.265E+07	1.361E+07	1.209E-01
46	4.606E-01	1.000E+00	6.517E-02	2.388E-01	-1.978E+01	2.828E-02	8.963E-01	1.232E+07	1.897E+07	4.544E-01
47	3.476E+00	1.000E+00	3.178E-01	2.606E-01	-1.904E+01	6.570E-03	1.412E-01	1.293E+07	1.648E+07	5.341E-01
48	7.708E+00	0.000E+00	4.551E-02	2.075E-01	-1.985E+01	2.239E-02	9.268E-01	1.288E+07	1.940E+07	1.113E-01
49	3.753E-01	1.000E+00	5.011E-02	6.990E-02	-1.816E+01	1.682E-03	9.470E-01	1.229E+07	1.415E+07	1.703E-01
50	3.539E-01	1.000E+00	1.899E-01	1.985E-01	-1.961E+01	1.289E-02	6.970E-01	1.266E+07	1.318E+07	2.231E-01
51	5.600E-01	1.000E+00	2.318E-02	1.181E-02	-1.639E+01	7.844E-03	3.078E-01	1.293E+07	1.631E+07	6.020E-01
52	3.237E+00	0.000E+00	1.504E-01	3.886E-01	-1.906E+01	4.713E-03	7.463E-01	1.297E+07	1.716E+07	1.251E+00
53	6.741E+00	1.000E+00	2.847E-01	1.806E-01	-1.811E+01	1.590E-02	3.382E-01	1.263E+07	1.731E+07	2.000E-02
54	4.720E-01	0.000E+00	1.659E-01	2.729E-01	-1.984E+01	1.450E-02	3.559E-01	1.259E+07	1.982E+07	1.000E-01
55	6.503E-01	0.000E+00	3.245E-01	3.033E-01	-1.699E+01	2.003E-02	5.037E-01	1.247E+07	1.689E+07	3.050E-01
56	4.848E+00	0.000E+00	9.277E-02	5.221E-02	-1.996E+01	1.165E-02	8.402E-01	1.276E+07	1.336E+07	3.112E-01
57	9.211E+00	1.000E+00	5.116E-03	2.777E-01	-2.028E+01	4.563E-03	4.489E-02	1.210E+07	1.907E+07	4.921E-01
58	6.406E-01	1.000E+00	3.488E-01	3.298E-01	-1.847E+01	8.711E-03	3.184E-01	1.239E+07	1.937E+07	2.852E-01
59	8.958E+00	1.000E+00	8.512E-02	3.127E-01	-1.910E+01	2.516E-02	9.379E-02	1.269E+07	1.711E+07	4.277E-01
60	9.862E+00	1.000E+00	7.038E-02	8.194E-02	-1.902E+01	8.260E-03	6.020E-01	1.283E+07	1.526E+07	2.881E-02
61	8.049E-01	1.000E+00	2.791E-01	1.389E-01	-1.938E+01	7.384E-03	1.695E-01	1.216E+07	1.835E+07	1.518E+00
62	2.863E-01	1.000E+00	3.599E-01	2.512E-01	-1.826E+01	1.225E-02	3.707E-01	1.289E+07	1.748E+07	1.920E-01
63	3.754E+00	0.000E+00	2.001E-01	2.836E-01	-1.602E+01	4.109E-03	6.620E-01	1.225E+07	1.616E+07	1.739E-01
64	2.495E+00	1.000E+00	2.932E-02	8.702E-02	-1.957E+01	3.739E-03	4.692E-01	1.285E+07	1.739E+07	4.756E-01
65	2.541E-01	1.000E+00	2.641E-01	3.510E-01	-1.943E+01	7.470E-03	5.998E-01	1.280E+07	2.072E+07	3.755E-01
66	6.915E-01	0.000E+00	1.238E-01	3.163E-01	-1.940E+01	3.533E-03	3.140E-03	1.236E+07	1.671E+07	1.027E+00
67	5.589E+00	0.000E+00	5.635E-02	2.537E-01	-1.886E+01	8.191E-03	2.424E-01	1.258E+07	1.326E+07	2.200E-01
68	4.520E+00	0.000E+00	3.024E-01	2.997E-01	-1.917E+01	1.076E-02	5.214E-01	1.263E+07	2.026E+07	2.027E-01

Table C-2. Seventy Values Sampled by LHS for 49 Parameters that Were Varied in December 1992 PA Calculations (Continued)

Material Parameter RUN NO.	BCEXP X(11)	BCFLG X(12)	BCBRSAT X(13)	BCGSSAT X(14)	MBPERM X(15)	MBPOR X(16)	TZPORF X(17)	MBPRES X(18)	BPPRES X(19)	BPSTOR X(20)
69	4.327E+00	1.000E+00	3.715E-01	4.839E-03	-1.948E+01	1.519E-02	1.780E-01	1.291E+07	1.658E+07	6.938E-02
70	6.277E-01	1.000E+00	1.013E-01	1.192E-01	-2.087E+01	1.489E-03	3.635E-02	1.203E+07	1.862E+07	1.034E-01

Material Parameter RUN NO.	BHPERM X(21)	DBDIAM X(22)	LAMBDA X(23)	BPAREAFR X(24)	SOLAM X(25)	SOLNP X(26)	SOLPU X(27)	SOLRA X(28)	SOLTH X(29)	SOLU X(30)
1	3.223E-13	4.087E-01	6.459E-01	2.756E-01	-9.664E+00	-9.454E+00	-8.853E+00	1.256E+00	-5.739E+00	-2.746E-01
2	2.683E-13	3.780E-01	3.485E-01	3.806E-01	-9.123E+00	-1.513E+01	-1.368E+01	1.094E+00	-6.470E+00	-3.643E+00
3	2.054E-13	4.214E-01	2.818E-01	3.888E-01	-9.693E+00	-6.185E+00	-1.359E+01	1.248E+00	-1.132E+01	-2.513E+00
4	1.000E-11	3.908E-01	6.879E-01	3.087E-01	-6.752E+00	-1.192E+01	-8.339E+00	1.110E+00	-1.138E+01	-5.123E+00
5	4.051E-12	2.788E-01	2.059E-01	2.964E-01	-8.758E+00	-6.916E+00	-6.509E+00	9.393E-01	-1.046E+01	-4.858E+00
6	2.328E-13	3.668E-01	4.707E-01	4.151E-01	-9.320E+00	-5.710E+00	-5.862E+00	1.251E+00	-6.704E+00	-4.508E+00
7	1.257E-12	4.100E-01	3.375E-02	4.445E-01	-9.300E+00	-4.863E+00	-7.801E+00	1.132E+00	-1.019E+01	-6.874E+00
8	7.713E-12	2.949E-01	1.731E-01	4.110E-01	-6.699E+00	-7.652E+00	-1.235E+01	1.043E+00	-9.188E+00	-4.763E+00
9	9.434E-14	2.762E-01	9.720E-01	4.628E-01	-9.277E+00	-1.019E+01	-1.045E+01	5.121E-01	-6.572E+00	-3.402E+00
10	1.322E-12	3.603E-01	4.759E-01	4.793E-01	-9.613E+00	-6.526E+00	-1.172E+01	1.107E+00	-9.756E+00	-2.987E+00
11	3.378E-14	3.320E-01	7.262E-01	3.501E-01	-1.740E+00	-4.591E+00	-1.193E+01	9.632E-01	-8.166E+00	-2.066E+00
12	2.016E-12	3.950E-01	6.321E-01	3.695E-01	-1.012E+01	-9.369E+00	-1.019E+01	1.015E+00	-1.068E+01	-1.081E+01
13	8.206E-14	4.189E-01	9.091E-01	2.689E-01	-9.926E+00	-3.360E+00	-8.118E+00	1.127E+00	-1.212E+01	-1.980E+00
14	1.646E-12	3.416E-01	7.358E-01	4.108E-01	-4.602E+00	-7.190E+00	-1.475E+01	1.234E+00	-7.740E+00	-2.399E+00
15	1.042E-12	3.357E-01	5.136E-01	4.016E-01	-6.398E+00	-9.919E+00	-1.062E+01	1.072E+00	-1.095E+01	-2.817E+00
16	8.788E-14	2.932E-01	1.927E-01	3.455E-01	-6.618E-01	-2.674E+00	-6.321E+00	1.258E+00	-9.910E+00	-2.327E+00
17	2.761E-13	2.847E-01	6.611E-01	3.468E-01	-1.019E+01	-6.337E+00	-1.081E+01	1.176E+00	-1.523E+01	-1.339E+01
18	2.585E-12	3.234E-01	9.689E-01	4.896E-01	-7.632E+00	-1.428E+01	-8.256E+00	1.163E+00	-1.444E+01	-4.146E+00
19	2.966E-13	4.262E-01	7.876E-01	4.204E-01	-4.225E+00	-2.066E+00	-7.325E+00	1.028E+00	-7.944E+00	-4.375E+00
20	2.257E-13	3.390E-01	2.651E-02	3.653E-01	-9.898E+00	-7.503E+00	-8.882E+00	9.832E-01	-9.571E+00	-4.058E+00
21	2.489E-13	3.090E-01	4.326E-01	3.356E-01	-1.027E+01	-5.897E+00	-7.599E+00	9.884E-01	-1.420E+01	-4.687E+00
22	8.276E-13	4.158E-01	4.229E-01	4.176E-01	-4.820E+00	-6.835E+00	-1.555E+01	8.333E-01	-1.376E+01	-1.781E+00
23	1.624E-13	3.058E-01	5.226E-01	4.589E-01	-9.760E+00	-5.568E+00	-6.234E+00	6.281E-01	-7.353E+00	-6.526E+00
24	3.118E-13	2.804E-01	8.593E-01	3.926E-01	-5.607E+00	-3.709E+00	-9.050E+00	1.057E+00	-6.334E+00	-6.016E+00
25	1.708E-13	4.326E-01	5.463E-01	3.837E-01	-1.132E+01	-5.467E+00	-7.503E+00	8.892E-01	-1.154E+01	-2.181E+00
26	4.007E-13	2.697E-01	3.010E-01	3.538E-01	-8.257E+00	-5.816E+00	-7.110E+00	1.242E+00	-9.030E+00	-2.048E+00
27	6.130E-13	2.689E-01	7.530E-01	3.966E-01	-9.486E+00	-8.816E+00	-1.518E+01	1.228E+00	-1.120E+01	-3.036E+00
28	8.499E-13	3.707E-01	2.271E-01	3.336E-01	-1.403E+00	-7.086E+00	-1.454E+01	8.135E-01	-1.045E+01	-2.485E+00
29	3.628E-13	3.340E-01	8.769E-01	3.255E-01	-8.532E+00	-1.355E+01	-7.762E+00	7.736E-01	-7.196E+00	-3.542E+00
30	1.334E-13	4.280E-01	4.486E-01	4.236E-01	-2.966E+00	-8.271E+00	-9.508E+00	9.546E-01	-1.185E+01	-2.299E+00
31	5.200E-13	3.932E-01	5.816E-02	5.669E-01	-9.447E+00	-9.102E+00	-1.500E+01	9.722E-01	-1.244E+01	-1.965E-01
32	3.473E-13	4.428E-01	4.029E-01	4.427E-01	-3.580E+00	-7.308E+00	-8.633E+00	6.622E-01	-1.335E+01	-7.758E+00
33	7.358E-14	2.877E-01	5.914E-01	3.673E-01	-1.004E+01	-6.684E+00	-8.610E+00	4.520E-01	-6.046E+00	-2.560E+00
34	4.264E-13	3.581E-01	8.248E-01	4.057E-01	-9.162E+00	-7.894E+00	-1.409E+01	1.201E+00	-8.763E+00	-3.749E+00
35	1.422E-13	3.740E-01	8.017E-02	4.330E-01	-1.107E+01	-7.348E+00	-1.591E+01	1.156E+00	-5.862E+00	-3.444E+00
36	2.846E-14	3.194E-01	9.552E-02	3.818E-01	-9.405E+00	-6.590E+00	-1.488E+01	1.100E+00	-1.110E+01	-5.092E+00
37	2.197E-14	3.832E-01	4.946E-01	3.291E-01	-9.817E+00	-1.154E+01	-4.335E+00	6.835E-01	-9.880E+00	-2.416E+00
38	9.957E-14	2.975E-01	3.215E-01	4.661E-01	-1.017E+01	-4.659E+00	-9.720E+00	1.171E+00	-1.299E+01	-1.695E+00

Table C-2. Seventy Values Sampled by LHS for 49 Parameters that Were Varied in December 1992 PA Calculations (Continued)

Material Parameter RUN NO.	BHPERM X(21)	DBDIAM X(22)	LAMBDA X(23)	BPAREAFR X(24)	SOLAM X(25)	SOLNP X(26)	SOLPU X(27)	SOLRA X(28)	SOLTH X(29)	SOLU X(30)
39	4.797E-12	4.398E-01	2.449E-01	2.877E-01	-9.050E+00	-5.345E+00	-9.307E+00	1.005E+00	-7.002E+00	-6.833E-01
40	2.160E-12	3.635E-01	7.612E-01	4.456E-01	-7.907E+00	-5.953E+00	-1.108E+01	1.206E+00	-1.209E+01	-5.830E+00
41	4.710E-13	2.826E-01	7.731E-01	4.525E-01	-8.640E-01	-5.218E+00	-1.290E+01	5.719E-01	-7.589E+00	-4.022E+00
42	3.221E-12	2.914E-01	6.280E-01	4.486E-01	-1.000E+01	-3.013E+00	-6.828E+00	3.350E-01	-8.923E+00	-1.357E+00
43	6.646E-14	3.968E-01	1.669E-01	3.749E-01	-3.156E+00	-6.788E+00	-6.742E+00	9.415E-01	-1.455E+01	-5.469E+00
44	5.226E-14	3.016E-01	9.254E-01	4.166E-01	-9.232E+00	-2.260E+00	-9.871E+00	1.183E+00	-1.163E+01	-5.276E+00
45	3.887E-13	4.034E-01	8.107E-01	3.986E-01	-9.006E+00	-8.645E+00	-6.077E+00	1.139E+00	-1.076E+01	-6.340E+00
46	5.483E-13	3.114E-01	3.988E-01	4.273E-01	-5.388E+00	-1.470E+01	-7.027E+00	1.189E+00	-1.291E+01	-1.213E+00
47	1.802E-12	4.134E-01	9.369E-01	4.336E-01	-9.372E+00	-5.527E+00	-9.985E+00	1.221E+00	-1.023E+01	-2.244E+00
48	1.023E-12	3.883E-01	9.918E-01	3.872E-01	-6.016E+00	-8.125E+00	-1.224E+01	1.087E+00	-1.010E+01	-1.434E+00
49	2.071E-13	3.150E-01	9.525E-01	3.422E-01	-1.204E+01	-7.061E+00	-1.088E+01	3.447E-01	-1.391E+01	-2.114E+00
50	1.146E-13	4.051E-01	5.620E-02	3.920E-01	-7.225E+00	-8.524E+00	-9.635E+00	1.244E+00	-1.345E+01	-6.980E+00
51	1.853E-13	3.150E-01	1.018E-01	3.712E-01	-8.886E+00	-1.039E+01	-9.217E+00	9.675E-01	-8.234E+00	-5.521E+00
52	7.378E-13	3.024E-01	3.290E-01	5.479E-01	-8.310E+00	-5.064E+00	-7.013E+00	1.027E+00	-7.531E+00	-2.687E+00
53	1.754E-13	3.516E-01	6.830E-01	4.295E-01	-2.568E+00	-1.001E+01	-5.636E+00	1.001E+00	-1.179E+01	-1.011E+00
54	9.068E-13	3.851E-01	8.436E-01	3.540E-01	-3.924E+00	-5.136E+00	-5.334E+00	1.147E+00	-1.430E+01	-2.736E+00
55	6.937E-13	3.293E-01	2.628E-01	4.032E-01	-2.032E+00	-9.169E+00	-6.906E+00	9.326E-01	-1.272E+01	-6.019E-01
56	5.605E-14	3.612E-01	8.309E-01	3.399E-01	-9.552E+00	-7.756E+00	-1.117E+01	1.121E+00	-9.535E+00	-4.278E+00
57	4.087E-14	3.450E-01	5.791E-01	4.975E-01	-6.351E+00	-1.010E+01	-7.276E+00	8.800E-01	-1.491E+01	-3.903E+00
58	1.125E-12	4.304E-01	6.134E-01	4.375E-01	-1.283E+01	-9.544E+00	-6.632E+00	5.178E-01	-7.088E+00	-6.654E+00
59	1.049E-13	3.476E-01	5.638E-01	2.559E-01	1.125E-01	-5.750E+00	-1.640E+01	4.217E-01	-9.366E+00	-6.291E+00
60	6.800E-13	3.257E-01	1.180E-01	4.259E-01	-1.181E+01	-3.981E+00	-9.468E+00	1.061E+00	-9.261E+00	-1.105E+00
61	1.546E-14	3.212E-01	2.890E-01	4.622E-01	-5.153E+00	-1.252E+01	-8.405E+00	1.251E+00	-6.910E+00	-3.247E+00
62	1.214E-13	4.239E-01	3.673E-01	3.780E-01	-8.009E+00	-8.928E+00	-1.122E+01	7.132E-01	-8.726E+00	-1.871E+00
63	1.511E-13	4.346E-01	7.078E-01	5.198E-01	-6.916E+00	-6.103E+00	-1.306E+01	1.012E+00	-7.818E+00	-6.161E+00
64	6.340E-14	3.483E-01	1.539E-01	4.396E-01	-5.982E+00	-6.030E+00	-3.565E+00	7.319E-01	-8.564E+00	-1.593E+00
65	4.483E-14	4.005E-01	8.983E-01	4.081E-01	-7.295E+00	-1.526E+01	-6.406E+00	1.212E+00	-8.355E+00	-3.795E+00
66	6.107E-13	3.543E-01	3.857E-01	3.620E-01	-1.288E+01	-6.225E+00	-1.052E+01	1.037E+00	-1.481E+01	-1.535E+00
67	1.434E-12	3.734E-01	1.422E-01	5.376E-01	-7.557E+00	-8.103E+00	-5.464E+00	9.945E-01	-8.466E+00	-3.316E+00
68	5.128E-13	2.726E-01	9.745E-03	3.596E-01	-9.110E+00	-9.712E+00	-1.028E+01	9.491E-01	-1.091E+01	-3.105E+00
69	1.000E-14	3.795E-01	5.364E-01	4.543E-01	-1.038E+01	-6.366E+00	-1.533E+01	1.050E+00	-1.503E+01	-2.625E+00
70	4.531E-13	4.387E-01	2.411E-01	3.577E-01	-9.599E+00	-6.020E+00	-7.968E+00	1.078E+00	-6.183E+00	-5.649E+00

Material Parameter RUN NO.	CULTRFLD X(31)	CULCLIM X(32)	CULFRPOR X(33)	CULFRSP X(34)	CULCLYF X(35)	CULCLYP X(36)	FKDAM X(37)	FKDNP X(38)	FKDPU X(39)	FKDTH X(40)
1	3.689E-01	1.347E-01	1.307E-03	3.149E+00	0.000E+00	9.844E-02	2.100E+00	-2.194E-01	1.137E+00	-1.263E+00
2	4.068E-01	5.823E-01	1.356E-03	1.078E-01	1.848E-01	4.169E-01	2.284E-01	-2.437E+00	2.874E+00	-3.127E+00
3	6.714E-01	8.879E-01	3.436E-03	3.478E-01	0.000E+00	3.011E-01	-9.079E-01	2.591E+00	-9.157E-01	9.695E-01
4	5.721E-01	3.106E-01	2.102E-03	4.629E+00	0.000E+00	2.892E-01	2.045E+00	-2.084E+00	2.942E+00	-7.889E-01
5	4.952E-01	5.394E-01	2.416E-03	7.314E+00	4.601E-01	4.119E-01	2.249E+00	2.370E+00	-1.004E-01	-1.208E+00
6	9.702E-01	1.115E-01	1.000E-02	6.791E+00	0.000E+00	1.458E-01	3.185E-01	1.058E+00	2.723E-01	3.758E-01
7	2.787E-01	2.758E-01	3.077E-04	3.104E-01	0.000E+00	3.002E-01	-2.487E-02	2.917E+00	2.668E+00	-2.930E+00
8	9.213E-01	7.240E-01	2.443E-04	1.133E-01	0.000E+00	2.134E-01	8.402E-01	2.522E+00	2.572E+00	2.835E-01

Table C-2. Seventy Values Sampled by LHS for 49 Parameters that Were Varied in December 1992 PA Calculations (Continued)

Material Parameter RUN NO.	CULTRFLD X(31)	CULCLIM X(32)	CULFRPOR X(33)	CULFRSP X(34)	CULCLYF X(35)	CULCLYP X(36)	FKDAM X(37)	FKDNP X(38)	FKDPU X(39)	FKDTH X(40)
9	6.322E-01	8.636E-01	1.471E-03	5.667E-01	0.000E+00	1.050E-01	1.631E-01	-2.822E+00	2.830E+00	-2.469E+00
10	8.899E-01	1.227E-01	3.077E-03	4.288E+00	2.777E-01	6.018E-02	2.138E+00	-3.622E+00	8.307E-01	-1.198E+00
11	9.365E-01	9.966E-01	4.324E-04	2.807E+00	0.000E+00	8.102E-02	9.633E-01	6.463E-02	-1.486E-02	-3.422E+00
12	9.128E-03	9.358E-01	3.571E-03	3.387E-01	8.276E-02	1.836E-01	2.314E+00	4.235E-01	6.207E-01	-1.693E+00
13	8.782E-01	9.174E-01	1.844E-03	9.675E-02	5.057E-02	1.946E-01	5.097E-01	-2.184E+00	2.114E+00	-1.676E+00
14	5.275E-01	7.538E-03	1.275E-03	2.589E+00	0.000E+00	4.739E-01	2.839E+00	2.420E-01	2.413E+00	5.278E-01
15	6.464E-02	4.629E-01	1.944E-03	3.750E+00	0.000E+00	4.237E-01	-1.944E+00	-2.335E+00	9.381E-02	3.394E-01
16	1.002E-01	5.997E-01	1.175E-03	3.312E-01	2.076E-01	2.446E-01	5.779E-01	-2.194E+00	2.888E+00	-1.085E+00
17	6.130E-01	5.713E-01	7.672E-04	2.635E-01	0.000E+00	3.395E-01	2.747E+00	2.686E+00	2.362E+00	-3.245E+00
18	7.468E-02	6.964E-01	9.308E-04	1.853E-01	6.629E-02	2.409E-01	2.077E+00	-2.010E+00	2.601E+00	8.519E-01
19	1.358E-01	6.647E-01	1.098E-03	2.927E-01	0.000E+00	4.047E-01	2.198E-02	-2.068E+00	8.928E-01	-2.913E+00
20	3.055E-01	4.519E-01	1.292E-04	8.809E-01	0.000E+00	1.478E-01	1.851E+00	1.662E-01	1.407E+00	7.119E-01
21	8.639E-01	6.504E-01	2.871E-03	1.981E-01	3.766E-02	4.654E-01	-3.934E-01	-2.127E+00	2.931E+00	7.650E-01
22	7.117E-01	5.489E-01	2.659E-04	1.685E-01	4.767E-01	4.013E-01	4.069E-01	-3.252E+00	-3.630E+00	-1.514E+00
23	5.492E-02	3.609E-01	1.427E-03	3.799E-01	1.475E-01	4.972E-01	7.533E-02	-2.254E+00	2.708E+00	2.400E-01
24	1.891E-01	6.105E-01	1.817E-03	1.610E-01	1.991E-01	2.791E-01	2.266E+00	5.886E-01	1.633E+00	-1.903E+00
25	3.704E-02	6.827E-01	1.701E-03	2.060E+00	0.000E+00	3.211E-01	2.672E+00	-7.864E-01	3.397E-01	-1.060E+00
26	8.072E-01	9.053E-01	5.944E-04	6.057E+00	0.000E+00	3.680E-01	2.443E+00	-1.975E+00	9.984E-01	-1.099E+00
27	5.662E-01	5.105E-01	2.522E-03	2.364E-01	1.629E-01	3.630E-01	1.231E+00	4.460E-01	7.365E-01	-3.938E+00
28	3.500E-01	2.168E-02	4.626E-03	6.637E-02	0.000E+00	3.145E-01	2.718E+00	1.864E+00	4.774E-01	-1.348E-01
29	4.453E-01	8.028E-01	3.027E-03	3.953E-01	3.330E-01	3.569E-01	2.403E+00	6.590E-01	1.783E-01	5.844E-01
30	6.472E-01	6.217E-01	2.274E-03	1.219E-01	3.679E-01	1.395E-01	2.930E+00	2.308E+00	9.142E-01	-1.227E+00
31	5.367E-01	9.768E-01	2.613E-03	5.169E+00	0.000E+00	3.088E-01	2.522E+00	7.498E-01	2.739E+00	-1.021E+00
32	9.048E-01	2.698E-01	5.894E-03	3.207E-01	0.000E+00	1.097E-01	2.592E+00	2.081E+00	2.497E+00	-2.254E+00
33	3.218E-01	4.387E-02	1.839E-04	1.555E+00	2.868E-01	2.228E-01	2.881E+00	-2.390E+00	2.392E+00	-1.016E+00
34	1.817E-01	8.466E-01	1.000E-04	2.277E-01	0.000E+00	4.303E-01	2.487E+00	-1.119E+00	1.944E+00	1.410E-01
35	7.374E-01	2.333E-01	6.994E-04	4.443E+00	0.000E+00	2.647E-01	-3.894E+00	1.026E+00	2.295E+00	-1.050E+00
36	1.243E-01	1.795E-01	6.654E-04	7.070E-02	0.000E+00	2.275E-01	1.335E-01	1.244E+00	2.764E+00	-1.181E+00
37	8.156E-01	3.528E-01	4.016E-03	1.444E-01	4.450E-01	1.561E-01	-7.678E-02	2.211E+00	2.445E+00	4.460E-01
38	5.551E-01	6.568E-02	2.028E-03	1.945E-01	2.488E-01	4.386E-01	9.195E-02	1.654E+00	-1.884E+00	-5.709E-01
39	3.355E-01	4.421E-01	1.546E-03	1.212E+00	9.509E-02	4.534E-01	1.803E-02	-1.891E+00	2.347E+00	-1.297E+00
40	4.853E-01	2.227E-01	1.024E-03	3.612E-01	2.600E-01	5.556E-02	1.870E-01	-1.825E+00	-1.014E+00	-1.241E+00
41	7.923E-01	9.005E-02	8.515E-04	2.800E-01	0.000E+00	7.060E-02	2.380E+00	2.798E+00	2.860E+00	-5.004E-02
42	2.366E-01	1.481E-01	6.353E-04	2.144E-01	0.000E+00	9.389E-02	4.665E-01	-1.735E+00	-2.685E+00	1.949E-01
43	3.907E-01	1.870E-01	5.579E-04	7.386E+00	0.000E+00	4.771E-01	7.765E-01	-2.771E+00	4.188E-02	-3.708E+00
44	8.378E-01	3.195E-01	4.624E-04	1.368E+00	4.333E-01	4.610E-01	2.579E+00	1.145E+00	2.462E+00	-6.334E-01
45	1.691E-01	1.642E-01	6.700E-04	2.524E-01	0.000E+00	1.320E-01	2.417E+00	-2.508E+00	-1.200E+00	-7.496E-01
46	6.676E-01	7.674E-01	7.987E-04	4.783E+00	3.280E-01	3.349E-01	2.187E+00	1.785E+00	2.487E+00	-3.650E+00
46	6.676E-01	7.674E-01	7.987E-04	4.783E+00	3.280E-01	3.349E-01	2.187E+00	1.785E+00	2.487E+00	-3.650E+00
47	4.224E-01	4.110E-01	3.989E-04	7.852E+00	3.862E-01	1.763E-01	2.562E-01	1.966E+00	2.994E+00	-1.274E+00
48	4.385E-01	3.782E-01	3.626E-04	6.452E+00	4.207E-01	2.578E-01	2.232E+00	8.375E-01	5.452E-01	-2.831E-01
49	7.578E-01	7.722E-01	8.756E-04	6.025E+00	0.000E+00	2.700E-01	3.579E-01	2.455E+00	7.299E-01	-1.713E-01
50	7.210E-01	5.186E-01	6.171E-04	3.304E+00	4.881E-01	1.261E-01	2.692E+00	-3.413E+00	4.172E-01	1.715E-02
51	6.205E-01	8.187E-01	1.611E-03	1.823E+00	0.000E+00	1.619E-01	1.977E+00	-1.950E+00	6.136E-01	-2.148E+00
52	2.939E-01	9.520E-01	6.659E-03	5.554E+00	0.000E+00	2.815E-01	2.148E+00	-2.317E+00	2.643E+00	-5.250E-01

Table C-2. Seventy Values Sampled by LHS for 49 Parameters that Were Varied in December 1992 PA Calculations (Continued)

Material Parameter RUN NO.	CULTRFLD X(31)	CULCLIM X(32)	CULFRPOR X(33)	CULFRSP X(34)	CULCLYF X(35)	CULCLYP X(36)	FKDAM X(37)	FKDNP X(38)	FKDPU X(39)	FKDTH X(40)
53	8.836E-02	2.940E-01	3.815E-04	1.281E-01	1.084E-01	3.886E-01	5.221E-02	2.020E+00	2.314E+00	-2.400E+00
54	9.512E-01	6.366E-01	3.283E-04	1.501E-01	0.000E+00	2.107E-01	2.027E+00	-3.932E+00	2.908E+00	7.848E-01
55	3.754E-01	7.419E-01	3.014E-04	5.735E+00	0.000E+00	1.989E-01	-2.214E+00	2.865E+00	2.704E+00	-9.494E-01
56	2.569E-01	2.058E-01	4.414E-04	2.211E-01	2.312E-02	1.147E-01	-3.157E+00	-1.324E+00	2.754E+00	-1.159E+00
57	7.443E-01	7.629E-02	1.070E-03	7.231E-01	0.000E+00	2.526E-01	-2.999E+00	-2.543E+00	2.387E+00	-1.126E+00
58	9.975E-01	4.856E-01	2.223E-04	2.199E+00	0.000E+00	4.464E-01	2.769E+00	1.453E+00	1.758E+00	-2.715E+00
59	5.879E-01	7.044E-01	9.522E-04	7.052E+00	1.229E-01	3.820E-01	6.146E-01	-1.870E+00	1.317E+00	9.363E-01
60	8.512E-01	7.893E-01	5.273E-04	8.214E-02	7.808E-03	3.472E-01	2.981E+00	-2.593E+00	2.662E+00	-6.702E-01
61	5.085E-01	7.507E-01	1.630E-03	3.520E-01	0.000E+00	3.738E-01	2.954E+00	1.567E+00	-4.994E-01	6.040E-01
62	6.872E-01	3.605E-02	4.837E-03	3.871E-01	2.159E-01	4.813E-01	2.889E+00	-1.934E+00	2.976E+00	-1.117E+00
63	2.096E-01	8.759E-01	9.785E-04	2.673E-01	3.076E-01	1.873E-01	6.946E-01	-5.562E-01	2.809E+00	4.670E-02
64	1.725E-02	4.210E-01	5.152E-04	3.611E+00	4.137E-01	8.630E-02	2.810E+00	1.325E+00	2.562E+00	-2.293E-01
65	7.809E-01	3.890E-01	1.775E-04	4.006E+00	0.000E+00	3.917E-01	9.076E-01	8.677E-01	-3.815E-01	-4.160E-01
66	1.453E-01	3.381E-01	7.300E-04	2.497E+00	0.000E+00	1.719E-01	2.554E+00	3.185E-01	2.508E+00	-8.453E-01
67	9.797E-01	8.423E-01	8.231E-04	3.017E-01	3.453E-01	4.905E-01	-1.380E+00	-2.036E+00	2.246E-01	-1.144E+00
68	4.706E-01	2.480E-01	1.134E-03	6.490E+00	2.408E-01	6.800E-02	1.563E+00	-3.004E+00	2.530E+00	-9.225E-01
69	2.602E-01	4.888E-01	1.228E-03	7.588E+00	1.395E-01	3.317E-01	2.618E+00	-3.263E-01	2.790E+00	-3.250E-01
70	2.270E-01	9.583E-01	4.925E-04	5.379E+00	3.802E-01	2.334E-01	2.345E+00	1.477E+00	2.609E+00	-4.852E-01

Material Parameter RUN NO.	FKDU X(41)	FKDRA X(42)	CULPOR X(43)	MKDAM X(44)	MKDNP X(45)	MKDPU X(46)	MKDTH X(47)	MKDU X(48)	MKDRA X(49)
1	-1.973E+00	-3.324E+00	1.143E-01	-5.213E-01	-2.949E+00	1.081E+00	-2.961E+00	-9.568E-01	-7.915E-01
2	-1.328E+00	-1.909E+00	1.822E-01	-1.557E+00	-3.164E+00	-1.633E+00	-1.348E+00	-3.044E+00	-1.630E+00
3	-2.687E+00	-2.978E+00	1.726E-01	-7.160E-01	-3.525E+00	-1.898E+00	-1.997E-01	-2.512E+00	-1.828E+00
4	-2.085E+00	-1.178E+00	1.284E-01	-9.199E-01	-1.183E+00	-1.090E+00	-3.000E-02	-4.026E-01	-6.370E-01
5	-2.208E+00	-1.406E+00	1.220E-01	1.583E+00	9.019E-01	-2.061E+00	-3.493E+00	-3.570E+00	-1.886E+00
6	-2.260E+00	-3.510E+00	1.783E-01	-8.983E-01	-2.889E+00	-2.012E+00	-1.968E+00	-3.023E+00	-9.798E-01
7	-2.393E+00	-2.639E-01	1.206E-01	-4.012E-01	-3.499E+00	-1.232E+00	-1.641E+00	-6.873E-01	-5.865E-01
8	-2.150E+00	-1.846E+00	1.045E-01	1.199E+00	-3.115E+00	1.638E+00	-2.146E+00	-2.873E+00	-2.569E+00
9	-2.221E+00	-8.716E-01	1.210E-01	-8.154E-01	-3.275E+00	-2.104E+00	-8.599E-01	-1.108E+00	-1.797E+00
10	-3.274E+00	5.759E-01	1.634E-01	-9.658E-01	-1.305E+00	-1.152E+00	-2.052E+00	-3.061E+00	-3.144E+00
11	-2.008E+00	-7.792E-01	1.788E-01	9.574E-01	1.949E+00	-1.230E-01	-2.225E+00	-1.026E+00	4.770E-01
12	-1.851E+00	-1.648E+00	1.374E-01	2.117E-01	-3.437E+00	-1.792E+00	-2.029E+00	-3.787E+00	-2.693E+00
13	-2.182E+00	2.384E-01	1.115E-01	1.799E+00	-9.035E-01	-7.714E-01	-2.412E+00	-2.830E+00	-2.651E+00
14	-2.042E+00	1.483E-01	1.259E-01	8.448E-01	1.102E+00	-3.750E+00	-3.756E+00	-3.262E+00	-3.232E+00
15	-2.115E+00	-1.763E+00	1.075E-01	-3.158E-01	-2.825E+00	9.417E-01	-2.862E+00	-6.235E-01	-2.179E+00
16	-2.414E+00	-1.397E+00	1.229E-01	-5.761E-01	-7.990E-01	-3.805E+00	-3.379E+00	-1.077E+00	-9.146E-01
17	-2.479E+00	7.485E-01	1.446E-01	-3.411E+00	-1.597E+00	-8.047E-01	-2.073E+00	-1.248E+00	9.659E-01
18	-3.923E+00	-1.916E+00	1.782E-01	1.136E+00	1.558E+00	-2.176E+00	-2.169E+00	-1.131E+00	-1.056E+00
19	-2.931E+00	-1.805E+00	7.602E-02	-8.255E-01	-1.283E+00	1.113E+00	-1.008E+00	-1.291E+00	-2.474E+00
20	-2.447E+00	-1.377E+00	2.052E-01	-8.912E-01	7.450E-01	1.309E+00	-3.085E+00	-1.154E+00	-4.022E-01
21	-2.311E+00	-1.599E+00	1.050E-01	3.747E-01	-3.720E+00	6.354E-01	-2.706E+00	-3.192E+00	-3.458E+00
22	-2.899E+00	-1.306E+00	1.311E-01	-1.002E+00	-3.196E+00	-2.878E+00	-2.133E+00	-9.999E-01	-1.586E+00
23	-1.685E+00	8.752E-01	1.422E-01	-1.254E-01	1.817E+00	1.748E+00	-1.699E+00	-1.364E-02	-1.859E+00

Table C-2. Seventy Values Sampled by LHS for 49 Parameters that Were Varied in December 1992 PA Calculations (Continued)

Material Parameter RUN NO.	FKDU X(41)	FKDRA X(42)	CULPOR X(43)	MKDAM X(44)	MKDNP X(45)	MKDPU X(46)	MKDTH X(47)	MKDU X(48)	MKDRA X(49)
24	-2.521E+00	-3.915E+00	1.451E-01	-1.690E+00	-3.683E+00	-9.208E-01	-1.124E+00	-9.652E-02	-1.960E+00
25	-1.892E+00	-1.516E+00	2.034E-01	-9.375E-01	-7.844E-01	8.066E-01	-3.880E+00	-3.297E+00	-3.759E+00
26	-3.430E+00	-1.341E+00	2.078E-01	-1.197E+00	-3.990E+00	-5.145E-01	-2.781E+00	-8.614E-01	-3.628E+00
27	-2.772E+00	-2.646E+00	1.647E-01	5.074E-01	-1.389E+00	1.863E+00	-3.269E+00	-1.216E+00	-3.257E+00
28	-3.605E-01	3.550E-01	1.889E-01	-9.915E-01	-3.889E+00	-3.191E+00	-2.616E+00	-4.194E-01	-1.908E+00
29	-3.642E+00	-1.452E+00	1.554E-01	1.352E+00	1.414E+00	-2.277E-01	-1.699E-01	-3.213E+00	-1.663E-02
30	-3.740E+00	-1.223E+00	1.662E-01	-6.191E-01	-1.020E+00	-4.121E-01	-8.300E-01	-1.051E+00	-3.835E+00
31	-2.054E+00	-1.674E+00	1.020E-01	-1.088E+00	2.580E-01	-3.806E-01	-3.684E+00	-2.781E-01	-1.538E+00
32	-2.507E+00	-2.124E+00	1.224E-01	6.149E-01	-3.105E+00	4.431E-01	-1.594E+00	-2.981E+00	-3.372E+00
33	-1.874E+00	-1.948E+00	1.255E-01	6.488E-01	-2.998E+00	-2.965E+00	-1.530E+00	-1.755E+00	-2.131E+00
34	-1.930E+00	-3.411E+00	1.458E-01	-7.348E-01	-3.074E+00	-5.174E-02	-2.254E+00	-3.536E+00	-3.572E+00
35	-2.595E+00	9.350E-01	2.021E-01	1.480E+00	-2.973E+00	2.266E-01	-5.313E-01	-3.657E+00	-1.402E+00
36	-1.839E+00	-3.820E+00	1.718E-01	1.699E+00	1.430E+00	-3.356E+00	-1.291E+00	-2.961E+00	-2.790E+00
37	-1.782E+00	-5.875E-01	1.099E-01	-1.399E+00	1.651E-01	-8.768E-01	-3.588E+00	-2.193E+00	-2.627E+00
38	-6.954E-01	-1.709E+00	1.196E-01	-1.214E+00	1.700E+00	-1.769E-01	-7.181E-01	-1.951E-01	-2.348E+00
39	-1.978E+00	-3.008E+00	1.328E-01	-1.986E+00	-2.677E-01	-6.431E-01	-2.050E+00	-3.868E+00	-1.443E+00
40	-6.488E-02	-1.734E+00	1.916E-01	-9.715E-02	-1.641E+00	1.368E+00	-1.840E+00	-1.358E+00	-1.995E+00
41	-3.132E+00	-3.663E+00	1.431E-01	-1.327E+00	1.246E+00	-9.698E-02	-2.342E+00	-3.402E+00	-2.321E+00
42	-2.357E+00	-1.363E+00	9.562E-02	-1.720E+00	-3.653E+00	-1.069E+00	-9.338E-01	-3.148E+00	-1.082E+00
43	-3.325E+00	-2.766E+00	1.215E-01	-7.704E-01	-1.136E+00	-9.655E-01	-7.951E-01	-3.463E+00	-1.712E+00
44	-4.902E-01	-1.416E+00	1.593E-01	-7.772E-01	-2.918E+00	-2.830E-02	-4.897E-01	-3.887E+00	-1.778E+00
45	-2.235E+00	4.820E-01	1.617E-01	-6.506E-01	-1.814E+00	4.050E-02	-2.534E+00	-2.826E+00	-2.944E+00
46	-1.243E+00	-1.155E-01	1.368E-01	-1.034E+00	-1.854E+00	1.440E+00	-1.202E+00	-3.958E+00	-1.147E+00
47	-2.096E+00	4.563E-02	7.999E-02	-7.023E-01	-1.082E+00	-2.603E+00	-1.394E+00	-7.574E-01	-3.807E+00
48	-1.514E+00	-2.353E+00	1.462E-01	-3.391E-01	4.024E-01	6.585E-02	-6.711E-01	-7.236E-01	-1.681E+00
49	-1.889E+00	-1.526E+00	1.231E-01	-8.642E-01	-3.026E+00	-1.417E+00	-2.215E+00	-1.529E+00	-2.282E+00
50	-1.820E+00	-2.019E+00	6.405E-02	-1.943E-01	-1.213E+00	-2.758E-01	-2.114E+00	-1.265E+00	-1.226E+00
51	-1.544E-01	-1.863E+00	1.065E-01	4.152E-02	-1.058E+00	-5.830E-01	-3.304E-01	-8.211E-01	-1.732E+00
52	-6.399E-01	-1.361E+00	2.452E-01	1.529E+00	-2.852E+00	-1.575E+00	-2.016E+00	-3.086E+00	-3.108E+00
53	-2.031E+00	-1.153E+00	1.618E-01	-1.312E+00	-8.421E-01	-6.104E-01	-4.110E-01	-3.330E+00	-2.997E+00
54	-9.314E-01	-1.558E+00	2.184E-01	-1.631E+00	-1.158E+00	6.242E-01	-1.051E+00	-1.466E+00	-2.069E+00
55	-8.030E-01	-1.089E+00	1.793E-01	1.036E+00	-3.343E+00	-5.505E-01	-1.913E+00	-1.350E+00	-3.343E+00
56	-3.560E+00	-1.482E+00	1.617E-01	-8.378E-01	-8.552E-01	-1.008E+00	-2.258E+00	-1.444E+00	-3.914E+00
57	-1.935E+00	-2.511E+00	1.488E-01	-4.477E-01	-3.388E+00	-1.318E+00	-2.183E+00	-3.487E+00	-3.368E-01
58	-1.906E+00	-3.232E+00	1.784E-01	-8.554E-01	1.081E+00	-1.844E+00	-3.188E+00	-7.868E-01	-2.875E+00
59	-1.995E+00	-6.297E-01	1.409E-01	-5.343E-01	-9.310E-01	-6.923E-01	-1.757E+00	-2.086E+00	-2.843E+00
60	-2.069E+00	-1.029E+00	9.787E-02	1.958E+00	-9.753E-01	-2.254E+00	-2.489E-01	-3.758E+00	-2.014E+00
61	-2.423E+00	-2.027E-01	1.171E-01	-1.755E+00	-7.094E-01	-3.331E-01	-5.990E-01	-2.889E+00	-3.511E+00
62	-3.083E+00	-1.624E+00	1.781E-01	1.244E+00	-3.853E+00	1.945E+00	-1.480E+00	-9.237E-01	-1.283E+00
63	-2.143E+00	-1.309E+00	1.151E-01	-1.849E+00	-2.768E+00	-3.154E-01	-3.938E+00	-3.683E+00	-1.921E-01
64	-2.544E+00	-1.436E+00	1.624E-01	1.851E+00	-3.598E+00	-2.137E-01	-2.092E+00	-2.327E+00	-1.336E+00
65	-2.346E+00	-3.999E-01	1.004E-01	-1.470E-02	-3.825E+00	-1.460E+00	-2.193E+00	-1.204E+00	-3.052E+00
66	-3.859E+00	-1.793E+00	2.062E-01	-9.802E-01	-4.791E-01	-4.331E-01	-3.969E-01	-1.660E+00	-1.175E+00
67	-2.563E+00	-2.268E+00	2.387E-01	-9.478E-01	-7.412E-01	-2.326E+00	-2.288E+00	-5.709E-01	-2.441E+00
68	-2.293E+00	-1.459E+00	1.238E-01	-1.881E+00	-1.606E-01	3.982E-01	-1.149E+00	-2.917E+00	-3.971E+00
69	-1.076E+00	-1.974E+00	1.780E-01	-1.045E+00	-3.282E+00	-1.684E+00	-1.774E+00	-9.031E-01	-1.480E+00
70	-1.960E+00	-1.322E+00	1.617E-01	-1.504E+00	-1.530E+00	-4.783E-01	-7.179E-02	-1.171E+00	-3.685E+00

Table C-3 lists the ranks of samples.

Table C-3. Ranks of 70 Values Sampled

Material Parameter RUN NO.	BRSAT X(1)	GRCORI X(2)	GRCORHF X(3)	STOICCOR X(4)	GRMICI X(5)	GRMICHF X(6)	STOICMIC X(7)	VWOOD X(8)	VMETAL X(9)	SALPERM X(10)
1	21.	9.	38.	34.	58.	31.	33.	21.	34.	55.
2	64.	21.	51.	15.	70.	60.	6.	58.	45.	67.
3	44.	5.	26.	4.	37.	54.	1.	40.	17.	44.
4	17.	55.	4.	31.	52.	18.	10.	12.	57.	45.
5	58.	2.	6.	49.	59.	19.	20.	33.	46.	26.
6	69.	64.	56.	46.	38.	35.	56.	68.	67.	6.
7	70.	57.	55.	44.	16.	44.	21.	6.	50.	15.
8	41.	36.	69.	53.	48.	17.	22.	16.	16.	32.
9	30.	10.	14.	22.	49.	1.	60.	69.	59.	5.
10	39.	48.	46.	56.	43.	5.	52.	20.	24.	56.
11	61.	50.	47.	1.	24.	38.	2.	3.	52.	64.
12	42.	61.	32.	29.	35.	22.	63.	22.	37.	66.
13	18.	25.	45.	68.	7.	55.	34.	29.	65.	7.
14	7.	62.	13.	9.	4.	62.	15.	49.	44.	13.
15	66.	12.	61.	24.	51.	29.	57.	52.	21.	4.
16	22.	33.	67.	25.	60.	56.	70.	13.	39.	48.
17	26.	16.	42.	64.	47.	16.	41.	47.	7.	17.
18	32.	3.	11.	16.	15.	36.	61.	18.	41.	36.
19	29.	45.	2.	3.	65.	8.	24.	48.	13.	11.
20	19.	32.	1.	11.	42.	15.	68.	45.	70.	68.
21	6.	60.	54.	14.	61.	24.	47.	36.	48.	69.
22	38.	11.	20.	48.	23.	46.	42.	56.	31.	60.
23	43.	44.	62.	51.	30.	59.	14.	50.	62.	34.
24	36.	24.	8.	37.	32.	70.	38.	7.	38.	43.
25	40.	41.	33.	42.	36.	42.	25.	19.	1.	63.
26	51.	63.	37.	41.	5.	2.	31.	59.	14.	47.
27	14.	58.	41.	17.	18.	64.	28.	70.	43.	33.
28	12.	37.	19.	40.	41.	27.	19.	44.	35.	31.
29	35.	70.	29.	69.	26.	65.	23.	37.	8.	50.
30	45.	65.	66.	36.	69.	33.	30.	55.	61.	38.
31	65.	39.	16.	67.	45.	28.	16.	42.	23.	28.
32	27.	1.	28.	28.	9.	66.	66.	54.	56.	62.
33	50.	19.	52.	32.	14.	50.	12.	62.	5.	40.
34	46.	59.	27.	63.	46.	32.	46.	32.	66.	24.
35	11.	26.	23.	58.	56.	58.	62.	34.	15.	54.
36	37.	51.	57.	47.	11.	7.	54.	41.	6.	19.
37	20.	40.	12.	5.	44.	4.	18.	39.	4.	39.
38	25.	7.	34.	54.	39.	23.	44.	51.	55.	59.
39	52.	22.	50.	62.	21.	10.	65.	28.	54.	37.
40	24.	67.	3.	45.	66.	41.	35.	46.	40.	10.
41	9.	17.	59.	57.	53.	11.	11.	31.	53.	61.
42	10.	66.	60.	8.	29.	57.	51.	11.	28.	35.
43	2.	29.	44.	59.	57.	39.	8.	53.	27.	51.
44	68.	6.	5.	30.	8.	13.	26.	23.	33.	57.
45	67.	4.	70.	6.	25.	40.	32.	30.	32.	53.

Table C-3. Ranks of 70 Values Sampled (Continued)

Material Parameter / RUN NO.	BRSAT X(1)	GRCORI X(2)	GRCORHF X(3)	STOICCOR X(4)	GRMICI X(5)	GRMICHF X(6)	STOICMIC X(7)	VWOOD X(8)	VMETAL X(9)	SALPERM X(10)
46	5.	20.	53.	2.	40.	63.	53.	25.	22.	1.
47	59.	56.	25.	20.	27.	61.	39.	66.	10.	70.
48	8.	15.	68.	60.	20.	3.	37.	14.	9.	52.
49	48.	53.	24.	55.	28.	67.	67.	8.	63.	22.
50	16.	69.	22.	21.	13.	9.	13.	38.	30.	21.
51	31.	30.	48.	50.	1.	48.	59.	60.	26.	65.
52	13.	18.	49.	52.	34.	6.	7.	2.	51.	49.
53	60.	68.	30.	35.	17.	12.	27.	35.	69.	58.
54	53.	28.	31.	66.	55.	69.	43.	61.	2.	29.
55	34.	31.	17.	13.	19.	45.	40.	64.	19.	18.
56	33.	35.	9.	61.	31.	37.	17.	1.	12.	2.
57	63.	47.	40.	38.	22.	25.	45.	15.	20.	30.
58	47.	42.	36.	7.	68.	43.	49.	24.	11.	9.
59	62.	46.	58.	18.	62.	26.	64.	43.	36.	8.
60	54.	23.	18.	12.	63.	49.	50.	27.	47.	14.
61	56.	54.	10.	39.	50.	34.	69.	10.	3.	41.
62	55.	34.	21.	19.	2.	14.	58.	4.	29.	16.
63	23.	38.	35.	43.	3.	53.	5.	65.	42.	27.
64	28.	27.	7.	70.	64.	51.	29.	63.	18.	20.
65	15.	13.	39.	65.	54.	30.	3.	17.	68.	46.
66	49.	49.	65.	10.	33.	21.	9.	67.	58.	12.
67	3.	52.	43.	26.	10.	47.	48.	26.	25.	42.
68	57.	14.	15.	33.	12.	68.	4.	9.	64.	23.
69	4.	43.	64.	27.	67.	52.	36.	5.	60.	25.
70	1.	8.	63.	23.	6.	20.	55.	57.	49.	3.

Material Parameter / RUN NO.	BCEXP X(11)	BCFLG X(12)	BCBRSAT X(13)	BCGSSAT X(14)	MBPERM X(15)	MBPOR X(16)	TZPORF X(17)	MBPRES X(18)	BPPRES X(19)	BPSTOR X(20)
1	69.	12.	16.	41.	66.	68.	2.	2.	22.	35.
2	21.	47.	26.	23.	16.	24.	34.	70.	14.	54.
3	34.	47.	33.	38.	65.	69.	50.	43.	23.	25.
4	52.	47.	31.	34.	37.	18.	70.	1.	19.	66.
5	15.	47.	35.	26.	8.	54.	5.	24.	27.	30.
6	56.	12.	59.	9.	14.	42.	68.	39.	69.	50.
7	37.	12.	7.	29.	17.	63.	19.	32.	10.	43.
8	57.	47.	68.	5.	54.	9.	40.	35.	51.	29.
9	16.	47.	60.	33.	10.	66.	31.	22.	1.	27.
10	39.	47.	14.	61.	67.	34.	21.	27.	59.	14.
11	22.	12.	48.	36.	11.	7.	45.	20.	63.	15.
12	61.	47.	25.	51.	56.	35.	39.	26.	70.	13.
13	41.	47.	64.	52.	36.	47.	6.	54.	48.	64.
14	8.	47.	2.	31.	5.	52.	32.	51.	34.	5.
15	18.	12.	41.	68.	20.	1.	61.	56.	21.	6.
16	24.	47.	67.	39.	61.	19.	54.	15.	5.	41.
17	55.	12.	20.	67.	40.	60.	60.	69.	45.	23.

Table C-3. Ranks of 70 Values Sampled (Continued)

Material Parameter RUN NO.	BCEXP X(11)	BCFLG X(12)	BCBRSAT X(13)	BCGSSAT X(14)	MBPERM X(15)	MBPOR X(16)	TZPORF X(17)	MBPRES X(18)	BPPRES X(19)	BPSTOR X(20)
18	28.	12.	52.	2.	42.	20.	28.	34.	65.	24.
19	40.	47.	21.	30.	35.	21.	56.	61.	66.	53.
20	33.	47.	23.	57.	34.	48.	52.	67.	46.	49.
21	2.	12.	4.	40.	51.	59.	16.	5.	58.	28.
22	38.	47.	39.	4.	44.	64.	51.	11.	61.	70.
23	60.	47.	42.	8.	30.	70.	58.	8.	55.	33.
24	17.	47.	11.	47.	41.	44.	14.	31.	62.	3.
25	43.	47.	54.	18.	28.	61.	62.	10.	7.	60.
26	53.	47.	44.	12.	22.	51.	57.	37.	17.	4.
27	64.	47.	38.	14.	21.	5.	35.	48.	42.	65.
28	63.	12.	61.	27.	18.	8.	15.	14.	44.	44.
29	29.	47.	58.	63.	27.	40.	9.	55.	8.	21.
30	1.	12.	3.	28.	45.	31.	64.	16.	24.	51.
31	10.	47.	37.	43.	3.	49.	27.	9.	52.	7.
32	66.	47.	55.	66.	6.	55.	66.	40.	12.	11.
33	23.	47.	19.	60.	60.	23.	69.	4.	49.	19.
34	65.	12.	45.	64.	9.	32.	41.	17.	9.	40.
35	14.	47.	51.	24.	26.	6.	55.	13.	43.	9.
36	6.	47.	65.	65.	19.	65.	44.	29.	67.	46.
37	59.	47.	40.	6.	24.	16.	38.	50.	41.	16.
38	44.	47.	32.	70.	53.	4.	46.	30.	13.	26.
39	5.	47.	29.	7.	39.	36.	48.	59.	30.	37.
40	3.	47.	43.	20.	55.	58.	8.	38.	18.	12.
41	27.	47.	24.	19.	59.	50.	11.	36.	16.	42.
42	25.	12.	70.	59.	2.	56.	29.	52.	25.	63.
43	48.	12.	69.	22.	57.	17.	30.	19.	26.	8.
44	12.	12.	46.	11.	38.	12.	18.	6.	15.	62.
45	9.	47.	28.	17.	50.	33.	20.	46.	6.	22.
46	19.	47.	12.	42.	15.	67.	63.	23.	53.	56.
47	46.	47.	56.	46.	48.	22.	10.	65.	31.	59.
48	62.	12.	8.	37.	12.	57.	65.	62.	57.	20.
49	13.	47.	9.	13.	63.	3.	67.	21.	11.	31.
50	11.	47.	34.	35.	23.	41.	49.	47.	2.	39.
51	26.	47.	5.	3.	69.	27.	22.	66.	29.	61.
52	45.	12.	27.	69.	47.	15.	53.	68.	37.	68.
53	58.	47.	50.	32.	64.	46.	24.	44.	38.	1.
54	20.	12.	30.	48.	13.	43.	25.	42.	60.	17.
55	32.	12.	57.	54.	68.	53.	36.	33.	35.	47.
56	51.	12.	17.	10.	7.	38.	59.	53.	4.	48.
57	68.	47.	1.	49.	4.	14.	4.	7.	54.	58.
58	31.	47.	62.	58.	58.	30.	23.	28.	56.	45.
59	67.	47.	15.	55.	46.	62.	7.	49.	36.	55.
60	70.	47.	13.	15.	49.	29.	43.	58.	20.	2.
61	36.	47.	49.	25.	33.	25.	12.	12.	47.	69.
62	7.	47.	63.	44.	62.	39.	26.	63.	40.	34.

Table C-3. Ranks of 70 Values Sampled (Continued)

Material Parameter / RUN NO.	BCEXP X(11)	BCFLG X(12)	BCBRSAT X(13)	BCGSSAT X(14)	MBPERM X(15)	MBPOR X(16)	TZPORF X(17)	MBPRES X(18)	BPPRES X(19)	BPSTOR X(20)
63	47.	12.	36.	50.	70.	13.	47.	18.	28.	32.
64	42.	47.	6.	16.	25.	11.	33.	60.	39.	57.
65	4.	47.	47.	62.	31.	26.	42.	57.	68.	52.
66	35.	12.	22.	56.	32.	10.	1.	25.	33.	67.
67	54.	12.	10.	45.	52.	28.	17.	41.	3.	38.
68	50.	12.	53.	53.	43.	37.	37.	45.	64.	36.
69	49.	47.	66.	1.	29.	45.	13.	64.	32.	10.
70	30.	47.	18.	21.	1.	2.	3.	3.	50.	18.

Material Parameter / RUN NO.	BHPERM X(21)	DBDIAM X(22)	LAMBDA X(23)	BPAREAFR X(24)	SOLAM X(25)	SOLNP X(26)	SOLPU X(27)	SOLRA X(28)	SOLTH X(29)	SOLU X(30)
1	36.	56.	46.	3.	19.	16.	39.	69.	70.	69.
2	32.	44.	25.	27.	32.	2.	11.	43.	65.	31.
3	27.	61.	20.	31.	18.	45.	12.	66.	24.	45.
4	70.	49.	49.	6.	48.	7.	43.	46.	23.	17.
5	67.	5.	15.	5.	37.	36.	60.	19.	31.	19.
6	30.	40.	33.	42.	27.	53.	65.	67.	63.	22.
7	58.	57.	3.	55.	28.	61.	47.	49.	34.	5.
8	69.	12.	13.	41.	49.	29.	15.	36.	43.	20.
9	15.	4.	69.	62.	29.	10.	26.	5.	64.	34.
10	59.	37.	34.	64.	20.	41.	18.	45.	38.	39.
11	5.	26.	51.	15.	66.	63.	17.	23.	52.	54.
12	63.	51.	45.	23.	11.	17.	28.	32.	30.	2.
13	13.	60.	64.	2.	14.	66.	45.	48.	17.	56.
14	61.	30.	52.	40.	58.	33.	8.	63.	55.	48.
15	56.	28.	36.	36.	50.	13.	24.	40.	27.	40.
16	14.	11.	14.	13.	69.	68.	62.	70.	36.	49.
17	33.	8.	47.	14.	9.	43.	23.	55.	1.	1.
18	65.	23.	68.	65.	43.	4.	44.	53.	6.	25.
19	34.	63.	56.	45.	59.	70.	51.	34.	53.	23.
20	29.	29.	2.	21.	15.	30.	38.	26.	39.	26.
21	31.	17.	31.	10.	8.	50.	49.	27.	8.	21.
22	52.	59.	30.	44.	57.	37.	3.	15.	10.	58.
23	23.	16.	37.	60.	17.	54.	63.	8.	58.	7.
24	35.	6.	61.	33.	54.	65.	37.	38.	66.	11.
25	24.	66.	39.	29.	5.	56.	50.	17.	22.	52.
26	40.	2.	22.	16.	40.	51.	53.	64.	44.	55.
27	48.	1.	53.	34.	23.	21.	5.	62.	25.	38.
28	53.	41.	16.	9.	67.	34.	9.	14.	32.	46.
29	38.	27.	62.	7.	38.	5.	48.	13.	59.	32.
30	20.	64.	32.	46.	63.	24.	33.	22.	19.	50.
31	45.	50.	5.	70.	24.	19.	6.	25.	16.	70.
32	37.	70.	29.	54.	61.	32.	40.	9.	12.	3.
33	12.	9.	42.	22.	12.	39.	41.	4.	68.	44.
34	41.	36.	58.	38.	31.	27.	10.	58.	46.	30.

Table C-3. Ranks of 70 Values Sampled (Continued)

Material Parameter RUN NO.	BHPERM X(21)	DBDIAM X(22)	LAMBDA X(23)	BPAREAFR X(24)	SOLAM X(25)	SOLNP X(26)	SOLPU X(27)	SOLRA X(28)	SOLTH X(29)	SOLU X(30)
35	21.	43.	6.	50.	6.	31.	2.	52.	69.	33.
36	4.	21.	7.	28.	25.	40.	7.	44.	26.	18.
37	3.	46.	35.	8.	16.	8.	69.	10.	37.	47.
38	16.	13.	23.	63.	10.	62.	31.	54.	13.	59.
39	68.	69.	18.	4.	34.	57.	35.	30.	61.	67.
40	64.	39.	54.	56.	42.	49.	21.	59.	18.	12.
41	43.	7.	55.	58.	68.	58.	14.	7.	56.	27.
42	66.	10.	44.	57.	13.	67.	57.	1.	45.	63.
43	11.	52.	12.	25.	62.	38.	58.	20.	5.	15.
44	8.	14.	65.	43.	30.	69.	30.	56.	21.	16.
45	39.	54.	57.	35.	35.	22.	64.	50.	29.	8.
46	46.	18.	28.	48.	55.	3.	54.	57.	14.	64.
47	62.	58.	66.	51.	26.	55.	29.	61.	33.	51.
48	55.	48.	70.	30.	52.	25.	16.	42.	35.	62.
49	28.	20.	67.	12.	3.	35.	22.	2.	9.	53.
50	18.	55.	4.	32.	46.	23.	32.	65.	11.	4.
51	26.	19.	8.	24.	36.	9.	36.	24.	51.	14.
52	51.	15.	24.	69.	39.	60.	55.	33.	57.	42.
53	25.	34.	48.	49.	64.	12.	66.	29.	20.	66.
54	54.	47.	60.	17.	60.	59.	68.	51.	7.	41.
55	50.	25.	19.	37.	65.	18.	56.	18.	15.	68.
56	9.	38.	59.	11.	22.	28.	20.	47.	40.	24.
57	6.	31.	41.	66.	51.	11.	52.	16.	3.	28.
58	57.	65.	43.	52.	2.	15.	59.	6.	60.	6.
59	17.	32.	40.	1.	70.	52.	1.	3.	41.	9.
60	49.	24.	9.	47.	4.	64.	34.	39.	42.	65.
61	2.	22.	21.	61.	56.	6.	42.	68.	62.	36.
62	19.	62.	26.	26.	41.	20.	19.	11.	47.	57.
63	22.	67.	50.	67.	47.	46.	13.	31.	54.	10.
64	10.	33.	11.	53.	53.	47.	70.	12.	48.	60.
65	7.	53.	63.	39.	45.	1.	61.	60.	50.	29.
66	47.	35.	27.	20.	1.	44.	25.	35.	4.	61.
67	60.	42.	10.	68.	44.	26.	67.	28.	49.	35.
68	44.	3.	1.	19.	33.	14.	27.	21.	28.	37.
69	1.	45.	38.	59.	7.	42.	4.	37.	2.	43.
70	42.	68.	17.	18.	21.	48.	46.	41.	67.	13.

Material Parameter RUN NO.	CULTRFLD X(31)	CULCLIM X(32)	CULFRPOR X(33)	CULFRSP X(34)	CULCLYF X(35)	CULCLYP X(36)	FKDAM X(37)	FKDNP X(38)	FKDAM X(39)	FKDTH X(40)
1	26.	10.	43.	48.	18.	8.	40.	35.	28.	20.
2	29.	41.	44.	5.	48.	58.	19.	11.	64.	6.
3	48.	63.	63.	30.	18.	40.	7.	66.	6.	70.
4	41.	22.	55.	55.	18.	38.	38.	19.	68.	39.
5	35.	38.	57.	67.	68.	57.	45.	63.	9.	23.
6	68.	8.	70.	65.	18.	15.	21.	48.	15.	60.

Table C-3. Ranks of 70 Values Sampled (Continued)

Material Parameter RUN NO.	CULTRFLD X(31)	CULCLIM X(32)	CULFRPOR X(33)	CULFRSP X(34)	CULCLYF X(35)	CULCLYP X(36)	FKDAM X(37)	FKDNP X(38)	FKDAM X(39)	FKDTH X(40)
7	20.	20.	9.	26.	18.	39.	10.	70.	54.	7.
8	65.	51.	6.	6.	18.	26.	30.	65.	49.	58.
9	45.	61.	46.	36.	18.	9.	17.	6.	62.	10.
10	63.	9.	62.	53.	55.	2.	41.	2.	24.	24.
11	66.	70.	14.	47.	18.	5.	32.	36.	10.	4.
12	1.	66.	64.	29.	41.	21.	47.	40.	21.	15.
13	62.	65.	52.	4.	39.	23.	25.	17.	34.	16.
14	37.	1.	42.	46.	18.	66.	65.	38.	41.	62.
15	5.	33.	53.	51.	18.	59.	5.	13.	12.	59.
16	8.	42.	40.	28.	50.	31.	26.	16.	65.	31.
17	43.	40.	28.	21.	18.	46.	62.	67.	38.	5.
18	6.	49.	33.	13.	40.	30.	39.	22.	50.	68.
19	10.	47.	38.	24.	18.	56.	12.	20.	25.	8.
20	22.	32.	2.	38.	18.	16.	35.	37.	30.	65.
21	61.	46.	60.	15.	38.	65.	8.	18.	67.	66.
22	50.	39.	7.	12.	69.	55.	23.	4.	1.	17.
23	4.	26.	45.	33.	46.	70.	14.	15.	56.	57.
24	14.	43.	51.	11.	49.	36.	46.	42.	31.	14.
25	3.	48.	50.	43.	18.	43.	59.	32.	16.	32.
26	57.	64.	21.	62.	18.	50.	52.	23.	27.	30.
27	40.	36.	58.	19.	47.	49.	33.	41.	23.	1.
28	25.	2.	66.	1.	18.	42.	61.	57.	18.	51.
29	32.	57.	61.	35.	59.	48.	50.	43.	13.	63.
30	46.	44.	56.	7.	61.	14.	68.	62.	26.	22.
31	38.	69.	59.	57.	18.	41.	54.	44.	57.	34.
32	64.	19.	68.	27.	18.	10.	57.	60.	45.	12.
33	23.	4.	4.	41.	56.	27.	66.	12.	40.	35.
34	13.	60.	1.	18.	18.	60.	53.	31.	33.	55.
35	52.	17.	26.	54.	18.	34.	1.	47.	35.	33.
36	9.	13.	24.	2.	18.	28.	16.	50.	59.	25.
37	58.	25.	65.	9.	67.	17.	9.	61.	42.	61.
38	39.	5.	54.	14.	53.	61.	15.	55.	3.	43.
39	24.	31.	47.	39.	42.	63.	11.	26.	37.	18.
40	34.	16.	36.	32.	54.	1.	18.	28.	5.	21.
41	56.	7.	31.	23.	18.	4.	49.	68.	63.	52.
42	17.	11.	23.	16.	18.	7.	24.	29.	2.	56.
43	28.	14.	20.	68.	18.	67.	29.	7.	11.	2.
44	59.	23.	16.	40.	66.	64.	56.	49.	43.	42.
45	12.	12.	25.	20.	18.	13.	51.	10.	4.	40.
46	47.	54.	29.	56.	58.	45.	43.	56.	44.	3.
47	30.	29.	13.	70.	63.	20.	20.	58.	70.	19.
48	31.	27.	11.	63.	65.	33.	44.	45.	19.	48.
49	54.	55.	32.	61.	18.	35.	22.	64.	22.	50.
50	51.	37.	22.	49.	70.	12.	60.	3.	17.	53.
51	44.	58.	48.	42.	18.	18.	36.	24.	20.	13.
52	21.	67.	69.	59.	18.	37.	42.	14.	52.	44.

Table C-3. Ranks of 70 Values Sampled (Continued)

Material Parameter RUN NO.	CULTRFLD X(31)	CULCLIM X(32)	CULFRPOR X(33)	CULFRSP X(34)	CULCLYF X(35)	CULCLYP X(36)	FKDAM X(37)	FKDNP X(38)	FKDAM X(39)	FKDTH X(40)
53	7.	21.	12.	8.	43.	53.	13.	59.	36.	11.
54	67.	45.	10.	10.	18.	25.	37.	1.	66.	67.
55	27.	52.	8.	60.	18.	24.	4.	69.	55.	36.
56	18.	15.	15.	17.	37.	11.	2.	30.	58.	26.
57	53.	6.	37.	37.	18.	32.	3.	9.	39.	28.
58	70.	34.	5.	44.	18.	62.	63.	52.	32.	9.
59	42.	50.	34.	66.	44.	52.	27.	27.	29.	69.
60	60.	56.	19.	3.	36.	47.	70.	8.	53.	41.
61	36.	53.	49.	31.	18.	51.	69.	54.	7.	64.
62	49.	3.	67.	34.	51.	68.	67.	25.	69.	29.
63	15.	62.	35.	22.	57.	22.	28.	33.	61.	54.
64	2.	30.	18.	50.	64.	6.	64.	51.	48.	49.
65	55.	28.	3.	52.	18.	54.	31.	46.	8.	46.
66	11.	24.	27.	45.	18.	19.	55.	39.	46.	38.
67	69.	59.	30.	25.	60.	69.	6.	21.	14.	27.
68	33.	18.	39.	64.	52.	3.	34.	5.	47.	37.
69	19.	35.	41.	69.	45.	44.	58.	34.	60.	47.
70	16.	68.	17.	58.	62.	29.	48.	53.	51.	45.

Material *Parameter* RUN NO.	FKDU X(41)	FKDRA X(42)	CULPOR X(43)	MKDAM X(44)	MKDNP X(45)	MKDPU X(46)	MKDTH X(47)	MKDU X(48)	MKDRA X(49)
1	46.	6.	14.	42.	24.	62.	11.	54.	62.
2	60.	20.	60.	9.	17.	18.	47.	21.	47.
3	14.	9.	52.	36.	9.	14.	67.	30.	41.
4	38.	50.	28.	25.	39.	25.	70.	66.	63.
5	32.	40.	21.	66.	61.	12.	6.	8.	39.
6	29.	4.	56.	26.	26.	13.	36.	22.	60.
7	24.	59.	18.	44.	10.	23.	42.	62.	64.
8	34.	22.	8.	61.	18.	67.	27.	27.	26.
9	31.	54.	19.	32.	15.	11.	55.	49.	42.
10	8.	67.	48.	22.	36.	24.	32.	20.	15.
11	43.	55.	58.	58.	70.	49.	22.	52.	69.
12	54.	29.	32.	52.	11.	16.	34.	4.	23.
13	33.	64.	13.	68.	47.	32.	17.	28.	24.
14	41.	63.	27.	57.	63.	2.	3.	15.	14.
15	36.	25.	11.	46.	28.	61.	12.	63.	32.
16	23.	41.	23.	40.	50.	1.	7.	50.	61.
17	20.	68.	36.	1.	33.	31.	31.	43.	70.
18	1.	19.	55.	60.	67.	10.	26.	48.	59.
19	11.	23.	2.	31.	37.	63.	53.	41.	27.
20	21.	42.	65.	27.	60.	64.	10.	47.	65.
21	27.	31.	9.	53.	5.	59.	14.	17.	10.
22	12.	48.	29.	19.	16.	6.	28.	53.	48.
23	58.	69.	34.	48.	69.	68.	41.	70.	40.

Table C-3. Ranks of 70 Values Sampled (Continued)

Material Parameter RUN NO.	FKDU X(41)	FKDRA X(42)	CULPOR X(43)	MKDAM X(44)	MKDNP X(45)	MKDPU X(46)	MKDTH X(47)	MKDU X(48)	MKDRA X(49)
24	18.	1.	37.	7.	6.	29.	51.	69.	37.
25	51.	34.	64.	24.	51.	60.	2.	14.	5.
26	6.	45.	67.	15.	1.	38.	13.	57.	7.
27	13.	11.	49.	54.	35.	69.	8.	44.	13.
28	68.	65.	61.	20.	2.	4.	15.	65.	38.
29	4.	37.	41.	63.	65.	46.	68.	16.	68.
30	3.	49.	50.	39.	44.	41.	56.	51.	3.
31	40.	28.	7.	16.	58.	42.	4.	67.	49.
32	19.	15.	22.	55.	19.	57.	43.	23.	11.
33	53.	18.	26.	56.	22.	5.	44.	34.	33.
34	49.	5.	38.	35.	20.	51.	21.	9.	8.
35	15.	70.	63.	64.	23.	55.	61.	7.	52.
36	55.	2.	51.	67.	66.	3.	48.	24.	22.
37	57.	57.	12.	11.	57.	30.	5.	32.	25.
38	65.	27.	17.	14.	68.	48.	58.	68.	29.
39	45.	8.	30.	2.	55.	34.	33.	3.	51.
40	70.	26.	62.	49.	32.	65.	38.	39.	36.
41	9.	3.	35.	12.	64.	50.	18.	12.	30.
42	25.	43.	4.	6.	7.	26.	54.	18.	58.
43	7.	10.	20.	34.	41.	28.	57.	11.	45.
44	67.	39.	42.	33.	25.	52.	62.	2.	43.
45	30.	66.	44.	38.	31.	53.	16.	29.	19.
46	61.	61.	31.	18.	30.	66.	49.	1.	57.
47	37.	62.	3.	37.	42.	7.	46.	60.	4.
48	59.	13.	39.	45.	59.	54.	59.	61.	46.
49	52.	33.	24.	28.	21.	21.	23.	36.	31.
50	56.	16.	1.	47.	38.	45.	29.	42.	55.
51	69.	21.	10.	51.	43.	36.	65.	58.	44.
52	66.	44.	70.	65.	27.	19.	35.	19.	16.
53	42.	51.	46.	13.	49.	35.	63.	13.	18.
54	63.	32.	68.	8.	40.	58.	52.	37.	34.
55	64.	52.	59.	59.	13.	37.	37.	40.	12.
56	5.	35.	45.	30.	48.	27.	20.	38.	2.
57	48.	12.	40.	43.	12.	22.	25.	10.	66.
58	50.	7.	57.	29.	62.	15.	9.	59.	20.
59	44.	56.	33.	41.	46.	33.	40.	33.	21.
60	39.	53.	5.	70.	45.	9.	66.	5.	35.
61	22.	60.	16.	5.	53.	43.	60.	26.	9.
62	10.	30.	54.	62.	3.	70.	45.	55.	54.
63	35.	47.	15.	4.	29.	44.	1.	6.	67.
64	17.	38.	47.	69.	8.	47.	30.	31.	53.
65	26.	58.	6.	50.	4.	20.	24.	45.	17.
66	2.	24.	66.	21.	54.	40.	64.	35.	56.
67	16.	14.	69.	23.	52.	8.	19.	64.	28.
68	28.	36.	25.	3.	56.	56.	50.	25.	1.
69	62.	17.	53.	17.	14.	17.	39.	56.	50.
70	47.	46.	43.	10.	34.	39.	69.	46.	6.

Table C-4 lists the total and percentage release for the 3 radionuclides contributing the most for each vector showing integrated discharge to the accessible environment for the E2 scenario assuming the dual porosity with chemical retardation conceptual model for contaminant transport in the Culebra Dolomite Member. Values are normalized by the EPA factor for each radionuclide. Vectors are ordered from most to least release. Vectors that have no release are omitted.

Table C-4. Vectors with Integrated Discharge through the Culebra Dolomite Member to the Accessible Environment for Scenario E2 and Assuming a Conceptual Model with Dual Porosity, Retardation, Clay, Matrix Diffusion, Intrusion at 1000 yr

Comp. Scen. ID	Vector	Total EPA-normalized, Integrated Discharge	Top 3 Radionuclides Contribution to Integrated Discharge								
01	55	1.5601E-06	RA226	1.5592E-06	100%	NP237	8.7829E-10	0%	PU239	7.2127E-12	0%
	10	1.2951E-10	RA226	9.4533E-11	73%	U233	3.3887E-11	26%	U234	9.8343E-13	1%
	1	1.8060E-11	TH229	9.2657E-12	51%	TH230	8.7942E-12	49%	RA226	8.0844E-17	0%
	47	3.9772E-12	TH229	2.9440E-12	74%	TH230	9.8663E-13	25%	U233	4.5353E-14	1%
	63	1.2484E-17	U233	1.0999E-17	88%	U234	1.4825E-18	12%	TH229	1.5601E-21	0%
	51	3.2655E-19	RA226	3.2653E-19	100%	U233	1.7647E-23	0%	PU239	3.8685E-24	0%
	32	2.1158E-20	RA226	2.1157E-20	100%	NP237	9.3466E-25	0%	U233	5.4155E-25	0%
	21	1.1627E-21	NP237	6.3619E-22	55%	RA226	4.4290E-22	38%	U233	7.7841E-23	7%
	12	1.2747E-22	RA226	6.6260E-23	52%	U233	5.6530E-23	44%	U234	2.5981E-24	2%
	41	5.0185E-23	U233	4.6164E-23	92%	U234	4.0125E-24	8%	TH229	7.2193E-27	0%
	20	2.0522E-23	TH229	1.1004E-23	54%	TH230	9.5181E-24	46%	U233	1.8413E-30	0%
	53	1.8459E-27	U233	1.5152E-27	82%	U234	3.2534E-28	18%	RA226	5.3614E-30	0%
	2	1.3229E-27	U233	1.0991E-27	83%	U234	2.2383E-28	17%			
	55	8.6746E-01	AM241	4.0456E-01	47%	U233	2.2463E-01	26%	U234	1.6182E-01	19%
	63	5.8316E-01	AM241	5.1702E-01	89%	U233	1.9999E-02	3%	U234	1.4437E-02	2%
	10	5.6803E-01	U233	2.8043E-01	49%	U234	2.0115E-01	35%	AM241	3.6609E-02	6%
	47	5.3812E-01	U233	2.9088E-01	54%	U234	2.0964E-01	39%	NP237	1.9271E-02	4%
	1	3.0538E-01	U233	1.1123E-01	36%	U234	8.0423E-02	26%	TH229	5.6951E-02	19%
	53	1.1882E-01	PU239	5.7959E-02	49%	U233	2.9360E-02	25%	U234	2.1251E-02	18%
	21	1.1481E-01	U233	6.2304E-02	54%	U234	4.5067E-02	39%	RA226	2.0227E-03	2%
	51	1.1373E-01	U233	5.4729E-02	48%	U234	3.9510E-02	35%	AM241	8.4059E-03	7%
	2	1.0707E-01	U233	4.0889E-02	38%	U234	2.9590E-02	28%	TH229	1.7937E-02	17%
	3	1.0372E-01	U233	5.7465E-02	55%	U234	4.1564E-02	40%	RA226	1.7829E-03	2%
	20	1.0007E-01	U233	9.9260E-02	99%	PU239	7.2152E-04	1%	AM241	3.7963E-05	0%
	41	8.8558E-02	U233	4.7047E-02	53%	U234	3.4002E-02	38%	NP237	2.2922E-03	3%
	12	3.2740E-03	RA226	3.0988E-03	95%	AM241	1.6372E-04	5%	PU239	4.8928E-06	0%
	32	1.7216E-03	RA226	1.2015E-03	70%	AM241	3.6873E-04	21%	PU239	6.1195E-05	4%
	47	3.9283E-01	U233	2.0411E-01	52%	U234	1.3539E-01	34%	TH229	1.8711E-02	5%
	55	1.9484E-01	U233	7.7691E-02	40%	U234	3.9633E-02	20%	PU239	2.7302E-02	14%
	51	2.8577E-02	U233	1.2640E-02	44%	U234	7.1274E-03	25%	TH229	4.5987E-03	16%
	10	1.1650E-02	U233	5.7654E-03	49%	TH229	3.0936E-03	27%	TH230	1.6631E-03	14%
	1	1.0092E-02	TH229	3.5024E-03	35%	TH230	3.1794E-03	32%	U233	2.5898E-03	26%
	63	6.0843E-10	AM241	3.8981E-10	64%	TH229	1.0160E-10	17%	TH230	7.7372E-11	13%
	12	2.6788E-10	RA226	2.1076E-10	79%	PU239	3.1347E-11	12%	PU240	2.3450E-11	9%
	3	1.1364E-11	U233	7.2824E-12	64%	U234	2.8670E-12	25%	TH229	6.3320E-13	6%

Table C-4. Vectors with Integrated Discharge through the Culebra Dolomite Member to the Accessible Environment for Scenario E2 and Assuming a Conceptual Model with Dual Porosity, Retardation, Clay, Matrix Diffusion, Intrusion at 1000 yr (Continued)

Comp. Scen. ID	Vector	Total EPA-normalized, Integrated Discharge	Top 3 Radionuclides Contribution to Integrated Discharge								
	21	3.3155E-14	U233	1.8388E-14	55%	U234	8.9303E-15	27%	PU239	3.0273E-15	9%
	32	1.9654E-14	PU239	9.4868E-15	48%	RA226	6.7524E-15	34%	PU240	1.8496E-15	9%
	20	2.1770E-16	PU239	1.1824E-16	54%	PU240	5.2106E-17	24%	U233	2.9388E-17	13%
	41	1.2839E-16	U233	4.8078E-17	37%	TH229	3.1209E-17	24%	TH230	2.3807E-17	19%
	2	6.9351E-18	U233	2.5481E-18	37%	U234	1.5823E-18	23%	TH229	1.4046E-18	20%
	53	2.2487E-19	PU239	1.5996E-19	71%	PU240	2.6297E-20	12%	U233	2.3418E-20	10%

Table C-5 lists the total and percentage release for the 3 radionuclides contributing the most for each vector showing integrated discharge to the accessible environment for the E1E2 scenario assuming the dual porosity with chemical retardation conceptual model for contaminant transport in the Culebra Dolomite Member. Values are normalized by the EPA factor for each radionuclide. Vectors are ordered from most to least release. Vectors that have no release are omitted.

Table C-5. Vectors with Integrated Discharge through the Culebra Dolomite Member to the Accessible Environment for Scenario E1E2 and Assuming a Conceptual Model with Dual Porosity, Retardation, Clay, Matrix Diffusion, Intrusion at 1000 yr

Comp. Scen. ID	Vector	Total EPA-normalized, Integrated Discharge	Top 3 Radionuclides Contribution to Integrated Discharge								
02	5	1.1828E-01	U233	6.3491E-02	54%	U234	2.2618E-02	19%	TH229	1.9558E-02	17%
	31	1.0155E-02	TH229	6.5324E-03	64%	TH230	3.6215E-03	36%	RA226	8.9532E-07	0%
	52	6.0021E-03	U233	5.3036E-03	88%	U234	4.9025E-04	8%	RA226	1.0069E-04	2%
	68	3.9493E-04	U233	3.8109E-04	96%	U234	1.1554E-05	3%	RA226	1.4480E-06	0%
	70	1.1963E-04	RA226	1.1963E-04	100%	NP237	1.0256E-16	0%	U233	7.4618E-17	0%
	43	7.0064E-05	U233	6.3893E-05	91%	U234	6.1699E-06	9%	TH229	1.4683E-09	0%
	25	8.3413E-06	TH229	5.0085E-06	60%	TH230	2.7607E-06	33%	RA226	5.6645E-07	7%
	26	6.0574E-06	NP237	4.3598E-06	72%	RA226	1.6974E-06	28%	TH229	1.2307E-10	0%
	15	5.6070E-06	TH229	3.4898E-06	62%	TH230	2.1084E-06	38%	RA226	5.7817E-09	0%
	55	3.6315E-06	RA226	3.6244E-06	100%	NP237	7.0716E-09	0%	U233	1.4572E-14	0%
	14	1.8426E-06	TH229	1.0264E-06	56%	TH230	8.1182E-07	44%	RA226	4.3964E-09	0%
	6	1.1396E-06	U233	9.3545E-07	82%	PU239	1.0569E-07	9%	U234	5.7744E-08	5%
	35	3.5419E-07	U233	3.4704E-07	98%	U234	7.1424E-09	2%	TH229	1.1195E-12	0%
	46	1.0551E-08	U233	9.2165E-09	87%	U234	1.3042E-09	12%	TH229	2.6075E-11	0%
	10	1.9074E-09	U233	1.1957E-09	63%	RA226	6.9553E-10	36%	U234	1.1530E-11	1%
	1	1.3264E-09	TH229	7.1628E-10	54%	TH230	6.1014E-10	46%	RA226	9.1101E-15	0%
	39	9.8486E-10	U233	9.7633E-10	99%	U234	8.3454E-12	1%	TH229	1.8781E-13	0%
	49	7.6570E-10	NP237	7.6493E-10	100%	RA226	5.2987E-13	0%	TH229	1.5280E-13	0%

Table C-5. Vectors with Integrated Discharge through the Culebra Dolomite Member to the Accessible Environment for Scenario E1E2 and Assuming a Conceptual Model with Dual Porosity, Retardation, Clay, Matrix Diffusion, Intrusion at 1000 yr (Continued)

Comp. Scen. ID	Vector	Total EPA-normalized, Integrated Discharge	Top 3 Radionuclides Contribution to Integrated Discharge								
	64	3.0805E-10	U233	3.0586E-10	99%	U234	1.7844E-12	1%	TH229	3.2846E-13	0%
	47	3.2280E-11	TH229	2.3698E-11	73%	TH230	8.3160E-12	26%	U233	2.5458E-13	1%
	4	3.0631E-11	PU239	2.6332E-11	86%	PU240	4.2924E-12	14%	AM241	5.6472E-15	0%
	59	2.3598E-11	U233	2.3405E-11	99%	U234	1.8425E-13	1%	RA226	5.8968E-15	0%
	48	9.5001E-13	RA226	9.5001E-13	100%	U234	1.3993E-19	0%	TH230	1.7653E-20	0%
	65	1.0586E-13	NP237	5.8251E-14	55%	RA226	4.7593E-14	45%	PU239	5.1619E-18	0%
	58	3.0946E-14	TH229	1.7760E-14	57%	TH230	1.3142E-14	42%	RA226	4.1869E-17	0%
	29	6.7815E-17	U233	6.3840E-17	94%	U234	3.9754E-18	6%	TH229	6.1612E-23	0%
	63	1.5077E-17	U233	1.3290E-17	88%	U234	1.7854E-18	12%	TH229	1.9138E-21	0%
	50	1.2251E-17	RA226	1.2121E-17	99%	U233	1.2432E-19	1%	U234	3.5309E-21	0%
	12	1.8679E-18	U233	1.8347E-18	98%	U234	2.1588E-20	1%	NP237	8.2324E-21	0%
	32	1.1875E-18	RA226	1.1870E-18	100%	NP237	3.2289E-22	0%	U233	1.6037E-22	0%
	57	4.0887E-19	U233	3.8426E-19	94%	U234	2.4527E-20	6%	TH229	7.8421E-23	0%
	51	3.5073E-19	RA226	3.5070E-19	100%	U233	1.9957E-23	0%	PU239	4.3904E-24	0%
	66	6.0965E-20	U233	5.7009E-20	94%	U234	3.9062E-21	6%	RA226	3.4558E-23	0%
	33	5.6963E-20	NP237	5.4450E-20	96%	RA226	2.1994E-21	4%	U233	1.6844E-22	0%
	42	1.9346E-20	NP237	1.8950E-20	98%	U233	3.7176E-22	2%	U234	2.3762E-23	0%
	11	3.8308E-21	TH229	2.0436E-21	53%	TH230	1.7854E-21	47%	U233	1.2593E-24	0%
	21	3.1981E-21	U233	2.4925E-21	78%	RA226	3.6286E-22	11%	U234	3.4266E-22	11%
	34	3.1981E-21	U233	2.4925E-21	78%	RA226	3.6286E-22	11%	U234	3.4266E-22	11%
	27	2.9053E-21	RA226	2.1703E-21	75%	TH229	4.7573E-22	16%	TH230	2.5929E-22	9%
	62	2.8047E-21	NP237	2.8047E-21	100%	U233	1.0084E-27	0%	TH229	2.3834E-28	0%
	60	2.0768E-21	U233	1.4616E-21	70%	U234	6.1526E-22	30%	RA226	4.7559E-28	0%
	20	9.1047E-22	TH229	5.2577E-22	58%	TH230	3.8470E-22	42%	RA226	5.9309E-29	0%
	24	8.0686E-22	NP237	8.0686E-22	100%	TH229	9.9112E-30	0%	U233	2.3114E-30	0%
	56	4.2492E-22	RA226	4.2492E-22	100%						
	44	3.3833E-22	U233	2.4447E-22	72%	U234	9.3438E-23	28%	RA226	4.1767E-25	0%
	28	6.1027E-23	NP237	6.1027E-23	100%	TH229	1.4684E-29	0%	U233	1.0105E-32	0%
	41	6.1027E-23	NP237	6.1027E-23	100%	TH229	1.4684E-29	0%	U233	1.0105E-32	0%
	30	5.3950E-23	RA226	5.3950E-23	100%						
	17	2.1233E-23	AM241	2.1233E-23	100%	NP237	1.3391E-30	0%			
	16	1.8958E-23	TH229	1.1168E-23	59%	TH230	7.7901E-24	41%	RA226	1.8494E-29	0%
	7	8.7737E-24	NP237	8.7737E-24	100%	TH229	2.8720E-31	0%			
	9	1.4889E-24	NP237	1.2603E-24	85%	PU239	1.1273E-25	8%	RA226	9.4959E-26	6%
	19	1.2786E-24	RA226	1.2786E-24	100%	U233	5.9915E-30	0%			
	45	5.8283E-25	RA226	5.5385E-25	95%	U233	2.7106E-26	5%	U234	1.6430E-27	0%
	67	3.1973E-25	RA226	1.1826E-25	37%	PU239	1.0921E-25	34%	TH229	3.7671E-26	12%
	53	1.9971E-25	U233	1.6527E-25	83%	U234	3.4201E-26	17%	RA226	2.3306E-28	0%
	2	9.5792E-26	U233	8.0505E-26	84%	U234	1.5286E-26	16%	TH229	1.2829E-30	0%
	22	9.7373E-27	NP237	9.7373E-27	100%						
	40	5.2502E-27	RA226	5.1259E-27	98%	TH229	5.8592E-29	1%	NP237	4.0679E-29	1%
	23	6.2438E-28	RA226	2.4878E-28	40%	TH229	2.0823E-28	33%	TH230	1.6737E-28	27%
	8	3.3002E-29	NP237	3.3002E-29	100%						

Table C-5. Vectors with Integrated Discharge through the Culebra Dolomite Member to the Accessible Environment for Scenario E1E2 and Assuming a Conceptual Model with Dual Porosity, Retardation, Clay, Matrix Diffusion, Intrusion at 1000 yr (Continued)

Comp. Scen. ID	Vector	Total EPA-normalized, Integrated Discharge	Top 3 Radionuclides Contribution to Integrated Discharge								
	36	1.3894E-30	U233	1.3573E-30	98%	U234	3.2119E-32	2%			
	38	9.1987E-31	RA226	9.1987E-31	100%						
02	54	5.0300E+01	PU239	2.7662E+01	55%	AM241	1.6566E+01	33%	PU240	5.5098E+00	11%
	22	2.3592E+01	AM241	2.2964E+01	97%	U233	3.5322E-01	1%	U234	2.5314E-01	1%
	8	2.1797E+01	AM241	2.1186E+01	97%	U233	3.2907E-01	2%	U234	2.3574E-01	1%
	4	1.9332E+01	AM241	1.8560E+01	96%	U233	3.3371E-01	2%	U234	2.3899E-01	1%
	48	1.9143E+01	AM241	1.8567E+01	97%	U233	3.2829E-01	2%	U234	2.3491E-01	1%
	14	1.8735E+01	AM241	1.8108E+01	97%	U233	3.2275E-01	2%	U234	2.3123E-01	1%
	64	1.8123E+01	PU239	1.5233E+01	84%	PU240	2.7304E+00	15%	U233	8.3300E-02	0%
	67	1.6270E+01	PU239	1.1978E+01	74%	PU240	2.3449E+00	14%	AM241	1.3633E+00	8%
	28	1.1190E+01	AM241	1.0576E+01	95%	U233	3.3862E-01	3%	U234	2.4268E-01	2%
	55	9.6472E+00	AM241	8.8167E+00	91%	PU239	2.8487E-01	3%	U233	2.8006E-01	3%
	19	8.8337E+00	AM241	8.0633E+00	91%	U233	3.0567E-01	3%	U234	2.1985E-01	2%
	46	7.8671E+00	AM241	7.0795E+00	90%	U233	3.2616E-01	4%	U234	2.3378E-01	3%
	15	6.6504E+00	AM241	6.1418E+00	92%	U233	2.8958E-01	4%	U234	2.0758E-01	3%
	18	4.4919E+00	AM241	3.8971E+00	87%	U233	2.9499E-01	7%	U234	2.1083E-01	5%
	5	4.0360E+00	PU239	2.6736E+00	66%	PU240	5.3952E-01	13%	AM241	3.4492E-01	9%
	58	3.3798E+00	PU239	2.3358E+00	69%	PU240	4.6454E-01	14%	TH229	1.7070E-01	5%
	32	3.0265E+00	AM241	3.0066E+00	99%	RA226	1.3014E-02	0%	PU239	2.3076E-03	0%
	41	2.6822E+00	AM241	2.0646E+00	77%	U233	2.9897E-01	11%	U234	2.1454E-01	8%
	24	2.6710E+00	AM241	2.2550E+00	84%	TH229	1.6329E-01	6%	TH230	1.2764E-01	5%
	6	2.2398E+00	PU239	1.2093E+00	54%	U233	3.2245E-01	14%	U234	2.3239E-01	10%
	42	2.2350E+00	PU239	1.3299E+00	60%	U233	3.0902E-01	14%	PU240	2.6319E-01	12%
	53	2.1395E+00	PU239	8.7786E-01	41%	AM241	6.4127E-01	30%	U233	2.5846E-01	12%
	40	1.9444E+00	AM241	1.4252E+00	73%	U233	2.7280E-01	14%	U234	1.9630E-01	10%
	39	1.1568E+00	AM241	5.1098E-01	44%	U233	3.1071E-01	27%	U234	2.2325E-01	19%
	52	1.0484E+00	U233	3.0219E-01	29%	U234	2.1733E-01	21%	PU239	2.0287E-01	19%
	45	9.0755E-01	PU239	6.8001E-01	75%	PU240	1.3384E-01	15%	U233	2.8106E-02	3%
	70	8.8969E-01	U233	3.2313E-01	36%	U234	2.3268E-01	26%	TH229	1.3685E-01	15%
	30	8.0558E-01	AM241	4.3508E-01	54%	U233	2.0857E-01	26%	U234	1.5027E-01	19%
	1	7.3146E-01	U233	3.3002E-01	45%	U234	2.3696E-01	32%	TH229	8.5585E-02	12%
	63	7.1551E-01	AM241	6.4078E-01	90%	U233	2.2719E-02	3%	U234	1.6400E-02	2%
	60	7.0063E-01	U233	3.7112E-01	53%	U234	2.6711E-01	38%	NP237	4.6131E-02	7%
	29	6.6141E-01	U233	2.7253E-01	41%	U234	1.9599E-01	30%	TH229	7.1920E-02	11%
	47	6.4328E-01	U233	2.6967E-01	42%	U234	1.9376E-01	30%	AM241	1.3012E-01	20%
	35	6.3165E-01	U233	2.5361E-01	40%	U234	1.8288E-01	29%	TH229	1.0164E-01	16%
	27	6.0961E-01	U233	3.3583E-01	55%	U234	2.4099E-01	40%	AM241	1.2347E-02	2%
	2	6.0892E-01	U233	2.5822E-01	42%	U234	1.8575E-01	31%	TH229	8.1899E-02	13%
	3	5.9995E-01	U233	3.3174E-01	55%	U234	2.3855E-01	40%	RA226	8.5920E-03	1%
	26	5.7868E-01	U233	2.7287E-01	47%	U234	1.9658E-01	34%	AM241	5.0188E-02	9%
	31	5.7764E-01	U233	3.1091E-01	54%	U234	2.2280E-01	39%	AM241	3.0944E-02	5%

Table C-5. Vectors with Integrated Discharge through the Culebra Dolomite Member to the Accessible Environment for Scenario E1E2 and Assuming a Conceptual Model with Dual Porosity, Retardation, Clay, Matrix Diffusion, Intrusion at 1000 yr (Continued)

Comp. Scen. ID	Vector	Total EPA-normalized, Integrated Discharge	Top 3 Radionuclides Contribution to Integrated Discharge								
	10	5.6803E-01	U233	2.8043E-01	49%	U234	2.0115E-01	35%	AM241	3.6609E-02	6%
	68	5.3173E-01	U233	2.8485E-01	54%	U234	2.0417E-01	38%	AM241	2.9595E-02	6%
	62	4.7248E-01	U233	2.3342E-01	49%	U234	1.6803E-01	36%	AM241	4.8164E-02	10%
	66	4.5604E-01	U233	2.4992E-01	55%	U234	1.7923E-01	39%	NP237	1.7269E-02	4%
	21	4.4697E-01	U233	2.3355E-01	52%	U234	1.6819E-01	38%	PU239	1.5544E-02	3%
	13	4.4662E-01	U233	2.3243E-01	52%	U234	1.6771E-01	38%	NP237	2.9304E-02	7%
	25	4.4433E-01	U233	2.3441E-01	53%	U234	1.6891E-01	38%	NP237	1.6014E-02	4%
	20	4.0991E-01	U234	4.0128E-01	98%	AM241	4.6955E-03	1%	TH229	3.4309E-03	1%
	49	3.6689E-01	U233	2.0807E-01	57%	U234	1.5011E-01	41%	RA226	6.1160E-03	2%
	7	3.1454E-01	AM241	7.4657E-02	24%	PU239	7.2978E-02	23%	U233	4.6748E-02	15%
	23	2.9013E-01	PU239	1.7934E-01	62%	PU240	3.3597E-02	12%	TH229	2.4695E-02	9%
	65	2.7809E-01	U233	1.1942E-01	43%	U234	8.6289E-02	31%	PU239	3.1322E-02	11%
	37	2.6454E-01	PU239	2.1702E-01	82%	PU240	3.2911E-02	12%	U233	8.0237E-03	3%
	33	1.6210E-01	U233	6.0685E-02	37%	U234	4.3846E-02	27%	TH229	2.9083E-02	18%
	51	1.2475E-01	U233	6.0116E-02	48%	U234	4.3395E-02	35%	AM241	9.2960E-03	7%
	43	1.0729E-01	AM241	4.4342E-02	41%	U233	2.2834E-02	21%	U234	1.6497E-02	15%
	50	1.0717E-01	AM241	9.8895E-02	92%	RA226	6.0852E-03	6%	U233	1.2382E-03	1%
	38	1.0622E-01	U233	5.5296E-02	52%	U234	3.9976E-02	38%	NP237	7.0201E-03	7%
	9	6.9506E-02	U233	3.0044E-02	43%	U234	2.1726E-02	31%	TH229	8.6543E-03	12%
	16	6.8157E-02	U233	2.8944E-02	42%	U234	2.0936E-02	31%	PU239	1.1265E-02	17%
	56	6.7705E-02	U233	3.8211E-02	56%	U234	2.7625E-02	41%	RA226	1.2161E-03	2%
	57	6.4570E-02	U233	3.4748E-02	54%	U234	2.5120E-02	39%	PU239	1.4873E-03	2%
	12	6.4309E-02	AM241	3.4036E-02	53%	RA226	2.8281E-02	44%	PU239	8.2614E-04	1%
	59	4.1731E-02	AM241	2.5102E-02	60%	U233	5.9522E-03	14%	U234	4.3001E-03	10%
	11	2.4469E-02	U233	1.2764E-02	52%	U234	9.2353E-03	38%	NP237	1.6258E-03	7%
	17	1.6855E-02	RA226	1.2892E-02	76%	NP237	2.6671E-03	16%	AM241	1.2859E-03	8%
	36	9.0879E-03	U233	4.9695E-03	55%	U234	3.5957E-03	40%	RA226	4.2488E-04	5%
	44	7.4099E-03	U233	2.8507E-03	38%	U234	2.0615E-03	28%	NP237	1.8861E-03	25%
02	64	7.4398E+00	PU239	6.3272E+00	85%	PU240	1.0757E+00	14%	U233	1.8908E-02	0%
	5	2.6223E+00	PU239	1.8323E+00	70%	PU240	3.5809E-01	14%	U233	1.8591E-01	7%
	48	1.5998E+00	AM241	1.2074E+00	75%	U233	1.8819E-01	12%	U234	1.1950E-01	7%
	15	1.4192E+00	AM241	9.0606E-01	64%	U233	2.4204E-01	17%	U234	1.7830E-01	13%
	55	1.1245E+00	AM241	6.3912E-01	57%	U233	1.5497E-01	14%	PU239	1.4422E-01	13%
	4	8.1018E-01	AM241	3.3669E-01	42%	U233	1.6562E-01	20%	U234	1.0902E-01	13%
	52	5.3199E-01	U233	1.6629E-01	31%	U234	1.0756E-01	20%	PU239	9.6773E-02	18%
	31	5.2176E-01	U233	2.5468E-01	49%	U234	1.8483E-01	35%	TH229	3.7762E-02	7%
	39	5.0865E-01	U233	1.8365E-01	36%	U234	1.1461E-01	23%	TH229	9.5212E-02	19%
	70	5.0663E-01	U233	1.7125E-01	34%	U234	1.0458E-01	21%	TH229	1.0453E-01	21%
	47	4.9744E-01	U233	2.2141E-01	45%	U234	1.5632E-01	31%	AM241	3.5945E-02	7%
	46	4.9697E-01	U233	2.2074E-01	44%	U234	1.5659E-01	32%	AM241	3.6518E-02	7%
	19	3.8423E-01	U233	1.4682E-01	38%	TH229	6.1683E-02	16%	AM241	5.6854E-02	15%
	68	3.5157E-01	U233	1.7063E-01	49%	U234	1.1140E-01	32%	TH229	3.4456E-02	10%

Table C-5. Vectors with Integrated Discharge through the Culebra Dolomite Member to the Accessible Environment for Scenario E1E2 and Assuming a Conceptual Model with Dual Porosity, Retardation, Clay, Matrix Diffusion, Intrusion at 1000 yr (Continued)

Comp. Scen. ID	Vector	Total EPA-normalized, Integrated Discharge	Top 3 Radionuclides Contribution to Integrated Discharge								
	6	3.2714E-01	PU239	2.2525E-01	69%	PU240	3.7739E-02	12%	U233	2.1199E-02	6%
	14	1.3659E-01	U233	5.2046E-02	38%	TH229	3.3106E-02	24%	TH230	2.5103E-02	18%
	49	1.2935E-01	U233	6.8289E-02	53%	U234	3.7181E-02	29%	TH229	1.2854E-02	10%
	10	9.5365E-02	U233	3.9891E-02	42%	TH229	2.1184E-02	22%	U234	1.5944E-02	17%
	1	7.3931E-02	U233	2.7756E-02	38%	TH229	2.2514E-02	30%	TH230	1.6522E-02	22%
	25	7.0795E-02	U233	3.2985E-02	47%	TH229	1.2671E-02	18%	U234	1.1847E-02	17%
	66	5.8591E-02	U233	2.8356E-02	48%	TH229	1.4991E-02	26%	TH230	8.6782E-03	15%
	26	5.6905E-02	U233	2.4752E-02	43%	TH229	9.0774E-03	16%	PU239	7.9224E-03	14%
	35	3.8868E-02	TH229	1.2217E-02	31%	U233	1.2050E-02	31%	TH230	1.0461E-02	27%
	65	3.4223E-02	U233	1.2769E-02	37%	PU239	9.9092E-03	29%	U234	3.6726E-03	11%
	51	3.1533E-02	U233	1.3969E-02	44%	U234	7.8247E-03	25%	TH229	5.1002E-03	16%
	43	3.1122E-02	PU239	9.5341E-03	31%	U233	8.3647E-03	27%	U234	4.5549E-03	15%
	58	1.9514E-02	PU239	1.6448E-02	84%	PU240	2.8386E-03	15%	TH229	1.1116E-04	1%
	42	1.6532E-02	PU239	1.3677E-02	83%	PU240	2.8462E-03	17%	TH229	4.2986E-06	0%
	50	7.5564E-03	AM241	5.2142E-03	69%	RA226	1.3324E-03	18%	U233	4.9539E-04	7%
	59	7.5457E-03	U233	2.1848E-03	29%	AM241	1.5770E-03	21%	U234	1.2179E-03	16%
	29	7.4028E-03	TH229	2.9104E-03	39%	U233	1.8528E-03	25%	TH230	1.7509E-03	24%
	23	3.9549E-03	PU239	3.3333E-03	84%	PU240	5.6213E-04	14%	TH229	2.6880E-05	1%
	33	2.2398E-04	TH229	9.8575E-05	44%	TH230	8.8017E-05	39%	U233	2.3950E-05	11%
	63	1.2267E-04	TH229	5.4031E-05	44%	TH230	4.5323E-05	37%	AM241	9.2966E-06	8%
	9	1.4765E-05	TH229	5.6827E-06	38%	TH230	4.9635E-06	34%	U233	3.3129E-06	22%
	16	8.8900E-06	PU239	7.6626E-06	86%	PU240	1.1887E-06	13%	TH229	1.4055E-08	0%
	11	4.0238E-06	U233	1.8497E-06	46%	TH229	1.1237E-06	28%	TH230	5.0738E-07	13%
	18	2.4501E-06	PU239	2.0224E-06	83%	PU240	4.2713E-07	17%	TH229	3.3858E-10	0%
	12	2.1123E-06	PU239	1.4349E-06	68%	PU240	3.0961E-07	15%	RA226	2.9390E-07	14%
	24	1.7199E-07	PU239	6.0899E-08	35%	TH229	5.1494E-08	30%	TH230	4.2481E-08	25%
	40	4.5393E-09	TH229	2.2883E-09	50%	TH230	8.8384E-10	19%	U233	4.5053E-10	10%
	44	2.5787E-09	TH229	8.1549E-10	32%	U233	4.9601E-10	19%	TH230	3.9865E-10	15%
	3	1.5489E-09	U233	9.4857E-10	61%	U234	3.7179E-10	24%	TH229	1.3461E-10	9%
	32	1.3706E-09	AM241	1.2268E-09	90%	PU239	8.9295E-11	7%	PU240	1.8095E-11	1%
	57	1.0122E-09	PU239	7.9878E-10	79%	PU240	1.5931E-10	16%	U233	3.0336E-11	3%
	67	9.6018E-11	PU239	7.8296E-11	82%	PU240	1.7638E-11	18%	U233	2.9731E-14	0%
	7	5.3780E-11	PU239	4.3661E-11	81%	PU240	1.0117E-11	19%	RA226	4.2362E-16	0%
	21	1.0735E-11	U233	4.8143E-12	45%	U234	2.2874E-12	21%	PU239	2.1974E-12	20%
	20	7.3981E-12	PU239	6.0215E-12	81%	PU240	1.3398E-12	18%	U233	1.5176E-14	0%
	45	6.4161E-12	PU239	5.2204E-12	81%	PU240	1.1932E-12	19%	RA226	1.3834E-15	0%
	13	3.4304E-12	U233	1.8367E-12	54%	U234	1.1541E-12	34%	NP237	2.2407E-13	7%
	62	2.4448E-12	U233	9.9724E-13	41%	TH229	7.3057E-13	30%	TH230	3.1740E-13	13%
	41	1.2315E-12	AM241	8.5370E-13	69%	U233	1.5725E-13	13%	TH229	1.1752E-13	10%
	28	6.1138E-13	U233	2.3314E-13	38%	AM241	1.7063E-13	28%	U234	1.6292E-13	27%
	27	2.0458E-13	U233	1.3850E-13	68%	U234	3.3816E-14	17%	TH229	1.9067E-14	9%
	53	6.8844E-14	PU239	5.6094E-14	81%	PU240	1.2691E-14	18%	AM241	4.4416E-17	0%
	22	2.0337E-14	AM241	1.9410E-14	95%	U233	5.8864E-16	3%	TH229	1.9363E-16	1%

Table C-5. Vectors with Integrated Discharge through the Culebra Dolomite Member to the Accessible Environment for Scenario E1E2 and Assuming a Conceptual Model with Dual Porosity, Retardation, Clay, Matrix Diffusion, Intrusion at 1000 yr (Continued)

Comp. Scen. ID	Vector	Total EPA-normalized, Integrated Discharge	Top 3 Radionuclides Contribution to Integrated Discharge								
	8	1.6813E-14	AM241	1.5920E-14	95%	U233	4.4742E-16	3%	TH229	2.4006E-16	1%
	30	1.2627E-14	AM241	8.4374E-15	67%	U233	2.6757E-15	21%	U234	1.2602E-15	10%
	37	7.6926E-15	PU239	6.5873E-15	86%	PU240	1.0775E-15	14%	U233	1.7715E-17	0%
	17	7.1648E-15	RA226	4.7673E-15	67%	PU239	1.3183E-15	18%	PU240	7.5391E-16	11%
	60	6.3257E-15	U233	3.7468E-15	59%	PU239	6.9432E-16	11%	TH229	5.3069E-16	8%
	2	1.6995E-15	U233	7.6826E-16	45%	U234	4.7135E-16	28%	TH229	2.4665E-16	15%
	38	1.0373E-15	U233	3.6615E-16	35%	PU240	2.4939E-16	24%	PU239	1.5507E-16	15%
	34	8.5961E-16	U233	5.2466E-16	61%	TH229	1.4732E-16	17%	RA226	8.8110E-17	10%
	54	2.6880E-16	PU239	2.1514E-16	80%	PU240	5.3100E-17	20%	AM241	5.4714E-19	0%
	56	3.0443E-18	U233	1.8870E-18	62%	RA226	6.8848E-19	23%	TH229	2.3680E-19	8%
	36	2.1027E-23	U233	1.2969E-23	62%	U234	5.2115E-24	25%	RA226	2.2437E-24	11%

Table C-6 lists total EPA summed normalized release and the percentages contribution for the 3 radionuclides contributing the most release for each vector when drilling into a CH waste drum with an average activity level. Vectors are ordered from most to least release. All vectors have some release when intruding into the repository from drilling.

Table C-6. Vectors with CH Cuttings Discharged to the Ground Surface

Comp. Scen. ID	Vector	Total EPA-normalized Cuttings	Top 3 Radionuclides Contribution to Integrated Discharge								
			(Time of Intrusion, 125 years)								
01	32	4.5271E-02	PU238	2.4764E-02	55%	AM241	1.2726E-02	28%	PU239	5.9680E-03	13%
	39	4.4913E-02	PU238	2.4568E-02	55%	AM241	1.2626E-02	28%	PU239	5.9208E-03	13%
	70	4.4782E-02	PU238	2.4496E-02	55%	AM241	1.2589E-02	28%	PU239	5.9035E-03	13%
	63	4.4294E-02	PU238	2.4230E-02	55%	AM241	1.2452E-02	28%	PU239	5.8392E-03	13%
	25	4.4057E-02	PU238	2.4100E-02	55%	AM241	1.2385E-02	28%	PU239	5.8079E-03	13%
	58	4.3796E-02	PU238	2.3957E-02	55%	AM241	1.2312E-02	28%	PU239	5.7735E-03	13%
	30	4.3512E-02	PU238	2.3802E-02	55%	AM241	1.2232E-02	28%	PU239	5.7361E-03	13%
	19	4.3299E-02	PU238	2.3685E-02	55%	AM241	1.2172E-02	28%	PU239	5.7080E-03	13%
	62	4.3028E-02	PU238	2.3537E-02	55%	AM241	1.2096E-02	28%	PU239	5.6723E-03	13%
	3	4.2733E-02	PU238	2.3376E-02	55%	AM241	1.2013E-02	28%	PU239	5.6334E-03	13%
	13	4.2439E-02	PU238	2.3215E-02	55%	AM241	1.1930E-02	28%	PU239	5.5947E-03	13%
	22	4.2076E-02	PU238	2.3016E-02	55%	AM241	1.1828E-02	28%	PU239	5.5467E-03	13%
	47	4.1794E-02	PU238	2.2862E-02	55%	AM241	1.1749E-02	28%	PU239	5.5096E-03	13%
	7	4.1397E-02	PU238	2.2645E-02	55%	AM241	1.1637E-02	28%	PU239	5.4572E-03	13%
	1	4.1245E-02	PU238	2.2562E-02	55%	AM241	1.1594E-02	28%	PU239	5.4372E-03	13%

Table C-6. Vectors with CH Cuttings Discharged to the Ground Surface (Continued)

Comp. Scen. ID	Vector	Total EPA-normalized Cuttings	Top 3 Radionuclides Contribution to Integrated Discharge								
			(Time of Intrusion, 125 years)								
	50	4.0826E-02	PU238	2.2332E-02	55%	AM241	1.1477E-02	28%	PU239	5.3820E-03	13%
	45	4.0628E-02	PU238	2.2224E-02	55%	AM241	1.1421E-02	28%	PU239	5.3559E-03	13%
	65	4.0291E-02	PU238	2.2040E-02	55%	AM241	1.1326E-02	28%	PU239	5.3115E-03	13%
	43	3.9863E-02	PU238	2.1806E-02	55%	AM241	1.1206E-02	28%	PU239	5.2550E-03	13%
	12	3.9655E-02	PU238	2.1692E-02	55%	AM241	1.1147E-02	28%	PU239	5.2276E-03	13%
	31	3.9447E-02	PU238	2.1578E-02	55%	AM241	1.1089E-02	28%	PU239	5.2002E-03	13%
	4	3.9170E-02	PU238	2.1427E-02	55%	AM241	1.1011E-02	28%	PU239	5.1637E-03	13%
	48	3.8883E-02	PU238	2.1269E-02	55%	AM241	1.0930E-02	28%	PU239	5.1258E-03	13%
	54	3.8515E-02	PU238	2.1068E-02	55%	AM241	1.0827E-02	28%	PU239	5.0773E-03	13%
	37	3.8297E-02	PU238	2.0949E-02	55%	AM241	1.0766E-02	28%	PU239	5.0486E-03	13%
	69	3.7874E-02	PU238	2.0718E-02	55%	AM241	1.0647E-02	28%	PU239	4.9928E-03	13%
	2	3.7703E-02	PU238	2.0624E-02	55%	AM241	1.0599E-02	28%	PU239	4.9702E-03	13%
	35	3.7247E-02	PU238	2.0375E-02	55%	AM241	1.0470E-02	28%	PU239	4.9101E-03	13%
	67	3.7179E-02	PU238	2.0337E-02	55%	AM241	1.0451E-02	28%	PU239	4.9011E-03	13%
	28	3.6872E-02	PU238	2.0169E-02	55%	AM241	1.0365E-02	28%	PU239	4.8607E-03	13%
	6	3.6430E-02	PU238	1.9928E-02	55%	AM241	1.0241E-02	28%	PU239	4.8024E-03	13%
	40	3.6056E-02	PU238	1.9723E-02	55%	AM241	1.0136E-02	28%	PU239	4.7532E-03	13%
	56	3.5797E-02	PU238	1.9581E-02	55%	AM241	1.0063E-02	28%	PU239	4.7190E-03	13%
	10	3.5695E-02	PU238	1.9526E-02	55%	AM241	1.0034E-02	28%	PU239	4.7056E-03	13%
	34	3.5448E-02	PU238	1.9390E-02	55%	AM241	9.9647E-03	28%	PU239	4.6730E-03	13%
	66	3.5021E-02	PU238	1.9157E-02	55%	AM241	9.8447E-03	28%	PU239	4.6167E-03	13%
	53	3.4718E-02	PU238	1.8991E-02	55%	AM241	9.7596E-03	28%	PU239	4.5768E-03	13%
	64	3.4349E-02	PU238	1.8790E-02	55%	AM241	9.6559E-03	28%	PU239	4.5282E-03	13%
	59	3.4271E-02	PU238	1.8747E-02	55%	AM241	9.6339E-03	28%	PU239	4.5179E-03	13%
	57	3.3981E-02	PU238	1.8588E-02	55%	AM241	9.5524E-03	28%	PU239	4.4796E-03	13%
	14	3.3603E-02	PU238	1.8381E-02	55%	AM241	9.4461E-03	28%	PU239	4.4298E-03	13%
	20	3.3314E-02	PU238	1.8223E-02	55%	AM241	9.3649E-03	28%	PU239	4.3917E-03	13%
	15	3.2948E-02	PU238	1.8023E-02	55%	AM241	9.2621E-03	28%	PU239	4.3435E-03	13%
	29	3.2760E-02	PU238	1.7920E-02	55%	AM241	9.2093E-03	28%	PU239	4.3187E-03	13%
	11	3.2539E-02	PU238	1.7800E-02	55%	AM241	9.1472E-03	28%	PU239	4.2896E-03	13%
	55	3.2242E-02	PU238	1.7637E-02	55%	AM241	9.0635E-03	28%	PU239	4.2504E-03	13%
	60	3.1846E-02	PU238	1.7420E-02	55%	AM241	8.9522E-03	28%	PU239	4.1982E-03	13%
	18	3.1593E-02	PU238	1.7282E-02	55%	AM241	8.8812E-03	28%	PU239	4.1649E-03	13%
	61	3.1352E-02	PU238	1.7150E-02	55%	AM241	8.8135E-03	28%	PU239	4.1331E-03	13%
	36	3.1155E-02	PU238	1.7043E-02	55%	AM241	8.7581E-03	28%	PU239	4.1071E-03	13%
	51	3.0675E-02	PU238	1.6780E-02	55%	AM241	8.6231E-03	28%	PU239	4.0438E-03	13%
	49	3.0675E-02	PU238	1.6780E-02	55%	AM241	8.6231E-03	28%	PU239	4.0438E-03	13%
	46	3.0283E-02	PU238	1.6565E-02	55%	AM241	8.5130E-03	28%	PU239	3.9922E-03	13%
	21	3.0023E-02	PU238	1.6423E-02	55%	AM241	8.4397E-03	28%	PU239	3.9578E-03	13%
	23	2.9676E-02	PU238	1.6233E-02	55%	AM241	8.3422E-03	28%	PU239	3.9121E-03	13%
	52	2.9309E-02	PU238	1.6032E-02	55%	AM241	8.2389E-03	28%	PU239	3.8637E-03	13%
	44	2.9222E-02	PU238	1.5985E-02	55%	AM241	8.2147E-03	28%	PU239	3.8523E-03	13%
	38	2.8781E-02	PU238	1.5743E-02	55%	AM241	8.0905E-03	28%	PU239	3.7941E-03	13%
	8	2.8501E-02	PU238	1.5591E-02	55%	AM241	8.0120E-03	28%	PU239	3.7573E-03	13%

Table C-6. Vectors with CH Cuttings Discharged to the Ground Surface (Continued)

Comp. Scen. ID	Vector	Total EPA-normalized Cuttings	Top 3 Radionuclides Contribution to Integrated Discharge								
			(Time of Intrusion, 125 years)								
	16	2.8319E-02	PU238	1.5491E-02	55%	AM241	7.9607E-03	28%	PU239	3.7332E-03	13%
	42	2.8126E-02	PU238	1.5385E-02	55%	AM241	7.9065E-03	28%	PU239	3.7078E-03	13%
	33	2.7731E-02	PU238	1.5169E-02	55%	AM241	7.7953E-03	28%	PU239	3.6557E-03	13%
	17	2.7411E-02	PU238	1.4994E-02	55%	AM241	7.7054E-03	28%	PU239	3.6135E-03	13%
	41	2.7187E-02	PU238	1.4872E-02	55%	AM241	7.6426E-03	28%	PU239	3.5840E-03	13%
	24	2.6953E-02	PU238	1.4744E-02	55%	AM241	7.5769E-03	28%	PU239	3.5532E-03	13%
	5	2.6784E-02	PU238	1.4651E-02	55%	AM241	7.5292E-03	28%	PU239	3.5308E-03	13%
	9	2.6508E-02	PU238	1.4500E-02	55%	AM241	7.4517E-03	28%	PU239	3.4945E-03	13%
	68	2.6128E-02	PU238	1.4292E-02	55%	AM241	7.3448E-03	28%	PU239	3.4444E-03	13%
	26	2.5822E-02	PU238	1.4125E-02	55%	AM241	7.2589E-03	28%	PU239	3.4041E-03	13%
	27	2.5738E-02	PU238	1.4079E-02	55%	AM241	7.2352E-03	28%	PU239	3.3930E-03	13%
			(Time of Intrusion, 175 years)								
02	32	3.2751E-02	PU238	1.3693E-02	42%	AM241	1.1299E-02	35%	PU239	5.9551E-03	18%
	39	3.2492E-02	PU238	1.3585E-02	42%	AM241	1.1210E-02	35%	PU239	5.9080E-03	18%
	70	3.2397E-02	PU238	1.3545E-02	42%	AM241	1.1177E-02	35%	PU239	5.8908E-03	18%
	63	3.2044E-02	PU238	1.3398E-02	42%	AM241	1.1056E-02	35%	PU239	5.8266E-03	18%
	25	3.1873E-02	PU238	1.3326E-02	42%	AM241	1.0996E-02	35%	PU239	5.7954E-03	18%
	58	3.1684E-02	PU238	1.3247E-02	42%	AM241	1.0931E-02	35%	PU239	5.7611E-03	18%
	30	3.1478E-02	PU238	1.3161E-02	42%	AM241	1.0860E-02	35%	PU239	5.7237E-03	18%
	19	3.1325E-02	PU238	1.3097E-02	42%	AM241	1.0807E-02	35%	PU239	5.6957E-03	18%
	62	3.1128E-02	PU238	1.3015E-02	42%	AM241	1.0740E-02	35%	PU239	5.6600E-03	18%
	3	3.0915E-02	PU238	1.2926E-02	42%	AM241	1.0666E-02	35%	PU239	5.6213E-03	18%
	13	3.0702E-02	PU238	1.2837E-02	42%	AM241	1.0593E-02	35%	PU239	5.5826E-03	18%
	22	3.0439E-02	PU238	1.2727E-02	42%	AM241	1.0502E-02	35%	PU239	5.5347E-03	18%
	47	3.0236E-02	PU238	1.2642E-02	42%	AM241	1.0432E-02	35%	PU239	5.4978E-03	18%
	7	2.9948E-02	PU238	1.2521E-02	42%	AM241	1.0332E-02	35%	PU239	5.4455E-03	18%
	1	2.9839E-02	PU238	1.2476E-02	42%	AM241	1.0295E-02	35%	PU239	5.4255E-03	18%
	50	2.9535E-02	PU238	1.2349E-02	42%	AM241	1.0190E-02	35%	PU239	5.3703E-03	18%
	45	2.9392E-02	PU238	1.2289E-02	42%	AM241	1.0141E-02	35%	PU239	5.3443E-03	18%
	65	2.9148E-02	PU238	1.2187E-02	42%	AM241	1.0056E-02	35%	PU239	5.3000E-03	18%
	43	2.8838E-02	PU238	1.2057E-02	42%	AM241	9.9495E-03	35%	PU239	5.2437E-03	18%
	12	2.8688E-02	PU238	1.1994E-02	42%	AM241	9.8976E-03	35%	PU239	5.2163E-03	18%
	31	2.8538E-02	PU238	1.1932E-02	42%	AM241	9.8457E-03	35%	PU239	5.1890E-03	18%
	4	2.8337E-02	PU238	1.1848E-02	42%	AM241	9.7767E-03	35%	PU239	5.1526E-03	18%
	48	2.8129E-02	PU238	1.1761E-02	42%	AM241	9.7048E-03	35%	PU239	5.1147E-03	18%
	54	2.7863E-02	PU238	1.1650E-02	42%	AM241	9.6131E-03	35%	PU239	5.0664E-03	18%
	37	2.7706E-02	PU238	1.1584E-02	42%	AM241	9.5588E-03	35%	PU239	5.0377E-03	18%
	69	2.7400E-02	PU238	1.1456E-02	42%	AM241	9.4531E-03	35%	PU239	4.9820E-03	18%
	2	2.7276E-02	PU238	1.1404E-02	42%	AM241	9.4103E-03	35%	PU239	4.9595E-03	18%
	35	2.6946E-02	PU238	1.1266E-02	42%	AM241	9.2966E-03	35%	PU239	4.8996E-03	18%
	67	2.6897E-02	PU238	1.1246E-02	42%	AM241	9.2795E-03	35%	PU239	4.8906E-03	18%
	28	2.6675E-02	PU238	1.1153E-02	42%	AM241	9.2029E-03	35%	PU239	4.8502E-03	18%

Table C-6. Vectors with CH Cuttings Discharged to the Ground Surface (Continued)

Comp. Scen. ID	Vector	Total EPA-normalized Cuttings	Top 3 Radionuclides Contribution to Integrated Discharge								
(Time of Intrusion, 175 years)											
	6	2.6355E-02	PU238	1.1019E-02	42%	AM241	9.0926E-03	35%	PU239	4.7920E-03	18%
	40	2.6085E-02	PU238	1.0906E-02	42%	AM241	8.9995E-03	35%	PU239	4.7430E-03	18%
	56	2.5897E-02	PU238	1.0828E-02	42%	AM241	8.9347E-03	35%	PU239	4.7088E-03	18%
	10	2.5824E-02	PU238	1.0797E-02	42%	AM241	8.9094E-03	35%	PU239	4.6955E-03	18%
	34	2.5644E-02	PU238	1.0722E-02	42%	AM241	8.8475E-03	35%	PU239	4.6629E-03	18%
	66	2.5336E-02	PU238	1.0593E-02	42%	AM241	8.7410E-03	35%	PU239	4.6067E-03	18%
	53	2.5117E-02	PU238	1.0501E-02	42%	AM241	8.6655E-03	35%	PU239	4.5669E-03	18%
	64	2.4850E-02	PU238	1.0390E-02	42%	AM241	8.5734E-03	35%	PU239	4.5184E-03	18%
	59	2.4793E-02	PU238	1.0366E-02	42%	AM241	8.5538E-03	35%	PU239	4.5081E-03	18%
	57	2.4583E-02	PU238	1.0278E-02	42%	AM241	8.4815E-03	35%	PU239	4.4700E-03	18%
	14	2.4310E-02	PU238	1.0164E-02	42%	AM241	8.3870E-03	35%	PU239	4.4202E-03	18%
	20	2.4101E-02	PU238	1.0077E-02	42%	AM241	8.3150E-03	35%	PU239	4.3822E-03	18%
	15	2.3836E-02	PU238	9.9660E-03	42%	AM241	8.2237E-03	35%	PU239	4.3341E-03	18%
	29	2.3700E-02	PU238	9.9091E-03	42%	AM241	8.1768E-03	35%	PU239	4.3094E-03	18%
	11	2.3540E-02	PU238	9.8423E-03	42%	AM241	8.1217E-03	35%	PU239	4.2803E-03	18%
	55	2.3325E-02	PU238	9.7523E-03	42%	AM241	8.0474E-03	35%	PU239	4.2412E-03	18%
	60	2.3039E-02	PU238	9.6325E-03	42%	AM241	7.9485E-03	35%	PU239	4.1891E-03	18%
	18	2.2856E-02	PU238	9.5562E-03	42%	AM241	7.8855E-03	35%	PU239	4.1559E-03	18%
	61	2.2682E-02	PU238	9.4833E-03	42%	AM241	7.8254E-03	35%	PU239	4.1242E-03	18%
	36	2.2539E-02	PU238	9.4237E-03	42%	AM241	7.7762E-03	35%	PU239	4.0983E-03	18%
	51	2.2192E-02	PU238	9.2784E-03	42%	AM241	7.6563E-03	35%	PU239	4.0351E-03	18%
	49	2.2192E-02	PU238	9.2784E-03	42%	AM241	7.6563E-03	35%	PU239	4.0351E-03	18%
	46	2.1908E-02	PU238	9.1599E-03	42%	AM241	7.5586E-03	35%	PU239	3.9836E-03	18%
	21	2.1720E-02	PU238	9.0811E-03	42%	AM241	7.4935E-03	35%	PU239	3.9493E-03	18%
	23	2.1469E-02	PU238	8.9762E-03	42%	AM241	7.4070E-03	35%	PU239	3.9037E-03	18%
	52	2.1203E-02	PU238	8.8651E-03	42%	AM241	7.3153E-03	35%	PU239	3.8553E-03	18%
	44	2.1141E-02	PU238	8.8390E-03	42%	AM241	7.2937E-03	35%	PU239	3.8440E-03	18%
	38	2.0821E-02	PU238	8.7054E-03	42%	AM241	7.1835E-03	35%	PU239	3.7859E-03	18%
	8	2.0619E-02	PU238	8.6209E-03	42%	AM241	7.1138E-03	35%	PU239	3.7491E-03	18%
	16	2.0487E-02	PU238	8.5657E-03	42%	AM241	7.0682E-03	35%	PU239	3.7252E-03	18%
	42	2.0348E-02	PU238	8.5074E-03	42%	AM241	7.0201E-03	35%	PU239	3.6998E-03	18%
	33	2.0061E-02	PU238	8.3878E-03	42%	AM241	6.9214E-03	35%	PU239	3.6478E-03	18%
	17	1.9830E-02	PU238	8.2910E-03	42%	AM241	6.8415E-03	35%	PU239	3.6057E-03	18%
	41	1.9668E-02	PU238	8.2234E-03	42%	AM241	6.7858E-03	35%	PU239	3.5763E-03	18%
	24	1.9499E-02	PU238	8.1527E-03	42%	AM241	6.7274E-03	35%	PU239	3.5455E-03	18%
	5	1.9376E-02	PU238	8.1014E-03	42%	AM241	6.6850E-03	35%	PU239	3.5232E-03	18%
	9	1.9177E-02	PU238	8.0180E-03	42%	AM241	6.6163E-03	35%	PU239	3.4870E-03	18%
	68	1.8902E-02	PU238	7.9030E-03	42%	AM241	6.5214E-03	35%	PU239	3.4369E-03	18%
	26	1.8681E-02	PU238	7.8105E-03	42%	AM241	6.4451E-03	35%	PU239	3.3967E-03	18%
	27	1.8620E-02	PU238	7.7850E-03	42%	AM241	6.4240E-03	35%	PU239	3.3856E-03	18%
(Time of Intrusion, 350 years)											
03	32	1.9671E-02	AM241	8.5346E-03	43%	PU239	5.9252E-03	30%	PU238	3.4362E-03	17%
	39	1.9516E-02	AM241	8.4671E-03	43%	PU239	5.8783E-03	30%	PU238	3.4090E-03	17%

Table C-6. Vectors with CH Cuttings Discharged to the Ground Surface (Continued)

Comp. Scen. ID	Vector	Total EPA-normalized Cuttings	Top 3 Radionuclides Contribution to Integrated Discharge								
(Time of Intrusion, 350 years)											
	70	1.9459E-02	AM241	8.4424E-03	43%	PU239	5.8611E-03	30%	PU238	3.3991E-03	17%
	63	1.9247E-02	AM241	8.3504E-03	43%	PU239	5.7973E-03	30%	PU238	3.3621E-03	17%
	25	1.9144E-02	AM241	8.3057E-03	43%	PU239	5.7662E-03	30%	PU238	3.3441E-03	17%
	58	1.9030E-02	AM241	8.2565E-03	43%	PU239	5.7321E-03	30%	PU238	3.3243E-03	17%
	30	1.8907E-02	AM241	8.2030E-03	43%	PU239	5.6949E-03	30%	PU238	3.3027E-03	17%
	19	1.8815E-02	AM241	8.1629E-03	43%	PU239	5.6671E-03	30%	PU238	3.2866E-03	17%
	62	1.8697E-02	AM241	8.1117E-03	43%	PU239	5.6316E-03	30%	PU238	3.2659E-03	17%
	3	1.8569E-02	AM241	8.0562E-03	43%	PU239	5.5930E-03	30%	PU238	3.2436E-03	17%
	13	1.8441E-02	AM241	8.0007E-03	43%	PU239	5.5545E-03	30%	PU238	3.2213E-03	17%
	22	1.8283E-02	AM241	7.9321E-03	43%	PU239	5.5069E-03	30%	PU238	3.1937E-03	17%
	47	1.8161E-02	AM241	7.8791E-03	43%	PU239	5.4701E-03	30%	PU238	3.1723E-03	17%
	7	1.7988E-02	AM241	7.8042E-03	43%	PU239	5.4181E-03	30%	PU238	3.1422E-03	17%
	1	1.7922E-02	AM241	7.7756E-03	43%	PU239	5.3982E-03	30%	PU238	3.1306E-03	17%
	50	1.7740E-02	AM241	7.6965E-03	43%	PU239	5.3433E-03	30%	PU238	3.0988E-03	17%
	45	1.7654E-02	AM241	7.6593E-03	43%	PU239	5.3175E-03	30%	PU238	3.0838E-03	17%
	65	1.7508E-02	AM241	7.5958E-03	43%	PU239	5.2734E-03	30%	PU238	3.0582E-03	17%
	43	1.7321E-02	AM241	7.5150E-03	43%	PU239	5.2173E-03	30%	PU238	3.0257E-03	17%
	12	1.7231E-02	AM241	7.4758E-03	43%	PU239	5.1901E-03	30%	PU238	3.0099E-03	17%
	31	1.7141E-02	AM241	7.4366E-03	43%	PU239	5.1629E-03	30%	PU238	2.9941E-03	17%
	4	1.7020E-02	AM241	7.3844E-03	43%	PU239	5.1267E-03	30%	PU238	2.9731E-03	17%
	48	1.6895E-02	AM241	7.3302E-03	43%	PU239	5.0890E-03	30%	PU238	2.9513E-03	17%
	54	1.6736E-02	AM241	7.2609E-03	43%	PU239	5.0409E-03	30%	PU238	2.9234E-03	17%
	37	1.6641E-02	AM241	7.2199E-03	43%	PU239	5.0124E-03	30%	PU238	2.9069E-03	17%
	69	1.6457E-02	AM241	7.1401E-03	43%	PU239	4.9570E-03	30%	PU238	2.8747E-03	17%
	2	1.6383E-02	AM241	7.1078E-03	43%	PU239	4.9346E-03	30%	PU238	2.8617E-03	17%
	35	1.6185E-02	AM241	7.0218E-03	43%	PU239	4.8749E-03	30%	PU238	2.8271E-03	17%
	67	1.6155E-02	AM241	7.0090E-03	43%	PU239	4.8660E-03	30%	PU238	2.8220E-03	17%
	28	1.6022E-02	AM241	6.9511E-03	43%	PU239	4.8258E-03	30%	PU238	2.7987E-03	17%
	6	1.5829E-02	AM241	6.8678E-03	43%	PU239	4.7680E-03	30%	PU238	2.7651E-03	17%
	40	1.5667E-02	AM241	6.7974E-03	43%	PU239	4.7191E-03	30%	PU238	2.7368E-03	17%
	56	1.5555E-02	AM241	6.7485E-03	43%	PU239	4.6851E-03	30%	PU238	2.7171E-03	17%
	10	1.5510E-02	AM241	6.7294E-03	43%	PU239	4.6719E-03	30%	PU238	2.7094E-03	17%
	34	1.5403E-02	AM241	6.6827E-03	43%	PU239	4.6395E-03	30%	PU238	2.6906E-03	17%
	66	1.5217E-02	AM241	6.6022E-03	43%	PU239	4.5836E-03	30%	PU238	2.6582E-03	17%
	53	1.5086E-02	AM241	6.5451E-03	43%	PU239	4.5440E-03	30%	PU238	2.6352E-03	17%
	64	1.4926E-02	AM241	6.4756E-03	43%	PU239	4.4957E-03	30%	PU238	2.6072E-03	17%
	59	1.4892E-02	AM241	6.4608E-03	43%	PU239	4.4854E-03	30%	PU238	2.6013E-03	17%
	57	1.4766E-02	AM241	6.4062E-03	43%	PU239	4.4475E-03	30%	PU238	2.5793E-03	17%
	14	1.4601E-02	AM241	6.3348E-03	43%	PU239	4.3980E-03	30%	PU238	2.5505E-03	17%
	20	1.4476E-02	AM241	6.2804E-03	43%	PU239	4.3602E-03	30%	PU238	2.5286E-03	17%
	15	1.4317E-02	AM241	6.2115E-03	43%	PU239	4.3123E-03	30%	PU238	2.5009E-03	17%
	29	1.4235E-02	AM241	6.1760E-03	43%	PU239	4.2877E-03	30%	PU238	2.4866E-03	17%
	11	1.4139E-02	AM241	6.1344E-03	43%	PU239	4.2588E-03	30%	PU238	2.4698E-03	17%
	55	1.4010E-02	AM241	6.0783E-03	43%	PU239	4.2199E-03	30%	PU238	2.4473E-03	17%

Table C-6. Vectors with CH Cuttings Discharged to the Ground Surface (Continued)

Comp. Scen. ID	Vector	Total EPA-normalized Cuttings	Top 3 Radionuclides Contribution to Integrated Discharge								
			(Time of Intrusion, 350 years)								
	60	1.3838E-02	AM241	6.0036E-03	43%	PU239	4.1680E-03	30%	PU238	2.4172E-03	17%
	18	1.3728E-02	AM241	5.9560E-03	43%	PU239	4.1350E-03	30%	PU238	2.3980E-03	17%
	61	1.3623E-02	AM241	5.9106E-03	43%	PU239	4.1034E-03	30%	PU238	2.3797E-03	17%
	36	1.3538E-02	AM241	5.8735E-03	43%	PU239	4.0777E-03	30%	PU238	2.3648E-03	17%
	51	1.3329E-02	AM241	5.7829E-03	43%	PU239	4.0148E-03	30%	PU238	2.3283E-03	17%
	49	1.3329E-02	AM241	5.7829E-03	43%	PU239	4.0148E-03	30%	PU238	2.3283E-03	17%
	46	1.3159E-02	AM241	5.7091E-03	43%	PU239	3.9635E-03	30%	PU238	2.2986E-03	17%
	21	1.3046E-02	AM241	5.6600E-03	43%	PU239	3.9294E-03	30%	PU238	2.2788E-03	17%
	23	1.2895E-02	AM241	5.5946E-03	43%	PU239	3.8841E-03	30%	PU238	2.2525E-03	17%
	52	1.2735E-02	AM241	5.5253E-03	43%	PU239	3.8360E-03	30%	PU238	2.2246E-03	17%
	44	1.2698E-02	AM241	5.5090E-03	43%	PU239	3.8247E-03	30%	PU238	2.2181E-03	17%
	38	1.2506E-02	AM241	5.4258E-03	43%	PU239	3.7669E-03	30%	PU238	2.1845E-03	17%
	8	1.2384E-02	AM241	5.3731E-03	43%	PU239	3.7303E-03	30%	PU238	2.1633E-03	17%
	16	1.2305E-02	AM241	5.3387E-03	43%	PU239	3.7064E-03	30%	PU238	2.1495E-03	17%
	42	1.2221E-02	AM241	5.3024E-03	43%	PU239	3.6812E-03	30%	PU238	2.1349E-03	17%
	33	1.2050E-02	AM241	5.2278E-03	43%	PU239	3.6294E-03	30%	PU238	2.1048E-03	17%
	17	1.1911E-02	AM241	5.1675E-03	43%	PU239	3.5876E-03	30%	PU238	2.0806E-03	17%
	41	1.1813E-02	AM241	5.1254E-03	43%	PU239	3.5583E-03	30%	PU238	2.0636E-03	17%
	24	1.1712E-02	AM241	5.0813E-03	43%	PU239	3.5277E-03	30%	PU238	2.0458E-03	17%
	5	1.1638E-02	AM241	5.0493E-03	43%	PU239	3.5055E-03	30%	PU238	2.0330E-03	17%
	9	1.1518E-02	AM241	4.9974E-03	43%	PU239	3.4694E-03	30%	PU238	2.0121E-03	17%
	68	1.1353E-02	AM241	4.9257E-03	43%	PU239	3.4197E-03	30%	PU238	1.9832E-03	17%
	26	1.1220E-02	AM241	4.8680E-03	43%	PU239	3.3796E-03	30%	PU238	1.9600E-03	17%
	27	1.1184E-02	AM241	4.8522E-03	43%	PU239	3.3686E-03	30%	PU238	1.9536E-03	17%
			(Time of Intrusion, 1000 years)								
04	32	1.0509E-02	PU239	5.8153E-03	55%	AM241	3.0092E-03	29%	PU240	1.6121E-03	15%
	39	1.0425E-02	PU239	5.7693E-03	55%	AM241	2.9854E-03	29%	PU240	1.5994E-03	15%
	70	1.0395E-02	PU239	5.7524E-03	55%	AM241	2.9767E-03	29%	PU240	1.5947E-03	15%
	63	1.0282E-02	PU239	5.6898E-03	55%	AM241	2.9443E-03	29%	PU240	1.5774E-03	15%
	25	1.0227E-02	PU239	5.6593E-03	55%	AM241	2.9285E-03	29%	PU240	1.5689E-03	15%
	58	1.0166E-02	PU239	5.6258E-03	55%	AM241	2.9112E-03	29%	PU240	1.5596E-03	15%
	30	1.0100E-02	PU239	5.5893E-03	55%	AM241	2.8923E-03	29%	PU240	1.5495E-03	15%
	19	1.0051E-02	PU239	5.5620E-03	55%	AM241	2.8782E-03	29%	PU240	1.5419E-03	15%
	62	9.9878E-03	PU239	5.5271E-03	55%	AM241	2.8601E-03	29%	PU240	1.5323E-03	15%
	3	9.9194E-03	PU239	5.4893E-03	55%	AM241	2.8405E-03	29%	PU240	1.5218E-03	15%
	13	9.8512E-03	PU239	5.4515E-03	55%	AM241	2.8210E-03	29%	PU240	1.5113E-03	15%
	22	9.7667E-03	PU239	5.4048E-03	55%	AM241	2.7968E-03	29%	PU240	1.4983E-03	15%
	47	9.7014E-03	PU239	5.3687E-03	55%	AM241	2.7781E-03	29%	PU240	1.4883E-03	15%
	7	9.6092E-03	PU239	5.3176E-03	55%	AM241	2.7517E-03	29%	PU240	1.4742E-03	15%
	1	9.5740E-03	PU239	5.2981E-03	55%	AM241	2.7416E-03	29%	PU240	1.4688E-03	15%
	50	9.4766E-03	PU239	5.2442E-03	55%	AM241	2.7137E-03	29%	PU240	1.4538E-03	15%
	45	9.4307E-03	PU239	5.2188E-03	55%	AM241	2.7006E-03	29%	PU240	1.4468E-03	15%
	65	9.3526E-03	PU239	5.1756E-03	55%	AM241	2.6782E-03	29%	PU240	1.4348E-03	15%
	43	9.2531E-03	PU239	5.1205E-03	55%	AM241	2.6497E-03	29%	PU240	1.4195E-03	15%
	12	9.2048E-03	PU239	5.0938E-03	55%	AM241	2.6359E-03	29%	PU240	1.4121E-03	15%
	31	9.1565E-03	PU239	5.0671E-03	55%	AM241	2.6221E-03	29%	PU240	1.4047E-03	15%
	4	9.0923E-03	PU239	5.0316E-03	55%	AM241	2.6037E-03	29%	PU240	1.3949E-03	15%

Table C-6. Vectors with CH Cuttings Discharged to the Ground Surface (Continued)

Comp. Scen. ID	Vector	Total EPA-normalized Cuttings	Top 3 Radionuclides Contribution to Integrated Discharge								
			(Time of Intrusion, 1000 years)								
	48	9.0255E-03	PU239	4.9946E-03	55%	AM241	2.5846E-03	29%	PU240	1.3846E-03	15%
	54	8.9402E-03	PU239	4.9474E-03	55%	AM241	2.5601E-03	29%	PU240	1.3715E-03	15%
	37	8.8897E-03	PU239	4.9194E-03	55%	AM241	2.5457E-03	29%	PU240	1.3638E-03	15%
	69	8.7914E-03	PU239	4.8651E-03	55%	AM241	2.5175E-03	29%	PU240	1.3487E-03	15%
	2	8.7517E-03	PU239	4.8431E-03	55%	AM241	2.5061E-03	29%	PU240	1.3426E-03	15%
	35	8.6458E-03	PU239	4.7845E-03	55%	AM241	2.4758E-03	29%	PU240	1.3264E-03	15%
	67	8.6300E-03	PU239	4.7757E-03	55%	AM241	2.4713E-03	29%	PU240	1.3240E-03	15%
	28	8.5588E-03	PU239	4.7363E-03	55%	AM241	2.4509E-03	29%	PU240	1.3130E-03	15%
	6	8.4561E-03	PU239	4.6795E-03	55%	AM241	2.4215E-03	29%	PU240	1.2973E-03	15%
	40	8.3695E-03	PU239	4.6316E-03	55%	AM241	2.3967E-03	29%	PU240	1.2840E-03	15%
	56	8.3093E-03	PU239	4.5982E-03	55%	AM241	2.3795E-03	29%	PU240	1.2747E-03	15%
	10	8.2857E-03	PU239	4.5852E-03	55%	AM241	2.3727E-03	29%	PU240	1.2711E-03	15%
	34	8.2282E-03	PU239	4.5534E-03	55%	AM241	2.3562E-03	29%	PU240	1.2623E-03	15%
	66	8.1291E-03	PU239	4.4986E-03	55%	AM241	2.3279E-03	29%	PU240	1.2471E-03	15%
	53	8.0589E-03	PU239	4.4597E-03	55%	AM241	2.3078E-03	29%	PU240	1.2363E-03	15%
	64	7.9732E-03	PU239	4.4123E-03	55%	AM241	2.2832E-03	29%	PU240	1.2232E-03	15%
	59	7.9551E-03	PU239	4.4023E-03	55%	AM241	2.2780E-03	29%	PU240	1.2204E-03	15%
	57	7.8878E-03	PU239	4.3650E-03	55%	AM241	2.2588E-03	29%	PU240	1.2101E-03	15%
	14	7.8000E-03	PU239	4.3164E-03	55%	AM241	2.2336E-03	29%	PU240	1.1966E-03	15%
	20	7.7330E-03	PU239	4.2793E-03	55%	AM241	2.2144E-03	29%	PU240	1.1863E-03	15%
	15	7.6481E-03	PU239	4.2324E-03	55%	AM241	2.1901E-03	29%	PU240	1.1733E-03	15%
	29	7.6044E-03	PU239	4.2082E-03	55%	AM241	2.1776E-03	29%	PU240	1.1666E-03	15%
	11	7.5532E-03	PU239	4.1798E-03	55%	AM241	2.1629E-03	29%	PU240	1.1588E-03	15%
	55	7.4841E-03	PU239	4.1416E-03	55%	AM241	2.1431E-03	29%	PU240	1.1482E-03	15%
	60	7.3922E-03	PU239	4.0907E-03	55%	AM241	2.1168E-03	29%	PU240	1.1341E-03	15%
	18	7.3336E-03	PU239	4.0583E-03	55%	AM241	2.1000E-03	29%	PU240	1.1251E-03	15%
	61	7.2776E-03	PU239	4.0273E-03	55%	AM241	2.0840E-03	29%	PU240	1.1165E-03	15%
	36	7.2319E-03	PU239	4.0020E-03	55%	AM241	2.0709E-03	29%	PU240	1.1095E-03	15%
	51	7.1204E-03	PU239	3.9404E-03	55%	AM241	2.0390E-03	29%	PU240	1.0924E-03	15%
	49	7.1204E-03	PU239	3.9404E-03	55%	AM241	2.0390E-03	29%	PU240	1.0924E-03	15%
	46	7.0295E-03	PU239	3.8900E-03	55%	AM241	2.0130E-03	29%	PU240	1.0784E-03	15%
	21	6.9690E-03	PU239	3.8566E-03	55%	AM241	1.9956E-03	29%	PU240	1.0691E-03	15%
	23	6.8885E-03	PU239	3.8120E-03	55%	AM241	1.9726E-03	29%	PU240	1.0568E-03	15%
	52	6.8032E-03	PU239	3.7648E-03	55%	AM241	1.9482E-03	29%	PU240	1.0437E-03	15%
	44	6.7832E-03	PU239	3.7537E-03	55%	AM241	1.9424E-03	29%	PU240	1.0406E-03	15%
	38	6.6807E-03	PU239	3.6970E-03	55%	AM241	1.9131E-03	29%	PU240	1.0249E-03	15%
	8	6.6158E-03	PU239	3.6611E-03	55%	AM241	1.8945E-03	29%	PU240	1.0149E-03	15%
	16	6.5735E-03	PU239	3.6377E-03	55%	AM241	1.8824E-03	29%	PU240	1.0085E-03	15%
	42	6.5287E-03	PU239	3.6129E-03	55%	AM241	1.8696E-03	29%	PU240	1.0016E-03	15%
	33	6.4369E-03	PU239	3.5621E-03	55%	AM241	1.8433E-03	29%	PU240	9.8750E-04	15%
	17	6.3627E-03	PU239	3.5210E-03	55%	AM241	1.8220E-03	29%	PU240	9.7611E-04	15%
	41	6.3108E-03	PU239	3.4923E-03	55%	AM241	1.8072E-03	29%	PU240	9.6815E-04	15%
	24	6.2565E-03	PU239	3.4623E-03	55%	AM241	1.7916E-03	29%	PU240	9.5983E-04	15%
	5	6.2171E-03	PU239	3.4405E-03	55%	AM241	1.7803E-03	29%	PU240	9.5379E-04	15%
	9	6.1532E-03	PU239	3.4051E-03	55%	AM241	1.7620E-03	29%	PU240	9.4398E-04	15%
	68	6.0649E-03	PU239	3.3562E-03	55%	AM241	1.7367E-03	29%	PU240	9.3043E-04	15%
	26	5.9939E-03	PU239	3.3170E-03	55%	AM241	1.7164E-03	29%	PU240	9.1954E-04	15%
	27	5.9744E-03	PU239	3.3061E-03	55%	AM241	1.7108E-03	29%	PU240	9.1654E-04	15%
			(Time of Intrusion, 3000 years)								
05	32	6.9712E-03	PU239	5.4897E-03	79%	PU240	1.3041E-03	19%	AM241	1.2175E-04	2%
	39	6.9161E-03	PU239	5.4463E-03	79%	PU240	1.2938E-03	19%	AM241	1.2078E-04	2%
	70	6.8959E-03	PU239	5.4304E-03	79%	PU240	1.2900E-03	19%	AM241	1.2043E-04	2%
	63	6.8208E-03	PU239	5.3713E-03	79%	PU240	1.2759E-03	19%	AM241	1.1912E-04	2%

Table C-6. Vectors with CH Cuttings Discharged to the Ground Surface (Continued)

Comp. Scen. ID	Vector	Total EPA-normalized Cuttings	Top 3 Radionuclides Contribution to Integrated Discharge								
(Time of Intrusion, 3000 years)											
	25	6.7842E-03	PU239	5.3425E-03	79%	PU240	1.2691E-03	19%	AM241	1.1848E-04	2%
	58	6.7441E-03	PU239	5.3109E-03	79%	PU240	1.2616E-03	19%	AM241	1.1778E-04	2%
	30	6.7003E-03	PU239	5.2764E-03	79%	PU240	1.2534E-03	19%	AM241	1.1702E-04	2%
	19	6.6676E-03	PU239	5.2506E-03	79%	PU240	1.2473E-03	19%	AM241	1.1644E-04	2%
	62	6.6258E-03	PU239	5.2177E-03	79%	PU240	1.2395E-03	19%	AM241	1.1571E-04	2%
	3	6.5804E-03	PU239	5.1820E-03	79%	PU240	1.2310E-03	19%	AM241	1.1492E-04	2%
	13	6.5352E-03	PU239	5.1463E-03	79%	PU240	1.2225E-03	19%	AM241	1.1413E-04	2%
	22	6.4791E-03	PU239	5.1022E-03	79%	PU240	1.2120E-03	19%	AM241	1.1315E-04	2%
	47	6.4358E-03	PU239	5.0681E-03	79%	PU240	1.2039E-03	19%	AM241	1.1240E-04	2%
	7	6.3746E-03	PU239	5.0199E-03	79%	PU240	1.1925E-03	19%	AM241	1.1133E-04	2%
	1	6.3513E-03	PU239	5.0015E-03	79%	PU240	1.1881E-03	19%	AM241	1.1092E-04	2%
	50	6.2867E-03	PU239	4.9507E-03	79%	PU240	1.1760E-03	19%	AM241	1.0979E-04	2%
	45	6.2562E-03	PU239	4.9267E-03	79%	PU240	1.1703E-03	19%	AM241	1.0926E-04	2%
	65	6.2044E-03	PU239	4.8859E-03	79%	PU240	1.1606E-03	19%	AM241	1.0836E-04	2%
	43	6.1384E-03	PU239	4.8339E-03	79%	PU240	1.1483E-03	19%	AM241	1.0720E-04	2%
	12	6.1064E-03	PU239	4.8087E-03	79%	PU240	1.1423E-03	19%	AM241	1.0664E-04	2%
	31	6.0744E-03	PU239	4.7835E-03	79%	PU240	1.1363E-03	19%	AM241	1.0608E-04	2%
	4	6.0317E-03	PU239	4.7499E-03	79%	PU240	1.1283E-03	19%	AM241	1.0534E-04	2%
	48	5.9874E-03	PU239	4.7150E-03	79%	PU240	1.1200E-03	19%	AM241	1.0457E-04	2%
	54	5.9309E-03	PU239	4.6705E-03	79%	PU240	1.1095E-03	19%	AM241	1.0358E-04	2%
	37	5.8973E-03	PU239	4.6441E-03	79%	PU240	1.1032E-03	19%	AM241	1.0299E-04	2%
	69	5.8321E-03	PU239	4.5927E-03	79%	PU240	1.0910E-03	19%	AM241	1.0185E-04	2%
	2	5.8058E-03	PU239	4.5720E-03	79%	PU240	1.0861E-03	19%	AM241	1.0139E-04	2%
	35	5.7356E-03	PU239	4.5167E-03	79%	PU240	1.0729E-03	19%	AM241	1.0017E-04	2%
	67	5.7250E-03	PU239	4.5084E-03	79%	PU240	1.0710E-03	19%	AM241	9.9984E-05	2%
	28	5.6778E-03	PU239	4.4712E-03	79%	PU240	1.0621E-03	19%	AM241	9.9159E-05	2%
	6	5.6097E-03	PU239	4.4176E-03	79%	PU240	1.0494E-03	19%	AM241	9.7970E-05	2%
	40	5.5523E-03	PU239	4.3723E-03	79%	PU240	1.0386E-03	19%	AM241	9.6966E-05	2%
	56	5.5123E-03	PU239	4.3408E-03	79%	PU240	1.0312E-03	19%	AM241	9.6268E-05	2%
	10	5.4967E-03	PU239	4.3285E-03	79%	PU240	1.0282E-03	19%	AM241	9.5996E-05	2%
	34	5.4585E-03	PU239	4.2985E-03	79%	PU240	1.0211E-03	19%	AM241	9.5329E-05	2%
	66	5.3928E-03	PU239	4.2467E-03	79%	PU240	1.0088E-03	19%	AM241	9.4181E-05	2%
	53	5.3462E-03	PU239	4.2101E-03	79%	PU240	1.0001E-03	19%	AM241	9.3368E-05	2%
	64	5.2894E-03	PU239	4.1653E-03	79%	PU240	9.8946E-04	19%	AM241	9.2375E-05	2%
	59	5.2773E-03	PU239	4.1558E-03	79%	PU240	9.8721E-04	19%	AM241	9.2165E-05	2%
	57	5.2327E-03	PU239	4.1207E-03	79%	PU240	9.7885E-04	19%	AM241	9.1385E-05	2%
	14	5.1744E-03	PU239	4.0748E-03	79%	PU240	9.6795E-04	19%	AM241	9.0368E-05	2%
	20	5.1300E-03	PU239	4.0398E-03	79%	PU240	9.5964E-04	19%	AM241	8.9591E-05	2%
	15	5.0737E-03	PU239	3.9954E-03	79%	PU240	9.4911E-04	19%	AM241	8.8608E-05	2%
	29	5.0447E-03	PU239	3.9726E-03	79%	PU240	9.4369E-04	19%	AM241	8.8102E-05	2%
	11	5.0107E-03	PU239	3.9458E-03	79%	PU240	9.3733E-04	19%	AM241	8.7508E-05	2%
	55	4.9649E-03	PU239	3.9098E-03	79%	PU240	9.2875E-04	19%	AM241	8.6708E-05	2%
	60	4.9039E-03	PU239	3.8617E-03	79%	PU240	9.1735E-04	19%	AM241	8.5643E-05	2%
	18	4.8650E-03	PU239	3.8311E-03	79%	PU240	9.1008E-04	19%	AM241	8.4964E-05	2%
	61	4.8279E-03	PU239	3.8019E-03	79%	PU240	9.0313E-04	19%	AM241	8.4316E-05	2%
	36	4.7976E-03	PU239	3.7780E-03	79%	PU240	8.9746E-04	19%	AM241	8.3786E-05	2%
	51	4.7236E-03	PU239	3.7198E-03	79%	PU240	8.8363E-04	19%	AM241	8.2495E-05	2%
	49	4.7236E-03	PU239	3.7198E-03	79%	PU240	8.8363E-04	19%	AM241	8.2495E-05	2%
	46	4.6633E-03	PU239	3.6723E-03	79%	PU240	8.7234E-04	19%	AM241	8.1441E-05	2%
	21	4.6232E-03	PU239	3.6407E-03	79%	PU240	8.6483E-04	19%	AM241	8.0740E-05	2%
	23	4.5698E-03	PU239	3.5986E-03	79%	PU240	8.5485E-04	19%	AM241	7.9808E-05	2%
	52	4.5132E-03	PU239	3.5541E-03	79%	PU240	8.4426E-04	19%	AM241	7.8820E-05	2%
	44	4.4999E-03	PU239	3.5436E-03	79%	PU240	8.4177E-04	19%	AM241	7.8587E-05	2%
	38	4.4319E-03	PU239	3.4900E-03	79%	PU240	8.2905E-04	19%	AM241	7.7400E-05	2%
	8	4.3889E-03	PU239	3.4562E-03	79%	PU240	8.2100E-04	19%	AM241	7.6648E-05	2%

Table C-6. Vectors with CH Cuttings Discharged to the Ground Surface (Continued)

Comp. Scen. ID	Vector	Total EPA-normalized Cuttings	Top 3 Radionuclides Contribution to Integrated Discharge								
(Time of Intrusion, 1000 years)											
	16	4.3608E-03	PU239	3.4341E-03	79%	PU240	8.1575E-04	19%	AM241	7.6158E-05	2%
	42	4.3311E-03	PU239	3.4107E-03	79%	PU240	8.1020E-04	19%	AM241	7.5640E-05	2%
	33	4.2702E-03	PU239	3.3627E-03	79%	PU240	7.9880E-04	19%	AM241	7.4576E-05	2%
	17	4.2209E-03	PU239	3.3239E-03	79%	PU240	7.8959E-04	19%	AM241	7.3715E-05	2%
	41	4.1865E-03	PU239	3.2968E-03	79%	PU240	7.8315E-04	19%	AM241	7.3114E-05	2%
	24	4.1505E-03	PU239	3.2685E-03	79%	PU240	7.7642E-04	19%	AM241	7.2486E-05	2%
	5	4.1244E-03	PU239	3.2479E-03	79%	PU240	7.7153E-04	19%	AM241	7.2029E-05	2%
	9	4.0820E-03	PU239	3.2145E-03	79%	PU240	7.6359E-04	19%	AM241	7.1289E-05	2%
	68	4.0234E-03	PU239	3.1684E-03	79%	PU240	7.5264E-04	19%	AM241	7.0266E-05	2%
	26	3.9763E-03	PU239	3.1313E-03	79%	PU240	7.4383E-04	19%	AM241	6.9443E-05	2%
	27	3.9633E-03	PU239	3.1211E-03	79%	PU240	7.4140E-04	19%	AM241	6.9217E-05	2%
(Time of Intrusion, 7250 years)											
06	32	5.7513E-03	PU239	4.8572E-03	84%	PU240	8.3097E-04	14%	U233	2.6554E-05	0%
	39	5.7058E-03	PU239	4.8188E-03	84%	PU240	8.2440E-04	14%	U233	2.6344E-05	0%
	70	5.6891E-03	PU239	4.8047E-03	84%	PU240	8.2199E-04	14%	U233	2.6268E-05	0%
	63	5.6272E-03	PU239	4.7524E-03	84%	PU240	8.1304E-04	14%	U233	2.5981E-05	0%
	25	5.5970E-03	PU239	4.7269E-03	84%	PU240	8.0868E-04	14%	U233	2.5842E-05	0%
	58	5.5639E-03	PU239	4.6990E-03	84%	PU240	8.0389E-04	14%	U233	2.5689E-05	0%
	30	5.5278E-03	PU239	4.6685E-03	84%	PU240	7.9868E-04	14%	U233	2.5523E-05	0%
	19	5.5007E-03	PU239	4.6457E-03	84%	PU240	7.9478E-04	14%	U233	2.5398E-05	0%
	62	5.4663E-03	PU239	4.6165E-03	84%	PU240	7.8979E-04	14%	U233	2.5239E-05	0%
	3	5.4289E-03	PU239	4.5849E-03	84%	PU240	7.8439E-04	14%	U233	2.5066E-05	0%
	13	5.3915E-03	PU239	4.5534E-03	84%	PU240	7.7899E-04	14%	U233	2.4893E-05	0%
	22	5.3453E-03	PU239	4.5143E-03	84%	PU240	7.7231E-04	14%	U233	2.4680E-05	0%
	47	5.3096E-03	PU239	4.4842E-03	84%	PU240	7.6715E-04	14%	U233	2.4515E-05	0%
	7	5.2591E-03	PU239	4.4415E-03	84%	PU240	7.5986E-04	14%	U233	2.4282E-05	0%
	1	5.2398E-03	PU239	4.4253E-03	84%	PU240	7.5707E-04	14%	U233	2.4193E-05	0%
	50	5.1865E-03	PU239	4.3803E-03	84%	PU240	7.4937E-04	14%	U233	2.3947E-05	0%
	45	5.1614E-03	PU239	4.3590E-03	84%	PU240	7.4574E-04	14%	U233	2.3831E-05	0%
	65	5.1186E-03	PU239	4.3229E-03	84%	PU240	7.3956E-04	14%	U233	2.3633E-05	0%
	43	5.0642E-03	PU239	4.2769E-03	84%	PU240	7.3170E-04	14%	U233	2.3382E-05	0%
	12	5.0377E-03	PU239	4.2546E-03	84%	PU240	7.2788E-04	14%	U233	2.3260E-05	0%
	31	5.0113E-03	PU239	4.2323E-03	84%	PU240	7.2406E-04	14%	U233	2.3138E-05	0%
	4	4.9762E-03	PU239	4.2026E-03	84%	PU240	7.1898E-04	14%	U233	2.2976E-05	0%
	48	4.9396E-03	PU239	4.1718E-03	84%	PU240	7.1370E-04	14%	U233	2.2807E-05	0%
	54	4.8929E-03	PU239	4.1323E-03	84%	PU240	7.0696E-04	14%	U233	2.2591E-05	0%
	37	4.8653E-03	PU239	4.1090E-03	84%	PU240	7.0296E-04	14%	U233	2.2464E-05	0%
	69	4.8115E-03	PU239	4.0635E-03	84%	PU240	6.9519E-04	14%	U233	2.2215E-05	0%
	2	4.7897E-03	PU239	4.0452E-03	84%	PU240	6.9205E-04	14%	U233	2.2115E-05	0%
	35	4.7318E-03	PU239	3.9963E-03	84%	PU240	6.8368E-04	14%	U233	2.1848E-05	0%
	67	4.7232E-03	PU239	3.9889E-03	84%	PU240	6.8243E-04	14%	U233	2.1808E-05	0%
	28	4.6842E-03	PU239	3.9560E-03	84%	PU240	6.7679E-04	14%	U233	2.1628E-05	0%
	6	4.6280E-03	PU239	3.9086E-03	84%	PU240	6.6868E-04	14%	U233	2.1368E-05	0%
	40	4.5806E-03	PU239	3.8685E-03	84%	PU240	6.6183E-04	14%	U233	2.1149E-05	0%
	56	4.5476E-03	PU239	3.8407E-03	84%	PU240	6.5706E-04	14%	U233	2.0997E-05	0%
	10	4.5347E-03	PU239	3.8298E-03	84%	PU240	6.5520E-04	14%	U233	2.0938E-05	0%
	34	4.5033E-03	PU239	3.8032E-03	84%	PU240	6.5066E-04	14%	U233	2.0792E-05	0%
	66	4.4490E-03	PU239	3.7574E-03	84%	PU240	6.4282E-04	14%	U233	2.0542E-05	0%
	53	4.4106E-03	PU239	3.7250E-03	84%	PU240	6.3727E-04	14%	U233	2.0364E-05	0%
	64	4.3637E-03	PU239	3.6854E-03	84%	PU240	6.3049E-04	14%	U233	2.0148E-05	0%
	59	4.3538E-03	PU239	3.6770E-03	84%	PU240	6.2906E-04	14%	U233	2.0102E-05	0%
	57	4.3170E-03	PU239	3.6459E-03	84%	PU240	6.2374E-04	14%	U233	1.9932E-05	0%

Table C-6. Vectors with CH Cuttings Discharged to the Ground Surface (Continued)

Comp. Scen. ID	Vector	Total EPA-normalized Cuttings	Top 3 Radionuclides Contribution to Integrated Discharge								
(Time of Intrusion, 7250 years)											
	14	4.2689E-03	PU239	3.6053E-03	84%	PU240	6.1679E-04	14%	U233	1.9710E-05	0%
	20	4.2322E-03	PU239	3.5743E-03	84%	PU240	6.1149E-04	14%	U233	1.9541E-05	0%
	15	4.1858E-03	PU239	3.5351E-03	84%	PU240	6.0478E-04	14%	U233	1.9326E-05	0%
	29	4.1619E-03	PU239	3.5149E-03	84%	PU240	6.0133E-04	14%	U233	1.9216E-05	0%
	11	4.1338E-03	PU239	3.4912E-03	84%	PU240	5.9727E-04	14%	U233	1.9086E-05	0%
	55	4.0960E-03	PU239	3.4593E-03	84%	PU240	5.9181E-04	14%	U233	1.8912E-05	0%
	60	4.0457E-03	PU239	3.4168E-03	84%	PU240	5.8454E-04	14%	U233	1.8680E-05	0%
	18	4.0136E-03	PU239	3.3897E-03	84%	PU240	5.7991E-04	14%	U233	1.8532E-05	0%
	61	3.9830E-03	PU239	3.3638E-03	84%	PU240	5.7548E-04	14%	U233	1.8390E-05	0%
	36	3.9580E-03	PU239	3.3427E-03	84%	PU240	5.7187E-04	14%	U233	1.8275E-05	0%
	51	3.8970E-03	PU239	3.2912E-03	84%	PU240	5.6305E-04	14%	U233	1.7993E-05	0%
	49	3.8970E-03	PU239	3.2912E-03	84%	PU240	5.6305E-04	14%	U233	1.7993E-05	0%
	46	3.8472E-03	PU239	3.2492E-03	84%	PU240	5.5586E-04	14%	U233	1.7763E-05	0%
	21	3.8141E-03	PU239	3.2212E-03	84%	PU240	5.5108E-04	14%	U233	1.7610E-05	0%
	23	3.7701E-03	PU239	3.1840E-03	84%	PU240	5.4472E-04	14%	U233	1.7407E-05	0%
	52	3.7234E-03	PU239	3.1446E-03	84%	PU240	5.3797E-04	14%	U233	1.7191E-05	0%
	44	3.7124E-03	PU239	3.1353E-03	84%	PU240	5.3639E-04	14%	U233	1.7141E-05	0%
	38	3.6563E-03	PU239	3.0879E-03	84%	PU240	5.2828E-04	14%	U233	1.6882E-05	0%
	8	3.6208E-03	PU239	3.0579E-03	84%	PU240	5.2315E-04	14%	U233	1.6718E-05	0%
	16	3.5976E-03	PU239	3.0384E-03	84%	PU240	5.1981E-04	14%	U233	1.6611E-05	0%
	42	3.5731E-03	PU239	3.0177E-03	84%	PU240	5.1627E-04	14%	U233	1.6498E-05	0%
	33	3.5229E-03	PU239	2.9753E-03	84%	PU240	5.0901E-04	14%	U233	1.6266E-05	0%
	17	3.4823E-03	PU239	2.9409E-03	84%	PU240	5.0313E-04	14%	U233	1.6078E-05	0%
	41	3.4539E-03	PU239	2.9170E-03	84%	PU240	4.9903E-04	14%	U233	1.5947E-05	0%
	24	3.4242E-03	PU239	2.8919E-03	84%	PU240	4.9474E-04	14%	U233	1.5810E-05	0%
	5	3.4026E-03	PU239	2.8737E-03	84%	PU240	4.9162E-04	14%	U233	1.5710E-05	0%
	9	3.3676E-03	PU239	2.8441E-03	84%	PU240	4.8657E-04	14%	U233	1.5549E-05	0%
	68	3.3193E-03	PU239	2.8033E-03	84%	PU240	4.7959E-04	14%	U233	1.5326E-05	0%
	26	3.2804E-03	PU239	2.7705E-03	84%	PU240	4.7398E-04	14%	U233	1.5146E-05	0%
	27	3.2697E-03	PU239	2.7615E-03	84%	PU240	4.7243E-04	14%	U233	1.5097E-05	0%

Table C-7 lists total EPA summed normalized release and the percentage contribution for the top 3 radionuclides for each vector when drilling into RH waste with an average activity level. Vectors are ordered from most to least release. All vectors have some small release when intruding into the repository from drilling.

Table C-7. Vectors with RH Cuttings Discharged to the Ground Surface

Comp. Scen. ID	Vector	Total EPA-normalized Cuttings	Top 3 Radionuclides Contribution to Integrated Discharge								
			(Time of Intrusion, 125 years)								
01	32	5.3080E-03	PU238	1.7186E-03	32%	PU239	1.1756E-03	22%	CS137	7.8303E-04	15%
	39	5.2660E-03	PU238	1.7050E-03	32%	PU239	1.1663E-03	22%	CS137	7.7684E-04	15%
	70	5.2507E-03	PU238	1.7000E-03	32%	PU239	1.1629E-03	22%	CS137	7.7457E-04	15%
	63	5.1935E-03	PU238	1.6815E-03	32%	PU239	1.1503E-03	22%	CS137	7.6614E-04	15%
	25	5.1656E-03	PU238	1.6725E-03	32%	PU239	1.1441E-03	22%	CS137	7.6203E-04	15%
	58	5.1351E-03	PU238	1.6626E-03	32%	PU239	1.1373E-03	22%	CS137	7.5752E-04	15%
	30	5.1018E-03	PU238	1.6518E-03	32%	PU239	1.1299E-03	22%	CS137	7.5260E-04	15%
	19	5.0768E-03	PU238	1.6437E-03	32%	PU239	1.1244E-03	22%	CS137	7.4893E-04	15%
	62	5.0450E-03	PU238	1.6334E-03	32%	PU239	1.1174E-03	22%	CS137	7.4423E-04	15%
	3	5.0105E-03	PU238	1.6222E-03	32%	PU239	1.1097E-03	22%	CS137	7.3914E-04	15%
	13	4.9760E-03	PU238	1.6111E-03	32%	PU239	1.1021E-03	22%	CS137	7.3405E-04	15%
	22	4.9333E-03	PU238	1.5973E-03	32%	PU239	1.0926E-03	22%	CS137	7.2776E-04	15%
	47	4.9004E-03	PU238	1.5866E-03	32%	PU239	1.0853E-03	22%	CS137	7.2290E-04	15%
	7	4.8538E-03	PU238	1.5715E-03	32%	PU239	1.0750E-03	22%	CS137	7.1602E-04	15%
	1	4.8360E-03	PU238	1.5658E-03	32%	PU239	1.0711E-03	22%	CS137	7.1340E-04	15%
	50	4.7868E-03	PU238	1.5498E-03	32%	PU239	1.0602E-03	22%	CS137	7.0614E-04	15%
	45	4.7636E-03	PU238	1.5423E-03	32%	PU239	1.0551E-03	22%	CS137	7.0272E-04	15%
	65	4.7241E-03	PU238	1.5295E-03	32%	PU239	1.0463E-03	22%	CS137	6.9690E-04	15%
	43	4.6739E-03	PU238	1.5133E-03	32%	PU239	1.0352E-03	22%	CS137	6.8949E-04	15%
	12	4.6495E-03	PU238	1.5054E-03	32%	PU239	1.0298E-03	22%	CS137	6.8589E-04	15%
	31	4.6251E-03	PU238	1.4975E-03	32%	PU239	1.0244E-03	22%	CS137	6.8229E-04	15%
	4	4.5927E-03	PU238	1.4870E-03	32%	PU239	1.0172E-03	22%	CS137	6.7751E-04	15%
	48	4.5590E-03	PU238	1.4761E-03	32%	PU239	1.0097E-03	22%	CS137	6.7253E-04	15%
	54	4.5159E-03	PU238	1.4621E-03	32%	PU239	1.0002E-03	22%	CS137	6.6617E-04	15%
	37	4.4903E-03	PU238	1.4538E-03	32%	PU239	9.9453E-04	22%	CS137	6.6241E-04	15%
	69	4.4407E-03	PU238	1.4378E-03	32%	PU239	9.8353E-04	22%	CS137	6.5508E-04	15%
	2	4.4206E-03	PU238	1.4313E-03	32%	PU239	9.7908E-04	22%	CS137	6.5212E-04	15%
	35	4.3672E-03	PU238	1.4140E-03	32%	PU239	9.6725E-04	22%	CS137	6.4424E-04	15%
	67	4.3592E-03	PU238	1.4114E-03	32%	PU239	9.6547E-04	22%	CS137	6.4306E-04	15%
	28	4.3232E-03	PU238	1.3997E-03	32%	PU239	9.5751E-04	22%	CS137	6.3775E-04	15%
	6	4.2713E-03	PU238	1.3829E-03	32%	PU239	9.4602E-04	22%	CS137	6.3010E-04	15%
	40	4.2276E-03	PU238	1.3688E-03	32%	PU239	9.3633E-04	22%	CS137	6.2365E-04	15%
	56	4.1972E-03	PU238	1.3589E-03	32%	PU239	9.2959E-04	22%	CS137	6.1916E-04	15%
	10	4.1853E-03	PU238	1.3551E-03	32%	PU239	9.2696E-04	22%	CS137	6.1740E-04	15%
	34	4.1562E-03	PU238	1.3457E-03	32%	PU239	9.2053E-04	22%	CS137	6.1312E-04	15%
	66	4.1062E-03	PU238	1.3295E-03	32%	PU239	9.0944E-04	22%	CS137	6.0574E-04	15%
	53	4.0707E-03	PU238	1.3180E-03	32%	PU239	9.0158E-04	22%	CS137	6.0050E-04	15%
	64	4.0274E-03	PU238	1.3040E-03	32%	PU239	8.9200E-04	22%	CS137	5.9412E-04	15%
	59	4.0183E-03	PU238	1.3010E-03	32%	PU239	8.8997E-04	22%	CS137	5.9277E-04	15%
	57	3.9843E-03	PU238	1.2900E-03	32%	PU239	8.8244E-04	22%	CS137	5.8775E-04	15%
	14	3.9399E-03	PU238	1.2756E-03	32%	PU239	8.7262E-04	22%	CS137	5.8121E-04	15%
	20	3.9060E-03	PU238	1.2647E-03	32%	PU239	8.6512E-04	22%	CS137	5.7621E-04	15%
	15	3.8632E-03	PU238	1.2508E-03	32%	PU239	8.5562E-04	22%	CS137	5.6989E-04	15%
	29	3.8411E-03	PU238	1.2436E-03	32%	PU239	8.5074E-04	22%	CS137	5.6664E-04	15%
	11	3.8152E-03	PU238	1.2353E-03	32%	PU239	8.4501E-04	22%	CS137	5.6282E-04	15%
	55	3.7803E-03	PU238	1.2240E-03	32%	PU239	8.3728E-04	22%	CS137	5.5767E-04	15%
	60	3.7339E-03	PU238	1.2089E-03	32%	PU239	8.2699E-04	22%	CS137	5.5082E-04	15%
	18	3.7043E-03	PU238	1.1993E-03	32%	PU239	8.2044E-04	22%	CS137	5.4645E-04	15%

Table C-7. Vectors with RH Cuttings Discharged to the Ground Surface (Continued)

Comp. Scen. ID	Vector	Total EPA-normalized Cuttings	Top 3 Radionuclides Contribution to Integrated Discharge								
			(Time of Intrusion, 125 years)								
	61	3.6760E-03	PU238	1.1902E-03	32%	PU239	8.1418E-04	22%	CS137	5.4229E-04	15%
	36	3.6530E-03	PU238	1.1827E-03	32%	PU239	8.0906E-04	22%	CS137	5.3888E-04	15%
	51	3.5966E-03	PU238	1.1645E-03	32%	PU239	7.9659E-04	22%	CS137	5.3057E-04	15%
	49	3.5966E-03	PU238	1.1645E-03	32%	PU239	7.9659E-04	22%	CS137	5.3057E-04	15%
	46	3.5507E-03	PU238	1.1496E-03	32%	PU239	7.8642E-04	22%	CS137	5.2380E-04	15%
	21	3.5202E-03	PU238	1.1397E-03	32%	PU239	7.7965E-04	22%	CS137	5.1929E-04	15%
	23	3.4795E-03	PU238	1.1266E-03	32%	PU239	7.7065E-04	22%	CS137	5.1329E-04	15%
	52	3.4364E-03	PU238	1.1126E-03	32%	PU239	7.6110E-04	22%	CS137	5.0694E-04	15%
	44	3.4263E-03	PU238	1.1093E-03	32%	PU239	7.5886E-04	22%	CS137	5.0544E-04	15%
	38	3.3745E-03	PU238	1.0926E-03	32%	PU239	7.4739E-04	22%	CS137	4.9780E-04	15%
	8	3.3418E-03	PU238	1.0820E-03	32%	PU239	7.4014E-04	22%	CS137	4.9297E-04	15%
	16	3.3204E-03	PU238	1.0750E-03	32%	PU239	7.3540E-04	22%	CS137	4.8982E-04	15%
	42	3.2978E-03	PU238	1.0677E-03	32%	PU239	7.3040E-04	22%	CS137	4.8648E-04	15%
	33	3.2514E-03	PU238	1.0527E-03	32%	PU239	7.2012E-04	22%	CS137	4.7964E-04	15%
	17	3.2139E-03	PU238	1.0406E-03	32%	PU239	7.1182E-04	22%	CS137	4.7411E-04	15%
			(Time of Intrusion, 175 years)								
02	32	3.2678E-03	PU239	1.1731E-03	36%	PU238	9.5030E-04	29%	AM241	5.4423E-04	17%
	39	3.2420E-03	PU239	1.1638E-03	36%	PU238	9.4278E-04	29%	AM241	5.3992E-04	17%
	70	3.2325E-03	PU239	1.1604E-03	36%	PU238	9.4003E-04	29%	AM241	5.3835E-04	17%
	63	3.1973E-03	PU239	1.1478E-03	36%	PU238	9.2979E-04	29%	AM241	5.3248E-04	17%
	25	3.1802E-03	PU239	1.1416E-03	36%	PU238	9.2481E-04	29%	AM241	5.2963E-04	17%
	58	3.1614E-03	PU239	1.1349E-03	36%	PU238	9.1933E-04	29%	AM241	5.2649E-04	17%
	30	3.1409E-03	PU239	1.1275E-03	36%	PU238	9.1337E-04	29%	AM241	5.2308E-04	17%
	19	3.1255E-03	PU239	1.1220E-03	36%	PU238	9.0890E-04	29%	AM241	5.2052E-04	17%
	62	3.1059E-03	PU239	1.1150E-03	36%	PU238	9.0321E-04	29%	AM241	5.1726E-04	17%
	3	3.0847E-03	PU239	1.1073E-03	36%	PU238	8.9702E-04	29%	AM241	5.1372E-04	17%
	13	3.0634E-03	PU239	1.0997E-03	36%	PU238	8.9085E-04	29%	AM241	5.1018E-04	17%
	22	3.0372E-03	PU239	1.0903E-03	36%	PU238	8.8322E-04	29%	AM241	5.0581E-04	17%
	47	3.0169E-03	PU239	1.0830E-03	36%	PU238	8.7731E-04	29%	AM241	5.0243E-04	17%
	7	2.9882E-03	PU239	1.0727E-03	36%	PU238	8.6897E-04	29%	AM241	4.9765E-04	17%
	1	2.9772E-03	PU239	1.0688E-03	36%	PU238	8.6579E-04	29%	AM241	4.9583E-04	17%
	50	2.9470E-03	PU239	1.0579E-03	36%	PU238	8.5698E-04	29%	AM241	4.9079E-04	17%
	45	2.9327E-03	PU239	1.0528E-03	36%	PU238	8.5283E-04	29%	AM241	4.8841E-04	17%
	65	2.9084E-03	PU239	1.0441E-03	36%	PU238	8.4576E-04	29%	AM241	4.8436E-04	17%
	43	2.8774E-03	PU239	1.0329E-03	36%	PU238	8.3677E-04	29%	AM241	4.7921E-04	17%
	12	2.8624E-03	PU239	1.0276E-03	36%	PU238	8.3240E-04	29%	AM241	4.7671E-04	17%
	31	2.8474E-03	PU239	1.0222E-03	36%	PU238	8.2804E-04	29%	AM241	4.7421E-04	17%
	4	2.8275E-03	PU239	1.0150E-03	36%	PU238	8.2223E-04	29%	AM241	4.7088E-04	17%
	48	2.8067E-03	PU239	1.0075E-03	36%	PU238	8.1619E-04	29%	AM241	4.6743E-04	17%
	54	2.7802E-03	PU239	9.9802E-04	36%	PU238	8.0848E-04	29%	AM241	4.6301E-04	17%
	37	2.7644E-03	PU239	9.9238E-04	36%	PU238	8.0390E-04	29%	AM241	4.6039E-04	17%
	69	2.7339E-03	PU239	9.8141E-04	36%	PU238	7.9502E-04	29%	AM241	4.5530E-04	17%
	2	2.7215E-03	PU239	9.7697E-04	36%	PU238	7.9142E-04	29%	AM241	4.5324E-04	17%
	35	2.6886E-03	PU239	9.6516E-04	36%	PU238	7.8185E-04	29%	AM241	4.4776E-04	17%
	67	2.6837E-03	PU239	9.6339E-04	36%	PU238	7.8042E-04	29%	AM241	4.4694E-04	17%
	28	2.6615E-03	PU239	9.5544E-04	36%	PU238	7.7398E-04	29%	AM241	4.4325E-04	17%
	6	2.6296E-03	PU239	9.4398E-04	36%	PU238	7.6470E-04	29%	AM241	4.3794E-04	17%
	40	2.6027E-03	PU239	9.3431E-04	36%	PU238	7.5687E-04	29%	AM241	4.3345E-04	17%

Table C-7. Vectors with RH Cuttings Discharged to the Ground Surface (Continued)

Comp. Scen. ID	Vector	Total EPA-normalized Cuttings	Top 3 Radionuclides Contribution to Integrated Discharge								
			(Time of Intrusion, 175 years)								
	56	2.5840E-03	PU239	9.2759E-04	36%	PU238	7.5142E-04	29%	AM241	4.3033E-04	17%
	10	2.5766E-03	PU239	9.2496E-04	36%	PU238	7.4929E-04	29%	AM241	4.2911E-04	17%
	34	2.5588E-03	PU239	9.1854E-04	36%	PU238	7.4409E-04	29%	AM241	4.2613E-04	17%
	66	2.5279E-03	PU239	9.0748E-04	36%	PU238	7.3513E-04	29%	AM241	4.2100E-04	17%
	53	2.5061E-03	PU239	8.9964E-04	36%	PU238	7.2878E-04	29%	AM241	4.1736E-04	17%
	64	2.4795E-03	PU239	8.9008E-04	36%	PU238	7.2103E-04	29%	AM241	4.1293E-04	17%
	59	2.4738E-03	PU239	8.8805E-04	36%	PU238	7.1939E-04	29%	AM241	4.1199E-04	17%
	57	2.4529E-03	PU239	8.8054E-04	36%	PU238	7.1330E-04	29%	AM241	4.0850E-04	17%
	14	2.4256E-03	PU239	8.7073E-04	36%	PU238	7.0536E-04	29%	AM241	4.0395E-04	17%
	20	2.4047E-03	PU239	8.6325E-04	36%	PU238	6.9930E-04	29%	AM241	4.0048E-04	17%
	15	2.3783E-03	PU239	8.5378E-04	36%	PU238	6.9163E-04	29%	AM241	3.9609E-04	17%
	29	2.3648E-03	PU239	8.4891E-04	36%	PU238	6.8768E-04	29%	AM241	3.9383E-04	17%
	11	2.3488E-03	PU239	8.4318E-04	36%	PU238	6.8304E-04	29%	AM241	3.9117E-04	17%
	55	2.3273E-03	PU239	8.3547E-04	36%	PU238	6.7679E-04	29%	AM241	3.8759E-04	17%
	60	2.2988E-03	PU239	8.2521E-04	36%	PU238	6.6848E-04	29%	AM241	3.8283E-04	17%
	18	2.2805E-03	PU239	8.1867E-04	36%	PU238	6.6318E-04	29%	AM241	3.7980E-04	17%
	61	2.2631E-03	PU239	8.1242E-04	36%	PU238	6.5812E-04	29%	AM241	3.7690E-04	17%
	36	2.2489E-03	PU239	8.0732E-04	36%	PU238	6.5399E-04	29%	AM241	3.7453E-04	17%
	51	2.2143E-03	PU239	7.9487E-04	36%	PU238	6.4391E-04	29%	AM241	3.6876E-04	17%
	49	2.2143E-03	PU239	7.9487E-04	36%	PU238	6.4391E-04	29%	AM241	3.6876E-04	17%
	46	2.1860E-03	PU239	7.8472E-04	36%	PU238	6.3568E-04	29%	AM241	3.6405E-04	17%
	21	2.1672E-03	PU239	7.7797E-04	36%	PU238	6.3021E-04	29%	AM241	3.6092E-04	17%
	23	2.1421E-03	PU239	7.6898E-04	36%	PU238	6.2294E-04	29%	AM241	3.5675E-04	17%
	52	2.1156E-03	PU239	7.5946E-04	36%	PU238	6.1522E-04	29%	AM241	3.5233E-04	17%
	44	2.1094E-03	PU239	7.5722E-04	36%	PU238	6.1341E-04	29%	AM241	3.5129E-04	17%
	38	2.0775E-03	PU239	7.4578E-04	36%	PU238	6.0414E-04	29%	AM241	3.4599E-04	17%
	8	2.0573E-03	PU239	7.3854E-04	36%	PU238	5.9828E-04	29%	AM241	3.4263E-04	17%
	16	2.0442E-03	PU239	7.3382E-04	36%	PU238	5.9445E-04	29%	AM241	3.4044E-04	17%
	42	2.0302E-03	PU239	7.2882E-04	36%	PU238	5.9040E-04	29%	AM241	3.3812E-04	17%
	33	2.0017E-03	PU239	7.1857E-04	36%	PU238	5.8210E-04	29%	AM241	3.3336E-04	17%
	17	1.9786E-03	PU239	7.1028E-04	36%	PU238	5.7538E-04	29%	AM241	3.2952E-04	17%
	41	1.9625E-03	PU239	7.0449E-04	36%	PU238	5.7069E-04	29%	AM241	3.2683E-04	17%
	24	1.9456E-03	PU239	6.9843E-04	36%	PU238	5.6578E-04	29%	AM241	3.2402E-04	17%
	5	1.9333E-03	PU239	6.9403E-04	36%	PU238	5.6222E-04	29%	AM241	3.2198E-04	17%
	9	1.9135E-03	PU239	6.8690E-04	36%	PU238	5.5644E-04	29%	AM241	3.1867E-04	17%
	68	1.8860E-03	PU239	6.7704E-04	36%	PU238	5.4845E-04	29%	AM241	3.1410E-04	17%
	26	1.8639E-03	PU239	6.6912E-04	36%	PU238	5.4204E-04	29%	AM241	3.1042E-04	17%
	27	1.8579E-03	PU239	6.6694E-04	36%	PU238	5.4027E-04	29%	AM241	3.0941E-04	17%
			(Time of Intrusion, 350 years)								
03	32	2.1649E-03	PU239	1.1672E-03	54%	AM241	4.1114E-04	19%	PU240	3.0632E-04	14%
	39	2.1478E-03	PU239	1.1580E-03	54%	AM241	4.0789E-04	19%	PU240	3.0389E-04	14%
	70	2.1415E-03	PU239	1.1546E-03	54%	AM241	4.0670E-04	19%	PU240	3.0301E-04	14%
	63	2.1182E-03	PU239	1.1420E-03	54%	AM241	4.0227E-04	19%	PU240	2.9971E-04	14%
	25	2.1069E-03	PU239	1.1359E-03	54%	AM241	4.0011E-04	19%	PU240	2.9810E-04	14%
	58	2.0944E-03	PU239	1.1292E-03	54%	AM241	3.9774E-04	19%	PU240	2.9633E-04	14%
	30	2.0808E-03	PU239	1.1218E-03	54%	AM241	3.9516E-04	19%	PU240	2.9441E-04	14%
	19	2.0706E-03	PU239	1.1164E-03	54%	AM241	3.9323E-04	19%	PU240	2.9297E-04	14%
	62	2.0577E-03	PU239	1.1094E-03	54%	AM241	3.9077E-04	19%	PU240	2.9114E-04	14%
	3	2.0436E-03	PU239	1.1018E-03	54%	AM241	3.8809E-04	19%	PU240	2.8914E-04	14%
	13	2.0295E-03	PU239	1.0942E-03	54%	AM241	3.8542E-04	19%	PU240	2.8715E-04	14%
	22	2.0121E-03	PU239	1.0848E-03	54%	AM241	3.8212E-04	19%	PU240	2.8469E-04	14%
	47	1.9987E-03	PU239	1.0776E-03	54%	AM241	3.7956E-04	19%	PU240	2.8279E-04	14%
	7	1.9797E-03	PU239	1.0673E-03	54%	AM241	3.7595E-04	19%	PU240	2.8010E-04	14%
	1	1.9724E-03	PU239	1.0634E-03	54%	AM241	3.7458E-04	19%	PU240	2.7907E-04	14%

Table C-7. Vectors with RH Cuttings Discharged to the Ground Surface (Continued)

Comp. Scen. ID	Vector	Total EPA-normalized Cuttings	Top 3 Radionuclides Contribution to Integrated Discharge								
(Time of Intrusion, 350 years)											
	50	1.9523E-03	PU239	1.0526E-03	54%	AM241	3.7077E-04	19%	PU240	2.7624E-04	14%
	45	1.9429E-03	PU239	1.0475E-03	54%	AM241	3.6897E-04	19%	PU240	2.7490E-04	14%
	65	1.9268E-03	PU239	1.0388E-03	54%	AM241	3.6591E-04	19%	PU240	2.7262E-04	14%
	43	1.9063E-03	PU239	1.0278E-03	54%	AM241	3.6202E-04	19%	PU240	2.6972E-04	14%
	12	1.8963E-03	PU239	1.0224E-03	54%	AM241	3.6013E-04	19%	PU240	2.6831E-04	14%
	31	1.8864E-03	PU239	1.0170E-03	54%	AM241	3.5824E-04	19%	PU240	2.6691E-04	14%
	4	1.8732E-03	PU239	1.0099E-03	54%	AM241	3.5573E-04	19%	PU240	2.6503E-04	14%
	48	1.8594E-03	PU239	1.0025E-03	54%	AM241	3.5312E-04	19%	PU240	2.6309E-04	14%
	54	1.8418E-03	PU239	9.9301E-04	54%	AM241	3.4978E-04	19%	PU240	2.6060E-04	14%
	37	1.8314E-03	PU239	9.8739E-04	54%	AM241	3.4780E-04	19%	PU240	2.5913E-04	14%
	69	1.8112E-03	PU239	9.7648E-04	54%	AM241	3.4396E-04	19%	PU240	2.5626E-04	14%
	2	1.8030E-03	PU239	9.7206E-04	54%	AM241	3.4240E-04	19%	PU240	2.5510E-04	14%
	35	1.7812E-03	PU239	9.6031E-04	54%	AM241	3.3826E-04	19%	PU240	2.5202E-04	14%
	67	1.7779E-03	PU239	9.5855E-04	54%	AM241	3.3764E-04	19%	PU240	2.5156E-04	14%
	28	1.7633E-03	PU239	9.5064E-04	54%	AM241	3.3486E-04	19%	PU240	2.4948E-04	14%
	6	1.7421E-03	PU239	9.3924E-04	54%	AM241	3.3084E-04	19%	PU240	2.4649E-04	14%
	40	1.7243E-03	PU239	9.2962E-04	54%	AM241	3.2745E-04	19%	PU240	2.4397E-04	14%
	56	1.7119E-03	PU239	9.2292E-04	54%	AM241	3.2510E-04	19%	PU240	2.4221E-04	14%
	10	1.7070E-03	PU239	9.2031E-04	54%	AM241	3.2417E-04	19%	PU240	2.4152E-04	14%
	34	1.6952E-03	PU239	9.1392E-04	54%	AM241	3.2193E-04	19%	PU240	2.3985E-04	14%
	66	1.6747E-03	PU239	9.0292E-04	54%	AM241	3.1805E-04	19%	PU240	2.3696E-04	14%
	53	1.6603E-03	PU239	8.9512E-04	54%	AM241	3.1530E-04	19%	PU240	2.3491E-04	14%
	64	1.6426E-03	PU239	8.8560E-04	54%	AM241	3.1195E-04	19%	PU240	2.3241E-04	14%
	59	1.6389E-03	PU239	8.8359E-04	54%	AM241	3.1124E-04	19%	PU240	2.3189E-04	14%
	57	1.6250E-03	PU239	8.7611E-04	54%	AM241	3.0861E-04	19%	PU240	2.2992E-04	14%
	14	1.6069E-03	PU239	8.6635E-04	54%	AM241	3.0517E-04	19%	PU240	2.2736E-04	14%
	20	1.5931E-03	PU239	8.5891E-04	54%	AM241	3.0255E-04	19%	PU240	2.2541E-04	14%
	15	1.5756E-03	PU239	8.4948E-04	54%	AM241	2.9923E-04	19%	PU240	2.2294E-04	14%
	29	1.5666E-03	PU239	8.4464E-04	54%	AM241	2.9752E-04	19%	PU240	2.2166E-04	14%
	11	1.5561E-03	PU239	8.3894E-04	54%	AM241	2.9551E-04	19%	PU240	2.2017E-04	14%
	55	1.5419E-03	PU239	8.3127E-04	54%	AM241	2.9281E-04	19%	PU240	2.1816E-04	14%
	60	1.5229E-03	PU239	8.2106E-04	54%	AM241	2.8921E-04	19%	PU240	2.1548E-04	14%
	18	1.5108E-03	PU239	8.1455E-04	54%	AM241	2.8692E-04	19%	PU240	2.1377E-04	14%
	61	1.4993E-03	PU239	8.0834E-04	54%	AM241	2.8473E-04	19%	PU240	2.1214E-04	14%
	36	1.4899E-03	PU239	8.0326E-04	54%	AM241	2.8294E-04	19%	PU240	2.1080E-04	14%
	51	1.4669E-03	PU239	7.9088E-04	54%	AM241	2.7858E-04	19%	PU240	2.0756E-04	14%
	49	1.4669E-03	PU239	7.9088E-04	54%	AM241	2.7858E-04	19%	PU240	2.0756E-04	14%
	46	1.4482E-03	PU239	7.8078E-04	54%	AM241	2.7502E-04	19%	PU240	2.0490E-04	14%
	21	1.4357E-03	PU239	7.7406E-04	54%	AM241	2.7266E-04	19%	PU240	2.0314E-04	14%
	23	1.4192E-03	PU239	7.6512E-04	54%	AM241	2.6951E-04	19%	PU240	2.0080E-04	14%
	52	1.4016E-03	PU239	7.5564E-04	54%	AM241	2.6617E-04	19%	PU240	1.9831E-04	14%
	44	1.3975E-03	PU239	7.5342E-04	54%	AM241	2.6539E-04	19%	PU240	1.9772E-04	14%
	38	1.3763E-03	PU239	7.4203E-04	54%	AM241	2.6138E-04	19%	PU240	1.9474E-04	14%
	8	1.3630E-03	PU239	7.3483E-04	54%	AM241	2.5884E-04	19%	PU240	1.9285E-04	14%
	16	1.3543E-03	PU239	7.3013E-04	54%	AM241	2.5718E-04	19%	PU240	1.9161E-04	14%
	42	1.3450E-03	PU239	7.2516E-04	54%	AM241	2.5543E-04	19%	PU240	1.9031E-04	14%
	33	1.3261E-03	PU239	7.1496E-04	54%	AM241	2.5184E-04	19%	PU240	1.8763E-04	14%
	17	1.3108E-03	PU239	7.0671E-04	54%	AM241	2.4894E-04	19%	PU240	1.8547E-04	14%
	41	1.3001E-03	PU239	7.0095E-04	54%	AM241	2.4691E-04	19%	PU240	1.8395E-04	14%
	24	1.2890E-03	PU239	6.9492E-04	54%	AM241	2.4478E-04	19%	PU240	1.8237E-04	14%
	5	1.2808E-03	PU239	6.9054E-04	54%	AM241	2.4324E-04	19%	PU240	1.8122E-04	14%
	9	1.2677E-03	PU239	6.8344E-04	54%	AM241	2.4074E-04	19%	PU240	1.7936E-04	14%
	68	1.2495E-03	PU239	6.7364E-04	54%	AM241	2.3728E-04	19%	PU240	1.7679E-04	14%
	26	1.2349E-03	PU239	6.6575E-04	54%	AM241	2.3451E-04	19%	PU240	1.7472E-04	14%
	27	1.2308E-03	PU239	6.6358E-04	54%	AM241	2.3374E-04	19%	PU240	1.7415E-04	14%

Table C-7. Vectors with RH Cuttings Discharged to the Ground Surface (Continued)

Comp. Scen. ID	Vector	Total EPA-normalized Cuttings	Top 3 Radionuclides Contribution to Integrated Discharge								
			(Time of Intrusion, 1000 years)								
04	32	1.6156E-03	PU239	1.1455E-03	71%	PU240	2.8591E-04	18%	AM241	1.4496E-04	9%
	39	1.6028E-03	PU239	1.1365E-03	71%	PU240	2.8365E-04	18%	AM241	1.4382E-04	9%
	70	1.5982E-03	PU239	1.1332E-03	71%	PU240	2.8282E-04	18%	AM241	1.4340E-04	9%
	63	1.5808E-03	PU239	1.1208E-03	71%	PU240	2.7974E-04	18%	AM241	1.4184E-04	9%
	25	1.5723E-03	PU239	1.1148E-03	71%	PU240	2.7825E-04	18%	AM241	1.4108E-04	9%
	58	1.5630E-03	PU239	1.1082E-03	71%	PU240	2.7660E-04	18%	AM241	1.4024E-04	9%
	30	1.5528E-03	PU239	1.1010E-03	71%	PU240	2.7480E-04	18%	AM241	1.3933E-04	9%
	19	1.5452E-03	PU239	1.0957E-03	71%	PU240	2.7346E-04	18%	AM241	1.3865E-04	9%
	62	1.5356E-03	PU239	1.0888E-03	71%	PU240	2.7175E-04	18%	AM241	1.3778E-04	9%
	3	1.5250E-03	PU239	1.0813E-03	71%	PU240	2.6989E-04	18%	AM241	1.3684E-04	9%
	13	1.5146E-03	PU239	1.0739E-03	71%	PU240	2.6803E-04	18%	AM241	1.3590E-04	9%
	22	1.5016E-03	PU239	1.0647E-03	71%	PU240	2.6573E-04	18%	AM241	1.3473E-04	9%
	47	1.4915E-03	PU239	1.0576E-03	71%	PU240	2.6396E-04	18%	AM241	1.3383E-04	9%
	7	1.4774E-03	PU239	1.0475E-03	71%	PU240	2.6145E-04	18%	AM241	1.3256E-04	9%
	1	1.4719E-03	PU239	1.0437E-03	71%	PU240	2.6049E-04	18%	AM241	1.3207E-04	9%
	50	1.4570E-03	PU239	1.0331E-03	71%	PU240	2.5784E-04	18%	AM241	1.3073E-04	9%
	45	1.4499E-03	PU239	1.0281E-03	71%	PU240	2.5659E-04	18%	AM241	1.3010E-04	9%
	65	1.4379E-03	PU239	1.0195E-03	71%	PU240	2.5446E-04	18%	AM241	1.2902E-04	9%
	43	1.4226E-03	PU239	1.0087E-03	71%	PU240	2.5176E-04	18%	AM241	1.2765E-04	9%
	12	1.4152E-03	PU239	1.0034E-03	71%	PU240	2.5044E-04	18%	AM241	1.2698E-04	9%
	31	1.4078E-03	PU239	9.9817E-04	71%	PU240	2.4913E-04	18%	AM241	1.2631E-04	9%
	4	1.3979E-03	PU239	9.9117E-04	71%	PU240	2.4738E-04	18%	AM241	1.2543E-04	9%
	48	1.3876E-03	PU239	9.8389E-04	71%	PU240	2.4557E-04	18%	AM241	1.2451E-04	9%
	54	1.3745E-03	PU239	9.7459E-04	71%	PU240	2.4324E-04	18%	AM241	1.2333E-04	9%
	37	1.3667E-03	PU239	9.6908E-04	71%	PU240	2.4187E-04	18%	AM241	1.2263E-04	9%
	69	1.3516E-03	PU239	9.5836E-04	71%	PU240	2.3920E-04	18%	AM241	1.2128E-04	9%
	2	1.3455E-03	PU239	9.5403E-04	71%	PU240	2.3811E-04	18%	AM241	1.2073E-04	9%
	35	1.3292E-03	PU239	9.4250E-04	71%	PU240	2.3524E-04	18%	AM241	1.1927E-04	9%
	67	1.3268E-03	PU239	9.4077E-04	71%	PU240	2.3480E-04	18%	AM241	1.1905E-04	9%
	28	1.3159E-03	PU239	9.3300E-04	71%	PU240	2.3287E-04	18%	AM241	1.1807E-04	9%
	6	1.3001E-03	PU239	9.2182E-04	71%	PU240	2.3007E-04	18%	AM241	1.1665E-04	9%
	40	1.2868E-03	PU239	9.1237E-04	71%	PU240	2.2772E-04	18%	AM241	1.1546E-04	9%
	56	1.2775E-03	PU239	9.0581E-04	71%	PU240	2.2608E-04	18%	AM241	1.1463E-04	9%
	10	1.2739E-03	PU239	9.0324E-04	71%	PU240	2.2544E-04	18%	AM241	1.1430E-04	9%
	34	1.2650E-03	PU239	8.9697E-04	71%	PU240	2.2387E-04	18%	AM241	1.1351E-04	9%
	66	1.2498E-03	PU239	8.8617E-04	71%	PU240	2.2118E-04	18%	AM241	1.1214E-04	9%
	53	1.2390E-03	PU239	8.7851E-04	71%	PU240	2.1927E-04	18%	AM241	1.1117E-04	9%
	64	1.2258E-03	PU239	8.6917E-04	71%	PU240	2.1694E-04	18%	AM241	1.0999E-04	9%
	59	1.2230E-03	PU239	8.6720E-04	71%	PU240	2.1644E-04	18%	AM241	1.0974E-04	9%
	57	1.2127E-03	PU239	8.5986E-04	71%	PU240	2.1461E-04	18%	AM241	1.0881E-04	9%
	14	1.1992E-03	PU239	8.5028E-04	71%	PU240	2.1222E-04	18%	AM241	1.0760E-04	9%
	20	1.1889E-03	PU239	8.4298E-04	71%	PU240	2.1040E-04	18%	AM241	1.0668E-04	9%
	15	1.1758E-03	PU239	8.3373E-04	71%	PU240	2.0809E-04	18%	AM241	1.0550E-04	9%
	29	1.1691E-03	PU239	8.2897E-04	71%	PU240	2.0690E-04	18%	AM241	1.0490E-04	9%
	11	1.1613E-03	PU239	8.2338E-04	71%	PU240	2.0551E-04	18%	AM241	1.0420E-04	9%
	55	1.1506E-03	PU239	8.1585E-04	71%	PU240	2.0363E-04	18%	AM241	1.0324E-04	9%
	60	1.1365E-03	PU239	8.0583E-04	71%	PU240	2.0113E-04	18%	AM241	1.0197E-04	9%
	18	1.1275E-03	PU239	7.9944E-04	71%	PU240	1.9953E-04	18%	AM241	1.0117E-04	9%
	61	1.1189E-03	PU239	7.9334E-04	71%	PU240	1.9801E-04	18%	AM241	1.0039E-04	9%
	36	1.1119E-03	PU239	7.8836E-04	71%	PU240	1.9676E-04	18%	AM241	9.9764E-05	9%
	51	1.0947E-03	PU239	7.7621E-04	71%	PU240	1.9373E-04	18%	AM241	9.8226E-05	9%
	49	1.0947E-03	PU239	7.7621E-04	71%	PU240	1.9373E-04	18%	AM241	9.8226E-05	9%
	46	1.0807E-03	PU239	7.6629E-04	71%	PU240	1.9126E-04	18%	AM241	9.6971E-05	9%
	21	1.0714E-03	PU239	7.5970E-04	71%	PU240	1.8961E-04	18%	AM241	9.6137E-05	9%
	23	1.0591E-03	PU239	7.5093E-04	71%	PU240	1.8742E-04	18%	AM241	9.5026E-05	9%

Table C-7. Vectors with RH Cuttings Discharged to the Ground Surface (Continued)

Comp. Scen. ID	Vector	Total EPA-normalized Cuttings	Top 3 Radionuclides Contribution to Integrated Discharge								
			(Time of Intrusion, 100 years)								
	52	1.0460E-03	PU239	7.4163E-04	71%	PU240	1.8510E-04	18%	AM241	9.3850E-05	9%
	44	1.0429E-03	PU239	7.3944E-04	71%	PU240	1.8456E-04	18%	AM241	9.3573E-05	9%
	38	1.0271E-03	PU239	7.2827E-04	71%	PU240	1.8177E-04	18%	AM241	9.2159E-05	9%
	8	1.0171E-03	PU239	7.2120E-04	71%	PU240	1.8000E-04	18%	AM241	9.1265E-05	9%
	16	1.0106E-03	PU239	7.1658E-04	71%	PU240	1.7885E-04	18%	AM241	9.0681E-05	9%
	42	1.0038E-03	PU239	7.1171E-04	71%	PU240	1.7763E-04	18%	AM241	9.0063E-05	9%
	33	9.8964E-04	PU239	7.0170E-04	71%	PU240	1.7513E-04	18%	AM241	8.8797E-05	9%
	17	9.7822E-04	PU239	6.9360E-04	71%	PU240	1.7311E-04	18%	AM241	8.7772E-05	9%
	41	9.7024E-04	PU239	6.8795E-04	71%	PU240	1.7170E-04	18%	AM241	8.7057E-05	9%
	24	9.6190E-04	PU239	6.8203E-04	71%	PU240	1.7023E-04	18%	AM241	8.6308E-05	9%
	5	9.5584E-04	PU239	6.7774E-04	71%	PU240	1.6915E-04	18%	AM241	8.5765E-05	9%
	9	9.4601E-04	PU239	6.7077E-04	71%	PU240	1.6742E-04	18%	AM241	8.4883E-05	9%
	68	9.3244E-04	PU239	6.6114E-04	71%	PU240	1.6501E-04	18%	AM241	8.3665E-05	9%
	26	9.2153E-04	PU239	6.5341E-04	71%	PU240	1.6308E-04	18%	AM241	8.2686E-05	9%
	27	9.1852E-04	PU239	6.5127E-04	71%	PU240	1.6255E-04	18%	AM241	8.2416E-05	9%
			(Time of Intrusion, 3000 years)								
05	32	1.3564E-03	PU239	1.0814E-03	80%	PU240	2.3128E-04	17%	U233	2.7246E-05	2%
	39	1.3457E-03	PU239	1.0729E-03	80%	PU240	2.2945E-04	17%	U233	2.7031E-05	2%
	70	1.3418E-03	PU239	1.0697E-03	80%	PU240	2.2878E-04	17%	U233	2.6952E-05	2%
	63	1.3271E-03	PU239	1.0581E-03	80%	PU240	2.2629E-04	17%	U233	2.6658E-05	2%
	25	1.3200E-03	PU239	1.0524E-03	80%	PU240	2.2508E-04	17%	U233	2.6515E-05	2%
	58	1.3122E-03	PU239	1.0462E-03	80%	PU240	2.2374E-04	17%	U233	2.6359E-05	2%
	30	1.3037E-03	PU239	1.0394E-03	80%	PU240	2.2229E-04	17%	U233	2.6188E-05	2%
	19	1.2973E-03	PU239	1.0343E-03	80%	PU240	2.2121E-04	17%	U233	2.6060E-05	2%
	62	1.2892E-03	PU239	1.0278E-03	80%	PU240	2.1982E-04	17%	U233	2.5896E-05	2%
	3	1.2804E-03	PU239	1.0208E-03	80%	PU240	2.1831E-04	17%	U233	2.5719E-05	2%
	13	1.2716E-03	PU239	1.0138E-03	80%	PU240	2.1681E-04	17%	U233	2.5542E-05	2%
	22	1.2607E-03	PU239	1.0051E-03	80%	PU240	2.1495E-04	17%	U233	2.5323E-05	2%
	47	1.2522E-03	PU239	9.9837E-04	80%	PU240	2.1352E-04	17%	U233	2.5154E-05	2%
	7	1.2403E-03	PU239	9.8887E-04	80%	PU240	2.1149E-04	17%	U233	2.4915E-05	2%
	1	1.2358E-03	PU239	9.8525E-04	80%	PU240	2.1071E-04	17%	U233	2.4823E-05	2%
	50	1.2232E-03	PU239	9.7523E-04	80%	PU240	2.0857E-04	17%	U233	2.4571E-05	2%
	45	1.2173E-03	PU239	9.7051E-04	80%	PU240	2.0756E-04	17%	U233	2.4452E-05	2%
	65	1.2072E-03	PU239	9.6246E-04	80%	PU240	2.0584E-04	17%	U233	2.4249E-05	2%
	43	1.1944E-03	PU239	9.5223E-04	80%	PU240	2.0365E-04	17%	U233	2.3991E-05	2%
	12	1.1881E-03	PU239	9.4726E-04	80%	PU240	2.0259E-04	17%	U233	2.3866E-05	2%
	31	1.1819E-03	PU239	9.4229E-04	80%	PU240	2.0152E-04	17%	U233	2.3741E-05	2%
	4	1.1736E-03	PU239	9.3568E-04	80%	PU240	2.0011E-04	17%	U233	2.3574E-05	2%
	48	1.1650E-03	PU239	9.2881E-04	80%	PU240	1.9864E-04	17%	U233	2.3401E-05	2%
	54	1.1540E-03	PU239	9.2003E-04	80%	PU240	1.9676E-04	17%	U233	2.3180E-05	2%
	37	1.1475E-03	PU239	9.1483E-04	80%	PU240	1.9565E-04	17%	U233	2.3049E-05	2%
	69	1.1348E-03	PU239	9.0472E-04	80%	PU240	1.9349E-04	17%	U233	2.2794E-05	2%
	2	1.1296E-03	PU239	9.0063E-04	80%	PU240	1.9261E-04	17%	U233	2.2691E-05	2%
	35	1.1160E-03	PU239	8.8974E-04	80%	PU240	1.9028E-04	17%	U233	2.2417E-05	2%
	67	1.1139E-03	PU239	8.8811E-04	80%	PU240	1.8994E-04	17%	U233	2.2376E-05	2%
	28	1.1047E-03	PU239	8.8078E-04	80%	PU240	1.8837E-04	17%	U233	2.2191E-05	2%
	6	1.0915E-03	PU239	8.7021E-04	80%	PU240	1.8611E-04	17%	U233	2.1925E-05	2%
	40	1.0803E-03	PU239	8.6130E-04	80%	PU240	1.8420E-04	17%	U233	2.1700E-05	2%
	56	1.0725E-03	PU239	8.5510E-04	80%	PU240	1.8288E-04	17%	U233	2.1544E-05	2%
	10	1.0695E-03	PU239	8.5268E-04	80%	PU240	1.8236E-04	17%	U233	2.1483E-05	2%
	34	1.0621E-03	PU239	8.4676E-04	80%	PU240	1.8109E-04	17%	U233	2.1334E-05	2%
	66	1.0493E-03	PU239	8.3656E-04	80%	PU240	1.7891E-04	17%	U233	2.1077E-05	2%
	53	1.0402E-03	PU239	8.2934E-04	80%	PU240	1.7737E-04	17%	U233	2.0895E-05	2%

Table C-7. Vectors with RH Cuttings Discharged to the Ground Surface (Continued)

Comp. Scen. ID	Vector	Total EPA-normalized Cuttings	Top 3 Radionuclides Contribution to Integrated Discharge								
			(Time of Intrusion, 3000 years)								
	64	1.0292E-03	PU239	8.2052E-04	80%	PU240	1.7548E-04	17%	U233	2.0673E-05	2%
	59	1.0268E-03	PU239	8.1865E-04	80%	PU240	1.7508E-04	17%	U233	2.0626E-05	2%
	57	1.0181E-03	PU239	8.1173E-04	80%	PU240	1.7360E-04	17%	U233	2.0451E-05	2%
	14	1.0068E-03	PU239	8.0269E-04	80%	PU240	1.7167E-04	17%	U233	2.0224E-05	2%
	20	9.9815E-04	PU239	7.9579E-04	80%	PU240	1.7019E-04	17%	U233	2.0050E-05	2%
	15	9.8719E-04	PU239	7.8706E-04	80%	PU240	1.6832E-04	17%	U233	1.9830E-05	2%
	29	9.8156E-04	PU239	7.8257E-04	80%	PU240	1.6736E-04	17%	U233	1.9717E-05	2%
	11	9.7494E-04	PU239	7.7729E-04	80%	PU240	1.6624E-04	17%	U233	1.9584E-05	2%
	55	9.6602E-04	PU239	7.7018E-04	80%	PU240	1.6472E-04	17%	U233	1.9405E-05	2%
	60	9.5416E-04	PU239	7.6072E-04	80%	PU240	1.6269E-04	17%	U233	1.9166E-05	2%
	18	9.4660E-04	PU239	7.5469E-04	80%	PU240	1.6140E-04	17%	U233	1.9014E-05	2%
	61	9.3937E-04	PU239	7.4893E-04	80%	PU240	1.6017E-04	17%	U233	1.8869E-05	2%
	36	9.3347E-04	PU239	7.4423E-04	80%	PU240	1.5917E-04	17%	U233	1.8751E-05	2%
	51	9.1908E-04	PU239	7.3276E-04	80%	PU240	1.5671E-04	17%	U233	1.8462E-05	2%
	49	9.1908E-04	PU239	7.3276E-04	80%	PU240	1.5671E-04	17%	U233	1.8462E-05	2%
	46	9.0735E-04	PU239	7.2340E-04	80%	PU240	1.5471E-04	17%	U233	1.8226E-05	2%
	21	8.9954E-04	PU239	7.1717E-04	80%	PU240	1.5338E-04	17%	U233	1.8069E-05	2%
	23	8.8915E-04	PU239	7.0889E-04	80%	PU240	1.5161E-04	17%	U233	1.7860E-05	2%
	52	8.7814E-04	PU239	7.0011E-04	80%	PU240	1.4973E-04	17%	U233	1.7639E-05	2%
	44	8.7555E-04	PU239	6.9805E-04	80%	PU240	1.4929E-04	17%	U233	1.7587E-05	2%
	38	8.6232E-04	PU239	6.8750E-04	80%	PU240	1.4703E-04	17%	U233	1.7322E-05	2%
	8	8.5395E-04	PU239	6.8083E-04	80%	PU240	1.4561E-04	17%	U233	1.7153E-05	2%
	16	8.4849E-04	PU239	6.7647E-04	80%	PU240	1.4467E-04	17%	U233	1.7044E-05	2%
	42	8.4271E-04	PU239	6.7187E-04	80%	PU240	1.4369E-04	17%	U233	1.6928E-05	2%
	33	8.3086E-04	PU239	6.6242E-04	80%	PU240	1.4167E-04	17%	U233	1.6690E-05	2%
	17	8.2127E-04	PU239	6.5478E-04	80%	PU240	1.4003E-04	17%	U233	1.6497E-05	2%
	41	8.1458E-04	PU239	6.4944E-04	80%	PU240	1.3889E-04	17%	U233	1.6363E-05	2%
	24	8.0757E-04	PU239	6.4385E-04	80%	PU240	1.3770E-04	17%	U233	1.6222E-05	2%
	5	8.0249E-04	PU239	6.3980E-04	80%	PU240	1.3683E-04	17%	U233	1.6120E-05	2%
	9	7.9424E-04	PU239	6.3322E-04	80%	PU240	1.3542E-04	17%	U233	1.5954E-05	2%
	68	7.8284E-04	PU239	6.2413E-04	80%	PU240	1.3348E-04	17%	U233	1.5725E-05	2%
	26	7.7368E-04	PU239	6.1683E-04	80%	PU240	1.3192E-04	17%	U233	1.5541E-05	2%
	27	7.7116E-04	PU239	6.1482E-04	80%	PU240	1.3149E-04	17%	U233	1.5490E-05	2%
			(Time of Intrusion, 7250 years)								
06	32	1.1421E-03	PU239	9.5682E-04	84%	PU240	1.4737E-04	13%	U233	2.6750E-05	2%
	39	1.1331E-03	PU239	9.4925E-04	84%	PU240	1.4621E-04	13%	U233	2.6538E-05	2%
	70	1.1298E-03	PU239	9.4648E-04	84%	PU240	1.4578E-04	13%	U233	2.6461E-05	2%
	63	1.1174E-03	PU239	9.3617E-04	84%	PU240	1.4419E-04	13%	U233	2.6172E-05	2%
	25	1.1115E-03	PU239	9.3115E-04	84%	PU240	1.4342E-04	13%	U233	2.6032E-05	2%
	58	1.1049E-03	PU239	9.2564E-04	84%	PU240	1.4257E-04	13%	U233	2.5878E-05	2%
	30	1.0977E-03	PU239	9.1964E-04	84%	PU240	1.4165E-04	13%	U233	2.5710E-05	2%
	19	1.0923E-03	PU239	9.1514E-04	84%	PU240	1.4095E-04	13%	U233	2.5584E-05	2%
	62	1.0855E-03	PU239	9.0941E-04	84%	PU240	1.4007E-04	13%	U233	2.5424E-05	2%
	3	1.0781E-03	PU239	9.0318E-04	84%	PU240	1.3911E-04	13%	U233	2.5250E-05	2%
	13	1.0707E-03	PU239	8.9697E-04	84%	PU240	1.3815E-04	13%	U233	2.5076E-05	2%
	22	1.0615E-03	PU239	8.8928E-04	84%	PU240	1.3697E-04	13%	U233	2.4861E-05	2%
	47	1.0544E-03	PU239	8.8334E-04	84%	PU240	1.3606E-04	13%	U233	2.4695E-05	2%
	7	1.0444E-03	PU239	8.7494E-04	84%	PU240	1.3476E-04	13%	U233	2.4460E-05	2%
	1	1.0405E-03	PU239	8.7173E-04	84%	PU240	1.3427E-04	13%	U233	2.4371E-05	2%
	50	1.0299E-03	PU239	8.6286E-04	84%	PU240	1.3290E-04	13%	U233	2.4123E-05	2%
	45	1.0250E-03	PU239	8.5869E-04	84%	PU240	1.3226E-04	13%	U233	2.4006E-05	2%
	65	1.0165E-03	PU239	8.5157E-04	84%	PU240	1.3116E-04	13%	U233	2.3807E-05	2%
	43	1.0057E-03	PU239	8.4251E-04	84%	PU240	1.2977E-04	13%	U233	2.3554E-05	2%

Table C-7. Vectors with RH Cuttings Discharged to the Ground Surface (Continued)

Comp. Scen. ID	Vector	Total EPA-normalized Cuttings	Top 3 Radionuclides Contribution to Integrated Discharge								
			(Time of Intrusion, 7250 years)								
	12	1.0004E-03	PU239	8.3811E-04	84%	PU240	1.2909E-04	13%	U233	2.3431E-05	2%
	31	9.9516E-04	PU239	8.3372E-04	84%	PU240	1.2841E-04	13%	U233	2.3308E-05	2%
	4	9.8818E-04	PU239	8.2787E-04	84%	PU240	1.2751E-04	13%	U233	2.3145E-05	2%
	48	9.8092E-04	PU239	8.2179E-04	84%	PU240	1.2658E-04	13%	U233	2.2975E-05	2%
	54	9.7165E-04	PU239	8.1403E-04	84%	PU240	1.2538E-04	13%	U233	2.2757E-05	2%
	37	9.6616E-04	PU239	8.0942E-04	84%	PU240	1.2467E-04	13%	U233	2.2629E-05	2%
	69	9.5548E-04	PU239	8.0048E-04	84%	PU240	1.2329E-04	13%	U233	2.2379E-05	2%
	2	9.5116E-04	PU239	7.9686E-04	84%	PU240	1.2274E-04	13%	U233	2.2277E-05	2%
	35	9.3966E-04	PU239	7.8722E-04	84%	PU240	1.2125E-04	13%	U233	2.2008E-05	2%
	67	9.3793E-04	PU239	7.8578E-04	84%	PU240	1.2103E-04	13%	U233	2.1968E-05	2%
	28	9.3019E-04	PU239	7.7929E-04	84%	PU240	1.2003E-04	13%	U233	2.1786E-05	2%
	6	9.1904E-04	PU239	7.6995E-04	84%	PU240	1.1859E-04	13%	U233	2.1525E-05	2%
	40	9.0962E-04	PU239	7.6206E-04	84%	PU240	1.1738E-04	13%	U233	2.1305E-05	2%
	56	9.0308E-04	PU239	7.5658E-04	84%	PU240	1.1653E-04	13%	U233	2.1151E-05	2%
	10	9.0052E-04	PU239	7.5443E-04	84%	PU240	1.1620E-04	13%	U233	2.1091E-05	2%
	34	8.9427E-04	PU239	7.4920E-04	84%	PU240	1.1539E-04	13%	U233	2.0945E-05	2%
	66	8.8350E-04	PU239	7.4018E-04	84%	PU240	1.1400E-04	13%	U233	2.0693E-05	2%
	53	8.7587E-04	PU239	7.3378E-04	84%	PU240	1.1302E-04	13%	U233	2.0514E-05	2%
	64	8.6656E-04	PU239	7.2598E-04	84%	PU240	1.1182E-04	13%	U233	2.0296E-05	2%
	59	8.6458E-04	PU239	7.2433E-04	84%	PU240	1.1156E-04	13%	U233	2.0250E-05	2%
	57	8.5727E-04	PU239	7.1820E-04	84%	PU240	1.1062E-04	13%	U233	2.0078E-05	2%
	14	8.4772E-04	PU239	7.1020E-04	84%	PU240	1.0939E-04	13%	U233	1.9855E-05	2%
	20	8.4044E-04	PU239	7.0410E-04	84%	PU240	1.0845E-04	13%	U233	1.9684E-05	2%
	15	8.3122E-04	PU239	6.9637E-04	84%	PU240	1.0726E-04	13%	U233	1.9468E-05	2%
	29	8.2647E-04	PU239	6.9240E-04	84%	PU240	1.0665E-04	13%	U233	1.9357E-05	2%
	11	8.2090E-04	PU239	6.8773E-04	84%	PU240	1.0593E-04	13%	U233	1.9227E-05	2%
	55	8.1339E-04	PU239	6.8144E-04	84%	PU240	1.0496E-04	13%	U233	1.9051E-05	2%
	60	8.0340E-04	PU239	6.7307E-04	84%	PU240	1.0367E-04	13%	U233	1.8817E-05	2%
	18	7.9703E-04	PU239	6.6774E-04	84%	PU240	1.0285E-04	13%	U233	1.8668E-05	2%
	61	7.9095E-04	PU239	6.6264E-04	84%	PU240	1.0206E-04	13%	U233	1.8525E-05	2%
	36	7.8598E-04	PU239	6.5848E-04	84%	PU240	1.0142E-04	13%	U233	1.8409E-05	2%
	51	7.7387E-04	PU239	6.4833E-04	84%	PU240	9.9858E-05	13%	U233	1.8125E-05	2%
	49	7.7387E-04	PU239	6.4833E-04	84%	PU240	9.9858E-05	13%	U233	1.8125E-05	2%
	46	7.6399E-04	PU239	6.4005E-04	84%	PU240	9.8583E-05	13%	U233	1.7894E-05	2%
	21	7.5741E-04	PU239	6.3454E-04	84%	PU240	9.7735E-05	13%	U233	1.7740E-05	2%
	23	7.4866E-04	PU239	6.2721E-04	84%	PU240	9.6606E-05	13%	U233	1.7535E-05	2%
	52	7.3939E-04	PU239	6.1945E-04	84%	PU240	9.5410E-05	13%	U233	1.7318E-05	2%
	44	7.3722E-04	PU239	6.1762E-04	84%	PU240	9.5129E-05	13%	U233	1.7267E-05	2%
	38	7.2607E-04	PU239	6.0829E-04	84%	PU240	9.3691E-05	13%	U233	1.7006E-05	2%
	8	7.1903E-04	PU239	6.0238E-04	84%	PU240	9.2782E-05	13%	U233	1.6841E-05	2%
	16	7.1443E-04	PU239	5.9853E-04	84%	PU240	9.2188E-05	13%	U233	1.6733E-05	2%
	42	7.0956E-04	PU239	5.9445E-04	84%	PU240	9.1560E-05	13%	U233	1.6619E-05	2%
	33	6.9958E-04	PU239	5.8609E-04	84%	PU240	9.0273E-05	13%	U233	1.6385E-05	2%
	17	6.9151E-04	PU239	5.7933E-04	84%	PU240	8.9231E-05	13%	U233	1.6196E-05	2%
	41	6.8587E-04	PU239	5.7461E-04	84%	PU240	8.8504E-05	13%	U233	1.6064E-05	2%
	24	6.7998E-04	PU239	5.6967E-04	84%	PU240	8.7743E-05	13%	U233	1.5926E-05	2%
	5	6.7569E-04	PU239	5.6608E-04	84%	PU240	8.7190E-05	13%	U233	1.5826E-05	2%
	9	6.6875E-04	PU239	5.6026E-04	84%	PU240	8.6294E-05	13%	U233	1.5663E-05	2%
	68	6.5915E-04	PU239	5.5222E-04	84%	PU240	8.5055E-05	13%	U233	1.5438E-05	2%
	26	6.5144E-04	PU239	5.4576E-04	84%	PU240	8.4060E-05	13%	U233	1.5258E-05	2%
	27	6.4931E-04	PU239	5.4398E-04	84%	PU240	8.3786E-05	13%	U233	1.5208E-05	2%

APPENDIX D: MEMORANDA REGARDING REFERENCE DATA

Referenced Memoranda

APPENDIX D: MEMORANDA REGARDING REFERENCE DATA

Marietta and Nowak, November 25, 1992

Date: 11/25/92
To: Distribution
From: M.G. Marietta, 6342, and E.J. Nowak, 6345
Subject: Joint Memorandum from SNL Departments 6342 and 6345 on WIPP Performance Assessment Needs, Priorities, and Thresholds for Solubility Tests

Marietta and Gelbard, December 14, 1992

Date: 12/14/92
To: Distribution
From: M.G. Marietta, 6342, and F. Gelbard, 6119
Subject: Joint Memorandum from SNL Departments 6342 and 6119 on WIPP Performance Assessment Needs, Priorities, and Thresholds for Tracer Column Experiments

Marietta and Nowak, November 25, 1992

Date: 11/25/92
To: Distribution
From: M.G. Marietta, 6342, and E.J. Nowak, 6345
Subject: Joint Memorandum from SNL Departments 6342 and 6345 on WIPP Performance Assessment Needs, Priorities, and Thresholds for Solubility Tests

Sandia National Laboratories

Albuquerque, New Mexico 87185

date: November 25, 1992

to: Distribution

from: M. G. Marietta (6342) and E. J. Nowak (6345)

subject: Joint Memorandum from SNL Departments 6342 and 6345 on WIPP Performance Assessment Needs, Priorities, and Thresholds for Solubility Tests

This memo (1) records present WIPP Performance Assessment (PA) needs concerning radionuclide concentrations in the waste-disposal panels and priorities of these needs, (2) documents PA guidance and requests for information from the radionuclide source term activities, and (3) discusses feasibility of providing these critical information needs.

BACKGROUND
(M. G. Marietta, 6342)

PA's needs for a quantitative understanding of radionuclide concentrations in the waste-disposal panels should be considered in the context of the present understanding of the Project's status with regard to regulatory compliance.

Performance assessments to date (Marietta et al., 1989; Bertram-Howery et al., 1990; WIPP PA Division, 1991) indicate that radionuclides will reach the accessible environment only if the repository is breached by human intrusion, and therefore only the Containment Requirements of 40 CFR 191B and the safety assessments needed for NEPA evaluations are of concern. The long-term requirements of RCRA (40 CFR 268.6) apply to the release of non-radioactive contaminants at the disposal-unit boundary (i.e., the top of the Salado Formation and the subsurface extension of the land-withdrawal boundary), and, as presently interpreted by the WIPP Project, only to the undisturbed performance of the disposal system. Calculations of undisturbed performance indicate that brine (and, by implication, radionuclides) does not migrate from the disturbed rock zone surrounding the panels (WIPP PA Department, 1992). Therefore, concentrations in brine are not needed for assessing compliance with the long-term requirements of RCRA.

Assessments to date indicate that, for the preferred choice of conceptual model (i.e., including gas generation in the waste and dual-porosity transport in the Culebra with chemical retardation), the shape and position of the CCDF used for comparison with 40 CFR 191B are determined primarily by the direct releases at the ground surface during drilling (cuttings) (WIPP PA Division, 1991; Helton et al., 1992). Figure 1 shows the CCDFs calculated for the 1991 performance assessment with and without groundwater transport in the Culebra. Note that the mean, median, and 10 and 90 quantile curves are relatively close together, their positions are essentially unchanged by the inclusion of subsurface groundwater releases, and normalized releases in the region of regulatory interest are approximately 10^{-1}. If subsurface releases are to affect the position of the CCDF, they must result in normalized releases comparable in magnitude to those caused by cuttings. Releases of radionuclides mobilized in brine that may flow directly to the ground surface following

borehole intrusion have not been included in CCDFs to date, but preliminary estimates indicate that they will be significantly less than particulate releases of cuttings.

These observations about the magnitude of the releases that may affect compliance lead to a recognition of PA priorities for information on radionuclide concentrations in disposal rooms. Releases orders of magnitude below the predicted cuttings releases are of little regulatory interest. Because radionuclide concentrations do not affect the quantity of particulate waste brought to the surface as cuttings and cavings, the primary impact of changes in concentrations will be on subsurface releases, and changes that result in relatively small changes in the subsurface release will have little effect on compliance. PA therefore recommends concentrating solubility research on those radionuclides with the potential to result in normalized releases greater than 10^{-2} (approximately one order of magnitude below the presently predicted cuttings releases).

Figure 2 shows the EPA-normalized inventory of the repository, radionuclide by radionuclide, as a function of time (based on the most recent IDB, as will be reported in Volume 3 of the 1992 Preliminary Performance Assessment). Note that the two portions of the figure are plotted at different scales, and that a horizontal line is drawn on each at an EPA-normalized value of 10^{-2}. Time-dependent inventories are shown to 10^5 yr, although a vertical line is drawn on each figure at 10^4 yr, indicating the end of the regulatory period specified by 40 CFR 191B. Radionuclides whose normalized inventories never exceed 10^{-2} during 10^4 yr cannot result in releases greater than 10^{-2}, and can therefore be dropped from further consideration in analyses for 40 CFR 191B.

Figure 2a shows that the normalized inventories of ^{239}Pu, ^{240}Pu, ^{241}Am, ^{233}U, ^{234}U, ^{237}Np, ^{229}Th, ^{230}Th, and ^{226}Ra all exceed 10^{-2} during the 10^4-yr period. Figure 2b shows normalized inventories for two additional radionuclides exceeding 10^{-2}; ^{238}Pu (which is high early in the regulatory period) and ^{210}Pb (which barely reaches 10^{-2} at very late times approaching 10^5 yr) exceeding 10^{-2}. PA modeling for 1991 examined transport to the accessible environment of 7 of these radionuclides (^{239}Pu, ^{240}Pu, ^{241}Am, ^{233}U, ^{234}U, ^{237}Np, and ^{230}Th) (WIPP PA Division, 1991, volume 2, section 6.5.2.10). Subsurface transport of two of the remaining radionuclides will be modeled in 1992, ^{229}Th and ^{226}Ra. Transport of ^{238}Pu in the Culebra will not be modeled because of its short half-life (87.7 yr). Subsurface transport of ^{210}Pb will not be modeled because of its low inventory at 10^4 yr and short half-life (22.3 yr), and consequent low impact on 40 CFR 191B compliance. ^{210}Pb may be considered for subsurface transport in future dose calculations as a daughter product created in the Culebra. Transport of both ^{238}Pu and ^{210}Pb in brine brought directly to the ground surface following intrusion (not yet included in performance assessments) also has the potential to contribute to doses.

Figure 3 shows cumulative (10^4 yr) normalized releases into the Culebra resulting from an intrusion borehole that occurs at 10^3 yr (1991 PA, as reported in Helton et al., 1992) for the seven transported radionuclides for the E1E2 scenario (upper row) and E1 scenario (lower row) for three different assumptions. Figure 4 shows the corresponding CCDF plots.

The first column in Figure 3 plots releases into the Culebra from the borehole, before any retardation can occur in the Culebra. The corresponding CCDFs are shown in the top row of Figure 4. The second column of Figure 3 shows releases to the accessible environment (5 km for this analysis) assuming no chemical retardation in the Culebra (i.e., $K_d = 0$, as stipulated in the Consultation and Cooperation (C & C) agreement between DOE and the State of New Mexico [US DOE and State of New Mexico, 1981 as modified]). Note that because a dual-porosity transport model was used, physical retardation does occur because of diffusion into the dolomite matrix. The corresponding CCDFs are shown in the middle row of Figure 4. The third column of Figure 3 shows releases to the accessible environment calculated using the sampled values for K_d, and the corresponding CCDFs are shown in the bottom row of Figure 4. These curves are incorporated in the total release CCDFs shown in

the top half of Figure 1, although the contribution of the groundwater release can be observed in only one realization shown in Figure 1a.

(In interpreting Figure 3, note that upper and lower bounds of the boxes for each radionuclide indicate the 25th and 75th percentiles from the total number of realizations, the vertical line within the box is the median value, and the black dot is the mean. The horizontal lines extending above the boxes extend to either the maximum value or the value representing $x_{.75} + 1.5(x_{.75} - x_{.25})$, which ever is lower, and the lines extending below the boxes indicate the comparable lower value. Observations falling outside these ranges are shown with individual "x" symbols. These plots do not contain information about the probability of scenario occurrence, and therefore assign equal weight to each scenario. [Helton et al., 1992])

Clearly, retardation in the Culebra may be an important contributor to increasing our confidence of complying with 40 CFR 191B and of defending the overall long-term safety of the WIPP. Given the stipulations of the C & C agreement, however, chemical retardation in the Culebra will not be assumed for a final compliance evaluation until confirmed by the tracer column experiments. To insure a defensible multi-barrier system, we recommend that radionuclide concentration research be designed assuming no credit for retardation in the Culebra. Therefore, we recommend that radionuclide concentration research be designed with respect to releases into the Culebra, as shown in the first column of Figure 3. These releases are calculated before any retardation can occur in the Culebra, and are primarily dependent on the available inventory and the sampled values for solubility limits (and quantity of brine flowing up the borehole, as calculated by the two-phase flow code BRAGFLO). Note that cumulative normalized releases of all seven radionuclides into the Culebra have the potential to exceed 10^{-2} for both scenarios. Cumulative releases for many radionuclides exceed 10^{0} in some realizations, resulting in the potential for a violation of 40 CFR 191B and causing some individual CCDFs in the top row of Figure 4 to exceed the EPA limits.

Concentrations of all radionuclides shown in Figure 3 are therefore important to PA, although special importance falls to U (which is the major contributor to the 1991 subsurface releases at the accessible environment assuming chemical retardation in the Culebra, as shown in the third column of Figure 3) and to Pu (which is an important contributor to releases into the Culebra, as shown in the first column of Figure 3, and could dominate releases to the accessible environment if chemical retardation were not allowed). Of the remaining radionuclides, Ra and Pb are relatively less important for compliance with 40 CFR 191B because of their lower inventories. Ra and Pb are important, however, in safety assessments because of their potential contributions to doses to humans through either subsurface transport or the direct release of brine at the ground surface during drilling. Because of the relatively short half-lives of ^{226}Ra and ^{210}Pb (1600 yr and 22.3 yr, respectively) their concentrations in disposal-room brine are primarily of concern for direct releases at the ground surface. Most subsurface transport of these isotopes will be of decay products of other radionuclides.

Solubility distributions used in the 1991 PA were based on the judgment of an expert panel (Trauth et al., 1992), and are shown in Figure 5. Distributions were provided for different oxidation states for the major radionuclides, reflecting uncertainty in the chemical conditions in the waste-panel environment. Solubilities used in the multiple simulations were selected from these distributions by Latin hypercube sampling after first sampling on Eh-pH conditions within the panel to determine the oxidation states present. (For additional information, see Sections 3.3.5 and 3.3.6 of Volume 3 of WIPP PA Division, 1991.) Concentrations of elements dissolved in waste-panel brine were then calculated assuming equilibrium conditions and uniform distribution of waste. Concentrations of individual isotopes of each element were proportional to their relative abundance in the solid phase of the element. (For additional information, see Section 5.3.2 of Volume 2 of WIPP PA Division, 1991).

As noted above, solubility, inventory, and the quantity of brine flowing up the borehole are the main factors controlling the magnitude of the releases into the Culebra shown in Figure 3. Sensitivity analyses provide a means to separate the relative contribution of brine flow and isolate the effects of uncertainty in solubility. As shown in Figure 6, far-field halite permeability in the Salado Formation (SALPERM) was one of the most important two-phase flow parameter affecting radionuclide migration up the borehole under the assumptions of the 1991 PA (Helton et al., 1992). Releases of ^{239}Pu do not occur for an E1-type intrusion at 10^3 yr for sampled values of SALPERM below approximately 5×10^{-21}. Above that value, the magnitude of release shows no apparent correlation with SALPERM. This "switch" effect, which is also observed for releases of other radionuclides, reflects the control of SALPERM over brine inflow from the far-field. At low values of SALPERM, the panel never becomes brine-saturated, in part because inflow is restricted by elevated gas pressures within the panel and in part because corrosion consumes what brine does enter, and less brine is available to transport radionuclides up the borehole.

Figure 7 (Helton et al., 1992) shows scatterplots of releases versus sampled values for solubility for ^{239}Pu for E1 and E1E2 intrusions at 10^3 yr. Releases on the vertical axis of Figure 7a, the E1 intrusion, are the same as those shown in Figure 6. Note the zero releases (plotted at 10^{-8}) corresponding to low values of SALPERM. Figure 7b shows the same relationship for the E1E2 intrusion at 10^3 yr. Note that there are far fewer zero releases, reflecting the abundant supply of brine from the Castile reservoir assumed in the E1E2 scenario. In both plots, for those realizations that do result in a release, the log of the magnitude of the release is linearly dependent on the log of the sampled value for solubility. Both plots show a solubility threshold for ^{239}Pu for releases of regulatory interest (above approximately 10^{-2}) between 10^{-8} and 10^{-7} mol/ℓ. PA therefore recommends that radionuclide concentration research concentrate on possible values above this threshold.

Figure 8 (Helton et al., 1992) shows a scatterplot of releases versus sampled values for solubility for ^{234}U for an E1E2 intrusion at 10^3 yr. In this case, sampled solubilities were high enough (see Figure 5, U^{+6}) and the inventory low enough that releases were in many realizations limited by the available inventory rather than by the sampled solubility value. Only below solubilities of approximately 10^{-5} mol/ℓ was a log-log linear relationship present between releases and solubilities, and a threshold of regulatory interest (i.e., releases below approximately 10^{-2}) does not occur until solubilities drop below approximately 10^{-6} mol/ℓ. The cutoff recommended for U is the same as that suggested above for Pu, between approximately 10^{-8} and 10^{-7} mol/ℓ.

RECOMMENDATIONS FROM PA FOR THE EXPERIMENTAL PROGRAM
(M. G. Marietta, 6342)

40 CFR 191B

With regard to 40 CFR 191B, PA needs data on concentrations above approximately 10^{-7} mol/ℓ for

U and Pu (highest priority)
Am, Np, and Th (high priority)
Ra and Pb (lower priority--not essential)

For all radionuclides, data on concentrations less than approximately 10^{-7} mol/ℓ are less important, because releases from this range will have essentially no impact on the location of the CCDF.

NEPA

With regard to NEPA, PA needs data for

U and Pu (highest priority)
Np and Th (high priority)
Am, Ra, and Pb (low priority)

Again, data on concentrations less than approximately 10^{-7} mol/ℓ will have little effect on the determination of disposal-system safety. Ra and Pb are given low priority here despite their potential to contribute to doses from subsurface releases because most transport of these radionuclides in the Culebra will be of decay products formed during transport of other radionuclides. Low initial inventories and relatively short half-lives of ^{226}Ra and ^{210}Pb will cause the amount of these radionuclides dissolved in repository brine to have little affect on doses following transport in the Culebra.

Overall Recommendations

Taking into account relative priorities of compliance evaluations with 40 CFR 191B (high) and safety evaluations (relatively lower), our composite recommendations are as follows:

U and Pu data are critical (highest priority)

Am, Np, and Th are important (high priority)

Ra and Pb should be included if possible and if their inclusion does not add significantly to the cost of the experiments or detract from the ultimate defensibility of data for the other elements. This judgement is based on some remaining uncertainty regarding possible brine flow directly to the surface during drilling. Assumptions about future drilling techniques and practices will be a concern of regulators and could change.

ACTINIDE SOURCE TERM PROGRAM RESPONSE TO RECOMMENDATIONS FROM PA

(E. J. Nowak, 6345)

The actinide source term program consists of laboratory tests with radionuclides in WIPP brines, source term model development, and a source term waste test program (STTP) with actual waste in WIPP brines. The laboratory tests produce data on species identification, stability constants of chemical complexes, solubilities, sorption on backfill materials that may be used in the WIPP, and colloid formation. An actinide source term model will be developed with data produced by laboratory tests. The model will predict the concentrations of actinide species in brines within the disposal rooms and panels, with particular emphasis on upper bounds. Results from the tests with actual waste (STTP) will be used to test the validity of the source term model. STTP data will be interpreted with the aid of the laboratory test data.

The actinide source term model will include isotopes of plutonium, americium, neptunium, thorium, and uranium. The model will reflect the complex chemical behavior of these elements, including radionuclide-containing colloid formation and sensitivities to parameters such as Eh, pH, and the concentrations of organic and inorganic ligands that can act as complexing agents. Numerical models that incorporate these parameters and thermodynamic relationships are being evaluated in the modeling effort.

Inclusion of radium and lead is not planned at this time, because significant additional resources would be required to do so, and the priority for data on these elements has not been established at a sufficiently high level to warrant the required expansion of the actinide source term program.

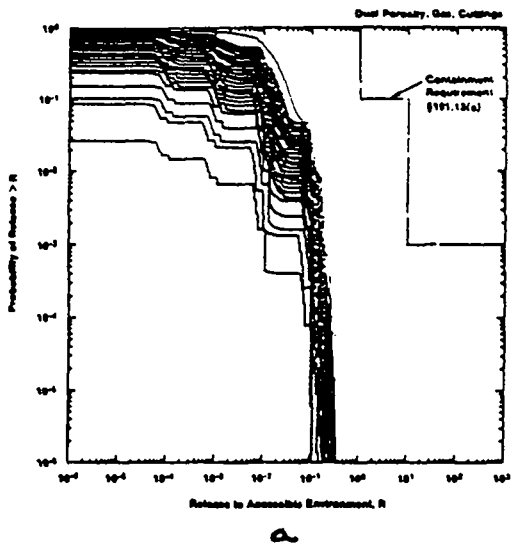

a

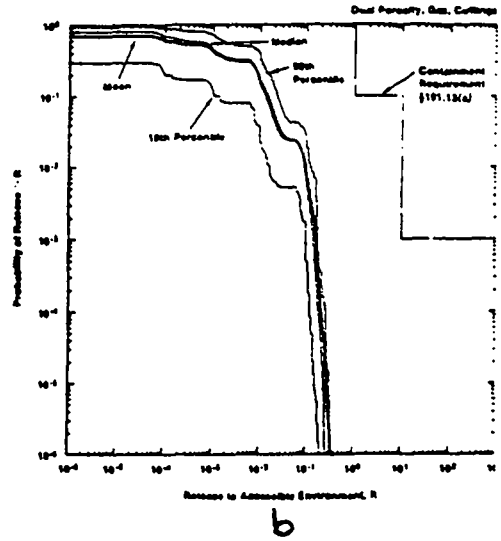

b

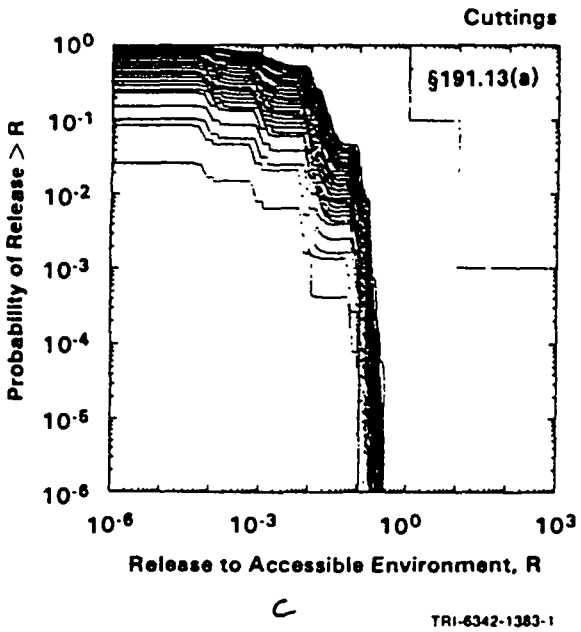

c

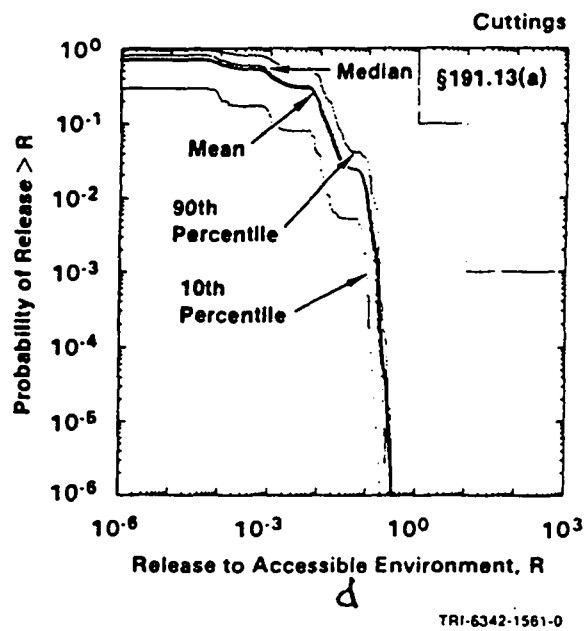

d

Figure 1. Distributions of CCDFs and summary CCDFs from the 1991 WIPP preliminary performance assessment. Figures 1a and 1b show total releases (subsurface and cuttings) assuming dual porosity transport with chemical retardation in the Culebra (Figures 2.1-2 and 4.1-1 in Helton et al., 1992). Figures 1c and 1d show the same curves without subsurface releases (i.e., cuttings only) (Figure 4-1.2 in Helton et al., 1992).

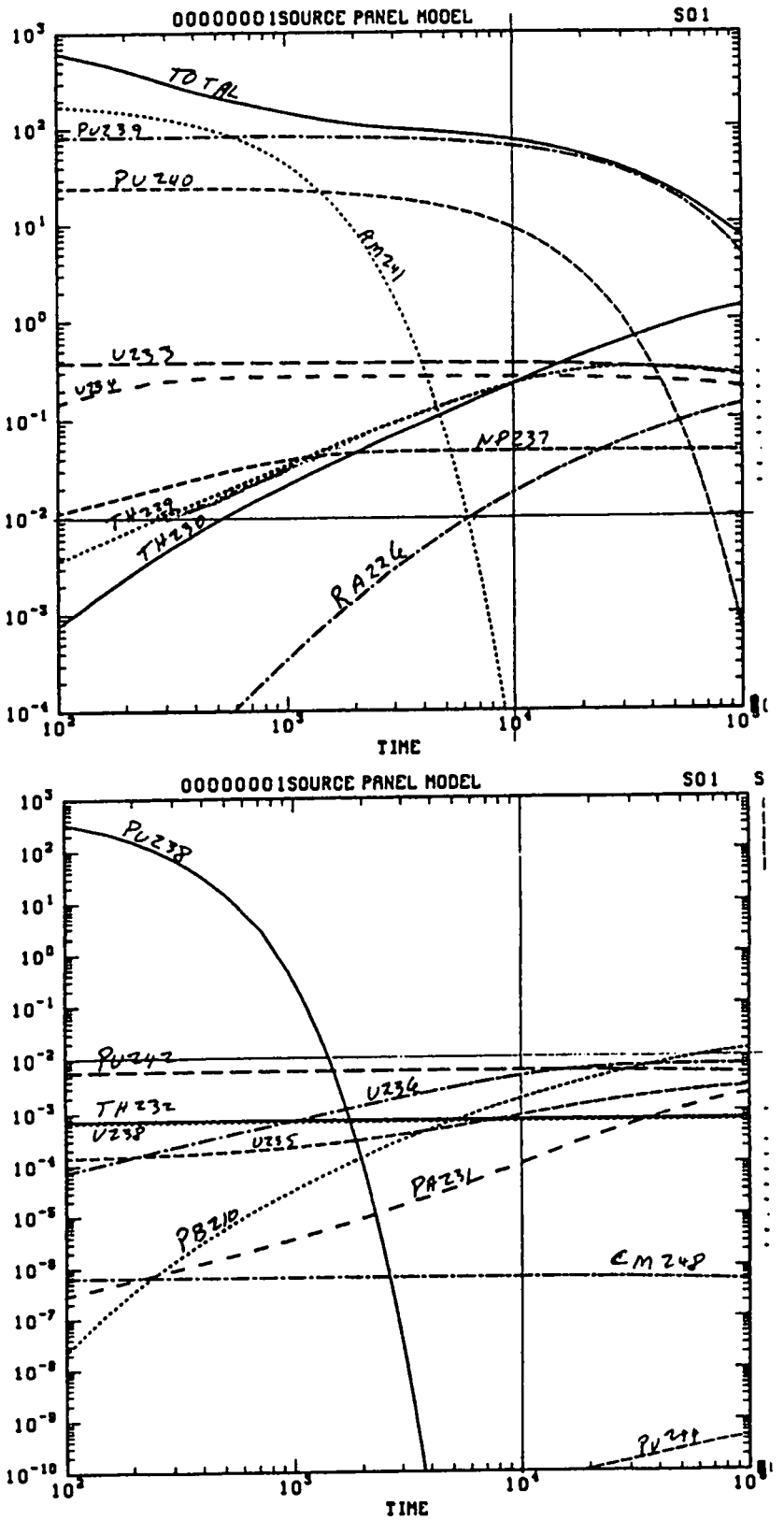

Figure 2. Decay histories for the present IDB inventory. Note scale change between Figures 2a and 2b. Horizontal line at 10^{-2} indicates threshold of importance for PA. Vertical line at 10^{4} yr indicates EPA regulatory time period.

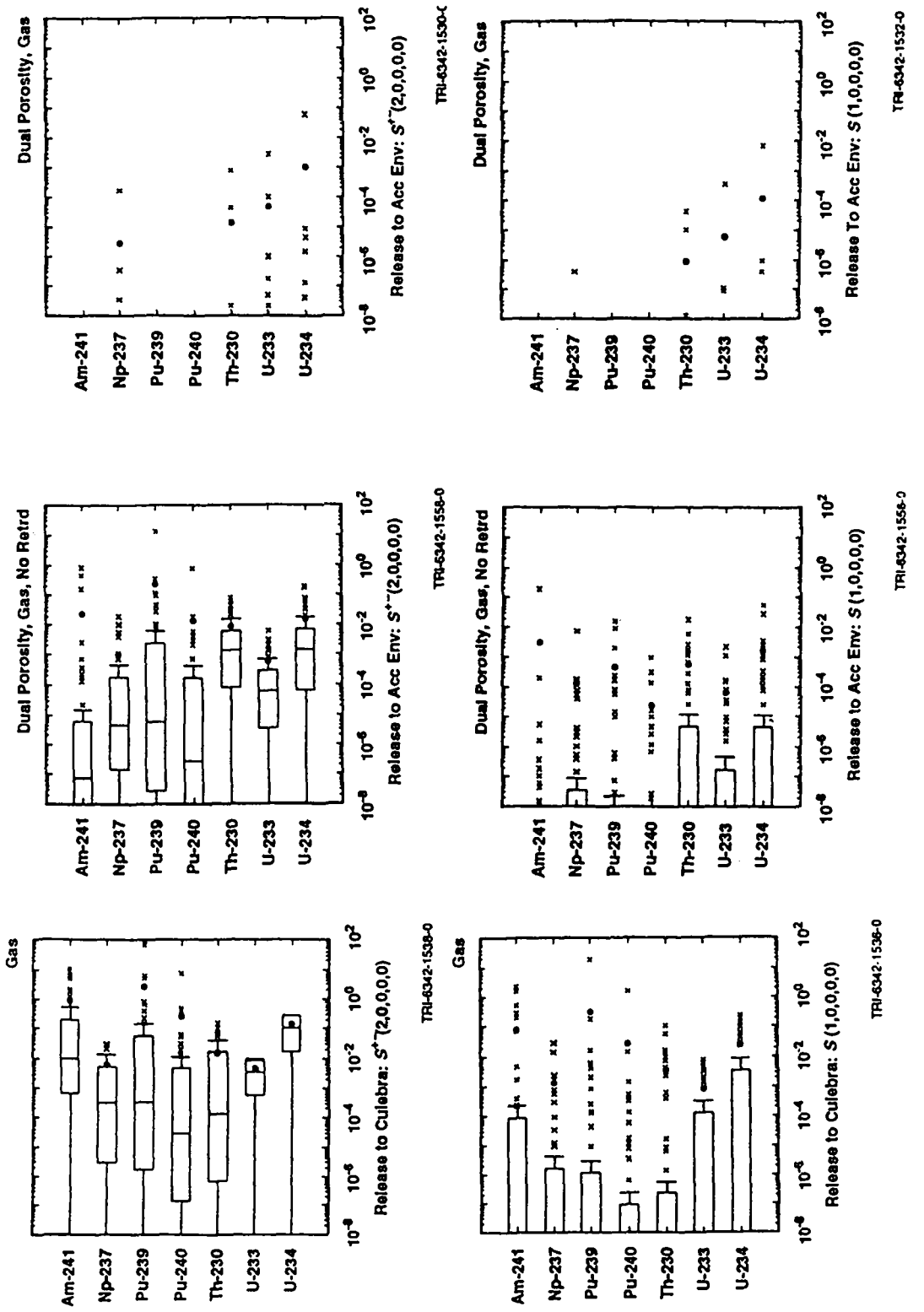

Figure 3. Cumulative normalized releases for radionuclides from E1E2 (upper row) and E1 (lower row) intrusions at 10^3 yr. (1991 WIPP preliminary performance assessment) (Helton et al., 1992).

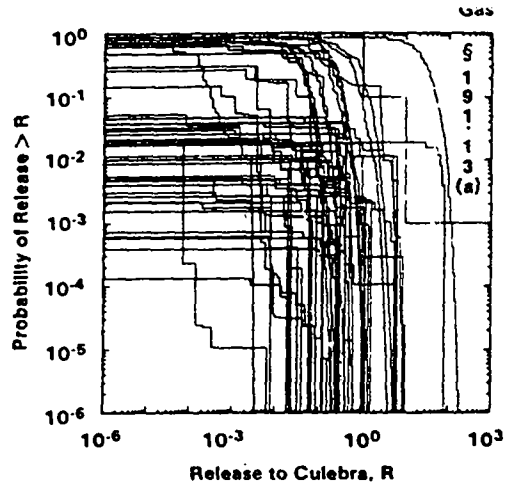

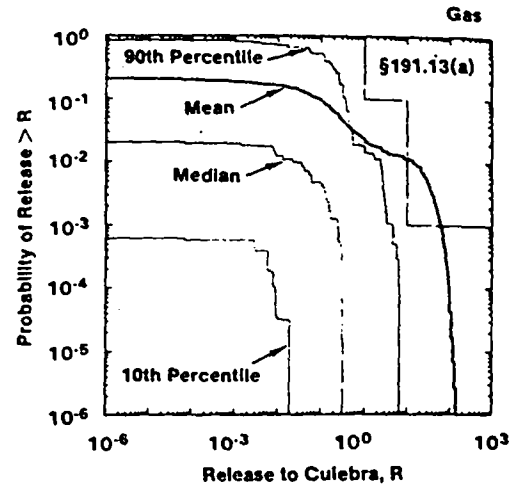

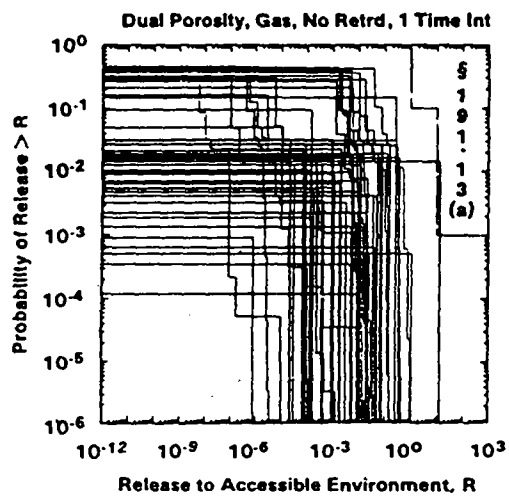

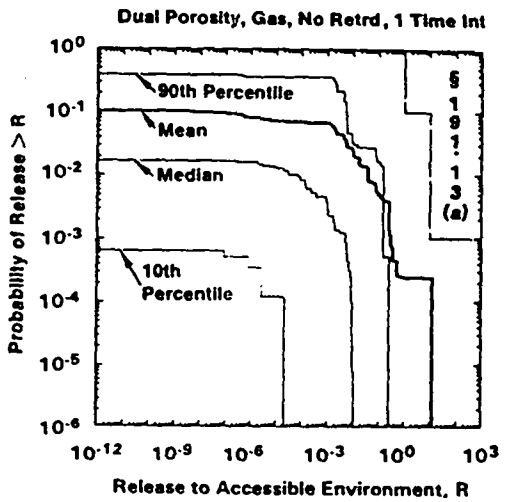

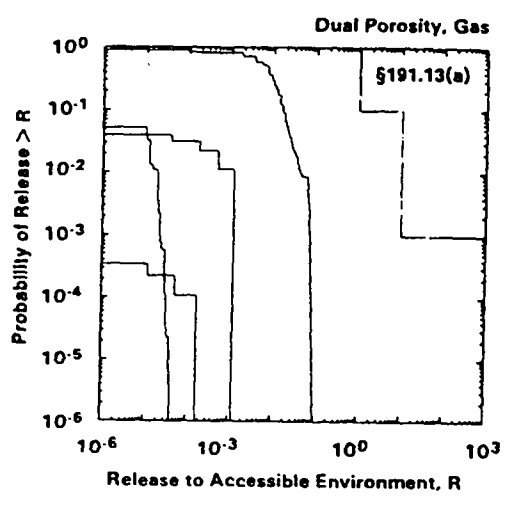

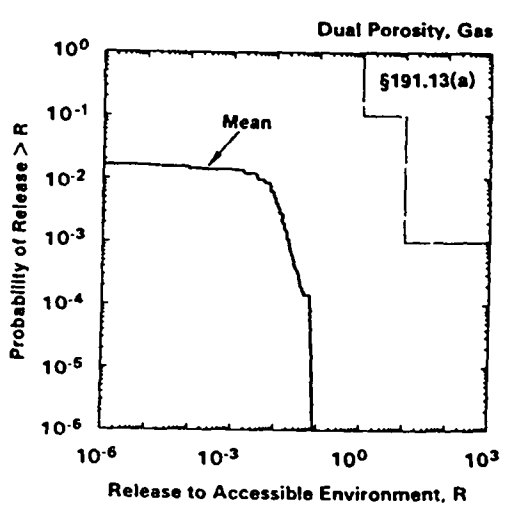

Figure 4. CCDFs corresponding to the releases plotted in Figure 3 (Helton et al., 1992).

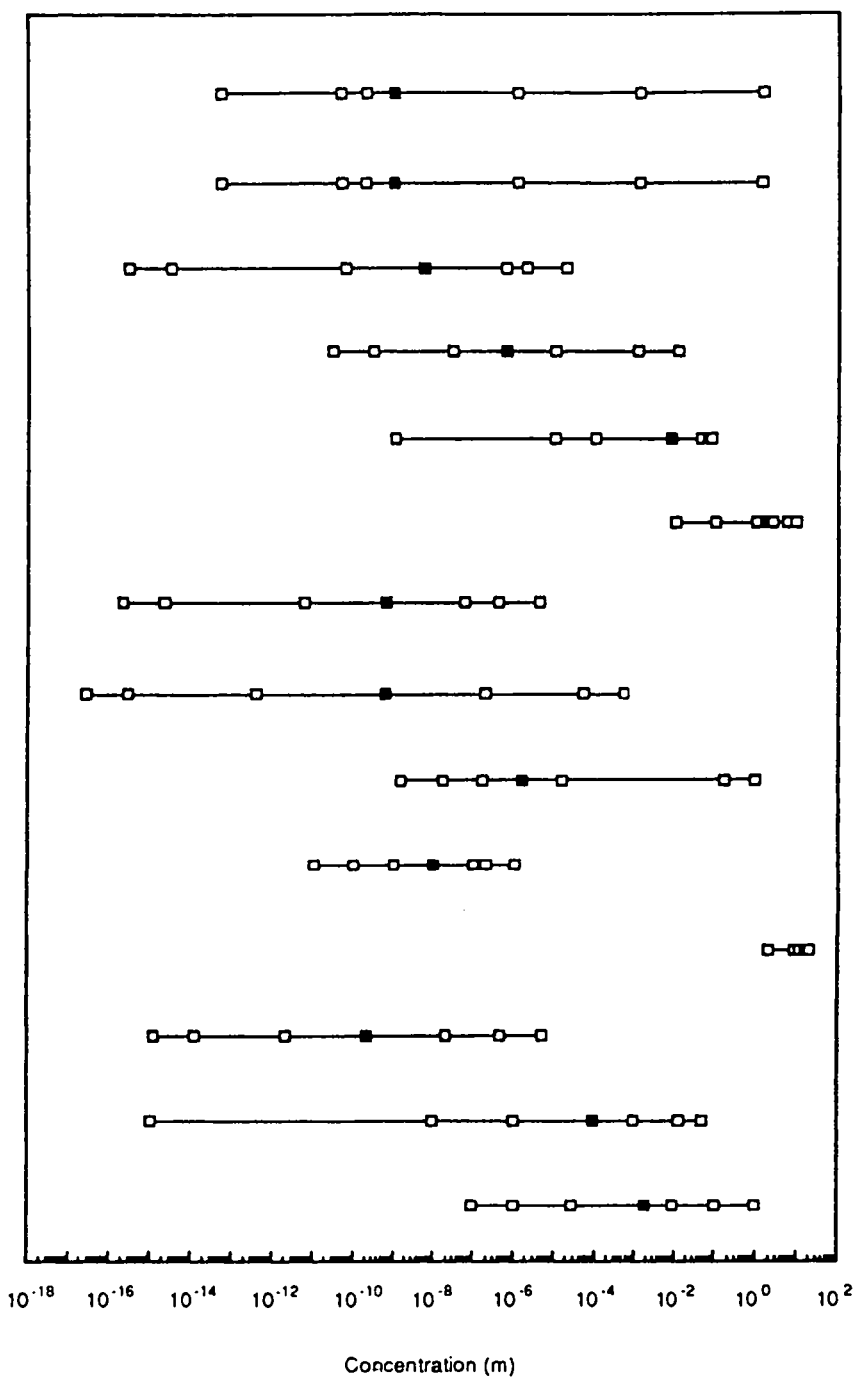

The blocks represent, from left to right, the 0.00, 0.10, 0.25, 0.50, 0.75, 0.90 and 1.00 fractiles

TRI-6342-1410-0

Figure 5. Distributions used for elemental solubilities in the 1991 PA (WIPP PA Division, 1991, Volume 3).

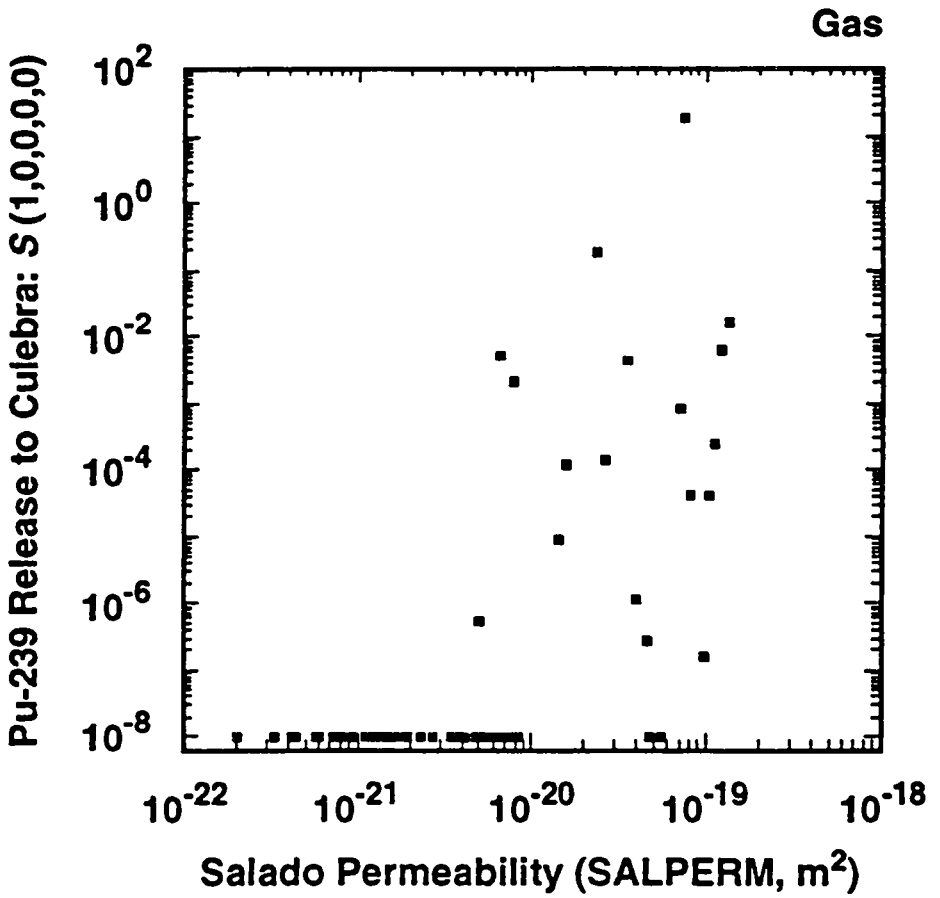

Figure 6. Scatterplot showing relationship between release of ^{239}Pu to the Culebra and sampled value for far-field halite permeability in the Salado Formation (Helton et al., 1992).

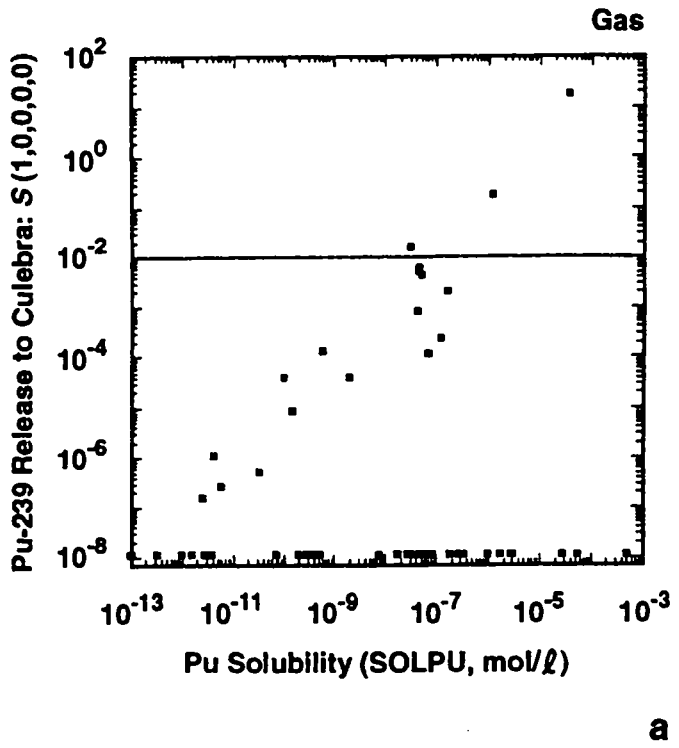

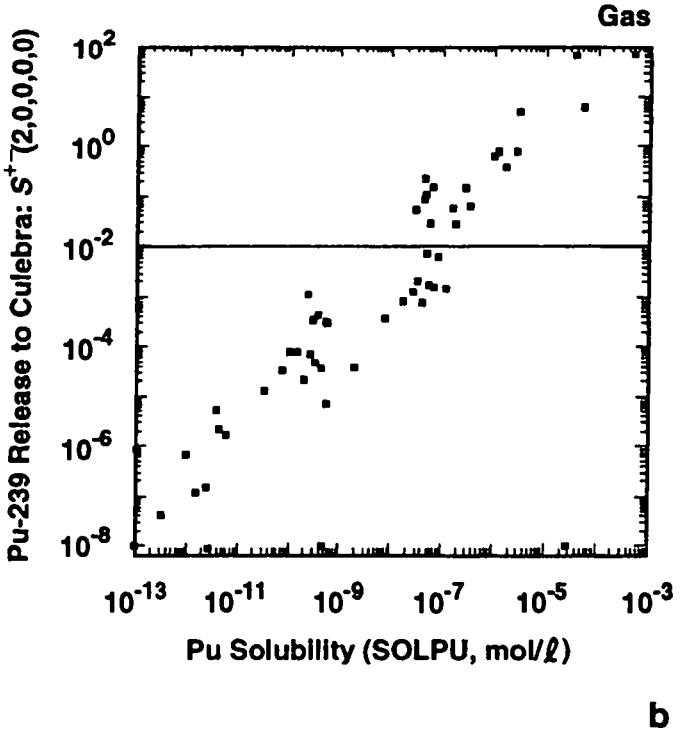

Figure 7. Scatterplots showing relationship between release of ^{239}Pu to the Culebra and sampled value for Pu solubility for E1 (Figure 7a) and E1E2 (Figure 7b) intrusions at 1000 yr (Helton et al, 1992). Horizontal lines at 10^{-2} indicate threshold of importance to PA.

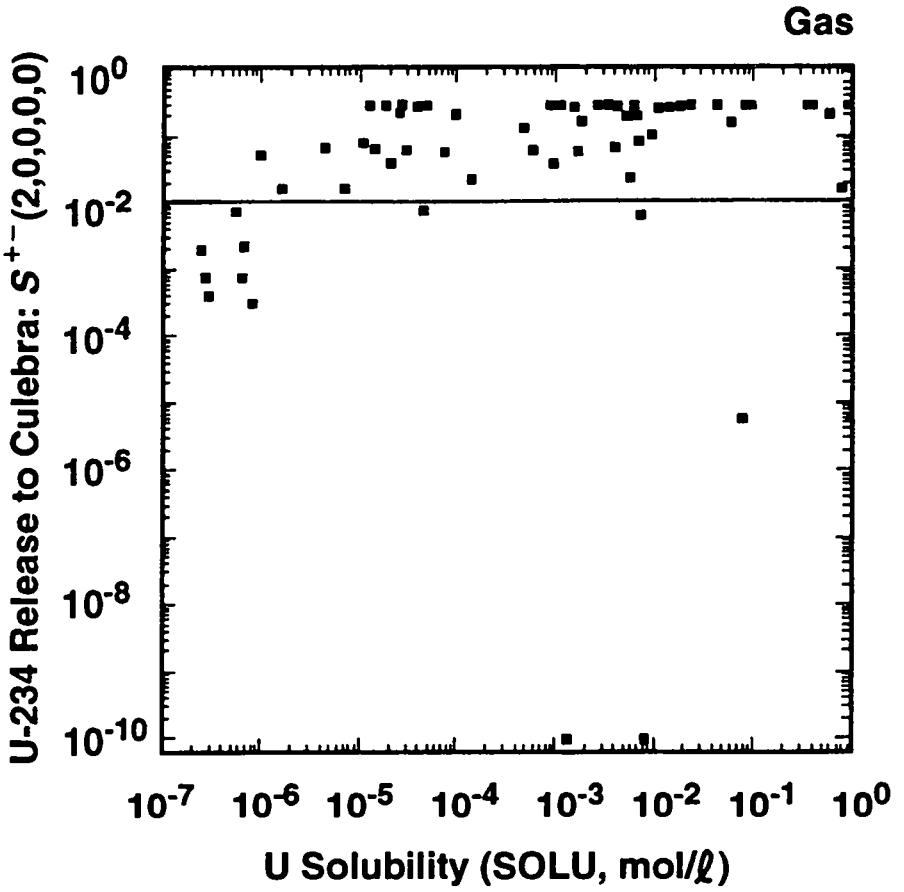

Figure 8. Scatterplot showing relationship between release of ^{234}U to the Culebra and sampled value for U solubility for E1E2 intrusion at 10^{3} yr (Helton et al., 1992). Horizontal line at 10^{-2} indicates threshold of importance to PA.

REFERENCES

Bertram-Howery, S. G., M. G. Marietta, R. P. Rechard, P. N. Swift, D. R. Anderson, B. L. Baker, J. E. Bean, W. Beyeler, K. F. Brinster, R. V. Guzowski, J. C. Helton, R. D. McCurley, D. K. Rudeen, J. D. Schreiber, and P. Vaughn. 1990. *Preliminary Comparison with 40 CFR Part 191, Subpart B for the Waste Isolation Pilot Plant, December 1990.* SAND90-2347. Albuquerque, NM: Sandia National Laboratories.

Marietta, M. G., S. G. Bertram Howery, D. R. Anderson, K. F. Brinster, R. V. Guzowski, H. Iuzzolino, and R. P. Rechard. 1989. *Performance Assessment Methodology Demonstration: Methodology Development for Purposes of Evaluating Compliance with EPA 40 CFR Part 191, Subpart B, for the Waste Isolation Pilot Plant.* SAND89-2027. Albuquerque, NM: Sandia National Laboratories.

Helton, J. C., J. W. Garner, R. P. Rechard, D. K. Rudeen, and P. N. Swift. 1992. *Preliminary Comparison with 40 CFR Part 191, Subpart B for the Waste Isolation Pilot Plant, December 1991. Volume 4: Uncertainty and Sensitivity Analysis Results.* SAND91-0893/4. Albuquerque, NM: Sandia National Laboratories.

Trauth, K. M., S. C. Hora, R. P. Rechard, and D. R. Anderson. 1992. *The Use of Expert Judgment to Quantify Uncertainty in Solubility and Sorption Parameters for Waste Isolation Pilot Plant Performance Assessment.* SAND92-0479. Albuquerque, NM: Sandia National Laboratories. (in review).

US DOE (Department of Energy). 1991. *Integrated Data Base for 1991: Spent Fuel and Radioactive Waste Inventories, Projects and Characterizations.* DOE/RW-006, Rev. 7.

US DOE (Department of Energy) and State of New Mexico. 1981, as modified. "Agreement for Consultation and Cooperation" on WIPP by the State of New Mexico and the U.S. Department of Energy, modified 11/30/84, 8/4/87, and 4/18/88.

WIPP PA (Performance Assessment) Department. 1992. *Long-Term Gas and Brine Migration at the Waste Isolation Pilot Plant: Preliminary Sensitivity Analyses for Post-Closure 40 CFR 268 (RCRA), May 1992.*SAND92-1933. Albuquerque, NM: Sandia National Laboratories.

WIPP PA (Performance Assessment) Division. 1991. *Preliminary Comparison with 40 CFR Part 191, Subpart B for the Waste Isolation Pilot Plant, December 1991. Volumes 1-3.* SAND91-0893/1,2,3. Albuquerque, NM: Sandia National Laboratories.

Distribution

D. E. Miller, 6300
W. D. Weart, 6303
D. R. Anderson, 6342
R. C. Lincoln, 6345
M. L. F. Phillips, 6345
SWCF/GENEXP

Marietta and Gelbard, December 14, 1992

Date: 12/14/92
To: Distribution
From: M.G. Marietta, 6342, and F. Gelbard, 6119
Subject: Joint Memorandum from SNL Departments 6342 and 6119 on WIPP Performance Assessment Needs, Priorities, and Thresholds for Tracer Column Experiments

Sandia National Laboratories

Albuquerque, New Mexico 87185

date: December 14, 1992

to: Distribution

from: M. G. Marietta, 6342, and F. Gelbard, 6119

subject: Joint Memorandum from SNL Departments 6342 and 6119 on WIPP Performance Assessment Needs, Priorities, and Thresholds for Tracer Column Experiments

This memo records present WIPP Performance Assessment (PA) needs concerning radionuclide retardation measurements in the Culebra Dolomite and priorities of these needs. The importance of both physical and chemical retardation is discussed, and threshold values for matrix distribution coefficients (assuming double porosity transport can be justified), as observed in sensitivity analyses of the 1991 preliminary PA, are provided. The feasibility of fulfilling PA needs is briefly discussed. The memo documents PA guidance and requests for information from the tracer column experiments.

BACKGROUND
(M. G. Marietta)

PA's needs for a quantitative understanding of radionuclide retardation in the Culebra should be considered in the context of the present understanding of the Project's status with regard to regulatory compliance.

Performance assessments to date (Marietta et al., 1989; Bertram-Howery et al., 1990; WIPP PA Division, 1991) indicate that radionuclides will reach the Culebra only if the repository is breached by human intrusion, and therefore only the Containment Requirements of 40 CFR 191B and the safety assessments needed for NEPA evaluations are of concern. The long-term requirements of RCRA (40 CFR 268.6) apply to the release of non-radioactive contaminants at the disposal-unit boundary (i.e., the top of the Salado Formation and the subsurface extension of the land-withdrawal boundary), and as presently interpreted by the WIPP Project, only to the undisturbed performance of the disposal system.

The conceptual model used in assessments to date has assumed that radionuclide transport in the Culebra occurs in a double-porosity medium, with both physical and chemical retardation occurring in the dolomite matrix (WIPP PA Division, 1991; Helton et al., 1992). Given the assumptions of this model, retardation during groundwater transport is sufficient to reduce subsurface releases in the Culebra below those estimated to occur directly at the ground surface during drilling (i.e., cuttings).

If present assumptions about transport mechanisms and retardation in the Culebra can be justified experimentally, subsurface releases may continue to have little affect on the position of the CCDF. If, however, assumptions about retardation change or cannot be defended, estimates of subsurface releases comparable in magnitude to or greater than those estimated for cuttings may result, and may affect regulatory compliance.

For the purposes of setting priorities, PA recommends concentrating retardation research on those radionuclides with the potential to result in normalized releases greater than 10^{-2} (approximately one order of magnitude below the presently predicted cutting releases). Figure 1 shows the EPA normalized inventory of the repository, radionuclide by radionuclide, as a function of time (based on the most recent IDB [US DOE, 1991], as will be reported in Volume 3 of the 1992 Preliminary Performance Assessment). Note that the two portions of the figure are plotted at different scales, and that a horizontal line is drawn on each at an EPA normalized value of 10^{-2}. Time-dependent inventories are shown to 10^5 yr, although a vertical line is drawn at 10^4 yr, indicating the end of the regulatory period specified by 40 CFR 191B. Radionuclides with normalized inventories that never exceed 10^{-2} during 10^4 yr cannot result in releases greater than 10^{-2}, and can therefore be dropped from further consideration.

Figure 1a shows that the normalized inventories of ^{239}Pu, ^{240}Pu, ^{241}Am, ^{233}U, ^{234}U, ^{237}Np, ^{229}Th, ^{230}Th, and ^{226}Ra all exceed 10^{-2} during the 10^4 yr period. Figure 1b shows ^{238}Pu and ^{210}Pb (just barely at very late times approaching 10^5 yr) exceeding 10^{-2}. PA modeling for 1991 examined transport of 7 of these radionuclides (^{239}Pu, ^{240}Pu, ^{241}Am, ^{233}U, ^{234}U, ^{237}Np, and ^{230}Th) (WIPP PA Division, 1991, volume 2, section 6.5.2.10). Subsurface transport of two of the remaining radionuclides will be modeled in 1992, ^{229}Th and ^{226}Ra. Transport of ^{238}Pu in the Culebra will not be modeled because of its short half-life (87.7 yr). Subsurface transport of ^{210}Pb will not be modeled because of its low inventory at 10^4 yr and therefore low impact on 40 CFR 191B compliance. ^{210}Pb may be considered for subsurface transport in future dose calculations as a daughter product created in the Culebra by the decay of ^{226}Ra. Transport of both ^{238}Pu and ^{210}Pb in brine brought directly to the ground surface following intrusion (not yet included in performance assessments) also has the potential to contribute to doses.

Figure 2 shows cumulative normalized releases (1991 PA, as reported in Helton et al., 1992) for the seven transported radionuclides for the E1E2 scenario (upper row) and E1 scenario (lower row) at 1000 yr for three different assumptions. Figure 3 shows the corresponding CCDF plots.

The first column in Figure 4 plots releases into the Culebra from the borehole, before any retardation can occur in the Culebra. These releases are calculated assuming gas generation in the repository and no pressure-dependent fracturing of anhydrite layers in the Salado Formation, which may underestimate radionuclide releases to the Culebra. The corresponding CCDFs are shown in the top row of Figure 3. The second column of Figure 2 shows releases to the accessible environment (5 km for this analysis) assuming no chemical retardation (i.e., $K_d = 0$, as stipulated in the Consultation and Cooperation agreement between DOE and the State of New Mexico [US DOE and State of New Mexico, 1981 as modified]). Note that because a double-porosity transport model was used, physical retardation does occur because of diffusion into the dolomite matrix. The corresponding CCDFs are shown in the middle row of Figure 3. The third column of Figure 2 shows releases to the accessible environment calculated using the sampled values for K_d. The corresponding CCDFs are shown in the bottom row of Figure 3.

(In interpreting Figure 2, note that upper and lower bounds of the boxes for each radionuclide indicate the 25th and 75th percentiles from the total number of realizations, the vertical line within the box is the median value, and the black dot is the mean. The horizontal lines extending above the boxes extend to either the maximum value or the value representing $x_{.75} + 1.5(x_{.75} - x_{.25})$, which ever is lower, and the lines extending below the boxes indicate the comparable lower value. Observations falling outside these ranges are shown with individual "x" symbols. These plots do not contain information about the probability of scenario occurrence, and therefore assign equal weight to each scenario. [Helton et al., 1992])

The first column of Figure 2 shows that cumulative normalized releases of all seven radionuclides into the Culebra have the potential to exceed 10^{-2} for both scenarios. Therefore, transport of all seven in the Culebra has the potential to affect regulatory compliance. (Note that cumulative releases for many radionuclides exceed 10^{0} in some realizations, resulting in the potential for a violation of 40 CFR 191B).

The second column of Figure 2 ($K_d = 0$) shows that physical retardation by matrix diffusion significantly lowers cumulative normalized releases. Most radionuclides still exceed 10^{-1} for some realizations, but mean values are now in all cases within the EPA limit. This observation indicates that verification of physical retardation may be important to defending compliance with 191B, and that physical retardation should receive special attention in the experimental program.

The third column of Figure 2 (sampled values for K_ds) shows that using chemical retardation estimates based on judgment from two experts (C. Novak and R. Dosch, as reported in Trauth et al., 1992) resulted in only one value close to 10^{-1} (^{234}U in a single E1E2 realization) and very few values greater than 10^{-3}. Although the experts' values represent the best information available at this point, there are no actual data to support these values rigorously. Chemical retardation has the potential to greatly reduce releases to the accessible environment, and defensible values for K_ds in the Culebra may be very important for building confidence in a demonstration of compliance with 191B.

All of the radionuclides listed in Figure 2 are important for consideration in the experimental program. Special importance falls to U, which is the main contributor to releases, and to Pu, which dominates the inventory but makes no subsurface contribution to the 1991 CCDF because of its assumed high chemical retardation in the Culebra (compare columns 2 and 3 of Figure 2). It may be critically important for PA to be able to defend the high K_d values for Pu. (Although not shown in Figure 2 and not discussed further in this memo, releases of Pu into the Culebra [column 1] are limited by the assumed solubility of Pu in the repository brine, and defensible solubilities are therefore also important.)

Figure 4 provides additional insight into the sensitivity of PA results to the assumed values for K_ds. As seen in the upper left scatterplot, K_d values greater than 10^{-2} m^3/kg imply essentially zero release of ^{234}U to the accessible environment. (Note that, in these scatterplots, cumulative normalized releases are given at one-quarter of the distance to the accessible environment, rather than at the accessible environment boundary.) K_d values greater than approximately 10^{-1} m^3/kg imply essentially zero release of ^{239}Pu and ^{241}Am.

A major purpose of the column experiments is to generate defensible information on chemical retardation in the Culebra. Therefore, column experiments should include all radionuclides that, in the absence of chemical and physical retardation, have the potential to reach the accessible environment in quantities large enough to violate the Standard. These include isotopes of Pu, Am, U, Np, Th, and Ra. Pb should be included because of its potential to contribute to long-term doses.

RECOMMENDATIONS FROM PA FOR THE EXPERIMENTAL PROGRAM
(M. G. Marietta)

1. With regard to 40 CFR 191B, PA needs transport data for:

   U and Pu (highest priority)
   Am, Np, and Th (high priority)
   Ra (lower priority--not essential)

2. With regard to NEPA, PA needs transport data for

   U (highest priority)
   Ra and Pb (high priority)
   Np and Th (low priority)
   (assuming retardation of Pu is defensible)

3. Taking into account relative priorities of compliance evaluations with 40 CFR 191B (high) and safety evaluations (relatively lower), PA's composite recommendations are as follows:

   U and Pu data are critical (highest priority)

   Am, Np, and Th are important (high priority)

   Ra and Pb should be included if possible and if their inclusion does not add significantly to the cost of the experiment or detract from the ultimate defensibility of data for the other elements.

FEASIBILITY
(F. Gelbard)

The radiation detectors purchased for the experiment are designed to detect, identify, and measure the concentration of individual radioisotopes in a mixture of radioisotopes. A germanium detector, cooled with liquid nitrogen, is used to analyze gamma radiation from a sample. Although in principle, our system should be able to distinguish an arbitrary number of radionuclides, we have not yet tested the system. Obviously, the fewer the number of radionuclides, the easier to distinguish a specific radionuclide. Furthermore, for ES&H considerations, we would like to minimize the total radioactivity, and thus reduce the number of radionuclides.

With these considerations, we expect that a mixture with the following radioisotopes can be measured with our equipment: ^{232}U, ^{228}Th, ^{241}Am and/or ^{243}Am, ^{237}Np, ^{226}Ra, ^{210}Pb, and ^{22}Na (nonsorbing tracer). We are investigating which isotope of Pu would be best to use. In addition, we may also include the following isotopes, ^{133}Ba (analog for Ra), a radioactive rare-earth metal (analog for radionuclides in the +3 oxidation state), and ^{243}Cm. If we encounter difficulty in the measurements, Ra, Ba, and/or Pb may be excluded from our measurements.

The number of experiments that can be performed is limited not only by time and cost, but also because it would be virtually impossible to obtain more core. Furthermore, ES&H requirements limit the number of experiments. All the liquid radioactive effluent, regardless of the activity level, is considered radioactive waste and must be stored in the laboratory indefinitely (or until SNL has an acceptable means for disposal). Because of the large volume of waste generated for each experiment, and our plans to perform destructive post-test analysis on the cores, it is crucial that the above list of radioisotopes be complete.

Based on the composite recommendations of the PA Department (6342) given previously, the only elements requiring retardation measurements in Culebra rock are U, Pu, Th, Am, Np, Ra, and Pb, with Ra and Pb of least importance. Both physical and chemical retardation measurements are needed for these elements. The oxidation states of the radionuclides in solution is determined by the brine composition, pH, and temperature. In the experiments these three variables will be controlled to be the same as that found in the Culebra from which the cores were taken. Therefore, retardation factors will be obtained for the radionuclides in whatever oxidation state they would be in in the field, but the oxidation state will not be measured.

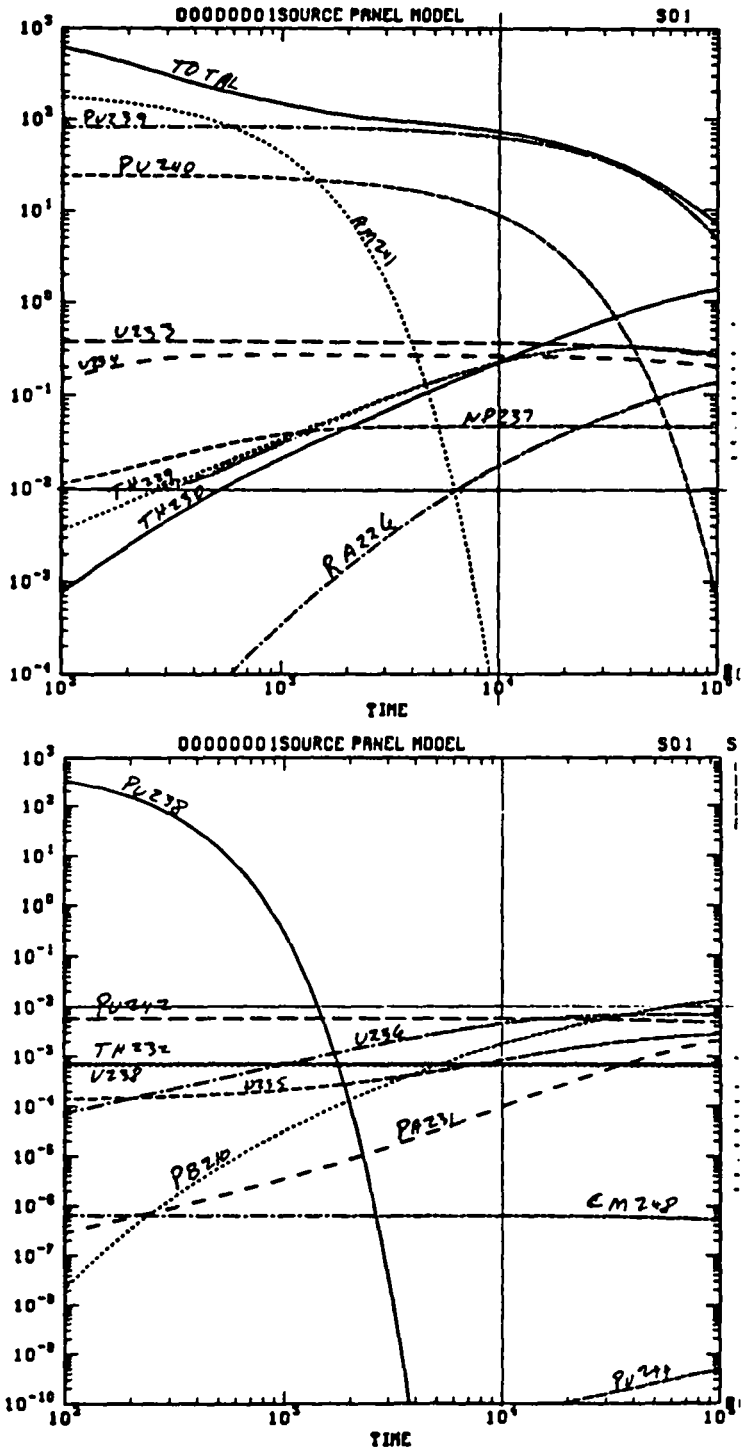

Figure 1. Decay histories for the present IDB inventory. Note scale change between Figures 2a and 2b. Horizontal line at 10^{-2} indicates threshold of importance for PA. Vertical line at 10^{4} yr indicates EPA regulatory time period.

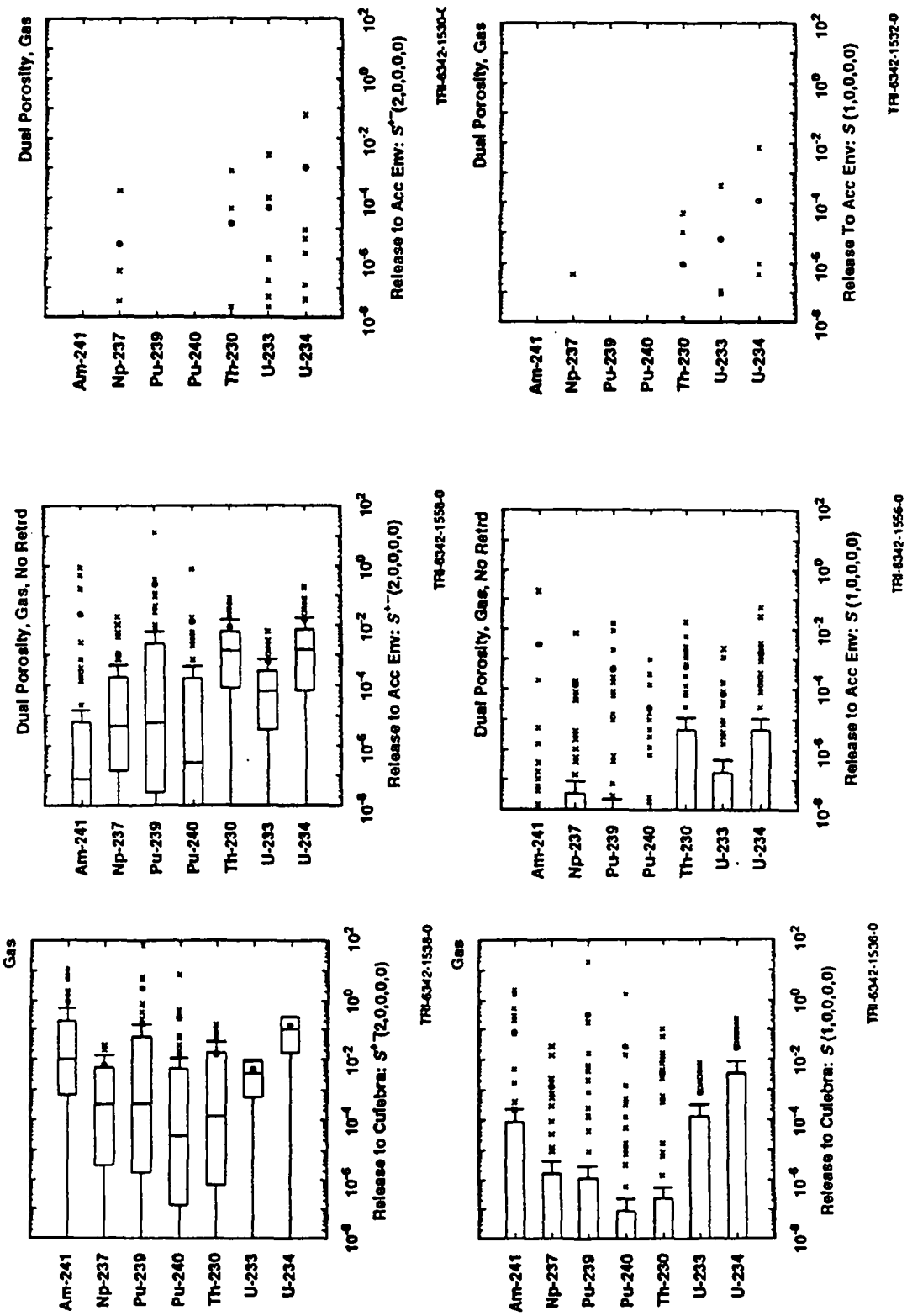

Figure 2. Cumulative normalized releases for radionuclides from E1E2 (upper row) and E1 (lower row) intrusions at 10^3 yr (1991 WIPP preliminary performance assessment) (Helton et al., 1992).

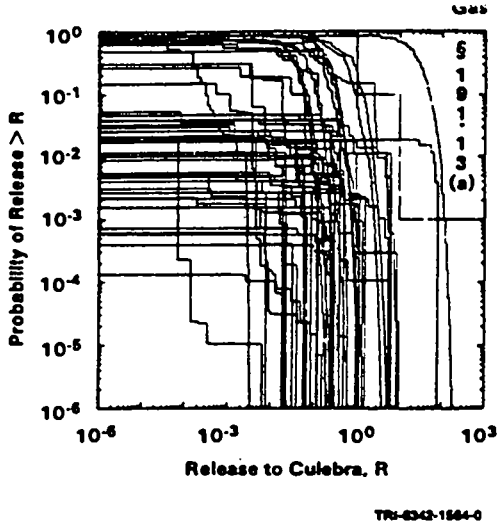

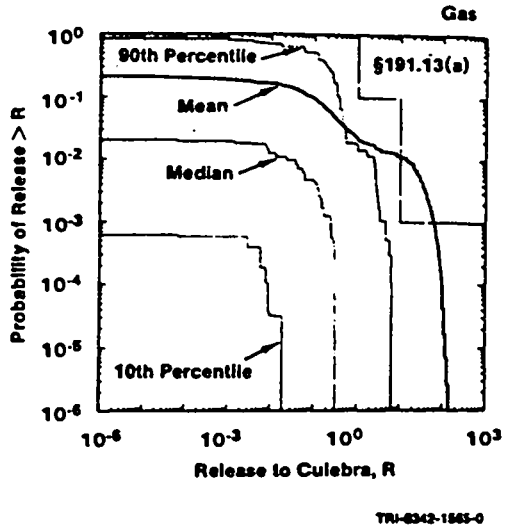

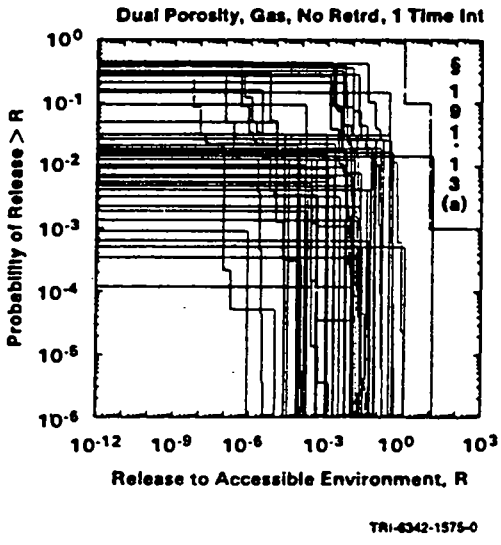

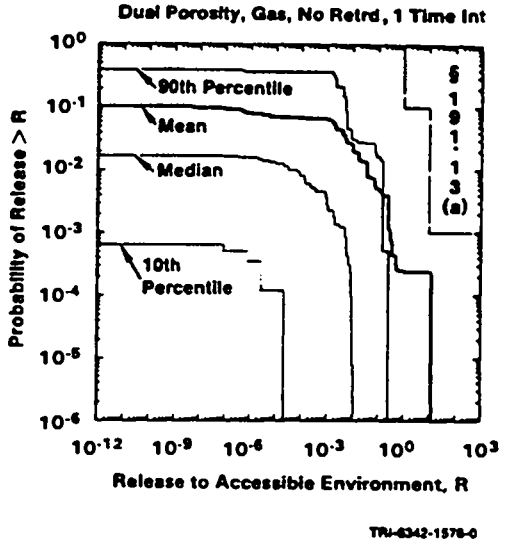

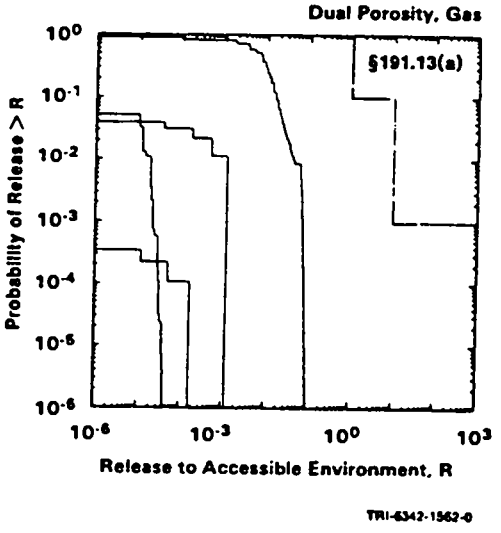

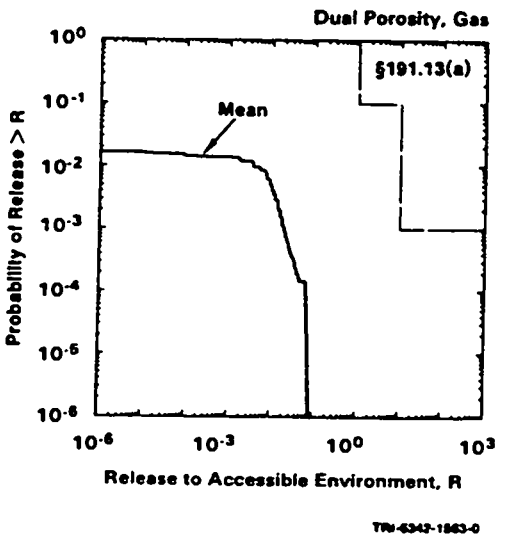

Figure 3. CCDFs corresponding to the releases plotted in Figure 2 (Helton et al., 1992).

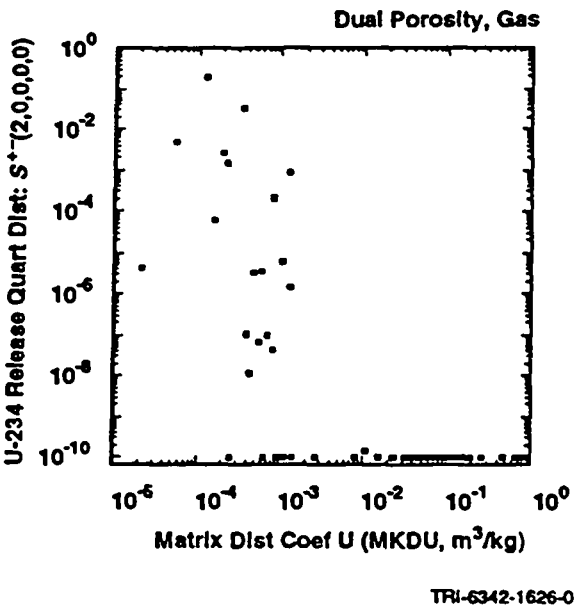

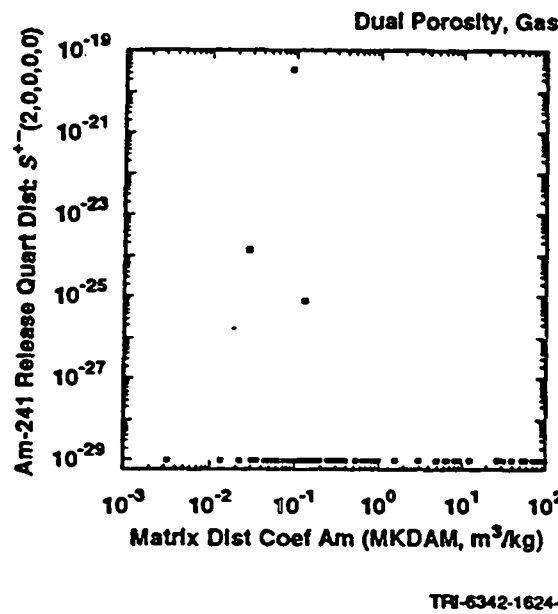

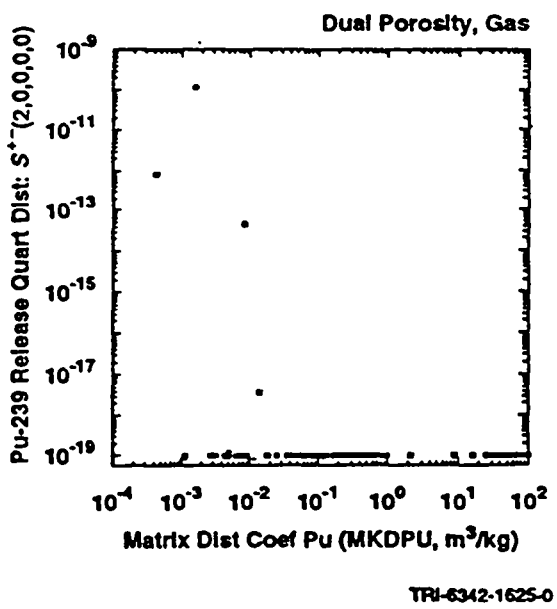

Figure 4. Scatterplots for radioisotope release versus matrix K_ds showing thresholds.

REFERENCES

Bertram-Howery, S. G., M. G. Marietta, R. P. Rechard, P. N. Swift, D. R. Anderson, B. L. Baker, J. E. Bean, W. Beyeler, K. F. Brinster, R. V. Guzowski, J. C. Helton, R. D. McCurley, D. K. Rudeen, J. D. Schreiber, and P. Vaughn. 1990. *Preliminary Comparison with 40 CFR Part 191, Subpart B for the Waste Isolation Pilot Plant, December 1990.* SAND90-2347. Albuquerque, NM: Sandia National Laboratories.

Marietta, M. G., S. G. Bertram Howery, D. R. Anderson, K. F. Brinster, R. V. Guzowski, H. Iuzzolino, and R. P. Rechard. 1989. *Performance Assessment Methodology Demonstration: Methodology Development for Purposes of Evaluating Compliance with EPA 40 CFR Part 191, Subpart B, for the Waste Isolation Pilot Plant.* SAND89-2027. Albuquerque, NM: Sandia National Laboratories.

Helton, J. C., J. W. Garner, R. P. Rechard, D. K. Rudeen, and P. N. Swift. 1992. *Preliminary Comparison with 40 CFR Part 191, Subpart B for the Waste Isolation Pilot Plant, December 1991. Volume 4: Uncertainty and Sensitivity Analysis Results.* SAND91-0893/4. Albuquerque, NM: Sandia National Laboratories.

Trauth, K. M., S. C. Hora, R. P. Rechard, and D. R. Anderson. 1992. *The Use of Expert Judgment to Quantify Uncertainty in Solubility and Sorption Parameters for Waste Isolation Pilot Plant Performance Assessment.* SAND92-0479. Albuquerque, NM: Sandia National Laboratories. (in review).

US DOE (Department of Energy). 1991. *Integrated Data Base for 1991: Spent Fuel and Radioactive Waste Inventories, Projects and Characterizations.* DOE/RW-006, Rev. 7.

US DOE (Department of Energy) and State of New Mexico. 1981, as modified. "Agreement for Consultation and Cooperation" on WIPP by the State of New Mexico and the U.S. Department of Energy, modified 11/30/84, 8/4/87, and 4/18/88.

WIPP PA (Performance Assessment) Department. 1992. *Long-Term Gas and Brine Migration at the Waste Isolation Pilot Plant: Preliminary Sensitivity Analyses for Post-Closure 40 CFR 268 (RCRA), May 1992.*SAND92-1933. Albuquerque, NM: Sandia National Laboratories.

WIPP PA (Performance Assessment) Division. 1991. *Preliminary Comparison with 40 CFR Part 191, Subpart B for the Waste Isolation Pilot Plant, December 1991. Volumes 1-3.* SAND91-0893/1,2,3. Albuquerque, NM: Sandia National Laboratories.

Distribution

R. W. Lynch, 6100
D. E. Miller, 6300
W. D. Weart, 6303
E. D. Gorham, 6119
C. F. Novak, 6119
D. R. Anderson, 6342
SWCF/GENEXP

DISTRIBUTION

(Send Distribution list changes to M.M. Gruebel, Dept. 6342, Sandia National Laboratories, PO Box 5800, Albuquerque, NM 87185-5800)

Federal Agencies

US Department of Energy (6)
Office of Civilian Radioactive Waste Management
Attn: Deputy Director, RW-2
Associate Director, RW-10/50
Office of Program and Resources Management
Office of Contract Business Management
Director, Analysis and Verification Division, RW-22
Associate Director, RW-30
Office of Systems and Compliance
Associate Director, RW-40
Office of Storage and Transportation
Director, RW-4/5
Office of Strategic Planning and International Programs
Office of External Relations
Forrestal Building
Washington, DC 20585

US Department of Energy
Albuquerque Operations Office
Attn: National Atomic Museum Library
PO Box 5400
Albuquerque, NM 87185

US Department of Energy (2)
Office of Environmental Restoration and Waste Management
Attn: EM-1
C. Frank, EM-50
Washington, DC 20585

US Department of Energy (3)
Office of Environmental Restoration and Waste Management
Attn: M. Frei, EM-34, Trevion II
Director, Waste Management Projects
Washington, DC 20585-0002

US Department of Energy
Office of Environmental Restoration and Waste Management
Attn: J. Lytle, EM-30, Trevion II
Washington, DC 20585-0002

US Department of Energy
Office of Environmental Restoration and Waste Management
Attn: S. Schneider, EM-342, Trevion II
Washington, DC 20585-0002

US Department of Energy (3)
WIPP Task Force
Attn: G.H. Daly
S. Fucigna
B. Bower
12800 Middlebrook Rd., Suite 400
Germantown, MD 20874

US Department of Energy (4)
Office of Environment, Safety and Health
Attn: R.P. Berube, EH-20
C. Borgstrum, EH-25
R. Pelletier, EH-231
K. Taimi, EH-232
Washington, DC 20585

US Department of Energy (6)
WIPP Project Integration Office
Attn: S. Alcorn
W.J. Arthur III
J. Coffey
L.W. Gage
P.J. Higgins
D.A. Olona
PO Box 5400
Albuquerque, NM 87115-5400

US Department of Energy (2)
WIPP Project Integration Satellite Office
Attn: R. Batra
R. Becker
PO Box 3090, Mail Stop 525
Carlsbad, NM 88221-3090

US Department of Energy (10)
WIPP Project Site Office (Carlsbad)
Attn: A. Hunt (4)
V. Daub (4)
J. Lippis
K. Hunter
PO Box 3090
Carlsbad, NM 88221-3090

US Department of Energy
Research & Waste Management Division
Attn: Director
PO Box E
Oak Ridge, TN 37831

US Department of Energy (2)
Idaho Operations Office
Fuel Processing and Waste
Management Division
785 DOE Place
Idaho Falls, ID 83402

US Department of Energy
Savannah River Operations Office
Defense Waste Processing
Facility Project Office
Attn: W.D. Pearson
PO Box A
Aiken, SC 29802

US Department of Energy (2)
Richland Operations Office
Nuclear Fuel Cycle & Production
Division
Attn: R.E. Gerton
825 Jadwin Ave.
PO Box 500
Richland, WA 99352

US Department of Energy
Office of Geologic Disposal
Yucca Mountain Project Office
Attn: Associate Director, RW-20
PO Box 98608
Las Vegas, NV 89193-8608

US Department of Energy (3)
Nevada Operations Office
Attn: J.R. Boland
D. Livingston
P.K. Fitzsimmons
2753 S. Highland Drive
Las Vegas, NV 89183-8518

US Department of Energy (2)
Technical Information Center
PO Box 62
Oak Ridge, TN 37831

US Department of Energy
Los Alamos Area Office
528 35th Street
Los Alamos, NM 87544

US Department of Energy (2)
Chicago Operations Office
Attn: J.C. Haugen
9800 South Cass Avenue
Argonne, IL 60439

US Department of Energy (3)
Rocky Flats Area Office
Attn: W.C. Rask
G. Huffman
T. Lukow
PO Box 928
Golden, CO 80402-0928

US Department of Energy
Dayton Area Office
Attn: R. Grandfield
PO Box 66
Miamisburg, OH 45343-0066

US Department of Energy
Attn: E. Young
Room E-178
GAO/RCED/GTN
Washington, DC 20545

US Bureau of Land Management
Carlsbad Office
101 E. Mermod
Carlsbad, NM 88220

US Bureau of Land Management
New Mexico State Office
PO Box 1449
Santa Fe, NM 87507

US Environmental Protection
Agency (2)
Radiation Protection Programs
Attn: M. Oge
ANR-460
Washington, DC 20460

US Environmental Protection
Agency, Region 6
Attn: C. Byrum, 6T-ET
1445 Ross Ave.
Dallas, TX 75202

US Geological Survey (2)
Water Resources Division
Attn: C. Peters
4501 Indian School NE
Suite 200
Albuquerque, NM 87110

US Nuclear Regulatory Commission
Division of Waste Management
Attn: H. Marson
Mail Stop 4-H-3
Washington, DC 20555

US Nuclear Regulatory Commission (4)
Advisory Committee on Nuclear Waste
Attn: D. Moeller
M.J. Steindler
P.W. Pomeroy
W.J. Hinze
7920 Norfolk Ave.
Bethesda, MD 20814

Defense Nuclear Facilities Safety Board
Attn: D. Winters
625 Indiana Ave. NW
Suite 700
Washington, DC 20004

Nuclear Waste Technical Review Board
Attn: Library (2)
1100 Wilson Blvd.
Suite 910
Arlington, VA 22209-2297

Energy and Science Division
Office of Management and Budget
Attn: K. Yuracko
725 17th Street NW
Washington, DC 20503

State Agencies

New Mexico Bureau of Mines
and Mineral Resources
Socorro, NM 87801

New Mexico Energy, Minerals and Natural Resources Department
Attn: Librarian
2040 South Pacheco
Santa Fe, NM 87505

New Mexico Energy, Minerals and Natural Resources Department
New Mexico Radioactive Task Force (2)
(Governor's WIPP Task Force)
Attn: A. Lockwood, Chairman
C. Wentz, Policy Analyst
2040 South Pacheco
Santa Fe, NM 87505

Bob Forrest
Mayor, City of Carlsbad
PO Box 1569
Carlsbad, NM 88221

Carlsbad Department of Development
Executive Director
Attn: C. Bernard
PO Box 1090
Carlsbad, NM 88221

New Mexico Environment Department
Secretary of the Environment (3)
Attn: J. Espinosa
PO Box 968
1190 St. Francis Drive
Santa Fe, NM 87503-0968

New Mexico Environment Department
Attn: P. McCasland
WIPP Project Site Office
PO Box 3090
Carlsbad, NM 88221-3090

New Mexico State Engineer's Office
Attn: M. Chudnoff
PO Box 25102
Santa Fe, NM 87504-5102

Environmental Evaluation Group (5)
Attn: R. Neill
7007 Wyoming Blvd. NE, Suite F-2
Albuquerque, NM 87109

Advisory Committee on Nuclear Facility Safety

John F. Ahearne
Executive Director, Sigma Xi
99 Alexander Drive
Research Triangle Park, NC 27709

James E. Martin
109 Observatory Road
Ann Arbor, MI 48109

WIPP Panel of National Research Council's Board on Radioactive Waste Management

Charles Fairhurst, Chairman
Department of Civil and
Mineral Engineering
University of Minnesota
500 Pillsbury Dr. SE
Minneapolis, MN 55455-0220

John O. Blomeke
3833 Sandy Shore Drive
Lenoir City, TN 37771-9803

John D. Bredehoeft
Western Region Hydrologist
Water Resources Division
US Geological Survey (M/S 439)
345 Middlefield Road
Menlo Park, CA 94025

Rodney C. Ewing
Department of Geology
University of New Mexico
Albuquerque, NM 87131

B. John Garrick
PLG, Inc.
4590 MacArthur Blvd.
Suite 400
Newport Beach, CA 92660-2027

Leonard F. Konikow
US Geological Survey
431 National Center
Reston, VA 22092

Jeremiah O'Driscoll
505 Valley Hill Drive
Atlanta, GA 30350

Chris G. Whipple
ICF Kaiser Engineers
1800 Harrison St.
Oakland, CA 94612-3430

National Research Council (3)
Board on Radioactive
Waste Management
RM HA456
Attn: P.B. Myers (2)
G.J. Grube
2101 Constitution Ave.
Washington, DC 20418

Performance Assessment Peer Review Panel

G. Ross Heath
College of Ocean and Fishery
Sciences, HN-15
583 Henderson Hall
University of Washington
Seattle, WA 98195

Thomas H. Pigford
Department of Nuclear Engineering
4159 Etcheverry Hall
University of California
Berkeley, CA 94720

Thomas A. Cotton
JK Research Associates, Inc.
4429 Butterworth Place NW
Washington, DC 20016

Robert J. Budnitz
President, Future Resources
Associates, Inc.
2000 Center Street, Suite 418
Berkeley, CA 94704

C. John Mann
Department of Geology
245 Natural History Bldg.
1301 West Green Street
University of Illinois
Urbana, IL 61801

Frank W. Schwartz
Department of Geology and Mineralogy
The Ohio State University
Scott Hall
1090 Carmack Rd.
Columbus, OH 43210

National Laboratories

Argonne National Laboratory (2)
Attn: A. Smith
D. Tomasko
9700 South Cass, Bldg. 201
Argonne, IL 60439

Battelle Pacific Northwest
Laboratory (2)
Attn: S. Bates
R.E. Westerman
MSIN P8-44
Battelle Boulevard
Richland, WA 99352

Idaho National Engineering
Laboratory (2)
Attn: H. Loo
R. Klinger
Mail Stop 5108
Idaho Falls, ID 83403-4000

Los Alamos National Laboratory (5)
Attn: B. Erdal, CNC-11
M. Ennis, HS-12
Mail Stop J900
S. Kosiewicz, EM-7
Mail Stop J595
L. Soholt, EM-13
Mail Stop M992
J. Wenzel, HS-12
Mail Stop K482
PO Box 1663
Los Alamos, NM 87545

Oak Ridge National Laboratory
Transuranic Waste Manager
Attn: D.W. Turner
Bldg. 3047
PO Box 2008
Oak Ridge, TN 37831-6060

Pacific Northwest Laboratory
Attn: B. Kennedy
PO Box 999
Richland, WA 99352

Westinghouse-Savannah River
Technology Center (4)
Attn: N. Bibler
J.R. Harbour
M.J. Plodinec
G.G. Wicks
Aiken, SC 29802

Corporations/Members of the Public

Battelle Memorial Institute
Attn: R. Root
J. Kircher
505 Marquette NW
Suite 1
Albuquerque, NM 87102

Benchmark Environmental Corp.
Attn: C. Frederickson
4501 Indian School NE
Suite 105
Albuquerque, NM 87110

Beta Corporation Int.
Attn: E. Bonano
6613 Esther NE
Albuquerque, NM 87109

City of Albuquerque
Public Works Department
Utility Planning Division
Attn: W.K. Summers
PO Box 1293
Albuquerque, NM 87103

Deuel and Associates, Inc.
Attn: R.W. Prindle
7208 Jefferson NE
Albuquerque, NM 87109

Disposal Safety, Inc.
Attn: B. Ross
1660 L Street NW, Suite 314
Washington, DC 20036

Ecodynamics (2)
Attn: P. Roache
R. Blaine
PO Box 9229
Albuquerque, NM 87119-9229

EG & G Idaho (3)
1955 Fremont Street
Attn: C. Atwood
C. Hertzler
T.I. Clements
Idaho Falls, ID 83415

Geomatrix
Attn: K. Coppersmith
100 Pine St., Suite 1000
San Francisco, CA 94111

Golder Associates, Inc.
Attn: R. Kossik
4104 148th Avenue NE
Redmond, WA 98052

INTERA, Inc.
Attn: A.M. LaVenue
1650 University Blvd. NE, Suite 300
Albuquerque, NM 87102

INTERA, Inc.
Attn: J.F. Pickens
6850 Austin Center Blvd., Suite 300
Austin, TX 78731

INTERA, Inc.
Attn: W. Stensrud
PO Box 2123
Carlsbad, NM 88221

INTERA, Inc.
Attn: W. Nelson
101 Convention Center Drive
Suite 540
Las Vegas, NV 89109

IT Corporation (2)
Attn: R.F. McKinney
J. Myers
Regional Office
Suite 700
5301 Central Avenue NE
Albuquerque, NM 87108

John Hart and Associates, P.A.
Attn: J.S. Hart
2815 Candelaria Road NW
Albuquerque, NM 87107

John Hart and Associates, P.A.
Attn: K. Lickliter
1009 North Washington
Tacoma, WA 98406

MAC Technical Services Co.
Attn: D.K. Duncan
8418 Zuni Road SE
Suite 200
Albuquerque, NM 87108

Newman and Holtzinger
Attn: C. Mallon
1615 L Street NW
Suite 1000
Washington, DC 20036

RE/SPEC, Inc. (2)
Attn: W. Coons
4775 Indian School NE
Suite 300
Albuquerque, NM 87110

RE/SPEC, Inc.
Attn: J.L. Ratigan
PO Box 725
Rapid City, SD 57709

Reynolds Electric and Engineering
Company, Inc.
Attn: E.W. Kendall
Building 790
Warehouse Row
PO Box 98521
Las Vegas, NV 89193-8521

Science Applications International
Corporation (SAIC)
Attn: H.R. Pratt
10260 Campus Point Drive
San Diego, CA 92121

Science Applications International
Corporation (2)
Attn: D.C.Royer
C.G. Pflum
101 Convention Center Dr.
Las Vegas, NV 89109

Science Applications International
Corporation (3)
Attn: M. Davis
R. Guzowski
J. Tollison
2109 Air Park Road SE
Albuquerque, NM 87106

Science Applications International
Corporation (2)
Attn: J. Young
D. Lester
18706 North Creek Parkway, Suite 110
Bothell, WA 98011

Southwest Research Institute
Center for Nuclear Waste Regulatory
Analysis (2)
Attn: P.K. Nair
6220 Culebra Road
San Antonio, TX 78228-0510

Systems, Science, and Software (2)
Attn: E. Peterson
P. Lagus
Box 1620
La Jolla, CA 92038

TASC
Attn: S.G. Oston
55 Walkers Brook Drive
Reading, MA 01867

Tech Reps, Inc. (7)
Attn: J. Chapman
C. Crawford
D. Marchand
T. Peterson
J. Stikar
D. Scott
M. Minahan
5000 Marble NE, Suite 222
Albuquerque, NM 87110

Tolan, Beeson & Associates
Attn: T.L. Tolan
2320 W. 15th Avenue
Kennewick, WA 99337

TRW Environmental Safety Systems (2)
Attn: I. Sacks, Suite 800
L. Wildman, Suite 1300
2650 Park Tower Drive
Vienna, VA 22180-7306

Sanford Cohen and Associates
Attn: J. Channell
7101 Carriage Rd NE
Albuquerque, NM 87109

Westinghouse Electric Corporation (5)
Attn: Library
C. Cox
L. Fitch
B.A. Howard
R.F. Kehrman
PO Box 2078
Carlsbad, NM 88221

Westinghouse Hanford Company
Attn: D.E. Wood, MSIN HO-32
PO Box 1970
Richland, WA 99352

Western Water Consultants
Attn: P.A. Rechard
PO Box 4128
Laramie, WY 82071

Western Water Consultants
Attn: D. Fritz
1949 Sugarland Drive #134
Sheridan, WY 82801-5720

P. Drez
8816 Cherry Hills Road NE
Albuquerque, NM 87111

David Lechel
9600 Allende Rd. NE
Albuquerque, NM 87109

C.A. Marchese
PO Box 21790
Albuquerque, NM 87154

Arend Meijer
3821 Anderson SE
Albuquerque, NM 87108

D.W. Powers
Star Route Box 87
Anthony, TX 79821

Shirley Thieda
PO Box 2109, RR1
Bernalillo, NM 87004

Jack Urich
c/o CARD
144 Harvard SE
Albuquerque, NM 87106

Universities

University of California
Mechanical, Aerospace, and
Nuclear Engineering Department (2)
Attn: W. Kastenberg
D. Browne
5532 Boelter Hall
Los Angeles, CA 90024

University of California
Engineering and Applied Science Attn:
D. Okrent
48-121A Engineering IV
Los Angeles, CA 90024-1597

University of California
Mine Engineering Department
Rock Mechanics Engineering
Attn: N. Cook
Berkeley, CA 94720

University of Hawaii at Hilo
Business Administration
Attn: S. Hora
Hilo, HI 96720-4091

University of New Mexico
Geology Department
Attn: Library
Albuquerque, NM 87131

University of New Mexico
Research Administration
Attn: H. Schreyer
102 Scholes Hall
Albuquerque, NM 87131

University of Wyoming
Department of Civil Engineering
Attn: V.R. Hasfurther
Laramie, WY 82071

University of Wyoming
Department of Geology
Attn: J.I. Drever
Laramie, WY 82071

University of Wyoming
Department of Mathematics
Attn: R.E. Ewing
Laramie, WY 82071

Libraries

Thomas Brannigan Library
Attn: D. Dresp
106 W. Hadley St.
Las Cruces, NM 88001

New Mexico State Library
Attn: N. McCallan
325 Don Gaspar
Santa Fe, NM 87503

New Mexico Tech
Martin Speere Memorial Library
Campus Street
Socorro, NM 87810

New Mexico Junior College
Pannell Library
Attn: R. Hill
Lovington Highway
Hobbs, NM 88240

Carlsbad Municipal Library
WIPP Public Reading Room
Attn: L. Hubbard
101 S. Halagueno St.
Carlsbad, NM 88220

University of New Mexico
Zimmerman Library
Government Publications Department
Albuquerque, NM 87131

NEA/Performance Assessment Advisory Group (PAAG)

P. Duerden
ANSTO
Lucas Heights Research Laboratories
Private Mail Bag No. 1
Menai, NSW 2234
AUSTRALIA

Gordon S. Linsley
Division of Nuclear Fuel Cycle and Waste Management
International Atomic Energy Agency
PO Box 100
A-1400 Vienna, AUSTRIA

Nicolo Cadelli
Commission of the European Communities
200, Rue de la Loi
B-1049 Brussels, BELGIUM

R. Heremans
Organisme Nationale des Déchets Radioactifs et des Matiéres Fissiles (ONDRAF)
Place Madou 1, Boitec 24/25
B-1030 Brussels, BELGIUM

J. Marivoet
Centre d'Etudes de l'Energie Nucléaire (CEN/SCK)
Boeretang 200
B-2400 Mol, BELGIUM

P. Conlon
Waste Management Division
Atomic Energy Control Board (AECB)
PO Box 1046
Ottawa, Ontario KIP 559, CANADA

A.G. Wikjord
Manager, Environmental and Safety Assessment Branch
Atomic Energy of Canada Limited
Whiteshell Research Establishment
Pinewa, Manitoba ROE 1LO
CANADA

Teollisuuden Voima Oy (TVO) (2)
Attn: Timo Äikäs
Jukka-Pekka Salo
Annankatu 42 C
SF-00100 Helsinki Suomi
FINLAND

Timo Vieno
Technical Research Centre of Finland (VTT)
Nuclear Energy Laboratory
PO Box 208
SF-02151 Espoo, FINLAND

Division de la Sécurité et de la
Protection de l'Environment (DSPE)
Commissariat á l'Energie Atomique
Agence Nationale pour la Gestion des
Déchets Radioactifs (ANDRA) (2)
Attn: Gérald Ouzounian
M. Claude Ringeard
Route du Panorama Robert Schuman
B. P. No. 38
F-92266 Fontenay-aux-Roses Cedex
FRANCE

Claudio Pescatore
Division of Radiation Protection and
Waste Management
OECD Nuclear Energy Agency
38, Boulevard Suchet
F-75016 Paris, FRANCE

M. Dominique Greneche
Commissariat á l'Energie Atomique
IPSN/DAS/SASICC/SAED
B.P. No. 6
F-92265 Fontenay-aux-Roses Cedex
FRANCE

Robert Fabriol
Bureau de Recherches Géologiques et
Miniéres (BRGM)
B.P. 6009
45060 Orléans Cedex 2, FRANCE

P. Bogorinski
Gesellschaft für Reaktorsicherheit
(GRS) MBH
Schwertnergasse 1
D-5000 Köln 1, GERMANY

R. Storck
GSF - Institut für Tieflagerung
Theodor-Heuss-Strabe 4
D-3300 Braunschweig, GERMANY

Ferrucio Gera
ISMES S.p.A
Via del Crociferi 44
I-00187 Rome, ITALY

Hiroyuki Umeki
Isolation System Research Program
Radioactive Waste Management Project
Power Reactor and Nuclear Fuel
Development Corporation (PNC)
1-9-13, Akasaka, Minato-ku
Tokyo 107, JAPAN

P. Carboneras Martinez
ENRESA
Calle Emilio Vargas, 7
R-28043 Madrid
SPAIN

Tönis Papp
Swedish Nuclear Fuel and Waste
Management Co.
Box 5864
S 102 48 Stockholm
SWEDEN

Conny Hägg
Swedish Radiation Protection
Institute (SSI)
Box 60204
S-104 01 Stockholm
SWEDEN

J. Hadermann
Paul Scherrer Institute
Waste Management Programme
CH-5232 Villigen PSI
SWITZERLAND

J. Vigfusson
HSK-Swiss Nuclear Safety Inspectorate
Federal Office of Energy
CH-5232 Villigen-HSK
SWITZERLAND

D.E. Billington
Departmental Manager—Assessment
Studies
Radwaste Disposal R&D Division
AEA Decommissioning & Radwaste
Harwell Laboratory, B60
Didcot Oxfordshire OX11 ORA
UNITED KINGDOM

P. Grimwood
Waste Management Unit
BNFL
Sellafield
Seascale, Cumbria CA20 1PG
UNITED KINGDOM

Alan J. Hooper
UK Nirex Ltd
Curie Avenue
Harwell, Didcot
Oxfordshire, OX11 ORH
UNITED KINGDOM

Jerry M. Boak
Yucca Mountain Project Office
US Department of Energy
PO Box 98608
Las Vegas, NV 89193

Seth M. Coplan (Chairman)
US Nuclear Regulatory Commission
Division of High-Level Waste Management
Mail Stop 4-H-3
Washington, DC 20555

A.E. Van Luik
INTERA/M&O
The Valley Bank Center
101 Convention Center Dr.
Las Vegas, NV 89109

NEA/Probabilistic System Assessment Group (PSAG)

Shaheed Hossain
Division of Nuclear Fuel Cycle and Waste Management
International Atomic Energy Agency
Wagramerstrasse 5
PO Box 100
A-1400 Vienna, AUSTRIA

Alexander Nies (PSAC Chairman)
Gesellschaft für Strahlen- und Institut für Tieflagerung
Abteilung für Endlagersicherheit
Theodor-Heuss-Strasse 4
D-3300 Braunschweig, GERMANY

Eduard Hofer
Gesellschaft für Reaktorsicherheit (GRS) MBH
Forschungsgelände
D-8046 Garching, GERMANY

Andrea Saltelli
Commission of the European Communities
Joint Resarch Centre of Ispra
I-21020 Ispra (Varese)
ITALY

Alejandro Alonso
Cátedra de Tecnología Nuclear
E.T.S. de Ingenieros Industriales
José Gutiérrez Abascal, 2
E-28006 Madrid, SPAIN

ENRESA (2)
Attn: M. A. Cuñado
F. J. Elorza
Calle Emilio Vargas, 7
E-28043 Madrid, SPAIN

Pedro Prado
CIEMAT
Instituto de Tecnología Nuclear
Avenida Complutense, 22
E-28040 Madrid, SPAIN

Nils A. Kjellbert
Swedish Nuclear Fuel and Waste Management Company (SKB)
Box 5864
S-102 48 Stockholm, SWEDEN

Björn Cronhjort
Royal Institute of Technology
Automatic Control
S-100 44 Stockholm, SWEDEN

Richard A. Klos
Paul-Scherrer Institute (PSI)
CH-5232 Villingen PSI, SWITZERLAND

Nationale Genossenschaft für die Lagerung Radioaktiver Abfälle (2)
Attn: C. McCombie
F. Van Dorp
Hardstrasse 73
CH-5430 Wettingen, SWITZERLAND

N. A. Chapman
Intera Information Technologies
Park View House
14B Burton Street
Melton Mowbray
Leicestershire LE13 1AE
UNITED KINGDOM

Daniel A. Galson
Galson Sciences Ltd.
35, Market Place
Oakham
Leicestershire LE15 6DT
UNITED KINGDOM

David P. Hodgkinson
Intera Information Technologies
45 Station Road, Chiltern House
Henley-on-Thames
Oxfordshire RG9 1AT
UNITED KINGDOM

Brian G.J. Thompson
Department of the Environment: Her Majesty's Inspectorate of Pollution
Room A5.33, Romney House
43 Marsham Street
London SW1P 2PY
UNITED KINGDOM

Intera Information Technologies
Attn: M.J.Apted
3609 South Wadsworth Blvd.
Denver, CO 80235

US Nuclear Regulatory Commission (2)
Attn: R. Codell
N. Eisenberg
Mail Stop 4-H-3
Washington, DC 20555

Battelle Pacific Northwest Laboratories
Attn: P.W. Eslinger
MS K2-32
PO Box 999
Richland, WA 99352

Center for Nuclear Waste Regulatory Analysis (CNWRA)
Southwest Research Institute
Attn: B. Sagar
PO Drawer 28510
6220 Culebra Road
San Antonio, TX 78284

Geostatistics Expert Working Group (GXG)

Rafael L. Bras
R.L. Bras Consulting Engineers
44 Percy Road
Lexington, MA 02173

Jesus Carrera
Universidad Politécnica de Cataluña
E.T.S.I. Caminos
Jordi, Girona 31
E-08034 Barcelona
SPAIN

Gedeon Dagan
Department of Fluid Mechanics and Heat Transfer
Tel Aviv University
PO Box 39040
Ramat Aviv, Tel Aviv 69978
ISRAEL

Ghislain de Marsily (GXG Chairman)
University Pierre et Marie Curie
Laboratorie de Geologie Applique
4, Place Jussieu
T.26 - 5^{e} etage
75252 Paris Cedex 05, FRANCE

Alain Galli
Centre de Geostatistique
Ecole des Mines de Paris
35 Rue St. Honore
77035 Fontainebleau, FRANCE

Christian Ravenne
Geology and Geochemistry Division
Institut Francais du Pétrole
1 & 4, Av. de Bois-Préau B.P. 311
92506 Rueil Malmaison Cedex
FRANCE

Peter Grindrod
INTERA Information Technologies Ltd.
Chiltern House
45 Station Road
Henley-on-Thames
Oxfordshire, RG9 1AT, UNITED KINGDOM

Alan Gutjahr
Department of Mathematics
New Mexico Institute of Mining and Technology
Socorro, NM 87801

C. Peter Jackson
Harwell Laboratory
Theoretical Studies Department
Radwaste Disposal Division
Bldg. 424.4
Oxfordshire Didcot Oxon OX11 ORA
UNITED KINDGOM

Rae Mackay
Department of Civil Engineering
University of Newcastle Upon Tyne
Newcastle Upon Tyne NE1 7RU
UNITED KINGDOM

Steve Gorelick
Department of Applied Earth Sciences
Stanford University
Stanford, CA 94305-2225

Peter Kitanidis
60 Peter Coutts Circle
Stanford, CA 94305

Dennis McLaughlin
Parsons Laboratory
Room 48-209
Department of Civil Engineering
Massachusetts Institute of Technology
Cambridge, MA 02139

Shlomo P. Neuman
College of Engineering and Mines
Department of Hydrology and Water Resources
University of Arizona
Tucson, AZ 85721

Yoram Rubin
Department of Civil Engineering
University of California
Berkeley, CA 94720

Foreign Addresses

Studiecentrum Voor Kernenergie
Centre D'Energie Nucleaire
Attn: A. Bonne
SCK/CEN
Boeretang 200
B-2400 Mol
BELGIUM

Atomic Energy of Canada, Ltd. (3)
Whiteshell Research Establishment
Attn: M.E. Stevens
B.W. Goodwin
D. Wushke
Pinewa, Manitoba ROE 1LO, CANADA

Juhani Vira
Teollisuuden Voima Oy (TVO)
Annankatu 42 C
SF-00100 Helsinki Suomi
FINLAND

Jean-Pierre Olivier
OECD Nuclear Energy Agency (2)
38, Boulevard Suchet
F-75016 Paris
FRANCE

D. Alexandre, Deputy Director
ANDRA
31 Rue de la Federation
75015 Paris
FRANCE

Claude Sombret
Centre D'Etudes Nucleaires
De La Vallee Rhone
CEN/VALRHO
S.D.H.A. B.P. 171
30205 Bagnols-Sur-Ceze, FRANCE

Bundesministerium fur Forschung und Technologie
Postfach 200 706
5300 Bonn 2, GERMANY

Bundesanstalt fur Geowissenschaften und Rohstoffe
Attn: M. Langer
Postfach 510 153
3000 Hanover 51, GERMANY

Gesellschaft fur Reaktorsicherheit (GRS) (2)
Attn: B. Baltes
W. Muller
Schwertnergasse 1
D-5000 Cologne, GERMANY

Institut fur Tieflagerung (2)
Attn: K. Kuhn
Theodor-Heuss-Strasse 4
D-3300 Braunschweig, GERMANY

Physikalisch-Technische Bundesanstalt
Attn: P. Brenneke
Postfach 33 45
D-3300 Braunschweig, GERMANY

Shingo Tashiro
Japan Atomic Energy Research Institute
Tokai-Mura, Ibaraki-Ken
319-11, JAPAN

Netherlands Energy Research Foundation (ECN)
Attn: L.H. Vons
3 Westerduinweg
PO Box 1
1755 ZG Petten, THE NETHERLANDS

Johan Andersson
Swedish Nuclear Power Inspectorate
Statens Kärnkraftinspektion (SKI)
Box 27106
S-102 52 Stockholm, SWEDEN

Fred Karlsson
Svensk Karnbransleforsorjning
AB SKB
Box 5864
S-102 48 Stockholm, SWEDEN

Nationale Genossenschaft für die
Lagerung Radioaktiver Abfälle (2)
Attn: S. Vomvoris
P. Zuidema
Hardstrasse 73
CH-5430 Wettingen, SWITZERLAND

AEA Technology
Attn: J.H. Rees
D5W/29 Culham Laboratory
Abington
Oxfordshire OX14 3DB, UNITED KINGDOM

AEA Technology
Attn: W.R. Rodwell
044/A31 Winfrith Technical Centre
Dorchester
Dorset DT2 8DH, UNITED KINGDOM

AEA Technology
Attn: J.E. Tinson
B4244 Harwell Laboratory
Didcot, Oxfordshire OX11 ORA
UNITED KINGDOM

D.R. Knowles
British Nuclear Fuels, plc
Risley, Warrington
Cheshire WA3 6AS, 1002607
UNITED KINGDOM

Internal

1 A. Narath
20 O.E. Jones
1502 J.C. Cummings
1511 D.K. Gartling
6000 D.L. Hartley
6115 P.B. Davies
6115 R.L. Beauheim
6119 E.D. Gorham
6119 Staff (14)
6121 J.R. Tillerson
6121 Staff (7)
6233 J.C. Eichelberger
6300 D.E. Ellis
6302 L.E. Shephard
6303 S.Y. Pickering
6303 W.D. Weart
6305 S.A. Goldstein
6305 A.R. Lappin
6306 A.L. Stevens
6312 F.W. Bingham
6313 L.S. Costin
6331 P.A. Davis
6341 Sandia WIPP Central Files (100)
6342 D.R. Anderson
6342 Staff (30)
6343 V. Harper-Slaboszewicz
6343 Staff (3)
6345 R.C. Lincoln
6345 Staff (9)
6347 D.R. Schafer
6348 J.T. Holmes
6348 Staff (4)
6351 R.E. Thompson
6352 D.P. Garber
6352 S.E. Sharpton
6400 N.R. Ortiz
6613 R.M. Cranwell
6613 R.L. Iman
6613 C. Leigh
6622 M.S.Y. Chu
6641 R.E. Luna, Acting
7141 Technical Library (5)
7151 Technical Publications
7613-2 Document Processing for
DOE/OSTI (10)
8523-2 Central Technical Files

☆ U.S. GOVERNMENT PRINTING OFFICE 1993—774-122/80240

THIS PAGE INTENTIONALLY LEFT BLANK